TECHNICAL UNIVERSITY OF CRETE

SCHOOL OF CHEMICAL AND ENVIRONMENTAL ENGINEERING

COMPUTATIONAL DYNAMICS & ENERGY RESEARCH GROUP

APPLICATION OF EXPANDED POLYSTYRENE (EPS) GEOFOAM FOR THE MITIGATION OF DYNAMIC VIBRATIONS AND DISTRESS OF CIVIL INFRASTRUCTURE

Ph.D. Thesis

Alexandros M. Lyratzakis

M.Eng. Civil Engineering, AUTH

M.Sc. School of Architecture, TUC

SUPERVISOR:

Professor Yiannis Tsompanakis

CHANIA, 2021

ΠΟΛΥΤΕΧΝΕΙΟ ΚΡΗΤΗΣ

ΣΧΟΛΗ ΧΗΜΙΚΩΝ ΜΗΧΑΝΙΚΩΝ ΚΑΙ ΜΗΧΑΝΙΚΩΝ ΠΕΡΙΒΑΛΛΟΝΤΟΣ

ΕΡΓΑΣΤΗΡΙΟ ΥΠΟΛΟΓΙΣΤΙΚΗΣ ΔΥΝΑΜΙΚΗΣ & ΕΝΕΡΓΕΙΑΣ

ΔΙΕΡΕΥΝΗΣΗ ΤΗΣ ΧΡΗΣΗΣ ΔΙΟΓΚΩΜΕΝΗΣ ΠΟΛΥΣΤΕΡΙΝΗΣ (EPS) ΣΕ ΤΕΧΝΙΚΑ ΕΡΓΑ ΥΠΟΔΟΜΗΣ ΚΑΙ ΤΗΝ ΑΠΟΜΕΙΩΣΗ ΔΥΝΑΜΙΚΩΝ ΦΟΡΤΙΩΝ ΚΑΙ ΤΑΛΑΝΤΩΣΕΩΝ

ΔΙΔΑΚΤΟΡΙΚΗ ΔΙΑΤΡΙΒΗ

Αλέξανδρου Μ. Λυρατζάκη
M.Eng. Civil Engineering
M.Sc. Architecture Engineering

ΕΠΙΒΛΕΠΩΝ:
Γιάννης Τσομπανάκης
Καθηγητής Πολυτεχνείου Κρήτης

ΧΑΝΙΑ, 2021

TECHNICAL UNIVERSITY OF CRETE

SCHOOL OF CHEMICAL AND ENVIRONMENTAL ENGINEERING
COMPUTATIONAL DYNAMICS & ENERGY RESEARCH GROUP

APPLICATION OF EXPANDED POLYSTYRENE (EPS) GEOFOAM FOR THE MITIGATION OF DYNAMIC VIBRATIONS AND DISTRESS OF CIVIL INFRASTRUCTURE

Ph.D. Thesis

Alexandros M. Lyratzakis

M.Eng. Civil Engineering, AUTH
M.Sc. School of Architecture, TUC

The Thesis is submitted to the School of Chemical and Environmental Engineering
of Technical University of Crete
in fulfillment of the requirements for the degree of doctor of philosophy

ADVISORY COMMITTEE:

1. Y. TSOMPANAKIS, Professor T.U.C. (supervisor)
2. N. LAGAROS, Professor N.T.U.A.
3. E. PLEVRIS, Professor OsloMet

EXAMINATION COMMITTEE:

1. Y. TSOMPANAKIS, Professor T.U.C. (supervisor)
2. N. LAGAROS, Professor N.T.U.A.
3. E. PLEVRIS, Professor OSLOMET
4. D. CHARMPIS, Associate Professor University of Cyprus
5. M. FRAGIADAKIS, Associate Professor N.T.U.A.
6. A. SEXTOS, Professor University of Bristol
7. C. PROVIDAKIS, Professor T.U.C.

CHANIA, 2021

ACKNOWLEDGMENTS

reference numerical models, which were further enhanced with the proposed mitigation measures. It should be stressed that the investigation of the HST-induced vibrations is a relatively new subject worldwide and this thesis consists the first specialized study in the field in Greece. Hence, the support by a top-expert in thse topics, such as Prof. Kouroussis, was extremely beneficial in the progress and completion of this research.

Last, but not least, I would like to acknowledge and express my deepest gratitude to the most patient people in the world, my parents. Except from the unconditional financial and psychological support, my parents endured and supported me in all the hard and easy moments during all these years. I'd like to thank my fiancé, Anna for being by my side in our effort for both of us to become doctors. Eventually we became doctors in 2021, it is just that Anna can also write medical prescriptions. Furthermore, a special thanks to my sister, Eleni, for her continuous assistance in the visual editing of the sketches of the dissertation.

Alexandros M. Lyratzakis

"If I have seen further,
it is by standing on the shoulders of Giants."
Isaac Newton

To my family,
for their invaluable support

ΠΟΛΥΤΕΧΝΕΙΟ ΚΡΗΤΗΣ

ΣΧΟΛΗ ΧΗΜΙΚΩΝ ΜΗΧΑΝΙΚΩΝ ΚΑΙ ΜΗΧΑΝΙΚΩΝ ΠΕΡΙΒΑΛΛΟΝΤΟΣ

ΕΡΓΑΣΤΗΡΙΟ ΥΠΟΛΟΓΙΣΤΙΚΗΣ ΔΥΝΑΜΙΚΗΣ and ΕΝΈΡΓΕΙΑΣ

Διδακτορική διατριβή του Αλέξανδρου Μ. Λυρατζάκη

Διερεύνηση της χρήσης διογκωμένης πολυστερίνης (EPS) σε τεχνικά έργα υποδομής για την απομείωση δυναμικών φορτίων και ταλαντώσεων.

Περίληψη

Η κυκλοφοριακή συμφόρηση αποτελεί ένα από τα πιο σημαντικά προβλήματα για τα συμβατικά μέσα μεταφοράς, όπως τα αυτοκίνητα και τα λεωφορεία. Το μειονέκτημα αυτό, οδηγεί όλο ένα και περισσότερο, στην αναζήτηση εναλλακτικών, άνετων, γρήγορων και φιλικών προς το περιβάλλον μέσων μεταφοράς. Τα τρένα υψηλής ταχύτητας (high-speed trains - HST) αποτελούν μια εξαιρετική εναλλακτική λύση σε αυτό το πρόβλημα, όμως θα πρέπει να διευθετηθούν κάποια ζητήματα ώστε να εξασφαλιστεί η σωστή λειτουργία τους. Το πιο σημαντικό πρόβλημα, το οποίο επηρεάζει την ασφάλεια των σιδηρόδρομων υποδομών υψηλής ταχύτητας, είναι τα ενισχυμένα επίπεδα κραδασμών που προκαλούνται λόγω της υψηλής ταχύτητας διέλευσης. Τις τελευταίες δεκαετίες, ο αναπτυσσόμενοι κραδασμοί κατά τη διέλευση HST θεωρούνται ως ένα ιδιαίτερα σημαντικό περιβαλλοντικό ζητήματα.

Για τον λόγο αυτό, έχουν πραγματοποιηθεί αρκετές μελέτες προκειμένου να προταθούν μέτρα περιορισμού των κραδασμών. Τα μέτρα αυτά μπορούν να ομαδοποιηθούν σε τέσσερις κατηγορίες: (α) την τροποποίηση της σιδηροτροχιάς, (β) την καλή και τακτική συντήρηση του σιδηροδρομικού δικτύου, (γ) την εφαρμογή μέτρων προστασίας σε θεμελίωση/σκελετό των κτιρίων, και (δ) την τοποθέτηση τάφρων με στόχο την απομείωση των επιφανειακών κυμάτων. Το πιο δημοφιλές μέτρο μετριασμού για τη μείωση του επιπέδου των κραδασμών είναι η κατασκευή τάφρων κατά μήκος του σιδηροδρομικού δικτύου. Τα τελευταία χρόνια, έχουν προταθεί διάφοροι τύποι τάφρων και υλικών πλήρωσης, ωστόσο, οι πιο αποτελεσματικές τάφροι έχουν υψηλό κόστος κατασκευής και συντήρησης. Ως εκ τούτου, η πρόταση ενός αποτελεσματικού και

οικονομικού μέτρου περιορισμού των κραδασμών εξακολουθεί να αποτελεί πρόκληση για την επιστημονική κοινότητα.

Μία ακόμη πρόκληση για τους ερευνητές είναι η εύρεση αριθμητικών, πειραματικών ή αναλυτικών μεθόδων, ικανών να προβλέψουν με ακρίβεια τα χαρακτηριστικά των κραδασμών. Για τον σκοπό αυτό, έχουν αναπτυχθεί διάφορα προσομοιώματα δύο (2D), δυόμιση (2.5D) και τριών διαστάσεων (3D) με τη χρήση των μεθόδων πεπερασμένων διαφορών, πεπερασμένων στοιχείων ή συνοριακών στοιχείων. Τα τελευταία χρόνια, οι προαναφερθείσες μεθοδολογίες χρησιμοποιήθηκαν για την εξέταση διαφόρων προβλημάτων, όπως η διερεύνηση της κρίσιμης ταχύτητας διέλευσης των HST, η επιρροή των γεωμετρικών και μηχανικών χαρακτηριστικών της σιδηροδρομικής γραμμής και του υπεδάφους, η εφαρμογή αποτελεσματικών μέτρων περιορισμού των κραδασμών, κ.λπ.

Βασικός στόχος της παρούσας διατριβής είναι η ανάπτυξη μίας αποτελεσματικής αριθμητικής μεθοδολογίας προσομοίωσης του σύνθετου δυναμικού φαινομένου, με σχετικά χαμηλό υπολογιστικό κόστος, ικανής να προβλέψει με ακρίβεια τους κραδασμούς του υπεδάφους κατά τη διέλευση HST. Για τον σκοπό αυτό, έχει επιλεγεί η μέθοδος των πεπερασμένων στοιχείων. Προκειμένου να διασφαλιστεί η αξιοπιστία της αριθμητικής μεθοδολογίας, τα αποτελέσματα του κάθε προσομοιώματος αναφοράς συγκρίθηκαν με διαθέσιμες επιτόπιες μετρήσεις. Συγκεκριμένα, χρησιμοποιήθηκαν μετρήσεις πεδίου κατά τη διέλευση του τρένου υψηλής ταχύτητας Thalys σε τρεις θέσεις της σιδηροδρομικής γραμμής Παρισιού-Βρυξελλών για την επαλήθευση της ορθότητας των αντίστοιχων αριθμητικών προσομοιωμάτων. Στη συνέχεια, πραγματοποιήθηκε εκτεταμένη διερεύνηση με στόχο την πρόταση αποτελεσματικών διατάξεων περιορισμού των κραδασμών με τη χρήση γεωαφρού διογκωμένης πολυστερίνης (expanded polystyrene – EPS) σε θέσεις επιχωμάτων και ορυγμάτων. Για τη διασφάλιση της αξιοπιστίας των προτεινόμενων διατάξεων, πραγματοποιήθηκε μια εκτενής διερεύνηση διαφόρων παραγόντων, όπως οι συνθήκες του υπεδάφους, η διάταξη της σιδηροτροχιάς, καθώς και η ταχύτητα διέλευσης του HST. Επιπροσθέτως, διερευνάται η προστασία γειτονικών κτιρίων και υπόγειων αγωγών με τη χρήση γεωαφρού EPS, όπου και πάλι αναδεικνύεται η συμβολή του προτεινόμενων μέτρων στην αντιμετώπιση των δυσμενών συνεπειών στις κατασκευές και στους ανθρώπους εξαιτίας των κραδασμών από τη διέλευση HST.

TECHNICAL UNIVERSITY OF CRETE

SCHOOL OF CHEMICAL AND ENVIRONMENTAL ENGINEERING

COMPUTATIONAL DYNAMICS and ENERGY RESEARCH GROUP

Ph.D. Thesis of Alexandros M. Lyratzakis

Application of expanded polystyrene (EPS) geofoam for the mitigation of dynamic vibrations and distress of civil infrastructure

Abstract

Traffic congestion is one of the most important issues related to the conventional means of transportation (e.g., cars or busses). This disadvantage has led to the development of alternative comfort, fast and environmentally friendly transportation means, such as high-speed trains (HST). Nonetheless, in order to safely operate relatively new transportation means such as HST, several important aspects should be properly addressed. The most important issue related to the safety of high-speed railway infrastructure and the disturbance/comfort of the residents of nearby buildings, is the vibrations developed due to the high passing velocity of the trains. In recent decades, the developing noise and vibrations induced by the HST passage, as well as their mitigation, are considered as very crucial issues in structural dynamics.

For this reason, several studies have been carried out aiming to propose optimal mitigation approaches in order to reduce ground-borne vibrations. These mitigation approaches can be grouped into four categories: (a) track modification, (b) track maintenance, (c) retrofitting to reduce vibrations of adjacent buildings and infrastructure, and (d) installation of wave barriers. The most popular mitigation measure to reduce the vibrations developed by the passage of HST is the construction of wave barriers/trenches across the railway. For this purpose, several types of wave barriers and filling materials have been proposed over the last decades. However, the most effective wave barriers have also high construction and maintenance costs. Hence, the proposal of an effective, low-cost mitigation measure is still a challenge for the engineering community.

An additional challenge for the researchers is to establish numerical, experimental or analytical approaches capable of predicting the developing vibrations in a reliable and accurate manner. For this purpose, several numerical approaches have been proposed, i.e., finite differences, finite element and boundary element-based methods. Furthermore, this complex phenomenon has been investigated via two-dimensional (2D), two-and-a-half-dimensional (2.5D) and three-dimensional (3D) models. Sophisticated computational models have been implemented in order to examine various issues, such as the critical speed of HST, the properties of the track and the subsoil, ground vibrations generated by two passing trains, mitigation measures of induced vibrations, train-structure interaction, etc.

One of the main aims of the current doctoral research is to present an efficient computational methodology, with low computational cost, capable of accurately predicting the HST-induced vibrations. For this purpose, the finite element method has been selected and advanced 3D models have been developed. In order to ensure the reliability of the numerical model, the numerical results have been compared with pre-available in-situ measurements. More specifically, field data from the passage of Thalys HST at three sites in Paris-Brussels line have been used in order to validate the developed numerical methodology. In the sequence, an extensive investigation of several mitigation measures based on the application of expanded polystyrene (EPS) geofoam at embankment and cutting sites has been performed in order to determine the optimal mitigation configuration. Accordingly, the impact of the subsoil conditions, the geometrical properties of the site or the HST passing speed have been investigated. Furthermore, the protection of nearby buildings and buried pipelines, using optimal configurations of EPS geofoam has been thoroughly examined and the results illustrate the efficiency of the proposed mitigation measures.

ΠΙΝΑΚΑΣ ΠΕΡΙΕΧΟΜΕΝΩΝ ΕΚΤΕΝΟΥΣ ΠΕΡΙΛΗΨΗΣ

ΕΚΤΕΝΗΣ ΠΕΡΙΛΗΨΗ

ΔΙΕΡΕΥΝΗΣΗ ΤΗΣ ΧΡΗΣΗΣ ΔΙΟΓΚΩΜΕΝΗΣ ΠΟΛΥΣΤΕΡΙΝΗΣ ΣΕ ΤΕΧΝΙΚΑ ΕΡΓΑ ΥΠΟΔΟΜΗΣ ΚΑΙ ΤΗΝ ΑΠΟΜΕΙΩΣΗ ΔΥΝΑΜΙΚΩΝ ΦΟΡΤΙΩΝ ΚΑΙ ΤΑΛΑΝΤΩΣΕΩΝ

Α.1. Εισαγωγή

Τα τελευταία χρόνια, οι σιδηροδρομικές γραμμές υψηλής ταχύτητας (high-speed rails - HSR) αναπτύσσονται διαρκώς, οπότε τα τρένα υψηλής ταχύτητας (high-speed trains - HST) χρησιμοποιούνται ευρέως σε πολλές χώρες. Για παράδειγμα, στην Κίνα το συνολικό μήκος των σιδηροδρομικών γραμμών υψηλής ταχύτητας φτάνει πλέον τα 38,000km. Ως ένα από τα πλέον σύγχρονα μέσα μεταφοράς, το HST αποτελεί μια επιλογή μετακίνησης υψηλής ποιότητας καθώς είναι ακριβές, βολικό και κυρίως γρήγορο. Η μέγιστη αναπτυσσόμενη ταχύτητα των HST αυξάνεται συνεχώς και σε δοκιμές φτάνει τα 600 km/h, ενώ αναμένεται να αυξηθεί περαιτέρω τις επόμενες δεκαετίες. Εξαιτίας αυτών των πλεονεκτημάτων, πολλές νέες γραμμές HSR πρόκειται να κατασκευαστούν παγκοσμίως, καθιστώντας τον 21ο αιώνα ως την εποχή των HST. Στην Ελλάδα -παρά τις μεγάλες οικονομικό-τεχνικές δυσκολίες εξαιτίας του δύσκολου τοπογραφικού ανάγλυφου- γίνεται σοβαρή προσπάθεια για να αναβαθμιστεί το σιδηροδρομικό δίκτυο και να εναρμονιστεί όσο γίνεται περισσότερο με τα σύγχρονα δεδομένα.

Από την άλλη πλευρά, όπως όλες οι καινοτόμες ιδέες, έτσι και τα HST χρήζουν αυξημένης προσοχής για την αντιμετώπιση διάφορων θεμάτων, όπως η εξασφάλιση της ασφαλούς λειτουργίας, η ανθεκτικότητα των αμαξωμάτων και οι επιπτώσεις στο περιβάλλον και στον άνθρωπο. Αρκετοί ερευνητές επικεντρώνονται στο ζήτημα των δονήσεων, και κυρίως των εδαφικών κραδασμών που προκαλούνται από τα HST, καθώς οι αναπτυσσόμενες δονήσεις, εκτός από το αίσθημα ανασφάλειας στους επιβάτες προκαλούν όχληση στους περίοικους, αλλά πιθανώς και βλάβες στις παρακείμενες

κατασκευές και στα τεχνικά έργα υποδομής. Υπό αυτό το πρίσμα, η παρούσα Διδακτορική Διατριβή (Δ.Δ.) στοχεύει στη διερεύνηση εναλλακτικών προτάσεων απόσβεσης των κραδασμών με τη χρήση ελαφροβαρών υλικών πληρώσεως. Στο πλαίσιο αυτό, διερευνάται η χρήση διογκωμένης πολυστερίνης (expanded polystyrene - EPS) ως "φραγμός" των δονήσεων που προκαλούνται από τη διέλευση των HST.

Η ταχύτητα της αμαξοστοιχίας συνδέεται άμεσα με τη λειτουργικότητα και την ασφάλεια των σύγχρονων σιδηροδρομικών γραμμών υψηλής ταχύτητας. Η λειτουργικότητα σχετίζεται με: (α) τον θόρυβο των σιδηροδρόμων που μπορεί να προκαλέσει σημαντικές επιπτώσεις-διαταραχές στους περιοίκους, και (β) τις ζημιές σε γειτονικές κατασκευές λόγω των επιβαλλόμενων κραδασμών. Η ασφάλεια σχετίζεται με την ακεραιότητα των σιδηροδρομικών επιχωμάτων ή ορυγμάτων και των άλλων έργων υποδομής των σιδηροδρομικών γραμμών. Ειδικότερα, οι προκαλούμενες δονήσεις μπορεί: (α) να έχουν αντίκτυπο στην ευστάθεια τους, ή/και (β) να προκαλέσουν διαφορικές καθιζήσεις στο σώμα του επιχώματος ή/και των υποκείμενων εδαφικών στρώσεων. Τα προβλήματα αυτά μπορούν να αντιμετωπισθούν με κατάλληλες συμβατικές ή/και νέες τεχνικές, όπως η προτεινόμενη χρήση EPS, η οποία μπορεί να αποτελέσει μία οικονομική και αποτελεσματική λύση, είτε αυτόνομα, είτε σε συνδυασμό με άλλες.

Τα τελευταία χρόνια, έχουν προταθεί διάφορα αριθμητικά προσομοιώματα για τη διερεύνηση του φαινομένου των κραδασμών που προκαλούνται από τη διέλευση HST. Τα 3D προσομοιώματα θεωρούνται πλέον απαραίτητα για τον υπολογισμό των κραδασμών που προκαλούνται από τη διέλευση των HST. Ωστόσο, η αύξηση της ακρίβειας των 3D προσομοιωμάτων συνεπάγεται και την αύξηση του υπολογιστικού κόστους. Στο πλαίσιο της Δ.Δ., χρησιμοποιήθηκαν προηγμένα 3D προσομοιώματα πεπερασμένων στοιχείων, με στόχο την εύρεση μιας χρυσής τομής μεταξύ ακρίβειας των αποτελεσμάτων και υπολογιστικού κόστους. Τα εν λόγω προσομοιώματα ελέγχθηκαν κυρίως με μετρήσεις πεδίου, αλλά και πειραματικά αποτελέσματα εργαστηριακών δοκιμών.

Εξαιτίας των αρνητικών επιπτώσεων που δύναται προκαλούν οι κραδασμοί από τη διέλευση τρένων υψηλής ταχύτητας, τίθενται καίρια επιστημονικά ερωτήματα που σχετίζονται με την αντιμετώπιση του φαινομένου. Στην προσπάθεια να απαντηθούν αυτά τα ερωτήματα από την επιστημονική κοινότητα έχουν προταθεί διάφορα μοντέλα πρόβλεψης και αποτίμησης της αύξησης των δονήσεων πριν από την κατασκευή νέων γραμμών ή την αναβάθμιση υφιστάμενων. Επίσης, έχουν ερευνηθεί και χρησιμοποιηθεί στην πράξη μέτρα περιορισμού των δυναμικών δονήσεων. Ο πιο αποτελεσματικός τρόπος

μετριασμού της δόνησης του εδάφους είναι η μείωση των ταχυτήτων της αμαξοστοιχίας σε θέσεις όπου οι ταχύτητες των κυμάτων Rayleigh στο έδαφος είναι πολύ χαμηλές. Εάν αυτό δεν είναι εφικτό (π.χ., για οικονομικούς λόγους), τότε μπορούν να εφαρμοστούν ορισμένα μέτρα προστασίας, όπως η ενίσχυση των σιδηροδρομικών επιχωμάτων ή η κατασκευή προστατευτικών τάφρων και φραγμών μεταξύ σιδηροδρόμων και παρακείμενων κατασκευών. Στην παρούσα Δ.Δ. διερευνήθηκε η διατύπωση μιας νέας αποτελεσματικότερης και οικονομικότερης πρότασης μέτρων για την απομείωση των δυναμικών κραδασμών. Συγκεκριμένα, ερευνήθηκε αν η εφαρμογή EPS θα μπορούσε να αποτελέσει μία τεχνο-οικονομικά αποτελεσματική λύση προς αυτήν την κατεύθυνση.

A.2. Βιβλιογραφική Ανασκόπηση

A.2.1. Εισαγωγή

Σε αυτήν την ενότητα παρουσιάζεται μια συνοπτική επισκόπηση της υφιστάμενης βιβλιογραφίας, σχετικά με το περίπλοκο φαινόμενο των παραγόμενων κραδασμών κατά τη διέλευση τρένων υψηλής ταχύτητας. Αρχικά, περιγράφεται η δημιουργία και η διάδοση των δονήσεων και γίνεται μια σύντομη αναφορά στη θεωρία της διάδοσης των κυμάτων. Εξετάζεται η επίδραση των δονήσεων στους ανθρώπους και τα κτίρια και παρουσιάζονται οι πιο κοινοί δείκτες για την εκτίμησή τους. Επιπλέον, πραγματοποιήθηκε μια αναλυτική ανασκόπηση της διαδικασίας συντήρησης της γραμμής και των διαθέσιμων προσεγγίσεων περιορισμού των κραδασμών. Τέλος, εξετάστηκαν εν συντομία υφιστάμενες αναλυτικές και αριθμητικές προσεγγίσεις για την περιγραφή του προβλήματος.

A.2.2. Μηχανισμός δημιουργίας και διάδοσης κραδασμών

Η κατανόηση του μηχανισμού δημιουργίας των κραδασμών, κατά την αλληλεπίδραση του διερχόμενου HST με τις ράγες, είναι ζωτικής σημασίας για την άρτια διερεύνηση του φαινομένου. Το βάρος, τα γεωμετρικά χαρακτηριστικά καθώς και το σύστημα ανάρτησης του HST επηρεάζουν έντονα τη μορφή των προκαλούμενων κραδασμών. Οι κραδασμοί εξαρτώνται άμεσα από παράγοντες όπως η τραχύτητα των τροχών και των ραγών, οι συνδέσεις των ραγών, η δυσκαμψία των υποστρώσεων της σιδηροτροχιάς, καθώς και τα μηχανικά χαρακτηριστικά του υπεδάφους (Nelson and Saurenman, 1983). Τα φορτία των παραγόμενων κραδασμών χωρίζονται συνήθως σε δύο κατηγορίες, τα στατικά και τα δυναμικά (Lombaert et al., 2003). Τα στατικά φορτία προκαλούνται λόγω του βάρους των αξόνων του διερχόμενου HST και είναι υπεύθυνα για τις δονήσεις στις χαμηλές

συχνότητες (0-20Hz). Τα στατικά φορτία εξαρτώνται από το βάρος του HST, επομένως δεν μεταβάλλονται ανάλογα με την ταχύτητα διέλευσης του HST.

Από την άλλη πλευρά, το δυναμικό μέρος του φορτίου επηρεάζεται έντονα από την ταχύτητα διέλευσης της αμαξοστοιχίας, καθώς οι κύριοι παράγοντες που το επηρεάζουν θεωρούνται η απόσταση μεταξύ των στρωτήρων, οι συνθήκες του υπεδάφους και η τραχύτητα της ράγας και των τροχών. Η απόσταση τοποθέτησης των στρωτήρων επηρεάζει άμεσα τη δυσκαμψία της ράγας, καθώς είναι προφανές ότι η δυσκαμψία είναι υψηλότερη όταν ο τροχός διέρχεται πάνω από τη θέση ενός στρωτήρα και μικρότερη κατά τη διέλευση από το κενό μεταξύ δυο διαδοχικών στρωτήρων. Ως εκ τούτου, είναι προφανές ότι προκαλούν περιοδική διέγερση, η οποία εξαρτάται άμεσα από την ταχύτητα διέλευσης, τα γεωμετρικά χαρακτηριστικά και το βάρος του HST. Επίσης, διάφοροι άλλοι παράμετροι, όπως οι θέσεις των συνδέσεων των ραγών ή οι προβληματικοί τροχοί μπορεί να επηρεάσουν το δυναμικό μέρος του φορτίου, προκαλώντας κραδασμούς υψηλών συχνοτήτων. Αξίζει να σημειωθεί ότι αυτοί οι παράμετροι καθίστανται όλο και λιγότερο σημαντικοί, καθώς το επίπεδο συντήρησης των σιδηροδρομικών γραμμών βελτιώνεται ραγδαία, ειδικά σε γραμμές υψηλών ταχυτήτων. Επιπλέον, η εκτεταμένη χρήση των συνεχώς συγκολλημένων ραγών έχει ελαχιστοποιήσει τις ανωμαλίες που οφείλονται στις συνδέσεις.

Μετά τη δημιουργία τους, οι κραδασμού διαδίδονται από τη σιδηροτροχιά στο έδαφος υπό τη μορφή εγκάρσιων, διαμηκών και επιφανειακών κυμάτων. Σύμφωνα με τον Woods (1968), το 67% των κραδασμών μεταδίδεται ως επιφανειακά κύματα Rayleigh. Το ποσοστό των εγκάρσιων και διαμηκών κυμάτων είναι ίσο με 7% και 26%, αντίστοιχα. Επομένως, τα κύματα Rayleigh είναι τα κυρίαρχα και αυτά που επηρεάζουν τις δραστηριότητες των περίοικων και τη λειτουργικότητα των γειτονικών κατασκευών. Εκτός από την ευρύτερη περιοχή πέριξ της σιδηροτροχιάς, ένα μέρος των δονήσεων μεταφέρονται προς τα πάνω, μέσα στο ίδιο το HST. Αυτό το φαινόμενο είναι εξίσου σημαντικό με τη διάδοση των δονήσεων στην επιφάνεια του εδάφους, καθώς οι δονήσεις διαταράσσουν τους επιβάτες της αμαξοστοιχίας. Συνεπώς, η μείωση των δονήσεων προς τα πάνω είναι ζωτικής σημασίας για την διασφάλιση της σωστής λειτουργίας της αμαξοστοιχίας. Για τον σκοπό αυτό, τα HST χρησιμοποιούν συνήθως δύο συστήματα ανάρτησης, το πρώτο συνδέει τους τροχούς και τα φορεία και το δεύτερο ενώνει τα φορεία με το αμάξωμα του αυτοκινήτου (Kouroussis et al., 2014). Στην περίπτωση των τρένων μεγάλης ταχύτητας, η άνεση του επιβάτη είναι ζωτικής σημασίας. Ως εκ τούτου, το HST πρέπει να παρέχει ένα κατάλληλο

περιβάλλον όπου οι επιβάτες θα μπορούσαν να διαβάζουν ή να γράφουν. Οι Pallord και Simons (1984) εξέτασαν τον ρόλο των αναρτήσεων στην άνεση του επιβάτη και κατέληξαν στο συμπέρασμα ότι οι κραδασμοί εντός του εύρους χαμηλών συχνοτήτων (0.8Hz-8Hz) και ειδικά κάτω των 5Hz, θα μπορούσαν να διαταράξουν την ανάγνωση ή τη γραφή των επιβατών.

Η σιδηροδρομική γραμμή έχει σημαντικό ρόλο στην διάδοση των κραδασμών καθώς αποτελεί την βάση έδρασης των ραγών. Υπάρχουν δυο βασικές κατηγορίες σιδηροδρομικής γραμμής, ανάλογα αν το σύστημα έδρασης είναι με ή χωρίς υπόβαση (ballasted και ballastless, αντίστοιχα). Τα συστήματα με υπόβαση είναι τα πιο συνηθισμένα και αποτελούνται από ράγες, στρωτήρες και το έρμα της υπόβασης. Το έρμα από αδρανή αυξάνει την ευκαμψία της σιδηροδρομικής γραμμής και μειώνει το επίπεδο των κραδασμών στο περιβάλλον έδαφος. Από την άλλη πλευρά, στα σύστήματα χωρίς έρμα, οι ράγες εδράζονται απευθείας σε πλάκες σκυροδέματος, όπου μπορούν να ενσωματωθούν και συστήματα απόσβεσης κραδασμών. Τα εν λόγω συστήματα αποτελούν πιο αποτελεσματική διάταξη για τη μείωση των κραδασμών και τα τελευταία χρόνια προτιμώνται σε χώρες με ραγδαίως αναπτυσσόμενα σιδηροδρομικά δίκτυα, όπως η Κίνα.

Τα μηχανικά χαρακτηριστικά των ραγών αποτελούν σημαντικό παράγοντα για τη διάδοση των κραδασμών. Για παράδειγμα, σε εύκαμπτες ράγες μπορεί να προκληθούν μεγάλες παραμορφώσεις, αυξάνοντας τον κίνδυνο εκτροχιασμού, ενώ εξαιτίας των παραμορφώσεων απαιτείται μεγαλύτερη ισχύ για την κίνηση του HST. Αντιθέτως, σε πολύ δύσκαμπτες ράγες μπορεί να προκληθεί συγκέντρωση τάσεων σε μια μικρή περιοχή ολίσθησης, οδηγώντας σε αυλάκωση των τροχών (Grossoni et al., 2018). Σε γενικές γραμμές, είναι δύσκολο να υπολογιστούν οι βέλτιστες τιμές δυσκαμψίας της τροχιάς, καθώς οι προτεινόμενες τιμές διαφέρουν ανάλογα με τα πρότυπα κάθε χώρας και τον τύπο των τρένων λειτουργίας. Συνεπώς, είναι ακόμα πιο δύσκολο να προταθεί μια βέλτιστη τιμή δυσκαμψίας για μια γραμμή HSR, την οποία χρησιμοποιούν διάφοροι τύποι αμαξοστοιχιών.

Ένας ακόμη σημαντικός παράγοντας που σχετίζεται με τη διάδοση των κραδασμών είναι το περιβάλλον έδαφος, καθώς αποτελεί το μέσο μετάδοσης των κραδασμών και στα γειτονικά κτίρια και τεχνικά έργα υποδομής. Ο βασικός παράγοντας επιρροής της απόκρισης του εδάφους είναι η ταχύτητα διέλευσης του HST, καθώς έχει παρατηρηθεί σημαντική αύξηση των κραδασμών εάν το HST διέρχεται με ταχύτητα υψηλότερη από την ταχύτητα των επιφανειακών κυμάτων του περιβάλλοντος εδάφους, η οποία είναι γνωστή

ως κρίσιμη ταχύτητα. Όπως είναι αναμενόμενο, καθώς η ταχύτητα των HST αυξάνεται, μεγαλώνει η πιθανότητα υπέρβασης της κρίσιμης ταχύτητας σε περισσότερες θέσεις του HSR. Η προκαλούμενη αύξηση του επιπέδου των κραδασμών λόγω της κρίσιμης ταχύτητας, μπορεί να προκαλέσει σημαντικά προβλήματα, τα οποία μπορεί να σχετίζονται με βλάβες της σιδηροτροχιάς καθώς και στην υγεία των περίοικων ή των χρηστών του HST.

Α.2.3. Επιπτώσεις των κραδασμών

Η ταχεία ανάπτυξη των γραμμών HSR κατά τις τελευταίες δεκαετίες οδήγησε διάφορους διεθνείς οργανισμούς, στην υιοθέτηση κατάλληλων δεικτών μέτρησης των παραγόμενων κραδασμών. Στην παρούσα ενότητα παρουσιάζονται οι κύριοι δείκτες που έχουν προταθεί για την διερεύνηση του αντίκτυπου των αναπτυσσόμενων δονήσεων σε ανθρώπους και κατασκευές. Τα δύο πιο κοινά ζητήματα τα οποία διερευνούν οι εν λόγω δείκτες, είναι η επιρροή στους ανθρώπους και οι βλάβες σε κοντινά κτίρια. Γενικά, η συνεχόμενη έκθεση στους κραδασμούς επηρεάζει άμεσα την υγεία και την άνεση των περίοικων. Ο Διεθνής Οργανισμός Τυποποίησης (ISO) εστιάζει στην ανθρώπινη έκθεση στους προκαλούμενους κραδασμούς. Το αντίστοιχο πρότυπο έχει ομαδοποιηθεί σε δύο μέρη: το ISO 2631-part 1, το οποίο διερευνά τους κραδασμούς που αισθάνονται οι επιβάτες της αμαξοστοιχίας και το ISO 2631-part 2, το οποίο εξετάζει την επίδραση των προκαλούμενων κραδασμών στα κοντινά κτίρια και στους κατοίκους τους. Σύμφωνα με το ISO2631-part 1, προτείνονται δείκτες που εξαρτώνται από τη συχνότητα και σχετίζονται με τις δραστηριότητες των επιβατών, τη στάση του σώματος (π.χ., όρθια, καθιστή ή ύπνου) και την κατεύθυνση των κραδασμών. Για την όχληση των περίοικων το ISO 2631- part 2 δεν λαμβάνει υπόψη την κατεύθυνση των δονήσεων και τη θέση του ανθρώπινου σώματος και εστιάζει στο εύρος χαμηλών συχνοτήτων από 1Hz έως 20 Hz.

Τα Γερμανικά πρότυπα (DIN), μέσω της οδηγίας DIN 4150-2, προτείνουν τη χρήση της σταθμισμένης μέσης τετραγωνικής ρίζας του σήματος ταχύτητας, λόγω του δυναμικού χαρακτήρα των κραδασμών. Σύμφωνα με το DIN 4150-2, το μέσο σταθμισμένο σήμα υπολογίζεται ως εξής:

$$KB_F(t) = \sqrt{\frac{1}{\tau} \int_0^T KB^2(\xi) e^{\frac{t-\xi}{\tau}} d\xi} \tag{A.1}$$

Το σταθμισμένο σήμα ταχύτητας, KB (t), λαμβάνεται μέσω του φίλτρου υψηλής διέλευσης ως το αρχικό σήμα ταχύτητας συναρτήσει της συχνότητας, f:

$$H_{KB}(f) = \frac{1}{\sqrt{1+(\frac{5.6}{f})^2}}$$

(A.2)

Από την άλλη πλευρά, το DIN 4150-3 εστιάζει στην επίδραση των κραδασμών στα κτίρια. Για τον σκοπό αυτό, εισάγεται ένας δεύτερος δείκτης, η μέγιστη ταχύτητα σωματιδίων (peak particle velocity - PPV). Η PPV ορίζεται ως η μέγιστη τιμή της χρονοϊστορίας ταχυτήτων στην κυρίαρχη κατεύθυνση της διέγερσης. Επομένως, σύμφωνα με το DIN, το PPV υπολογίζεται ως εξής:

$$PPV = \max|v(t)|$$

(A.3)

Πίνακας Α.1. Σύνοψη οριακών τιμών δεικτών επιπέδου κραδασμών (Kouroussis et al., 2014).

Κανονισμός	Δείκτης	Οριακή τιμή	Είδος χρήσης
Επίδραση στα κτίρια			
DIN 4150-3	Μέγιστη ταχύτητα σωματιδίου (κύρια διεύθυνση)	3 mm/s	Πολύ ευαίσθητα κτίρια
		5 mm/s	Συγκροτήματα κατοικιών
SN 640 312a	Μέγιστη ταχύτητα σωματιδίου	3 mm/s	Ευαίσθητα κτίρια σε συχνή έκθεση σε κραδασμούς
		6 mm/s	Ευαίσθητα κτίρια σε κανονική έκθεση σε κραδασμούς
Επίδραση στους ανθρώπους			
ISO 2631-2	Σταθμισμένη μέση τετραγωνική Επιτάχυνση	0.315 m/s²	Καθόλου ή μικρή όχληση
		2 m/s²	Σημαντική όχληση
USDT	Σταθμισμένη μέση τετραγωνική ταχύτητα	0.10 mm/s	Αστική περιοχή Συχνή (>70 διελεύσεις/ημέρα)
		0.26 mm/s	Αστική περιοχή Σπάνια (>70 διελεύσεις/ημέρα)
DIN 4150-2	Σταθμισμένο $KB_{F,max}$	0.15 mm/s	Αστική περιοχή
		0.10 mm/s	Ευαίσθητη περιοχή

Αξίζει να σημειωθεί ότι οι Ελβετικές οδηγίες (Schweizerische Normen-Vereinigung, 1992), σε αντίθεση με το DIN, λαμβάνουν υπόψη και τις τρείς συντεταγμένων του PPV. Ακολούθως, ο PPV προκύπτει ως εξής:

$$PPV = \max\left[\sqrt{v_x^2(t) + v_y^2(t) + v_z^2(t)}\right]$$

(A.4)

Προφανώς, στην περίπτωση που υπάρχει μία κυρίαρχη κατεύθυνση, οι τιμές που προκύπτει από τις εξισώσεις Α.3 και Α.4 είναι σχεδόν ίδιες.

Το Υπουργείο Μεταφορών των Ηνωμένων Πολιτειών έχει παρουσιάσει μια κλίμακα ντεσιμπέλ για να διερευνήσει την επίδραση των επιπτώσεων των προκαλούμενων κραδασμών σε γειτονικά κτίρια. Το επίπεδο των ντεσιμπέλ υπολογίζεται ως εξής:

$$V_{dB} = 20 \log_{10} \frac{V_{rms}}{V_0} \qquad\qquad (A.5)$$

Ο Πίνακας Α.1. συνοψίζει τις προτεινόμενες οριακές τιμές των προαναφερόμενων διεθνών προτύπων.

Α.2.4. Μέθοδοι περιορισμού των κραδασμών

Οι αρνητικές επιπτώσεις των κραδασμών στην υγεία των περίοικων καθώς και στη δομική κατάσταση των γειτονικών κτιρίων οδήγησε την παγκόσμια επιστημονική κοινότητα στη διερεύνηση διάφορων μέτρων περιορισμού των αναπτυσσόμενων κραδασμών (Feng et al., 2019a; Gao et al., 2020; Thompson et al., 2016a; With et al., 2009). Τα μέτρα περιορισμού των κραδασμών ομαδοποιούνται σε τρεις κατηγορίες: α) στις τροποποιήσεις του HST και στη συντήρηση των ραγών (Ferreira and López-Pita, 2015), β) στην τοποθέτηση τάφρων ή άλλων φραγμών των κραδασμών στη διαδρομή μετάδοσης (Garinei et al., 2014; Takemiya, 2004; Yarmohammadi et al., 2018), γ) σε τοπικά μέτρα έναντι κραδασμών περιμετρικά σε ευαίσθητα κτίρια (Yang et al., 2019). Η βέλτιστη λύση θα πρέπει να λαμβάνει υπόψη τόσο τις τεχνικές όσο και τις οικονομικές πτυχές του εξεταζόμενου προβλήματος.

Η πρώτη κατηγορία μέτρων περιλαμβάνει τόσο λύσεις σχεδιασμού νέων HSR όσο και συντήρησης υφισταμένων. Σε νέες σιδηροδρομικές γραμμές με κατάλληλο σχεδιασμό διαδρομών, επιλέγονται οι βέλτιστες θέσεις για διακόπτες, στροφές και διασταυρώσεις, όπου συνήθως αυξάνεται το επίπεδο κραδασμών. Επιπλέον, εξετάζονται στο στάδιο του σχεδιασμού διάφορες λύσεις, όπως καλύτερος σχεδιασμός τροχών/αξόνων χρησιμοποιώντας υλικά υψηλότερης απόδοσης. Η χρήση ελαστικών τροχών (resilient wheels) (Pita et al., 2004) ή συστημάτων ελέγχου δονήσεων (Dahlberg, 2010) θα μπορούσε να έχει ευεργετικό ρόλο στη μείωση των δονήσεων. Έχει αναφερθεί ότι η εφαρμογή ελαστικών συστημάτων στερέωσης οδηγεί σε μείωση θορύβου μεταξύ 3dB και 6dB, σε σύγκριση με το κλασικό σύστημα τροχών (Federal Transit Administration, 1997). Ένα ακόμα αποτελεσματικό μέτρο είναι η χρήση αποσβεστήρων ράγας (rail dampers). Οι αποσβεστήρες μπορούν να συγκολληθούν ή να συνδεθούν εύκολα σε υπάρχουσες και νέες σιδηροδρομικές γραμμές. Ο κύριος μηχανισμός αυτής της μεθόδου βασίζεται στην αύξηση του βάρους της ράγας προκειμένου να αποφευχθούν οι δονήσεις. Τέλος, όπως έχει ήδη αναφερθεί, η χρήση συνεχούς ράγας μπορεί επίσης να μειώσει το επίπεδο κραδασμών. Σε υφιστάμενες γραμμές, όπου τα προαναφερόμενα μέτρα δεν μπορούν να εφαρμοστούν,

προτείνεται η μείωση της ταχύτητας διέλευσης του HST στις επικίνδυνες θέσεις της διαδρομής.

Η δεύτερη κατηγορία μέτρων αφορά την τοποθέτηση κάποιου «φράγματος» κραδασμών παράλληλα με τη σιδηροτροχιά. Τα τελευταία χρόνια έχουν προταθεί πολυάριθμα μέτρα περιορισμού, προκειμένου να αποφευχθεί η διάδοση των κραδασμών στη γύρω περιοχή (Connolly et al., 2015; Dijckmans et al., 2015; Karlström and Boström, 2007). Η πιο συχνά χρησιμοποιούμενη προσέγγιση είναι η διάνοιξη μιας ή πολλαπλών τάφρων οι οποίες έχουν ως βασικό στόχο να ανακλούν και να απορροφούν τις δονήσεις (Sitharam et al., 2018). Η ασυνέχεια μεταξύ του εδάφους και του υλικού πλήρωσης της τάφρου οδηγεί στον περιορισμό των κραδασμών στη διεπιφάνεια τους. Οι ανοικτές τάφροι θεωρούνται οι πιο αποτελεσματικές στον περιορισμό των κραδασμών (Hung et al., 2004; Yang et al., 2018). Όμως, προβλήματα όπως η διατήρηση της αρχικής γεωμετρίας τους, η αποφυγή φυτών ή πλήρωσης με νερό ή άλλα υλικά, είναι δύσκολο να αντιμετωπιστούν. Επομένως, για τεχνικούς λόγους αρκετές φορές προτιμούνται οι - λιγότερο αποτελεσματικές- πληρωμένες τάφροι. Αναμφίβολα, η αποτελεσματικότητα μιας πληρωμένης τάφρου εξαρτάται άμεσα από τις ιδιότητες του υλικού πλήρωσης. Αρκετά υλικά έχουν χρησιμοποιηθεί για την πλήρωση των τάφρων, όπως σκυρόδεμα ή μπεντονίτης (Al-Hussaini and Ahmad, 1996), αεροστεγείς σάκοι αερίου (gas-filled cushions) (Massarsch, 2005), νερό (Ekanayake et al., 2014), μείγμα άμμου-καουτσούκ (Chew et al., 2019), πολυουρεθάνη (Alzawi et al., 2011) ή διογκωμένη πολυστερίνη (Bo et al., 2014).

Όπως έχει αναφερθεί, οι κραδασμοί μεταδίδονται μέσω του εδάφους σε κοντινά κτίρια και έργα υποδομής. Επομένως, είναι απαραίτητο να εφαρμοστούν περαιτέρω τοπικά μέτρα σε κτίρια και έργα υψηλής σημασίας. Υπάρχει πάντοτε η επιλογή να κατασκευαστεί ένα κέλυφος μεταξύ της θεμελίωσης του κτιρίου και του εδάφους. Αυτή είναι μια εξαιρετική λύση για την προστασία υφιστάμενων κτιρίων, αν και, στην περίπτωση νέων κατασκευών κοντά σε γραμμές HSR, είναι δυνατή η μείωση των δομικών δονήσεων μέσω κατάλληλων μέτρων κατά τον σχεδιασμό τους. Αυτή η προσέγγιση χρησιμοποιείται συνήθως για κατασκευές πάνω από υπόγειες γραμμές. Η βασική αρχή του σχεδιασμού, είναι η απομόνωση της ανωδομής με τη χρήση της μεθόδου της σεισμικής μόνωσης βάσης με στόχο την τροποποίηση των κύριων συχνοτήτων του κτιρίου.

A.2.5. Γεωαφρός διογκωμένης πολυστερίνης

Στην παρούσα διατριβή διερευνάται η χρήση γεωαφρού διογκωμένης πολυστερίνης σε διάφορες διατάξεις ως μέτρο περιορισμού των κραδασμών. Σύμφωνα με τον Horvarth (1994), ο όρος γεωαφρός έχει εισαχθεί στην επιστημονική κοινότητα για να εντάξει σε μια κατηγορία όλους τους πλαστικούς αφρούς, οι οποίοι χρησιμοποιούνται σε γεωτεχνικές εφαρμογές. Αξίζει να σημειωθεί ότι από την δεκαετία του 1960, ο γεωαφρός EPS χρησιμοποιείται ως υλικό πλήρωσης σε μια πληθώρα γεωτεχνικών έργων, όπως οδικά και σιδηροδρομικά επιχώματα, σταθεροποίηση κλίσης πρανών, μείωση πλευρικών ωθήσεων, απόσβεση κραδασμών και πλήρωση υπόβασης οδών, κυρίως λόγω του μικρού του βάρους. Συγκεκριμένα, το βάρος του EPS είναι περίπου ίσο με το 1% του βάρους του εδάφους και λιγότερο από 10% του βάρους εναλλακτικών ελαφροβαρών υλικών πλήρωσης (Stark et al., 2012).

Ο ευεργετικός ρόλος του γεωαφρού EPS είναι εμφανής στη μείωση του κόστους και του χρονοδιαγράμματος των τεχνικών έργων, λόγω της ευκολίας στη χρήση του και την ανθεκτικότητα του σε διάφορες καιρικές συνθήκες. Ως εκ τούτου, είναι σε θέση να διατηρεί μακροπρόθεσμα τις μηχανικές του ιδιότητες, ενώ και η διάρκεια ζωής του είναι παρόμοια με άλλα εναλλακτικά υλικά. Η ευρεία χρήση του γεωαφρού EPS οδήγησε στην παραγωγή διαφόρων τύπων, εξειδικευμένων για κάθε εφαρμογή.

Σε σύγκριση με τις εφαρμογές του γεωαφρού σε τεχνικά έργα, όπως γέφυρες και αυτοκινητόδρομοι, το EPS δεν έχει χρησιμοποιηθεί ακόμη ευρέως στην περίπτωση των σιδηροδρομικών έργων. Ωστόσο, οι μηχανικές του ιδιότητες έχουν προσελκύσει το ενδιαφέρον αρκετών ερευνητών στον τομέα της σιδηροδρομικής μηχανικής. Ο γεωαφρός EPS μπορεί να χρησιμοποιηθεί για τη διαχείριση παρόμοιων ζητημάτων με τις εφαρμογές σε αυτοκινητόδρομους, όπως η έδραση της σιδηροδρομικής γραμμής σε θέσεις με προβληματικό υπέδαφος. Ο γεωαφρός EPS μπορεί να χρησιμοποιηθεί ως υλικό πλήρωσης σιδηροδρομικών επιχωμάτων για τον περιορισμό της καταπόνησης των υποκείμενων εδαφών ή για τη σταθεροποίηση των πλαγιών σιδηροδρομικών ορυγμάτων. Για παράδειγμα, στην Utah στις Η.Π.Α., χρησιμοποιήθηκε γεωαφρός EPS για την έδραση του σιδηροδρόμου, στην κοιλάδα του Salt Lake. Αυτό το έργο ήταν η πρώτη εφαρμογή σε σιδηροδρομικό έργο και ένα από τα μεγαλύτερα έργα όσον αφορά τη χρήση EPS στις ΗΠΑ. Πρέπει να αναφερθεί ότι αυτό το έργο έχει ολοκληρωθεί με μικρότερο από τον αρχικό προϋπολογισμό και νωρίτερα από το χρονοδιάγραμμα λόγω της εύκολης χρήσης

του γεωαφρού EPS. Στην παρούσα διατριβή ο γεωαφρός χρησιμοποιείται ως φράγμα για τον περιορισμό των κραδασμών από τη διέλευση τρένων υψηλής ταχύτητας.

Α.2.6. Μέθοδοι πρόβλεψης κραδασμών

Η περιπλοκότητα του φαινομένου των προκαλούμενων κραδασμών από τη διέλευση HST οδήγησε την επιστημονική κοινότητα στην ανάπτυξη κατάλληλων πειραματικών, αναλυτικών και αριθμητικών μοντέλων πρόβλεψης. Το ιδανικό μοντέλο πρέπει να προβλέπει με ακρίβεια το συχνοτικό περιεχόμενο και το μέγεθος των κραδασμών σε ένα μεγάλο εύρος αποστάσεων από την σιδηροτροχιά, λαμβάνοντας υπόψη τόσο τη γεωμετρία όσο και την απόσβεση του υλικού. Στη συνέχεια, παρουσιάζεται μια σύντομη ανασκόπηση των υφιστάμενων μεθοδολογιών. Οι μετρήσεις πεδίου είναι η πιο άμεση προσέγγιση. Ο διεθνής οργανισμός πιστοποίησης (ISO) μέσω του πρότυπου ISO 14837-1 (2005), προτείνει ένα πρόγραμμα εργασιών για την καταγραφή των κραδασμών. Σύμφωνα με το προτεινόμενο πρόγραμμα εργασιών, μια σειρά αισθητήρων τοποθετείται σε αυξανόμενη απόσταση από την σιδηροτροχιά για να υπολογιστεί ο βαθμός απομείωσης της ταχύτητας σε αυξανόμενη απόσταση.

Οι Degrande και Schillemans (2001) διεξήγαγαν μια σειρά μετρήσεων πεδίου με στόχο τη διερεύνηση της απόκριση του εδάφους κατά την διέλευση του Thalys HST με ταχύτητα μεταξύ 223km/h και 214km/h. Αυτές οι μετρήσεις συνέβαλαν σημαντικά στην κατανόηση του φαινομένου, καθώς πολλοί ερευνητές τις χρησιμοποίησαν για να επαληθεύσουν τα αριθμητικά τους μοντέλα. Πιο πρόσφατα, ο Connolly et al. (2014) πραγματοποίησε μια νέα σειρά μετρήσεων πεδίου, μελετώντας τα HST Thalys, TGV και Eurostar σε διάφορες θέσεις (σε επίπεδο, επίχωμα, όρυγμα και διάβαση πεζών) στη γραμμή HSR Παρισιού-Βρυξελλών. Πρέπει να αναφερθεί ότι οι συγγραφείς παρέχουν δωρεάν πρόσβαση σε ένα μέρος των δεδομένων των μετρήσεων για ερευνητές που ασχολούνται στον τομέα των σιδηροδρομικών δονήσεων.

Οι μετρήσεις πεδίου αποτελούν ένα εξαιρετικό εργαλείο, καθώς παρέχουν ακριβή αποτελέσματα, τα οποία θα μπορούσαν να χρησιμοποιηθούν για την κατασκευή νέων HSR. Από την άλλη πλευρά, ο χρόνος και το κόστος αποτελούν το βασικό τους μειονέκτημα. Επιπλέον, οι πειραματικές αναλύσεις περιορίζονται συνήθως σε μια πολύ συγκεκριμένη θέση για τη διέλευση ενός συγκεκριμένου HST. Παρ' όλα αυτά είναι αδύνατο να επιλεχθεί μια τοποθεσία, όπου οι στόχοι της έρευνας αντιστοιχούν σε υπερκρίσιμα φαινόμενα. Ένας σημαντικός περιορισμός είναι η καταγραφή του

εξωτερικού θορύβου από άλλες πηγές (π.χ., διερχόμενα αυτοκίνητα), οι οποίες αλλοιώνουν τα αποτελέσματα. Ωστόσο, οι μετρήσεις πεδίου είναι εξαιρετικά χρήσιμες στην επαλήθευση αναλυτικών ή αριθμητικών προσομοιωμάτων.

Επομένως, οι ερευνητές εκτός από τις μετρήσεις πεδίων, στράφηκαν σε εναλλακτικές, λιγότερο κοστοβόρες και χρονοβόρες μεθόδους πρόβλεψης των κραδασμών. Η πρώτη εναλλακτική λύση που χρησιμοποιήθηκε ήταν μέσω αναλυτικών μοντέλων. Το βασικό πλεονέκτημα των αναλυτικών μοντέλων είναι το χαμηλό υπολογιστικό κόστος, ως εκ τούτου, πριν από την ανάπτυξη της σύγχρονης τεχνολογίας υπολογιστών, τα αναλυτικά μοντέλα ήταν η κυρίαρχη προσέγγιση. Η πρώτη προσέγγιση χρησιμοποίησε ένα ομοιογενές σώμα τροχιάς, στο οποίο η ράγα στηριζόταν μέσω ελατηρίων Winkler. Αυτή η προσέγγιση είναι γνωστή ως μέθοδος ενός στρώματος (single layer) και εξακολουθεί να χρησιμοποιείται για τη διερεύνηση των προκαλούμενων δονήσεων στην περιοχή των χαμηλών συχνοτήτων (Popp et al., 1999). Αυτή η μεθοδολογία έδωσε μερικά πρώτα χρήσιμα αποτελέσματα στο πεδίο των δονήσεων, ωστόσο, υπήρχε ανάγκη βελτίωσης της για να ληφθεί υπόψη η επιρροή κάθε υπόστρωσης της σιδηροτροχιάς στη διάδοση των κραδασμών. Στην περίπτωση των μεθόδων μονής ή διπλής στρώσης, γίνεται η υπόθεση ότι η σιδηροτροχιά είναι πακτωμένη. Αυτή η υπόθεση ισχύει στην περίπτωση του υποβάθρου με δυσκαμψία υψηλότερη ή ίση με τη δυσκαμψία της σιδηροτροχιάς (Kouroussis et al., 2011). Ωστόσο, στην περίπτωση ενός πιο μαλακού υλικού υπεδάφους, αυτές οι προσεγγίσεις δεν είναι ακριβείς.

Τα τελευταία χρόνια, η τεχνολογική εξέλιξη, κατέστησε δυνατή τη διερεύνηση περισσότερων παραμέτρων στη διάδοση των κραδασμών μέσω αριθμητικών προσομοιωμάτων. Ως εκ τούτου, το περίπλοκο πρόβλημα των δονήσεων προσεγγίζεται συνήθως μέσω αριθμητικών προσομοιωμάτων με τη χρήση μεθόδων, όπως η μέθοδος πεπερασμένων διαφορών (FDM), η μέθοδος πεπερασμένων στοιχείων (FEM) ή η μέθοδος συνοριακών στοιχείων (BEM). Η μέθοδος πεπερασμένων διαφορών έχει σχετικά χαμηλό υπολογιστικό κόστος, καθώς η διακριτοποίηση είναι καλά καθορισμένη, επομένως είναι δυνατός ο διαχωρισμός της ανάλυσης σε πολλαπλούς επεξεργαστές. Επιπλέον, η δυνατότητα χρήσης οριακών συνθηκών με δυνατότητες απόσβεσης καθιστά την FDM μια ανταγωνιστική εναλλακτική λύση σε σύγκριση με τη μέθοδο των πεπερασμένων στοιχείων. Το κύριο πρόβλημα της FDM είναι η δυσκολία προσομοίωσης σύνθετων γεωμετριών και ελεύθερων επιφανειών. Ως εκ τούτου, είναι δύσκολο να προσομοιωθεί επακριβώς ένα λεπτομερές μοντέλο σιδηροτροχιάς / εδάφους, καθώς απαιτεί πολλές

απλουστεύσεις. Για τον λόγο αυτό, οι περισσότεροι ερευνητές προτιμούν πλέον να χρησιμοποιούν άλλες αριθμητικές προσεγγίσεις αντί της FDM.

Ως εναλλακτική λύση, εφαρμόσθηκε η μέθοδος πεπερασμένων στοιχείων, η οποία μπορεί να προσομοιώσει σχετικά εύκολα περίπλοκες γεωμετρίες. Επιπροσθέτως, υπάρχει πληθώρα σχετικών λογισμικών (π.χ., ABAQUS, ANSYS, MSC Marc), τα οποία προσφέρουν ένα εύχρηστο γραφικό περιβάλλον. Προφανώς, τα λογισμικά FEM είναι ένα εξαιρετικό αριθμητικό εργαλείο για τους ερευνητές των δονήσεων που προκαλούνται από HST, καθώς η περίπλοκη γεωμετρία του προβλήματος μπορεί να σχεδιαστεί λεπτομερώς. Για τον λόγο αυτό, έχουν παρουσιαστεί τα τελευταία χρόνια πολλές σχετικές μελέτες με τη χρήση προσομοιωμάτων FEM (Connolly et al., 2013; El Kacimi, et al., 2013; Sayeed and Shahin, 2016a). Ωστόσο, επειδή το μέγεθος του μοντέλου πρέπει να είναι εξ ορισμού πεπερασμένο, δεν είναι εύκολο να προσομοιωθεί ένας ημι-άπειρος χώρος με ακρίβεια, χρησιμοποιώντας απλά μοντέλα FEM. Για αυτόν τον λόγο, χρειάζεται να χρησιμοποιηθούν οριακές συνθήκες απορρόφησης των κραδασμών προκειμένου να αποφευχθούν οι ανανακλάσεις στις άκρες του μοντέλου.

Τα πρώιμα μοντέλα FEM, χρησιμοποίησαν πακτώσεις στα όρια του προσομοιώματος, αρκετά μακριά από τη θέση φόρτισης για να μην επηρεάσουν τη λύση. Αυτό δεν είναι εφικτό σε δυναμικές προσομοιώσεις, καθώς οι πακτώσεις ανακλούν τους κραδασμούς, οδηγώντας σε λανθασμένα αποτελέσματα. Η προσομοίωση με ιξώδεις συνοριακές συνθήκες (viscous boundaries) είναι μια από τις πρώτες προσεγγίσεις για την απορρόφηση των κραδασμών στα όρια του προσομοιώματος (Kouroussis et al., 2011). Μια εναλλακτική επιλογή για την αποφυγή των ανακλάσεων των κραδασμών στα όρια του μοντέλου, είναι η χρήση ημιάπειρων στοιχείων. Η μέθοδος πεπερασμένων στοιχείων αποτελεί ένα υπολογιστικό εργαλείο υψηλής ακρίβειας, όμως απαιτεί υψηλούς υπολογιστικούς πόρους, επομένως αποτελεί μια αρκετά χρονοβόρα διαδικασία. Όμως είναι θέμα χρόνου να αντιμετωπιστεί αυτό το πρόβλημα λόγω της ταχείας εξέλιξης των δυνατοτήτων των σύγχρονων υπολογιστών.

Η χρήση της μεθόδου συνοριακών στοιχείων έχει το συγκριτικό πλεονέκτημα σε σχέση με την FEM, της αντιμετώπισης του προβλήματος των συνοριακών συνθηκών. Ωστόσο, όπως προαναφέρθηκε, η χρήση της μεθόδου BEM έχει αρκετές αδυναμίες, κυριότερη εκ των οποίων η δυσκολία προσομοίωσης ασυνεχών δομών, όπως η σιδηροδρομική γραμμή. Αυτό το μειονέκτημα οδήγησε αρκετούς ερευνητές να συνδυάσουν τις προσεγγίσεις BEM και FEM προκειμένου να εκμεταλλευτούν τα πλεονεκτήματα και των δύο μεθόδων.

Σύμφωνα με αυτήν την προσέγγιση, το υπέδαφος προσομοιώνεται χρησιμοποιώντας BEM και η σιδηροτροχιά χρησιμοποιώντας FEM. Βέβαια, όπως στην περίπτωση των προσομοιωμάτων FEM, τα προσομοιώματα BE-FE εξακολουθούν να έχουν σχετικά υψηλό υπολογιστικό κόστος. Επίσης, είναι δύσκολο να συνδεθεί το μοντέλο BEM με ένα τμήμα του προβλήματος, όπως ένα κτίριο κοντά στην τροχιά, με στόχο τη διερεύνηση της απόκρισης του.

A.3. Επαλήθευση αριθμητικών προσομοιωμάτων

A.3.1. Λεπτομέρειες θέσεων επαλήθευσης

Η διασφάλιση της αξιοπιστίας των αποτελεσμάτων των αριθμητικών προσομοιωμάτων πολυπαραμετρικών προβλημάτων, όπως είναι η διερεύνηση των παραγόμενων κραδασμών από τη διέλευση HST, είναι ένα πολύ σημαντικό βήμα της οποιαδήποτε διερεύνησης. Για τον λόγο αυτό, η ακρίβεια των προσομοιωμάτων επιτυγχάνεται με τη σύγκριση των αριθμητικών αποτελεσμάτων με μετρήσεις πεδίου σε τρεις θέσεις της γραμμής Παρίσι-Βρυξέλλες (Connolly et al., 2014). Οι μετρήσεις πεδίου που χρησιμοποιήθηκαν στην παρούσα διατριβή, αποτελούν μέρος μιας σειράς μετρήσεων από την επιστημονική ομάδα στην οποία συμμετείχε ο καθηγητής κ. G. Kouroussis, του Πανεπιστημίου του Mons.
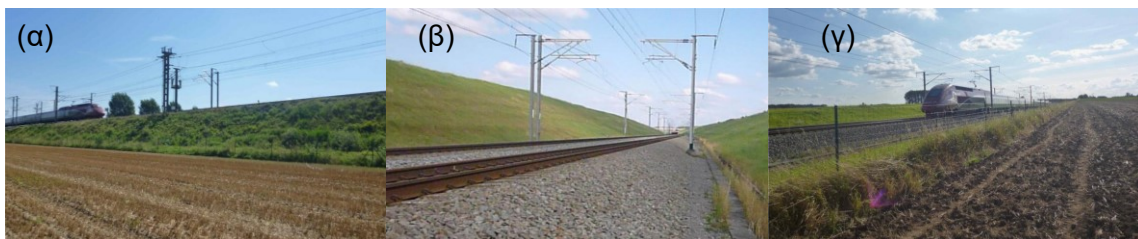
Σχήμα Α.1. Θέσεις μετρήσεων πεδίου σε: (α) επίχωμα, (β) όρυγμα, (γ) επίπεδη θέση (Connolly et al., 2014).

Η πρώτη θέση βρίσκεται βορειοανατολικά της πόλης Braffe, όπου η HSR διέρχεται από σιδηροδρομικό επίχωμα ύψους 5.5 μέτρων και κλίση 30° όπως απεικονίζεται στο Σχήμα Α.1α. Από την άλλη πλευρά, στη θέση 2 η σιδηροτροχιά περνάει από όρυγμα με ύψος 7.2m και κλίση 25° (Σχήμα Α.1β). Στην τελευταία περίπτωση (Θέση 3), η σιδηροτροχιά διέρχεται από επίπεδη θέση, 4 χιλιόμετρα νότια του Leuze-en-Hainaut (βλ. Σχήμα Α.1γ). Η σιδηροδρομική γραμμή υψηλής ταχύτητας Παρίσι - Βρυξέλλες είναι μια κλασικού τύπου τροχιά με υπόβαση, αποτελούμενο από έρμα, υπο-έρμα και υπόβαση, με πάχη 30cm, 20cm και 50cm, αντίστοιχα. Οι συνεχείς συγκολλημένες ράγες UIC60 εδράζονται σε στρωτήρες σκυροδέματος. Έχει γίνει η υπόθεση ότι οι ασυνέχειες και οι

γεωμετρικές ανωμαλίες των ραγών και των τροχών είναι πολύ μικρές σε όλες τις εξεταζόμενες θέσεις, καθώς είχε προηγηθεί συντήρηση της σιδηροτροχιάς οκτώ ημέρες πριν από τις μετρήσεις πεδίου (Connolly et al., 2014).

Οι Conolly et al. (2014), για τις ίδιες επιτόπιες μετρήσεις, κατέγραψε την ταχύτητα διέλευσης των HST από πληροφορίες που ελήφθησαν από τον φορέα εκμετάλλευσης της αμαξοστοιχίας, Infrabel. Τέσσερις τύποι αμαξοστοιχιών (TGV, Eurostar, Thalys και double-Thalys) χρησιμοποιούνταν στον σιδηρόδρομο κατά τη διάρκεια των μετρήσεων (Σχήμα Α.2). Για τους σκοπούς της παρούσας έρευνας, ο καθηγητής κ. G. Kouroussis παρείχε δεδομένα πεδίου για ένα πέρασμα των Thalys και TGV HST σε καθεμία από τις τρεις τοποθεσίες που εξετάστηκαν. Το Thalys διέρχεται με 284km/h, 297km/h και 299km/h στις θέσεις επιχώματος, ορύγματος και στο επίπεδο, αντίστοιχα.


Σχήμα Α.2. (α) TGV, (β) Thalys, (γ) Eurostar.

Α.3.2. Προσομοίωση διέλευσης HST

Τα εξεταζόμενα HST (Thalys και TGV), συνολικού μήκους περίπου 200 μέτρων, έχουν την ίδια γεωμετρία, καθώς αποτελούνται από τρεις τύπους βαγονιών, δύο κινητήρια βαγόνια (Y230A) και οκτώ βαγόνια επιβατών (δύο Y237A και έξι Y237B). Τα γεωμετρικά χαρακτηριστικά των HST, οι θέσεις των αξόνων και το μέγεθος των αξονικών φορτίων που ασκούνται στις ράγες παρουσιάζονται στο Σχήμα Α.3. Για την εισαγωγή των κινητών φορτίων του διερχόμενου HST, αναπτύχθηκε μια υπορουτίνα χρήστη Vdload σε γλώσσα υπολογιστή Fortran. Για να εξασφαλιστεί η αριθμητική σταθερότητα του μοντέλου, το χρονικό βήμα Δt ορίστηκε ίσο με $1,3 \times 10^{-6}$s.

Δεδομένου ότι τα ευθεία τμήματα αποτελούν το μεγαλύτερο μέρος των σιδηροδρομικών γραμμών παγκοσμίως, το παρόν μοντέλο λαμβάνει υπόψη κυρίως τα κατακόρυφα φορτία στις ράγες. Το συνολικό φορτίο αμαξοστοιχίας, το οποίο κατανέμεται σε μια σειρά 26 αξονικών φορτίων, εφαρμόζεται στα σημεία διεπαφής τροχού-

σιδηροτροχιάς, ενώ η ταχύτητα διέλευσης έχει θεωρηθεί σταθερή. Το συνολικό φορτίο του HST προκύπτει ως εξής:

$$f_{total} = \sum_{n=1}^{26} f_n$$
(A.6)

(α)

ΦΟΡΤΙΑ ΑΞΟΝΩΝ [Ν]

(β)
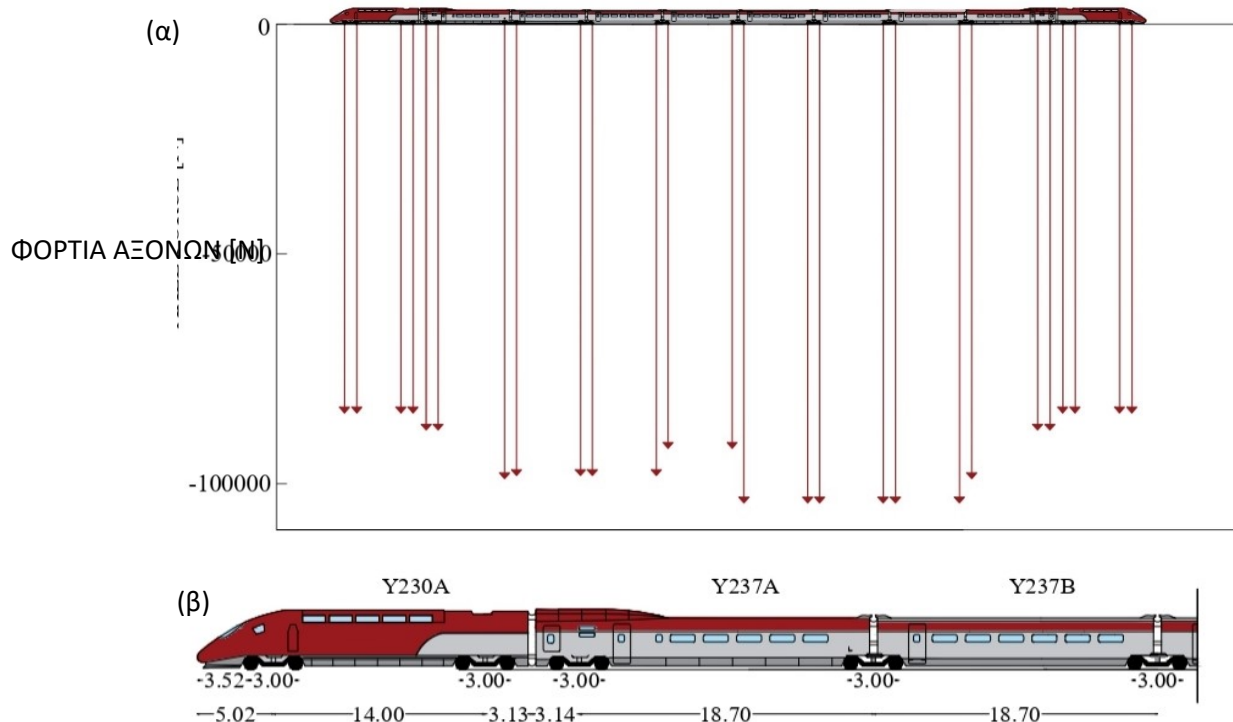
Σχήμα Α.3. (α) Αξονικά φορτία Thalys HST (Kouroussis and Verlinden, 2013); (β) Διαστάσεις βαγονιών (Degrande and Schillemans, 2001).

Η θέση του κάθε άξονα του HST σε κάθε βήμα (t) υπολογίζεται από την ακόλουθη σχέση:

$$y_n = vt - d_n$$
(A.7)

όπου:

v: ταχύτητα διέλευσης,

d_n: απόσταση μεταξύ του πρώτου και του ν άξονα.

Το μέγεθος κάθε επιμέρους αξονικού φορτίου f_n που ασκείται σε κάθε σημείο της ράγας προκύπτει ως εξής:

$$f_p = \sum_{n=1}^{26} f_n \delta(y_n - y_p)$$
(A.8)

όπου:

δ: σταθερά του Dirac,

y_p: η θέση εφαρμογής.

A-16

Α.3.3. Προσομοίωση σιδηροτροχιάς & εδάφους

Για τους σκοπούς της παρούσας διατριβής, επιλέχθηκε η μέθοδος των πεπερασμένων στοιχείων, λόγω της ευχέρειας της στην προσομοίωση περίπλοκων γεωμετριών. Για να ελαχιστοποιηθεί το υπολογιστικό κόστος, προσομοιώθηκε ένα μέρος του μοντέλου λόγω συμμετρίας κατά την κατακόρυφη κατεύθυνση, ενώ για την αποφυγή των ανακλάσεων των κραδασμών στα όρια του μοντέλου, χρησιμοποιήθηκαν ημι-άπειρα στοιχεία (βλ. Σχήμα Α.3). Η ράγα έχει προσομοιωθεί ως δοκός Euler Bernoulli, ορθογωνικής διατομής με διαστάσεις 0.153 m x 0.078 m. Η ράγα έχει μάζα 60kg/m και εδράζεται σε στρωτήρες σκυροδέματος με διαστάσεις 0.242m x 0.2m x 2.42m. Για την προσομοίωση του υπόλοιπου μοντέλου, έχουν χρησιμοποιηθεί 3D πεπερασμένα στοιχεία. Οι στρωτήρες έχουν τοποθετηθεί κατά μήκος της ράγας με διάκενο 60cm. Όλα τα μέλη του μοντέλου θεωρούνται ως γραμμικά ελαστικά και οι ιδιότητές τους παρατίθενται στον Πίνακα Α.2.
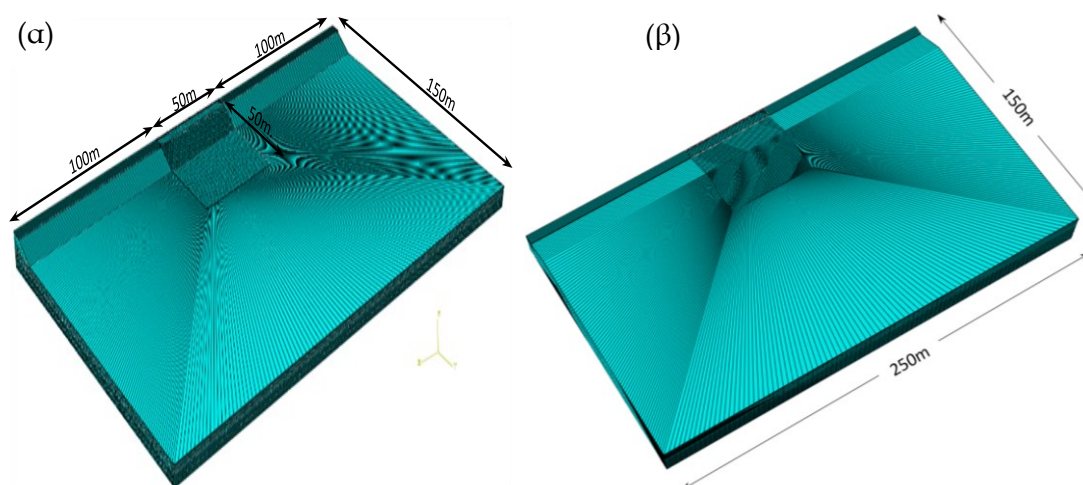
Σχήμα Α.4. 3D μοντέλο πεπερασμένων στοιχείων: (α) Επίχωμα (β) Όρυγμα.

Πίνακας Α.2. Ιδιότητες υλικών σιδηροτροχιάς.

	Πάχος στρώσης (m)	Μέτρο Ελαστικότητας (GPa)	Λόγος Poisson	Πυκνότητα (kg/m³)
Ράγα	-	210	0.25	7900
Στρωτήρες	-	30	0.4	2400
Έρμα	0.3	0.1	0.35	1800
Υπο-έρμα	0.2	0.3	0.35	2200
Υπόβαση	0.5	0.127	0.35	2100

Ο Πίνακας Α.3 παρουσιάζει τα μηχανικά χαρακτηριστικά κάθε στρώσης, τα οποία χρησιμοποιήθηκαν για την προσομοίωση του εδαφικού προφίλ κάθε εξεταζόμενης θέσης. Οι εξεταζόμενες θέσεις έχουν παρόμοια στρωματογραφία, καθώς οι υπερκείμενες χαλαρές αργιλικές αποθέσεις εδράζονται σε ενδιάμεσες στρώσεις άμμου, ενώ οι βαθύτερες στρώσεις αποτελούνται από σκληρότερες αργιλικές αποθέσεις.

Πίνακας Α.3. Ιδιότητες εδαφικών υλικών.

| Θέση 1: Επίχωμα			Θέση 2: Όρυγμα			Θέση 3: Επίπεδο		
h (m)	v	E (MPa)	h (m)	v	E (MPa)	h (m)	v	E (MPa)
1.3	0.33	132	1.35	0.23	126	1.5	0.14	157
1.3	0.25	149	1.35	0.17	136	1	0.38	113
1.2	0.27	145	3.1	0.29	257	1.7	0.42	191
2.85	0.3	259	3.1	0.16	315	2.5	0.29	277
2.85	0.16	297	Inf.	0.29	3278	Inf.	0.33	419

Α.3.4. Αποτελέσματα προσομοίωσης

#### Α.3.4.1. Επαλήθευση χρονοϊστοριών και φασμάτων ταχυτήτων

Η επαλήθευση των αριθμητικών αποτελεσμάτων πραγματοποιήθηκε σε οκτώ αποστάσεις μεταξύ 15 και 35 μέτρα από την τροχιά σε όλα τα εξεταζόμενα σημεία της σιδηροτροχιάς. Για λόγους συντομίας, στην εκτενή ελληνική περίληψη παρουσιάζονται τα αποτελέσματα κατά τη διέλευση του Thalys HST σε σιδηροδρομικό επίχωμα, σε δυο χαρακτηριστικές αποστάσεις παρατήρησης, στα 15 μέτρα και στα 35 μέτρα από την σιδηροτροχιά. Τα αριθμητικά αποτελέσματα συγκρίνονται με τις μετρήσεις πεδίου τόσο ως χρονοϊστορίες όσο και ως φάσματα Fourier των κατακόρυφων ταχυτήτων. Αναλυτικότερα αποτελέσματα για όλες τις εξεταζόμενες αποστάσεις και θέσεις μπορούν να αναζητηθούν στο κυρίως κείμενο της διατριβής.

Στο Σχήμα Α.5 παρουσιάζονται οι χρονοϊστορίες κατακόρυφων ταχυτήτων σύμφωνα με τα αριθμητικά αποτελέσματα και τις μετρήσεις πεδίου για τη διέλευση του Thalys HST από τη θέση σιδηροδρομικού επιχώματος (Θέση 1). Παρατηρείται πολύ καλή ταύτιση μεταξύ των αριθμητικών αποτελεσμάτων και των μετρήσεων πεδίου. Για παράδειγμα, η μέγιστη κατακόρυφη ταχύτητα στα 15 μέτρα είναι ίση με 1.3mm/s σύμφωνα με τις μετρήσεις πεδίου, και 1.1mm/s βάσει των αριθμητικών αποτελεσμάτων. Επίσης, σύμφωνα με το αριθμητικό μοντέλο, λόγω του μεγαλύτερου βάρους του πρώτου και του τελευταίου βαγονιού, παρατηρήθηκαν υψηλότερες ταχύτητες κατά τη διέλευσή

τους. Το Σχήμα Α.5 απεικονίζει τις χρονοϊστορίες κατακόρυφων ταχυτήτων στο μακρινό πεδίο. Σε αυτήν τη θέση, η χρονοϊστορία έχει παρόμοιο μέγεθος και μορφή με τις μετρήσεις πεδίου. Όπως ήταν αναμενόμενο, οι κραδασμοί αποσβένονται ανάλογα με την απόσταση από την τροχιά, επομένως οι ταχύτητες στα 35 μέτρα από την τροχιά είναι αρκετά μικρότερες από τα 15 μέτρα. Ωστόσο, υπάρχει μια μικρή απόκλιση μεταξύ των μέγιστων τιμών των μετρήσεων πεδίου και των αριθμητικών αποτελεσμάτων. Συγκεκριμένα, η μέγιστη ταχύτητα είναι ίση με 0.27mm/s, ενώ είναι ίση με 0.19mm/s, σύμφωνα με το αριθμητικό μοντέλο. Παρά ταύτα αυτές οι τιμές είναι της ίδιας τάξης μεγέθους, επομένως η σύγκληση θεωρείται ικανοποιητική.
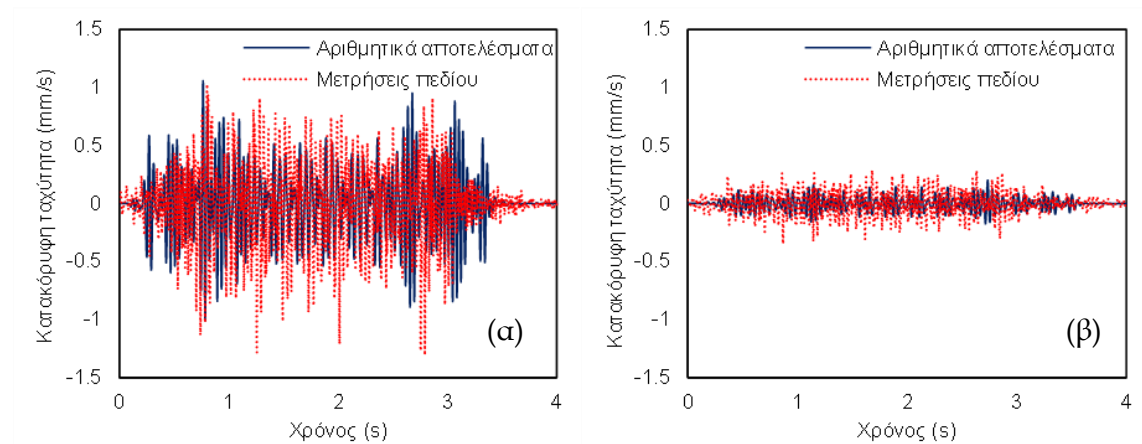
Σχήμα Α.5. Διέλευση Thalys HST από θέση 1: Χρονοϊστορίες κατακόρυφων ταχυτήτων στα: (α) 15 μέτρα, (β) 35 μέτρα από την τροχιά.
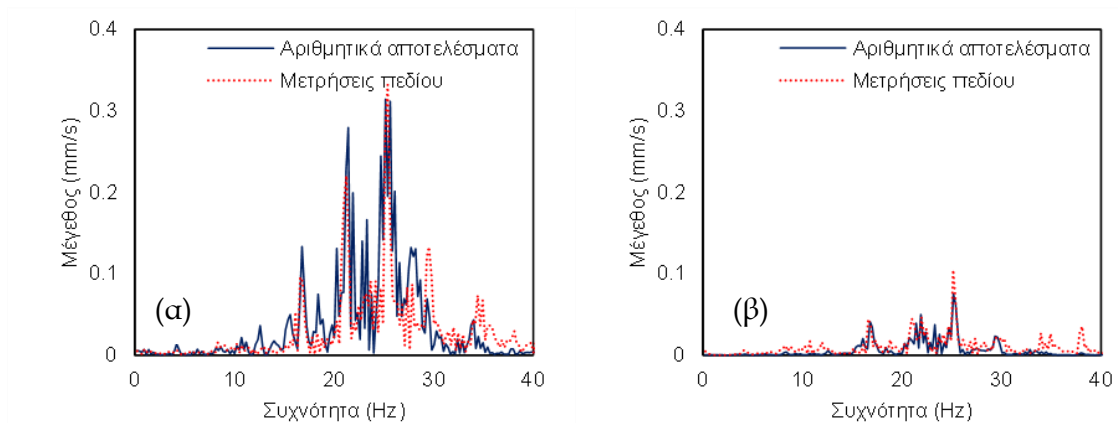
Σχήμα Α.6. Διέλευση Thalys HST από θέση 1: Φάσματα Fourier κατακόρυφων ταχυτήτων στα: (α) 15 μέτρα, (β) 35 μέτρα από την τροχιά.

Εκτός από τις χρονοϊστορίες, διερευνάται η σύγκληση του συχνοτικού περιεχόμενου των κραδασμών μεταξύ του αριθμητικού προσομοιώματος και των μετρήσεων πεδίου. Με βάση τα διεθνή πρότυπα, οι δονήσεις χαμηλής συχνότητας είναι οι πιο κρίσιμες (Kouroussis et al., 2011). Τα φάσματα Fourier είναι σε συμφωνία μεταξύ των δεδομένων πεδίου και των αριθμητικών υπολογισμών για τις εξεταζόμενες θέσεις. Το αριθμητικό

μοντέλο έχει απεικονίσει με επιτυχία τις κορυφές των κραδασμών στο χαμηλό εύρος συχνοτήτων μεταξύ 10 και 40 Hz. Οι κύριες συχνότητες (21.4 Hz και 25.2 Hz) είναι ίδιες σε όλες τις εξεταζόμενες αποστάσεις και υπάρχει ικανοποιητική συσχέτιση μεταξύ των αριθμητικών αποτελεσμάτων και των δεδομένων πεδίων. Επιπλέον, ορισμένες δευτερεύουσες κορυφές των μετρήσεων (16,7 Hz, 29,6 Hz, 34Hz) επαληθεύονται και αριθμητικά. Στην περίπτωση των κοντινών θέσεων, οι αιχμές των κραδασμών είναι κοντά στις μετρήσεις πεδίου.

Α.3.4.2. Διερεύνηση επιπέδου ντεσιμπέλ

Σε αυτήν την ενότητα, παρουσιάζεται έναν ευρέως αποδεκτός δείκτης για τη διερεύνηση κραδασμών από τη διέλευση HST, που αντιστοιχεί στα ντεσιμπελ της ταχύτητας (V_{dB}) στην κεντρική συχνότητα κάθε 1/3 οκτάβας, για τη σύγκριση των αριθμητικών αποτελεσμάτων με τις διαθέσιμες μετρήσεις πεδίου. Το V_{db} σε κάθε εξεταζόμενη οκτάβα υπολογίζεται σύμφωνα με την ακόλουθη σχέση:

$$V_{db} = 20 \log_{10} \frac{v_{rms}}{v_0} \qquad\qquad (A.9)$$

όπου:

v_{rms}: μέση τετραγωνική ρίζα των ταχυτήτων κάθε οκτάβας,

v_{rms}: επίπεδο αναφοράς ταχυτήτων.

Το Σχήμα Α.7 απεικονίζει το επίπεδο των ντεσιμπελ σε κάθε 1/3 οκτάβα με κεντρική συχνότητα από 1.25Hz και 50Hz στα 15 και 35 μέτρα από την τροχιά λόγω της διέλευσης του Thalys HST από τις τρεις εξεταζόμενες θέσεις. Οι υψηλότερες τιμές κραδασμών παρουσιάζονται μεταξύ 12ης και 15ης οκτάβας σε όλες τις εξεταζόμενες θέσεις. Σε γενικές γραμμές τα αριθμητικά αποτελέσματα έχουν μια καλή αντιστοιχία με τις μετρήσεις πεδίου και στις 3 θέσεις στα 15 μέτρα από την τροχιά. Η σύγκληση των αποτελεσμάτων είναι εντυπωσιακή στο κοντινό πεδίο, ιδιαίτερα στην περίπτωση του επιχώματος όπως απεικονίζεται στο Σχήμα Α.7α. Στο κοντινό πεδίο η κυρίαρχη οκτάβα είναι η 14η, φτάνοντας τιμές μεταξύ 70dB και 75dB.

Κυρίαρχη συχνότητα παραμένει η 14η στο μακρινό πεδίο, όμως -όπως ήταν αναμενόμενο- το επίπεδο των ντεσιμπελ μειώνεται σημαντικά σε σύγκριση με το κοντινό πεδίο. Το μέγιστο επίπεδο ντεσιμπελ στην περίπτωση του επιχώματος είναι ίσο με 56dB (Σχήμα Α.7β), η τιμή αυτή είναι σε συμφωνία με τις μετρήσεις πεδίου. Στη θέση του ορύγματος, το μέγιστο επίπεδο ντεσιμπελ αυξάνεται στα 62dB σύμφωνα με τις μετρήσεις

πεδίου και παραμένει στην ίδια οκτάβα με το επίχωμα. Το αριθμητικό μοντέλο πλησιάζει αρκετά αυτήν την τιμή.
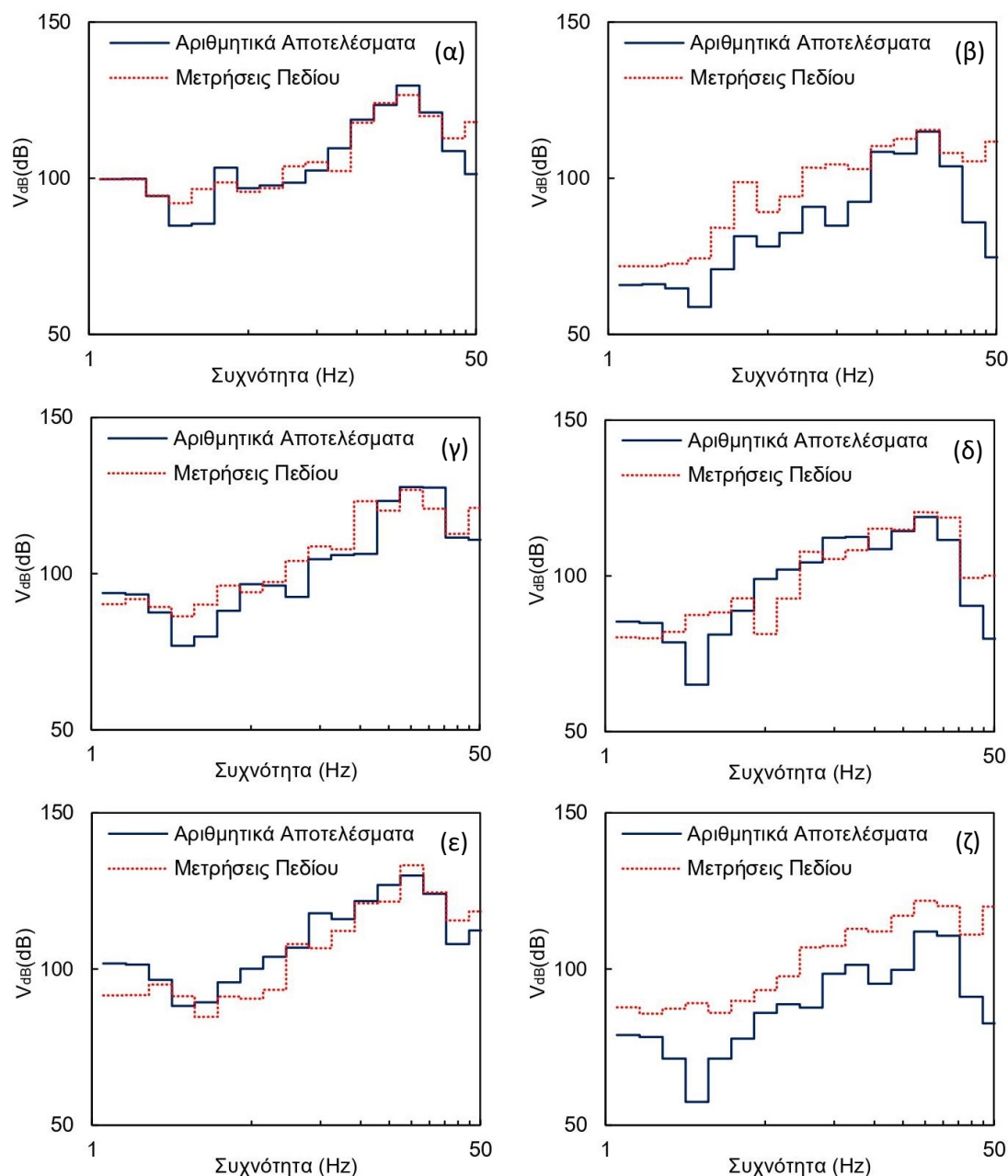

Σχήμα Α.7. Σύγκριση V_{dB} κάθε οκτάβας ων αριθμητικών αποτελεσμάτων και των μετρήσεων πεδίου σε επίχωμα ((a), (b)), όρυγμα ((c), (d)) και επίπεδο ((e), (f)).

Από την άλλη πλευρά, στην τρίτη εξεταζόμενη θέση (στο επίπεδο), το μοντέλο δεν προβλέπει με ακρίβεια το επίπεδο των κραδασμών στο μακρινό πεδίο. Πιο συγκεκριμένα, το επίπεδο των ντεσιμπέλ κορυφής είναι 10dB χαμηλότερο από τις μετρήσεις πεδίου στις περισσότερες οκτάβες, όπως απεικονίζεται στο Σχήμα Α.7ζ. Σε αυτήν την περίπτωση η απόκλιση ίσως οφείλεται στην υψηλή απόσβεση της επιφανειακής εδαφικής στρώσης της

τρίτης θέσης, ωστόσο, σε γενικές γραμμές, το αριθμητικό μοντέλο είναι ικανό να προβλέψει με ακρίβεια το επίπεδο των κραδασμών.

A.3.4.3. Διερεύνηση μεταβολης ταχυτήτων PPV

Στη συνέχεια παρουσιάζεται ένας κοινά χρησιμοποιούμενος δείκτης μέτρησης των παραγόμενων κραδασμών, η μέγιστη ταχύτητα σωματιδίων (PPV) σε αυξανόμενη απόσταση από την τροχιά. Το Σχήμα Α.8α απεικονίζει τις τιμές της PPV στην περίπτωση του σιδηροδρομικού επιχώματος. Είναι προφανές ότι το αριθμητικό προσομοίωμα είναι ικανό να προβλέψει με ακρίβεια το επίπεδο της PPV σε όλο το εύρος αποστάσεων μεταξύ 15 μέτρα και 35 μέτρα από την σιδηροτροχιά. Ειδικά στις κοντινές θέσεις οι τιμές της PPV είναι σχεδόν πανομοιότυπες.
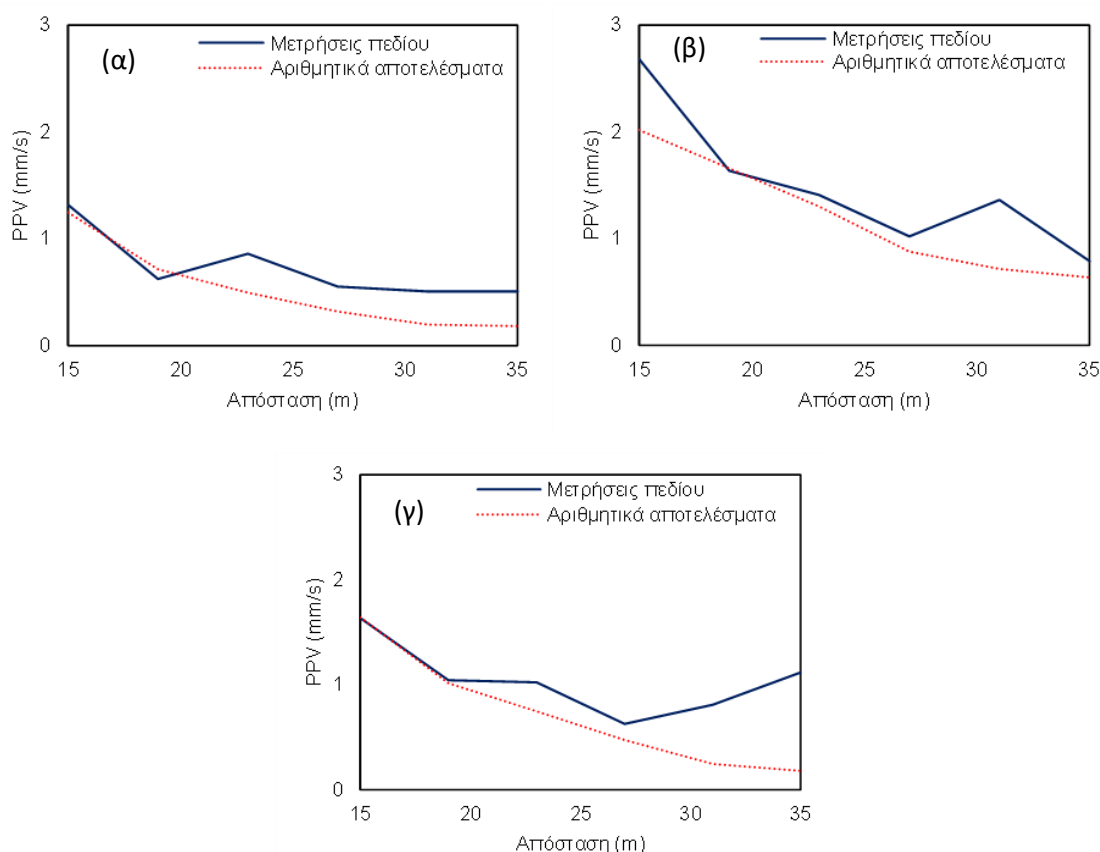
Σχήμα Α.8. Σύγκριση PPV σε αυξανόμενη απόσταση από την τροχιά σε: (α) επίχωμα, (β) όρυγμα και (γ) επίπεδη θέση.

Το Σχήματα Α.8β δείχνει την εξασθένηση του PPV, σε αυξανόμενη απόσταση στην θέση του σιδηροδρομικού ορύγματος. Οι τιμές της PPV σε αυτήν την περίπτωση είναι αρκετά υψηλότερες σε σύγκρισή με το επίχωμά. Αυτό μπορεί να δικαιολογηθεί λόγω της χαμηλότερης απόσβεσης της εδαφικής στρώσης αυτής της θέσης. Σε γενικές γραμμές, τα

αριθμητικά αποτελέσματα είναι αρκετά κοντά στις μετρήσεις πεδίου και σε αυτήν την περίπτωση. Τέλος, στην τελευταία θέση το μοντέλο προβλέπει επιτυχώς την PPV στο κοντινό πεδίο. Ωστόσο, σε μεγαλύτερες αποστάσεις η PPV αυξάνεται αρκετά σύμφωνα με τις μετρήσεις πεδίου. Για παράδειγμα, η PPV στα 19 μέτρα είναι χαμηλότερη σε σχέση με τα 35 μέτρα από την τροχιά. Εάν οι ιδιότητες του εδάφους είναι σταθερές σε ολόκληρη την απόσταση και δεν υπάρχουν άλλες πηγές κραδασμών, αυτό το φαινόμενο δεν είναι λογικό. Επομένως, γίνεται η υπόθεση ότι οι μετρήσεις πεδίου σε αυτήν τη θέση δεν είναι ακριβείς. Από την άλλη πλευρά, σύμφωνα με τα αριθμητικά αποτελέσματα, η διαβάθμιση της PPV φαίνεται να είναι πιο λογική, καθώς οι τιμές μειώνονται με την απόσταση από την τροχιά.

Α.3.5. Βασικά συμπεράσματα

Τα κύρια συμπεράσματα της διαδικασίας επαλήθευσης της αριθμητικής μεθοδολογίας είναι τα ακόλουθα:

- Η μορφή και η διάρκεια των χρονοϊστοριών είναι παρόμοια με τις μετρήσεις και για τις τρεις θέσεις, ειδικά στο κοντινό πεδίο.

- Υπάρχει υψηλή συσχέτιση μεταξύ των κυρίαρχων συχνοτήτων στο χαμηλό εύρος συχνοτήτων μεταξύ 0Hz και 40Hz.

- Το επίπεδο των ντεσιμπελ στα 15 μέτρα από την τροχιά είναι κοντά στα 75dB και μειώνεται στα 56-63dB στα 35 μέτρα. Το επίπεδο των κραδασμών των αριθμητικών αποτελεσμάτων είναι πάρα πολύ κοντά στις μετρήσεις πεδίου, ειδικά στις κοντινές θέσεις.

- Σε γενικές γραμμές, η τάση της PPV σε όλο το εύρος των αποστάσεων σύμφωνα με τα αριθμητικά αποτελέσματα, ακολουθεί τα δεδομένα πεδίου.

Μετά την επαλήθευση των αριθμητικών αποτελεσμάτων με τις διαθέσιμες μετρήσεις πεδίου, είναι προφανές ότι το αριθμητικό μοντέλο είναι ικανό να αναπαραστήσει τη διέλευση του HST με ακρίβεια. Ορισμένες διαφορές, που έχουν επίσης αναφερθεί σε σχετικές μελέτες (π.χ., (Kouroussis et al., 2011)), είναι εύλογες, λαμβάνοντας υπόψη την πολυπλοκότητα αυτού του δυναμικού προβλήματος και τις αβεβαιότητες για τις δυσκολίες στην αναπαραγωγή των πραγματικών συνθηκών ή ακόμα και πιθανά σφάλματα κατά τη διάρκεια των μετρήσεων. Ως εκ τούτου, μπορεί να διερευνηθεί η εφαρμογή διαφόρων μέτρων μετριασμού, τροποποιώντας κατάλληλα τα βασικά προσομοιώματα αναφοράς στις διάφορες θέσεις.

A.4.   Ενίσχυση επιχώματος με τη χρήση γεωαφρού EPS

A.4.1. Προτεινόμενη διάταξη

Στη συνέχεια, εξετάζονται εναλλακτικές διατάξεις με τη χρήση γεωαφρού EPS για τον περιορισμό των κραδασμών σε σιδηροδρομικό επίχωμα, προκειμένου να προταθεί μια βέλτιστη διάταξη. Αρχικά, εξετάστηκε η πλήρης αντικατάσταση του επιχώματος με γεωαφρό EPS, όμως η μέθοδος αυτή αποκλείστηκε λόγω αυξημένης πιθανότητας εκτροχιασμού του HST, εξαιτίας των αυξημένων παραμορφώσεων. Αντίστοιχα, αποκλείστηκε και η πλήρωση του κεκλιμένου τμήματος του επιχώματος με EPS, λόγω περιορισμένης αποτελεσματικότητας και πιθανής αστάθειας στο κέντρο του επιχώματος. Για τον λόγο αυτό, προτείνεται η χρήση περιορισμένου αριθμού τεμαχών γεωαφρού EPS, θαμμένων σε μικρό βάθος στο πρανές του επιχώματος. Με αυτήν τη διαμόρφωση, επιτυγχάνεται η ευστάθεια του επιχώματος και δεν αυξάνονται σημαντικά οι κατακόρυφες μετατοπίσεις. Σημειώνεται ότι αυτή είναι μια εύκολα εφαρμόσιμη και οικονομική λύση που μπορεί να χρησιμοποιηθεί σε νέα και υφιστάμενα σιδηροδρομικά επιχώματα.
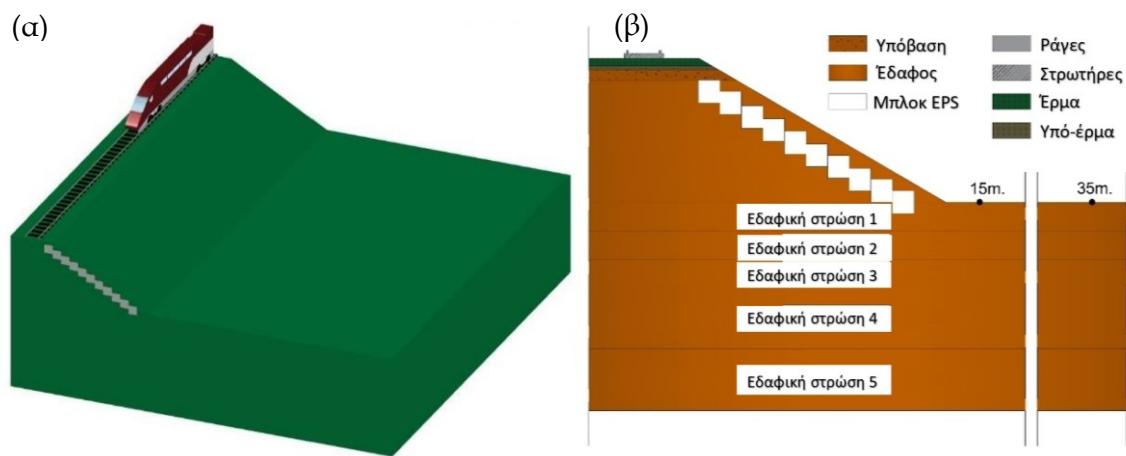

Σχήμα A.9. Προτεινόμενη διατομή.

Η προτεινόμενη διάταξη με τη χρήση γεωαφρού EPS απεικονίζεται στο Σχήμα A.9. Εξετάζεται η αποτελεσματικότητα δύο τύπων γεωαφρού: EPS19 και EPS46. Το EPS46 είναι το πιο στιβαρό μεταξύ των επτά διαθέσιμων τύπων EPS, καθώς η πυκνότητά του είναι ίση με 45.7 kg/m³ και το μέτρο ελαστικότητας του είναι 12800kPa. Από την άλλη πλευρά, το EPS19 είναι υλικό χαμηλής πυκνότητας (18.4 kg/m³) με μέτρο ελαστικότητας ίσο με 4000kPa. Σημειώνεται ότι ο λόγος Poisson και των δύο υλικών είναι πολύ χαμηλός, καθώς ισούται με μόλις 0,05, ενώ η απόσβεση του EPS είναι ίση με 2%.Με στόχο τη διασφάλιση

της αποτελεσματικότητας της προτεινόμενης διάταξης, εξετάστηκε η επιρροή διάφορων παραγόντων επιρροής, όπως η ταχύτητα διέλευσης του HST, οι μηχανικές ιδιότητες του EPS και του εδάφους και τα γεωμετρικά χαρακτηριστικά του επιχώματος.

Α.4.2. Επιρροή μηχανικών ιδιοτήτων EPS

Ο περιορισμός των κραδασμών από τη διέλευση του Thalys HST χρησιμοποιώντας την προτεινόμενη διάταξη γεωαφρού EPS απεικονίζεται στο Σχήμα Α.10. Οι δύο πρώτες χρονοϊστορίες κατακόρυφων ταχυτήτων (Σχήματα Α.10α και Α.10γ) απεικονίζουν τη βελτίωση της απόκρισης του εδάφους στα 15 μέτρα και στα 35 μέτρα από την τροχιά που επιτυγχάνεται με τη χρήση τεμαχών EPS46. Αντίθετα, η χρήση των τεμαχών EPS19, μειώνει μόνο ελαφρώς τις δονήσεις. Πιο συγκεκριμένα, στο κοντινό πεδίο (15 μέτρα από την τροχιά), κατά τη διέλευση των κινητήριων βαγονιών (τα οποία είναι τα βαρύτερα), η κατακόρυφη ταχύτητα μειώνεται σημαντικά.
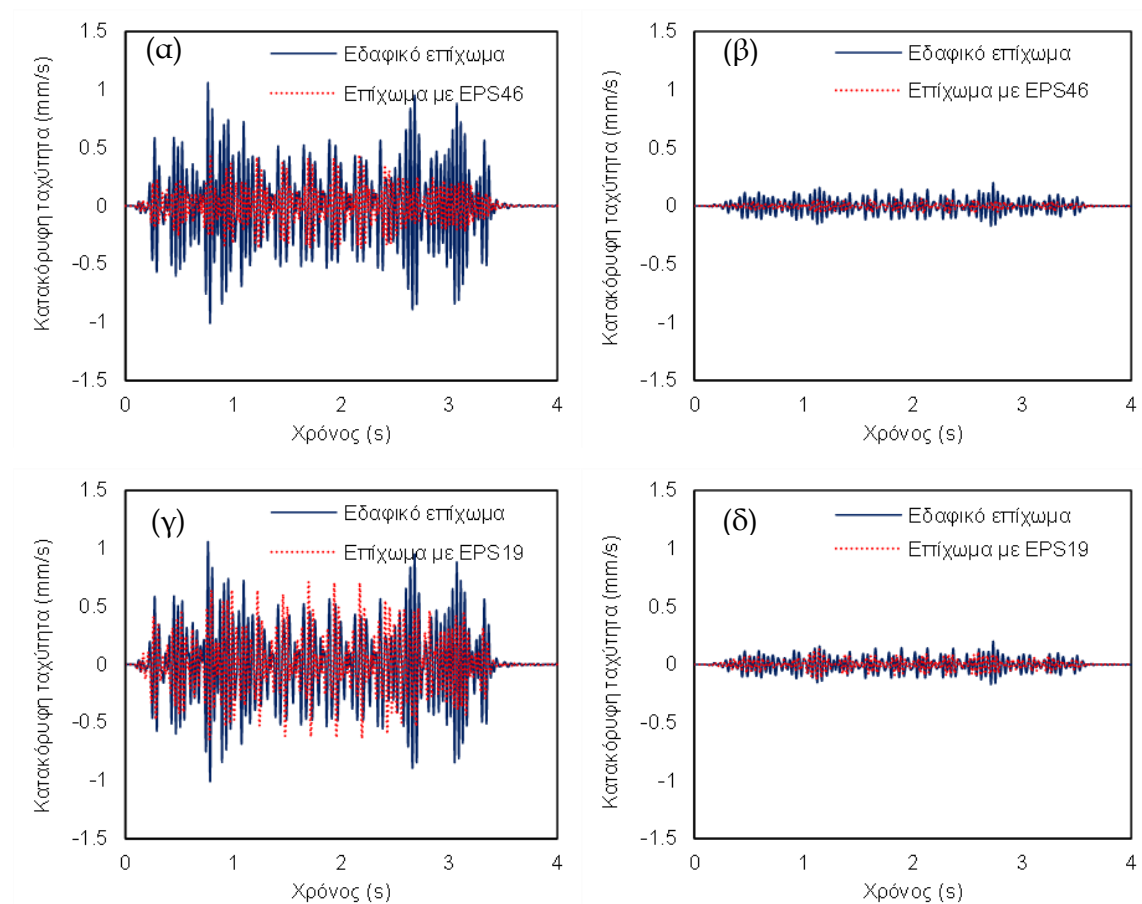
Σχήμα Α.10. Σύγκριση χρονοϊστοριών κατακόρυφων ταχυτήτων εδαφικού και ενισχυμένου με EPS επιχώματος: EPS46 ((α) στα 15 μέτρα, (β) στα 35 μέτρα από την τροχιά), EPS19 ((γ) στα 31 μέτρα, (δ) στα 35 μέτρα από την τροχιά).

Ωστόσο, η ταχύτητα στο μέσο της χρονοϊστορίας είναι ελαφρώς αυξημένη. Η μέγιστη κατακόρυφη ταχύτητα έχει μειωθεί από 1.1mm/s σε 0.7mm/s και 0.45mm/s στα 15 μέτρα από την τροχιά, μετά την εφαρμογή των EPS19 και EPS46, αντίστοιχα. Στη συνέχεια, παρουσιάζονται οι χρονοϊστορίες κατακόρυφων ταχυτήτων στο μακρινό πεδίο. Όπως φαίνεται στο Σχήμα Α.10δ, και σε αυτήν την περίπτωση το EPS19 παραμένει αρκετά αποτελεσματικό και σε μεγάλες αποστάσεις. Όμως, η μείωση των κραδασμών είναι ακόμα πιο μεγάλος με την χρήση του EPS46 και σε αυτήν τη θέση (Σχήμα Α.11β). Πιο συγκεκριμένα, το επίπεδο μείωσης φτάνει σε ορισμένες περιπτώσεις κοντά στο 50%. Προκύπτει το συμπέρασμα ότι το EPS46 είναι η βέλτιστη επιλογή υλικού, καθώς μειώνει την κατακόρυφη ταχύτητα σε όλο το εύρος αποστάσεων μεταξύ 15 και 35 μέτρων από την τροχιά.
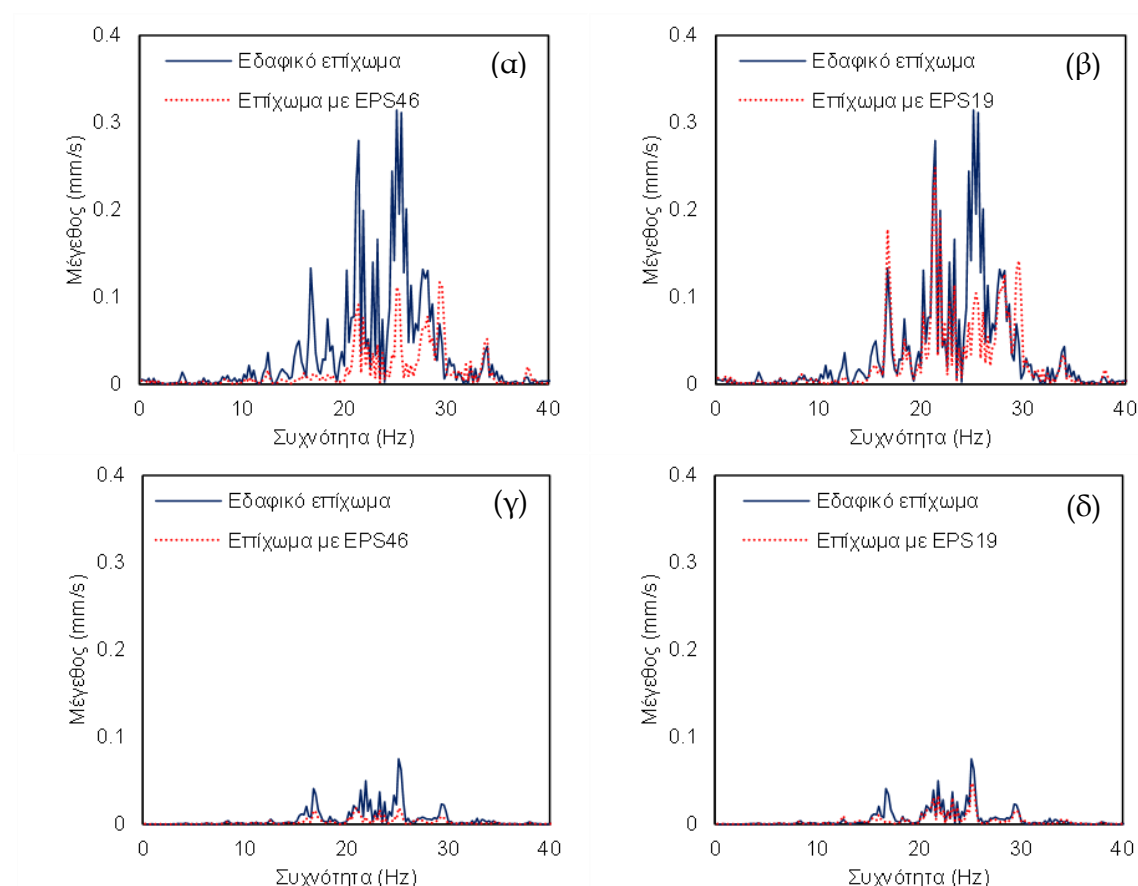
Σχήμα Α.11. Σύγκριση φασμάτων Fourier εδαφικού και ενισχυμένου με EPS επιχώματος: EPS46 ((α) στα 15 μέτρα, (β) στα 35 μέτρα από την τροχιά), EPS19 ((γ) στα 31 μέτρα, (δ) στα 35 μέτρα από την τροχιά).

Στο Σχήμα Α.11 παρουσιάζεται η σύγκριση των φασμάτων ταχύτητας του αρχικού επιχώματος και των ενισχυμένων με γεωαφρό EPS επιχωμάτων. Στην πλησιέστερη απόσταση (15 μέτρα από την τροχιά), η κορυφή της κυρίαρχης συχνότητας (25.2Hz) περιορίζεται σημαντικά μετά την εφαρμογή των τεμαχών EPS19. Από την άλλη πλευρά,

οι κορυφές στα 16.8Hz και 21.4Hz είναι κοντά στις τιμές του αρχικού επιχώματος. Στην περίπτωση του EPS46, οι περισσότερες από τις κορυφές στο εύρος χαμηλών συχνοτήτων 10 έως 40 Hz έχουν μειωθεί σημαντικά. Πιο συγκεκριμένα, οι κορυφές στις δύο κυρίαρχες συχνότητες στα 15 μέτρα από την τροχιά, μειώνονται από 0.28mm/s σε 0.09mm/s και από 0.31mm/s σε 0.1mm/s στα 21.4Hz και 25.2Hz, αντίστοιχα.

Επιπλέον, οι κορυφές στα 16.8Hz και 28.1Hz έχουν σχεδόν εξαφανιστεί. Θα πρέπει να σημειωθεί ότι η φασματική ταχύτητα στο μακρινό πεδίο (Σχήματα Α.11γ και Α.11δ) μειώνεται σε όλο το εξεταζόμενο εύρος συχνοτήτων (10 έως 40 Hz) με τη χρήση γεωαφρού EPS. Ο ευεργετικός ρόλος της προτεινόμενης προσέγγισης περιορισμού των κραδασμών, ειδικά στην περίπτωση του δύσκαμπτου EPS46, είναι εμφανής. Πιο συγκεκριμένα, η εφαρμογή τεμαχών EPS46 περιορίζει την κρίσιμη κορυφή στα 25.2Hz από 0.08mm/s σε 0.02mm / s στα 35 μέτρα από την τροχιά. Στην περίπτωση του EPS19, η τιμή αυτή μειώνεται, όμως όχι τόσο αποτελεσματικά όσο με το EPS46.

Α.1.1. Σύγκριση επιπέδων κραδασμού με οριακές τιμές κανονισμών

Σε αυτήν την ενότητα, χρησιμοποιήθηκαν εγκεκριμένοι δείκτες από διεθνείς κανονισμούς για τη διερεύνηση των επιπτώσεων των κραδασμών στην ανθρώπινη υγεία και στην απόκριση των κτιρίων, με στόχο την περαιτέρω διερεύνηση της αποτελεσματικότητας της προτεινόμενης διάταξης. Σύμφωνα με το Γερμανικό Ινστιτούτο Τυποποίησης (DIN 4150-3, 1999b), προτείνεται η οριακή τιμή των 3mm/s για την PPV για την προστασία ευαίσθητων κτιρίων από πιθανές ζημιές. Όπως φαίνεται στο Σχήμα Α.12α, η τιμή της PPV του αρχικού μοντέλου είναι χαμηλότερο από αυτό το όριο σε όλο το εξεταζόμενο εύρος αποστάσεων. Είναι προφανές ότι και μετά την εφαρμογή του γεωαφρού EPS, η PPV παραμένει χαμηλότερη από την οριακή τιμή του DIN.

Εκτός από τις πιθανές ζημιές σε κοντινά κτίρια, θα πρέπει να εκτιμηθεί ο βαθμός ενόχλησης των κατοίκων από τη διέλευση του HST. Σύμφωνα με το Υπουργείο Μεταφορών των Ηνωμένων Πολιτειών (USDT, 1998), το όριο της v_{rms} για την προστασία των περίοικων είναι 0.10mm/s για λίγες διελεύσεις (<70 ανά ημέρα). Αυτή η τιμή αυξάνεται στα 0.26mm/s για περισσότερες από 70 διελεύσεις ανά ημέρα. Το v_{rms} του αρχικού επιχώματος είναι χαμηλότερο από το όριο USDT για συχνές διόδους σε αποστάσεις μεγαλύτερες από 21m από την τροχιά. Η τοποθέτηση τεμαχών EPS46 στην πλαγιά του επιχώματος συμβάλλει στη μείωση των v_{rms} κάτω από αυτό το όριο για όλες τις αποστάσεις μεταξύ 15 και 35 μέτρα (βλ. Σχήμα Α.12β). Σύμφωνα με τον Παγκόσμιο

Οργανισμό Υγείας (ΠΟΥ, 2018), οι δονήσεις άνω των 55dB είναι αρκετά επικίνδυνες για τη δημόσια υγεία. Στην περίπτωση του αρχικού μοντέλου, το V_{dB} είναι υψηλότερο από το όριο των 55dB σε όλες τις εξεταζόμενες αποστάσεις. Η εφαρμογή των τεμαχών EPS46 μειώνει το V_{dB} κάτω από το όριο των 55dB για αποστάσεις μεγαλύτερες από 23 μέτρα από την τροχιά. Από την άλλη πλευρά, το Γερμανικό Ινστιτούτο Τυποποίησης (DIN4150-2, 1999) προτείνει τη σύγκριση μεταξύ του $KB_{F,max}$ και του ορίου των 0.15mm/s για κατοικημένες περιοχές. Το $KB_{F,max}$ μειώνεται κάτω από αυτό το όριο για αποστάσεις μεγαλύτερες από 21m με την χρήση τεμαχών EPS.
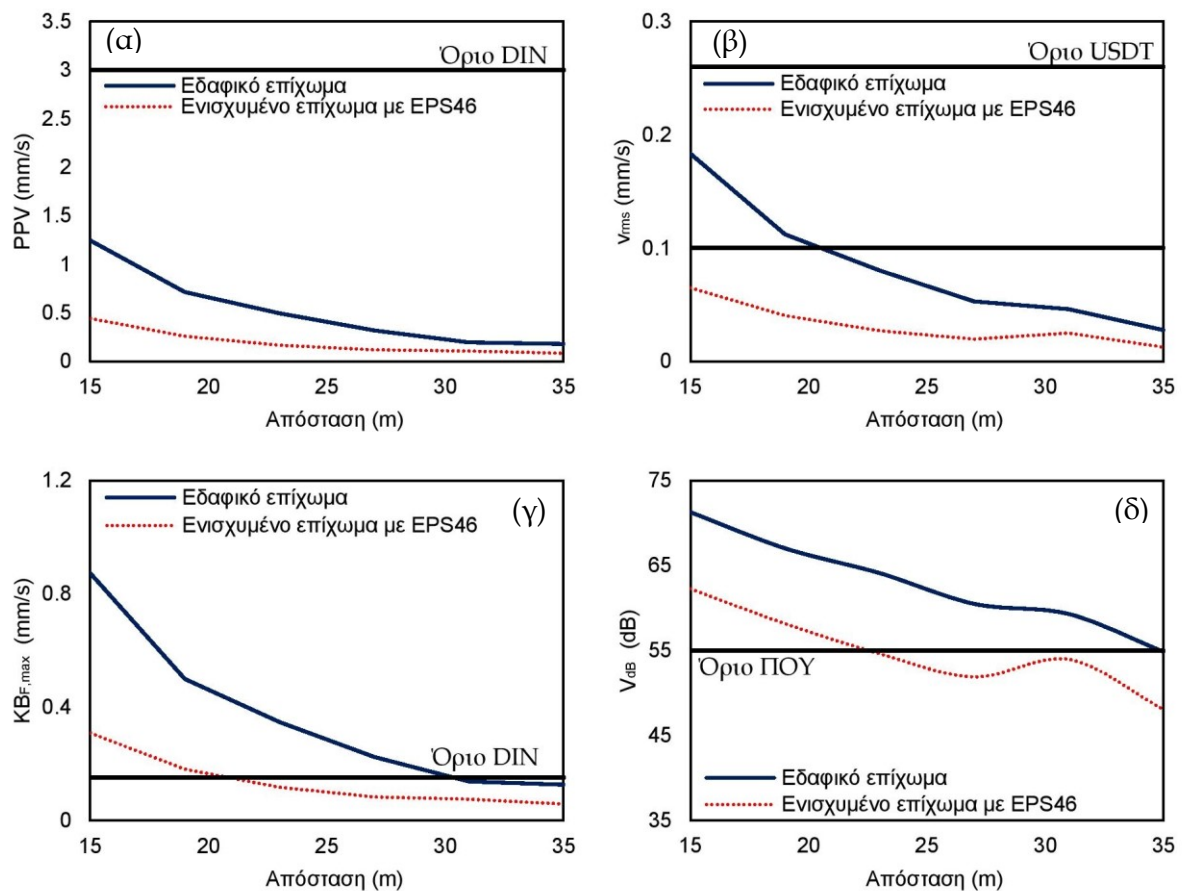
Σχήμα Α.12. Σύγκριση επιπέδου κραδασμού με οριακές τιμές: (α) PPV, (β) v_{rms}, (γ) V_{dB}, (δ) $KB_{F,max}$.

Α.4.3. Επιρροή γεωμετρικών χαρακτηριστικών του επιχώματος

Προκειμένου να εξεταστεί η επίδραση του ύψους του επιχώματος στην αποτελεσματικότητα του εξεταζόμενου μέτρου μετριασμού, εξετάζονται και συγκρίνονται διάφορα ύψη επιχώματος μεταξύ 3.5 και 5.5 μέτρων. Όλα τα εξεταζόμενα επιχώματα έχουν κλίση πρανών 30°. Για λόγους συντομίας στην εκτενή περίληψη παρουσιάζονται τα αποτελέσματα επιχωμάτων στα 15 και 35 μέτρα από την τροχιά.

Στο σχήμα Α.13 παρουσιάζεται το επίπεδο της μείωσης των ντεσιμπέλ στις δυο αποστάσεις. Οι οκτάβες με κεντρικές συχνότητες 16Hz, 20Hz και 25Hz είναι οι πιο κρίσιμες και στις δυο εξεταζόμενες αποστάσεις. Σύμφωνα με το Σχήμα Α.13α, στις πρώτες 4 οκτάβες, το επίπεδο μείωσης των ντεσιμπέλ είναι υψηλότερο στις περιπτώσεις των χαμηλότερων συχνοτήτων στα 15 μέτρα από την τροχιά. Η εφαρμογή του γεωαφρού EPS46 αυξάνει ελαφρώς το επίπεδο κραδασμών στις οκτάβες με κεντρικές συχνότητες υψηλότερες από 31.5Hz στα χαμηλά επιχώματα. Με την εφαρμογή του γεωαφρού EPS στο επίχωμα με ύψος μεγαλύτερο από 5m, το επίπεδο των ντεσιμπέλ παραμένει το ίδιο ή μειώνεται σε όλο το εξεταζόμενο φάσμα. Το Σχήμα Α.13β δείχνει το επίπεδο των ντεσιμπέλ στα 35 μέτρα από την τροχιά, όπου το επίπεδο μείωσης εξακολουθεί να είναι υψηλότερο στα επιχώματα με μεγαλύτερα ύψη. Είναι προφανές ότι σε αυτήν την περίπτωση, το επίπεδο των ντεσιμπέλ για όλες τις εξεταζόμενες οκτάβες έχει περιοριστεί κάτω από 50dB, ανεξάρτητα από το ύψος του επιχώματος.
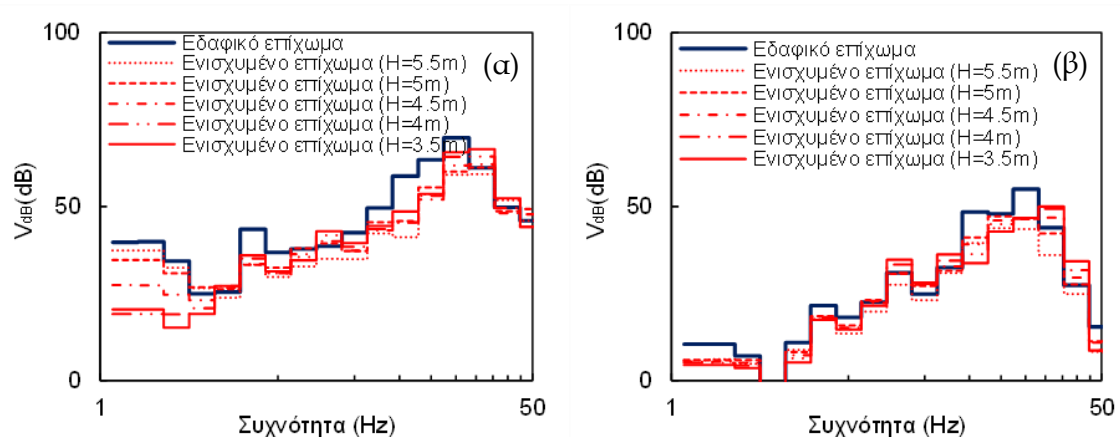
Σχήμα Α.13. Σύγκριση επιπέδου ντεσιμπέλ για επιχώματα με ύψη από 3.5 μέτρα έως 5.5 μέτρα: (α) στα 15 μέτρα, (β) στα 35μέτρα από την τροχιά.

Στη συνέχεια, παρουσιάζεται η επίδραση της κλίσης του επιχώματος στην αποτελεσματικότητα της προτεινόμενης διατομής στον περιορισμό των κραδασμών. Διερευνώνται δύο επιχώματα, ένα με μεγαλύτερη (45°) και ένα με μικρότερη κλίση (20°) από το αρχικό επίχωμα. Η απόκριση του εδάφους στα 15 μέτρα από την τροχιά λόγω των αναπτυσσόμενων δονήσεων παρουσιάζεται στην περίπτωση επιχώματος με κλίση 20° στο Σχήματος Α.14α. Το επίπεδο των ντεσιμπέλ των κύριων συχνοτήτων (13η, 14η και 15η), κυμαίνεται μεταξύ 65dB και 70dB πριν την εφαρμογή των τεμαχών EPS. Αυτές οι τιμές έχουν περιοριστεί κάτω από 60dB μετά την εφαρμογή της προτεινόμενης διάταξης. Σε ορισμένες περιπτώσεις, όπως στις δύο τελευταίες οκτάβες, το επίπεδο των ντεσιμπέλ

αυξήθηκε ελαφρώς. Ωστόσο, ο ευεργετικός ρόλος της προτεινόμενης διάταξης είναι ουσιαστικός, καθώς το επίπεδο των ντεσιμπέλ μειώνεται στην πλειονότητα των οκτάβων.

Το Σχήμα Α.14β απεικονίζει το επίπεδο των ντεσιμπέλ στην περίπτωση επιχώματος με κλίση 45°. Είναι προφανές ότι το επίπεδο των ντεσιμπέλ του αρχικού επιχώματος είναι μειωμένο σε σύγκριση με το επίχωμα με κλίση ίση με 20°. Για παράδειγμα, το επίπεδο ντεσιμπέλ στις πρώτες πέντε οκτάβες είναι σχεδόν το μισό σε σύγκριση με την προηγούμενη περίπτωση (βλ. Σχήμα Α.14α). Ωστόσο, το επίπεδο των ντεσιμπέλ στις κυρίαρχες οκτάβας (13η, 14η, 15η) παραμένει υψηλότερο από 60dB. Η εφαρμογή του γεωαφρού EPS δεν αλλάζει σημαντικά το ήδη χαμηλό επίπεδο των ντεσιμπέλ στις οκτάβες με τις χαμηλότερες κεντρικές συχνότητες. Από την άλλη πλευρά, ο ευεργετικός ρόλος του στη μείωση των δονήσεων είναι εμφανής στις πιο κυρίαρχες οκτάβες.
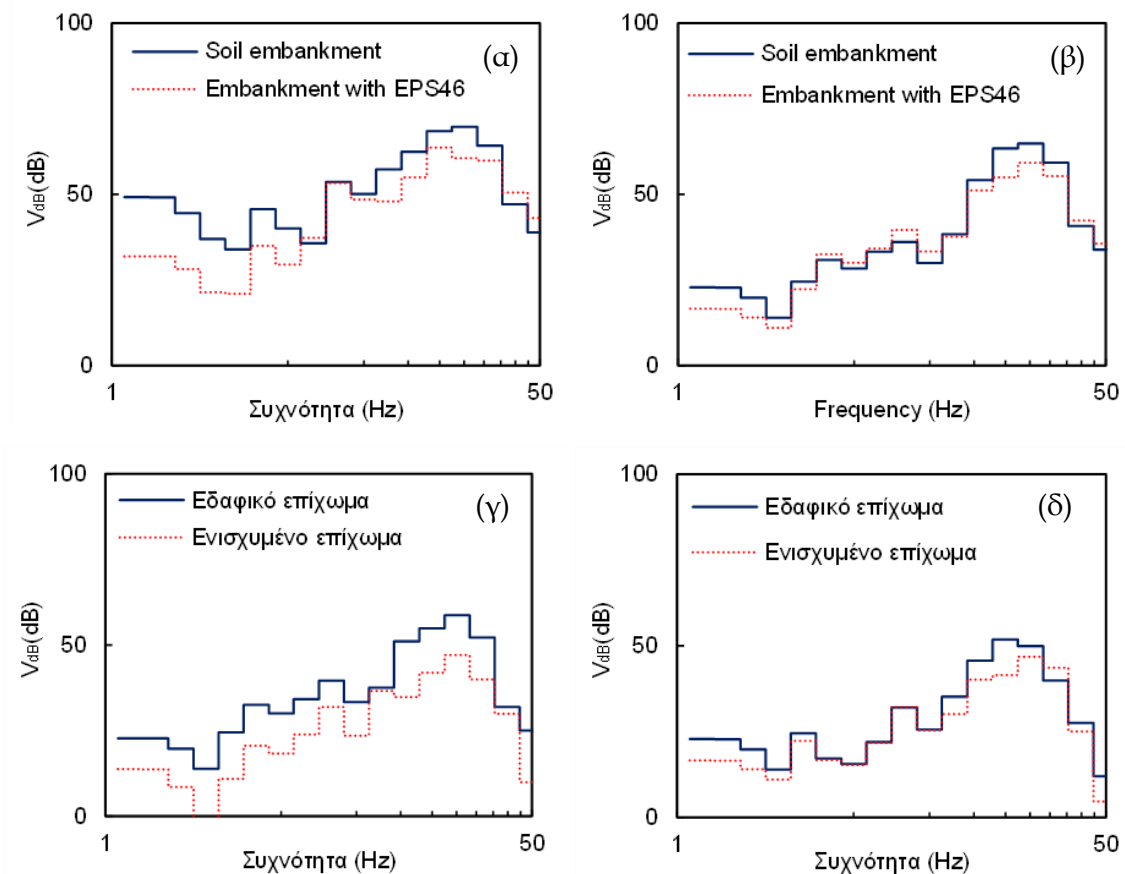
Σχήμα Α.14. Σύγκριση επιπέδου ντεσιμπέλ στα 15μέτρα από την τροχιά για επιχώματα με κλίση: (α) 20°, (b) 45°, στα 35μέτρα από την τροχιά για επιχώματα με κλίση: (γ) 20°, (δ) 45°.

Το επίπεδο των ντεσιμπέλ στο μακρινό πεδίο παρουσιάζεται στα Σχήματα Α.14γ και Α.14δ. Στην περίπτωση του αρχικού επιχώματος με κλίση 20°, το επίπεδο των ντεσιμπέλ είναι υψηλότερο από 60dB στις οκτάβες με κεντρικές συχνότητες 12.5Hz, 16Hz, 20Hz και 25Hz. Η μείωση αυτών των τιμών μετά την εφαρμογή του EPS46 είναι αξιοσημείωτη,

καθώς κυμαίνεται μεταξύ 11dB και 14dB. Αξίζει να σημειωθεί, ότι το επίπεδο των ντεσιμπέλ παραμένει χαμηλότερο από 47dB σε ολόκληρο το εύρος συχνοτήτων. Στην περίπτωση του επιχώματος με κλίση 45ο κλίσης, το αρχικό επίπεδο των ντεσιμπέλ είναι χαμηλότερο από 51dB, όπως φαίνεται στο Σχήμα Α.14δ. Επιπλέον, η εφαρμογή του EPS46 μειώνει περαιτέρω το επίπεδο των ντεσιμπέλ. Η μείωση των ντεσιμπέλ είναι μικρή στις χαμηλότερες οκτάβες, αν και είναι υψηλότερη από 3dB στην κυρίαρχη οκτάβα.

Α.4.4. Επιρροή ταχύτητας διέλευσης

Η ταχύτητα διέλευσης του HST έχει καθοριστικό ρόλο στο επίπεδο των δονήσεων. Η μέγιστη ταχύτητα λειτουργίας των Thalys και TGV HST, στην γραμμή Παρίσι-Βρυξέλλες, είναι ίση με 300km/h. Για αυτόν τον λόγο, έγινε η υπόθεση ότι ο Thalys μπορεί να διέλθει από την εξεταζόμενη θέση με ταχύτητες από 0km/h έως 300km/h. Ως εκ τούτου, εξετάζεται το επίπεδο κραδασμών και η αποτελεσματικότητα της προτεινόμενης διάταξης για τη διέλευση του Thalys με διάφορες ταχύτητες χαμηλότερες από 300km/h. Το Σχήμα Α.15 δείχνει την αύξηση της PPV για αυξανόμενη ταχύτητα διέλευσης πριν και μετά την εφαρμογή των τεμαχών EPS. Είναι προφανές ότι για χαμηλότερες ταχύτητες η PPV παραμένει χαμηλή. Για παράδειγμα, το επίπεδο της PPV είναι μόλις 0.3mm/s, στην περίπτωση διέλευσης με 100km/h πριν την εφαρμογή του EPS. Η τιμή αυτή αυξάνεται στα 1.3mm/s για διέλευση με ταχύτητα 200km/h. Επιπλέον, η PPV παραμένει περίπου στο ίδιο επίπεδο για ταχύτητες διέλευσης μεταξύ 200km/h και 300km/h. Η εφαρμογή του γεωαφρού EPS στην πλαγιά του επιχώματος μειώνει το επίπεδο δονήσεων για διελεύσεις με χαμηλή ταχύτητα. Από την άλλη πλευρά, η αποτελεσματικότητα της προτεινόμενης διάταξης είναι ακόμη πιο μεγάλη για ταχύτητες υψηλότερες από 150km/h.
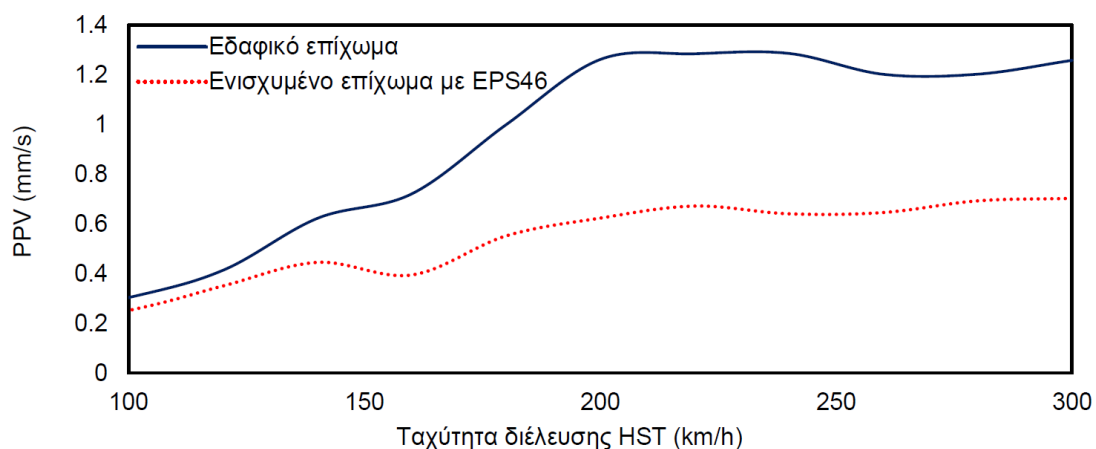
Σχήμα Α.15. Επίπεδο PPV για διάφορες ταχύτητες διέλευσης.

A.4.5. Επιρροή συνθηκών υπεδάφους

Σε αυτήν την ενότητα διερευνώνται οι εδαφικές συνθήκες προκειμένου να εξεταστεί η αποτελεσματικότητα της προτεινόμενης διάταξης (Διάταξη 1) σε διάφορα εδάφη έδρασης. Επιπλέον, η χρήση γεωαφρού EPS για τον περιορισμό των κραδασμών, επεκτείνεται περαιτέρω εξετάζοντας την εφαρμογή του ως υλικού πλήρωσης τάφρου (Διάταξη 2) και ο συνδυασμός της με την τοποθέτηση τεμαχών EPS στις πλαγιές του επιχώματος (Διάταξη 3). Στην εκτενή περίληψη παρουσιάζονται δυο χαρακτηριστικά εδαφικά υλικά, η χαλαρή άργιλος και η πυκνή άμμος με κροκάλες. Οι μηχανικές ιδιότητες των εξεταζόμενων εδαφών δίνονται στον Πίνακα A.4.

Πίνακας A.4. Μηχανικά χαρακτηριστικά εδαφών.

Τύπος εδάφους	Πυκνότητα (kg/m³)	Μέτρο ελαστικότητας (MPa)	Λόγος Poisson (-)	Συντελεστής απόσβεσης ξ (%)
Πυκνή άμμος με κροκάλες	2100	1000	0.20	5
Χαλαρή άργιλος	1850	170	0.35	5

Το επίπεδο των ντεσιμπέλ των τριών εξεταζόμενων διατάξεων περιορισμού των κραδασμών συγκρίνεται με το αρχικό επίπεδο ντεσιμπέλ στην περίπτωση που το επίχωμα εδράζεται σε χαλαρή άργιλο. Η απόκριση του εδάφους στα 15 μέτρα από την τροχιά φαίνεται στο Σχήμα A.16α. Οι κυρίαρχες οκτάβες είναι οι 13η, 14η και 15η, όπου το επίπεδο των κραδασμών στην περίπτωση του αρχικού εδαφικού επιχώματος κυμαίνεται μεταξύ 60dB και 64dB. Η εφαρμογή της Διάταξης 1 συμβάλει στη μείωση αυτών των τιμών, για παράδειγμα το επίπεδο των ντεσιμπέλ μειώνεται από 64dB σε 48dB στην οκτάβα με κεντρική συχνότητα 31.5Hz. Επιπλέον, η χρήση τάφρου EPS (Διάταξη 2) μείωσε ελαφρώς το επίπεδο των κραδασμών, ωστόσο αυτή η διάταξη είναι λιγότερο αποτελεσματική σε σύγκριση με τη Διάταξη 1. Η πιο αποτελεσματική μέθοδος περιορισμού των κραδασμών είναι η ταυτόχρονη τοποθέτηση EPS στο πρανές του επιχώματος και ως υλικό πλήρωσης της τάφρου. Αυτή η διάταξη περιορίζει το επίπεδο των ντεσιμπέλ κάτω από 52dB σε όλο το εξεταζόμενο εύρος.

Όπως ήταν αναμενόμενο, το αρχικό επίπεδο ντεσιμπέλ στα 35 μέτρα από την τροχιά είναι αρκετά χαμηλότερο σε σύγκριση με το κοντινό πεδίο, (Σχήμα A.16b). Οι οκτάβες με κεντρικές συχνότητες μεταξύ 16Hz και 31Hz είναι οι κυρίαρχες σε αυτήν την περίπτωση. Επιπλέον, το επίπεδο ντεσιμπέλ παραμένει κάτω από 52dB για ολόκληρο το εύρος συχνοτήτων. Είναι αξιοσημείωτο ότι και οι τρείς εξεταζόμενες διατάξεις περιορίζουν

επιτυχώς το επίπεδο κραδασμών. Πιο συγκεκριμένα, οι διατάξεις 1 και 3 περιορίζουν το επίπεδο των ντεσιμπέλ όλων των εξεταζόμενων οκτάβων κάτω από τα 46dB. Όμως, η πιο αποτελεσματική διάταξη παραμένει η τρίτη, καθώς καταφέρνει να μειώσει το επίπεδο των ντεσιμπέλ κάτω από τα 42dB.
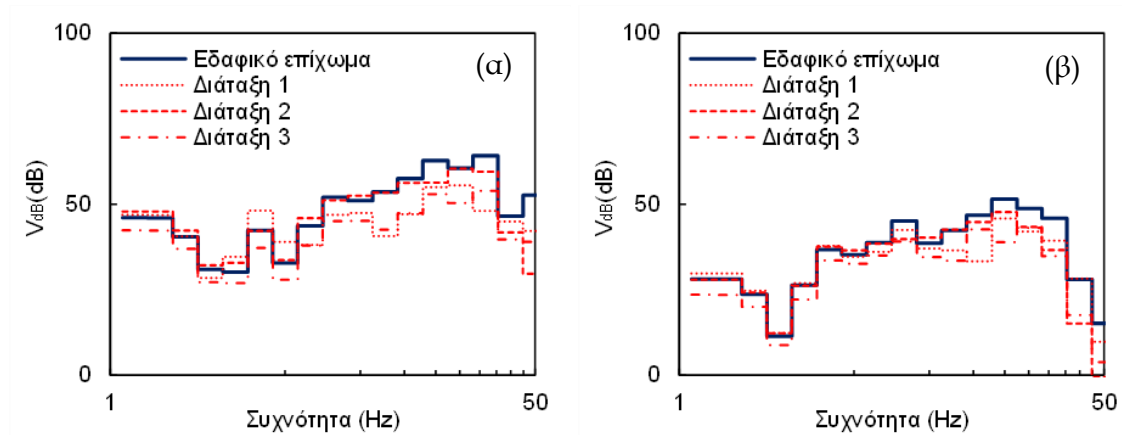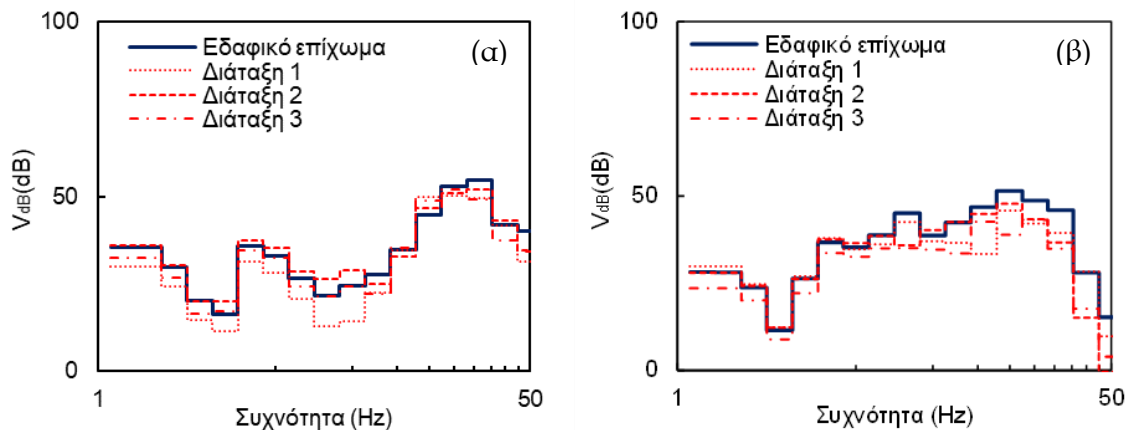

Σχήμα Α.16. Σύγκριση επιπέδου ντεσιμπέλ για επιχώματα εδραζόμενο σε χαλαρή άργιλο: (α) στα 15 μέτρα, (β) στα 35 μέτρα από την τροχιά.

Στη συνέχεια, παρουσιάζεται το επίπεδο των ντεσιμπέλ στην περίπτωση που το επίχωμα εδράζεται σε σκληρό αμμώδες έδαφος με κροκάλες. Σε αυτήν την περίπτωση το επίπεδο των ντεσιμπέλ του κανονικού επιχώματος είναι μειωμένο σε σύγκριση με τα πιο χαλαρά εδάφη. Ειδικότερα, το μέγιστο επίπεδο ντεσιμπέλ στα 15 μέτρα από την τροχιά είναι ίσο με 53dB σε σύγκριση με τα 64dB στην περίπτωση της χαλαρής αργίλου. Ως εκ τούτου, δεν είναι απαραίτητη η εφαρμογή οποιουδήποτε μέτρου περιορισμού λόγω του χαμηλού επιπέδου των ντεσιμπέλ. Σε γενικές γραμμές, το επίπεδο των κραδασμών παραμένει κοντά στο αρχικό επίπεδο σε ολόκληρο το εξεταζόμενο εύρος συχνοτήτων. Στα 35 μέτρα από την τροχιά, το επίπεδο μείωσης των δονήσεων είναι υψηλότερο, αν και δεν υπάρχει ανάγκη για εφαρμογή μέτρων περιορισμού των κραδασμών, καθώς το αρχικό επίπεδο είναι χαμηλότερο από 50dB.

Α.4.6. Βασικά συμπεράσματα

Συνοψίζοντας, σε αυτήν την ενότητα παρουσιάστηκε μια οικονομική και απλή προσέγγιση προκειμένου να περιοριστούν οι προκαλούμενες δονήσεις από τη διέλευση HST. Η προτεινόμενη διάταξη περιλαμβάνει την εφαρμογή ενός περιορισμένου αριθμού τεμαχών EPS και μπορεί εύκολα να εφαρμοστεί στην κατασκευή νέων ή/και στην αναβάθμιση υπαρχόντων επιχωμάτων. Τα κύρια ευρήματα από τη διερεύνηση την χρήσης EPS για τον περιορισμό των κραδασμών σε θέσεις επιχωμάτων συνοψίζονται ως εξής:

- Η εφαρμογή της προτεινόμενης διάταξης με την χρήση EPS περιορίζει σημαντικά τους κραδασμούς σε αποστάσεις από 15 έως 35 μέτρα από την τροχιά. Η χρήση σκληρότερου EPS είναι η βέλτιστη επιλογή καθώς οδηγεί στα χαμηλότερα επίπεδα κραδασμών.

- Η εφαρμογή των τεμαχών EPS συμβάλλει στον περιορισμό των δονήσεων για όλα τα εξεταζόμενα ύψη και κλίσεις πρανών επιχωμάτων.

- Το επίπεδο των κραδασμών είναι χαμηλότερο όταν η σιδηροτροχιά εδράζεται σε σκληρά εδάφη.

Σχήμα Α.17. Σύγκριση επιπέδου ντεσιμπέλ για επιχώματα εδραζόμενο σε σκληρή άμμο με κροκάλες: (α) στα 15 μέτρα, (β) στα 35μέτρα από την τροχιά.

Α.5. Ενίσχυση ορύγματος με χρήση γεωαφρού EPS

Στην προηγούμενη ενότητα διερευνήθηκε η χρήση γεωαφρού EPS για την απομείωση των κραδασμών σε θέσεις σιδηροδρομικού επιχώματος. Στη συνέχεια, λόγω της ευεργετικής συμβολής των προτεινόμενων μέτρων σε θέσεις επιχωμάτων, η διερεύνηση επεκτείνεται σε θέσεις σιδηροδρομικών ορυγμάτων. Αρχικά, η επικρατέστερη διάταξη στην περίπτωση του επιχώματος τροποποιείται για να χρησιμοποιηθεί και σε θέσεις ορυγμάτων. Διερευνάται η χρήση περιορισμένου αριθμού τεμαχών EPS στην πλαγιά του ορύγματος (Διάταξη S), η τοποθέτηση τάφρου EPS στην βάση του ορύγματος (Διάταξη T) και η ταυτόχρονη εφαρμογή των δυο διατάξεων (Διάταξη ST).

Επιπλέον, στη συνέχεια διερευνάται η αντικατάσταση της επιφανειακής εδαφικής στρώσης του ορύγματος με EPS με στόχο την εύρεση της βέλτιστης διάταξης. Διερευνώνται διάφορα πάχη στρώσεων μεταξύ 0.5 μέτρων και 2 μέτρων. Στην εκτενή περίληψη παρουσιάζονται οι δύο ακραίες περιπτώσεις. Συγκεκριμένα εξετάζεται η αντικατάσταση στρώματος εδάφους ύψους 0.5 μέτρων (Διάταξη Α) και 2 μέτρων (Διάταξη Β) και

παρουσιάζεται η αποτελεσματικότητα αυτών των προσεγγίσεων στη μείωση των δονήσεων σε δυο κρίσιμες θέσεις. Η πρώτη εξεταζόμενη θέση βρίσκεται επί του κεκλιμένου τμήματος του ορύγματος στα 15 μέτρα από την τροχιά και η δεύτερη στα 23 μέτρα από την τροχιά, κοντά στο άνω τμήμα του ορύγματος.

A.5.1. *Χρήση EPS στην πλαγιά του πρανούς*

Αρχικά, στο Σχήμα A.18 παρουσιάζονται οι χρονοϊστορίες των κατακόρυφων ταχυτήτων στα 15 μέτρα από την τροχιά, στις περιπτώσεις των Διατάξεων S, T και ST. Το επίπεδο των κραδασμών μετά την εφαρμογή τεμαχών EPS στην πλαγιά του ορύγματος (Διάταξη S), αντί να μειωθεί, αυξάνεται. Για παράδειγμα, η μέγιστη κατακόρυφη ταχύτητα αυξάνεται από τα 1.45mm/s στα 1.6mm/s. Από την άλλη πλευρά, η εφαρμογή της τάφρου EPS (Διάταξη T), περιορίζει τη μέγιστη κατακόρυφη ταχύτητα στα 0.7mm/s, όπως φαίνεται στο Σχήμα A.18β. Τέλος, η αποτελεσματικότητα της διάταξης ST, είναι ανάμεσα στις δυο προαναφερθείσες απλούστερες διατάξεις, περιορίζοντας τη μέγιστη κατακόρυφη ταχύτητα στα 0.95mm/s (Σχήμα A.18γ).
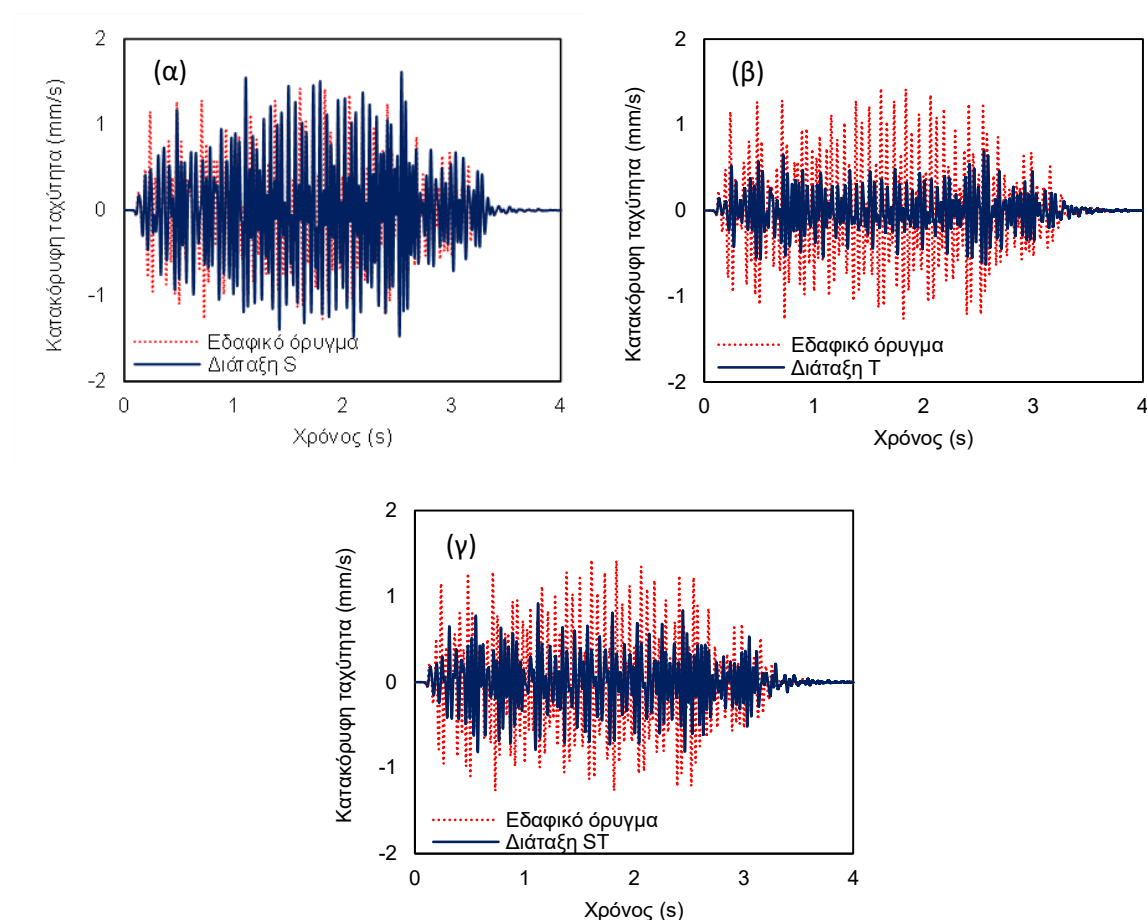
Σχήμα A.18. Σύγκριση χρονοϊστοριών κατακόρυφων ταχυτήτων στα 15 μέτρα από την τροχιά πριν και μετά την εφαρμογή των διατάξεων: (α) S, (β) T, (γ) ST.

Το Σχήμα Α.19 απεικονίζει τις χρονοϊστορίες των κατακόρυφων ταχυτήτων, στα 23 μέτρα από την τροχιά. Η θέση αυτή βρίσκεται στο άνω επίπεδο τμήμα του ορύγματος. Σε αυτό το σημείο, η αποτελεσματικότητα της Διάταξης ST αλλάζει αισθητά σε σύγκριση με τα 15 μέτρα από την τροχιά. Για παράδειγμα, η μέγιστη κατακόρυφη ταχύτητα μειώνεται από το 1mm/s στα 0.33mm/s, όπως φαίνεται στο Σχήμα Α.19α. Ακόμα πιο χαμηλή τιμή της μέγιστης κατακόρυφης ταχύτητας, η οποία φτάνει έως 0.33mm/s, καταγράφεται για τη διάταξη ST (Σχήμα Α.19β). Σε αντίθεση με τα 15 μέτρα από την τροχιά, η διάταξη T είναι η λιγότερο αποτελεσματική, περιορίζοντας τη μέγιστη κατακόρυφη ταχύτητα στα 0.44mm/s.
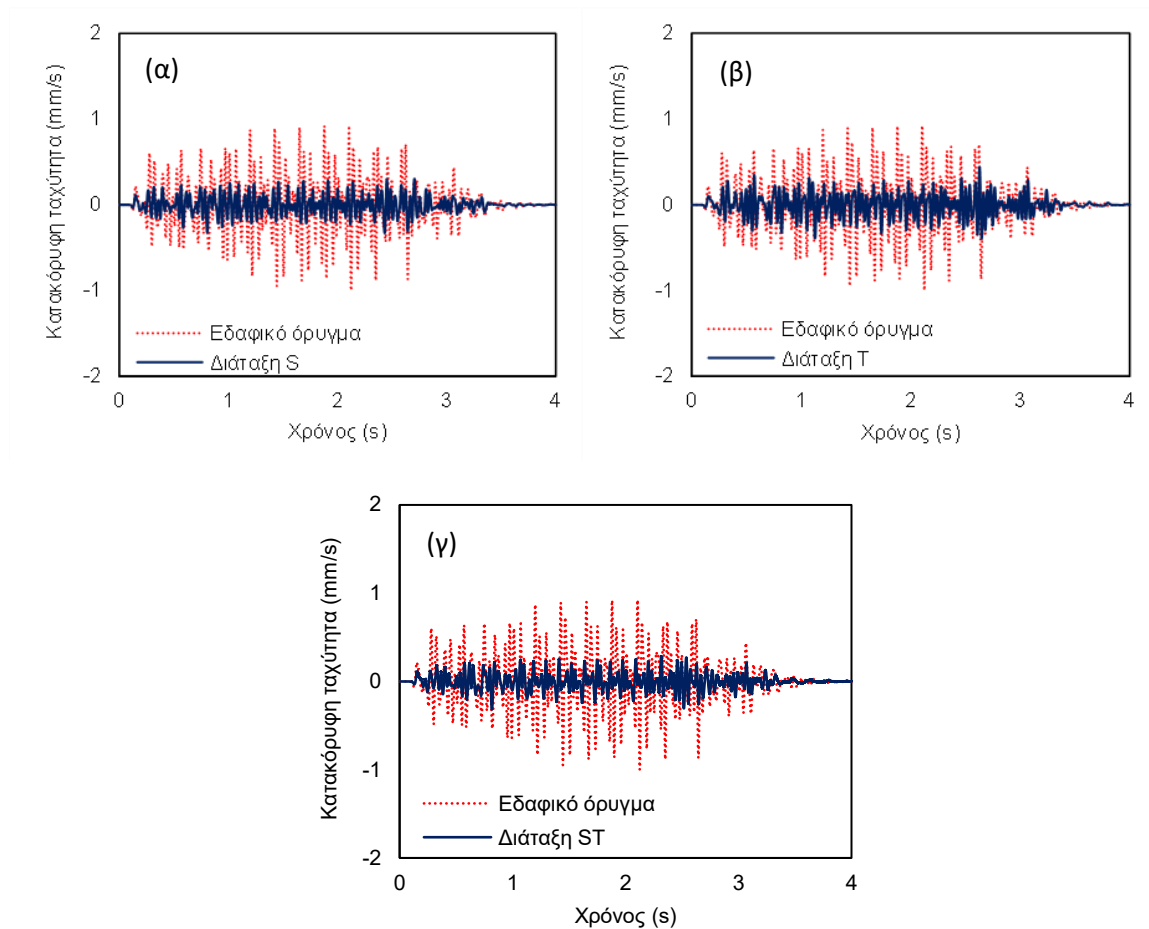
Σχήμα Α.19. Σύγκριση χρονοϊστοριών κατακόρυφων ταχυτήτων στα 23 μέτρα από την τροχιά πριν και μετά την εφαρμογή των διατάξεων: (α) S, (β) T, (γ) ST.

Είναι φανερό από τα Σχήματα Α.18 και Α.19 ότι η αποτελεσματικότητα των διατάξεων S και ST, διαφοροποιείται σημαντικά από την κεκλιμένη επιφάνεια του ορύγματος στο άνω επίπεδο τμήμα. Για τον λόγο αυτό, στο Σχήμα Α.20 παρουσιάζεται η μεταβολή της μέγιστης κατακόρυφης ταχύτητας σε αυξανόμενη απόσταση από την τροχιά, μεταξύ 15 μέτρων και 35 μέτρων. Όπως έχει ήδη αναφερθεί, το επίπεδο των

κραδασμών του αρχικού ορύγματος ελαττώνεται όσο αυξάνεται η απόσταση από την τροχιά. Η εφαρμογή της διάταξης S αυξάνει σταδιακά το επίπεδο κραδασμών σε όλο το κεκλιμένο τμήμα του ορύγματος, δηλαδή για αποστάσεις μικρότερες των 19 μέτρων από την τροχιά. Όμως, στη συνέχεια μειώνει απότομα το επίπεδο των κραδασμών σε τιμές μικρότερες από 0.5 mm/s. Η ίδια τάση παρατηρείται στην περίπτωση της διάταξης ST, όπου οι κατακόρυφες ταχύτητες παραμένουν χαμηλότερες από το αρχικό όρυγμα σε όλες τις εξεταζόμενες αποστάσεις από την τροχιά. Ωστόσο, η κατακόρυφη ταχύτητα φτάνει τιμές ίδιες με αυτές που παρατηρούνται στο αρχικό όρυγμα στην κορυφή της πλαγιάς. Αξίζει να σημειωθεί ότι αυτή η διάταξη φτάνει τις χαμηλότερες τιμές σε αποστάσεις μεγαλύτερες των 19 μέτρων. Αντίθετα, στις κοντινές θέσεις επί του πρανούς του ορύγματος, η πιο αποτελεσματική διάταξη είναι η τάφρος με EPS (Διάταξη T).
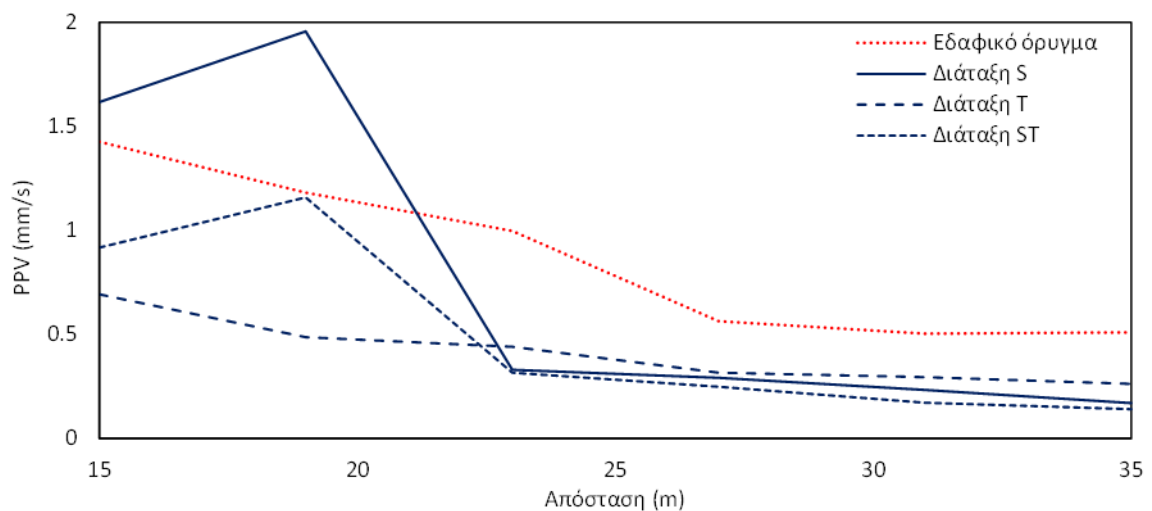
Σχήμα Α.20. Σύγκριση PPV σε διάφορες αποστάσεις από την τροχιά.

Α.5.2. Αντικατάσταση επιφανειακής στρώσης του πρανούς με EPS

Είναι προφανές ότι καμία από τις προαναφερθείσες διατάξεις δεν είναι η βέλτιστη για το σύνολο των εξεταζόμενων αποστάσεων, καθώς η Διάταξη T είναι πιο αποτελεσματική για τη μείωση των δονήσεων στο πρανές, ενώ οι άλλες δύο προσεγγίσεις στις πιο μακρινές θέσεις. Η βασική αιτία της αύξησης των κραδασμών στο πρανές είναι ο μεγάλος συντελεστή σεισμικής ανάκλασης (R_c=0.95) στην διεπαφή EPS-εδάφους, προκαλώντας την ανάκλαση των κυμάτων από το EPS πίσω στην επιφανειακή στρώση του εδάφους. Ως εκ τούτου, ένα μεγάλο ποσοστό των κραδασμών «παγιδεύεται» στο έδαφος κάλυψης των τεμαχών EPS, οδηγώντας σε αυξημένο επίπεδο δονήσεων. Για να αποφευχθεί αυτό, διερευνάται μια εναλλακτική διάταξη για να διατηρηθεί ο ωφέλιμος ρόλος της διάταξης S στη μείωση των κραδασμών στο μακρινό πεδίο και να επιλυθεί το ζήτημα των

αυξημένων επιπέδων κραδασμών στο πρανές. Πιο συγκεκριμένα, η επιφανειακή εδαφική στρώση του πρανούς έχει αντικατασταθεί με EPS46 για να αποφευχθεί η συγκέντρωση των κραδασμών στο έδαφος. Στο πλαίσιο της διατριβής έχουν διερευνηθεί αρκετά πάχη EPS προκειμένου να εξεταστεί η επίδραση του πάχους του στο επίπεδο περιορισμού των κραδασμών. Στο πλαίσιο της εκτενούς περίληψης παρουσιάζονται τα δύο ακραία πάχη 0.5 μέτρα (Διάταξη Α) και 2 μέτρα (Διάταξη Β).
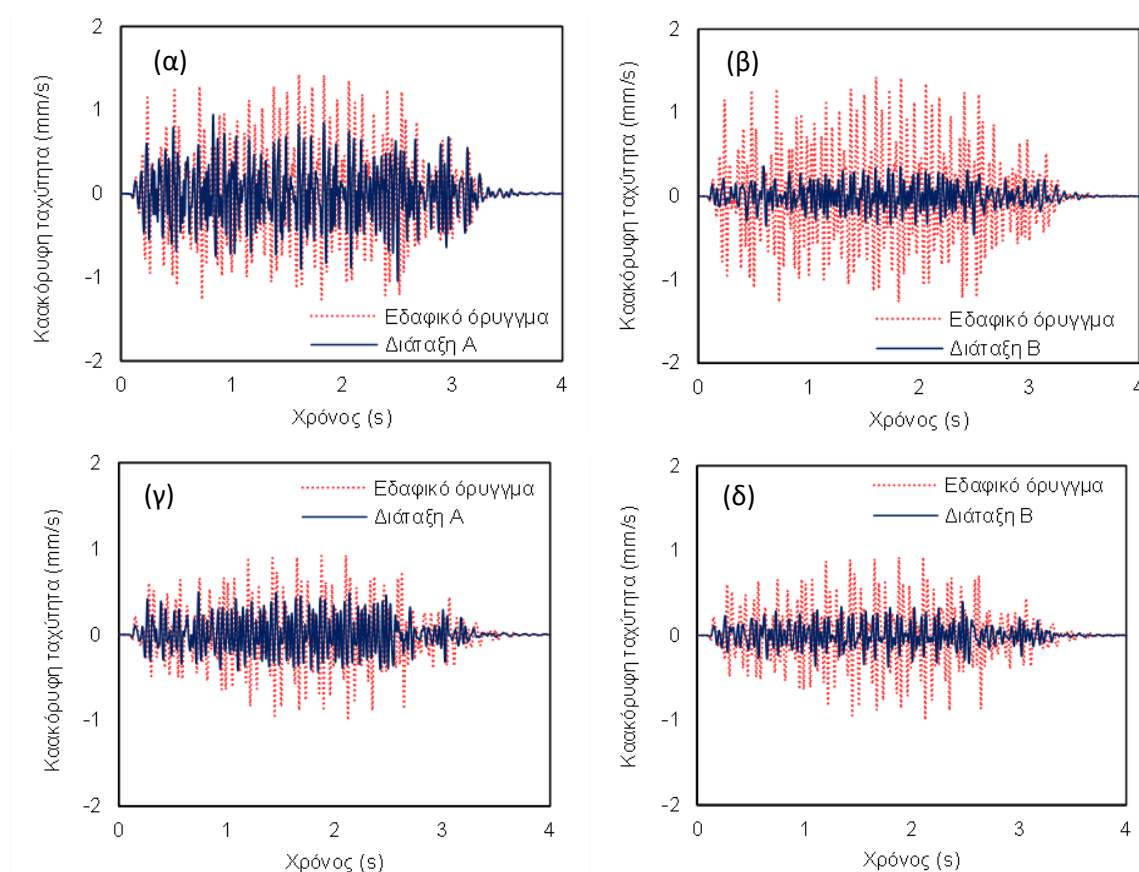

Σχήμα Α.21. Σύγκριση χρονοϊστοριών κατακόρυφων ταχυτήτων στα 15 μέτρα από την τροχιά ((α) Διάταξη Α, (β) Διάταξη Β) και στα 23 μέτρα από την τροχιά ((γ) Διάταξη Α, (δ) Διάταξη Β).

Η επίδραση του πάχους του EPS στο επίπεδο των κραδασμών στα 15 και 23 μέτρα από την τροχιά παρουσιάζεται στις χρονοϊστορίες κατακόρυφων ταχυτήτων του Σχήματος Α.21. Όπως φαίνεται από το Σχήμα Α.21α, η προσθήκη μιας λεπτής στρώσης με πάχος 0.5 μέτρων (Διάταξη Α) οδηγεί σε μια μικρή μείωση των τιμών της χρονοϊστορίας. Η μέγιστη κατακόρυφη ταχύτητα έχει μειωθεί από 1.4mm/s σε 1.05mm/s. Αντίθετα, η εφαρμογή μιας στρώσης 2 μέτρων EPS είναι πιο αποτελεσματική στη μείωση των κραδασμών, καθώς η μέγιστη κατακόρυφη ταχύτητα περιορίζεσαι στα 0.52mm/s. Εκτός από το πρανές, στη συνέχεια παρουσιάζονται στα Σχήματα Α.21γ και Α.21δ οι χρονοϊστορίες κατακόρυφων ταχυτήτων στο επίπεδο τμήμα στην κορυφή του πρανούς. Η εφαρμογή της προτεινόμενης

διάταξης εξακολουθεί να είναι αποτελεσματική και σε αυτήν τη θέση. Όπως φαίνεται στο Σχήμα Α.21γ, η μέγιστη κατακόρυφη ταχύτητα υποδιπλασιάζεται από 1mm/s στα 0.5mm/s με την εφαρμογή 0.5m πάχους EPS. Αυτή η τιμή μειώνεται ακόμη περισσότερο όσο αυξάνεται το πάχος του EPS φτάνοντας τα 0.33mm/s (Σχήμα Α.21δ).

Το Σχήμα Α.22 απεικονίζει δυο στιγμιότυπα των κατακόρυφων ταχυτήτων στην επιφάνεια του εδάφους, στα 0.6 δευτερόλεπτα μετά από την έναρξη της ανάλυσης. Τα πιο έντονα χρώματα αντιπροσωπεύουν τις ζώνες όπου οι κατακόρυφες ταχύτητες έχουν απόλυτες τιμές μεγαλύτερες από 0.5mm/s. Όπως φαίνεται στο Σχήμα Α.21, η μέγιστη απόλυτη κατακόρυφη ταχύτητα των διατάξεων Α και Β, είναι 0.73mm/s και 0.42mm/s, αντίστοιχα, στα 23 μέτρα από την τροχιά. Είναι εμφανές ότι τα επιφανειακά κύματα είναι πιο έντονα στην περίπτωση της διάταξης Α, φτάνοντας σε τιμές υψηλότερες από 0.5mm/s στην κορυφή του πρανούς. Αντίθετα, η σκέδαση των κυμάτων της διάταξης Β, είναι λιγότερο έντονη όπως φαίνεται στο Σχήμα Α.22β. Επομένως, μπορεί να εξαχθεί το συμπέρασμα ότι η αποτελεσματικότητα αυτής της διάταξης εξαρτάται από το πάχος της στρώσης EPS, οδηγώντας αναπόφευκτα και στην αύξηση του κόστους. Ωστόσο, το κόστος του EPS είναι γενικά χαμηλό και ποικίλλει ανάλογα με τον τύπο του υλικού, τις απαιτούμενες ποσότητες για έργα μεγάλης κλίμακας, το κόστος μεταφοράς, κ.α. Επομένως, η διαφορά στον προϋπολογισμό του έργου δεν θα είναι σημαντική.
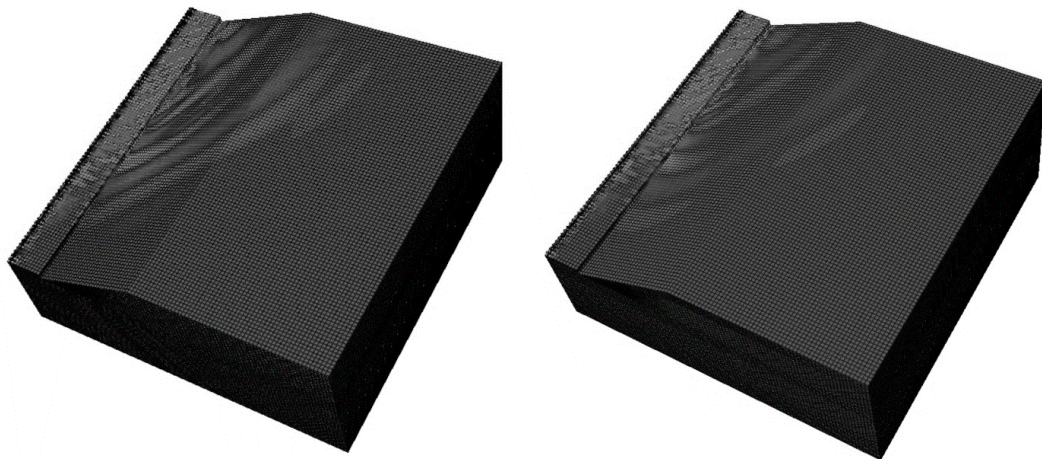
Σχήμα Α.22. Στιγμιότυπα κατακόρυφων ταχυτήτων στην επιφάνεια του εδάφους μετά την εφαρμογή των διατάξεων Α (αριστερά) και Β (δεξιά).

A.5.3. Σύγκριση διατάξεων

Όπως έχει ήδη αναφερθεί, η διάταξη Β έχει διερευνηθεί ως εναλλακτική της διάταξης S, με στόχο να αντιμετωπίσει την αύξηση των κραδασμών στο πρανές του ορύγματος. Το σχήμα Α.23 συγκρίνει τη μέγιστη κατακόρυφη ταχύτητα των διατάξεων S, Τ και ST σε

αυξανόμενες αποστάσεις από την τροχιά, όπου φαίνεται η αυξημένη αποτελεσματικότητα της διάταξη B. Πιο συγκεκριμένα, αυτή η διάταξη είναι πιο αποτελεσματική από την τάφρο EPS (Διάταξη T) στο πρανές του ορύγματος. Επιπλέον, καταφέρνει να φτάσει στο ίδιο επίπεδο περιορισμού των κραδασμών με τη διάταξη ST στο μακρινό πεδίο. Είναι προφανές ότι η διάταξη B είναι η βέλτιστη προσέγγιση, καθώς μειώνει το επίπεδο των κραδασμών περίπου 70% στις περισσότερες από τις εξεταζόμενες αποστάσεις.
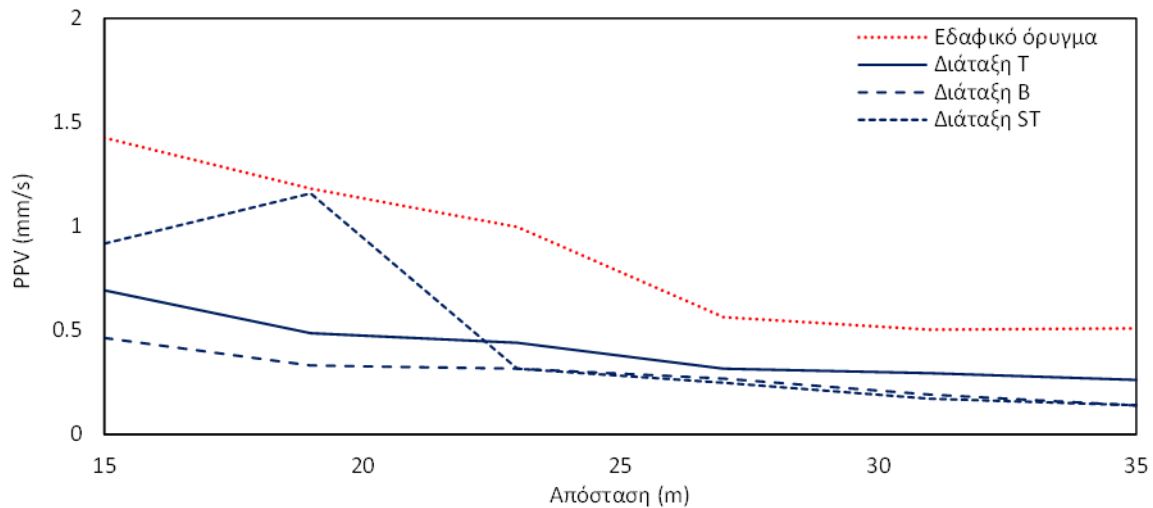
Σχήμα Α.23. Μέγιστη κατακόρυφη ταχύτητα σε αυξανόμενη απόσταση από την τροχιά.
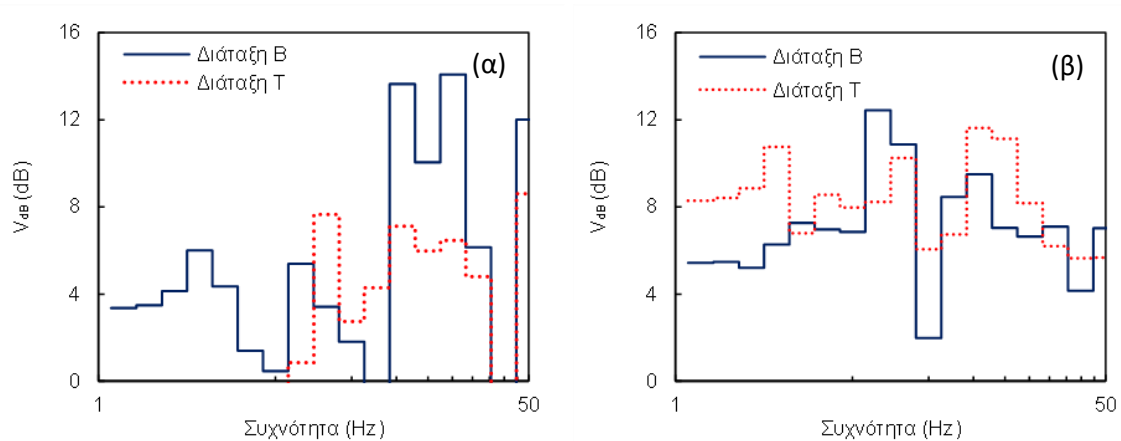
Σχήμα Α.24. (α) Σύγκριση IL διατάξεων D και T στα 15 μέτρα από την τροχιά, (β) Σύγκριση IL διατάξεων D και S στα 23 μέτρα από την τροχιά.

Το Σχήμα Α.24α απεικονίζει τις καμπύλες IL των διατάξεων B και T επί της πλαγιάς στα 15 μέτρα από την τροχιά. Η μείωση των κραδασμών κυμαίνεται μεταξύ 0dB έως 7dB σε όλο το εύρος των εξεταζόμενων οκτάβων. Τα υψηλότερα επίπεδα μείωσης των κραδασμών παρατηρούνται στις οκτάβες με κεντρικές συχνότητες 8Hz, 16Hz και 25Hz, όπου φτάνουν σε επίπεδα υψηλότερα από 6dB. Επιπλέον, η τάφρος με EPS είναι πιο αποτελεσματική από τη διάταξη B στις οκτάβες με κεντρικές συχνότητες μεταξύ 8Hz και

12.5Hz. Από την άλλη πλευρά, η διάταξη B επιτυγχάνει μεγαλύτερα επίπεδα μείωσης των κραδασμών σε όλες τις άλλες οκτάβες. Αξίζει να σημειωθεί ότι παρατηρείται μείωση των κραδασμών μεγαλύτερη από 13dB στην 12η και 14η οκτάβα. Στη συνέχεια, στο Σχήμα A.24β το επίπεδο μείωσης των κραδασμών στα 23 μέτρα από την τροχιά μετά την εφαρμογή της διάταξης B συγκρίνεται με την αποτελεσματική, στο μακρινό πεδίο, Διάταξη S. Η αποτελεσματικότητα της διάταξης S σε αυτή τη θέση είναι αξιοσημείωτη, καθώς η μείωση του ντεσιμπέλ είναι υψηλότερη από 6dB σε όλες τις εξεταζόμενες οκτάβες. Επιπροσθέτως, η IL φτάνει ελαφρώς κάτω από 12dB στην 12η και 13η οκτάβα. Η IL της διάταξης B είναι επίσης ικανοποιητική στα 23 μέτρα από την τροχιά, αν και η μείωση των ντεσιμπέλ, σε γενικές γραμμές, είναι χαμηλότερη από την διάταξη S.

A.5.4. Βασικά συμπεράσματα

Τα κύρια συμπεράσματα που μπορούν να εξαχθούν από την αριθμητική διερεύνηση συνοψίζονται ως εξής:

- Η εφαρμογή τάφρου EPS αποτελεί ένα εξαιρετικό μέτρο περιορισμού των κραδασμών.

- Η εφαρμογή περιορισμένου αριθμού τεμαχών EPS στην πλαγιά αυξάνει το επίπεδο δονήσεων στο πρανές λόγω της "παγίδευσης" της δόνησης στην επιφανειακή εδαφική στρώση. Ωστόσο, το επίπεδο μείωσης είναι υψηλότερο συγκριτικά με την τάφρο στο μακρινό πεδίο. Επιπλέον, εάν αυτή η προσέγγιση συνδυάζεται με μια τάφρο EPS, το επίπεδο μείωσης των κραδασμών στο μακρινό πεδίο είναι ακόμη υψηλότερο.

- Η αντικατάσταση της επιφανειακής στρώσης εδάφους του ορύγματος με EPS αντιμετωπίζει αποτελεσματικά τα υψηλά επίπεδα κραδασμών στο πρανές. Επίσης, όσο μεγαλύτερο πάχος έχει η στρώση EPS, τόσο μεγαλύτερη είναι η αποτελεσματικότητα της.

A.6. Προστασία υπόγειου αγωγού

A.6.1. Εισαγωγή

Στις προηγούμενες ενότητες, αποτυπώθηκε με ακρίβεια το φαινόμενο των κραδασμών που προκαλούνται από τη διέλευση HST στην επιφάνεια του εδάφους και προτάθηκαν μέτρα περιορισμού. Στη διεθνή βιβλιογραφία, η συντριπτική πλειοψηφία των ερευνητών επικεντρώνεται στη διάδοση των επιφανειακών δονήσεων (Celebi, 2006; Gao et al., 2019;

Singh and Seth, 2017). Από την άλλη πλευρά, λίγες μόνο μελέτες εξετάζουν τις επιπτώσεις των αναπτυσσόμενων δονήσεων από τη διέλευση των HST στο υπέδαφος και στα υπόγεια τεχνικά έργα (Liolios et al., 2002; Saboya et al., 2020). Ως εκ τούτου, σε αυτήν την ενότητα γίνεται μια πρώτη προσπάθεια διερεύνησης της δυναμικής απόκρισης των υπόγειων αγωγών που βρίσκονται θαμμένοι κάτω από μια γραμμή HSR. Στη συνέχεια, διερευνάται η χρήση EPS για τη διασφάλιση της δομικής του ακεραιότητας.

Α.6.2. Επαλήθευση απόκρισης αγωγού σε κυκλοφοριακά φορτία

Στη διεθνή βιβλιογραφία δεν έχουν καταγραφεί πειραματικά δεδομένα ή μετρήσεις πεδίου σχετιζόμενα με την απόκριση υπόγειων αγωγών στις δονήσεις που προκαλούνται από τη διέλευση HST. Ωστόσο, υπάρχει μια σειρά πειραματικών δεδομένων που προσομοιώνουν την απόκριση των υπόγειων αγωγών λόγω φορτίων οδικής κυκλοφορίας (Tafreshi et al., 2020, Khalaj et al., 2020). Τα αποτελέσματα αυτά χρησιμοποιήθηκαν στην παρούσα διατριβή για τη διασφάλιση της αξιοπιστίας του αριθμητικού προσομοιώματος των υπόγειων αγωγών. Σύμφωνα με τη διάταξη των Tafreshi et al. (2020), ένας αγωγός πολυαιθυλενίου υψηλής πυκνότητας (HDPE 100) διαμέτρου 250mm έχει τοποθετηθεί σε βάθος μισού μέτρου. Για την προσομοίωση των ισοδύναμων φορτίων ενός φορτηγού, έχει εφαρμοστεί στην επιφάνεια του εδάφους πίεση ίση με 800kPa, μέσω μεταλλικής πλάκας φόρτισης διαμέτρου 250mm. Ο αγωγός υποβλήθηκε σε 150 κύκλους φόρτισης. Οι Khalaj et al. (2020) χρησιμοποίησαν μια σχεδόν πανομοιότυπη διάταξη, όμως εφάρμοσαν έναν μόνο κύκλο φόρτισης αυξάνοντας σταδιακά το φορτίο από 0 σε 800kPa σε χρονικό διάστημα 5 δευτερολέπτων. Περισσότερες λεπτομέρειες για τα χαρακτηριστικά του προσομοιώματος και τις ιδιότητες των υλικών, παρέχονται στο κυρίως κείμενο της διατριβής.

Το Σχήμα Α.25 παρουσιάζει την επαλήθευση του αριθμητικού προσομοιώματος με τα πειραματικά αποτελέσματα της δοκιμής των Tafreshi et al. (2020). Συγκεκριμένα, η κάθετη και η οριζόντια μεταβολή της διαμέτρου του αγωγού σύμφωνα με τα πειραματικά αποτελέσματα (Tafreshi et al., 2020) απεικονίζεται στο Σχήμα Α.26α. Σύμφωνα με τα πειραματικά αποτελέσματα, το ποσοστό αλλαγής της διαμέτρου αυξάνεται από 0 σε 6% μετά από 25 κύκλους φόρτωσης και στις δυο διευθύνσεις. Στη συνέχεια, ο ρυθμός αύξησης των οριζόντιων και κατακόρυφων μεταβολών της διαμέτρου μειώνεται, φτάνοντας έως 7% και 8%, αντίστοιχα, μετά από 150 κύκλους φόρτωσης. Το αριθμητικό προσομοίωμα καταγράφει με ακρίβεια το ποσοστό αλλαγής της διαμέτρου μετά από 150 κύκλους φόρτωσης, όπως φαίνεται στο Σχήμα Α.25β. Από την άλλη πλευρά, τα αριθμητικά

αποτελέσματα δείχνουν μια μικρή απόκλιση από τα πειραματικά όσο αφορά την κλίση της γραφικής παράστασης. Είναι προφανές ότι το αριθμητικό προσομοίωμα χρειάζεται τους διπλάσιους κύκλους φόρτισης για να φτάσει σε ποσοστό 6% σε σχέση με τα πειραματικά αποτελέσματα. Ωστόσο, σε γενικές γραμμές, το αριθμητικό μοντέλο είναι σχετικά αξιόπιστο για τη διερεύνηση της απόκρισης υπόγειων αγωγών από τη διέλευση HST.
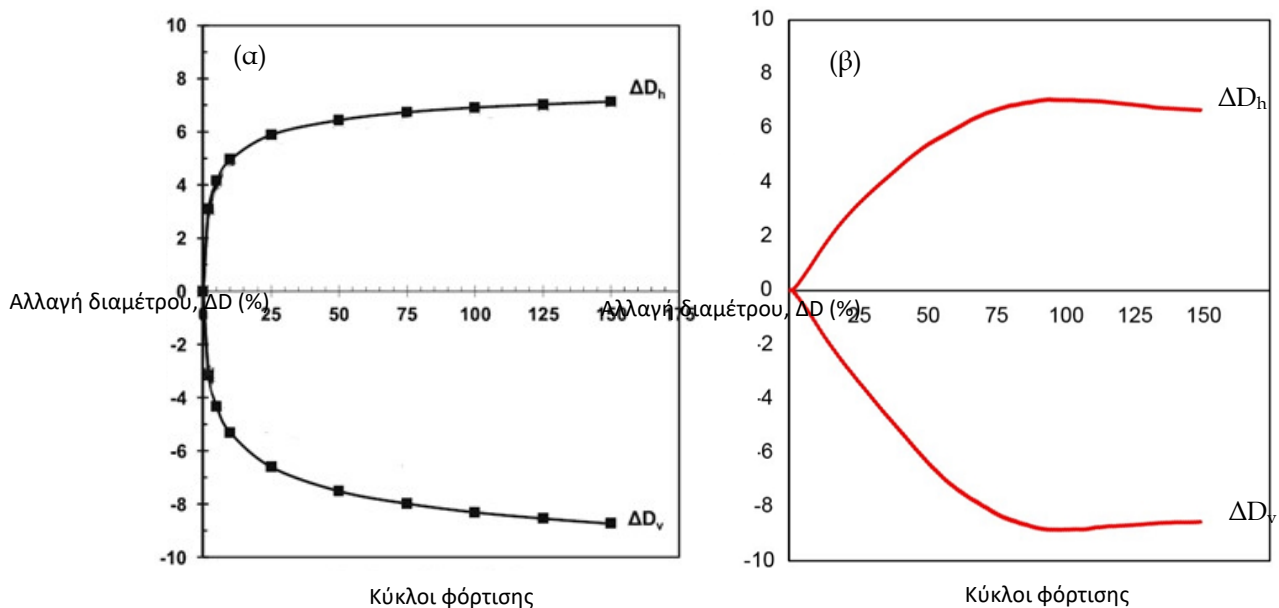
Σχήμα Α.25. Κατακόρυφη (ΔD$_v$) και οριζόντια (ΔD$_h$) αλλαγή διαμέτρου αγωγού σύμφωνα με (α) τα πειραματικά δεδομένα (Tafreshi et al., 2020), (β) το μοντέλο πεπερασμένων στοιχείων.
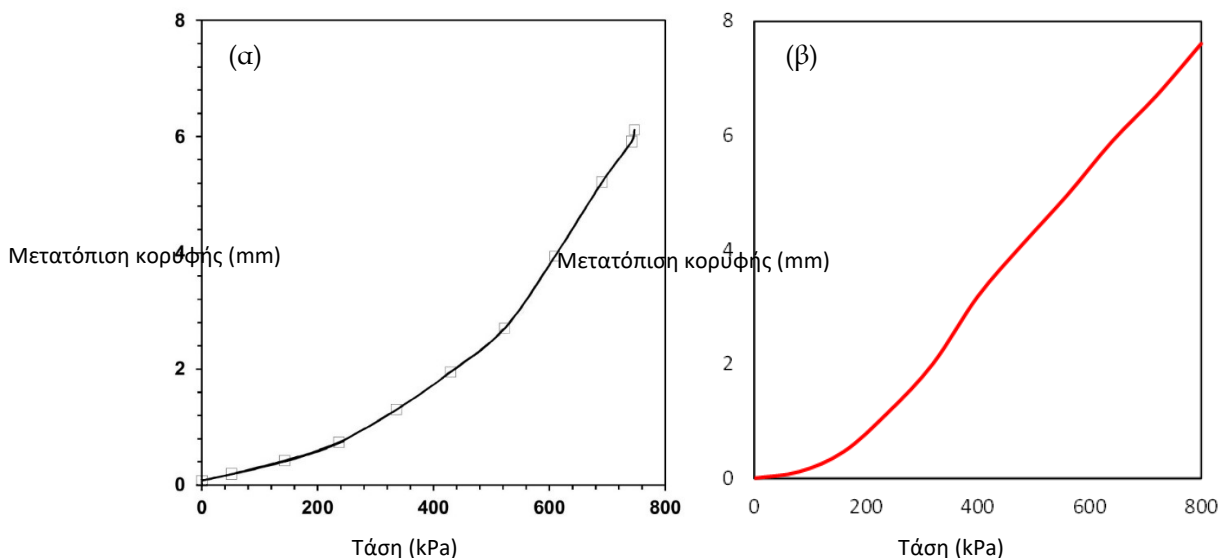
Σχήμα Α.26. Μετακίνηση κορυφής αγωγού σύμφωνα με: (α) τα πειραματικά δεδομένα (Khalaj et al., 2020), (β) το μοντέλο πεπερασμένων στοιχείων.

Στη συνέχεια, τα αριθμητικά αποτελέσματα συγκρίνονται με τα πειραματικά δεδομένα της διερεύνησης των Khalaj et al. (2020). Το Σχήμα Α.26α παρουσιάζει τη

μετακίνηση της κορυφής του αγωγού σύμφωνα με τα διαθέσιμα πειραματικά αποτελέσματα. Η μετακίνηση αυξάνεται ελαφρώς από 0 σε 2mm όταν το μισό του συνολικού φορτίου εφαρμόζεται στον αγωγό. Ακολούθως, ο ρυθμός αύξησης της μετακίνησης είναι μεγαλύτερος, καθώς η μέγιστη μετακίνηση κατά την εφαρμογή του συνόλου του φορτίου είναι ίση με 6mm. Όπως φαίνεται στο Σχήμα Α.26β, το αριθμητικό μοντέλο υπερεκτιμά ελαφρώς τις μετατοπίσεις σε σύγκριση με τα πειραματικά δεδομένα. Ωστόσο, η μορφή του διαγράμματος έχει αναπαραχθεί με αρκετά καλή ακρίβεια και τα αριθμητικά αποτελέσματα είναι της ίδιας τάξης μεγέθους με τα πειραματικά.

Α.6.3. Οριζόντια τάφρος EPS

Μετά την επαλήθευση των αριθμητικών αποτελεσμάτων, το προσομοίωμα χρησιμοποιείται για τη διερεύνηση της απόκρισης του αγωγού στη διέλευση HST και την αποτελεσματικότητα της διάταξης της οριζόντιας τάφρου στην προστασία του αγωγού. Το Σχήμα Α.27 απεικονίζει την προτεινόμενη διάταξη, η οποία βασίστηκε στη γνωστή ως «Imperfect trench» μέθοδο, όπως προτείνεται από το NPRA (2010). Σύμφωνα με το NPRA, μια οριζόντια τάφρος EPS με πλάτος 1.5D τοποθετείται στα 0.2D πάνω από τον αγωγό, όπου D είναι η διάμετρος του.
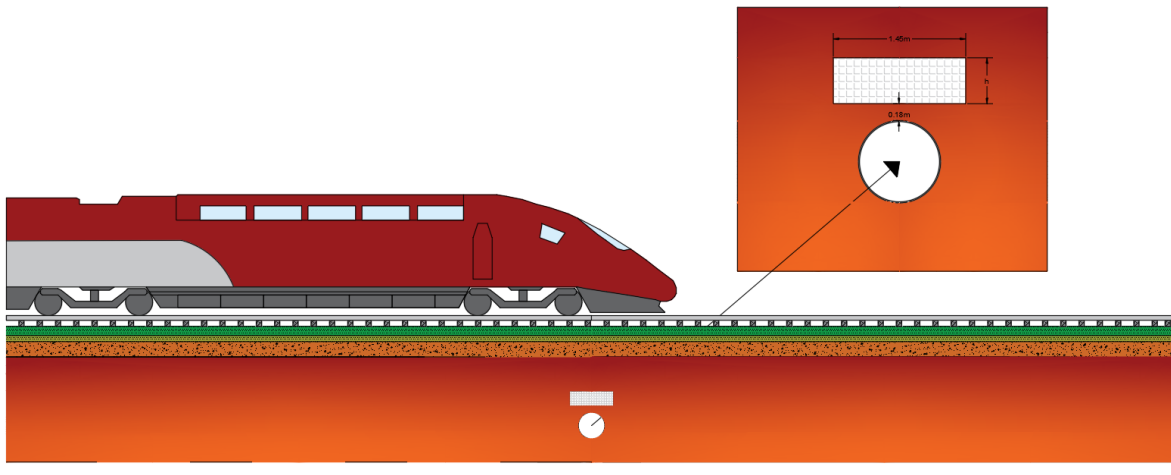
Σχήμα Α.27. Οριζόντια τάφρος EPS (Imperfect trench method).

Α.6.4. Επιρροή πάχους τάφρου EPS και ταχύτητας διέλευσης

Αρχικά διερευνήθηκε η αποτελεσματικότητα της οριζόντιας τάφρου EPS στον περιορισμό των κραδασμών στην επιφάνεια ενός μεταλλικού αγωγού ποιότητας Χ-65. Η εξωτερική διάμετρος και το πάχος των αγωγών Χ-65 είναι 914mm και 12.7mm, αντίστοιχα. Ο αγωγός έχει τοποθετηθεί σε βάθος ίσο με το διπλάσιο της διαμέτρου του (Mohitpour et al., 2007). Περισσότερες πληροφορίες σχετικά με τα μηχανικά χαρακτηριστικά του αγωγού και του

εδάφους παρέχονται στο πλήρες κείμενο της διατριβής. Παρουσιάζονται τρία πάχη στρώσεων (12.5cm, 25cm και 50cm) για να μελετηθεί η επιρροή του πάχους της στρώσης στην αποτελεσματικότητα της μεθόδου.

Στο σχήμα Α.28 παρουσιάζεται η μείωση των ντεσιμπέλ που επιτυγχάνεται μετά την τοποθέτηση της οριζόντιας τάφρου για όλες τις εξεταζόμενες ταχύτητες διέλευσης. Τα διαγράμματα της IL έχουν υπολογιστεί για τις οκτάβες με κεντρικές συχνότητες από 1.25Hz έως 125Hz. Στην πρώτη περίπτωση, όπου το πάχος της τάφρου ισούται με 12.5cm, η μείωση των κραδασμών παραμένει στο ίδιο επίπεδο, κοντά στα 4.8dB για όλες τις εξεταζόμενες ταχύτητες σε όλες τις οκτάβες με κεντρικές συχνότητες χαμηλότερες από 31.5Hz. Στις οκτάβες με υψηλότερες κεντρικές συχνότητες, η μείωση των ντεσιμπέλ παρουσιάζει διακυμάνσεις, καθώς κυμαίνεται μεταξύ εξαιρετικά χαμηλών ή υψηλών τιμών. Γενικά, η χρήση τάφρου EPS με πάχος 12.5 εκατοστών μειώνει ελαφρώς το επίπεδο κραδασμών στο πάνω μέρος του αγωγού, αν και αυτή η μείωση δεν είναι ικανοποιητική.
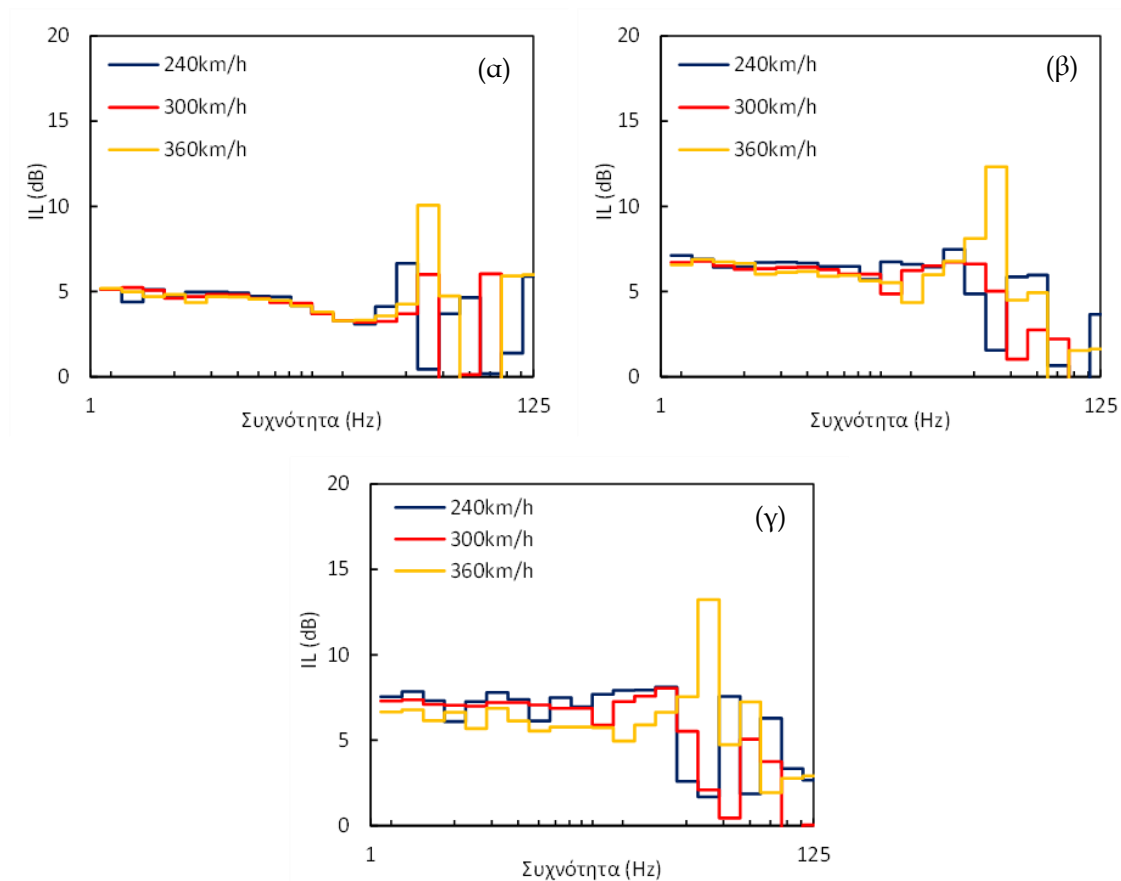
Σχήμα Α.28. IL στην επιφάνεια του αγωγού για πάχος οριζόντιας τάφρου: (α) 12.5cm, (β) 25cm, (γ) 50cm.

Στη συνέχεια, παρουσιάζεται το επίπεδο μείωσης των ντεσιμπέλ στην περίπτωση εφαρμογής τάφρου EPS πάχους 25mm. Είναι προφανές από το Σχήμα Α.28β ότι η

αποτελεσματικότητα της μεθόδου είναι καλύτερη σε σύγκριση με την προηγούμενη περίπτωση, καθώς η μείωση των ντεσιμπέλ αυξάνεται στα 6.7dB για οκτάβες με κεντρική συχνότητα μικρότερη από 31.5 Hz. Η μείωση των ντεσιμπέλ φτάνει τη μέγιστη τιμή των 12dB στην οκτάβα με κεντρική συχνότητα 40Hz όταν το τρένο διέρχεται με 360km/h. Τέλος, στο Σχήμα Α.28γ απεικονίζονται τα ίδια αποτελέσματα στην περίπτωση εφαρμογής της παχύτερης εξεταζόμενης τάφρου EPS. Στις χαμηλές οκτάβες, η απώλεια των ντεσιμπέλ κυμαίνεται γύρω στα 7.3dB. Αυτές οι τιμές παραμένουν στο ίδιο επίπεδο για όλες τις εξεταζόμενες συχνότητες.

Α.6.5. Επιρροή πάχους και υλικού κατασκευής αγωγού στις παραμορφώσεις

Όπως έχει αναφερθεί στην προηγούμενη ενότητα, η εφαρμογή της οριζόντιας τάφρου μειώνει επιτυχώς το επίπεδο των κραδασμών στην επιφάνεια του αγωγού. Ωστόσο, για τη διασφάλιση της δομικής του ακεραιότητας είναι σημαντικό να διερευνηθεί η επίδραση των φορτίων του HST στην αλλαγή της διαμέτρου του αγωγού, καθώς μεγάλες παραμορφώσεις μπορούν να οδηγήσουν σε βλάβες του αγωγού. Ως εκ τούτου, στην παρούσα ενότητα διερευνώνται αγωγοί θαμμένοι σε μικρό βάθος, οι οποίοι θεωρούνται ως πιο ευάλωτοι σε μεγάλες παραμορφώσεις. Συγκεκριμένα, αγωγός HDPE100 πάχους τοιχωμάτων 3mm, ο οποίος χρησιμοποιήθηκε και για την επαλήθευση των αποτελεσμάτων, τοποθετήθηκε σε βάθος 0.5 μέτρων. Επίσης, για να διερευνηθεί η επίδραση του πάχους του σωλήνα στην απόκριση του αγωγού, έχει διερευνηθεί ένας όμοιος αγωγός με πάχος τοιχωμάτων 9mm. Τέλος, μελετήθηκαν δύο μεταλλικοί αγωγοί με διάμετρο 250mm και πάχη 3mm και 9mm. Οι μηχανικές ιδιότητες αυτών των αγωγών είναι τύπου X-65.

Αρχικά, παρουσιάζεται η μεταβολή της διαμέτρου των πλαστικών αγωγών πριν και μετά την εφαρμογή οριζόντιας τάφρου EPS με πάχος 25cm στο Σχήμα Α.29. Κατά τη διέλευση του πρώτου άξονα του HST, η κατακόρυφη αλλαγή της διαμέτρου πριν την εφαρμογή της τάφρου είναι ίση με 1.6mm για αγωγό πάχους 3mm. Η τιμή αυτή αυξάνεται σταδιακά, φτάνοντας τη μέγιστη τιμή των 7mm κατά τη διέλευση του τελευταίου βαγονιού. Παρατηρείται ότι μετά τη διέλευση του HST, παρατηρείται παραμένουσα παραμόρφωση ίση με 0.8mm. Τέλος, πρέπει να αναφερθεί ότι το πλάτος ταλάντωσης της μέγιστης παραμόρφωσης είναι κοντά στα 6mm. Η εφαρμογή της τάφρου EPS έχει ευεργετική επίδραση στη μείωση της μεταβολής διαμέτρου του αγωγού, καθώς μειώνει τη μέγιστη κατακόρυφη παραμόρφωση από 7mm σε 3mm, ενώ το πλάτος ταλάντωσης περιορίζεται στο 1mm. Η αύξηση του πάχους του αγωγού στα 9mm μειώνει τις κάθετες

μεταβολές στη διάμετρο του αγωγού κάτω από 3mm και το πλάτος ταλάντωσης στα 5mm, όπως φαίνεται στο Σχήμα Α.29β. Ο ευεργετικός ρόλος της οριζόντιας τάφρου είναι εμφανής και σε αυτήν την περίπτωση, καθώς το μέγιστο πλάτος ταλάντωσης έχει μειωθεί κάτω από 0.4mm.
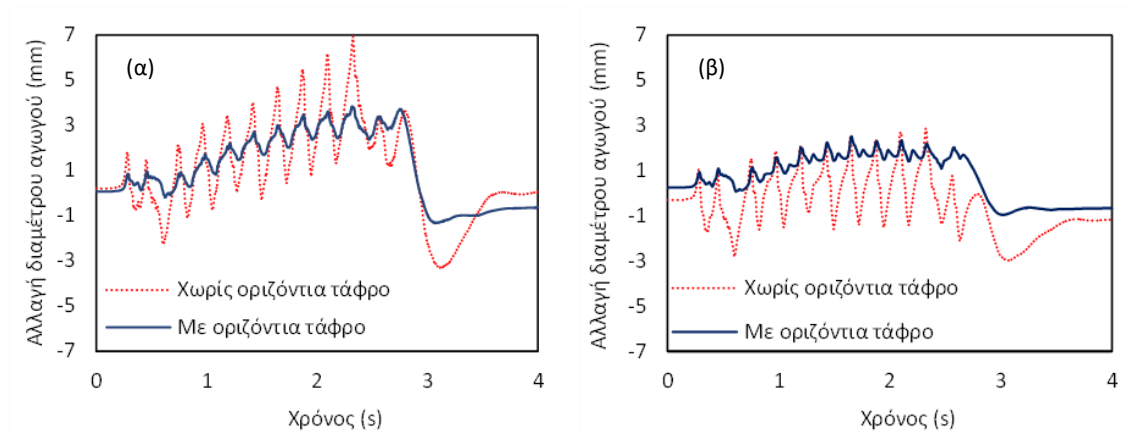
Σχήμα Α.29. Κατακόρυφη αλλαγή διαμέτρου αγωγού PVC πάχους (α) 3mm και (β) 10mm.

Η μεταβολή της διαμέτρου των μεταλλικών αγωγών παρουσιάζεται στο Σχήμα Α.30. Η μέγιστη αλλαγή διαμέτρου του αγωγού με πάχος 3 mm είναι ίση με 3 mm, όπως φαίνεται στα σχήματα Α.30α. Επιπλέον, το πλάτος ταλάντωσης είναι ίσο με 3 mm και η παραμένουσα παραμόρφωση είναι ίση με 0.8 mm. Είναι προφανές ότι ο μεταλλικός αγωγός είναι αρκετά πιο ανθεκτικός σε σύγκριση με τον αγωγό PVC. Η εφαρμογή της οριζόντιας τάφρου μειώνει σημαντικά τις προκαλούμενες παραμορφώσεις, ενώ σχεδόν μηδενίζει την παραμένουσα παραμόρφωση. Στην περίπτωση μεταλλικού αγωγού με πάχος 9mm, η αλλαγή της διαμέτρου παραμένει χαμηλότερη από 1mm και δεν υπάρχει παραμένουσα παραμόρφωση (Σχήμα Α.30β), επομένως δεν είναι απαραίτητη η χρήση οριζόντιας τάφρου.
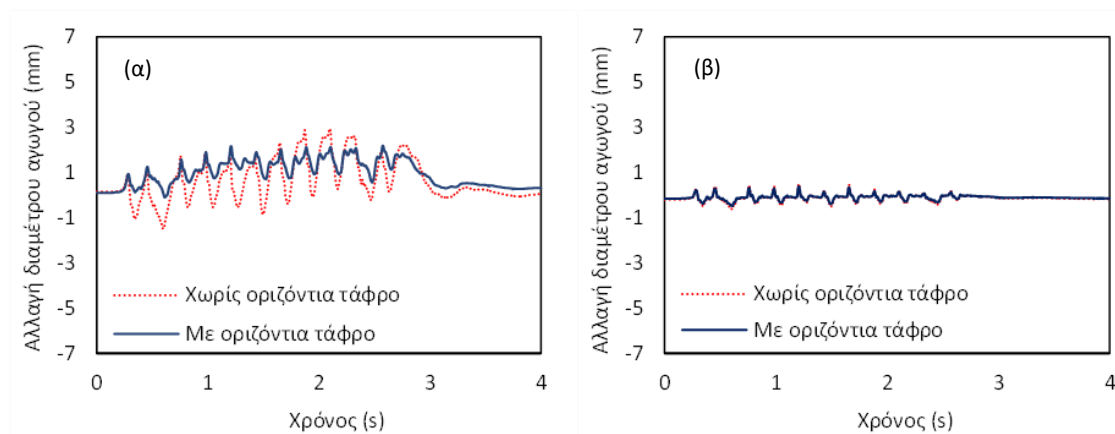
Σχήμα Α.30. Κατακόρυφη αλλαγή διαμέτρου μεταλλικού αγωγού πάχους (α) 3mm και (β) 10mm.

A.6.6. Βασικά συμπεράσματα

Τα κύρια συμπεράσματα που προκύπτουν από τη διερεύνηση της απόκρισης αγωγών κατά τη διέλευση HST, συνοψίζονται ως εξής:

- Η εφαρμογή οριζόντιας τάφρου EPS μεταξύ της σιδηροδρομικής γραμμής και του υπόγειου αγωγού περιορίζει τους κραδασμούς στην επιφάνεια του αγωγού κατά την διέλευση του HST. Το ποσοστό μείωσης εξαρτάται άμεσα από το πάχος της τάφρου EPS, καθώς οι παχύτερες τάφροι είναι οι πιο αποτελεσματικές.

- Η παραμένουσα παραμόρφωση των αγωγών PVC είναι υψηλότερη σε σύγκριση με τους μεταλλικούς. Επιπλέον, η αύξηση του πάχους των αγωγών οδηγεί σε μείωση της αλλαγής της διαμέτρου.

- Η οριζόντια τάφρος μειώνει επιτυχώς τη μεταβολή της διαμέτρου όλων των εξεταζόμενων αγωγών. Η εφαρμογή αυτής της διάταξης σε έναν παχύ και δύσκαμπτο μεταλλικό αγωγό δεν είναι απαραίτητη, καθώς η παραμόρφωση του είναι μικρή.

A.7. Προστασία κτιρίων με χρήση γεωαφρού EPS

A.7.1. Εισαγωγή

Σε αυτήν την ενότητα παρουσιάζεται η αριθμητική διερεύνηση της απόκρισης κτιρίων κατά την διέλευση τρένων υψηλής ταχύτητας. Όπως έχει ήδη αναφερθεί, η επίδραση των κραδασμών στα γειτονικά κτίρια κοντά στη σιδηροτροχιά είναι ένα σημαντικό περιβαλλοντικό ζήτημα που σχετίζεται με την άνεση και την υγεία των κατοίκων. Για τον λόγο αυτό, το επικυρωμένο προσομοίωμα πεπερασμένων στοιχείων από επίπεδη θέση της σιδηροτροχιάς Παρίσι - Βρυξέλλες τροποποιείται κατάλληλα προκειμένου να διερευνηθεί η απόκριση κτιρίων οπλισμένου σκυροδέματος και φέρουσας τοιχοποιίας κατά τη διέλευση του Thalys HST με 240km/h. Στη συνέχεια, μελετάται η εφαρμογή διάφορων διατάξεων τάφρου EPS, με στόχο την ελαχιστοποίηση του επιπέδου των κραδασμών σε κρίσιμες θέσεις του κτιρίου. Επιπλέον, έχει διερευνηθεί η επίδραση της απόστασης από την τροχιά στη δομική απόκριση των κτιρίων, για να προσδιοριστεί σε ποια απόσταση θα μπορούσαν να κατασκευαστούν τα κτίρια για να μην υπάρχουν προβλήματα στους κατοίκους εξαιτίας των δονήσεων.

Α.7.2. Πολυώροφα κτίρια Ο/Σ

Αρχικά, διερευνάται η απόκριση πολυώροφων κτιρίων οπλισμένου σκυροδέματος κατά τη διέλευση του HST. Στην εκτενή περίληψη παρουσιάζεται η απόκριση ενός τετραώροφου και ενός οκταώροφου κτιρίου που έχουν κατασκευαστεί σε απόσταση 10 και 30 μέτρων από την τροχιά. Στη συνέχεια, κατασκευάζεται μονή ή διπλή τάφρος EPS μεταξύ του κτιρίου και της τροχιάς για τη μείωση των κραδασμών της ανωδομής. Τα εξεταζόμενα κτίρια εδράζονται σε πλάκα πάχους 0.2 μ., ενώ το τυπικό ύψος ορόφου έχει οριστεί στα 3 μέτρα. Η κάτοψη των κτιρίων είναι ορθογωνική με πλάτος 12 μέτρων. Τα δύο κτίρια αποτελούνται από ορθογωνικά υποστυλώματα και δοκάρια με διατομές 0.6 μέτρα x 0.4 μέτρα και 0.4 μέτρα x 0.2 μέτρα, αντίστοιχα, όπως φαίνεται στο Σχήμα Α.31. Επιπλέον, στην όψη των κτιρίων από την πλευρά διέλευσης του HST, υπάρχει ένας πρόβολος μήκους 1.5 μέτρων. Για τον περιορισμό των κραδασμών αρχικά τοποθετήθηκε τάφρος βάθους 60 εκατοστών, το οποίο θεωρείται ως ένα βέλτιστο βάθος σύμφωνα με τους Alzawi et al. (2011), παράλληλα με την τροχιά. Σύμφωνα με τους Yarmohammadi et al. (2019), η διπλή τάφρος αυξάνει το επίπεδο μείωσης των δονήσεων σε σύγκριση με τη μονή τάφρο. Ως εκ τούτου, μια δεύτερη τάφρος κατασκευάστηκε σε απόσταση 3 μέτρων από την πρώτη για την περαιτέρω μείωση του επιπέδου των κραδασμών.
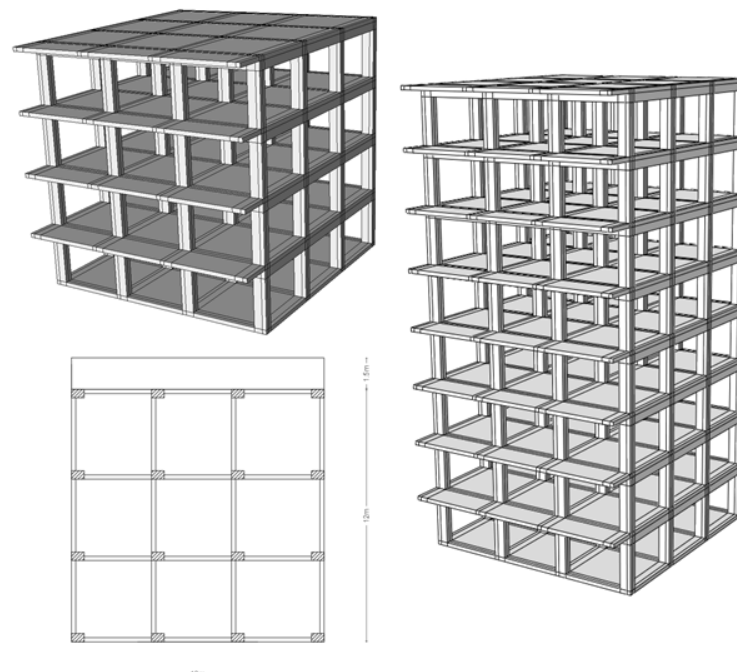
Σχήμα Α.31. Εξεταζόμενα κτίρια Ο/Σ.

Το Σχήμα Α.32 απεικονίζει την επίδραση της διέλευσης του HST στην απόκριση του μέσου της κεντρικής πλάκας στα επίπεδα της βάσης και του τελευταίου ορόφου του

τετραώροφου κτιρίου. Είναι εμφανές ότι στις περισσότερες εξεταζόμενες οκτάβες οι κραδασμοί αυξάνονται στον τελευταίο όροφο του κτιρίου. Στη στάθμη του εδάφους η κυρίαρχη οκτάβα είναι η 14η. Από την άλλη πλευρά, το επίπεδο κραδασμών της 13ης οκτάβας αυξάνεται σημαντικά στον 4ο όροφο, μετατρέποντας αυτήν την οκτάβα στην κύρια. Όταν το κτίριο εδράζεται στα 10 μέτρα από την τροχιά (Σχήμα Α.32α), το επίπεδο των ντεσιμπέλ στην 12ης και 13ης οκτάβα αυξήθηκε κατά 9dB και 12dB στον 4ο όροφο σε σχέση με το έδαφος.

Το Σχήμα Α.32β απεικονίζει το επίπεδο των ντεσιμπέλ στη βάση και στον 4ο όροφο του κτιρίου στην περίπτωση που το κτίριο εδράζεται στα 30 μέτρα από την τροχιά. Το επίπεδο των κραδασμών είναι σημαντικά χαμηλότερο σε σχέση με την προηγούμενη εξεταζόμενη απόσταση, καθώς το επίπεδο των ντεσιμπέλ στη βάση του κτιρίου έχει μειωθεί σε τιμές χαμηλότερες από 47dB σε όλες εξεταζόμενες οκτάβες. Το επίπεδο των ντεσιμπέλ αυξάνεται σε όλο το εξεταζόμενο εύρος στην κορυφή του κτιρίου. Συγκεκριμένα, το επίπεδο των ντεσιμπέλ στην κύρια οκτάβα (13η) φτάνει τα 55dB.
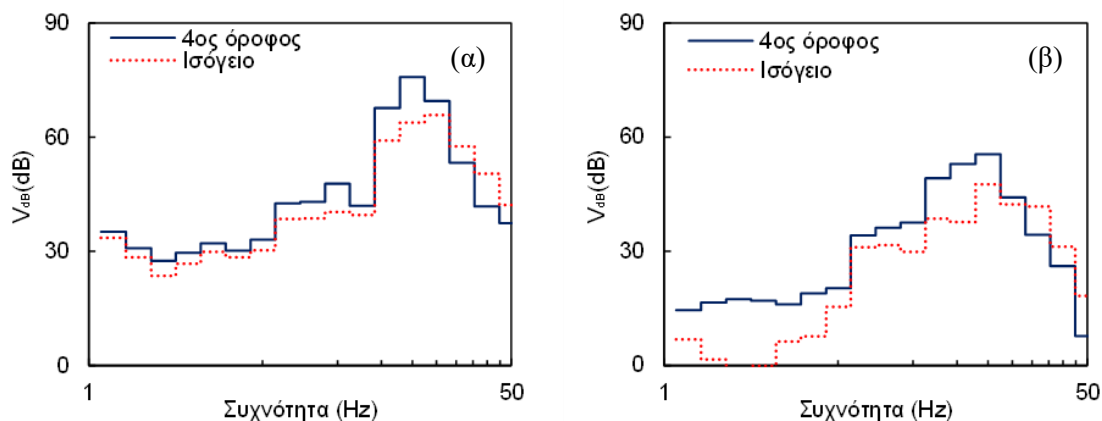
Σχήμα Α.32. Επίπεδο ντεσιμπέλ στο μέσο την κεντρική πλάκας του κτιρίου (α) στα 10 μέτρα, (β) στα 30 μέτρα από την τροχιά.
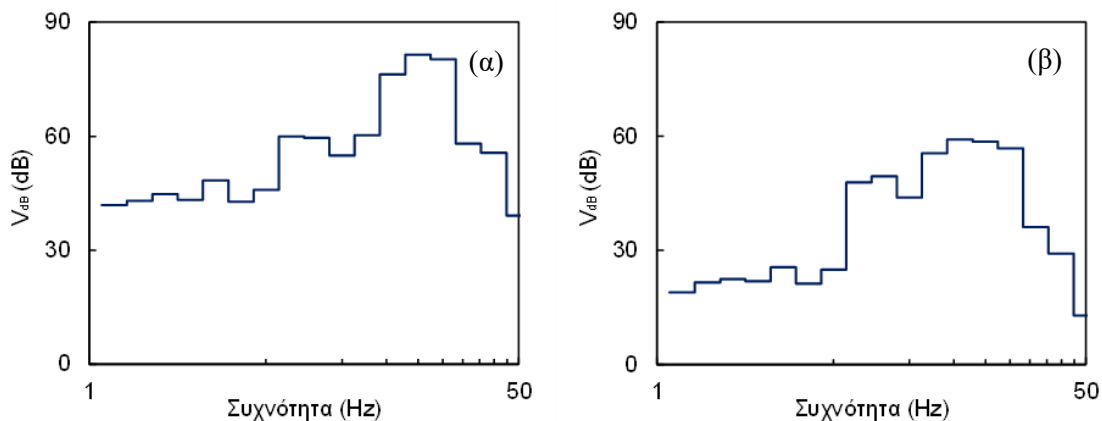
Σχήμα Α.33. Επίπεδο ντεσιμπέλ στην άκρη του προβόλου (α) στα 10 μέτρα, (β) στα 30 μέτρα από την τροχιά.

Στη συνέχεια, παρουσιάζεται το επίπεδο των ντεσιμπέλ στην πιο κρίσιμη θέση του κτιρίου, στην άκρη του προβόλου. Για κτίριο εδραζόμενο στα 10 μέτρα από την τροχιά, το επίπεδο των ντεσιμπέλ φτάνει τα 83dB και 81dB, στην 13η και 14η οκτάβα αντίστοιχα, όπως φαίνεται στο Σχήμα Α.33α. Αξίζει να σημειωθεί ότι το επίπεδο των ντεσιμπέλ είναι υψηλότερο από 40dB σε ολόκληρο το εξεταζόμενο φάσμα συχνοτήτων. Το επίπεδο των κραδασμών είναι μειωμένο όταν το κτίριο βρίσκεται σε απόσταση 30 μέτρων από την τροχιά, όπως φαίνεται στο Σχήμα Α.33β, καθώς το επίπεδο των ντεσιμπέλ είναι χαμηλότερο από 60dB σε ολόκληρο το εξεταζόμενο εύρος συχνοτήτων.

A.7.2.1. Μονή τάφρος

Προκειμένου να μειωθεί το επίπεδο των ντεσιμπέλ, αρχικά εφαρμόζεται παράλληλα με την τροχιά μια τάφρος EPS. Στο Σχήμα Α.34 παρουσιάζονται οι καμπύλες IL της τάφρου EPS στα τρία σημεία παρατήρησης στον 4ο όροφο του κτιρίου για τις δυο εξεταζόμενες αποστάσεις. Στην περίπτωση ενός κτιρίου κατασκευασμένου στα 10 μέτρα από την τροχιά, παρατηρούνται υψηλές μειώσεις των ντεσιμπέλ για όλες τις εξεταζόμενες θέσεις στις οκτάβες με κεντρικές συχνότητες υψηλότερες από 16Hz. Από την άλλη πλευρά, η μείωση των ντεσιμπέλ είναι χαμηλότερη από 4dB για τις πρώτες 11 οκτάβες, όπως φαίνεται στο Σχήμα Α.34α.
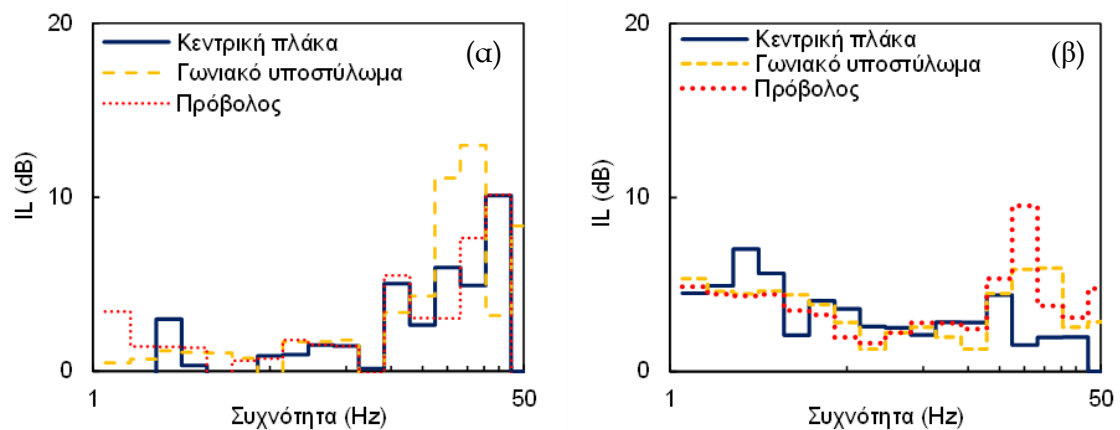
Σχήμα Α.34. Καμπύλες IL μονής τάφρου στον 4ο όροφο, τετραώροφου κτιρίου: (α) στα 10 μέτρα, (β) στα 30 μέτρα από την τροχιά.

Στο κέντρο της πλάκας παρατηρείται μείωση ίση με 10dB στη 16η οκτάβα. Επιπλέον, στις κύριες οκτάβες (11η, 12η και 13η), η μείωση των ντεσιμπέλ κυμαίνεται μεταξύ 4dB και 6dB. Στην κορυφή του γωνιακού υποστυλώματος, παρατηρείται η υψηλότερη μείωση των ντεσιμπέλ. Πιο συγκεκριμένα, η μείωση του επιπέδου των κραδασμών έφτασε τα 11dB και τα 13dB στην 14η και 15η οκτάβα, αντίστοιχα. Στην άκρη του προβόλου, η μείωση είναι

ελαφρώς χαμηλότερη σε σύγκριση με τις άλλες δυο θέσεις. Ωστόσο, η μείωση των ντεσιμπέλ φτάνει τα 10dB στην 16η οκτάβα.

Το Σχήμα Α.34β δείχνει τις καμπύλες IL για κτίριο κατασκευασμένο στα 30 μέτρα από την τροχιά. Η μείωση του επιπέδου των κραδασμών στις οκτάβες με κεντρικές συχνότητες μικρότερες από 5Hz είναι υψηλότερη από την προηγούμενη περίπτωση σε όλα τα εξεταζόμενα σημεία παρατήρησης. Σε ορισμένες περιπτώσεις, η IL στις χαμηλότερες συχνότητες είναι υψηλότερη από 5dB. Από την άλλη πλευρά, η μείωση του επιπέδου των ντεσιμπέλ είναι ελαφρώς χαμηλότερη στις υψηλότερες οκτάβες.

A.7.2.2. Διπλή τάφρος

Το Σχήμα Α.35 απεικονίζει τις καμπύλες IL της διπλής τάφρου. Είναι προφανές ότι η μείωση των κραδασμών έχει αυξηθεί σε σύγκριση με τη μονή τάφρο. Πιο συγκεκριμένα, στην κορυφή του γωνιακού υποστυλώματος, η μείωση φτάνει τιμές κοντά στα 15dB και 12dB στις οκτάβες με κεντρικές συχνότητες 20Hz και 25Hz, αντίστοιχα. Υψηλό επίπεδο μείωσης των κραδασμών έχει επίσης παρατηρηθεί και στα άλλα δύο σημεία παρατήρησης ,φτάνοντας τιμές μεταξύ 9dB και 12dB στις κύριες οκτάβες.   Στο Σχήμα Α.35β παρουσιάζεται η μείωση των κραδασμών στην περίπτωση κτιρίου κατασκευασμένου στα 30 μέτρα από την τροχιά. Η μείωση του επιπέδου των ντεσιμπέλ είναι ελαφρώς χαμηλότερη από την προηγούμενη περίπτωση. Το υψηλότερο επίπεδο μείωσης έχει παρατηρηθεί στην άκρη του προβόλου, στην οκτάβα με κεντρική συχνότητα 20Hz. Επιπροσθέτως, η απώλεια είναι υψηλότερη από 5dB στις τρεις κυρίαρχες οκτάβες για όλα τα εξεταζόμενα σημεία παρατήρησης. Λαμβάνοντας υπόψη τη σχετικά υψηλή απόσταση από την τροχιά, το επίπεδο των ντεσιμπέλ ήταν ήδη χαμηλό πριν από την εφαρμογή της τάφου.
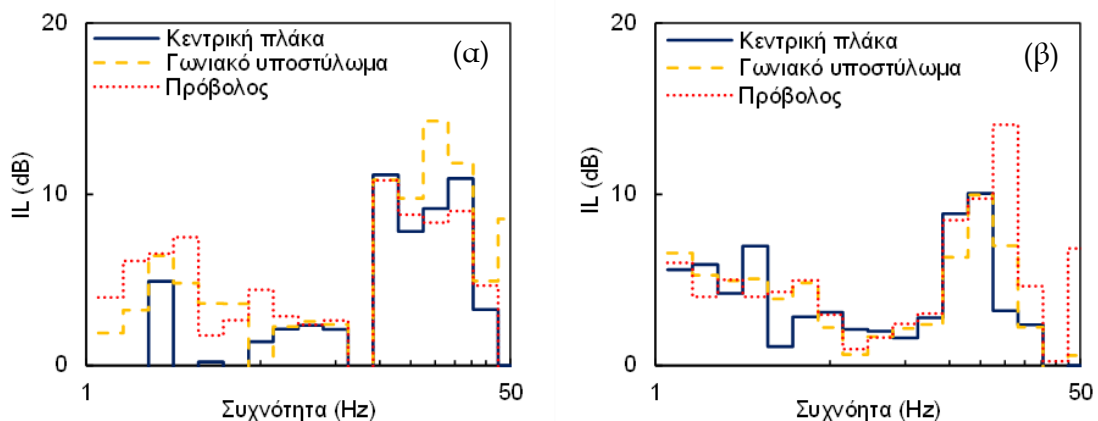
Σχήμα Α.35. Καμπύλες IL διπλής τάφρου στον 4ο όροφο, τετραώροφου κτιρίου: (α) στα 10 μέτρα, (β) στα 30 μέτρα από την τροχιά.

Στη συνέχεια, παρουσιάζεται η μείωση των κραδασμών μετά την εφαρμογή της διπλής τάφρου στον 4ο και τον 8ο όροφο του οκταώροφου κτιρίου. Στο Σχήμα Α.36α παρουσιάζονται οι καμπύλες IL σε όλες τις εξεταζόμενες θέσεις στον 4ο όροφο του κτιρίου στα 10 μέτρα από την τροχιά. Στις οκτάβες με κεντρικές συχνότητες μεταξύ 1.25Hz και 5Hz, η μείωση των κραδασμών φτάνει σε ορισμένες περιπτώσεις, τιμές υψηλότερες από 5dB. Για παράδειγμα, η IL είναι κοντά στα 6dB στην 5η οκτάβας στο γωνιακό υποστύλωμα και στην 6η οκτάβα στην άκρη του προβόλου. Από την άλλη πλευρά, η διπλή τάφρος δεν είναι αποτελεσματική στις οκτάβες με κεντρικές συχνότητες μεταξύ 6.3Hz και 12.5Hz.

Όπως προαναφέρθηκε, τα υψηλότερα επίπεδα κραδασμών βρίσκονται στις οκτάβες με κεντρικές συχνότητες 16Hz, 20Hz και 25Hz. Είναι προφανές ότι η εφαρμογή της διπλής τάφρου οδηγεί σε εξαιρετικά υψηλές τιμές IL. Συγκεκριμένα, η μείωση των ντεσιμπέλ σε αυτές τις οκτάβες κυμαίνεται μεταξύ 7dB και 9dB στις δύο πρώτες θέσεις παρατήρησης. Η ίδια παρατήρηση έγινε στα 30 μέτρα από την τροχιά, όπως φαίνεται στο Σχήμα Α.36β. Στις πρώτες 6 οκτάβες, η μείωση των κραδασμών φτάνει κοντά στα 10dB. Επιπλέον, η μείωση είναι υψηλότερη στις οκτάβες με υψηλότερες κεντρικές συχνότητες, φτάνοντας σε ορισμένες περιπτώσεις τιμές υψηλότερες από 15dB. Σε γενικές γραμμές, η εφαρμογή της διπλής τάφρου έχει ευεργετικό ρόλο στη μείωση των δομικών δονήσεων στον 4ο όροφο του κτιρίου.
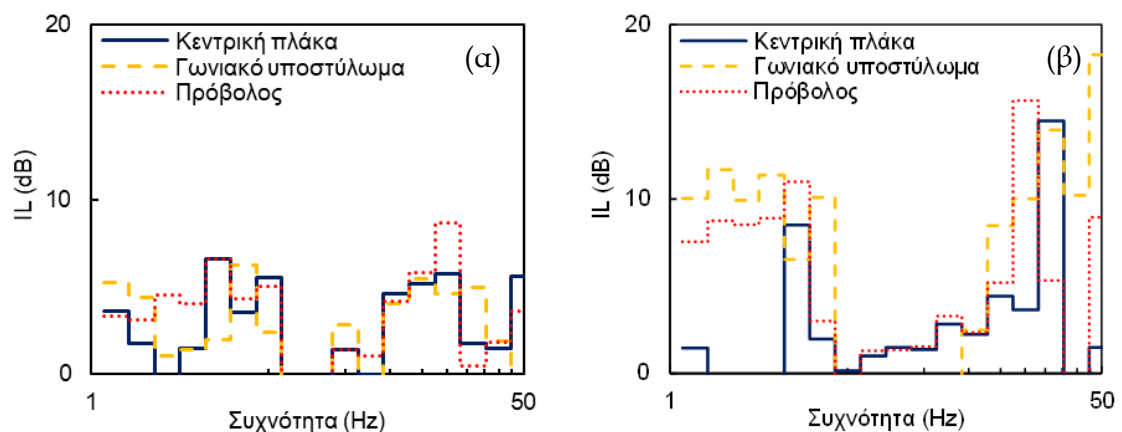
Σχήμα Α.36. Καμπύλες IL διπλής τάφρου στον 4ο όροφο, οκταώροφου κτιρίου: (α) στα 10 μέτρα, (β) στα 30 μέτρα από την τροχιά.

Στο Σχήμα Α.37 παρουσιάζεται η μείωση των ντεσιμπέλ στον 8ο όροφο του κτιρίου μετά την τοποθέτηση της διπλής τάφρου. Είναι προφανές ότι η μείωση των ντεσιμπέλ είναι χαμηλότερη σε σχέση με τον 4ο όροφο. Εάν το κτίριο κατασκευαστεί στα 10 μέτρα από την τροχιά (Σχήμα Α.37α), η μείωση των κραδασμών στις κύριες οκτάβες (π.χ., 12η, 13η, 14η) είναι μεγαλύτερη από 5dB σε όλες τις εξεταζόμενες θέσεις. Επιπλέον, στην άκρη του

προβόλου, η μείωση φτάνει κοντά στα 10dB στην 14ης οκτάβας. Οι μεγαλύτερες μειώσεις έχουν παρατηρηθεί στην περίπτωση κατά την οποία το κτίριο έχει κατασκευαστεί στα 30 μέτρα από την τροχιά, όπως φαίνεται στο Σχήμα Α.37β. Πιο συγκεκριμένα, η μείωση των κραδασμών στις οκτάβες με χαμηλές κεντρικές συχνότητες κυμαίνεται μεταξύ 10dB και 15dB στην άκρη του προβόλου. Επίσης, η μείωση του επιπέδου των ντεσιμπέλ στις κυρίαρχες συχνότητες (13η, 14η) φτάνει τα 9dB.
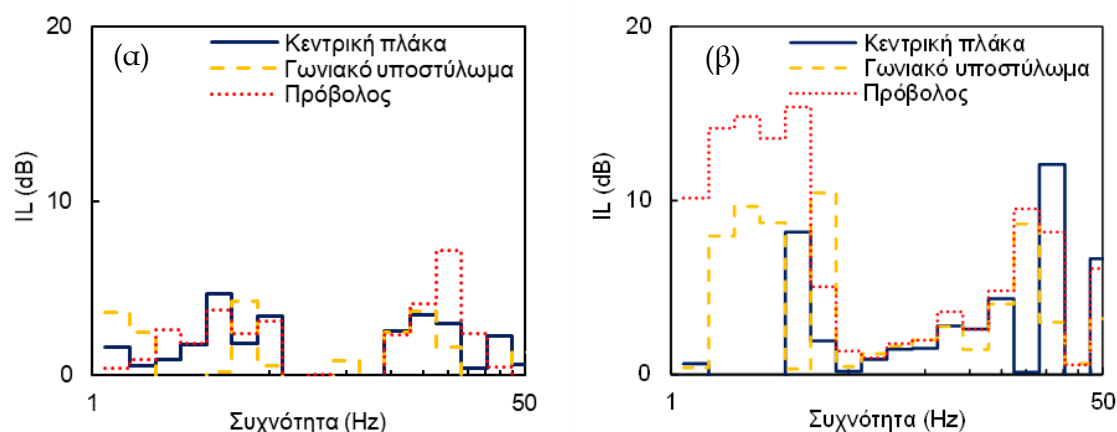
Σχήμα Α.37 Καμπύλες IL διπλής τάφρου στον 8ο όροφο, οκταώροφου κτιρίου: (α) στα 10 μέτρα, (β) στα 30 μέτρα από την τροχιά.

Α.7.3. Κτίριο υποδομών Φ/Τ

Στην προηγούμενη ενότητα παρουσιάστηκε η απόκριση πολυώροφων κτιρίων οπλισμένου σκυροδέματος κατά την διέλευση HST για να εξεταστεί η βέλτιστη απόσταση κατασκευής για την προστασία των κατοίκων από τις δυσμενείς επιπτώσεις στην υγεία. Είναι εμφανές ότι η χρήση τάφρων EPS έχει μετριάσει σημαντικά τις αναπτυσσόμενες δονήσεις. Για τον λόγο αυτό, διερευνώνται τα δομικά χαρακτηριστικά των υφισταμένων κτιρίων κατά μήκος της γραμμής Παρίσι - Βρυξέλλες. Σε αυτήν την περιοχή, η πλειονότητα των κτιρίων είναι κατασκευασμένα από φέρουσα τοιχοποιία (Φ/Τ) ενός ή δύο ορόφων με ορθογωνική κάτοψη.

Σχήμα Α.38. Κτίριο φέρουσας τοιχοποιίας κοντά στην γραμμή Παρίσι – Βρυξέλλες.

Εκτός από τα κτίρια με χρήση κατοικίας, τα οποία συνήθως βρίσκονται στα 30-35 μέτρα από την τροχιά, υπάρχουν αρκετά μονώροφα κτίρια υποδομών των HSR σε αποστάσεις μεταξύ 10m και 15m από την τροχιά, όπως φαίνεται στο Σχήμα Α.38. Προκειμένου να προστατευτούν τα υφιστάμενα κτίρια φέρουσας τοιχοποιίας, διερευνώνται διάφορες διατάξεις με τη χρήση EPS. Η πρώτη διάταξη αποτελεί μια μονή τάφρο EPS κατασκευασμένη παράλληλα με την τροχιά, ιδίων γεωμετρικών και μηχανικών χαρακτηριστικών με την περίπτωση του κτιρίου Ο/Σ. Σύμφωνα με τη δεύτερη διάταξη, ένα περίβλημα EPS έχει κατασκευαστεί περιμετρικά της θεμελίωσης του κτιρίου. Η τελευταία διάταξη αποτελεί μια υβριδική προσέγγιση, κατά την οποία χρησιμοποιούνται παράλληλα και η τάφρος EPS και το περίβλημα περιμετρικά από το κτίριο.
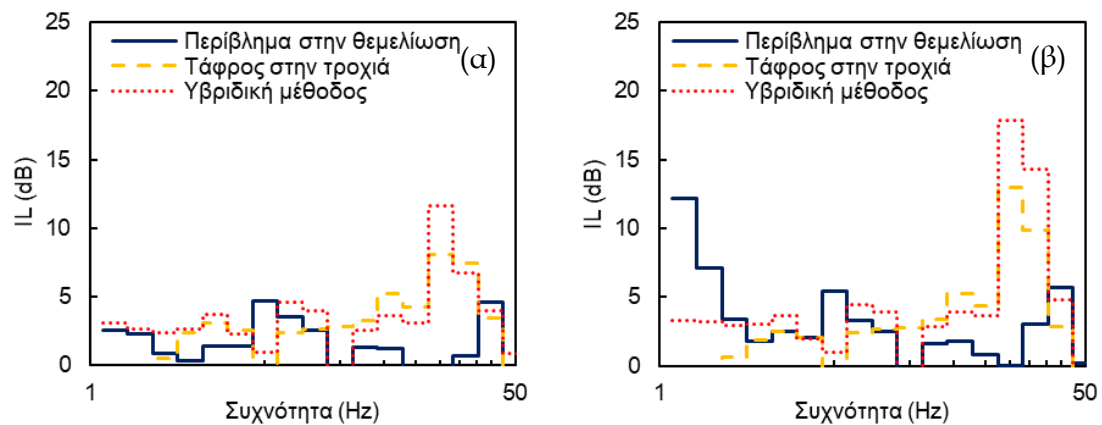
Σχήμα Α.39. Καμπύλες IL κτιρίου φέρουσας τοιχοποιίας (a) στη βάση, (b) στην οροφή.

Στο Σχήμα Α.39 συγκρίνονται τα επίπεδα των ντεσιμπέλ των τριών διατάξεων στην κορυφή του εξεταζόμενου κτιρίου φέρουσας τοιχοποιίας. Το περίβλημα EPS περιμετρικά της θεμελίωσης αποτελεί την λιγότερο αποτελεσματική προσέγγιση καθώς το επίπεδο των ντεσιμπέλ στις περισσότερες οκτάβες δεν ξεπερνάει τα 5dB. Για τον λόγο αυτό, δεν προτείνεται η εφαρμογή αυτής της διάταξης. Αντίθετα, η κατασκευή τάφρου EPS παράλληλα με την τροχιά είναι πολύ πιο αποτελεσματική, ειδικά στις κύριες οκτάβες. Πιο συγκεκριμένα, η μείωση των ντεσιμπέλ φτάνει κοντά στα 8dB και 11dB στην οκτάβα με κεντρική συχνότητα 25Hz, στη βάση και στην κορυφή του κτιρίου, αντίστοιχα. Η χρήση της υβριδικής μεθόδου αυξάνει ακόμη περισσότερο τη μείωση των ντεσιμπέλ στην 14η οκτάβα, φθάνοντας τη μέγιστη τιμή των 18dB στην κορυφή του κτιρίου. Επομένως, η μείωση των κραδασμών μπορεί να είναι ικανοποιητική για κτίρια υποδομών, HSR προκειμένου να προστατευθεί ευαίσθητος εξοπλισμός.

A.7.4. Βασικά συμπεράσματα

Στην παρούσα ενότητα, εξετάζεται η προστασία κτιρίων κοντά σε HSR με τη χρήση γεωαφρού EPS. Σύμφωνα με τα αριθμητικά αποτελέσματα, τα κύρια ευρήματα της μελέτης παρατίθενται ως εξής:

- Σε όλα τα εξεταζόμενα κτίρια, το επίπεδο των δονήσεων που προκαλούνται από τη διέλευση HST αυξάνεται στον τελευταίο όροφο του κτιρίου σε σύγκριση με το έδαφος.

- Στην πιο κοντινή απόσταση από την τροχιά, το επίπεδο των κραδασμών φτάνει πάνω από 80dB στις κύριες οκτάβες. Από την άλλη πλευρά, στην περίπτωση κτιρίων εδραζόμενων στα 30 μέτρων από την τροχιά, το επίπεδο των ντεσιμπέλ μειώνεται κάτω από 60dB.

- Η τοποθέτηση μονής τάφρου EPS μεταξύ του HSR και του κτιρίου οπλισμένου σκυροδέματος μειώνει αποτελεσματικά το επίπεδο των κραδασμών, ενώ η κατασκευή δυο παράλληλων τάφρων οδηγεί σε περεταίρω μείωση του επιπέδου των κραδασμών.

- Στην περίπτωση υφισταμένων κτιρίων φέρουσας τοιχοποιίας η βέλτιστη διάταξη μετριασμού των κραδασμών είναι η ταυτόχρονη τοποθέτηση τάφρου EPS παράλληλα με την τροχιά και περιβλήματος EPS περιμετρικά της θεμελίωσης. Αντίθετα, η εφαρμογή μόνο του περιβλήματος EPS δεν προτείνεται λόγω της περιορισμένης αποτελεσματικότητάς του.

A.8. Συμπεράσματα – Προτάσεις

A.8.1. Γενικά συμπεράσματα

Στην παρούσα ενότητα συνοψίζονται τα κύρια συμπεράσματα της παρούσας διατριβής, όπως προκύπτουν από τις προηγούμενες ενότητες. Στο πρώτο στάδιο της διατριβής, πραγματοποιήθηκε ανασκόπηση της σχετικής βιβλιογραφίας, με στόχο να εντοπιστούν οι κατάλληλες μέθοδοι προσομοίωσης του σύνθετου φαινομένου των παραγόμενων κραδασμών από τη διέλευση τρένων υψηλής ταχύτητας. Επιπλέον, κατά το στάδιο αυτό κατανοήθηκαν τα χαρακτηριστικά των παραγόμενων κραδασμών και η ανάγκη πρότασης νέων τρόπων περιορισμού τους. Στη συνέχεια, αναπτύχθηκαν κατάλληλα 3Δ προσομοιώματα πεπερασμένων στοιχείων με στόχο την ακριβή προσομοίωση του φαινομένου. Τα αριθμητικά αποτελέσματα που προέκυψαν συγκρίθηκαν με μετρήσεις

πεδίου ώστε να διασφαλιστεί η αξιοπιστία τους. Η διαδικασία επαλήθευσης των αποτελεσμάτων ανέδειξε τα ακόλουθα συμπεράσματα:

- Ως μια πρώτη ένδειξη της αξιοπιστίας των προσομοιωμάτων, οι θέσεις των κύριων συχνοτήτων κατά τη διέλευση του HST στα φάσματα Fourier, εντοπίζονται με ακρίβεια.

- Η διάρκεια και η μορφή των χρονοϊστοριών κατακόρυφων ταχυτήτων είναι σε συμφωνία με τις μετρήσεις πεδίου, ειδικά στο κοντινό πεδίο.

- Σύμφωνα με τα πειραματικά δεδομένα, οι κύριες συχνότητες βρίσκονται στο φάσμα χαμηλών συχνοτήτων μεταξύ 0Hz και 40Hz. Τα αριθμητικά προσομοιώματα επιτυγχάνουν να προβλέψουν τη θέση και το μέγεθος των κραδασμών σε αυτό το εύρος.

- Υπάρχει υψηλή συσχέτιση σε όρους PPV και $KB_{F,max}$ μεταξύ των αριθμητικών αποτελεσμάτων και των δεδομένων πεδίου σε αυξανόμενη απόσταση από την τροχιά.

- Ορισμένες αποκλίσεις μεταξύ των αριθμητικών και των πειραματικών αποτελεσμάτων είναι εύλογες λόγω της πολυπλοκότητας του εξεταζόμενου φαινομένου, ωστόσο οι αποκλίσεις είναι περιορισμένες σε σύγκριση με αριθμητικές προσεγγίσεις άλλων ερευνητών.

Πρέπει να αναφερθεί στο σημείο αυτό, ότι οι μετρήσεις πεδίου χρησιμοποιήθηκαν αυτούσιες, δηλαδή χωρίς την εφαρμογή κάποιου φίλτρου για τον καθαρισμό από πιθανό θόρυβο, το οποίο ενδεχομένως να βελτίωνε την -ήδη αρκετά καλή- ταύτιση των αριθμητικών αποτελεσμάτων και των μετρήσεων πεδίου. Ως εκ τούτου, μπορεί να θεωρηθεί ότι η αναπτυχθείσα διαδικασία προσομοίωσης είναι σε θέση να προβλέψει με ακρίβεια τις δονήσεις που προκαλούνται από τη διέλευση HST.

Στη συνέχεια, η ίδια υπολογιστική μεθοδολογία χρησιμοποιήθηκε για τη διερεύνηση εναλλακτικών διατάξεων με τη χρήση γεωαφρού EPS για τον περιορισμό των κραδασμών σε θέσεις σιδηροδρομικού επιχώματος ή ορύγματος. Η διαδικασία αυτή οδήγησε στα ακόλουθα ευρήματα:

- Η τοποθέτηση ενός περιορισμένου αριθμού τεμαχών γεωαφρού EPS στην πλαγιά του επιχώματος προτείνεται ως η βέλτιστη διάταξη, καθώς οδηγεί σε αξιοσημείωτη μείωση των κραδασμών.

- Συγκρίθηκε η αποτελεσματικότητα διαφόρων τύπων γεωαφρού EPS και προέκυψε ότι το πιο δύσκαμπτο EPS46 είναι το βέλτιστο υλικό πλήρωσης.

- Η ταυτόχρονη εφαρμογή της προτεινόμενης προσέγγισης και μίας τάφρου EPS μειώνει περαιτέρω το επίπεδο κραδασμών.

- Όταν η κλίση της πλαγιάς είναι σταθερή και το υλικό πλήρωσης του επιχώματος είναι το ίδιο με το υπέδαφος, το ύψος του επιχώματος έχει μικρή επιρροή στη διάδοση των δονήσεων, ενώ η προτεινόμενη διάταξη παραμένει αποτελεσματική σε όλα τα εξεταζόμενα ύψη επιχώματος.

- Το επίπεδο κραδασμών μειώνεται όταν η κλίση είναι πιο απότομη. Η χρήση τεμαχών EPS μειώνει το επίπεδο των κραδασμών αποτελεσματικά για όλες τις κλίσεις μεταξύ 20° και 45°.

- Το πιο συχνά χρησιμοποιούμενο μέτρο περιορισμού των κραδασμών, η τάφρος EPS, δεν είναι τόσο αποτελεσματική σε θέσεις επιχωμάτων, καθώς λόγω τις γεωμετρία της θέσης δεν μπορεί να τοποθετηθεί κοντά στην τροχιά. Αντίθετα, σε θέσεις ορυγμάτων, όπου είναι δυνατή η τοποθέτηση της δίπλα στην τροχιά, η τάφρος αποτελεί μια αξιόπιστη εναλλακτική διάταξη.

- Η αντικατάσταση της επιφανειακής στρώσης του ορύγματος με γεωαφρό EPS περιορίζει ικανοποιητικά το επίπεδο των κραδασμών. Επιπλέον, μια παχύτερη στρώση EPS οδηγεί σε μεγαλύτερη μείωση των κραδασμών.

- Το επίπεδο των κραδασμών είναι χαμηλό σε θέσεις όπου η HSR εδράζεται σε σκληρά εδάφη και αυξάνεται σημαντικά σε θέσεις με χαλαρά εδάφη. Οι προτεινόμενες διατάξεις σε θέσεις επιχωμάτων και ορυγμάτων είναι αποτελεσματικές ανεξάρτητα από τις συνθήκες υπεδάφους, ιδιαίτερα για χαλαρά εδάφη.

Επιπροσθέτως, ο γεωαφρός EPS χρησιμοποιήθηκε για την προστασία υπόγειων αγωγών και γειτονικών κτιρίων από τους παραγόμενους κραδασμούς. Από αυτήν τη διερεύνηση προέκυψαν τα ακόλουθα συμπεράσματα:

- Για την ακριβή προσομοίωση της απόκρισης υπόγειων αγωγών, τα αριθμητικά αποτελέσματα συγκρίθηκαν με πειραματικές μετρήσεις ισοδύναμων φορτίων κίνησης, εξαιτίας έλλειψης δεδομένων πεδίου αναφορικά με την απόκριση υπόγειων αγωγών στις δονήσεις που προκαλούνται από HST.

- Η χρήση οριζόντιας τάφρου EPS μεταξύ της τροχιάς και του αγωγού οδηγεί στη μείωση των παραμορφώσεων του αγωγού κατά τη διέλευση του HST.

- Η διέλευση του HST προκαλεί μεγαλύτερη παραμένουσα παραμόρφωση σε πλαστικούς αγωγούς σε σύγκριση με μεταλλικούς.

- Αγωγοί με μεγαλύτερο πάχος τοιχωμάτων είναι πιο ανθεκτικοί στις μεταβολές της διαμέτρου τους από τη διέλευση HST.

- Η εφαρμογή οριζόντιας τάφρου EPS σε έναν παχύ και δύσκαμπτο αγωγό δεν είναι απαραίτητη λόγω της αρχικής ελάχιστης παραμόρφωσης του αγωγού.

- Το επίπεδο κραδασμών από τη διέλευση HST αυξάνεται στην κορυφή όλων των εξεταζόμενων γειτονικών κτιρίων σε σύγκριση με το έδαφος, ενώ τα μεγαλύτερα επίπεδα κραδασμών παρουσιάζονται στους προβόλους των κτιρίων.

- Το επίπεδο των κραδασμών στους ορόφους κτιρίων οπλισμένου σκυροδέματος περιορίζεται σημαντικά με την τοποθέτηση μιας τάφρου EPS παράλληλα στην τροχιά. Η χρήση δυο παράλληλων τάφρων μειώνει ακόμα περισσότερο το επίπεδο των κραδασμών στους ορόφους των κτιρίων.

- Στην περίπτωση κτιρίων φέρουσας τοιχοποιίας, η πιο αποτελεσματική διάταξη είναι η ταυτόχρονη εφαρμογή τάφρου EPS παράλληλα με την τροχιά και περιβλήματος EPS περιμετρικά της θεμελίωσης του κτιρίου.

Α.8.2. *Συμβολή στην πρόοδο της επιστήμης της μηχανικής*

Η παρούσα διατριβή και οι δημοσιεύσεις που προέκυψαν στο πλαίσιο της, αποτελούν ένα πρώτο ολοκληρωμένο εγχείρημα για τη διερεύνηση του περίπλοκου φαινομένου των παραγόμενων κραδασμών από την διέλευση τρένων υψηλής ταχύτητας από ερευνητές στην Ελλάδα. Οι γνώσεις και τα αποτελέσματα που συγκεντρώθηκαν τα τελευταία τέσσερα χρόνια είναι μια εξαιρετική βάση για μελλοντικούς ερευνητές στον τομέα. Η κύρια συμβολή στην επιστήμη της μηχανικής, που προκύπτουν από την παρούσα διδακτορική διατριβή συνοψίζεται ως ακολούθως:

- Δημιουργήθηκαν πλήρως επαληθευμένα υπολογιστικά προσομοιώματα, ικανά να προβλέψουν με ακρίβεια τις δονήσεις που προκαλούνται από HST.

- Προτάθηκε ένα συχνά χρησιμοποιούμενο υλικό σε πολλές γεωτεχνικές εφαρμογές, όπως ο γεωαφρός EPS, για πρώτη φορά ως εναλλακτική επιλογή για τη μείωση των αναπτυσσόμενων δονήσεων εξαιτίας των HST. Οι προτεινόμενες διατάξεις περιορισμού των κραδασμών σε επιχώματα και ορύγματα παρουσιάζονται για πρώτη φορά στο πλαίσιο της παρούσας διατριβής.

- Έγινε μια πρώτη προσπάθεια προκειμένου να διερευνηθεί η απόκριση των υπόγειων αγωγών στις δονήσεις που προκαλούνται από τη διέλευση HST. Στη διεθνή βιβλιογραφία δεν υπάρχουν σχετικές διερευνήσεις της απόκρισης αγωγών

κατά τη διέλευση HST, για τον λόγο αυτό, η παρούσα διερεύνηση αποτελεί τη βάση ενός νέου ερευνητικού πεδίου με πολλές προεκτάσεις.

▪ Μελετήθηκε η επιρροή των κραδασμών στη λειτουργία γειτονικών κτιρίων και προτάθηκαν μέτρα περιορισμού των κραδασμών με στόχο τη μείωση της επιτρεπόμενης απόστασης κατασκευής τους από την τροχιά.

Α.8.3. Συμβολή στην πρόοδο της μηχανικής πρακτικής

Τις τελευταίες δεκαετίες, έχουν αυξηθεί ραγδαία οι κατασκευές νέων HSR παγκοσμίως. Επιπλέον, όλο και περισσότερες συμβατικές σιδηροδρομικές γραμμές αναβαθμίζονται προκειμένου να εξυπηρετούν HST. Για παράδειγμα στην Κίνα έως το τέλος του 2020, λειτουργούσαν περίπου 38,000χλμ., ενώ μέσα στα επόμενα 15 χρόνια αναμένεται να ξεπεράσουν τα 70,000χλμ. Στην κεντρική Ευρώπη, οι HSR εξυπηρετούν έως και το 40% των δρομολογίων μεσαίων αποστάσεων. Επιπλέον, σε πολλές δημοφιλείς διαδρομές όπως το Λονδίνο-Παρίσι ή το Παρίσι-Βρυξέλλες, το ποσοστό αυτό είναι ακόμη υψηλότερο. Στην Ανατολική Ευρώπη και στην Ελλάδα, η ανάπτυξη γραμμών HSR είναι ακόμη περιορισμένη. Ωστόσο, αναμένεται ραγδαία ανάπτυξη των γραμμών HSR τα επόμενα χρόνια λόγω των οικονομικών και κοινωνικών οφελών τους, ιδίως στον τουρισμό.

Είναι προφανές ότι οι κατασκευαστές HSR αναζητούν διατάξεις ικανές να μειώσουν τις προκαλούμενες δονήσεις με χαμηλό κόστος εφαρμογής. Οι προτεινόμενες διατάξεις θα μπορούσαν να μειώσουν σημαντικά το επίπεδο των κραδασμών σε χαλαρά εδάφη, όπου οι προκαλούμενες δονήσεις είναι υψηλές. Σε αυτές τις θέσεις, η κατασκευή HST θα ήταν αδύνατη χωρίς την εφαρμογή κάποιας διάταξης περιορισμού των κραδασμών. Επιπλέον, προκειμένου να αναβαθμιστεί μια υπάρχουσα γραμμή για την εξυπηρέτηση του HST, θα πρέπει πρώτα να προστατευθούν τα υπάρχοντα κτίρια και οι υποδομές περιμετρικά της τροχιάς. Οι προτεινόμενες προσεγγίσεις για την προστασία αγωγών και κτιρίων διευκολύνουν την αναβάθμιση των σιδηροδρόμων. Αξίζει να σημειωθεί ότι όλες οι προτεινόμενες διατάξεις είναι εύκολες στην εφαρμογή, σχετικά οικονομικές και ο γεωαφρός EPS είναι ένα υλικό ευρείας χρήσης και εφαρμογής σε όλες τις κατασκευές στις ανεπτυγμένες χώρες -και όχι μόνο- παγκοσμίως.

Α.8.4. Προτάσεις για περαιτέρω έρευνα

Είναι προφανές ότι οποιαδήποτε έρευνα είναι αδύνατο να καλύψει πλήρως ένα πολυπαραμετρικό και σύνθετο ερευνητικό πεδίο, όπως οι κραδασμοί που προκαλούνται από HST. Μια διδακτορική διατριβή μπορεί να συμβάλει στην κατανόηση ορισμένων

επιστημονικών ζητημάτων, αλλά ταυτόχρονα να αποτελέσει και τη βάση για την περαιτέρω ανάπτυξη της έρευνας στον επιστημονικό τομέα που πραγματεύται. Με βάση τα προαναφερθέντα ευρήματα της παρούσας διατριβής, θα μπορούσαν να προκύψουν οι ακόλουθες μελλοντικές επεκτάσεις:

▪ Δεδομένου ότι είναι η πρώτη φορά που χρησιμοποιείται γεωαφρός EPS με τις προτεινόμενες διατάξεις, πρέπει να διεξαχθεί περαιτέρω διερεύνηση για την αποτελεσματικότητα των προτεινόμενων διατάξεων μέσω μετρήσεων πεδίου ή εργαστηριακών δοκιμών.

▪ Στην παρούσα μελέτη, διερευνώνται μόνο τρένα υψηλής ταχύτητας. Ωστόσο, θα μπορούσαν να διερευνηθούν αρκετοί άλλοι τύποι αμαξοστοιχιών, όπως φορτηγά τρένα, συμβατικά τρένα κανονικής ταχύτητας ή τραμ. Επιπλέον, υπάρχουν γραμμές HSR που εξυπηρετούν περισσότερους από έναν τύπους HST. Ως εκ τούτου, προτείνεται η διερεύνηση της αποτελεσματικότητας των προτεινόμενων διατάξεων για διαφορετικούς τύπους αμαξοστοιχιών.

▪ Τα τελευταία χρόνια, η χρήση συνεχούς ράγας και το υψηλό επίπεδο συντήρησης των σιδηροδρομικών γραμμών υψηλής ταχύτητας, περιορίζει αρκετές πηγές κραδασμών, όπως είναι οι ασυνέχειες στις ράγες και στους τροχούς του HST.Για τον λόγο αυτό, οι παράμετροι αυτοί δεν λήφθηκαν υπόψη στην παρούσα διατριβή. Ωστόσο, θα μπορούσε να διερευνηθεί η επίδραση των παραμέτρων αυτών στην αποτελεσματικότητα των προτεινόμενων διατάξεων.

▪ Εκτός από τον γεωαφρό EPS, πραγματοποιήθηκε μια πρώτη προσπάθεια προκειμένου να διερευνηθεί η αποτελεσματικότητα μιας τάφρου νερού στον περιορισμό των αναπτυσσόμενων δονήσεων. Μια πιο λεπτομερής διερεύνηση αυτής της προσέγγισης θα μπορούσε να διεξαχθεί ως επέκταση της παρούσας μελέτης.

▪ Στην παρούσα διερεύνηση, η στρώση EPS θεωρήθηκε ότι είναι μονολιθική και πακτωμένη στο υπέδαφος. Η εν λόγω υπόθεση θεωρείται ρεαλιστική, αφού στην πράξη χρησιμοποιούνται σύνδεσμοι για τη σύνδεση των τεμαχών EPS. Ωστόσο, στο μέλλον θα μπορούσε να πραγματοποιηθεί λεπτομερέστερη διερεύνηση για την πιο ακριβή προσομοίωση της διεπαφής εδάφους / EPS και την εξέταση του ρόλου των πιθανών κινηματικών μηχανισμών μεταξύ των τεμαχών EPS.

Εκτενής Περίληψη

TABLE OF CONTENTS

LIST OF FIGURES

Chapter 3

Chapter 4

Chapter 5

Chapter 6

Chapter 7

LIST OF TABLES

NOTATIONS LIST

EU:	European Union
f_{cl}:	Logarithmic Center Frequency of the Octave Band
FDM:	Finite Difference Method
TEN-T:	Trans-European Transport Network
URM:	Unreinforced Masonry
[C]:	Damping Matrix
[K]:	Structural Stiffness Matrix
[M]:	Structural Mass Matrix
2.5D:	Two-And-A-Half-Dimensional
2D:	Two-Dimensional
3D:	Three-Dimensional
ASTM:	American Society for Testing and Materials
a_w:	Weighted Acceleration
BE:	Boundary Element
BEM:	Boundary Element Method
c:	Waves Velocity
CLM:	Coupled lumped Mass
c_p:	P Waves Velocity
c_r:	Surface Waves Velocity
cs:	S Waves Velocity
DD:	Doctoral Dissertation
DFM:	Dominant Frequency Method
DIN:	Deutsches Institut Fur Normung
E:	Young's Modulus
EPS:	Expanded Polystyrene
E_r:	Euler Beam Elastic Modulus
f_a:	Fundamental Axle Passage Frequency
$f_{b,n}$:	Fundamental Bogie Passage Frequency
f_{ca}:	Arithmetic Mean Frequency
FD:	Finite Difference
FE:	Finite Element
FEM:	Finite Element Method
f_s:	Sleeper Passing Frequency
F_{V0}:	Static Wheel Force
FV_{db}:	Contribution Due to Braking

FV$_{dh}$:	Dynamic Contribution Due to Wheel
FV$_{ds}$:	Dynamic Contribution Due to Rail Roughness
FV$_{j}$:	Contribution Due to Asymmetries
FV$_{k}$:	Quasi-Static Contribution in Curves
HSR:	High-Speed Railway
HST:	High-Speed Trains
IL:	Insertion Loss
I$_{r}$:	Euler Beam Second Moment of Area
ISO:	International Organization for Standardization
KB (t):	Weighted Velocity Signal
K$_{f}$:	Stiffness of The Winkler Foundation
NPRA:	Norwegian Public Roads Administration
P:	Axle Force
PPV:	Peak Partial Velocity
R:	Reflection Coefficient
RC:	Reinforced Concrete
SSI:	Soil-Structure Interaction
USDT:	US Department of Transportation
v$_{0}$:	HST Passing Velocity
v$_{dB}$:	Velocity Decibel Level
VED:	Viscoelastic Damper
V$_{LdB}$:	Equivalent Velocity Decibel Level
v$_{rms}$:	Root Mean Square of The Measured Velocity Time Hibase
v$_{x}$(t), v$_{y}$(t), v$_{z}$(t):	The Longitudinal, The Transversal and The Vertical Velocity Time Histories
w(x,t):	Track Deflection at Position X and Time T
WHO:	World Health Organization
WIB:	Wave Impeding Block
XPS:	Extruded Polystyrene
α:	Mass Proportional Rayleigh Damping Coefficient
β:	Stiffness Proportional Rayleigh Damping Coefficient.
H$_{KB}$(f):	Original Velocity Signal
λ:	Wavelength
λ:	Bulk Modulus
μ:	Shear Modulus
ν:	Poisson's Ratio
ξ:	Damping Coefficient
ξ$_{i}$:	Hysteretic Material Damping Ratio of the First Frequency
ξ$_{j}$:	Hysteretic Material Damping Ratios of the Second Frequency
ρ:	Soil Density
ω$_{i}$:	First Frequency Limit

ω_j: Second Frequency Limit

INTRODUCTION

1.1. Subject of the Doctoral Dissertation

In recent decades, High-Speed Railways (HSR) have constantly been growing, as High-Speed Trains (HST) are widely used in many countries worldwide. For instance, in China, the total length of high-speed railway lines reaches up to 38,000 km by the end of 2020. As one of the most modern means of transportation, the HST is a high-quality transportation choice as it is less expensive than airplanes, more convenient than the highways and primarily significantly fast. The peak operational speed of HST is constantly increasing and nowadays reaches 600 km/h, while it is expected to increase even further in the coming decades. Because of these advantages, many new HSR lines are going to be constructed worldwide, making the 21st century the HST era. In Greece -despite the great economic-technical difficulties due to the non-smooth landscape- a serious effort is made to upgrade the railway network and to harmonize as much as possible with the modern data.

Increasing number of HSR projects are being developed in Europe. The European Union (EU) aims to develop an HSR network that will serve the least developed regions and connect them to major European financial centers. The Maastricht Treaty established the Trans-European Transport Network (TEN-T) program by Decision 1692/96/E.C. in 1996, in which the development of high-speed trains has a prominent place, in order to ensure optimal transport infrastructure between EU countries. It is worth mentioning that the number of passengers in the new EU HSR constantly increases. Today, HST account

for about 40% of the continent medium-distance traffic. Even higher rates have been observed on some routes, such as London-Paris, Paris-Brussels and Madrid-Seville. For trips that take less than three hours, HST are now very competitive, as the waiting time is much shorter than air travel, while the travel time is shorter than traveling by car.

Figure 1.1 L0-Series Maglev: the fastest train in the world.

In Greece and the wider Balkan region, the development of HSR networks is still discussed at a theoretical level. Nevertheless, due to the common policy of the EU, in combination with the economic and social benefits mentioned above, it is a given that in the coming years, HSR networks will be developed both in Greece and in the wider region. At this time, the benefits would be significant for the tourism and the trade sectors. Connecting Athens with other Balkan capitals with a cheaper and faster means of transportation would boost the economy. The benefits to domestic travel would also be significant, as the increased safety combined with high speeds would lead many people to use HST over road transport, reducing emissions and fatal road accidents.

However, as it happens in the early years of all innovative ideas, several issues related to the HST should be addressed to ensure safe operation, the durability of the HST and tracks, and the environmental and human impacts of their operations. For this purpose, numerous researchers focus on vibrations, especially the ground vibrations caused by HST passage. The developing vibrations, except from the discomfort of the passengers, cause disturbance to the locals and possibly damage the neighboring buildings and the railways infrastructure. HST operating speed is directly related to the functionality and safety of modern high-speed railway lines. Functionality is related to: (a) railway

vibrations that can cause significant impact-disturbance to the neighbors and (b) in extreme cases, damage to adjacent structures due to the imposed vibrations. Safety is related to the integrity of railway embankments or ditches and other railway infrastructure. In particular, the induced vibrations could: (a) affect their stability or (b) cause differential subsidence in the embankment body or the underlying soil layers. These problems can be addressed with appropriate conventional or new techniques.

Figure 1.2 Operational high-speed lines in Europe.

Numerous numerical approaches have been proposed to investigate the complex phenomenon of the developing vibrations by the passage of HST. Initially, two-dimensional (2D) finite element simulations were proposed. Then, a more efficient numerical simulation (2.5D) methodology was developed, based on the assumption that if the cross-section of the rail and ground is constant in length, then the load from train movement can be described using Fourier transform. Both 2D and 2.5D simulations, despite their relatively low computational cost, now have a limited range of applications due to the many limitations and simulation simplifications. Therefore, more and more three-dimensional (3D) simulations have been proposed to increase simulation possibilities and the accuracy of the results. 3D simulations are now considered necessary

to calculate the vibrations caused by the passage of HST. However, increasing the accuracy of 3D simulations also means increasing computing costs.

Due to the potential negative effects of vibrations caused by the passage of high-speed trains, key scientific questions arise related to the treatment of the phenomenon. The scientific community has proposed various models for predicting and estimating vibrations increases before constructing new lines or upgrading existing ones to answer these questions. Also, measures to reduce dynamic vibrations have been researched and used in practice. The most effective way to mitigate ground vibrations is to reduce train speeds in locations where Rayleigh wave velocities on the ground are very low. If this is not possible (e.g., for financial reasons), certain protection measures could be applied, such as reinforcing railway embankments or constructing protective barriers between railways and adjacent structures.

1.2.   *Objectives of the Doctoral Dissertation*

In this context, the present Doctoral Dissertation (DD) aims to investigate alternative mitigation approaches to reduce the induced vibrations by using lightweight materials, such as Expanded Polystyrene (EPS) "barrier". EPS geofoam is an industrially produced material with great mechanical properties and high reliability in its behavior. The use of EPS in geotechnical applications began in the early 1970s, when it was realized that, with proper use of its lightweight and mechanical behavior, it offers technically reliable and cost-effective solutions in cases where construction time is critical or alternatives approaches require significant natural soil preparation/improvement projects. The total volume of EPS that has been integrated worldwide in geotechnical constructions and related technical projects over the last thirty years is estimated to be many tens of millions of cubic meters. The majority of applications concern the construction of road construction embankments on compacted soils, reducing the load on structures and pipelines, and improving slope stability. In recent years, many applications are concerned with the operation of EPS as a compact casing to reduce horizontal ground thrusts in structures. Finally, the possibility of protecting buildings and retaining walls from dynamic stresses is investigated with very positive indications using EPS. EPS is an industrial material, which could be an advantageous and effective solution for dealing with subsoil vibrations during the passage of high-speed trains due to its characteristics and low cost.

As it was aforementioned, there are several numerical approaches capable of predicting the HST-induced vibrations accurately. One main objective of the present Ph.D. Thesis is to find the balance between results accuracy and computational of the proposed 3D prediction models. The results are primarily compared with field measurements and experimental results of laboratory tests to ensure the accuracy of the proposed models. Furthermore, the investigation tries to formulate a new, more effective and economical proposal for mitigation measures to reduce the induced vibrations. In particular, it is investigated whether the application of EPS could be a techno-cost-effective solution in this direction. The main objectives of the current Ph.D. Thesis could be listed as follows:

- Proposal of an optimal prediction model in terms of accuracy and low computational cost.
- Validation of the examined models with reliable in-situ measurements and experimental results.
- Proposal of an ideal EPS geofoam configuration to reduce the developing vibrations on railway cuttings and embankments.
- Investigation of the optimal parameters such as the mechanical properties and the geometrical properties of the proposed mitigation schemes.
- Examination of the effect of parameters, such as the subsoil condition or the train speed, on the efficiency of the proposed mitigation measures.
- Investigation of the buried pipelines protection, passing below the HSR line with the implementation of an EPS layer between the track and the pipe.
- The study of the effects of the induced vibrations on human health and structural response as well as the reduction of the decibel level at nearby buildings by using EPS-filled trenches.

1.3. *Outline of the Doctoral Dissertation*

The present Ph.D. Thesis could be divided into four main parts: (a) a literature review of previous work relevant to this research, (b) the development and validation of a three-dimensional model to simulate HST induced vibrations, (c) the mitigation of HST vibrations with the use of EPS, (d) the protection of infrastructure and building with the use of EPS.

Chapter 2 contains a literature review of previous work relating to ground-borne vibrations induced by the passage of HST. Topics of interest include the impact of

vibrations on humans, vibrations excitation mechanisms associated with rail track, and analytic and numerical methods for simulating ground problems. Furthermore, the existed mitigation and maintenance approaches of the HST-induced vibrations are reviewed. Lastly, a brief presentation of EPS geofoam existing applications on several geotechnical applications and their advantages against other commonly used material is presented.

Chapter 3 presents the validations of the proposed numerical approach. An efficient three-dimensional numerical model has been developed in conjunction with a user-developed subroutine for applying the moving loads to calculate the dynamic response of the coupled soil model accurately. The numerical results have been compared to pre-available in-situ measurements in terms of vertical velocity time histories, Fourier Spectra and PPV charts at several distances from the track. As case studies, three Paris-Brussel High-Speed Railway line sites have been examined under the passage of Thalys and TGV high-speed trains. The three examined sites concern the passage of the HST from a railway embankment, a railway cutting and a horizontal site, i.e., at grade.

Chapter 4 investigates several countermeasures configurations to minimize the induced vibrations on railway embankments by using an alternative low-density material as an embankment fill to minimize HST vibrations. For this purpose, the application of expanded polystyrene (EPS) blocks is investigated. A new optimal mitigation configuration is presented in order to minimize the developed vibrations due to HST passage. This simple, economical and fast intervention approach can protect the railway embankments and soil layers from HST-induced vibrations. Aiming to examine its efficiency, a typical railway embankment has been "reinforced" with EPS blocks and the impact of this mitigation measure on the dynamic response of the system has been investigated numerically. The soil response (in terms of ground velocity) is investigated at various distances from the track with and without the proposed mitigation measure (via properly positioned EPS blocks) and a detailed parametric study is performed. In the sequence, the mitigation approach is implemented for different subsoil and railway embankment material conditions.

Four typical soil types - categorized as rock, dense sand with gravels, stiff and soft clay are investigated. In addition, the mechanical properties of the embankment material have been altered to assess to what extent they can affect the HST vibrations. One more crucial parameter, which influences the effectiveness of the proposed mitigation approach, is the

geometrical properties of the embankment. Therefore, to ensure an optimal design, a robust procedure that considers the impact of these factors is necessary. Hence, the implementation of EPS blocks on several embankments with different geometry, in terms of height and slope angle, has been investigated. More specifically, several embankment heights between 3.5m and 5.5m and slope angle between 20° and 45°, have been investigated.

Chapter 5 investigates the mitigation of the developing vibration from the passage of HST from cutting sites. Several mitigation configurations with the use of EPS geofoam have been investigated in order to propose a new optimal mitigation scheme. More specifically, in the case of the railway cutting, the application of expanded polystyrene (EPS) blocks at the cutting slopes has been proposed to reduce the levels of vibrations. The efficiency of this measure has been investigated via advanced three-dimensional numerical simulations. The retrofitted models have been compared with a typical cutting without mitigation measures in the Paris-Brussels line in Belgium. Several thicknesses of the EPS layer have been examined and the optimal configuration in terms of economy and efficacy has been presented. Furthermore, the effect of the soil conditions on the efficacy of the proposed mitigation approach has been investigated. For this purpose, several subsoils conditions have been applied to the cutting site. The presented results illustrate that EPS consists of an efficient solution for mitigating HST-ground vibrations in HSR cuttings.

Chapter 6 examines the level of traffic-induced vibrations on the surface of buried pipelines crossing the railway line vertically. Firstly, the 3D numerical model has been validated with pre-available experimental data in order to predict traffic loads accurately. In the sequence, the model has been modified in order to represent the HST moving loads, aiming to investigate the pipe response to the HST-induced vibrations. Subsequently, mitigation approaches are suggested to minimize the developing vibrations. EPS geofoam blocks have been implemented between the HSR line and the buried pipeline in order to mitigate the induced vibrations. This approach assumes that the HST-induced vibrations are reflected on the EPS blocks, preventing them from reaching the pipeline surface. Finally, useful conclusions are drawn about the mechanical properties and the geometry of the EPS layer.

Chapter 7 presents a numerical investigation of the building response due to HST-induced vibrations passage. The effect of the HST-induced vibrations on the neighboring

buildings close to the railway is a vital environmental issue related to the residents comfort. The effect of the distance of the track on the propagation and transition of the vibrations is examined in the case of typical RC buildings. Furthermore, the efficacy of the implementation of a single EPS–filled and a double trench is compared to examine its impact on the dynamic response of the structural system. The vibrations on a 4-story and an 8-story RC building in terms of dB are investigated. Furthermore, the insertion loss of the proposed mitigation scheme is presented. In the case of the masonry buildings, the effect of the induced vibrations, on two typical infrastructure buildings located in the vicinity of the track area, is presented. Several EPS configurations using EPS geofoam at the track and the building foundation have been examined to propose the optimal approach.

In the sequence, except from the mitigation of HST-induced vibrations, the EPS geofoam is implemented on traditional masonry buildings in order to investigate its effect on the seismic response by taking into account the impact of dynamic soil-structure interaction (SSI). More specifically, the dynamic response of a typical unreinforced masonry (URM) building constructed over a silty sand layer is examined. The main novelty of the investigation is that it considers time-varying soil mechanical properties, i.e., depending on the soil saturation level, which usually varies with time. In addition, a new structural assessment approach, which aims to accurately assess the performance levels (Limit States) of historic buildings and monuments after performing certain seismic rehabilitation measures, has been applied.

The conclusions of the present Ph.D. Thesis are summarized in Chapter 8. This chapter includes a brief presentation of the findings of this research and recommendations for mitigating the HST-induced vibrations. Furthermore, some useful remarks and ideas for further investigation are proposed. Lastly, the journal publications and the participation at international conferences are listed. The structure of the Ph.D. Thesis is presented in the flowchart of Figure 1.3.
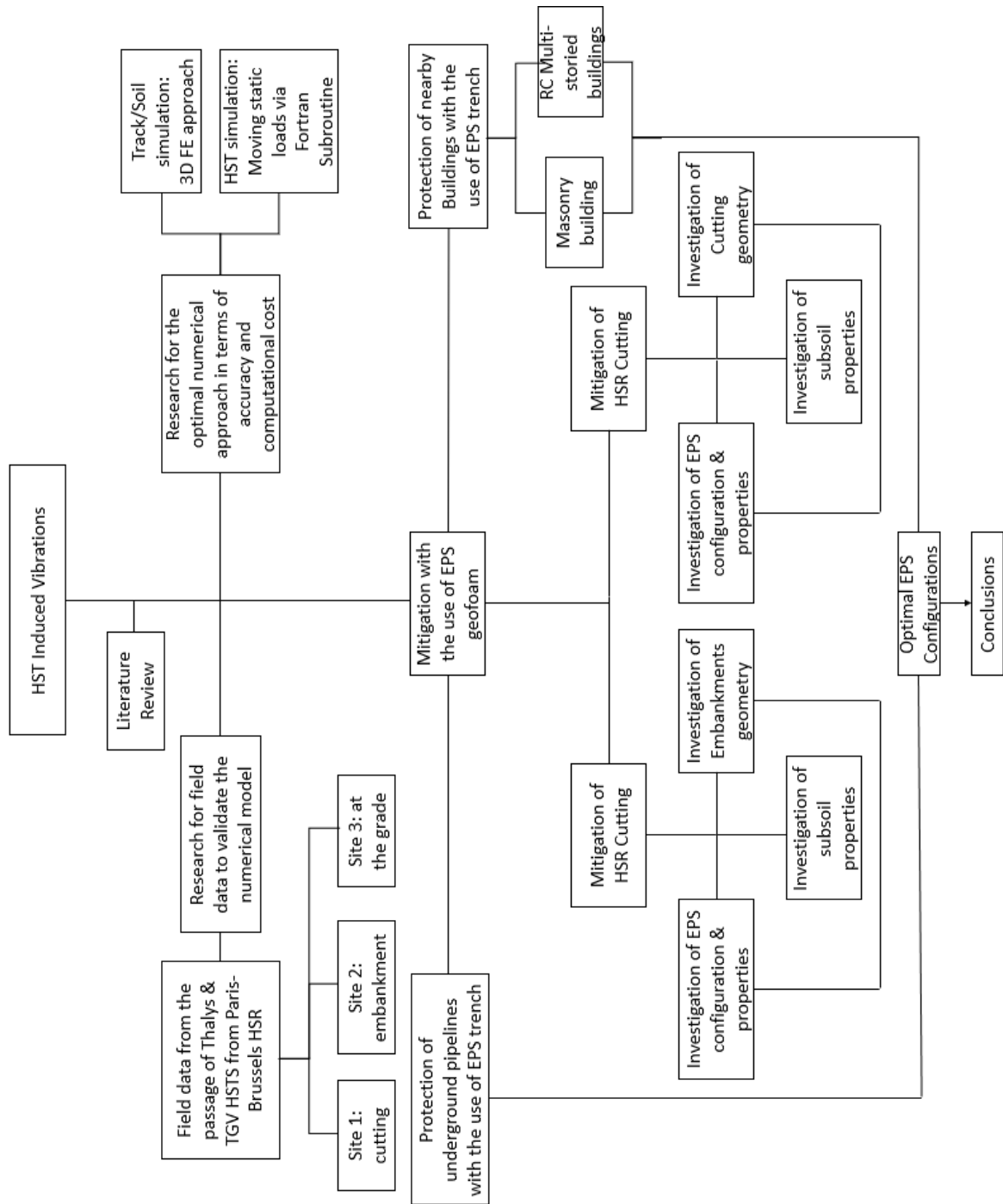
Figure 1.3 Flowchart of Ph.D. Thesis structure.

LITERATURE REVIEW

2.1. Introduction

In this chapter, a brief review of the previously published relevant literature review of the complex phenomenon of the induced vibrations due to the high-speed trains passage is presented. Initially, the generation and the propagation of the vibrations are discussed and a brief overview on waves propagation theoretical aspects is given. The vibrations impact on humans and buildings is reviewed, and the most common indicator for their estimation is presented. Furthermore, a state-of-the-art review of the track maintenance procedure and the available mitigation approaches against the developing vibrations have been carried out. Finally, analytical and numerical approaches, which have been used to describe the problem, have been briefly reviewed.

2.2. Ground-borne vibrations due to HST passage

2.2.1. Vibration source - Vibration excitation mechanisms

It is vital to investigate the excitation mechanism of train-induced vibrations generation. Generally, the interaction of the moving train with the rails is the main reason for the vibrations. The weight, the geometry of the train, and the suspension systems strongly affect the induced vibrations. The car body is connected to the bogie via the secondary suspension, which usually consists of an airbag in the case of modern passenger trains. In the sequence, the wheels propagate the loads to the track. The ground-borne vibrations developed by the train passage are dependent on factors as wheel and rail roughness, the discrete track supports, the dynamic characteristics of the rolling stock, the rail support

stiffness, the railway structure design and soil characteristics (Nelson and Saurenman, 1983). Remington (1976, 1988), Rudd (1976) and Ver et al. (1976) made the first attempt to group the mechanism of the developing vibrations by trains passage and identified three different vibrations excitation mechanisms (e.g., the quasi-static loading, parametric loading, and general wheel/rail roughness). The generated vertical force on the rail could be calculated as follows (Bahrekazemi, 2004):

$$FV = FV_0 + FV_k + FV_{ds} + FV_{dh} + FV_{db} + FV_j \tag{2.1}$$

where:

FV_0: Static wheel force,

FV_k: Quasi-static contribution in curves,

FV_{ds}: Dynamic contribution due to rail roughness,

FV_{dh}: Dynamic contribution due to wheel flat,

FV_{db}: Contribution due to braking,

FV_j: Contribution due to asymmetries.

As earlier mentioned, an HST passage from a railway line generates forces at the contact surface among the rail and the wheels of the HST. The acting forces are commonly separated into two categories, the quasi-static and the dynamic part of the force (Lombaert et al., 2003). The quasi-static loads of the passing train axles along the rail are responsible for the low-frequency vibrations (e.g., 0, 20Hz). Figure 2.1 depicts the quasi-static load of the train moving along the track. More specifically, the loads from the bogies weight at the interface between the rail and the wheel generate deflections, producing harmonic excitation as the train moves past an observation point. The quasi-static part of the force depends on the HST weight, although it is not altered by the HST passing velocity. Considering the railway track as an Euler beam laid on elastic foundations, the quasi-static loads are defined as follows (Connolly et al., 2015):

$$w(x,t) = w(x - v_o, t) \tag{2.2}$$

$$w(x,t) = [\cos(\beta|x - v_o t|) + \sin(\beta|x - v_o t|)] \frac{P + m_w g}{8E_r I_r \beta^3} e^{-\beta|x - v_o t|} \tag{2.3}$$

where:

w(x,t) : track deflection at position x and time t,

E_r: Euler beam Elastic modulus,

I_r: Euler beam second moment of area,

P: axle force,

v_0: HST passing velocity,

K_f: stiffness of the Winkler foundation,

b is calculated as:

$$\beta = \sqrt[4]{\frac{K_f}{4E_r I_r}} \qquad (2.4)$$
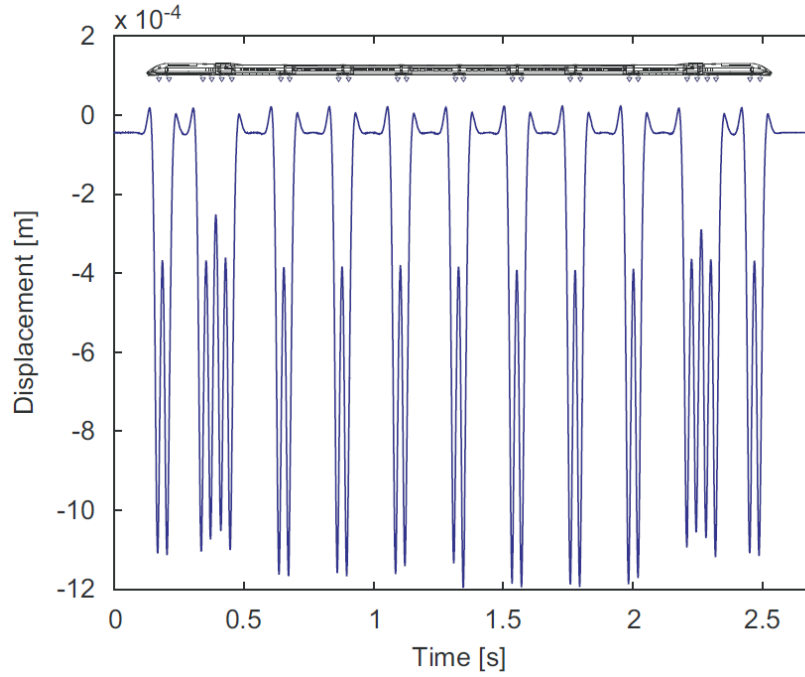
Figure 2.1 Rail deflection during the passage of the Thalys HST (adopted by (Kouroussis et al., 2011).

On the other hand, the dynamic part of the load is strongly affected by the train passing velocity as the main factors that affect the dynamic component of the force are considered the sleepers placements, the subsoil conditions and the unevenness at the interface between the wheels and the rail. Regarding the sleepers placements effect, the supported track where the rails have been based is responsible for the change of the rails effective stiffness. The rails are commonly based on equally spaced sleepers, which are supported by the ballast. Hence, it is obvious that the stiffness is higher when the wheel is passing over a sleeper and lower when it is passing from the spam between the sleepers, leading to the periodic excitation. Heckl et al. (1996) carried out a series of experimental measurements to investigate the effect of the periodic excitation mechanism and captured the resulting characteristic peaks from the sleeper spacing in the acceleration spectra.

The second main vibrations mechanism is the Parametric excitation, which is caused by the periodic altering of the rails effective stiffness. As mentioned above, several other parametric excitation mechanisms, such as problematic rail joints or wheel, are illustrated in Figure 2.2. These discontinuities, known as rail irregularities, occur high-frequency vibrations when the wheels pass over a rail joint or when the spot of the wheel flat is in contact with the rail.

(a)   (b)

Figure 2.2(a) Problematic rail joint, (b) wheel flat.
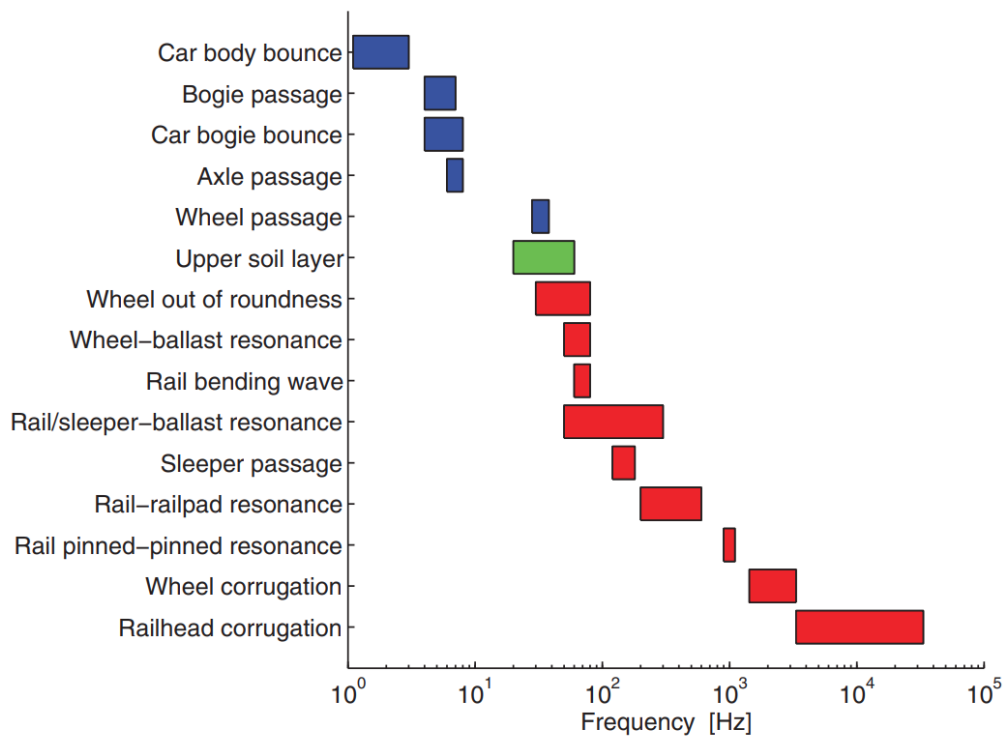
Figure 2.3 The main contribution of dynamic vehicle/track and soil interactions (adopted by Kouroussis et al. (2015)).

The quasi-static and dynamic components of the train force are strongly dependent on the train characteristics. Accordingly, the induced vibrations are widely varying. For instance, underground trains induce vibrations at a higher frequency range in comparison with regular trains. Furthermore, the dominant issue of high-frequency vibrations is the generation of noise within the tunnel and the response of infrastructure and buildings above the underground line. On the other hand, the low-speed tramways generate low-frequency vibrations, although their passage close to buildings might cause disturbance to the residents or negative structural effects. Due to their high weight and low speed, the freight trains generate low frequency and high amplitude vibration, which propagate to high distances from the railway line. The frequency range of each vibrations excitation mechanism is summarized in Figure 2.3, as presented by Kouroussis et al. (2015).

2.2.1.1. *Rail irregularities & defects*

The most commonly observed irregularities and defects can be classified in the following categories:

- **Complete switch mechanism:** Comprises of successive step-up joints and pulse joints.
- **Crossings and diamond crossings**: They are used in double junction and are often found on tram or streetcar networks where lines cross or split. They are considered approximatively as two successive negative pulse joints.
- **Foundation transition zone:** This is similar to a ramp which may occur at track–bridge or ballast–slab track transitions due to a change in track stiffness. A local foundation compaction can induce variation in height of rail.
- **Rail joint:** The force on the rail arising from a typical rail joint increases almost linearly with the product of train speed and the angle of the dip, whereas the force arising from a chordal flat increase with increasing severity of the flat, but not in proportion with the vehicle speed. The higher loads which are normally encountered by the track are those due to irregularities on the wheel tread. They could be due to manufacturing faults, the wheel sliding on the rail, tread braking or faulty turning and grinding during maintenance and repair.
- **Wheel flat:** Wheel irregularities are commonly defined into three categories: out-of-roundness of the wheel, tread damage from loss of metal and flat zones on the circumference caused by sliding. The typical wheel flat, caused by

wheelset lock-up, has a simple geometrical relationship between the depth and length. Flats have been observed in service with lengths extending significantly around the wheel and it is thought that such flats are produced by the dynamic forces modifying the shape of the original flat. Unlikely dynamic forces at dipping joints, wheel flat forces do no increase linearly with speed. Maximum force levels are produced when the wheel flat resonant frequency and the frequency of the track response coincide.
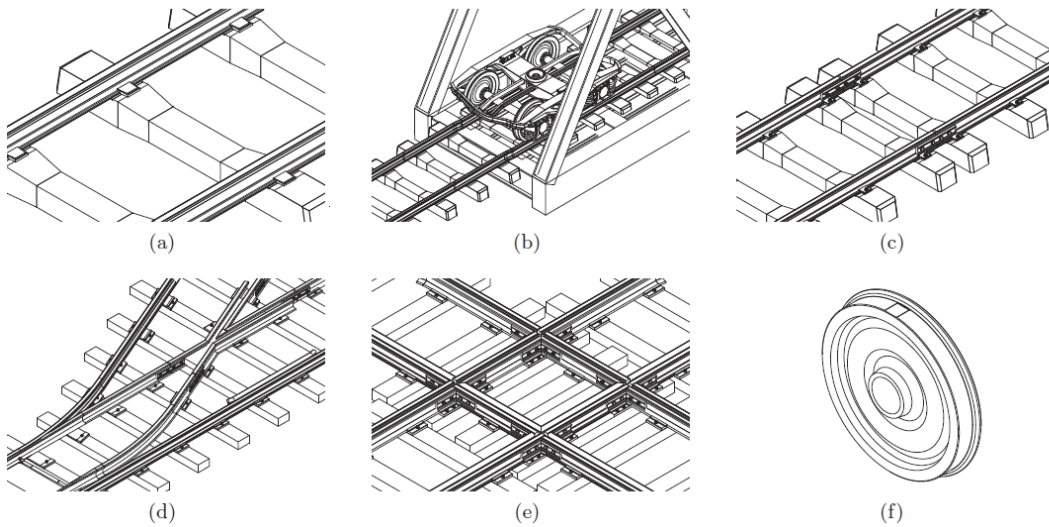
Figure 2.4 Overview of possible surface defects encountered in practice: (a) reference (no defect), (b) foundation transition, (c) fishplated rail joints, (d) turnout, (e) crossing and (f) wheel flat (adopted by Kouroussis et al. (2015)).

It should be mentioned that those types of excitation mechanisms are becoming a less and less important factor, in comparison with the other excitation sources as the level of railway lines maintenance has been improved through the years. Furthermore, the extensive use of the continuously welded rails has minimized the irregularities due to the rail joints and wheel flats.

2.2.2. *Propagation path of HST-induced vibrations*

2.2.2.1. *Wave types: Basics of the Wave Theory*

After the generation, the train-induced vibrations are propagated from the track to the soil. The vibrations could be separated into body and surface waves. The body waves are traveling under the soil surface, in contrast with the surface wave, as illustrated in Figure 2.5. The first noteworthy investigations in the field of vibrations propagation have been carried out by Rayleigh (1885) and (1904), who aimed to categorize the wave types in the

elastic half-space into three types: the dilation waves (pressure or P-wave), the equivoluminal waves (shear or S-wave), and the surface waves. The most common body waves are the compressional waves (P-waves) and the shear waves (S-waves). P-waves are the fastest waves and are travelling in longitudinal direction where the particles in the solid move in the same direction as the wavefront.
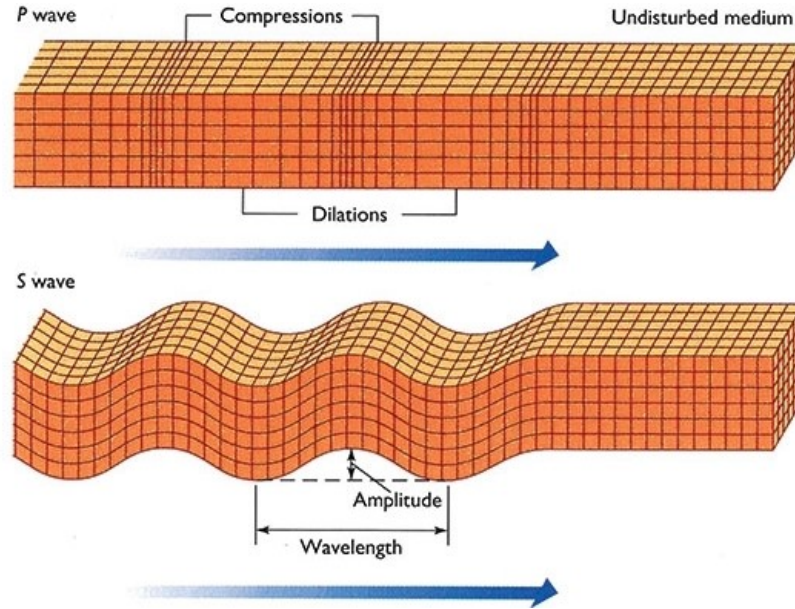
Figure 2.5 Propagation of P-waves and S-waves.

On the other hand, S-waves are slower than the P-waves and propagate in a transverse direction where the particles move perpendicular to the wavefront. The shear waves could also group into two subcategories, the horizontal plane (SH-waves) and the vertical plane (SV-waves). Furthermore, the variations of the layered soil medium lead to the generation of the P-SV wave (e.g., the coupling of the P and the SV waves); on the other hand, the SH waves remain uncoupled. Figure 2.5. demonstrates the propagation mechanism of the S-waves and the P-waves. The body waves speed is defined as follows:

$$C_P = \sqrt{\frac{\lambda + 2\mu}{\rho}} \tag{2.5}$$

$$C_S = \sqrt{\frac{\mu}{\rho}} \tag{2.6}$$

where:

    ρ: soil density,

    λ: bulk modulus,

    μ: shear modulus.
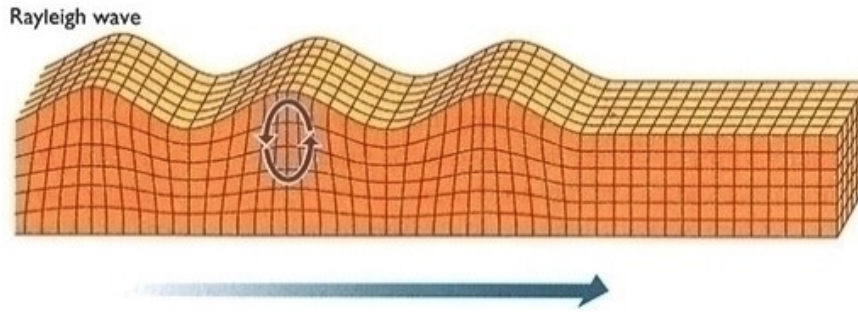
Figure 2.6 Propagation of R-waves.

The most dominant surface waves are the Rayleigh waves (R-wave). The propagation of Rayleigh waves is caused by the elliptical movement of the medium particles with in-plane longitudinal and transverse components, as illustrated in Figure 2.6. These waves propagate on the surface to a depth of approximately one wavelength. They are the slowest type of waves, and for linear elastic materials with a positive Poisson's ratio lower than 0.3, their speed is calculated by:

$$C_R = C_C \frac{0.862 + 1.14v}{1+v} \tag{2.7}$$

where:

v: Poisson's ratio.

Apart from the Compressional, Shear and Rayleigh waves, which are the most common, there are several other types of waves, such as Lamb waves, Love waves or Stoneley waves. The spread of the Love waves on the medium surface takes place in the out-of-plane direction. On the other hand, Stoneley waves are located at the interface area between different medium layers. However, those three types are the most dominant; according to Woods (1968), 67% of the total excitation energy is transmitted as Rayleigh waves. The percentage of P-waves and S-waves are equal to 7% and 26%, respectively. Therefore, Rayleigh waves are the most dominant and could affect the residents and the nearby structures.

2.2.2.2. *Damping*

The amplitude of the waves is minimized as the waves spread from the vibrations source to the surrounding medium due to radiation damping and medium damping. The induced waves widely spread at increasing distances from the source. The expansion of the wavefront causes the reduction of the waves energy; this phenomenon is the radiation damping. According to Woods (1968), who investigated the three-dimensional spread of

waves induced by a surface point load, the body waves amplitude reduces inversely as the square of the radian from the source and at depth as the converse to the radian (see Figure 2.7.). On the other hand, Rayleigh waves decay contrariwise of the square root of the radian from the waves source. Hence, it is obvious that the reduction of the waves energy is a function of geometry and is independent of the material properties of the medium. This theory also holds for propagation at depth, assuming that the radius r for body wavefronts is measured from the source, while the radius of the surface wavefront is measured from the surface vibrations epicenter.

On the other hand, material damping strongly depends on the material properties of the propagation medium and is associated with the spread of waves energy through mechanisms such as soil particles friction. The most common material damping models are the viscous and the hysteretic model. Viscous damping is the dissipation of energy that occurs when a soil particle is resisted by a constant force. Furthermore, viscous damping is independent of displacement and velocity, and its direction is opposite to the direction of the particles velocity.
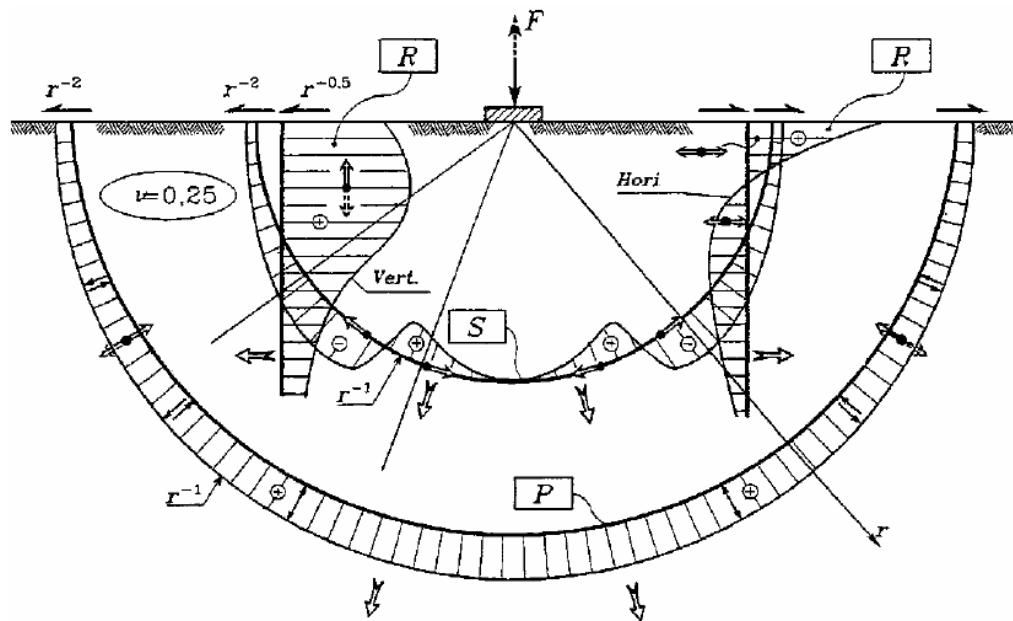
Figure 2.7 Different types of waves from a circular footing and their theoretical geometrical damping (adopted by (Woods, 1968)).

Material damping is non-linear in the frequency range. Hence, the dependence of frequency leads to complex modeling for time-domain approaches, in contrast with frequency-domain modeling. Furthermore, it is observed that at the surface layer of the soil, the damping is increased in comparison with deeper layers. The main reason of this

difference is the lower compact of the upper soil layer particle, as the waves lose higher amounts of energy when it passes through the air voids. In addition, in the case of saturated soils, increased viscous damping values are observed at the high-frequency range. Regarding the track, damping is dependent on a combination of rails, sleepers and ballast materials.

2.2.3. *HST role on the wave propagation*

As it has been thoroughly presented in the previous section, the waves propagate into the track and the surrounding soil upon their generation. However, apart from the HSR lines surrounding area, a part of the vibrations is propagated upwards to the HST bogies. This phenomenon is equally important with the propagation of the vibrations on the soil surface, as the vibrations disturb the passengers of the train. Hence, the reduction of the upwards vibrations is a vital issue to ensure the proper operation of the train. For this purpose, HST commonly use two suspension systems, the first connect the wheels and the bogies and the second joins the bogies with the car body (Kouroussis et al., 2014). This system has been first used only on high-speed trains, although they are going to be used on other train types in recent years. In the case of the high-speed trains, which commonly serve business and luxury customers, the passengers comfort is vital; hence the HST should provide a suitable environment where the passengers could read or write. For this purpose, several researchers have investigated the effect of the induced vibrations on the passengers comfort.

Pallord and Simons (1984) examined the role of the suspensions on the passengers comfort and concluded that vibrations within the low-frequency range (0.8Hz-8Hz) and especially below 5Hz, could disturb the passengers reading or writing tasks. A similar observation has been made by Griffin and Hayward (1994), who proposed a critical frequency range (1.25Hz, 6.3Hz) for the passengers reading. Furthermore, Corbridge and Griffin (1991) found that the probability of spilling liquid from a hand-held cup was also affected by the low-frequency range. Khan and Sundstrom (2007) concluded that low vibrations levels could reduce the ability to perform sedentary activities. Except for the reading and the writing, the induced vibrations might cause sickness to the passengers. Suzuki et al. (2005) carried out a poll of four thousand train passengers and vibrations measurements have been taken on each train involved. This investigation concluded that the ratio of passengers who felt motion sickness on tilting trains was higher than that on

non-tilting trains. Additionally, Low-frequency lateral vibrations between 0.25Hz and 0.32 Hz have been found to have a high influence on the degree of motion sickness.

In order to investigate the propagated vibrations to the train, the time-domain multibody approach is commonly used. Kargarnovin et al. (2005) examined the comfort of HST passengers when the train passes over bridges and concluded that the rail unevenness has a crucial role in this case. Furthermore, several researchers have examined the vibrations transmission of train seats in either vertical, lateral or fore-and-aft directions (Corbridge et al., 1989; Jalil and Griffin, 2007; Lo et al., 2013). Lee et al. (2009) presented a structural equation model for the ride comfort of the Korea Train Express in South Korea HSR.

2.2.4. Track role on the wave propagation

The railway track has a vital role in the waves propagations as it acts as the foundation of the whole railway track system. The basic HSR track commonly consists of the rails and their foundation layers. The two commonly used tracks are the ballasted and the ballastless track, as illustrated in Figure 2.8. There are several differences in the response, the composition, the construction, the maintenance and the cost of the ballasted and ballastless track.

(a) (b)

Figure 2.8 (a) Ballasted track, (b) ballastless track.

The ballasted track is the most commonly used and consists of steel rails, sleepers and ballast bed. Generally, multi-layered ballast is preferred in order to reduce the stress on the subsoil. Furthermore, the ballast bed improves the flexibility of the railway track and reduces the propagating vibrations level to the surrounding soil. On the other hand, the ballastless track is the railway track whose bed is composed of concrete. Generally, a

ballastless track consists of steel rail, fasteners and slab, on which the concrete sleepers are based. The ballastless tracks are a more advanced track than the ballasted and preferred in constructing new HSR lines worldwide. However, nowadays, the majority of the operating HSR lines are still based on ballasted tracks.

The track properties are one of the most important factors for wave propagation, as the track supports the moving HST and propagates the vibrations to the surrounding soil. A track with low stiffness occurs with high values of deformation, increasing the risk of derailment. Furthermore, HSR needs increased power in order to move. On the other hand, stiff track lead to wheel corrugation due to the concentration of stresses on a small slide area on the rail (Grossoni et al., 2018). In addition, Dahlberg (2010) investigated the track stiffness variations and concluded that when the stiffness of the track varies drastically, it leads to track corruption and an increase of the vibrations level. In general, there are no optimal values of track stiffness, as the proposed values differ according to each county standards and the type of the operating trains. Hence, it is obvious that it is hard to propose an optimal stiffness value for an HSR line, where several different types of trains are operating.

As mentioned earlier, the interaction of the train with the track is the source of the induced vibrations; therefore, it is vital to model the track components accurately. Obviously, inaccurate modeling of the track could lead to errors on the vibrations level at the surrounding soil. Several analytical and numerical approaches have been proposed through the years, aiming to represent the track accurately. Those models are commonly separated on either frequency or time domain.

2.2.5. *Surrounding soil role on the wave propagation*

One more important factor related to the propagation of the HST-induced vibrations is the surrounding soil, as it is the transmission path for vibration to reach nearby buildings and infrastructure. The most crucial amplitude related to the soil response is the HST passing velocity. More specifically, a substantial increase in the vibrations has occurred if the HST is running with a velocity higher than the surface wave speed of the surrounding soil. This passing speed is well known as critical speed. The critical speed is a factor that is becoming more and more important as the HST operational speeds increase through the years. Obviously, as the HST speed increases, approaching the 'critical velocity' at more sites of the HSR is also increased. The site with loose surface layers is more vulnerable тo high

vibrations levels due to their low Rayleigh waves velocity. The incredible rise of the vibrations level related to the critical speed except for a source of detrimental environmental effect and human disturbance also affects the HSR operation, as several issues such as degradation/deformation of track foundations, fatigue failure of rails and interruption of power supply to trains could be observed.

Numerous researches have examined the phenomenon of critical speed. For example, the Swedish Rail Administration (SRA) investigated the passage of X-2000 HST at the Ledsgard site, where the HSR track is founded on loose soil and extreme vibrations level in the HSR embankment surrounding soil have been observed. According to the investigation of Woldringh and New (1999), the passing velocity of X-2000 HST approached the critical speed of the subsoil; hence, SRA immediately reduced the passing velocity. This observation led several authors to investigate this site, aiming to assess the critical speed and associated issues (Auersch, 2008; Bian et al., 2016; Costa et al., 2015).

2.3. *Effects of vibrations*

In recent decades, the rapid growth of the HSR lines made their adverse effects related to potential structural damage in nearby buildings and the users of the buildings and the railway infrastructure even more pronounced. Hence, it is crucial to investigate the existed appropriate indicators proposed by the relevant international standards. Those indicators are relevant to the impact of the developing vibrations on the residents of buildings located in the vicinity of the HSR area. The complex transmission path from the HST/source to the receiver/building is demonstrated in the schematic diagram of Figure 2.9.
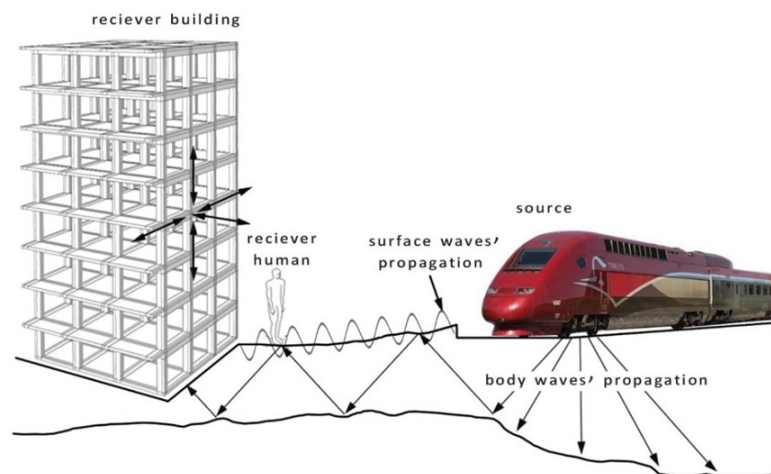
Figure 2.9 Scheme of vibrations transmission from HST passage to buildings and humans.

The two most common issues, which are assessed via proper indicators, are the human perception and the damages on nearby buildings. In the case of residents of nearby buildings, their health and comfort are in danger due to the consecutive reception of the developing vibrations. Furthermore, the vibrations could affect the dynamic behavior of the structures. In some cases, the induced vibrations could cause structural fatigue. Thus, it is crucial to ensure that the level of the receiving vibrations in structures by the passage of HST will not affect the health and the comfort of the residents. For this purpose, several international standards and guidelines have investigated this issue. For instance, the international standards (ISO (International Organization for Standardization), 1997, 2003) investigates the comfort evaluation and the Swiss standards (Schweizerische Normen-Vereinigung, 1992) is focused on building damages. In central Europe, the German standards (DIN (Deutsches Institut für Normung), 1999a, 1999b) are used and in the USA, the recommendations of the United States Department of Transportation (USDT, 1998).

2.3.1. *International Organization for Standardization standards (ISO 2631)*

The International Organization for Standardization is focused on human exposure to the induced vibrations. The standards are grouped into two parts, ISO 2631 part 1, which investigates the vibrations felt by the train passengers and s ISO 2631 part 2, which examines the effect of the induced vibrations on the nearby structure and their residents. According to ISO, frequency-dependent filters related to human activities inside the buildings, the body position (e.g., standing, sitting or sleeping) and the direction of vibrations are proposed. This methodology is based on the assumption that a root mean square of the weighted acceleration (a_w) from the measured accelerations time hibase is considered in order to describe the smoothed vibrations amplitude of the human response. The weighted acceleration is calculated by:

$$a_w = \sqrt{\frac{1}{T} \int_0^T a_w^2(t)dt)} \tag{2.8}$$

where T is the total time of the acceleration time hibase.

In comparison with the vehicle passengers, just one single filter is presented to estimate the vibrations level inside the buildings. Furthermore, this value does not consider the direction of the vibrations and human body position and is focused on the low-frequency range from 1Hz to 20 Hz.

2.3.2. *European standards*

The German standards use a running root mean square of the velocity signal as the vibrations are often non-stationary. According to DIN, the weighted time-averaged signal is calculated as follows:

$$KB_F(t) = \sqrt{\frac{1}{\tau} \int_0^T KB^2(\xi) e^{\frac{t-\xi}{\tau}} d\xi} \tag{2.9}$$

The weighted velocity signal KB (t) is obtained through the high-pass filter as the original velocity signal:

$$H_{KB}(f) = \frac{1}{\sqrt{1+(\frac{5.6}{f})^2}} \tag{2.10}$$

The filter is a function of the frequency f and the integration time τ to run the averaging is equal to 0.125s. This value considers phenomena like impacts or shocks that would otherwise be ignored if a simple rms had been used. Furthermore, the standards propose three thresholds to compare the captured maximum level of KB_F (e.g., A_u, A_o, A_r) to examine the level of comfort. On the other hand, DIN 4150-3 focuses on the effect of traffic vibrations on buildings. For this purpose, a second indicator, the peak particle velocity PPV, is introduced. PPV is defined as the maximum value of the velocity-time signal. This value is compared to thresholds depending on the dominant frequency of the vibrations. This standard examines the maximum value of the most dominant direction of the vibrations. According to DIN, PPV is calculated as follows:

$$PPV = \max|v(t)| \tag{2.11}$$

It is worth noting that Switzerland standards (Schweizerische Normen-Vereinigung, 1992), in contrast with DIN, are taking under consideration all the three components of PPV. Thus, PPV is defined by:

$$PPV = \max\left[\sqrt{v_x^2(t) + v_y^2(t) + v_z^2(t)}\right] \tag{2.12}$$

Obviously, in the case for which there is a dominant direction, Eq. 2.11 and 2.12 are almost equivalent.

2.3.3. USS Department of Transportation recommendations

The Department of Transportation of the United States presented a decibel scale to investigate the effect of the HST-induced vibrations impact of passing high-speed trains on buildings. In order to describe the velocity level, the proposed scale decrease the range of the required values and the decibel level is calculated as follows:

$$V_{dB} = 20 \log_{10} \frac{v_{rms}}{v_0} \qquad (2.13)$$

where v_{rms} is the root mean square of the measured velocity time hibase by the HST passage. In comparison with the ISO standards, USDT proposed an equivalent (V_{LdB}) be applied to the decibel level. For instance, in Japan, the standardized weighted vibration level for all the frequencies higher than 8Hz is defined by:

$$VL_{dB} = V_{dB} - 21 \qquad (2.14)$$

Accordingly, Table 2.1. summarizes the proposed limits in the international standards (Kouroussis et al., 2014).

Table 2.1. Standard analysis summary for ground-borne vibration assessment (adopted by (Kouroussis et al., 2014)).

Standard	Parameter	Limits	Conditions of use
DIN 4150-3	peak particle velocity (the higher component)	3 mm/s 5 mm/s	(very) sensitive building dwelling place
SN 640 312a	peak particle velocity (the higher component)	3 mm/s 6 mm/s	frequently excited sensitive building normally excited building
ISO 2631-2	weighted rms acceleration rms velocity	0.315 m/s² 2 m/s² 0.10 mm/s	not or a little uncomfortable extremely uncomfortable residential area
USDT		0.26 mm/s	frequent (>70 passbys per day) residential aera infrequent (<70 passbys per day)
DIN 4150-2	weighted dose KB$_{F,max}$	0.15 mm/s 0.10 mm/s	residential area sentitive area

2.4. Vibrations mitigation methods

As mentioned, the HST passage developing vibrations are a crucial environmental issue, which affects the passenger comfort, the health of the nearby residents and might occur, in some cases, structural damages to nearby buildings or HSR infrastructure. Hence,

several researchers have proposed numerous mitigation approaches in order to reduce the developing vibrations (Feng et al., 2019a; Gao et al., 2020; Thompson et al., 2016a; With et al., 2009). Several isolation measures have been proposed in recent decades in order to minimize the ground-born vibrations. Generally, those remedial solutions could be summarized into three categories: a) train modification and track maintenance (Ferreira and López-Pita, 2015), b) installing wave barriers in the transmission path (Garinei, Risitano, and Scappaticci, 2014; Takemiya, 2004; Yarmohammadi, Rafiee-Dehkharghani, Behnia, and Aref, 2018), c) retrofitting against vibrations of the nearby infrastructure (Yang et al., 2019). The optimal approach should consider both technical and financial aspects of each examined problem.

2.4.1. *Train modification and track maintenance*

The main strategies for the mitigation of the HST-induced vibrations involve design and maintenance solutions. In new railway lines with appropriate route design, the optimal locations are selected for track parts such as switches, turnouts, and crossovers, where the vibrations level is usually increased. At the stage of the design of new HST lines, it is easier to provide a high vibrations level. Optimal solutions to prevent the generation and propagation of vibrations are the correct choice of railway track superstructure elements (fastenings, sleepers, ballast). The increase of the flexibility of those parts could increase their vibrations damping ability generated at the wheel-rail interface. Solutions such as reducing the unsprung mass or better wheel/axle design using higher performance materials should be considered in the design stage.
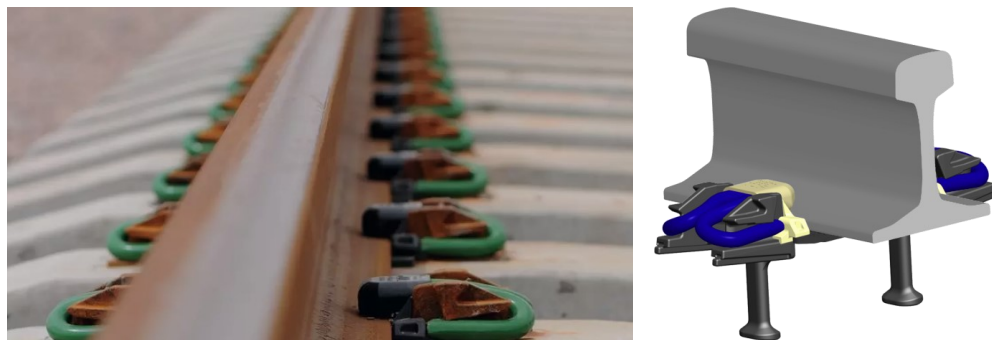
Figure 2.10 The resilient pre-loaded fastening system was adopted by www.pandrol.com).

Furthermore, the use of Resilient wheels (Pita et al., 2004) or active vibration control systems (Dahlberg, 2010) could have a beneficial role in the reduction of the induced vibrations. It has been reported that the implementation of resilient fastening systems leads to noise reduction between 3dB and 6dB, in comparison with the classic fastening

system (Federal Transit Administration, 1997). Resilient rail fastenings have been implemented at several sites on the lines of the Pan-European Corridor X, which passes from Retkovec and an average reduction equal to 2dB has been achieved. According to them, elastic elements are placed below the rail, the implementation of high-resilience fastenings prevents the contact of the sleepers and the rails. This approach increases the vertical deflection of the rail and reduces the induced vibrations up to 10dB at higher frequencies than 30Hz(Hanson et al., 2006). Figure 2.10 illustrates a discrete rail fastener with a highly resilient under base-plate pad, known as a resilience pre-loaded fixation system. This system could achieve even higher reduction of the vibrations level.

Figure 2.11 Rail vibration dampers.

Rail dampers are prefabricated elements implemented to the rail to reduce noise generated by railway rolling stock, as illustrated in Figure 2.11. The dampers can be easily glued or clipped on existing and new rail tracks. The main mechanism of this method is based on the increase of the rail weight in order to prevent rail vibrations. More specifically, the implementation of rail dampers minimizes the deflections along the rail, followed by isolating the vibrating length of the rail and ending in reducing the induced vibrations. The dampers are constructed by steel components, acting as springs under the influence of vibrations, and elastomeric material that absorbs the energy of rail (springs) oscillations. The use of continuously welded rail could also reduce the vibrations level as it was aforementioned.

On the other hand, in the case of existing HSR lines, the mitigation approaches are based on the maintenance of the track (e.g., rail grinding) and the wheels (e.g., wheel truing). In addition, the reduction of the passing speed of the train at problematic sites leads to the reduction of the vibrations level. One more effective approach is implementing

highly damped pads (Alves Costa et al., 2012) between track components (e.g., rail/sleepers or sleepers/ballast) to minimize the vibrations. This approach moves the vibrations to the lower frequency range, although it should be avoided close to buildings. Moliner et al. (2012) proposed a mitigation technic using viscoelastic dampers (VEDs) to protect existing railway bridges from the HST induced vibrations. Furthermore, floating slab tracks are commonly implemented instead of ballasted tracks in tunnels in order to isolate the induced vibrations.

Figure 2.12 Rail gridding.

Table 2.2. Effect of noise and vibration mitigation measures (adopted by Lakušić and Ahac (2012)).

Mitigation measure	Noise reduction /dB(A)	Vibration reduction/dB
Reduction at source – permanent way		
Resilient rail fastenings	3÷6	5 ÷ 10 (20)
Embedded rail system	3÷10	8÷18
Rail dampers	5÷6	7÷9
Wooden sleepers	1÷2	3÷5
Under sleeper pads	0÷3	8÷15
Ballast bed height increase	3÷5	0÷6
Ballast mats	8÷18	10÷15
Elimination of the rail running surface discontinuities	6÷10	0÷5
Maintaining smooth rail running surface	10÷15	10÷20
Reduction at source – rail vehicles		
Wheel re-profiling	5÷10	5÷10
Reduction of speed	3÷7(10)	3÷6
Disc brakes	10÷15	-
Composite brakes	8÷10	-
Resilient wheels	3÷20	3÷4

In practice, the implementation of just one of those mitigation approaches cannot significantly reduce the vibrations level; hence commonly, a combination of some of those approaches is used. The most common combination is the implementation of welded rail with resilient fixation to the track, which is used in order to upgrade existing lines. Furthermore, each mitigation approach is more effective at different frequency ranges. Hence, for instance, in order to reduce vibrations at frequencies higher than 100, the truing of wheel and rail grinding are the most appropriate solutions. Table 2.2 summarizes the level of noise and vibrations reduction of several mitigation approaches at the source (Lakušić and Ahac, 2012).

2.4.2. Installing wave barriers in the transmission path

The reduction of the induced vibrations by modifying the source is partially effective, although the mitigation level is limited. For this purpose, except for the modifications at the source, numerous mitigation schemes have been proposed through the years in order to prevent the spread of the vibrations on the surrounding area. Numerous researchers have focused on the proposal of mitigation approaches that can be used to reduce HST-induced vibrations (Connolly et al., 2015; Dijckmans et al., 2015; Karlström and Boström, 2007). The most commonly used mitigation approach is implementing one or more trenches -open or filled- in the direction of wave propagation to reflect and absorb the vibrations (Sitharam et al., 2018). The discontinuity between the soil and the trench fill material leads to the mitigation of the soil vibrations at the trench-soil interface. Yao et al. (2019) investigated the reflection at the interface of the soil material and the trenches filled material and concluded that a high difference between soil and fill material Young's Modulus and density leads to a higher reduction of the traffic vibrations. Numerous investigations have been carried out to investigate the optimum trench geometry and various filling materials have been proposed.

Beskos et al. (1986) compared filled with open trenches and concluded that trench depth must be higher than 60cm for open trenches. Furthermore, the normalized product (by Rayleigh wavelength) depth and width must be more than 1.5 for a trench filled with concrete. In another relevant study (Adam and von Estorff, 2005), it has been noted that the increase of trench width is less effective than its depth. Nevertheless, the implementation of very narrow trenches allows a significant part of the vibrations to pass (Bo e al., 2014). Feng et al. (2019b) examined the efficiency of open buried trenches also

covered with an extending plate and concluded that the source- and receiver-oriented extending plate is an effective mitigation approach, especially when the trench is buried at a depth equal to 0.2–0.3 Rayleigh wavelength. The most effective trenches for the mitigation of the traffic-induced vibrations are considered open ones (Hung et al., 2004; Yang et al., 2018). Nevertheless, several issues (e.g., maintaining their initial geometry intact, avoiding plants and filling with water or other materials) need to be properly addressed in order to ensure their continuous operation as initially planned.

(a) (b)
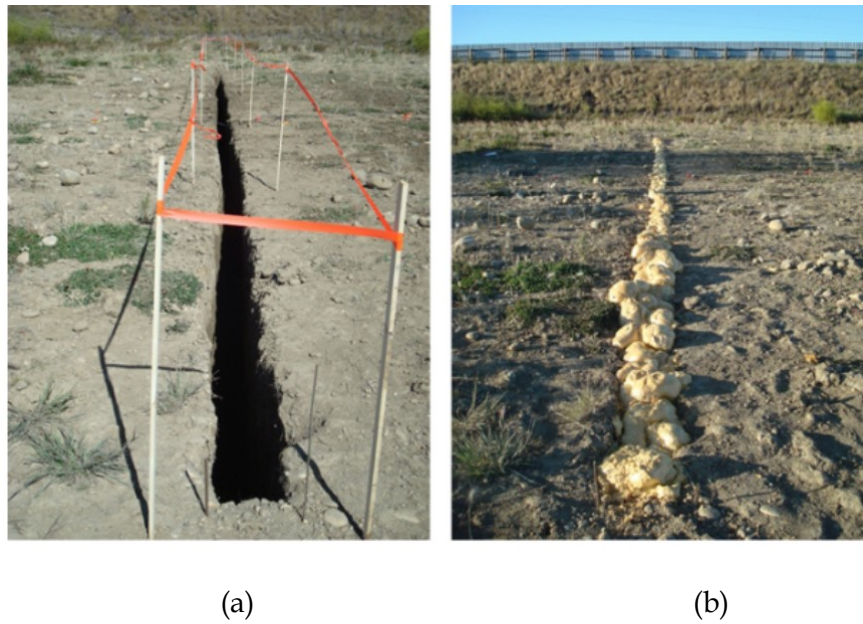
Figure 2.13 Trench barriers from the full-scale experimental study: (a) open trench and (b) Geofoam trench (adopted by Alzawi et al. (2011)).

(a) (b)
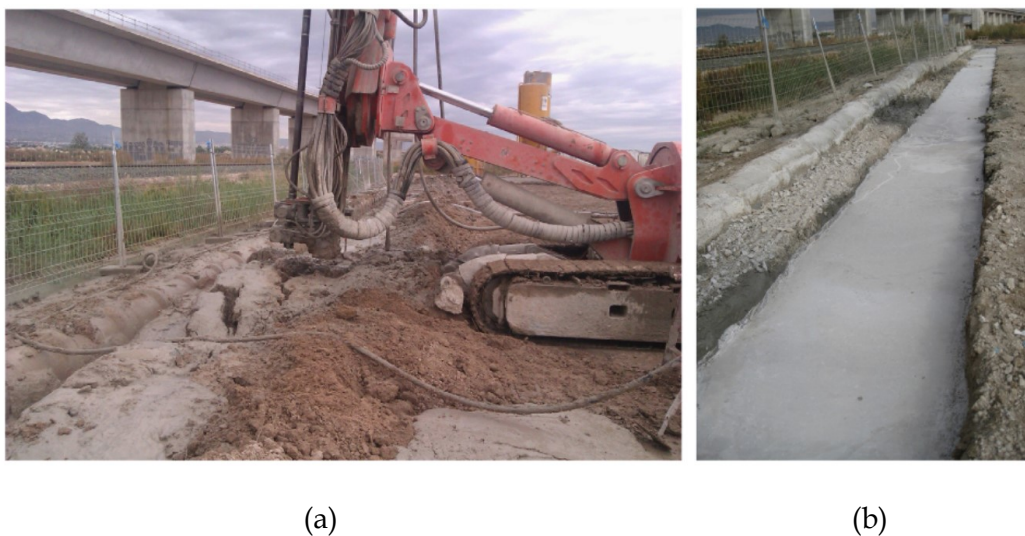
Figure 2.14 (a) Construction of the jet grout columns and (b) the stiff wave barrier upon completion at El Realengo (adopted by Coulier e al. (2013)).

Undoubtedly, the efficiency of a filled trench depends on filling material properties. Several types of filled trenches, such as concrete or bentonite trenches (Al-Hussaini and Ahmad, 1996), gas-filled cushions (Massarsch, 2021), water (Ekanayake et al., 2014), sand-rubber mixture (Chew et al., 2019), polyurethane (Alzawi et al., 2011) or expanded polystyrene (EPS) (Bo et al., 2014) have been proposed over the last decades. François et al. (2012) investigated the efficiency of a sandwich in-filled trench, using polystyrene as core material and concrete side panels and concluded that this method is less effective than an open trench. On the other hand, Kanda et al. (2006) studied the impact of gas cushion trench on vibrations isolation; according to this study, the examined barrier of the gas cushion is as effective as open trenches for the low-frequency range.

Yamohammadi et al. (2019) compared single, double and triple trenches and concluded that the double trench increases the vibrations reduction compared to the single trench. Moreover, double trenches require a lower depth in order to achieve a similar reduction of the vibrations as a single trench (Jayawardana et al., 2019). Bo et al. (2014) presented a numerical investigation of several parameters impact (e.g., trenches depth and width) in mitigating vibrations induced by a dynamic load, using a trench filled with EPS blocks. According to this investigation, larger depth leads to a higher reduction of the vibrations, while trenches with a slight inclination from the vertical direction are more efficient than the vertical cuts. Trenches filled with Fontainebleau sand were investigated and some guidelines regarding the design of geofoam infilled trenches were proposed by Murillo et al. (2009). Moreover, the effectiveness of the geometrical properties of open and geofoam-filled trenches was compared via a full-scale field experiment by Alzawi and EI-Naggar (2011).

There exist some alternative approaches for the mitigation of vibrations, aiming, for instance, to improve soil stiffness (Coulier e al., 2013) (e.g., deep vibro-compaction, grouting consolidation (Coulier et al., 2015), lime–cement columns (With et al., 2009) or deep subsoil mix), which can be quite effective, but they are not commonly applied due to their high cost. In addition, several studies have concluded that trenches provide a higher reduction of the train-induced vibrations, compared to the local soil stiffening beneath the embankment (Andersen and Nielsen, 2005; Pflanz et al., 2002). The heavy mass placement, such as a gabion wall across the track, has been proposed by Dijckmans et al. (2015).

The implementation of a sheet-pile wall as a stiff wave barrier has been studied by Dijckmans et al. (2016). This mitigation approach effectiveness is determined by the depth

and the stiffness contrast between the barrier and the surrounding soil. Thompson et al. (2015) examined the mitigation of the HST induced vibrations by stiffening the track subgrade. The implementation of a horizontal wave barrier, known as wave impeding blocks (WIBs), has been investigated by several authors (Antes and von Estorff, 1994; Gao et al., 2015; Takemiya, 2004). WIBs are placed under the track parts, as is illustrated in Figure 2.15 and their effectiveness depends on the position and the material properties of the blocks (Çelebi and Göktepe, 2012).
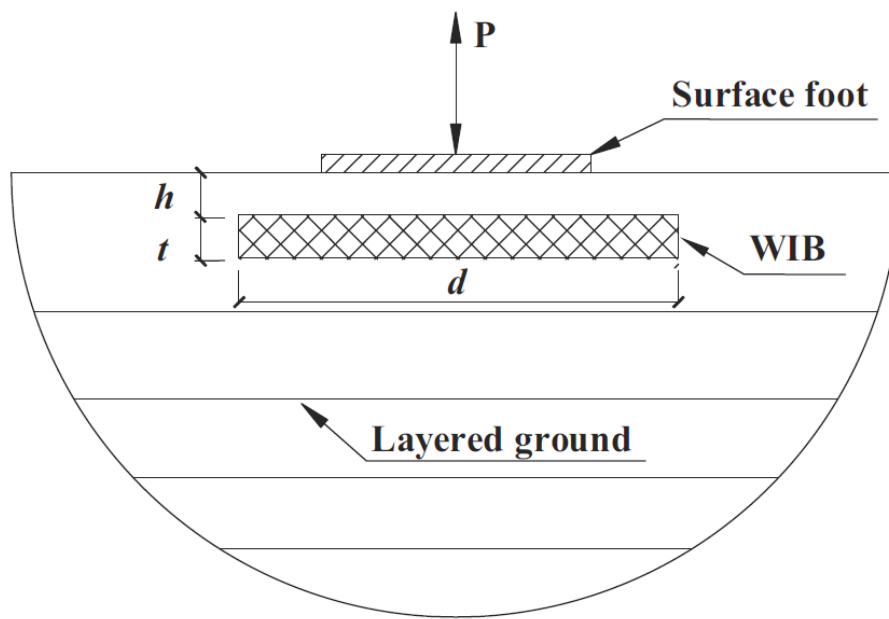
Figure 2.15 Schematic representation of WIB in the layered ground for vibration isolation (adopted by Gao et al., 2015).

2.4.3. *Retrofitting against vibrations of the nearby infrastructure and buildings*

The HST-induced vibration propagates through the surrounding soil to the nearby buildings and railway infrastructure, resulting in re-radiated ground-borne noise. According to Stiebel et al. (2012), this is a significant environmental issue internationally; thus, it is vital to implement further local countermeasure to reduce the vibration level on important structures. There is always the option to implement a trench between the building foundation and the surrounding soil to protect against the developing vibrations.

This is an efficient retrofitting approach in the case of pre-existed buildings, although, in the case of new structures close to HSR lines, it is possible to reduce the structural vibrations via optimal structural design. This approach is commonly used for structures above underground lines. One solution that can be followed during the structural design

is to apply base isolation to modify the frequencies and the response of the building. The selection of the optimal isolation system is a complex procedure as it depends on the foundation properties, structural flexibility and building damping (Talbot and Hunt, 2003a). The most common isolation methods are mounting the new building on suitable isolators (Talbot and Hunt, 2003b) and increasing the thickness of the lower floor (Zhao et al., 2010).

2.5. *EPS Geofoam materials*

According to Horvarth (1994), geofoams have been introduced to the scientific community to group in one category all the plastic foam, which are used in geotechnical applications. There are two basic types of geofoams, the expanded polystyrene (EPS), which is the most commonly used and the extruded polystyrene (XPS). The implementation of EPS geofoam at multiple geotechnical applications as fill material is used from the 60s. The primary usage of the geofoam is to provide lightweight fill material for numerous geotechnical applications, as its weight is approximately 1% the weight of soil and less than 10% the weight of other lightweight fill alternatives (Stark et al., 2012). The capability of EPS geofoam to minimize the applied loads to the subsoil and infrastructure makes it a very popular solution for several engineering challenges. Due to its mechanical behavior, energy dissipation characteristics, low density, low permeability and ease of use, EPS geofoam is ideal to be used for lightweight embankments construction, slope stabilization, lateral and vertical pressures reduction, vibrations damping and sub-base fill material.

Figure 2.16 Implementation of EPS at the field with bare hands.

The beneficial role of the EPS geofoam on the construction cost and schedule is observed, as it is easy to handle, in some cases with bare hands without special equipment (see Figure 2.16), and is not affected by the weather conditions. Furthermore, the life cycle of EPS geofoam is similar to other competitive materials. Hence it is capable of retaining long-term mechanical properties under designed conditions of use. The widespread EPS geofoam usage leads to the production of several types of geofoams, ideal for each specific application. Table 2.3 summarises the mechanical properties of the seven EPS types, classified by ASTM D6817 (2017). Worldwide, there are numerous EPS geofoam producers. Hence it is easy to find EPS in the majority of the countries. The geofoam is formed into blocks with various shapes and sizes to fill the needs of each project.

Table 2.3. Physical properties of EPS geofoam according to ASTM D6817 (2017).

	Units	EPS12	EPS15	EPS19	EPS22	EPS29	EPS39	EPS46
Density	kg/m3	11.2	14.4	18.4	21.6	28.8	38.4	45.7
Compressive Resistance, at 1 %	kPa	15	25	40	50	75	103	128
Compressive Resistance, at 5 %	kPa	35	55	90	115	170	241	300
Compressive Resistance, at 10 %	kPa	40	70)	110	135	200	276	345
Flexural Strength	kPa	69	172	207	240	345	414	517
Oxygen index, volume	%	24	24	24	24	24	24	24

2.5.1. EPS impact on the Environment

Commonly, in order to caegorize a material as ecological and environmentally friendly, the raw production materials are examined. Furthermore, the energy spent for its production and its application in construction as well as if the matterial can be easily recycled are taken under consideration. EPS is a 100% recyclable and environmentally

friendly material as EPS is non-toxic, completely inert. It does not contain chlorofluorocarbons (CFCs) or hydrofluorocarbons (HCFCs) throughout its life. In addition, EPS does not contain any nutritional value and therefore there is no risk of fungi or microorganisms.

Furthermore, EPS can be recycled in many ways when it can no longer be used in its original form. It can be recycled directly into new construction products or it can be used as a clean fuel in order to recover its energy content. The choice of recycling method is based on technical, environmental and economic studies. The environmental impact of the manufacture of raw materials (expanding polystyrene drop) and their conversion into EPS insulation is very small. Throughout the life of EPS, the only environmental aspects are those of gases released into the atmosphere for the required energy for its production.

It should be mentioned that EPS does not endanger health both during installation and during its function. EPS does not affect the health of workers, e.g., it does not irritate the skin or mucous membranes. The rules of working conditions do not require the use of gloves or a mask when using such a soft and compact material. EPS is biologically neautral and does not produce any pathogenic dust, even in the long-term conditions. As a result, EPS is equally safe for those who install it and for those who use it.

2.5.2. *EPS Geofoam geotechnical applications*

2.5.2.1. *EPS applications in highways engineering*

As it was aforementioned, EPS geofoam is a multi-functional material, which is ideal for several geotechnical applications. The geofoam applications to railways projects are still limited, although it is most commonly used in highway applications to prevent similar issues with the railways. For instance, EPS has been used to construct highways over loose soil, which cannot manage supplementary loads. For this purpose, heavy road-fill materials should be avoided. Hence, the use of lightweight fill material, such as EPS geofoam, is the optimal choice. Furthermore, the high compressive resistance makes the EPS geofoam able to support high highway traffic loadings effectively.

The EPS geofoam has already been used on numerous highways worldwide. For instance, in the USA, EPS has been selected for the Borman Expressway reconstruction in a site with loose subsoil close to Michigan lake. In this case, just 32 truckloads of EPS have been implemented. It is evident that if common soil fill has been used instead of EPS geofoam, four hundred truckloads would be needed. In addition, at the coastal area of

Great Yarmouth in the UKK, the native soft alluvial clayey soil level was needed to be raised above sea level. For this purpose, EPS has been implemented to address this sensitivity issue. In Greece, EPS geofoam has been used as large-scale road embankments fill in the new highway in Maliakos Gulf on loose native soil (see Figure 2.17).

Figure 2.17 EPS application on Maliakos Gulf as highway embankment fill material.

Figure 2.18 Widening of roads with the use of EPS geofoam.

Except for the highway settlement of loose soil, EPS has also been used to widen existing roads. In such cases, the use of EPS instead of traditional fill materials significantly minimizes the construction schedule. In some locations, several underground utilities such as gas lines, water mains and communication cables are pre-existing and must remain in use during the widening schedule. The EPS implementation in the sites where those utilities are passing makes the fast procedure of the construction without expensive interruption or relocation of those utilities. An example of EPS geofoam use to widen a highway is interstate 15 (I-15), which runs north-south in Utah, US. The widening

working schedule started in 1997 at a part of the highway close to Salt Lake City. This is the biggest EPS project in the USA as close to 100,000 m³ EPS has been implemented on the highway.

2.5.2.2. *EPS applications in bridge engineering*

In more geotechnical applications, where the EPS geofoam is commonly used is the construction of highway or railway bridges. The advantages of EPS geofoam, such as its low weight, make it a great fill material for bridge abutments or underfills. The high compressive resistance of EPS geofoam leads to lower differential displacements at the bridge/abutment interface. Hence, the maintenance cost of the bridge is reduced in the long term compared with the soil abutments. Furthermore, due to its low weight, the lateral forces on abutment walls are reduced. Hence, there are lower expectations in the dynamic design of new abutments.

Figure 2. 19 EPS as bridge abutment.

In several cases, EPS geofoam has been used as bridge underfills in order to support them. More specifically, in the case of existing bridges, which are no longer capable of carrying the required traffic loads, the underfill could further support the span and transfer the traffic load to the subsoil; EPS geofoam is a great solution. This approach was implemented on a masonry bridge along Tucker Boulevard at Saint Louis, USA, which was no longer capable of supporting a common soil underfill.

2.5.2.3. *Rail embankment*

Compared to the bridges and the highways applications, in the case of the railway projects, the implementation of EPS is not yet commonly used. However, its mechanical

properties attract the interest of several researchers in the field of railway engineering. As mentioned in the section with the mitigation approaches of HST induced vibrations, EPS geofoam has been used as trenches fill material (Khan and Dasaka, 2020; Majumder and Bhattacharyya, 2021) with great results. Except for the mitigation of the HST-induced vibrations, EPS geofoam can be used to manage similar issues with the highway applications, such as the settlement of the railway track on loose soils.

Figure 2.20 EPS Geofoam Embankment, UTA light-rail system, West Valley Line.

More specifically, the EPS geofoam can construct railway embankments that do not overload the underlying soils or stabilize the slopes of railway embankments or cuttings. Utah Transit Authority based its light-rail system on an EPS-filled embankment in Salt Lake Valley, as illustrated in Figure 2.20. This project is the first application in the railway system and one of the largest projects in terms of EPS geofoam usage in the USA. It should be mentioned that this project has been finished under budget and ahead of schedule due to the easy use of EPS geofoam application.

2.6. *Calculation of vibrations*

The complex phenomenon of the HST-induced vibrations has led the researcher to the proposal of several experimental, analytical and numerical prediction models. The ideal prediction model should accurately predict the amplitude of vibrations at several distances from the source, considering both the geometrical and material damping. In the sequence, a brief review of the existed prediction model is presented.

2.6.1. *Experimental Investigation*

The experimental investigations are the first approaches, which have been used to investigate the phenomenon of track-induced vibrations. A general guideline for predicting the developing vibrations in a variety of cases has been provided by ISO 14837-1 (2005). According to the proposed work schedule, a series of sensors is placed in increasing distance from the track to calculate the velocity or acceleration decrease level with the distance from the track. Degrande and Schillemans (2001) carried out an experimental investigation to examine the induced vibrations at the surface of the track and the surrounding soil in the cases of Thalys HST passage with speed between 223km/h and 214km/h. Those measurements greatly contributed to the field, as numerous researchers used them to validate their numerical models.

One more experimental investigation, which provided helpful information, was Auerch (2010) work, who also examined the reduction of the vibrations at increasing distance. More recently, Connolly et al. (2014) carried out an experimental analysis of ground-borne vibrations level generated by Thalys, TGV and Eurostar HST on several sites (at-grade, embankment, cutting and overpass) of Paris-Brussels HSR. Figure 2.21 illustrates the component geophone, which has been used in the in-situ measurements. It should be mentioned that the authors provide free access to the dataset of measurements for researchers working in the area of railway vibrations.

(a)   (b)
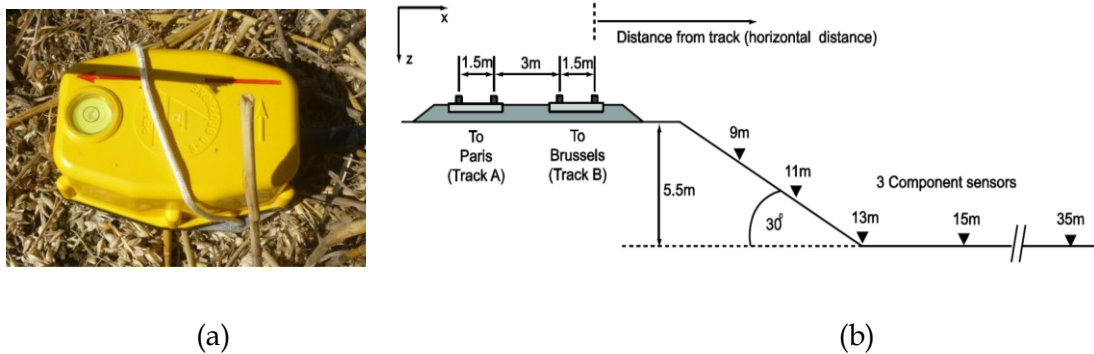
Figure 2.21 (a) In-field deployment of the three-component geophone, (b) Geophone configuration (adopted by Connolly et al. (2014).

One interesting practical method to investigate dynamic characteristics of the track is the receptance test. This test is performed using a hammer test aiming to investigate the transfer from force on rail to the associated displacement. This approach characterizes the global track behavior for a range of frequencies and allows the identification of the main

resonances of the structure, as it characterizes the structure sensitivity to vibrations and the dynamic flexibility of the track. However, this approach is not able to provide full information on track dynamic behavior under passing trains. More specifically, receptance could be a first fast and relatively easy measurement in order to estimate the track behavior, although the knowledge of the vehicle/track interaction and of the force acting on the track should also be investigated. On a realistic track model, receptance could be used in order to detail the relation between peaks visible in receptance curves and propagating waves in the track (Lesgidis et al., 2020).

The experimental investigations are a great tool for the researchers, as they provide accurate results, which could be used to construct new HSR and validate numerical prediction models. On the other hand, the time and cost limit the experimental analyses. Furthermore, experimental analyses are commonly limited to a particular case in which one phenomenon is expected to be emphasized. However, it is impossible to select an exact location where the objectives of the investigation correspond to supercritical phenomena. One important constraint is to capture the external noise from other sources such as cars or construction excitation, which alter the results. Nevertheless, in-situ measurements are incredibly useful in the validation of analytical or numerical models. Furthermore, receptance test has been also used in order to validate numerical models (Arlaud e al., 2020).

2.6.2. *Analytical modelling*

The main advantage of the analytical track modeling approach is its low computational cost in comparison with the lower cost-efficient numerical models. Hence, before the development of modern computing technology, analytical models were the most dominant approach in the early years. The first approach used a homogenous track layer, in which the rail was resting via the Winkler foundation. This approach was known as the single-layer method and it is still used to investigate the induced vibrations in the low-frequency range (Popp et al., 1999). Furthermore, according to this methodology, the assumption was made that the rail is a typically Euler–Bernoulli beam (Clark, 1982). In the sequence, to improve the efficacy of this method, various beams have been investigated and it was concluded that the use of Timoshenko beam instead of Euler-Bernoulli led to more accurate results due to its additional degrees of freedom (Zhang et al., 2020).

The single-layer method gave some first useful results in the field of the train-induced vibrations. However, there was a need for improvement of this methodology to consider the effect of each component of the track (e.g., the sleepers and the ballast layers) in the waves propagation. For this purpose, the two-layer method was developed, according to which the rail pads and the ballast were assumed to be massless. However, this methodology does no still take under consideration the effect of sleepers. Hence, dispute of this problem (Knothe and Grassie, 1993), this approach is useful only in the case of ballasted tracks. It is worth mentioning that, except for the track, the subgrade strongly affects the stiffness of the track components. In the case of the single-layer or double-layer methods, the assumption is made that the track is rigid. This assumption is valid in the case of the subgrade with stiffness higher or equal to the track stiffness (Kouroussis et al., 2011). However, in the case of a softer subgrade material, those approaches are not valid; hence, attempts were made to consider the subgrade as elastic half-space (Cao et al., 2011).

(a)

(b)
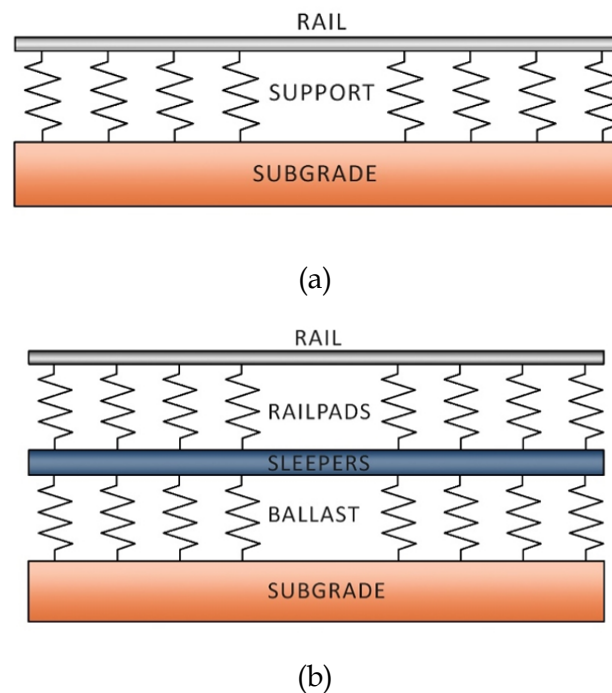
Figure 2.22 (a) Single-layer track model, (d) Double-layer track model.

2.6.3. *Numerical modelling*

According to the previous section, the analytical models in some cases are suitable to accurately predict the response of the track, especially at simple track geometries. However, the complexity of the required calculation to take into account parameters such as the layering of the track and the subsoils or irregular geometries makes the analytical

methods outdated. Nowadays, technological evolution, made possible the investigation of more parameters through numerical models. Hence, the complex problem of HST-induced vibrations is commonly approached via numerical methods such as the Finite difference (FD) method, Finite element (FE) method or the boundary element (BE) method.

2.6.3.1. *Finite Difference Method*

The finite difference method (FDM) has been introduced in structural vibrations prediction primarily to exceed complex continuum problems by finding closed-form solutions to the differential equations. FDM is one of the most straightforward numerical approaches, which resolves the motion equations numerically at specified nodes of the continuous structure by replacing the derivatives with finite-difference expressions of the functions. The finite-differential equation governs displacements are applied at each examined node of the meshed structure, connecting the displacements at the examined node and its neighboring nodes to the externally applied loads. This methodology results in a specific number of simultaneous equations to determine the displacements (Ghali et al., 2017).
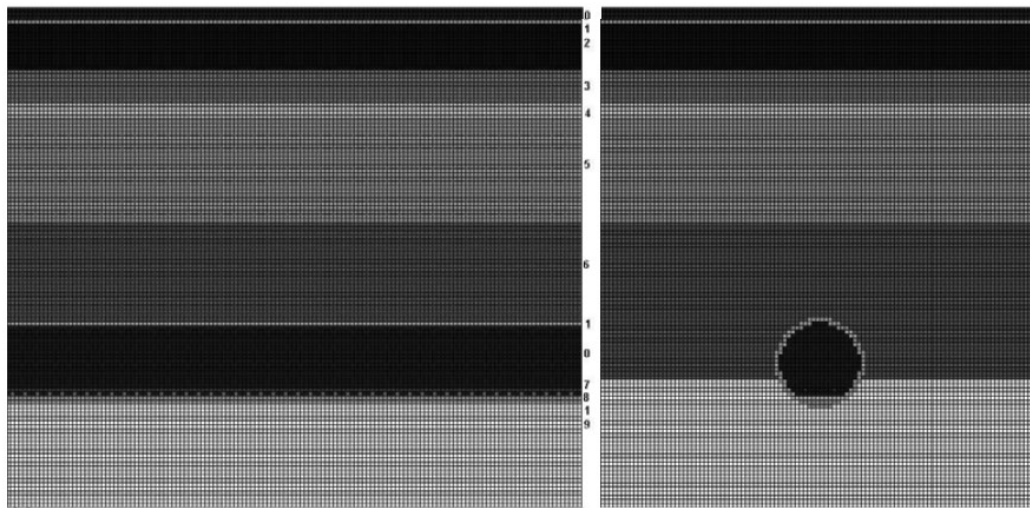
Figure 2.23 Sections through FDM model of the underground railway (left: longitudinal; right: transverse) (adopted by (Thornely-Taylor, 2004).

FDM has a relatively low computational cost, as the discretization is well defined, hence the separation of the analysis to multiple processors is possible. Furthermore, absorbing boundary conditions makes FDM a competitive alternative to the more computational costly finite element method. Those benefits led several researchers to use

the FDM in order to solve the problem of HST-induced vibrations. There are some investigations related to the field of HST-induced vibrations with the use of this method (Katou et al., 2008; Thornely-Taylor, 2004). The main problem of FDM is the reduced performance in simulating complex geometries and free surfaces. However, the FDM offers reduced performance in modelling domains with complex geometries and free surfaces. Hence, it is difficult to simulate a detailed track/soil model, as it requires numerous assumptions. For this reason, researchers in recent decades prefer to use other numerical approaches instead of FDM.

2.6.3.2. Finite Element Method

As an alternative to FDM, the finite element method (FEM) has been developed; this method can simulate relatively easily complex geometries. Furthermore, there is a great availability of numerous commercial software (e.g., ABAQUS, ANSYS, MSC Marc), which offer a graphical interface to the users. FEM has been created to numerically resolve models in differential method, a form that allows for easy boundary condition incorporation. FE necessitates the discretization of the whole model into smaller finite-sized components with basic governing equations. Matrix algebra is used to find the displacement solution to a given loading condition for all of the elements simultaneously. FEM is a great option in order to simulate complex geometries that cover a finite volume.

Obviously, FEM is a great numerical tool for the researchers of the HST-induced vibrations field as the complex geometry of the track and the soil could be detailed designed. For this reason, numerous relevant studies have been presented in recent years in the field with the use of the time-domain FEM approach (Connolly et al., 2013; El Kacimi, et al., 2013; Sayeed and Shahin, 2016a). Furthermore, this method is ideal for investigating issues such as rail irregularities (Kouroussis et al., 2011). However, since the model size must be finite by definition, it is not easy to simulate a semi-infinite domain using simple FE theory accurately. For this reason, absorbing boundary conditions are mandatory in order to avoid the reflections at the edges of the model.

Early FE models of semi-infinite media under static loads used rigid, artificial boundaries which were "far enough" from the loading position to not affect the solution. This is not achievable in dynamic simulations since the artificial boundaries reject waves, resulting in incorrect results. The viscous boundary is one of the first approaches to absorbing boundary simulation (Kouroussis et al., 2011). According to this approach, a

series of dashpots are coupled to the boundaries of the model instead of rigid constraints in order to absorb the reflection of the waves at the edges of the model. Lysmer et al. (1971) proposed an alternative approach according to which the problem is transformed to the domain of the frequency-wavenumber. The separation of variables is used to find a transcendental solution to the wave equation for the semi-infinite layer of soil represented by the absorbing boundary.

For layered media, equations are required for each layer and must meet compatibility conditions for adjoining layers. Contour integration can be used to find closed-form solutions in simple cases and numerical solutions are needed for arbitrarily layered soils. The stuffiness matrix method used to calculate this form of absorbing boundary is deemed exact because it does not introduce any additional approximation to the model. Drake (1972) calculated Rayleigh wave reflection and transmission factors in nonhorizontally layered media using FEM according to the stuffiness matrix approach; this necessitates absolute FEM discretization of the non-horizontal portion. Furthermore, this method has also been used for anisotropic media (Rokhlin and Wang, 2002) and transient analyses (Park and Kausel, 2004). In addition, the thin-layer method has been developed in the sequence as an expansion of the stuffiness matrix method (Hamdan, 2013).

(a)   (b)
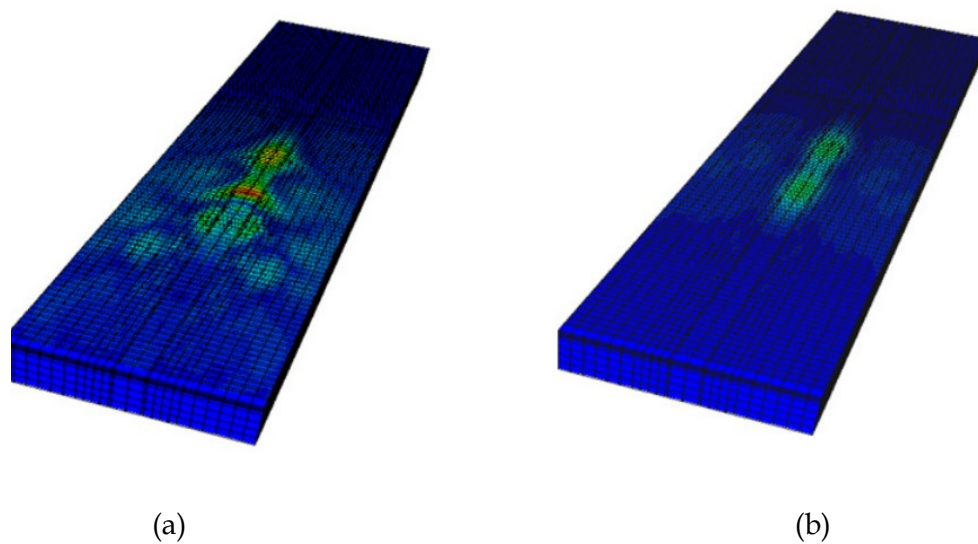
Figure 2.24 FEM method: contour plots of the displacement for the HST passing speeds: (a) 80m/s, (b) 40 m/s (adopted by (El Kacimi et al., 2013)).

In the case of FE models, which are used to simulate the complex phenomenon of HST-induced vibrations, several approaches capable of leading to valid results, have been used. More specifically, methods such as the combined FE-thin layer method (Barbosa et al., 2012), the scaled boundary FE method or the implementation of infinite elements

(Astley, 2000; Bettess and Zienkiewicz, 1977) have been proposed through the last decades. Several researchers have used the method of the infinite elements in recent years; some of those approaches are illustrated in Figure 2.25.

| (a) | (b) |
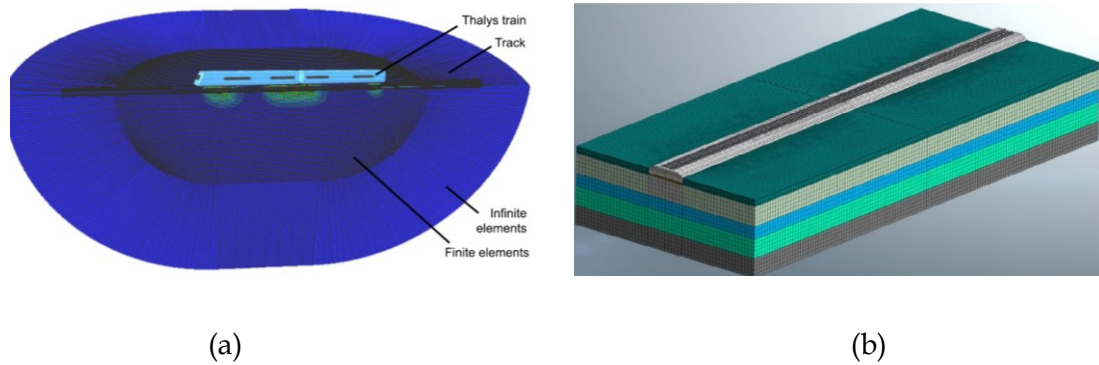
Figure 2.25 Symmetrical soil finite/infinite element solution (a) adopted by (Connolly et al., 2013), (b) adopted by (Sayeed and Shahin, 2016b).

As was aforementioned, the main disadvantage of the FEM approach is the high computational cost, especially in complex problems such as the HST-induced vibrations. Nowadays, 3D time or frequency domain FEM models are used in order to predict the vibrations spread. The frequency-domain models are less computationally expensive, although the majority of the absorbing boundary conditions cannot be implemented in the frequency domain simulations. On the other hand, the time-domain FEM models are a more accurate solution in terms of absorbing boundary conditions. However, this approach requires large computing resources at each timestep, leading to high running times. It is a matter of time before this problem is addressed due to the rapid evolution of modern computers capabilities.

2.6.3.3. *Coupled BE-FE Method*

Boundary Element Method (BEM) has an advantage compared to FEM in investigating infinite or semi-infinite domains. According to BEM, just the boundary of the domain is discretized in order to resolve the plane-strain problem. Furthermore, when BEM is used, there are not required artificial boundaries; hence there are no reflections at the edge of the domain. However, the use of the BEM approach has some weaknesses compared to the FEM approach, such as the inconvenience of simulating irregular bodies, such as the railway track.

This disadvantage led several researchers to couple the BEM and the FEM approaches in order to take the advantages of both methods. According to this approach, the soil

region is modeled using BEM and the track by using FEM. Some investigations use the coupled FE-BE method in the time domain (Galvín and Domínguez, 2009), although the majority of the researchers are using the frequency domain approach (Sheng et al., 2006). However, as in the case of the FEM approach, the BE-FE approach still has a relatively high computational cost. Additionally, it is not easy to couple the BEM model with a finite structure, such as a building close to the track, in order to investigate the structural vibrations.
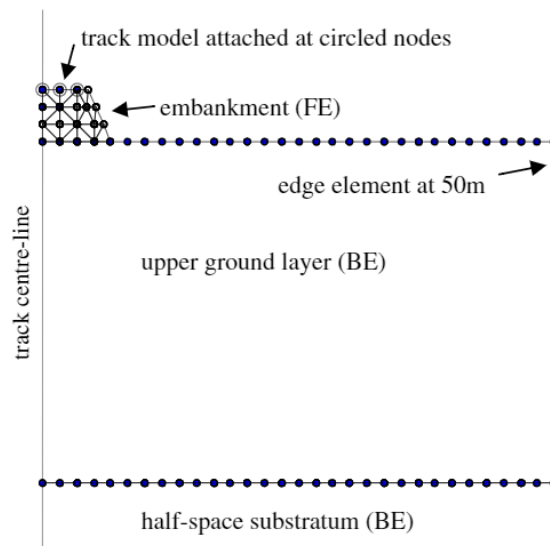
Figure 2.26 Sketch of FE/BE model adopted by (Sheng et al., 2006).

2.6.3.4. *2.5D method*

As mentioned, the 3D FEM and the coupled BE-FE approach are computational tools with high accuracy, although they have some limitations due to their high computational cost. For this purpose, several researchers examined alternative methods. Hanazato et al. (1991) investigated the combination of both two-and three-dimensional (3D) simulation approaches aiming to achieve a more efficient computational methodology. This approach, known as two-and-a-half-dimensional (2.5D) simulation, is based on the assumption that the track components are constant along the HST passage direction. Furthermore, the transformation between 2D and 3D is performed via Fourier Transformations. Subsequent studies (Coulier et al., 2014; Gao et al., 2018, 2012) examined the coupling of the 2.5D modeling approach with absorbing boundary conditions using infinite elements. This approach is incredibly efficient in the case of invariant track geometries, such as slab track, although in ballasted tracks, the accurate simulations of the

stress distribution associated with the sleepers is still a challenge. Recently, the rapid growth of computational capabilities has led to a limited use of 2D and 2.5D models.
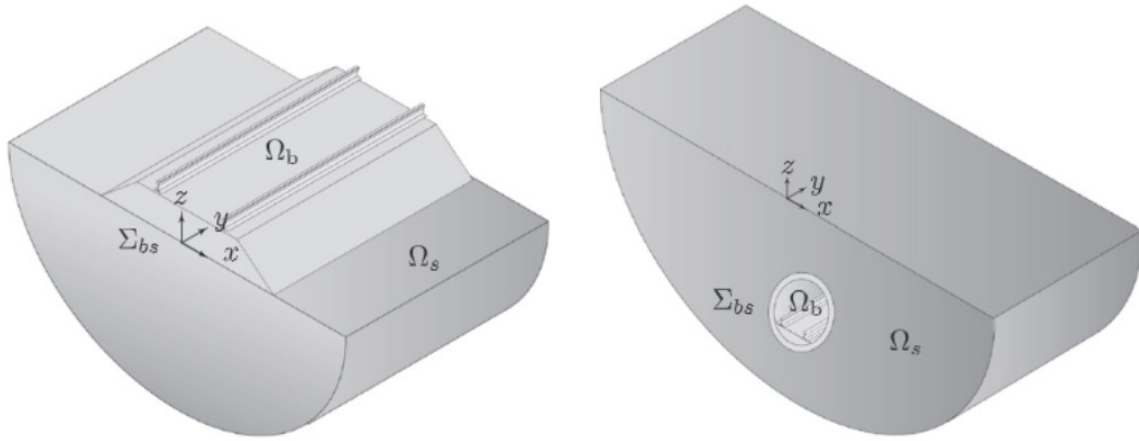
Figure 2.27 The 2.5D coupled FE-BE models: (a) a ballasted track at grade and (b) a tunnel in a half-space (adopted by (Galvín et al., 2010)).

CHAPTER 3

NUMERICAL MODEL VALIDATION

3.1. *Field data*

The importance and criticality of the numerical model validation are well recognized in the scientific community. Hence, the accuracy of the numerical model at three existing sites from Thalys Paris–Brussels line is captured by comparing the numerical results with in situ measurements (Connolly et al., 2014). For this purpose, field measurements, which had been carried out earlier by our colleges for Thalys and TGV HST passage from three sites near Braffe, Belgium, have been used. The authors are most appreciative of Prof. G. Kouroussis, University of Mons, Belgium, for providing the in-situ measurements. According to the in-situ measurements, in order to determine the material properties of the soils at each site, MASW had been used in conjunction with a desktop survey of existing soil data. Excitation was provided using a 12lbPCB086D50 impact hammer with an onboard accelerometer.

The accelerometer was connected to a data acquisition unit using a microdot connector. This allowed for the calculation of the input force exerted by each hammer blow. Twenty-four low frequency (4.5Hz), vertical component, SM-6 geophones were placed parallel to the railway track, in the same line as the geophones used for recording train vibrations. The array was placed far enough from the track to ensure that the results were not contaminated from potential artifacts close to the line but close enough to ensure that the soil properties were representative of those beneath the track. No MASW measurements were undertaken during train passage. Geophone spacing was 1m as

recommended by (Park Seismic, 2013) and each sensor was coupled to the ground using 150mm spikes (Stiebel, 2011). Excitation was performed at seven individual locations by striking an embedded metal impact plate. All results were amplified using a high gain setting and recorded using a Panasonic Toughbook in SEG-2 format. The gain was removed during post-processing.

3.2. Test site details

Site 1 consists of an embankment railway section located on the Paris–Brussels line, North-East of the town of Braffe (see Figure 3.1a). The track configuration consists of an embankment 5.5m high with a slope of 30°. On the other hand, site 2 is a cutting with a height equal to 7.2m at a gradient of 25°, as is illustrated in Figure 3.1b. In the last case (Site 3), the railway section is at-grade, located at 4km south of Leuze-en-Hainaut (see Figure 3.1c). The track on the Paris – Brussel HSR is a classically ballasted track with three layers, e.g., ballast, sub-ballast and subgrade, with thicknesses 30cm, 20cm and 50cm, respectively. The track cross-section is illustrated in Figure 3.2. A continuously welded UIC60 rail is typically used on the examined sites. The rails are fixed to the prestressed concrete sleepers via Pandrol clips. The assumption has been made that the rail unevenness is very low on all the examined sites; hence, griding was performed eight days before the in situ measurements (Connolly et al., 2014).
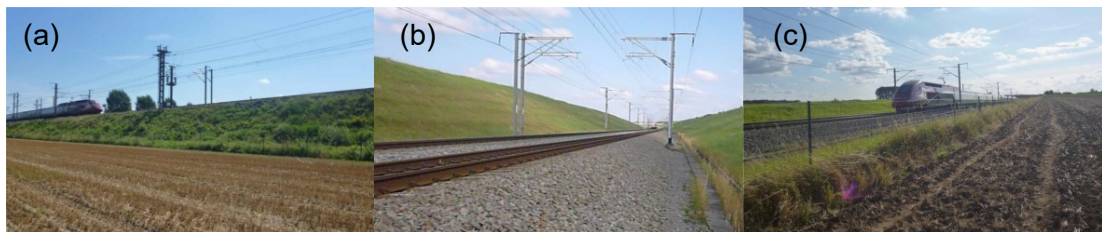
Figure 3.1 Examined sites (a) embankment, (b) cutting, (c) at grade (adopted by (Connolly et al., 2014)).

According to our colleges, who carried out the in-situ measurements, Geopsy (Wathelet, 2008b) (a graphical user interface capable of generating plots from the recorded signals) was used to analyze the MASW results. In the sequence, the plots have been used in the sub-program Dinver (Wathelet, 2008a). For the purposes of this investigation, the assumption has been made that the soil density has a constant value equal to 2000kg/m^3 in order to increase the reliability of the process. This assumption is valid as the S-wave speed is independent of density. Then, the layer thickness and the wave velocity were carried out through inversions. The researchers used the software package,

SiesImager/2D, to validate the Compressional wave (P-wave) profiles through refraction analysis. The soil layer wave velocities of the examined sites are summarized in Table 3.1.
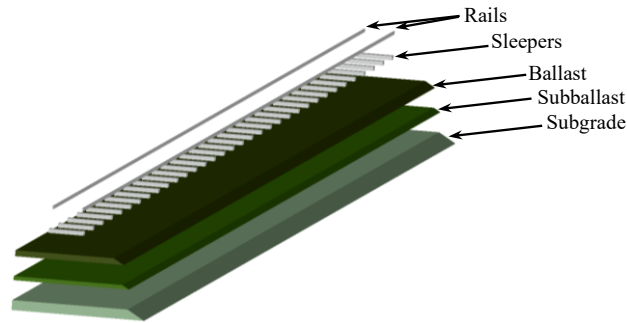
Figure 3.2 Sketch of track parts.

Table 3.1. Soil layers wave velocity.

Site 1: Embankment			Site 2: Cutting			Site 3: At-Grade		
h	V_s	V_p	h	V_s	V_p	h	V_s	V_p
(m)	(m/s)	(m/s)	(m)	(m/s)	(m/s)	(m)	(m/s)	(m/s)
1.3	142	280	1.35	160	270	1.5	175	270
1.3	162	280	1.35	171	270	1	120	270
1.2	157	280	3.1	223	410	1.7	202	550
2.85	280	520	3.1	260	410	2.5	300	550
2.85	330	520	Inf.	798	1460	Inf.	450	900
Inf.	598	940						

Table 3.2. HST passage speed.

	Thalys	TGV
Site 1	284	290
Site 2	297	299
Site 3	299	280

Conolly et al. (2014), in the same in-situ measurements, captured approximately the HST passing velocity by information obtained from the train operator, Infrabel. Four train types (TGV, Eurostar, Thalys and double-Thalys) have been recorded across the three sites during the in-situ measurements. Figure 3.3 shows the three train sets which are operating at the Paris-Brussels railway line. For the purposes of the present investigation, Prof. G. Kouroussis provided field data of one passage of Thalys and TGV HST on each of the three

examined sites. Table 3.2 summarizes the HST speed for each passage. The damping of the subsoil is an important factor of the vibrations attenuation. The damping ratio proposed for the soil layers of the three examined sites is summarized in Table 3.3.

Figure 3.3 (a) TGV, (b) Thalys, (c) Eurostar.

Table 3.3. Soil layers damping coefficients.

Site 1: Embankment		Site 2: Cutting		Site 3: at-grade	
h (m)	ξ	h (m)	ξ	h (m)	ξ
1.3	0.074	1.35	0.0775	0.8	0.105
2.5	0.07	1.35	0.07	1.5	0.0742
2.85	0.05	3.1	0.0309	1.5	0.09
2.85	0.0344	3.1	0.05	1.6	0.08
				1.5	0.07
Inf.	0.02	Inf.	0.03	5	0.04
				Inf.	0.01

3.3.   Review of previously validated numerical models

Connolly et al. (2014) have first publicized the pre-available field data in 2014, a part of which has been used to validate the proposed numerical model. In the sequence, the field data have been used by several authors in order to validate their numerical approaches. For instance, Kouroussis and Verlinden (2013) have used the field measurements of Thalys passage with 300 km/h on the Belgian site of Mevergnies in order to compare the efficacy of three different numerical approaches. The first model (e.g., Model A) did not illustrate the pitch motion of the bogies and used the Winkler foundation for the track subgrade (Kouroussis et al., 2011). Model B adopts the CLM model for the track subgrade and model C is a CLM model with pitch motion of bogies and car bodies. Figure 3.4 illustrates the publicized Fourier spectra and the 1/3 octave bands of the three examined models and the field data at 9m from the track. According to this investigation, the positions of the

vibrations peaks are in good agreement between the field data and the numerical results. As shown in Figure 3.4, the vibrations peaks predicted in the frequency range 20–30Hz and 50–60Hz are significantly larger than their field counterparts. The researchers have assumed that the reason for this difference is due to the adopted soil damping model.
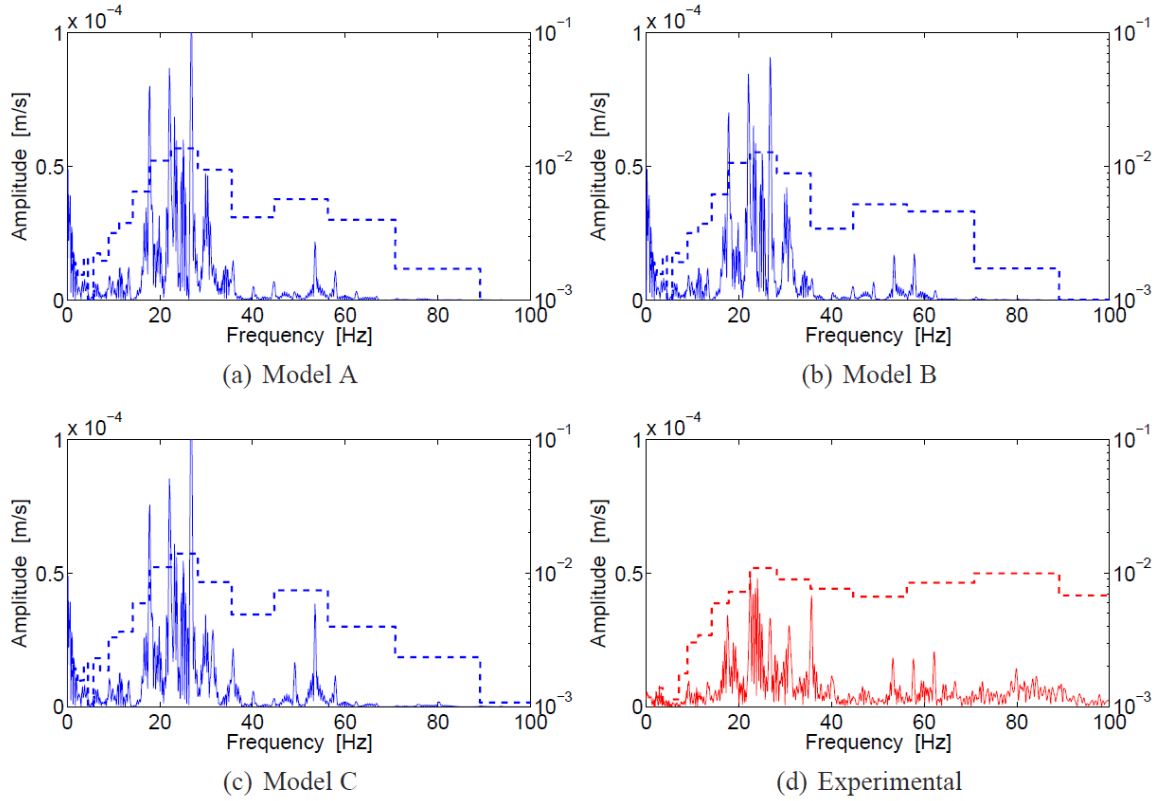
Figure 3.4 Predicted and measured frequency content (spectra in solid line and one-third octave band in dashed line) of vertical ground velocity at 9m from the track (adopted by Kouroussis and Verlinden (2013)).

Connolly et al. (2013) have used a part of the field data from an embankment site in Belgium on the Brussels to Paris high-speed line in order to validate their numerical model for the passage of Thalys HST with 265km/h. For the purpose of the analyses, the authors have used the software Abaqus along with a user-defined VDload subroutine. In this investigation, the velocity-time histories and the Fourier spectra at 19m of the track have been presented. The correlation between the field data and the numerical results, in this case, was remarkable, as the response of the soil to the passage of every HST wheel was visible and the timing of the passage is well captured. Furthermore, this numerical approach has successfully simulated the response to the heavier locomotives. Figure 3.5b illustrates the response of the soil at 19m from the track in terms of velocity Fourier spectra. Obviously, this numerical approach has captured the vibrations peaks value more

accurately at the frequency range between 0 and 40Hz. However, it is clear that several peaks were significantly higher than the field data. Hence, this numerical approach is quite accurate, although some modifications could lead to a higher correlation at the low-frequency range.
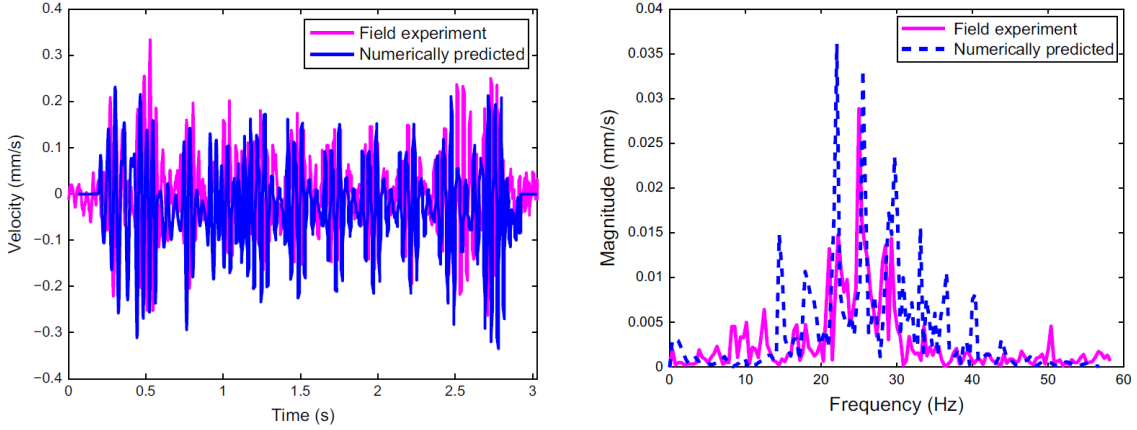
Figure 3.5 Comparison between field data and numerical model in terms of (a) Velocity time histories, (b) Fourier Spectra at 19m from the track (adopted by (Connolly et al., 2013)).
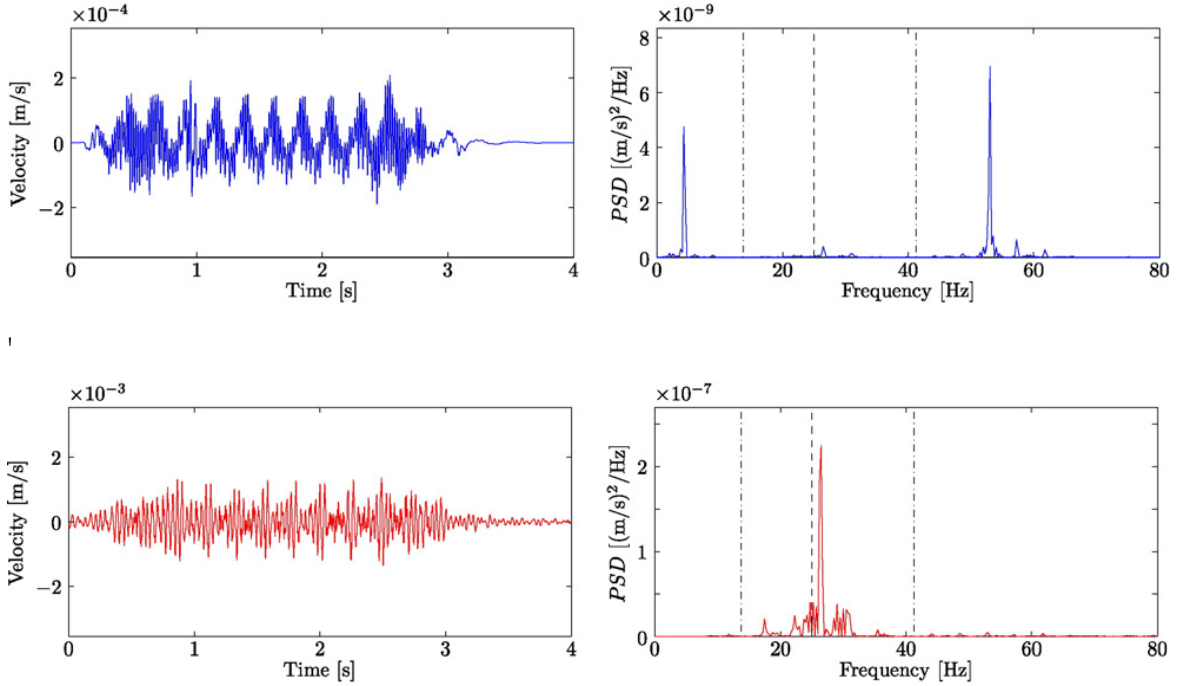
Figure 3.6 Vertical ground velocity at 11m from the track with cutting due to the passing of a Thalys HST at speed v_0=297 km/h: (a) Predicted time hibase. (b) Predicted frequency content. (c) Measured time hibase. (d) Measured frequency content.

One more attempt has been made by Connolly et al. (2016) in order to validate a coupled numerical model. According to this study, a vehicle multi-body model has been used, assuming that each of its parts is rigid and interconnected with spring and damper

elements defining the suspensions and a finite element model has been used for the simulation of the track components. The numerical model has been validated for the passage of Thalys HST from three sites (e.g., an embankment, a cutting, at grade). The researchers have concluded that this numerical approach had not performed well in the case of the HSR cutting sites. As illustrated in Figure 3.6, the shaping and timing of the time histories were significantly different from the in-situ measurements. The same observation has been made in the spectra, where the vibrations peaks were located in completely different frequencies.
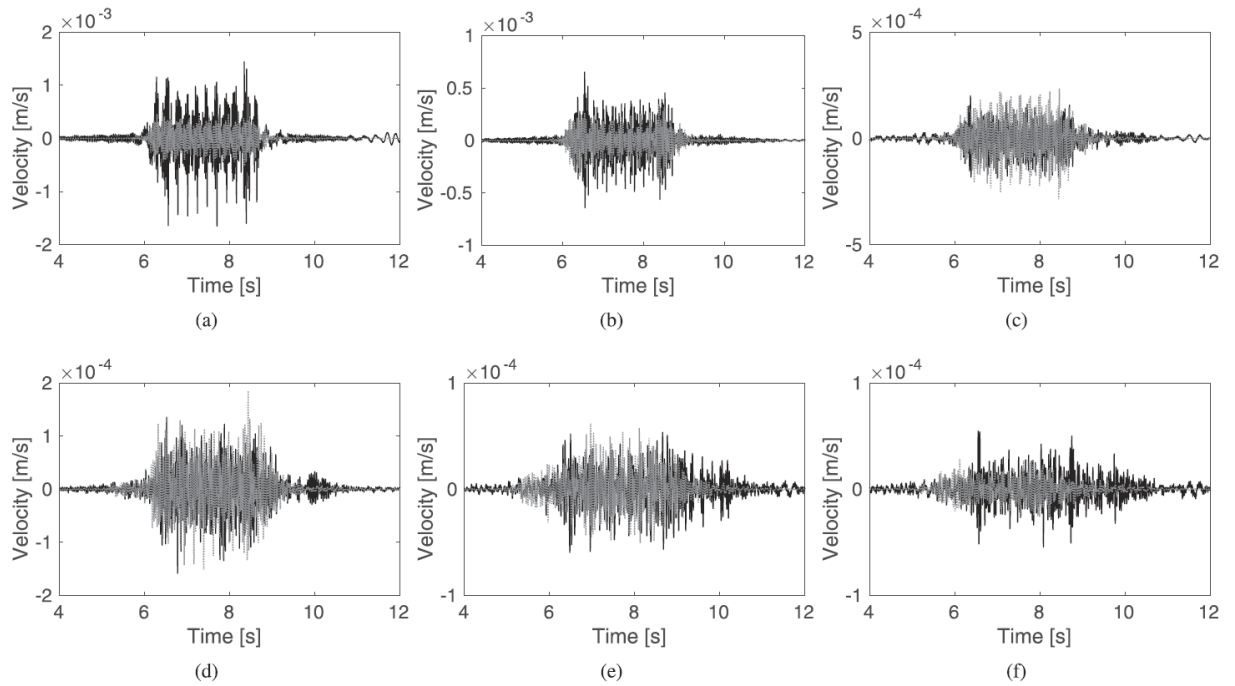
Figure 3.7 (Blackline) the experimental and (grey line) computed with the scoping model time hibase of the vertical velocity at the free field at a distance of: (a) 8 m; (b) 16 m; (c) 24 m; (d) 32 m; (e) 48 m and (f) 64 m from the track centerline during the passage of the Thalys HST at a speed v = 294 km/h.

More recently, a two-and-a-half dimensional (2.5D) finite element model has been used by Galvin et al. (2018) to accurately predict the induced vibration and reduce the high computational cost. The model has been validated by comparing the soil response with the experimental data at several distances between 8m and 64m from the track for the passage of Thalys HST with 294km/h. The model has captured the timing and the shaping of the time hibase at all the examined points. It should be mentioned that the numerical model has slightly underestimated the peak values of the vertical velocity at the near field (e.g., 8m, 16m from the track) and have overestimated these values at distances higher than 24m from the track, as it is presented in Figure 3.7. Nevertheless,

this research proposed a numerical approach with a great balance between the accuracy and the computational cost. As mentioned, several numerical models have been used to predict the induced vibrations by Thalys HST passage. Some of those great contributions to the field have been presented in this section. In the present investigation, an effort has been made to propose an equally accurate model by trying to overcome issues such as the effect of the soil damping simulation on the accuracy of the numerical approach.

3.4. HST moving load simulation

As it was aforementioned, the examined HST (Thalys and TGV) have the same geometry. More specifically, the HST have commonly consisted of three types of bogies, two locomotives (Y230A motor bogie) and eight passenger bogies (two Y237A trailing bogie and six Y237B trailing bogie) and their total length is equal to 200 m. Figure 3.8a depicts a sketch of the HST geometry and the axle loads acting on the tracks, which have been used in the present investigation. Figure 3.8b displays the axles distances and bogies lengths are also shown. Regarding HST moving loads, which have been simulated with a user-developed VDload subroutine, the time step Δt has been set equal to 1.3×10^{-6} s to ensure the FE model numerical stability. The colleagues who had performed the field measurements reported that (Connolly et al., 2014; Kouroussis et al., 2016): "…rail grinding operation maintenance restoring the profile and removing irregularities was performed one week before the measurement campaign…". Therefore, it has also been assumed herein that the track had no geometric irregularities and track defects and the dynamic responses were computed for a uniform track geometry.

Since the straight railway lines account for a large proportion, this model mainly considers the vertical loads on the rails. The total train load f_{total}, which is represented by a series of 26 axles load located in the wheels-rail contact points, has been formulated with a constant moving velocity for each examined HST passage (see Table 3.3). The geometry of typical Thalys or TGV HST is illustrated in Figure 3.8a. The total train load is described as:

$$f_{total} = \sum_{n=1}^{26} f_n \tag{3.1}$$

The position of each HST axle for each timestep (t) is derived as follows:

$$y_n = vt - d_n \tag{3.2}$$

where:

v is the HST constant velocity,

d_n is the distance between the first axle and the n axle.

The amount of each HST axle load f_n acting on each rail point has been determined as:

$$f_p = \sum_{n=1}^{26} f_n \delta(y_n - y_p) \tag{3.3}$$

where:

δ is the Dirac delta function,

y_p is the position of the point on the rail.
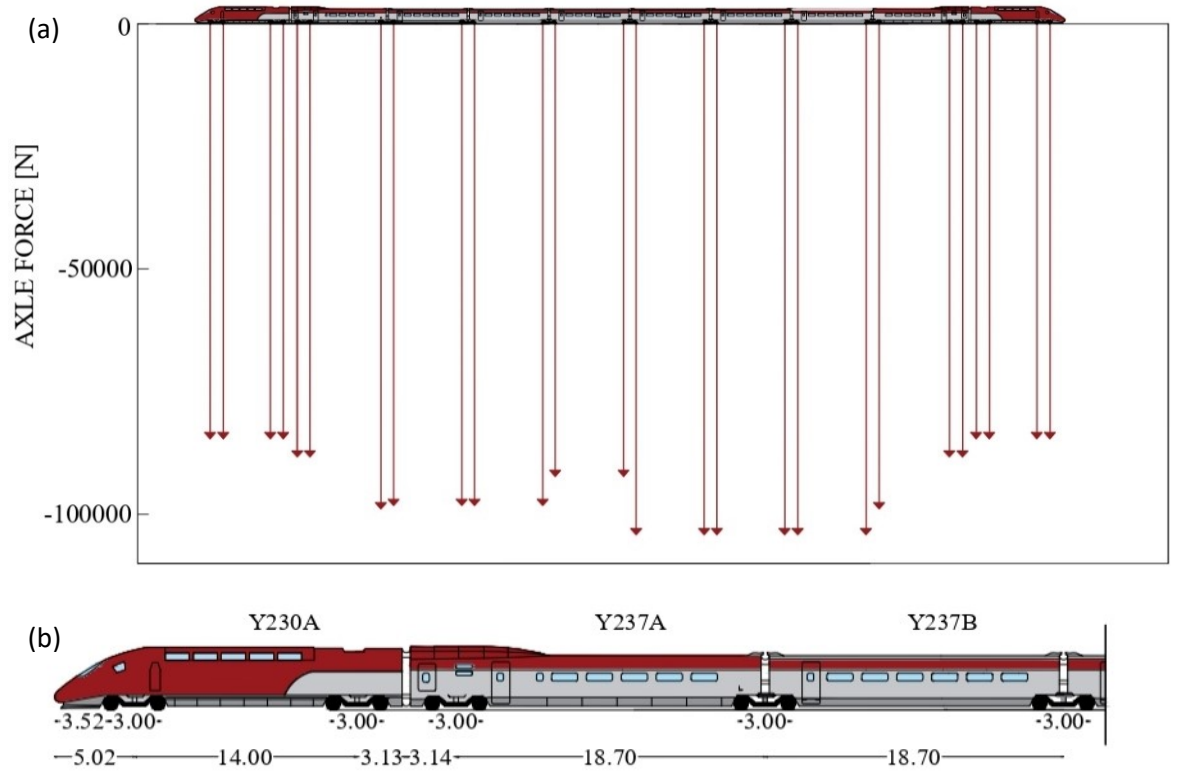
Figure 3.8 (a) Thalys train axle loads (adopted by (Kouroussis and Verlinden, 2013)); (b) Thalys bogies dimensions (adopted by (Degrande and Schillemans, 2001)).

3.5. *Numerical model details*

In this section, the proposed numerical approach is presented, which has been used in order to predict the HST-induced vibrations. As mentioned in the previous sections, the moving loads approach has been used to minimize the computational cost. According to Feng et al. (2017), this approach leads to comparable results to the most commonly used,

more detailed multi-body approach (Connolly et al., 2013). In the present investigation, an asymmetric finite/infinite element model (see Figure 3.9) has been developed utilizing commercial software ABAQUS (2014) in order to examine the vibrations due to HST passage. A user-developed Vdload subroutine has been implemented in order to simulate HST multiple moving loads. This numerical modelling approach can provide reliable results, as in the sequence, it is validated with field measurements from Paris-Brussels HSR line sites in Belgium. In order to minimize the computational cost, a part of the model has been used due to symmetry along the vertical direction of the track.

For the purpose of validation, the three sites at Paris- Brussels HSR, as they have been described in the previous sections, have been simulated. Figure 3.9 presents the finite/infinite 3D numerical model, which has been developed to simulate the examined problem in the case of soil embankment and cutting. All the examined sites models consist of two parts: the finite and the infinite. The finite part is located at the center of the model and has dimensions equal to 50 m in the longitudinal and horizontal directions and 20 m in the vertical direction. A relevant parametric study has been performed, in which it has been discovered that increased dimensions of the finite-element domain do not alter the results due to the presence of the surrounding infinite elements. Note that even smaller geometry dimensions have been used in similar studies (Khan and Dasaka, 2019).

The rail has been modeled as an Euler Bernoulli beam with a rectangular section with dimensions 0.153 m x 0.078 m running across the length of the modeled track. A typical UIC60 section, commonly used in Thalys HSR track, has been assumed for the rail. The rail has a mass of 60 kg/m and is fixed to reinforced concrete sleepers with dimensions 0.242 m x 0.2 m x 2.42 m. Three-dimensional solid elements have been used to model the track components (sleeper, ballast, sub-ballast and subgrade). The sleepers have been placed along the rail with a spacing equal to 60 cm. All track components are assumed as linear elastic materials and their properties are listed in Table 3.4. The soil density (ρ) is equal to 2000kg/m³ for all the examined soil layers. Furthermore, according to the density and the wave velocities, the Shear modulus (G), the poison ratio (v) and the Young's Modulus have been calculated as follows (see Table 3.5):

$$G = V_S^2 \rho \tag{3.4}$$

$$V_P = \sqrt{\frac{2G(1-v)}{\rho(1-2v)}} \tag{3.5}$$

$$E = 2G(1 + v) \tag{3.6}$$
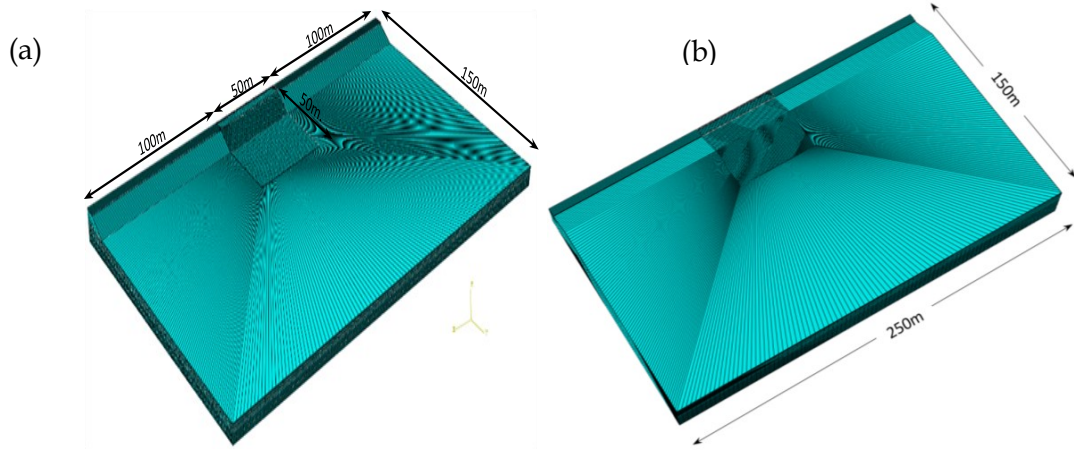
Figure 3.9 Finite/infinite 3D numerical model: (a) embankment, (b) cutting.

Table 3.4 Parameters of the examined HSR model.

Track Part	Layer Thickness (m)	Young's Modulus (GPa)	Poisson's Ratio	Density (kg/m³)
Rail	-	210	0.25	7900
Sleepers	-	30	0.4	2400
Ballast	0.3	0.1	0.35	1800
Subballast	0.2	0.3	0.35	2200
Subgrade	0.5	0.127	0.35	2100

Table 3.5 illustrates the Poisson's ratio and the Young's Modulus, which is used in order to validate the numerical model with the field data. All the examined sites have quite similar soil layer profiles. More specifically, the upper silty layers are led on deposits of sand and lower layers as consisting of soft or stiff clay. In order to ensure the accuracy of the results, the element size has been properly selected. Generally, the element size of the examined FE model is small enough to allow the propagation of the vibrations in the examined frequency range. The FE size could be estimated from the smallest wavelength as (Galavi and Brinkgreve, 2014):

$$\lambda = \frac{c}{f_{max}} \tag{3.7}$$

where c is the velocity of waves in the medium and f_{max} is the highest frequency of interest.

Table 3.5 Soil layers Poisson's ratio and Young's Modulus.

Site 1: Embankment			Site 2: Cutting			Site 3: At-grade		
h (m)	v	E (MPa)	h (m)	v	E (MPa)	h (m)	v	E (MPa)
1.3	0.33	132	1.35	0.23	126	1.5	0.14	157
1.3	0.25	149	1.35	0.17	136	1	0.38	113
1.2	0.27	145	3.1	0.29	257	1.7	0.42	191
2.85	0.3	259	3.1	0.16	315	2.5	0.29	277
2.85	0.16	297	Inf.	0.29	3278	Inf.	0.33	419

3.6. *Preliminary investigation of soil damping properties*

For the modelling of all track components except for the rail, 8-node cuboidal finite elements with 0.2m length along each axis have been used, capable of predicting the vibration level according to Equation (3.8) for the examined frequency range. The rails have been simulated with Euler–Bernoulli beam elements with 0.1m lengths. One of the most important parameters in order to capture reliable results of induced vibrations at the far-field is the damping properties of the soil layers. As it was aforementioned, the damping coefficient (ξ) for each soil layer have been adopted by the in-situ measurements. On the other hand, Abaqus uses as inputs the mass and stiffness proportional Rayleigh damping coefficients. For this purpose, a preliminary investigation is required to select the optimal coefficients. Hence, soil damping has been defined utilizing the classical Rayleigh damping model. More specifically, the damping matrix has been calculated via the generalized equation of the Classical Rayleigh damping model:

$$[C] = a[M] + \beta[K] \tag{3.8}$$

where:

[C]: model damping matrix,

[M]: model structural mass matrix,

[K]: model structural stiffness matrix,

α: mass proportional Rayleigh damping coefficient,

β: stiffness proportional Rayleigh damping coefficient.

The optimal values of stiffness and mass proportional Rayleigh damping coefficient have been chosen, aiming to keep the damping curve close to the damping coefficient value (ξ) in the examined low-frequency range (10-50Hz). It should be mentioned that in

the cases of high damping coefficients (e.g., layer 1 of Site 3), the model is less accurate for low frequencies (<10Hz), in order to achieve a specific value of damping with very low variations within this pre-defined target frequency range, suitable values of the parameters in Equations (3.9) and (3.19) (i.e., very high values for ω_2 and ξ and a very low value of ω_1) have been used for the calculation of α and β. Table 3.6 shows the optimal values of damping coefficients for each soil layer. The mass and stiffness proportional Rayleigh damping coefficients, which are listed in Table 3.6, have been defined as follows (Nakamura, 2017):

$$\alpha = \frac{2\omega_i\omega_j(\xi_i\omega_j - \xi_j\omega_i)}{(\omega_j^2 - \omega_i^2)} \tag{3.9}$$

$$\beta = \frac{2(\xi_j\omega_j - \xi_i\omega_i)}{(\omega_j^2 - \omega_i^2)} \tag{3.10}$$

where:

ω_i: first frequency limit,

ω_j: second frequency limit,

ξ_i: hysteretic material damping ratio of the first frequency,

ξ_j: hysteretic material damping ratios of the second frequency.

Table 3.6. Soil layers Rayleigh damping coefficients.

Site 1: Embankment			Site 2: Cutting			Site 3: At-grade		
h (m)	α	B	h (m)	A	B	h (m)	α	β
1.3	11.9	0.0004	1.35	12	0.0004	0.8	15	0.00045
2.5	10.3	0.0003	1.35	10.3	0.0003	1.5	14	0.0004
2.85	10.3	0.0003	3.1	4.8	0.0002	1.5	14	0.0005
2.85	7.5	0.00023	3.1	7.5	0.00023	1.6	13	0.0004
						1.5	10.3	0.0003
Inf.	4.6	0.00015	Inf.	4.4	0.0002	5	6.2	0.0002
						Inf.	1.4	0.0001

3.7. *Examined model validation*

3.7.1. *Rail dominant frequencies investigation*

Before comparing the results with the field data, it is important to investigate the rail dominant frequencies. More specifically, the rail peak frequencies could be derived via

the dominant frequency method (Kouroussis et al., 2015b). This approach is based on the assumption that the rail Fourier spectrum depends on HST passing speed and bogies geometry. According to this method, the HST moving speed and the dimensions of the HST bogies define the shape of the response spectrum of the theoretical rail deflections, i.e., the so-called quasi-static deflections (Kouroussis et al., 2014a). Several fundamental frequencies are defined according to this methodology, such as the fundamental bogie passage frequency, $f_{b,n}$, with zero amplitude at frequencies $\frac{2k+1}{2}f_b$ (where $k \in \mathbb{N}$), the fundamental axle passage frequency, f_a, with zero amplitude at frequencies $\frac{2k+1}{2}f_a$ and the sleeper passing frequency, f_s. The fundamental passage frequencies are calculated from (Kouroussis et al., 2015):

$$f_{b,n} = n\frac{V_0}{l_b} \tag{3.11}$$

$$f_a = \frac{V_0}{l_a} \tag{3.12}$$

$$f_s = \frac{V_0}{l_s} \tag{3.13}$$

where l_b is the bogie distance, l_a is the axle distance, l_s is the sleeper bay, n=1,2,3,..., and v_0 is HST moving speed. Thompson et al. (2019) demonstrated the amplitude modulation at f_a, with zero amplitude at frequencies $\frac{2k+1}{2}f_a$, and noted that this "beating" effect represents a single bogie force moving at speed equal to v_0. In the first examined case, Thalys passing speed from Site 1 is equal to 78.9 m/s and the distance of the bogie axle is 18.7 m; thus, from (3.11), $f_{b,1}$ is equal to 4.22 Hz for Thalys passage.

As shown in Figure 3.10a, the bogies passing frequency are well captured. These frequencies are also depicted in the obtained Fourier spectrum. Especially, the sleeper passing frequency is the most important frequency at the high-frequency range (f_s=138.9Hz). It should be mentioned that these frequencies are commonly investigated at small distances from the track and are attenuated at higher distances from the railway. Furthermore, the sleeper passing frequency is quite high and it is not captured by the numerical model at remote distances (>15 m from the track) due to soil material damping. In the case of Thalys passing from Site 2, the operating speed is equal to 83.05 m/s; thus, $f_{b,1}$ is equal to 4.44Hz. The dominant passing frequencies are captured from the numerical model, as illustrated in the Fourier spectra in Figure 3.10b.
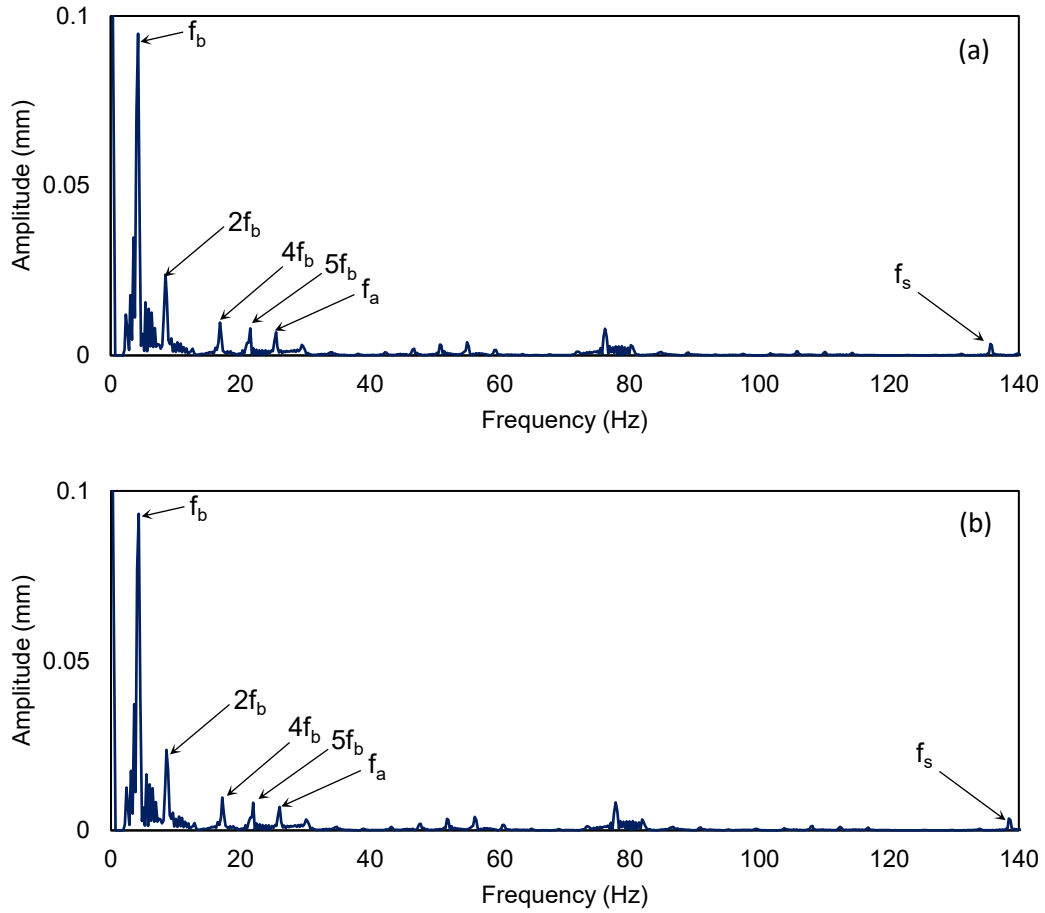
Figure 3.10 Fourier spectrum of rail deflection during the passage of (a) Thalys HST for the passing speed of 284 km/h, (b) TGV HST for the passing speed of 290 km/h from site 1 (embankment).

3.7.2. *Vertical velocity and Fourier Spectra validation*

In this section, the accuracy of the numerical model of the existing embankment from Thalys Paris–Brussels line, North-East of the town of Braffe, has been validated by comparing the numerical results with in situ measurements. More specifically, the induced vibrations by Thalys and TGV passage with speed equal to 284km/h and 290km/h have been examined. A comparison between field data and numerical calculations regarding the velocity time-histories at several distances (i.e., 15 m, 19 m, 23 m, 27 m, 31 m and 35 m from the track) has been carried out. The observation points are categorized into three groups, near (15m, 19m), middle (23m, 27m) and far-field (31m, 25m). The time histories of vertical velocity and the Fourier spectra have been compared in all the examined points with the in-situ measurements in order to ensure the accuracy of the results.

63

In the sequence, the validation of the proposed approach is expanding in the case of a train passing from a railway cutting (e.g., Site 2). As it was aforementioned, in this case, Thalys HST is passing with 297km/h (see Table 3.2). The comparison of the numerical results and the field data has been carried out at the same observation points with Site 1 (e.g., 15m, 19m, 23m, 27m, 31m and 35m from the track) are investigated. It should be mentioned that in this case, near field positions (e.g., 15m and 19m from the track) are located on the slope of the cutting. Lastly, the same results have been captured for the passage of Thalys HST from Site 3 (at grade) for passing velocity equal to 299km/h.

Figure 3.11 Thalys HST passage from Site 1: Comparison of field data and numerical results in terms of vertical velocity time-histories: (a) at 15 m, (b) at 19 m from the track.

3.7.2.1. *Site 1: Thalys HST passage*

The numerical results of the Thalys HST passage from Site 1 are presented. It can be noticed that the numerical results are in agreement with the available field measurements. Especially at the near-field locations (i.e., close to the track), the numerical time-histories are very close to the corresponding records. Figure 3.11 presents the time histories at 15m and 19m from the track, similar to the in-situ measurements. For instance, the peak vertical velocity at 15m is equal to 1.3mm/s according to field data, while the numerical value is 1.1mm/s. Moreover, due to the higher weight of the first and the last carriages (traction cars), a higher near-field ground response has been observed when those carriages are passing, captured by the numerical model. Furthermore, at 19m from the track, the accuracy of the numerical results is even higher. In this case, the peak vertical velocity of the field data is equal to the numerical results, close to 0.6mm/s and the shape of the time histories are similar.

Figure 3.12 Thalys HST passage from Site 1: Comparison of field data and numerical results in terms of vertical velocity time-histories: (a) at 23m, (b) at 27m from the track.

Figure 3.13 Thalys HST passage from Site 1: Comparison of field data and numerical results in terms of vertical velocity time-histories: (a) at 31 m, (b) at 35 m from the track.

The same observation is made at the middle field positions (e.g., 23m and 27m from the track), as illustrated in Figure 3.12. At 23m from the trach, the timing of the time hibase has been well captured by the model. Furthermore, the amplitude of the time hibase, in general, is close to the numerical results. However, there are some peak values, which have not been capture from the model. For instance, at 1.8s, the vertical velocity is close to 0.7mm/s, according to the field data. On the other hand, the vertical velocity remains at the whole time hibase below 0.5mm/s, according to the numerical results. Figure 3.12b demonstrates the vertical velocity time histories at 27m from the track. Herein, the vertical velocities have been minimized below 0.5mm/s. The numerical model has captured the shaping and the timing of the time hibase. Figure 3.13 illustrates the vertical velocity time histories in the case of far-field locations. In this case, the time-histories are also similar to the field data and -as expected- exhibit much less values compared to near-field. However, there is a more significant difference between field data and numerical values. For

example, the peak vertical velocity at 35 m from the track is recorded to be equal to 0.27 mm/s, while the numerical value is 0.19 mm/s.

Apart from the time histories, it is crucial to investigate the most critical vibrations for adjacent structures, infrastructure and the population close to HSR. Based on international standards, low-frequency vibrations are the most critical ones (Kouroussis et al., 2011). Accordingly, the Fourier spectra at all the examined positions (see Figures 3.14 - 3.16) present a good agreement between field data and numerical calculations. The numerical model has successfully captured the vibrations peaks in the low-frequency range between 10 and 40 Hz. The main frequencies (21.4 Hz and 25.2 Hz) are the same at all the examined distances and there is a satisfactory correlation between the numerical results and the field data. It should be mentioned that the most dominant frequency at 25.2 Hz is close to the axle passing frequency. Furthermore, some lower peaks at several frequencies (16.7 Hz,29.6 Hz, 34 Hz) are also numerically validated. In the case of the near field, the vibrations peaks are close to the field data. As mentioned, the most dominant frequencies at 21.4 Hz and 25.2 Hz are the same at both the examined positions (see Figure 3.14). The vibrations peaks at 15m are equal to 0.29mm/s and 0.32mm/s, respectively. Those values are significantly reduced at 19m from the track. In his case, the vibrations peaks are reduced under the 0.1mm/s for both dominant frequencies.
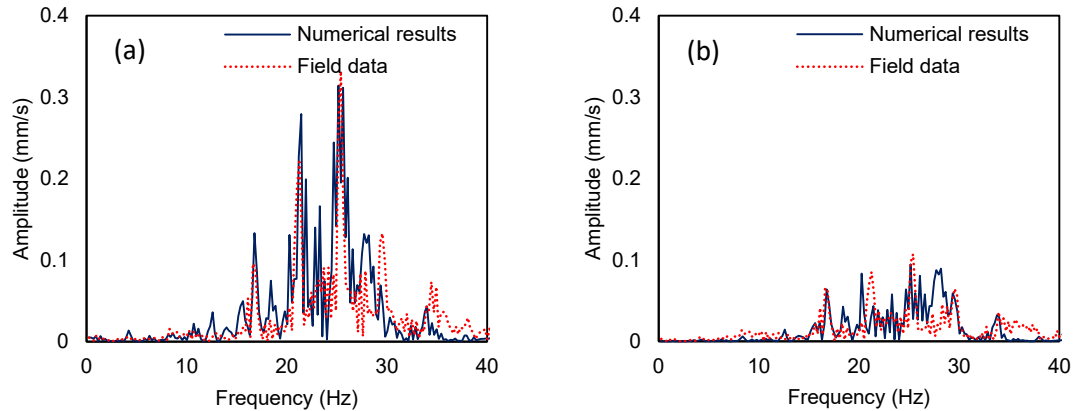
Figure 3. 14 Thalys HST passage from Site 1: Comparison of field data and numerical results in terms of vertical velocity Fourier spectra: (a) at 15m, (b) at 19m from the track.

Figure 3.15 depicts the vibrations peaks at the middle field as they have been successfully captured. In this case, the field data middle dominant frequencies (e.g., 21.4 Hz, 25.2 Hz) remain close to 0.1mm/s. Except for those frequencies, the vibrations peaks at 16.7Hz, 29.6Hz and 34Hz are also close to 0.1mm/s. It should be mentioned that the vibration peaks at 23m and 27m from the track have similar values. Hence, the assumption

could be made that the damping rate is lower in the middle field. Concluding, the numerical model is valid in the middle field. Figure 3.16 shows the Fourier spectra of vertical velocities at the far-field from the track. Specifically, as shown in Figure 3.16a, the convergence of the predicted vibrations with the field measurements is very high in the whole examined range at 31 m from the track.
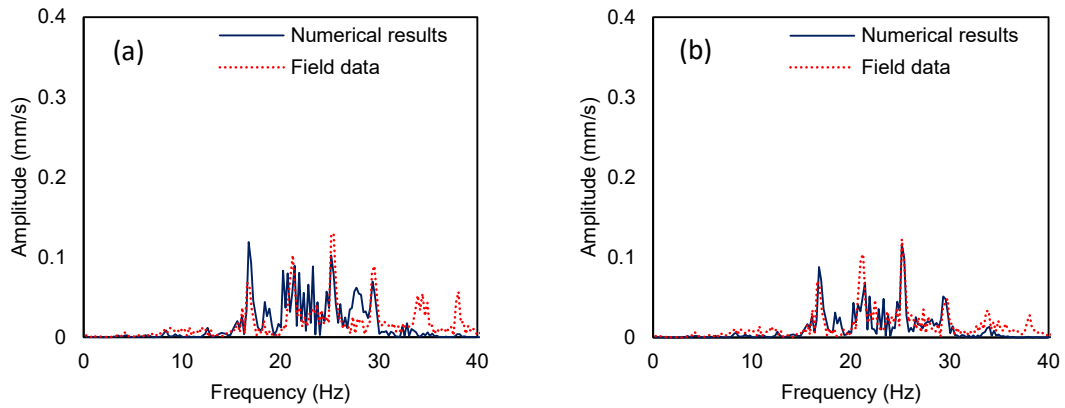
Figure 3.15 Thalys HST passage from Site 1: Comparison of field data and numerical results in terms of vertical velocity Fourier spectra: (a) at 23 m, (b) at 27 m from the track.
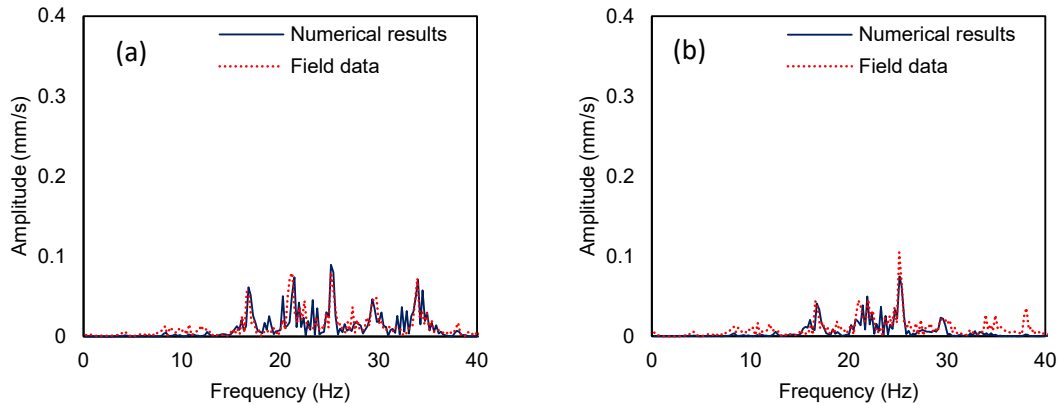
Figure 3.16 Thalys HST passage from Site 1: Comparison of field data and numerical results in terms of vertical velocity Fourier spectra: (a) at 31m, (b) at 35m from the track.

In addition, the spectral velocities are lower than the same values in the middle field positions. More specifically, at the whole low-frequency range, the spectral velocities remain below 0.1 mm/s. At 35m from the track, the spectrum has significantly decreased. Herein, except for the most dominant frequency at 25.2Hz, where the spectral velocity remains close to 0.1mm/s, in the rest of the spectrum, the spectral velocity remains below 0.04mm/s.

3.7.2.2. *Site 1: TGV HST passage*

In the sequence, the passage of a second HST from Site 1 has been examined in order to expand the validation. More specifically, the passage of TGV at the same embankment with a velocity equal to 290km/h has been investigated. TGV has identical geometry with Thalys; hence the time-histories are similar to the diagrams of the previous section. Fig 3.17 depicts the time histories at the near field, where it is clearly illustrated, the numerical results are in good agreement with the field data from Site 1. More specifically, the peak vertical velocity is close to 1.2mm/s for both the numerical model and the field measurements at 15m from the track. Furthermore, the duration of the event is the same (about 3.4s) as the in-situ measurements. In addition, similar to the passage of Thalys HST, when the heavier of the locomotive bogies are passing, higher vertical velocities have been observed. Figure 3.17b illustrates the vertical velocity time histories at 19m from the track. The convergence between the numerical results and the field data is remarkable at 19m from the track. The peak values and the shape of the two time-histories are notably similar.
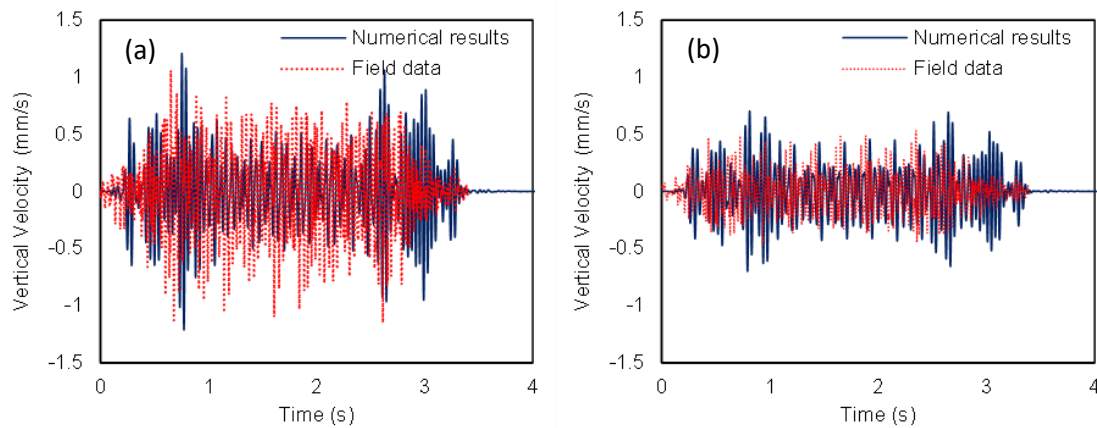
Figure 3.17 TGV HST passage from Site 1: Comparison of field data and numerical results in terms of vertical velocity time-histories: (a) at 15 m, (b) at 19 m from the track.

The response of the soil at the middle field is presented in terms of vertical velocity time-histories in Figure 3.18. Again, the numerical results are significantly close to the in-situ measurements. At 23m from the track, the peak vertical velocity of the numerical results is slightly lower than the field measurements, although the shaping and the duration are similar. The difference of the peak vertical velocity is minimized at 27m from the track. Herein, the peak vertical velocity value is equal to 0.48 mm/s according to the in-situ measurements and 0.41 mm/s according to the numerical results. The vertical velocity time histories at the far-field locations (31m and 35m from the track) in the case of HST TGV passage are depicted in Figure 3.19. In this case, the numerical results are

close to the field data, although similar to the case of Thalys passage, the peak vertical velocity according to the numerical data is just 0.19mm/s in contrast to the field record this value is equal to 0.31mm/s.
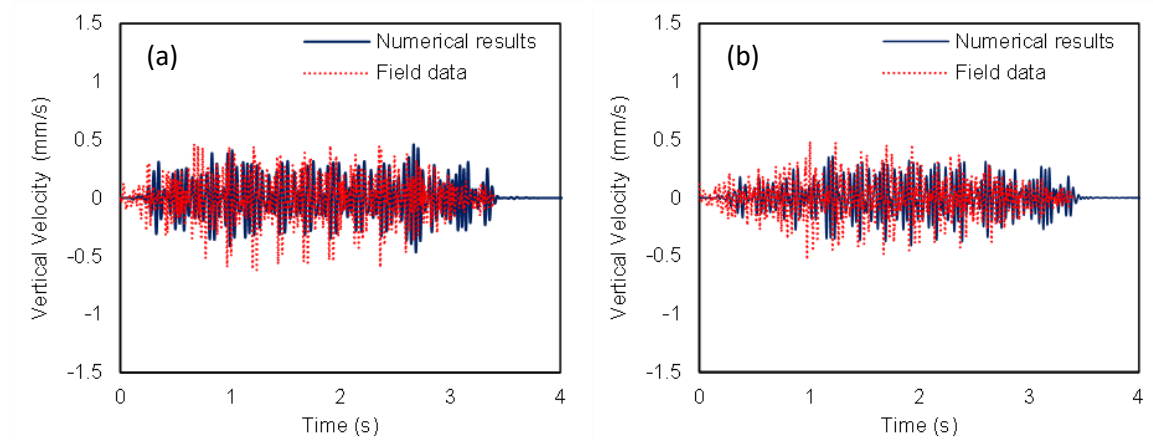
Figure 3.18 TGV HST passage from Site 1: Comparison of field data and numerical results in terms of vertical velocity time-histories: (a) at 23m, (b) at 27m from the track.
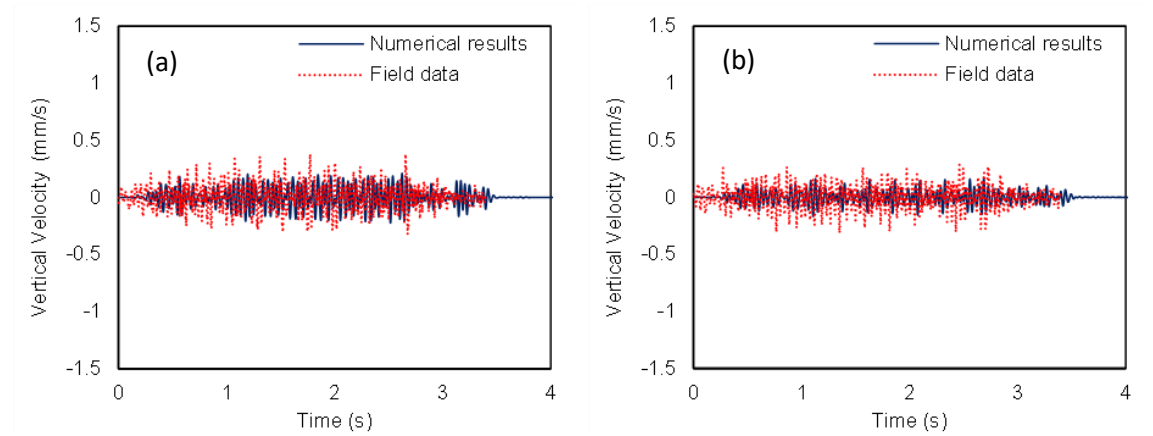
Figure 3.19 TGV HST passage from Site 1: Comparison of field data and numerical results in terms of vertical velocity time-histories: (a) at 31 m, (b) at 35 m from the track.

Subsequently, the response of the subsoil has been investigated in terms of Fourier spectra. In this modeling scenario, the TGV HST is passing faster than the passage of Thalys HST. More specifically, according to the in-situ measurement, TGV is passing with 6km/h higher speed than Thalys HST. For this reason, the most dominant vibration peaks have been moved to higher frequencies. According to the field data, the most dominant peak has been located at 25.8Hz for all the examined positions. Furthermore, three more vibrations peaks have been observed at 17.1Hz, 21.7Hz and 30Hz. Figure 3.20a illustrates the comparison of the field data and the numerical model Fourier Spectra at 15m from the track. The model has well captured the most dominant vibration peak at 25.8Hz. The

spectral velocity at this frequency is equal to 0.33mm/s according to the field measurements and 0.34mm/s according to the numerical model.
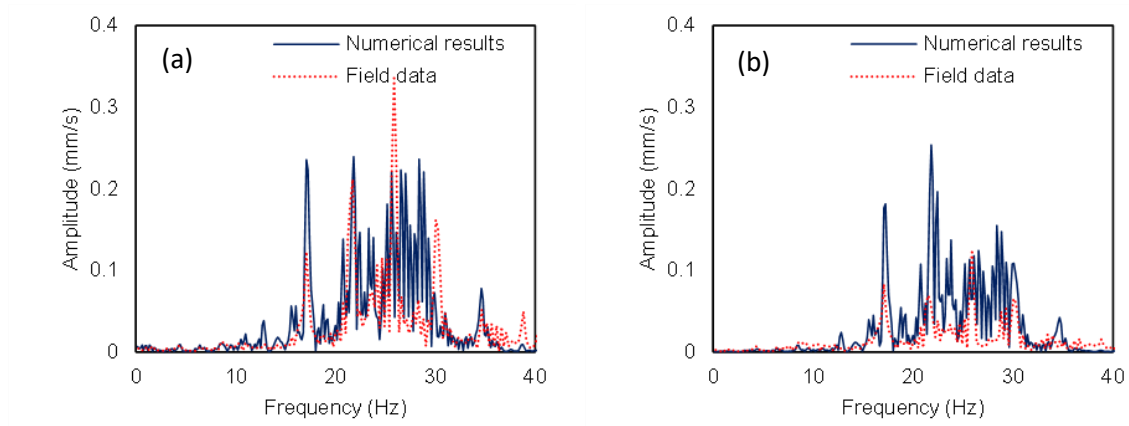
Figure 3.20 TGV HST passage from Site 1: Comparison of field data and numerical results in terms of vertical velocity Fourier spectra: (a) at 15m, (b) at 19m from the track.

The same observation is made for the dominant frequencies at 17.1Hz, 21.7Hz. In those cases, the captured spectral velocity is remarkably close to the field data. On the other hand, the vibrations peak at 30Hz according to the field data has been slightly moved to lower frequencies than the numerical results. The vibrations peaks remain at the same frequencies, although they are significantly lower at 19m from the track (see Figure 3.20b). The dominant peak at 25.8Hz has been reduced to 0.12mm/s and all the other peaks remain lower than 0.1mm/s. The numerical model has captured well the vibrations peaks at the whole examined low-frequency range.
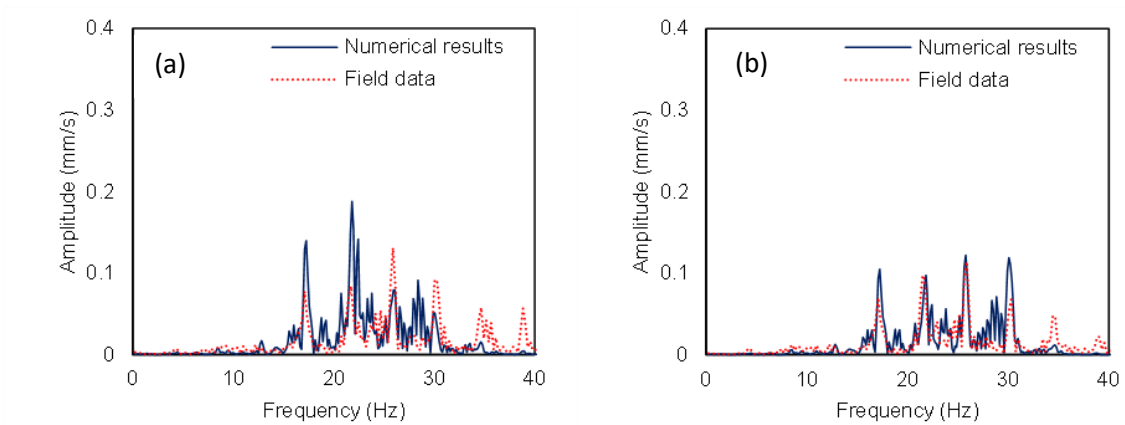
Figure 3.21 Thalys HST passage from Site 1: Comparison of field data and numerical results in terms of vertical velocity Fourier spectra: (a) at 23m, (b) at 27m from the track.

In the sequence, the validation of TGV passage has been examined in terms of Fourier spectra at middle field positions. Figure 3.21 illustrates the Fourier spectra at 23m and 27m

from the track; as observed, the soil response at those positions is not significantly altered compared with 19m from the track. The vibrations peaks remain at the same frequencies and the spectral acceleration of those peaks is close to 0.1mm/s. It should be mentioned that the vibrations peaks at the lower dominant frequencies (e.g., 17.1Hz and 21.7Hz) according to the field data are slightly lower than the captured spectral velocities by the numerical model at 23m from the track as it is presented in Figure 3.21a. For instance, the captured value of the spectral velocity at 17.1Hz is equal to 0.08 mm/s in comparison with 0.1 mm/s, according to the field data. The opposite phenomenon is observed at the two higher dominant frequencies, at 25.8 Hz and 30 Hz. In those cases, the vibration peaks according to the numerical model are slightly lower than the in-situ measurements.

As illustrated in Figure 3.21b, the accuracy of the numerical model is even higher at 27m from the track. More specifically, the vibration peaks at 21.7Hz and 25.8Hz of the numerical results and the field measurements are almost identical. Figure 3.22 shows the comparison between the Fourier spectra of the field data and the numerical results at the far-field positions. All the vibration peaks are significantly reduced in comparison with the middle field results. The vibration peaks remain lower than 0.1mm/s at all the vibration peaks at the whole examined low-frequency range for distances higher than 31m. It could be concluded that the proposed numerical approach can simulate the propagation of the induced vibration accurately by both TGV and Thalys HST at Site 1.
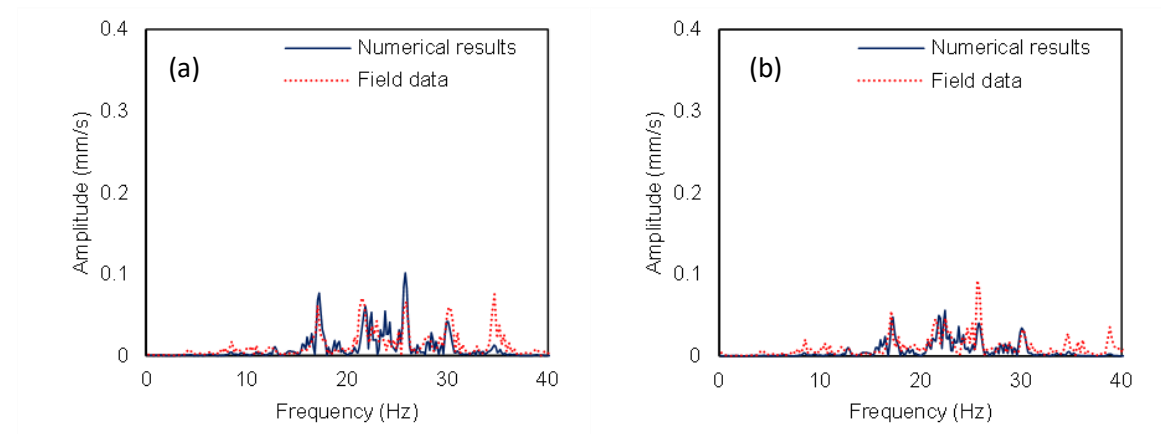
Figure 3.22 Thalys HST passage from Site 1: Comparison of field data and numerical results in terms of vertical velocity Fourier spectra: (a) at 31m, (b) at 35m from the track.

3.7.2.3. *Site 2: TGV HST passage*

Similar to Site 1, pre-available field data have been used to assess whether the numerical model can accurately predict the HST-induced vibrations at Site 2 (cutting site) in Braffe,

Belgium, during the passage of HST (Kouroussis et al., 2016). The numerical simulation has generated a series of vertical velocity time histories in varying distances between 15m and 35m from the railway track. Figure 3.23 presents indicative vertical velocity time histories at the near field, at 15m and 19m from the track. At 15m from the track, the numerical model captures the shape and the timing of the time hibase, although the peak values are lower than the field data. Figure 3.23b demonstrates the same values at the second observation position, at 19m from the track. Herein, the amplitude of the time hibase is significantly closer to the field data.
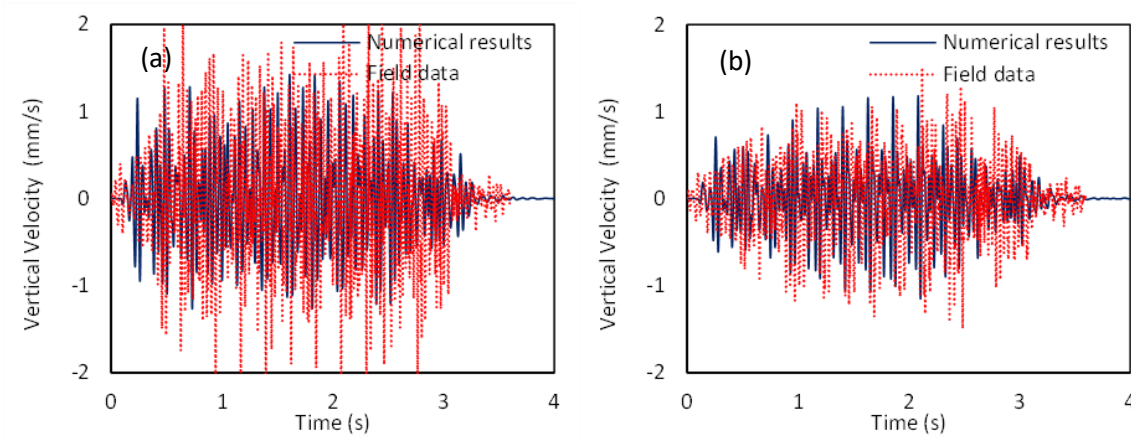
Figure 3.23 Thalys HST passage from Site 2: Comparison of field data and numerical results in terms of vertical velocity time-histories: (a) at 15 m, (b) at 19 m from the track.
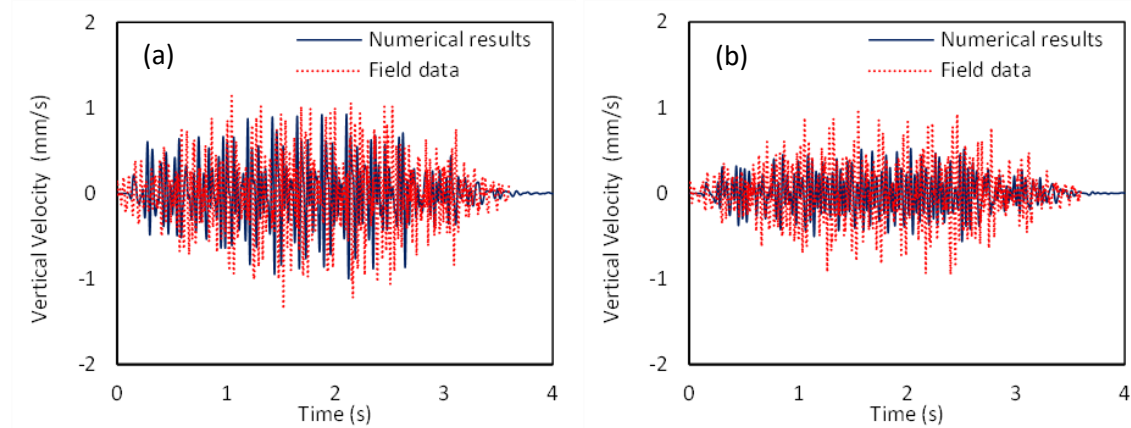
Figure 3.24 Thalys HST passage from Site 2: Comparison of field data and numerical results in terms of vertical velocity time-histories: (a) at 23 m, (b) at 27 m from the track.

The vertical velocity time histories at the middle field locations, at 23m and 27m from the track, are presented in the sequence. In this case, the convergence of results is even more pronounced in comparison with the near field. More specifically, in the middle of the time hibase, the vertical velocities are approximately 1.05mm/s and 0.9mm/s at 23 m and 27 m from the track, respectively. As it is clearly illustrated in Figure 3.24, the

numerical values are in good agreement with the in-situ measurements. The same observation is made at the far-field positions, as it is illustrated in Figure 3.25. More specifically, the peak vertical velocity at 31m from the track according to the numerical data is equal to 0.45mm/s, close enough to the 0.48mm/s according to the in-situ measurements. It could be concluded that the proposed numerical approach is capable to reliably capture the vertical velocity time histories in the modeling scenario for which Thalys HST is passing from Site 2, in a big range of distances between 15m and 35m from the track.
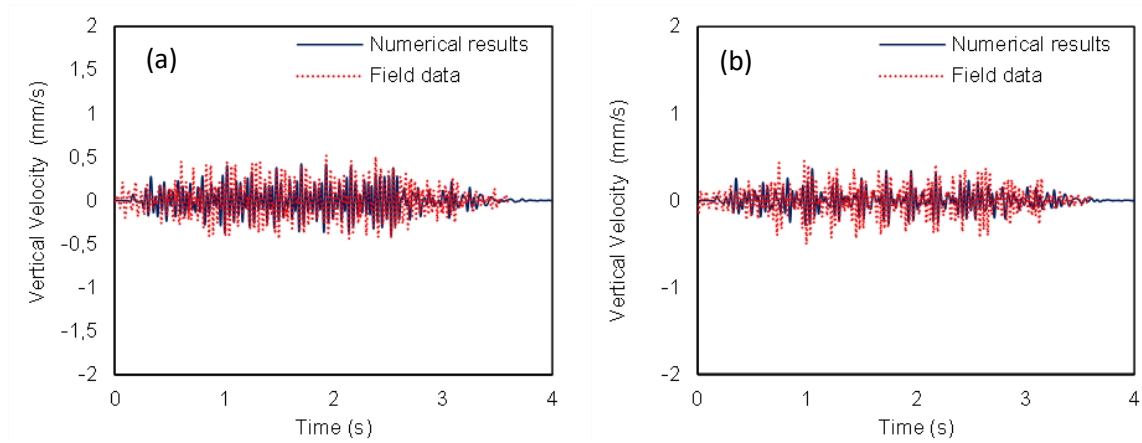
Figure 3.25 Thalys HST passage from Site 2: Comparison of field data and numerical results in terms of vertical velocity time-histories: (a) at 31 m, (b) at 35 m from the track.

Similarly, the frequency content has been well represented, with the dominant frequencies being located close to 30Hz. More specifically, the main frequency at 26.4Hz is the same at all examined distances and has been well identified by the numerical model. Furthermore, the secondary frequency peaks (e.g., 17.7Hz, 22.4Hz, 30.2Hz) also exhibit a satisfactory matching. As it is illustrated in Figure 3.26, the vibrations peak at the dominant frequency is equal to 0.6mm/s and 0.5mm/s at 15m and 19m from the track, respectively. Furthermore, the secondary vibration peaks in the near field are between 0.2mm/s and 0.4mm/s at 15m from the track. The vibrations peaks are located at the same frequencies as the field data. Furthermore, the first two peaks at 17.7Hz and 22.4Hz have been captured by the model. The last peak at 30.2Hz has been capture, although its amplitude is significantly lower than the field data. Figure 3.26b shows the Fourier spectra at 19m from the track. In this case, the vibration peaks are located at the same positions as the previously examined observation position. Herein, all the vibrations peaks are captured by the model.

.
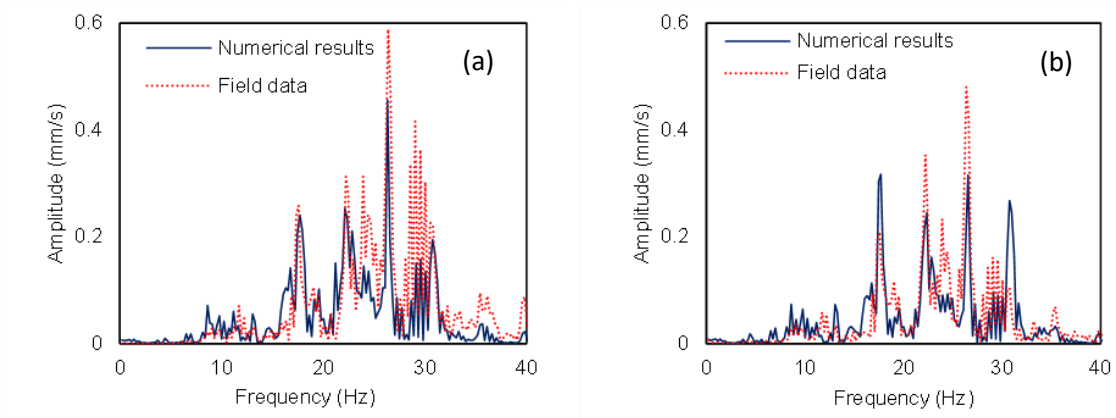
Figure 3.26 Thalys HST passage from Site 2: Comparison of field data and numerical results in terms of vertical velocity Fourier spectra: (a) at 15 m, (b) at 19 m from the track.
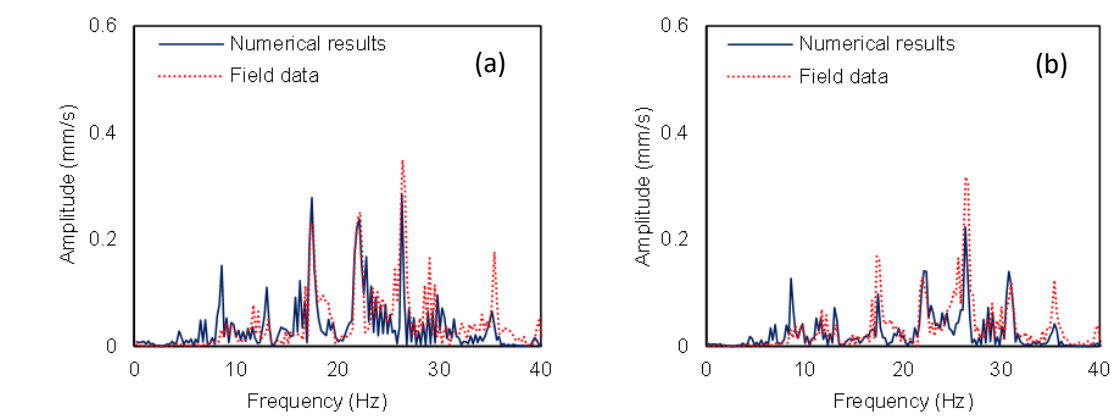
Figure 3.27 Thalys HST passage from Site 2: Comparison of field data and numerical results in terms of vertical velocity Fourier spectra: (a) at 23m, (b) at 27m from the track.
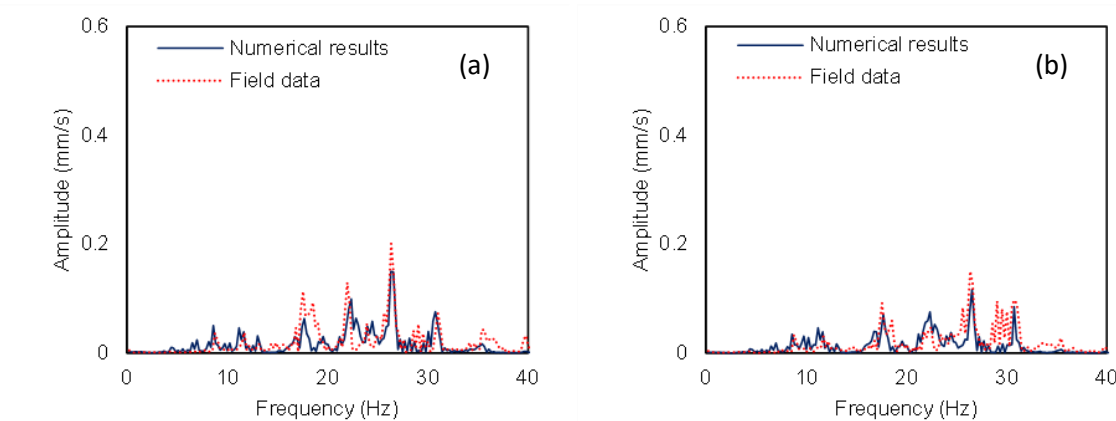
Figure 3.28 Thalys HST passage from Site 1: Comparison of field data and numerical results in terms of vertical velocity Fourier spectra: (a) at 31m, (b) at 35m from the track.

The vibrations peaks remain at the same frequencies at the middle field as the observation points at the near field. It should be mentioned that the amplitude at the most dominant frequency has been significantly reduced below 0.4mm/s. It is obvious from

Figure 3.27 that all the other vibrations peaks at the examined frequency range have also been significantly reduced. Especially at 27m from the track, the vibrations peaks at 17.7Hz, 22.4Hz and 30.2Hz from the track have been minimized below 0.2mm/s. The numerical model is in good agreement with the field data at the middle field positions. Figure 3.28 illustrates the vertical velocity Fourier spectra at the far-field positions. At 31 m from the track, the vibrations level has been significantly minimized at the bigger part of the examined frequency range. Nevertheless, the vibrations peak at the dominant frequency remains close to 0.2mm/s. Furthermore, the vibrations peaks at the secondary frequencies at 19.2Hz and 22Hz have been minimized below 0.1mm/s. Respectively, at 35m from the track, the dominant frequencies remain the same. According to the numerical results, the position and amplitude of the vibrations peaks at the examined low-frequency range are quite close to the field data.
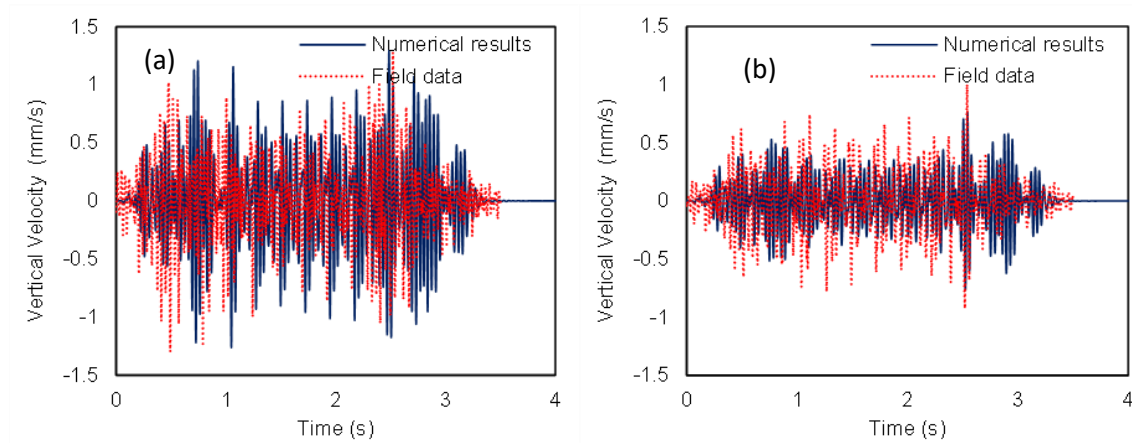
Figure 3.29 Thalys HST passage from Site 3: Comparison of field data and numerical results in terms of vertical velocity time-histories: (a) at 15 m, (b) at 19 m from the track.

3.7.2.4. *Site 3: Thalys HST passage*

In this section, the vertical velocity time histories at the last examined site (Site 3: at grade) for the passage of Thalys HST with 299km/h are presented. It should be mentioned that the main difference between Site 3 with the previously validated sites is the mechanical properties of the upper soil layer. More specifically, the damping ratio is equal to 10.5% compared to 7.4% and 7.75% at Site 2 and Site 3, respectively. For this reason, a higher reduction of the vibration level is expected at the fairest observation points. Figure 3.29a compares the field data and the numerical results in terms of vertical velocity time histories. The timing and the shaping of the time hibase are in good agreement with the field data. More specifically, the peak vertical velocity is equal to 1.3mm/s at 15m from the track, according to both numerical results and numerical data. According to the

numerical results, the agreement with the in-situ measurements is even more pronounced at 19m from the track (see Figure 3.29b), although the peak vertical velocity, according to the numerical results, is slightly lower than the field data.
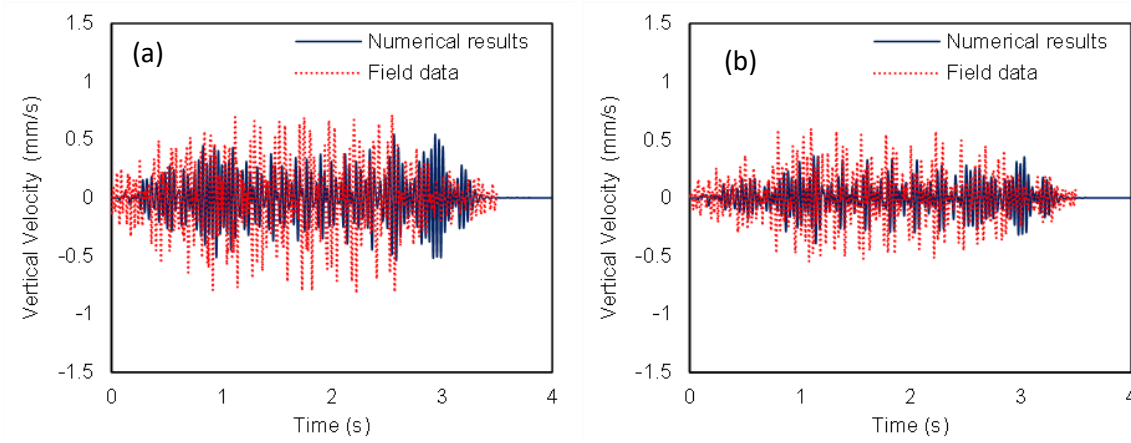
Figure 3.30 Thalys HST passage from Site 3: Comparison of field data and numerical results in terms of vertical velocity time-histories: (a) at 23 m, (b) at 27 m from the track.

At the middle observation positions, at 23m and 27m from the track, the shaping and the timing of the time hibase still agree with the numerical data (see Figure 3.30). At 23m from the track, the peak vertical velocity is equal to 0.7mm/s compared to the field data, where this value is just 0.5mm/s. The shaping of the time hibase is similar to the field data at 27m from the track, although there is a significant difference at the peak values of the numerical and field time histories. Especially in the middle of the time hibase, the captured vertical velocities from the numerical results, in some cases, are about 40% lower than the field data. As mentioned, the reason for those reduced values is the high damping ratio of the soil in this site.
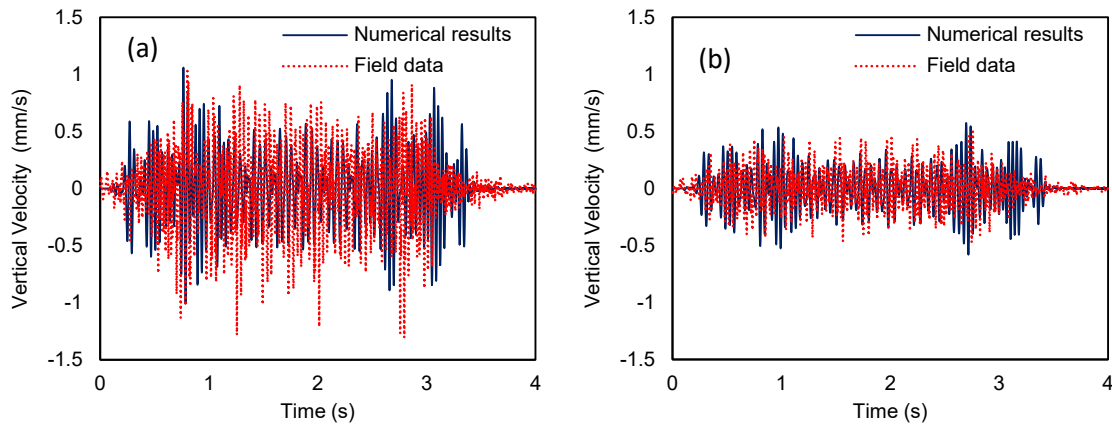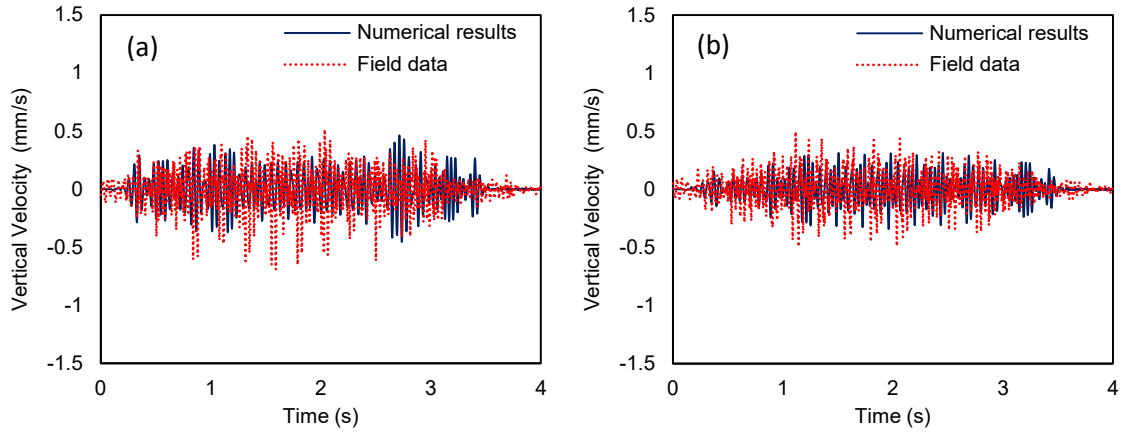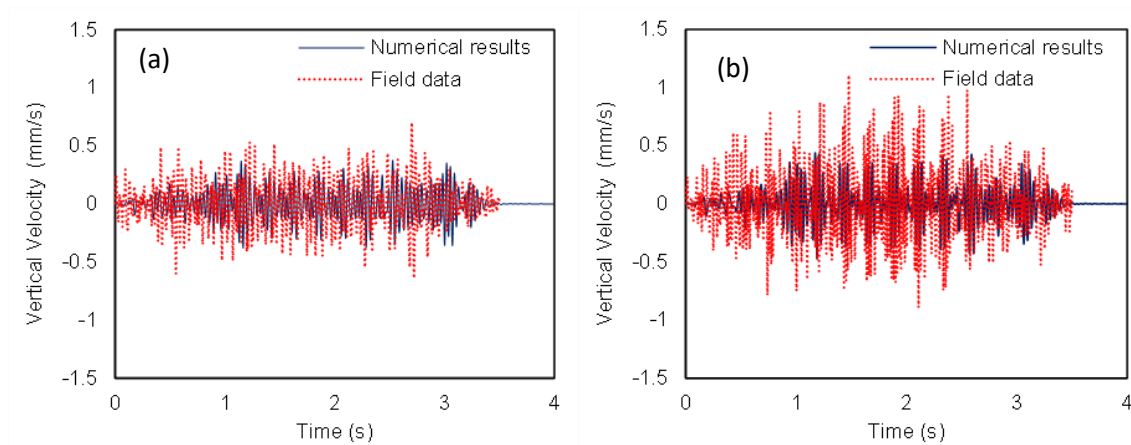

Figure 3.31 Thalys HST passage from Site 1: Comparison of field data and numerical results in terms of vertical velocity time-histories: (a) at 31 m, (b) at 35 m from the track.

The same observation is made at the far-field as it is illustrated in Figure 3.31. The time hibase mean amplitude at 31m from the track has been slightly underestimated due to the modelling of the soil damping. More specifically, the peak vertical velocity is close to 0.7mm/s, according to the field data. The same value has been computed just 0.4mm/s, according to the numerical results. At 35m from the track, the recorded time hibase in the field is significantly higher than all the closer observation points. This phenomenon is not reasonable; hence the assumption has been made that the high recorded level of vibration may be due to a possible change of the soil properties in this position or a secondary vibrations source, irrelevant with the passage of the HST.
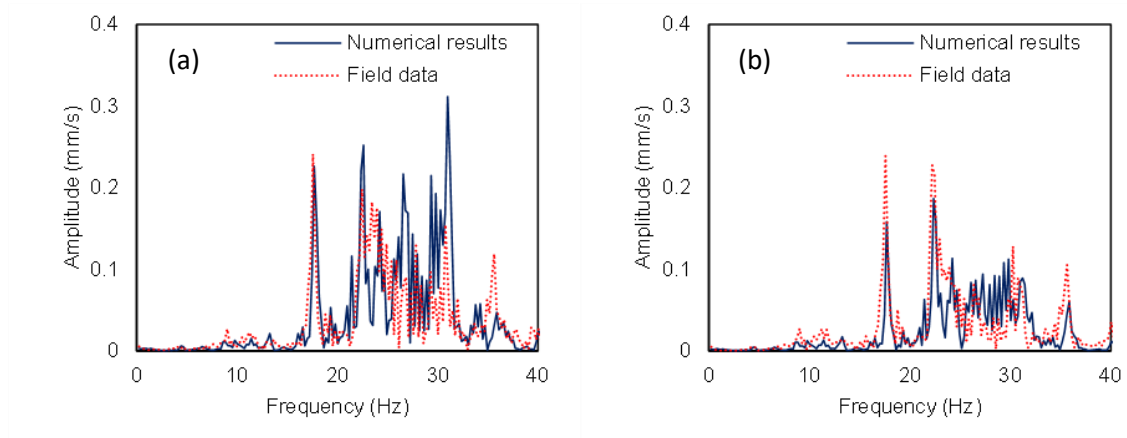
Figure 3.32 Thalys HST passage from Site 1: Comparison of field data and numerical results in terms of vertical velocity Fourier spectra: (a) at 15m, (b) at 19 m from the track.

Figure 3.32 depicts the comparison of the field data and numerical model in terms of Fourier spectra at the near field. There is a high correlation between the numerical results and the field data. The most dominant frequency peaks are located at 17.6Hz, 22.6Hz and 30.8Hz at both near field positions. Furthermore, a slightly lower secondary peak is observed at 35.7Hz, according to the field data. The numerical model accurately captures the locations of the vibrations peaks at the low-frequency range. At 15m from the track (see Figure 3.32a), the numerical model is slightly overestimating the vibrations peaks at 22.6Hz and 30.8Hz. Furthermore, at 19m, the correlation between the numerical results and the field data is even more pronounced. The location of the most dominant peaks remains at the same frequencies as the near field positions. The numerical model has captured the position of the vibrations peaks at 17.6Hz, 22.6Hz and 30.8Hz. It should be mentioned that the recorded amplitude according to the field measurements is higher than the predicted values according to the numerical model. This phenomenon is even more pronounced in the case of the vibrations peaks at 17.6Hz and 22.6Hz at 23m from the track,

where the field values are 50% higher than the numerical values. As mentioned, the reduced vibrations level could be attributed to the high damping ratio of the soil.
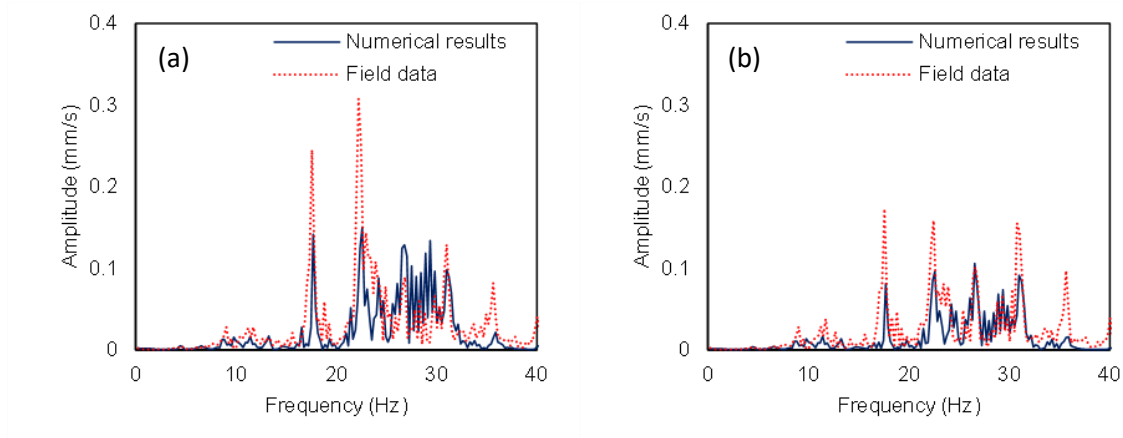
Figure 3.33 Thalys HST passage from Site 3: Comparison of field data and numerical results in terms of vertical velocity Fourier spectra: (a) at 23m, (b) at 27m from the track.
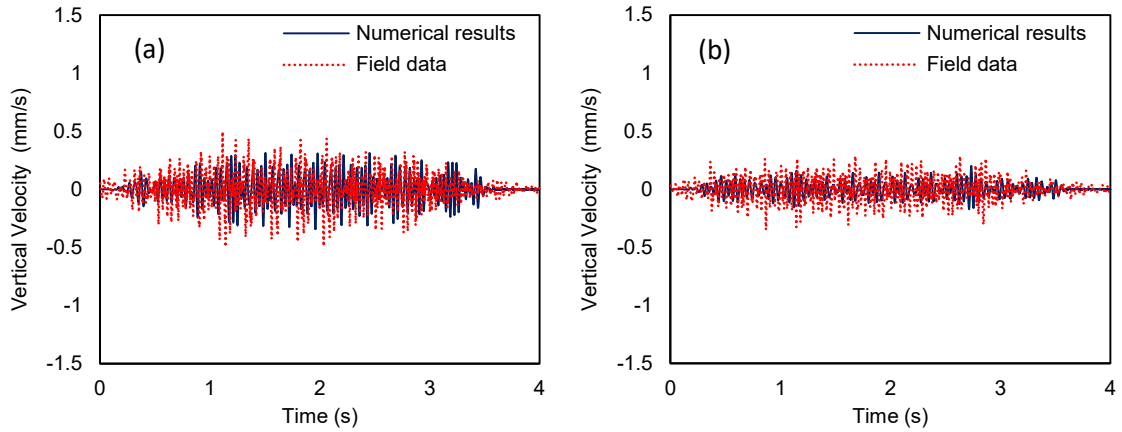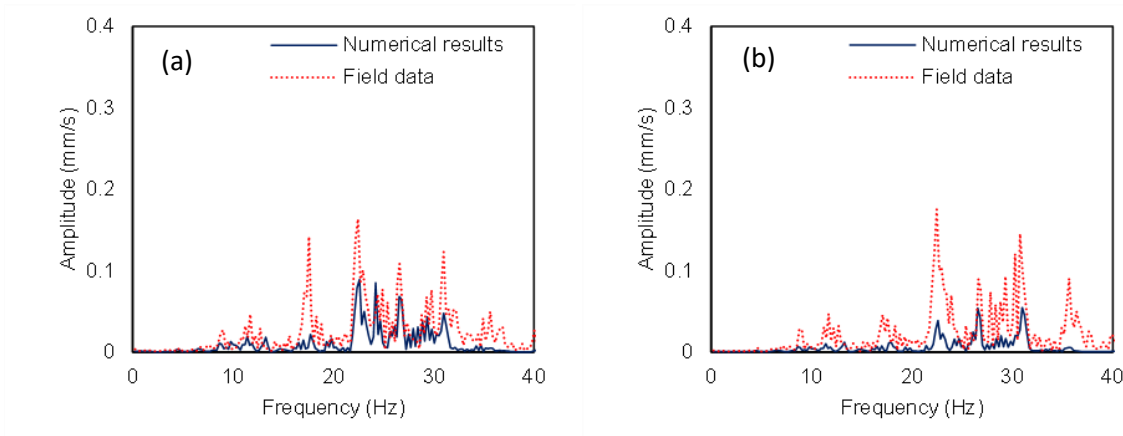

Figure 3.34 Thalys HST passage from Site 1: Comparison of field data and numerical results in terms of vertical velocity Fourier spectra: (a) at 31m, (b) at 35m from the track.

Figure 3.34 illustrates the Fourier spectra of vertical velocities at 31m and 35m from the track. The convergence of the predicted vibrations with the in-situ measurement is satisfactory in the whole examined range at 31 m from the track regarding the vibrations peaks. However, it is obvious that the numerical model slightly underestimates the amplitude of the vibrations peaks. The same observation could be made at 35m from the track (see Figure 3.34b). As mentioned, the authors are skeptical about field data at 35m from the track due to their suspiciously high vibrations levels. Concluding, in general, the numerical model is capable of predicting the HST-induced vibrations, especially in the near field in the case of Site 3.

3.7.3. *One third octave bands investigation*

In this section, a commonly used metric, the octave bands of the induced vibration, has been used in order to compare the numerical results with the pre-available field data. Accordingly, the vibrations frequency range is divided into unequal parts called octaves. Every next octave band central frequency is a doubling of the previous octave band centre frequency. Octave bands can be separated into three ranges - referred to as one-third-octave bands. As aforementioned, octaves are not linear scaled; hence higher-frequency bands are wider than lower-frequency bands. For this reason, the logarithmic center frequency (f_{cl}) of the octave band is always lower than the arithmetic mean frequency (f_{ca}). In the case of 1/3 octave bands, their center frequencies are approximately in the ratio 5:3. In this case, f_{cl} is calculated as follows (Pierce, 1989):

$$f_{cl} = 2^{1/6} f_a \qquad (3.13)$$

Table 3.7. 1/3 Octave Bands.

Band Number	Lower Band Limit (Hz)	Center Frequency (Hz)	Upper Band Limit (Hz)
1	1.12	1.25	1.41
2	1.41	1.6	1.78
3	1.78	2	2.24
4	2.24	2.5	2.82
5	2.82	3.15	3.55
6	3.55	4	4.47
7	4.47	5	5.62
8	5.62	6.3	7.08
9	7.08	8	8.91
10	8.91	10	11.2
11	11.2	12.5	14.1
12	14.1	16	17.8
13	17.8	20	22.4
14	22.4	25	28.2
15	28.2	31.5	35.5
16	35.5	40	44.7
17	44.7	50	56.2

Furthermore, the relationship between the lower (f_a) and the upper (f_b) frequency limit of each 1/3 octave band is defined as follows:

$$\frac{f_b}{f_a} = 2^{1/3} \qquad\qquad (3.14)$$

Table 3.7 summarizes the first 17 1/3 octave bands with central frequencies from 1.25Hz to 50Hz, which are examined in the case of the HST passing. As it was aforementioned, the present investigation is focused on the low-frequency range in order to evaluate the vibrations felt by the residents of nearby buildings and the users of nearby infrastructure and according to international standards that the low-frequency vibrations are considered as the most critical in terms of human exposure or buildings damage.

In the sequence, the velocity decibels (V_{db}) on each examined octave band central frequency have been calculated according to the following expression:

$$V_{db} = 20 \log_{10} \frac{V_{rms}}{V_0} \qquad\qquad (3.15)$$

where:

v_{rms}: root mean square of the spectral velocity at the center frequency of each 1/3 octave band,

v_0: the reference velocity level, equal to $5*10^{-8}$ m/s according to USDT (1998).

Figure 3.35 illustrates the one-third octave band center frequencies of the free-field response at 15m and 35m from the track due to the passage of Thalys HST from the three examined sites. The frequency content is concentrated between the 12th and the 15th octave bands for numerical results and in-situ measurements at all the examined sites. The one-third octave bands at 15m from the track show, on the whole, a good correspondence between experimental and numerical results in the low-frequency range [0–50Hz] at all the examined sites. The correlation at the near field is remarkable, especially in the railway embankment, as illustrated in Figure 3.35a. Furthermore, the numerical results are significantly close to the field data, especially at the most dominant octave bands (12th-15th). At the near field positions of all the examined sites, the most dominant octave is the 14th. In this band, the decibel level reaches close to 70-75dB.
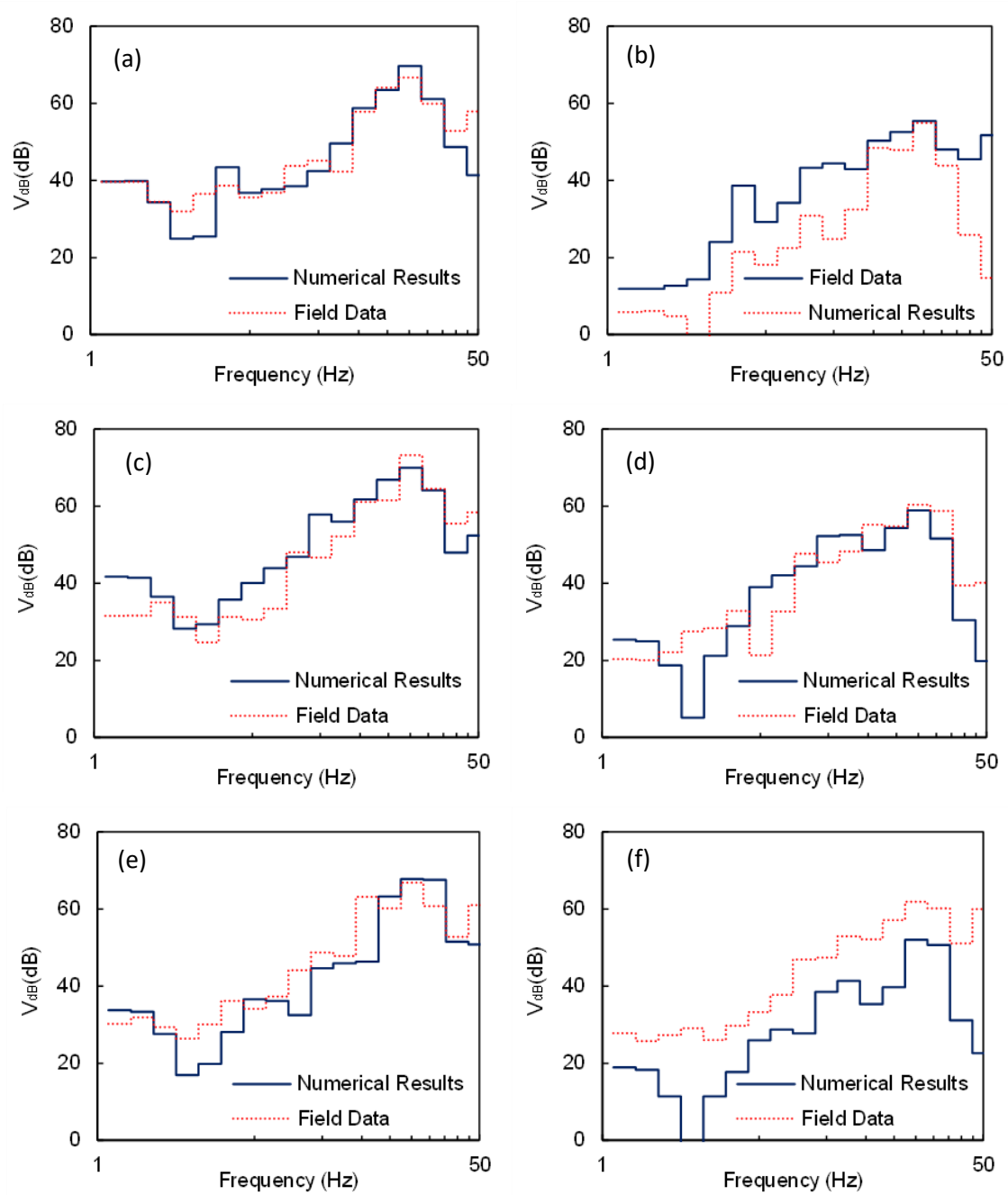
Figure 3.35 Comparison of field data and numerical results at increasing distance from the track in terms of 1/3 octave bands at Site 1 ((a), (b)), Site 2 ((c), (d)) and ((e), (f)).

The most dominant frequency remains at the 14th octave bands at the far-field, although the peak decibel level is reduced compared to the near field as it was expected. The peak decibel level in the case of Site 1 is equal to 56dB; according to the field data, the value has been captured the same according to the predicting model. This value is slightly higher at the other two examined sites. According to the numerical results in Site 2 (see Figure 3.35d), the peak decibel level is equal to 61dB according to the field data and 62dB. On the other hand, at the third examined site, the prediction model underestimates the

vibrations level, as the peak decibel level is 10dB lower than the field data, as depicted in Figure 3.35f. In the last site, the prediction model underestimates the decibel level at the whole examined band due to the high damping ratio of the upper soil layer. However, in general, the numerical model is a good agreement with the field data.
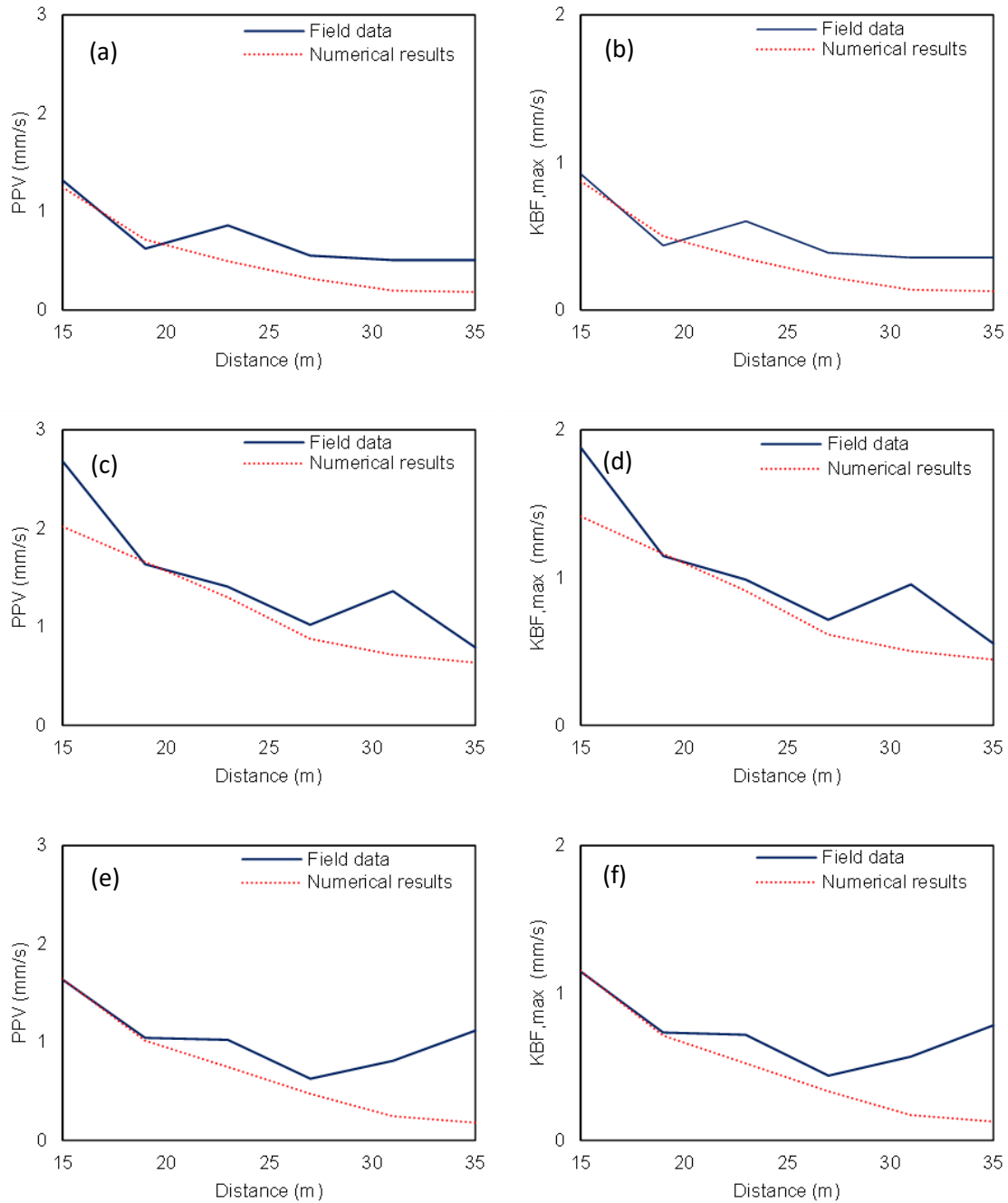
Figure 3.36 Comparison of field data and numerical results at increasing distance from the track in terms of PPV and $KB_{F,max}$ at Site 1 ((a), (b)), Site 2 ((c),(d)) and ((e),(f)).

3.7.4. *PPV investigation*

In conclusion, two commonly used vibrations metrics have also been used to examine the propagation of the HST induced vibrations at increasing distances from the track. Namely, the peak particle velocity (PPV) and the maximum level of the weighted time-averaged signal ($KB_{F,max}$), which are commonly used to measure the impact of vibration on structures and humans, respectively, are presented for the three examined sites. Figure 3.36a and 3.36c illustrate the numerical results and the field data comparison in terms of PPV for increasing distance from the track in the modelling scenario of Site 1 and Site 2. It is evident that the numerical approach is capable of predicting quite accurately PPV at both near and far distances in those cases.

Figures 3.36b and 3.36d display the attenuation of $KB_{F,max,}$ in increasing distance from the track for the same sites. Similarly, the predicted values are consistent with those obtained from the measurements. Furthermore, as it is clearly illustrated, the PPV and $KB_{F,max}$ level, according to both numerical model and field data, is increased in the case of Site 2. The lower damping ratio of Site 2 compared with the increased passing speed of the HST on this side could explain the increased values. In the case of site 3, the numerical approach successfully captures the PPV and $KB_{F,max}$ level at the near field. However, at higher distances, the field values are significantly increased. For instance, PPV at 19m from the track is lower than the same value at 35m from the track. If the soil properties are constant at the whole examined site and there are no other vibrations sources, this phenomenon is not reasonable. On the other hand, according to the numerical results, the PPV seems to be more reasonable, as the PPV values are reduced with the distance from the track.

3.8.   Discussion of the results

In this chapter, the validation of the proposed numerical model with pre-available field data is presented. In order to ensure the accuracy of the numerical approach, three different Sites from Paris-Brussels HSR have been investigated as case studies. The main conclusions of the validations are as follows:

- The numerical model captures the rail dominant frequencies. The bougies and sleepers passing frequency is visible at the rail Fourier spectrum of displacements.

- The time histories shaping and timing align with the field data for all the examined sites in the near field. At the far-field, the numerical model is still reliable at the first two sites. On the other hand, at site 3, the vertical velocity is underestimated by the model due to the high damping ratio of the upper soil layer.

- There is a high correlation between the dominant frequencies at the low-frequency range between 0Hz and 40Hz for all the examined cases. The correlation is even more pronounced in the case of Site 1.

- The peak decibel level is located at the 1/3 octave band with a central frequency equal to 25Hz for all the examined sites. The dB level at 15m from the track is close to 75dB and is reduced to 56-63dB at 35m from the track. The octave bands at 15m from the track are, in general, remarkably close to the field data.

- In general, the trend of PPV and $KB_{F,max}$ at increasing distance from the track of the numerical results follow the field data.

After validating the numerical results with the available field measurements, it is evident that the developed numerical model is reliable for representing the passage of Thalys HST. Some differences, which have also been reported in relevant studies (e.g., (Kouroussis et al., 2011)), are reasonable considering the complexity of this dynamic problem and the uncertainties the difficulties in reproducing the real conditions totally occurred during the measurements. In addition, the velocity time-histories have been used as measured in the field, without filtering them to remove any external noise. Filtered field data could lead to further improvement of the accuracy of the proposed numerical methodology. Hence, applying various mitigation measures on the examined sites can be investigated, following the validated numerical methodology for performing the required numerical simulations, as presented in the subsequent Chapters.

HSR EMBANKMENTS MITIGATION WITH EPS GEOFOAM

4.1. Introduction

In the present Chapter, alternative mitigation schemes are examined in order to propose an optimal mitigation approach against HST-induced vibrations. The investigation of the efficacy of such mitigation measures is vital due to their negative impact on the users of the HST, the nearby residents, as well as nearby buildings and HSR infrastructure. The main aim of the present study is to investigate the EPS geofoam application as an efficient alternative mitigation approach against the developing vibrations by the HST passage on the railway embankment. EPS has been selected as it is a high-performance, low-cost geosynthetic material, which is commonly used in various engineering applications. Herein, the three-dimensional numerical model, which has been presented in Chapter 3, has been used, utilizing the commercial FE software ABAQUS in conjunction with a user-developed subroutine to accurately simulate this complex dynamic phenomenon of surrounding soil response during the passage of HST. In order to propose the optimal EPS configurations, several schemes have been compared, aiming to find an optimal placement of EPS blocks on the embankment that is capable of minimizing the developing vibrations.

In the sequence, the efficiency of this new mitigation scheme has been investigated for various embankment geometries. More specifically, the soil response has been

numerically studied for various embankment heights and slope inclinations, with and without the proposed mitigation scheme. Furthermore, the efficacy of the examined mitigation approach has been examined for various underlying and embankment soil conditions. Four different typical soil types, classified as rock, dense sand with gravels, stiff and soft clay, have been investigated. In addition, the embankment material properties have been altered to assess to what extent they affect the propagation of HST vibrations and the effectiveness of the application of EPS blocks for their mitigation.

4.2.   Existing mitigation measures

Over the last decades, various measures have been proposed to mitigate soil vibrations induced by HST passage, as it is presented in Chapter 3. Most frequently wave barriers have been used (Çelebi and Göktepe, 2012; François et al., 2012; Kanda et al., 2006; With et al., 2009). Wave barriers are usually trenches (see Figure 4.1a) located at various distances from the embankment, aiming to block the developing waves at the soil surface. In order to increase their effectiveness, these barriers are often filled with low-density material, such as polyurethane (Alzawi and Hesham El Naggar, 2011), which increases wave reflections between soil and this filling material. The filling material should have lower acoustic impedance compared to the surrounding soil. This mitigation approach has been implemented at several railway lines in Europe (Sweden or Germany). The effectiveness of this technique has been investigated by several researchers, who concluded that the trench depth should be less than half of the dominant Rayleigh wavelength (Karlström and Boström, 2007; Yang and Hung, 1997).

(a)   (b)
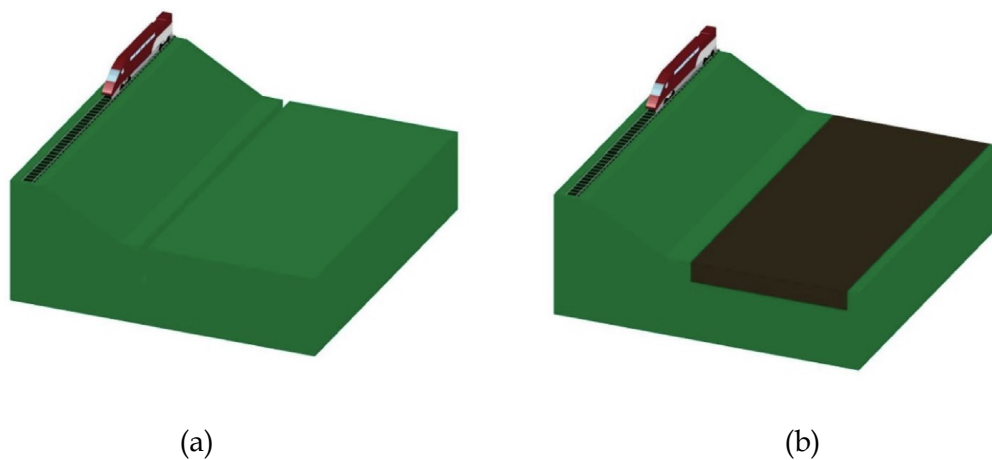
Figure 4.1 Mitigation of the railway embankment with: (a) a trench and (b) an extensive soil replacement (stiffening).

There are also alternative mitigation approaches, e.g., stone columns, deep vibro-compaction, grouting consolidation or deep subsoil mixing. Such mitigation measures increase the stiffness of the soil and reduce the developed vibrations. Nonetheless, a comprehensive soil stiffening approach, such as the one in Figure 4.1b, should be avoided due to its higher cost. Furthermore, it is worth mentioning that proper maintenance of HST wheels and rails could lead to some additional decrease of ground-born vibrations.

4.3. *Mitigation with expanded polystyrene blocks*

The present investigation proposes a new mitigation method using expanded polystyrene (EPS) as an alternative embankment fill material to reduce HST-induced ground vibrations. EPS is a high-performance, lightweight material consisting of closed-cell polystyrene foam. Its high density, combined with its low weight and highly affordable cost, can make EPS material an excellent alternative for reducing HST vibrations. It should be mentioned that the application of EPS blocks has several advantages compared to alternative approaches (e.g., subgrade stiffening), which can lead to overall cost and construction time savings. More specifically, there is no need for extensive mechanical equipment since the EPS can be placed easily and fast, even at sites with difficult access, while the maintenance cost is low. For this reason, the application of various possible configurations of EPS blocks within the examined embankment has been thoroughly investigated. Several configurations have been rejected due to various inefficiencies.

4.4. *Non-optimal EPS configurations*

Initially, several different embankment mitigation approaches have been investigated. In this Section, three non-optimal configurations are examined and the reasons for their rejection are presented. Those typical configurations are illustrated in Figure 4.2. The first sketch (Figure 4.2a) depicts a total replacement of soil with EPS. Figure 4.2b presents an alternative EPS layout, where only the side parts of the embankment have been constructed with EPS blocks in order to avoid the high vertical deflections under the tracks. Lastly, as shown in Figure 4.2c, only the soil subgrade has been replaced with EPS blocks. As embankment fill material, a high-density EPS geofoam (EPS46) has been selected. EPS46 is a high-performance, lightweight, geosynthetic fill material with 45.7kg/m^3 density, 0.05 Poison's ratio and 12.8MPa Young's Modulus.
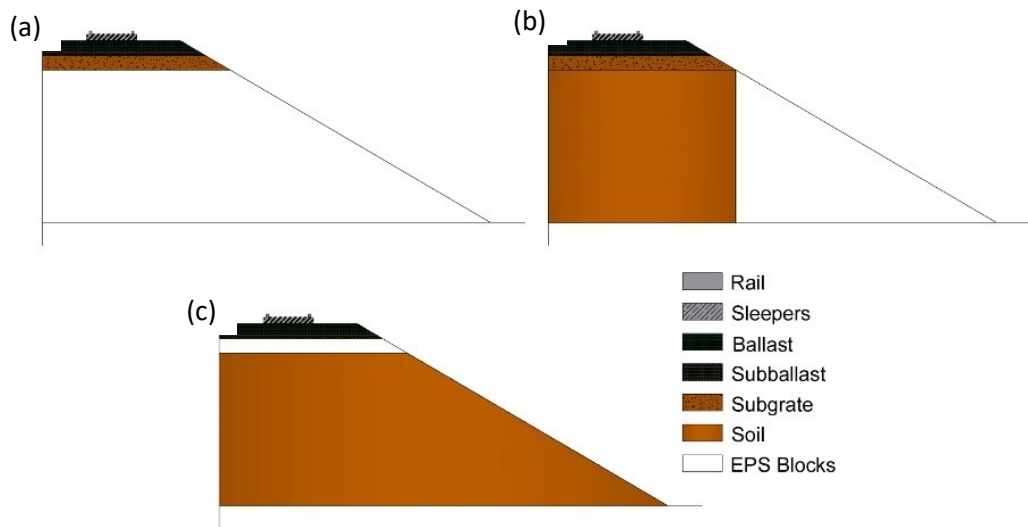
Figure 4.2 Embankment cross-sections with non-optimal EPS configurations: (a) full EPS embankment, (b) side-fill with EPS blocks, (c) limited EPS placement under the tracks.

4.4.1. *Full EPS embankment*

The change of the soil response to Thalys HST induced vibrations is clearly shown in Figure 4.3, in which the soil vertical velocity time hibase at 15m from the track for the initial soil embankment and the full EPS filled embankment are compared. The application of EPS geofoam improves the subsoil dynamic response by reducing the velocity at the soil surface. It is observed from Figure 4.3a that the vertical vibration level is significantly lower in the case of the full EPS-filled embankment. More specifically, the peak vertical velocity is reduced from 1.1mm/s to just 0.2mm/s after replacing the embankment soil fill with EPS geofoam at 15m from the track. The same observation is made at the far-field location, at 35m from the track. As it is clearly illustrated in Figure 4.3b, the peak vertical velocity has been reduced almost to zero. The assumption could be made that this mitigation approach has practically disappeared from the HST-induced vibrations.

This is further illustrated in the comparative Fourier spectrum of Figure 4.4, in which the improvement of the subsoil response by replacing the embankment fill with EPS geofoam is shown. In the case of the soil-filled embankment, two domain frequencies (21.4Hz, 25.2Hz) are observed. Obviously, in the near field vibrations at 15m from the track, the mitigated embankment first dominant frequency at 21.4Hz has been virtually disappeared. Moreover, the second domain frequency amplitude at 25.2Hz has been remarkably improved since the spectral velocity of the model with the EPS embankment is more than three to four times lower than the soil embankment. In the far-field case, there are three domain frequencies (16.7Hz, 21.9Hz, 25.2Hz). The dominant frequencies are even

more pronounced in the soil-filled embankment. The vibrations peaks have been significantly reduced with the use of EPS geofoam.
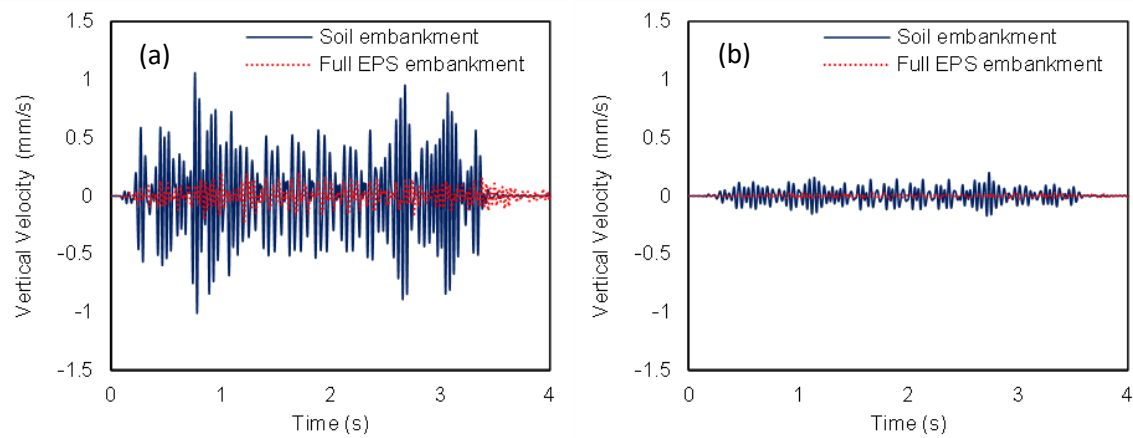
Figure 4.3 Vertical velocity time hibase of soil embankment and full EPS embankment at (a) 15m, (b) 35m from the track.
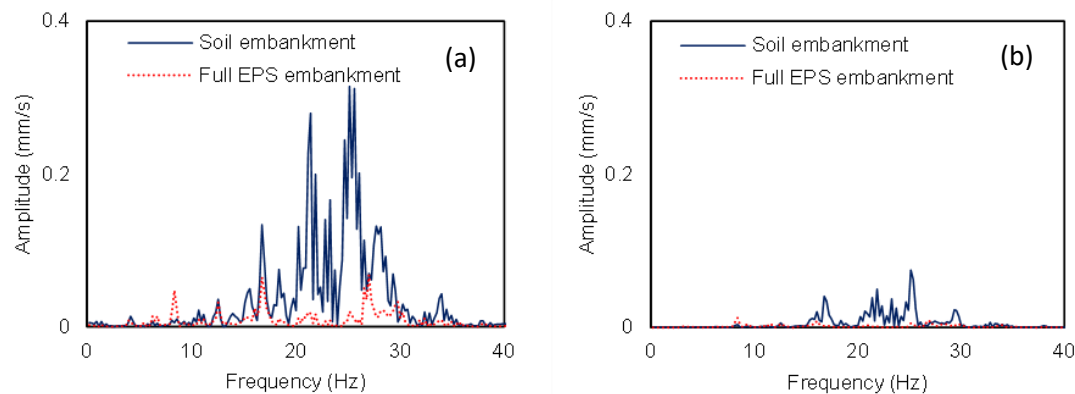
Figure 4.4 Fourier spectrum of soil embankment and full EPS embankment at a) 15m, b) 35m from the track.

4.4.2. Side-fill with EPS block

Figure 4.5a illustrates the soil vertical velocity time hibase at 15m from the track in the modeling scenario for which the side part of the embankment has been replaced with EPS geofoam. In this case, the vibration level has been slightly decreased, although the reduction level is significantly lower than the full EPS embankment (see Figure 4.3.). More specifically, at the near field, the peak vertical velocity has been reduced from 1.1mm/s to 0.65mm/s. The same observation is made at the far-field vibrations, where the reduction is even more pronounced, as illustrated in Figure 4.5b. The peak vertical velocity at 35m from the track has been reduced by 60%.

The soil embankment partial replacement with EPS geofoam has led to the limitation of the vibration peaks in the low-frequency range of 10-30Hz, as is illustrated in Figure

4.6. The two dominant frequencies spectral velocity has been limited from 0.28mm/s and 0.32mm/s to 0.1mm/s and 0.18mm/s, at 15m from the track (see Figure 4.6a). On the other hand, there is a new vibration peak at 8.4Hz for Model B at both distances from the track. In contrast with Model B, the spectral velocity of the model is higher than the soil-filled embankment for higher frequencies (35Hz). Nevertheless, it can be concluded that the use of an embankment formed from EPS geofoam significantly reduces the subsoil vibration level.
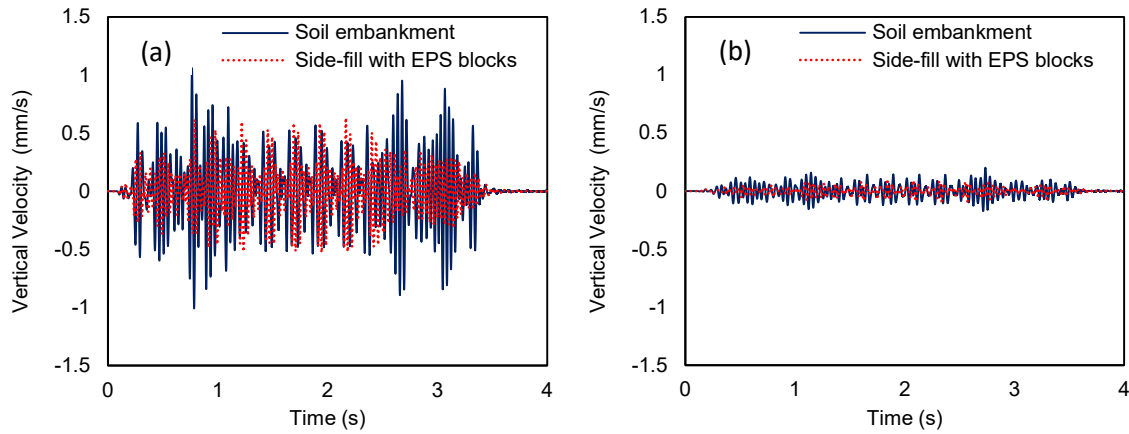
Figure 4.5 Vertical velocity time hibase at 15m from the track: (a) Soil embankment, (b) Full EPS embankment.
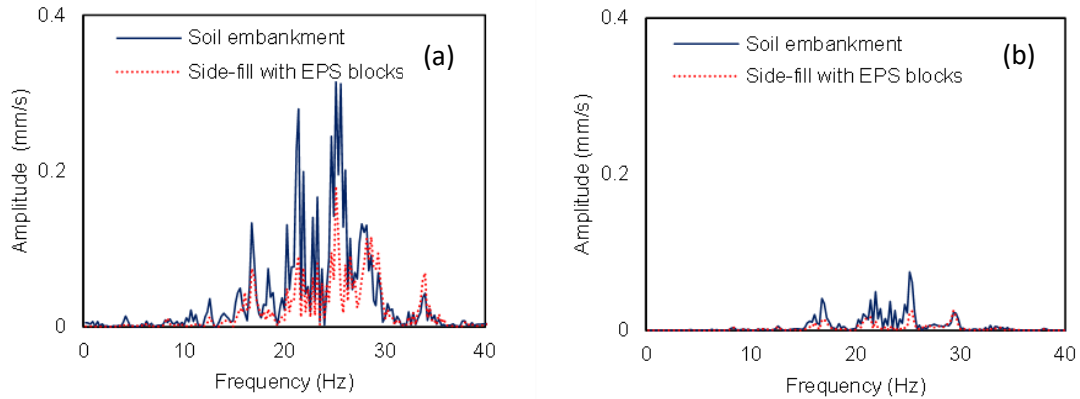
Figure 4.6 Fourier spectrum at (a) 15m from the track, (b) 35m from the track.

4.4.3. Comparison of Full EPS embankment and side-fill with EPS blocks

According to the previous sections, the assumption could be made that the full EPS embankment is significantly more effective than the side fill. Although, the use of lightweight material with lower elastic modulus than soils, as EPS geofoam, increases the risk of HST derailment. Therefore, the increase of the track deflection must be investigated. The rate of the ballast degradation is investigated in order to estimate the track response. The vertical ballast displacement during the passage of Thalys HST is shown in Figure 4.7.

The passage of each wheel can be seen in the diagram. In the case of a fully EPS-filled embankment, the rail vertical displacement is increased significantly compared to the soil-filled embankment. The deflection during the passing of locomotives and carriages is about five to six times higher in the case of the full EPS embankment. On the other hand, the deflection in the case of the side-fill with EPS blocks is the same as the initial soil embankment.
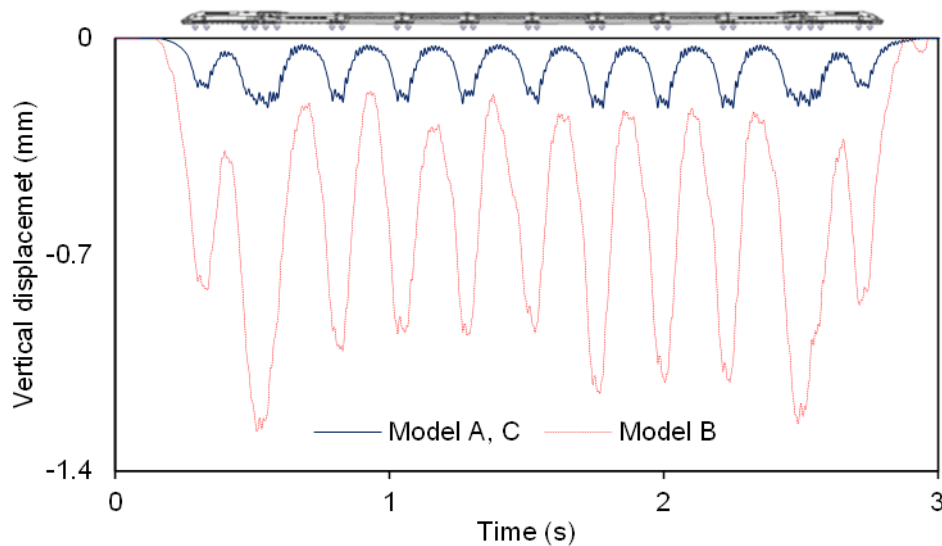
Figure 4.7 Ballast vertical deflection.
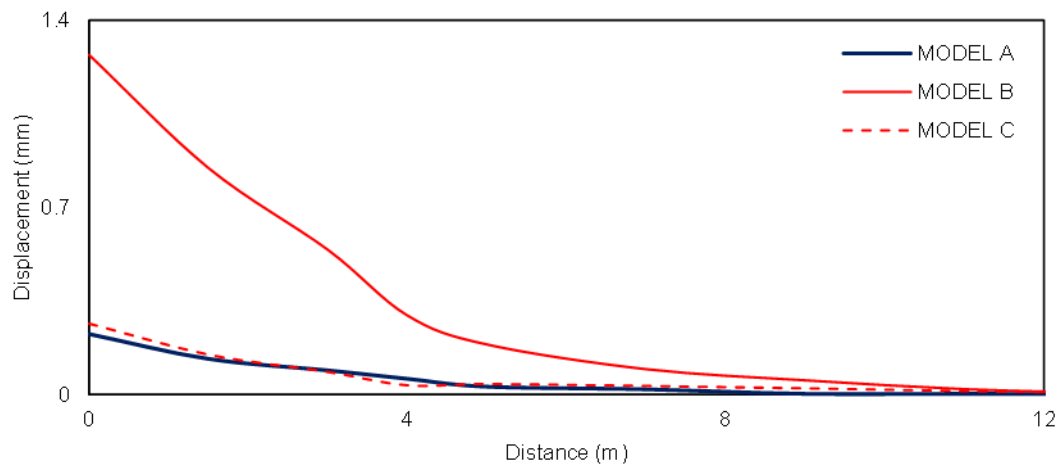
Figure 4.8 Embankment Displacements.

Figure 4.8 shows the peak embankment vertical displacement at several distances from the track, between 0–12 m from the rails. As expected, peak displacement declines rapidly with distance from the embankment. Fully EPS-filled embankment causes significantly higher vertical displacement at the whole embankment surface. Moreover, it has to be noticed that at the first five meters from the rails, the vertical displacements are significantly higher in the case of the full EPS embankment. On the other hand, the

difference between EPS embankment and soil embankment displacements is decreased for higher distances. Nevertheless, vertical displacement remains lower in the case of the soil-filled embankment. In the case of the side-fill with EPS geofoam, vertical displacement at all the distances from the track remains at the same level as in the case of the soil embankment.

The results have confirmed the original hypothesis that the subsoil vibrations induced by the passage of the HST are reduced with the EPS embankment application. This is attributed to the decrease of vertical velocities using a practical, high-performance, low-cost material as EPS geofoam. The reduction of the subsoil vibration is higher in the case of the embankment fully filled with EPS geofoam in comparison with the side-fill. On the other hand, in the case of the full EPS embankment, the use of the EPS geofoam as embankment fill material significantly increases the rate of track degradation. Embankment vertical displacements have also been increased after the application of the EPS embankment. This problem is not observed in the case of the side fill embankment, in which the vertical displacements are similar to the soil embankment.

The first approach (Figure 4.2a) depicts a total replacement of soil with EPS, which successfully minimized the developed vibrations but is rejected due to the resulting high vertical displacements since such excessive deformations under the tracks could lead to the derailment of HST. Figure 4.2b presents an alternative EPS layout, where only the side parts of the embankment have been constructed with EPS blocks in order to avoid the high vertical deflections under the tracks. Although the displacements are successfully limited, this embankment is expected to have instabilities, which could be alleviated via reinforcement with geosynthetics, but this would increase construction time and cost. In this case, the capability of the EPS blocks to retain the soil should be investigated. Lastly, as shown in Figure 4.2c, only the soil subgrade has been replaced with EPS blocks, but there is no significant ground vibration level reduction. It is evident that none of these mitigation schemes with the use of EPS geofoam is optimal; hence alternative approaches are investigated in the sequence.

4.5. *Optimal EPS configurations*

In this Section, an optimal configuration (of only a limited number of EPS blocks) has been placed on the soil embankment slopes and has been covered with a thin surface layer of soil, is proposed, as illustrated in Figure 4.9. The observation points are shown on the

existing embankment in Figure 4.9a and on the mitigated with EPS blocks in Figure 4.9b. With this configuration, the stability of the embankment is achieved and the vertical displacements are not significantly increased. Note that this is an easy and cost-efficient solution that can be applied to new and existing railway embankments. In addition, the variation of EPS properties has also been examined in the present Section. The effectiveness of two geofoam types is presented: EPS19 and EPS46. As mentioned in the previous section, EPS46 is the stiffest among the seven available EPS types, as its density is equal to 45.7 kg/m^3 and its Young's Modulus is equal to 12800 kPa. On the other hand, EPS19 is a low-density material (18.4 kg/m^3) with Young's Modulus equal to 4000 kPa. Note that for both EPS46 and EPS19 materials, the Poisson's ratio is very low, as it is equal to 0.05, while material damping is taken equal to 2%.
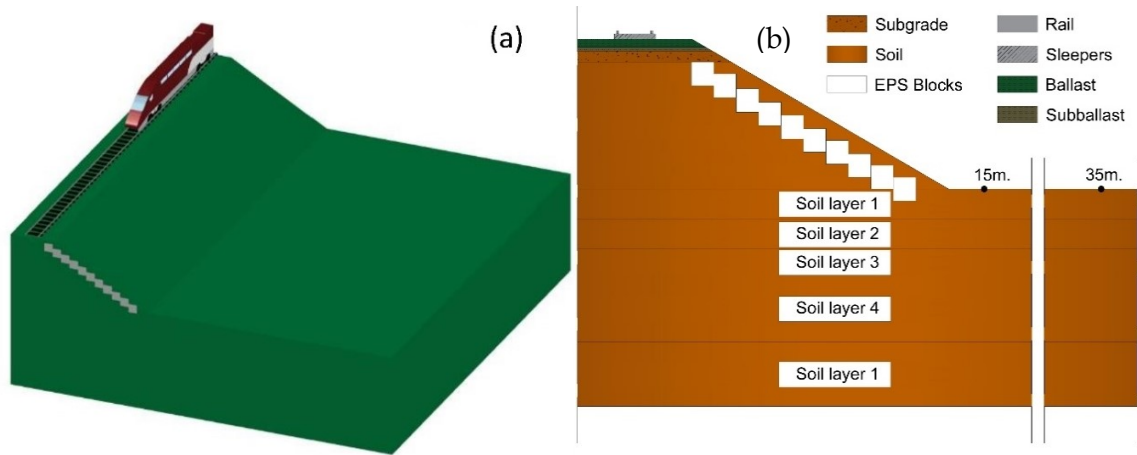
Figure 4.9 (a) Optimal mitigation of HST vibrations in the examined site with EPS blocks, (b) details of the EPS blocks placement along the embankment side.
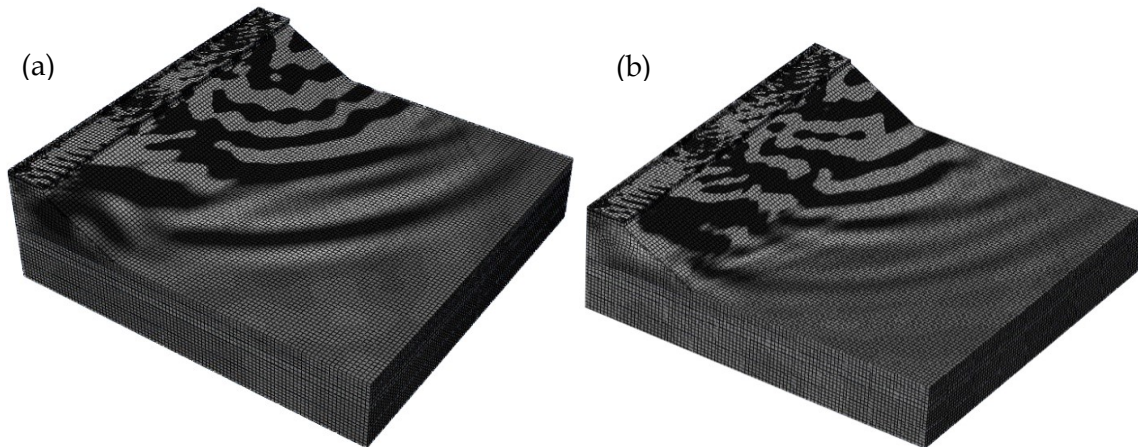
Figure 4. 10 Typical contour plots of vertical velocity at soil surface: (a) soil embankment, (b) EPS-mitigated embankment.

In order to illustrate the impact of the proposed mitigation measure, contour plots of the predicted soil surface velocity are shown in Figure 4.10 in the case of EPS46 blocks placement along the sides of the embankment. The effect that this light intervention on the embankment has on the wave propagation is demonstrated. More specifically, Figure 4.10a depicts the typical soil embankment, where a wide spreading of the surface waves is observed since the waves are reaching a distance of 40 m away from Thalys moving axle. On the other hand, the scattering of surface waves is much less in the case of the EPS-mitigated embankment (Figure 4.10b).
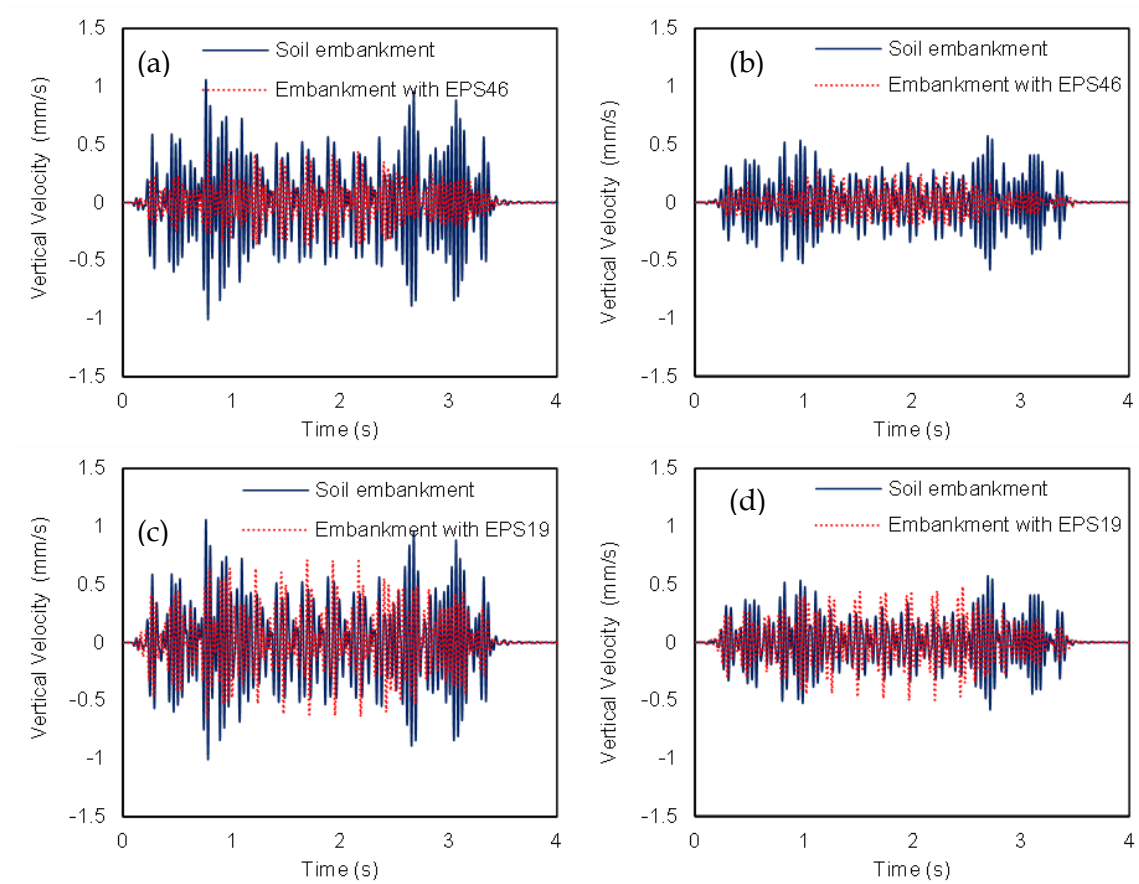
Figure 4.11 Comparison of soil and EPS-retrofitted embankments in terms of vertical velocity time-histories: EPS46 ((a) at 15 m, (b) at 19m from the track), EPS19 ((c) at 15 m, (d) at 19m from the track).

4.6. *Investigation of the optimal EPS geofoam*

4.6.1. *Vertical velocity time histories*

The mitigation of the vibrations induced by HST passage using the proposed EPS configuration at the near field positions is depicted in Figure 4.11. The first two vertical velocity time-histories (e.g., Figure 4.11a and Figure 4.11b) demonstrate the improvement of soil response at several distances from the track when using the stiffer EPS46 blocks. In

contrast, the usage of EPS19 blocks reduces only slightly the developed vibrations. More specifically, at 15m and 19m from the track, during locomotives passage (which are the heavier bogies), the vertical velocity is significantly reduced. However, the velocity at the middle of the time hibase is slightly increased. It is evident that the peak vertical velocity has been reduced from 1.1mm/s to 0.7mm/s and 0.45mm/s at 15m from the track, respectively, after the implementation of EPS19 and EPS46.
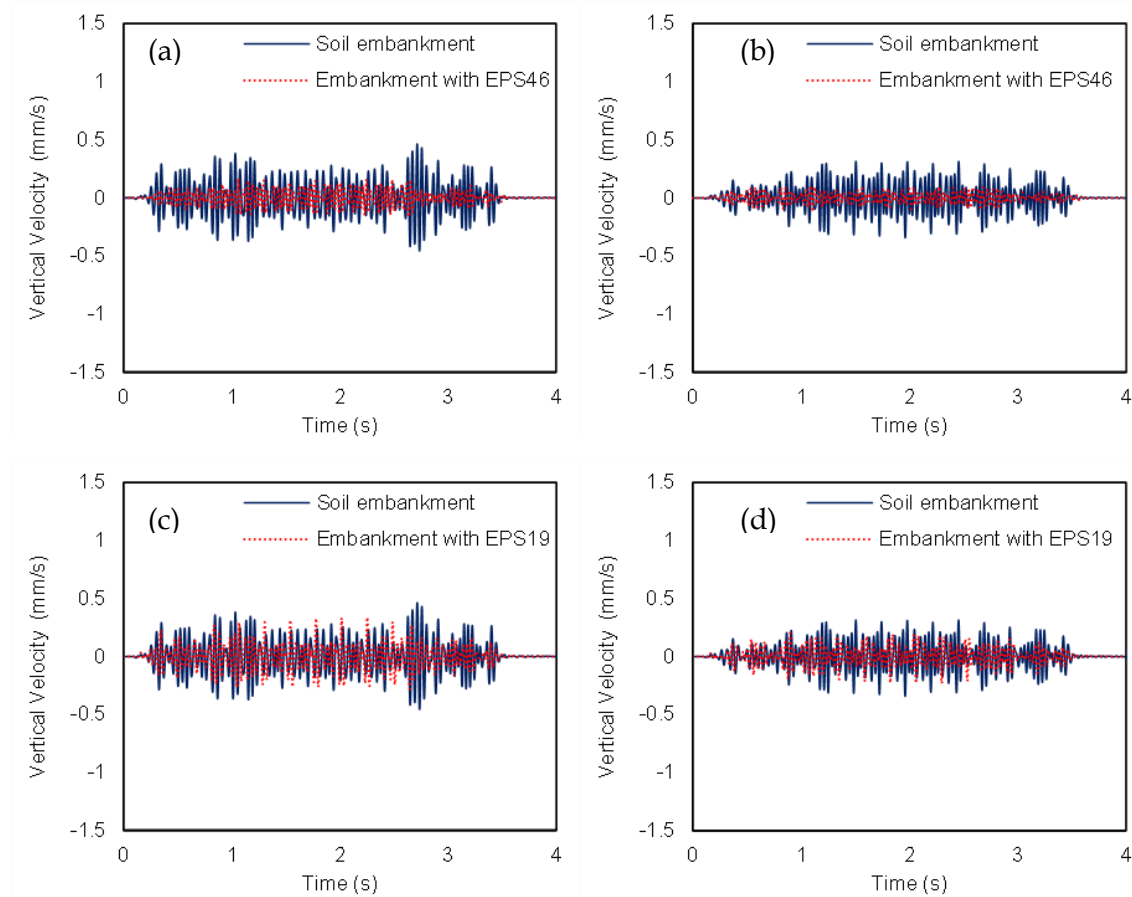
Figure 4.12 Comparison of soil and EPS-retrofitted embankments in terms of vertical velocity time-histories: EPS46 ((a) at 23 m, (b) at 27 m from the track), EPS19 ((c) at 23 m, (d) at 27 m from the track).

The addition of -a limited number- EPS46 blocks at the slope of the embankment substantially improves its dynamic response by minimizing the vertical surface velocity at the middle field positions, as is depicted in Figure 4.12. In particular, it is observed that the velocity has drastically reduced up to 60%, at 23m from the track, during the first and last two heavier bogies passage. In addition, the vertical velocity is also reduced during the passage of the middle bogies. The beneficial influence of the mitigation with EPS46 blocks is even more apparent at 27m, in which the peak vertical velocity is significantly reduced. Furthermore, in the middle field, EPS19 is more effective in comparison with the

nearest positions. EPS19 reduces the peak vertical velocity up to 30% at both examined positions. Nevertheless, EPS46 is still the optimal option.

Figure 4.13 depicts the vertical velocity time histories at the higher examined distances from the track. As shown in Figure 4.13a, the usage of EPS46 material still mitigated the HST ground-borne vibrations more effectively than EPS19 material. The usage of EPS19 slightly reduced the vibration level at the far-field positions. More specifically, the level of reduction reaches in some cases close to 20%. It is evident that EPS46 remarkably reduces the vibration level more effectively, especially at 35m from the track. In this case, the time hibase has been optically disappeared. It could be concluded that the proposed configuration with the use of EPS46 is the most efficacy as it reduces the vertical velocity up to 50% at all the examined observation points between 15m and 35m from the track.
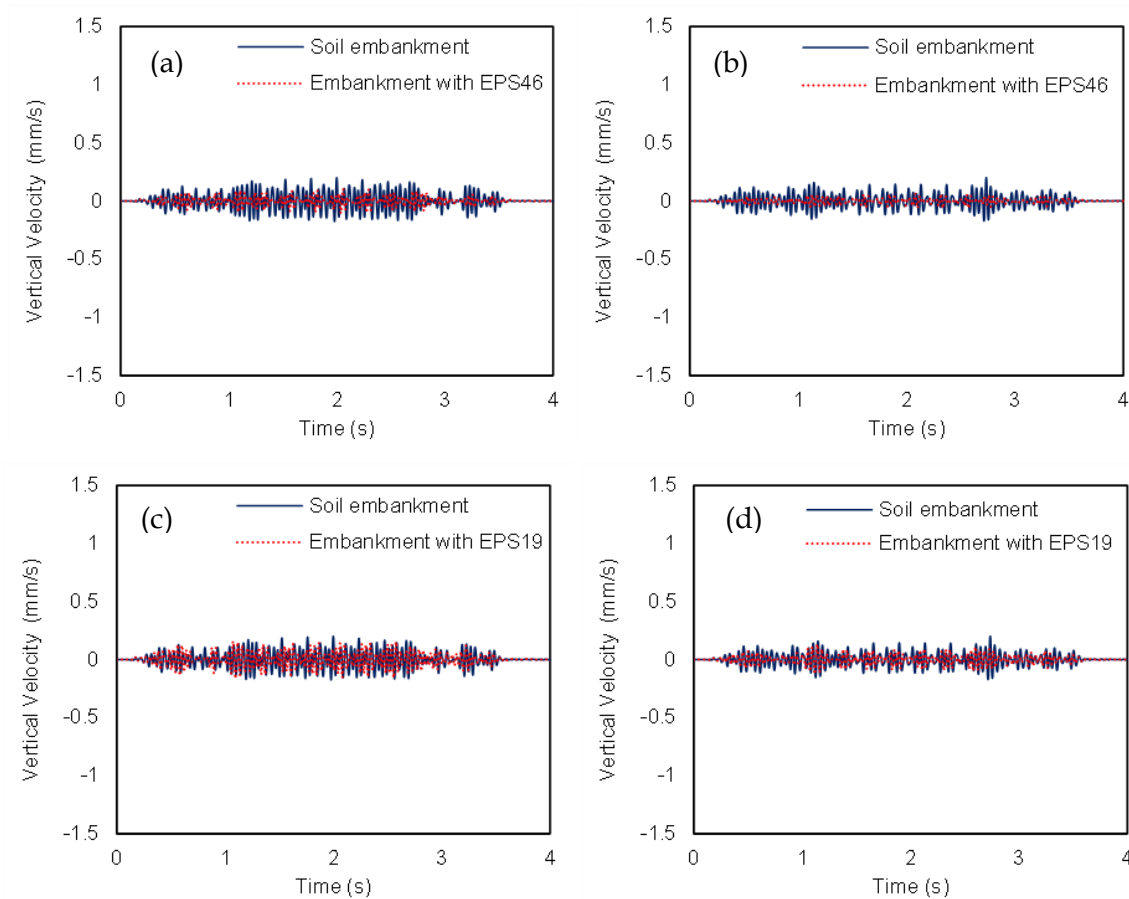
Figure 4. 13 Comparison of soil and EPS-retrofitted embankments in terms of vertical velocity time-histories: EPS46 ((a) at 31 m, (b) at 35 m from the track), EPS19 ((c) at 31 m, (d) at 35 m from the track).

4.6.2. *Fourier Spectra*

Figure 4.14 compares the velocity spectra between the initial soil and the EPS-retrofitted embankments at the near field. At the closest distance (15 m from the track), the most dominant peak at 25.2 Hz is significantly reduced after the implementation of EPS19. On the other hand, the peaks at 16.8 Hz and 21.4 Hz remains the same as the soil embankment. Conversely, at 19m from the track, the soil response is worsened at the frequency range between 15 and 24 Hz. The peaks in the frequency range of 10 to 40 Hz are slightly reduced in the rest of the observation points. In the case of EPS46, most of the peaks in the low-frequency range (10 to 40 Hz) have been significantly reduced. More specifically, the peaks at the two most dominant frequencies at 15 m from the track are notably reduced from 0.28mm/s to 0.09 mm/s and from 0.31 mm/s to 0.1 mm/s for 21.4 Hz and 25.2 Hz, respectively. Furthermore, the peaks at 16.8 Hz and 28.1 Hz have been almost disappeared.

Figure 4.14 Comparison of soil and EPS-retrofitted embankments in terms of vertical velocity Fourier spectra: EPS46 ((a) at 15 m, (b) at 19 m from the track), EPS19 ((c) at 15 m, (d) at 19 m from the track).

As mentioned earlier, most of the peaks at the low-frequency range are slightly reduced or remain at the same level in most observation points when using the less stiff

EPS19 blocks. The vibration peak at the dominant frequency, 21.4Hz, is the only exception. In this case, the vibration peak has been slightly increased. This trend remains at the middle-frequency range. The peaks at the range from 10 Hz to 30 Hz are sufficiently reduced, at 23 m from the track (see Figure 4.15a), in the case of the stiffer EPS46. It should be mentioned that a new significant frequency at 33.7 Hz is observed for both examined fill materials. For higher distances, as at 27m from the track, all the peaks in dominant frequencies have been notably reduced, as illustrated in Figure 4.15b.

Figure 4.15 Comparison of soil and EPS-retrofitted embankments in terms of vertical velocity Fourier spectra: EPS46 ((a) at 23 m, (b) at 27 m from the track), EPS19 ((c) at 23 m, (d) at 27 m from the track).

Moreover, it should be noted that the far-field (see Figure 4.16) spectral velocity of the EPS-mitigated embankment is reduced in the whole range of the critical frequencies (10 to 40 Hz). Hence, it is evident that the implementation of the EPS46 blocks generally reduces soil vibrations in a very efficient manner. The beneficial role of the proposed mitigation approach, especially in the case of the stiffer EPS material is used, is obvious in the frequency range of interest. More specifically, the implementation of EPS46 blocks has reduced the most dominant peak at 25.2 Hz from 0.1mm/s to 0.03mm/s at 31m from the

track. On the other hand, in the case of EPS19, there is a marginal reduction of this value. The same observation is made at the most remote position, at 35m from the track. In this observation position, the implementation of EPS46 geofoam almost disappeared all the vibrations peak.

Figure 4.16 Comparison of soil and EPS-retrofitted embankments in terms of vertical velocity Fourier spectra: EPS46 ((a) at 31 m, (b) at 35 m from the track), EPS19 ((c) at 31 m, (d) at 35 m from the track).

4.6.3. *Velocity decibels*

Figure 4.17 illustrates the relationship between velocity decibels (V_{db}) and the frequency at 15m from the track for the two examined geofoam materials. It is clearly shown that both of the examined materials reduce the vibrations level in the majority of the low-frequency octave bands. In the case of EPS19, the decibel level at the most dominant octave band, with a centre frequency 25Hz, is reduced from 69 dB to 64 dB. Furthermore, the highest level of reduction, equal to 12 dB, is observed at the 11th octave band, as depicted in Figure 4.17b. The beneficial effect of the vibrations reduction is even more pronounced in the case of EPS46. In the majority of the octave bands, the decibel level has been decreased. The highest level of reduction, equal to 17dB, is observed at the 12th octave

band, while the dB level at the most dominant octave band has been reduced up to 10dB. In general, the level of decibel reduction is higher in the case of the stiffer, EPS46 in comparison with EPS19.
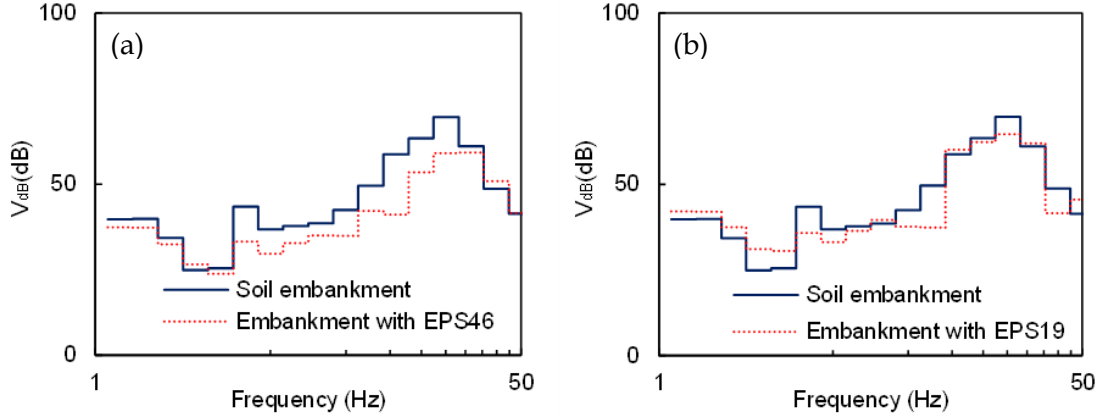
Figure 4. 17 Comparison of soil and EPS-retrofitted embankments in terms of velocity decibels (V_{db}): at 15m (a) EPS46 and (b) EPS19.
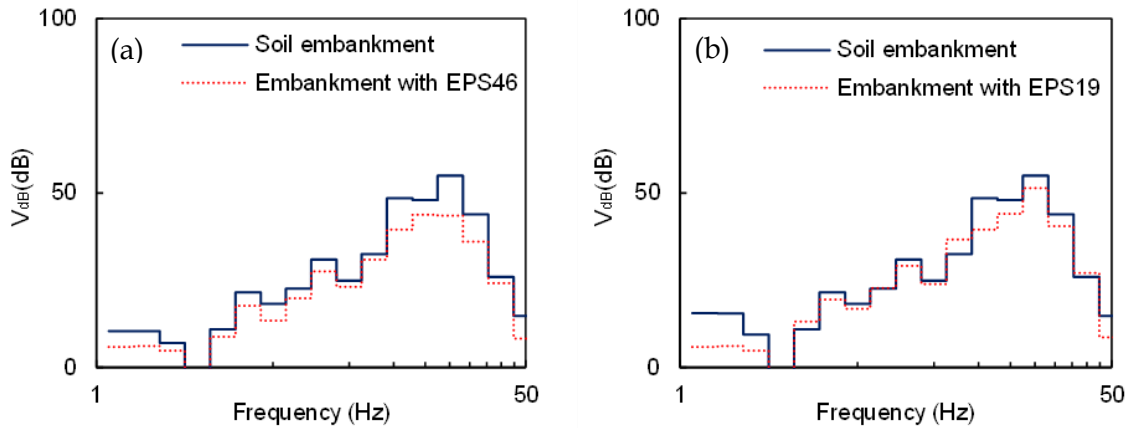
Figure 4. 18 Comparison of soil and EPS-retrofitted embankments in terms of velocity decibels (V_{db}): at 35m (a) EPS46 and (b) EPS19.

The same observation is made at the far-field position (e.g., 35m from the track), as illustrated in Figure 4.18. In this case, the implementation of EPS19 managed to decrease the vibrations level at most of the examined octave bands. The most dominant peak at the 14th octave band, the decibel level, has been reduced from 55dB to 51dB. Furthermore, the level of reduction at the octave bands with central frequencies, 16Hz and 20Hz, the reduction of the decibel level is equal to 9dB and 4dB, respectively. Figure 4.18a illustrates the reduction of the decibel level at the low-frequency range after the implementation of the stiffer EPS material. The beneficial role of the proposed mitigation approach is obvious in this case, as the decibel level is reduced at the whole examined frequency range. The

reduction is even more pronounced at the most dominant octave band, where the decibel level has been reduced from 55dB to 43dB.
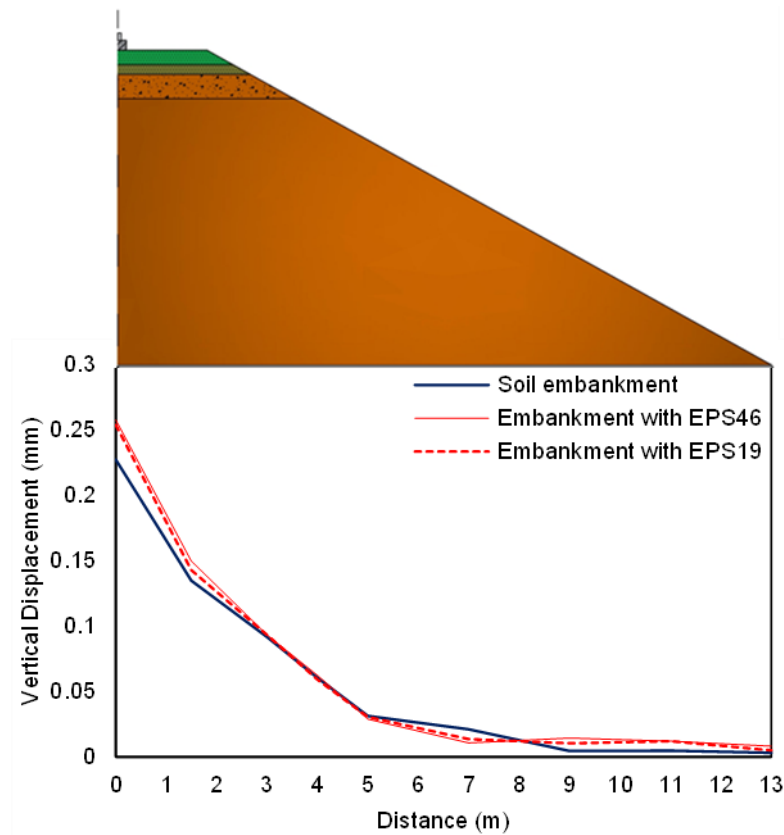
Figure 4.19 Comparison of vertical displacements of soil and EPS-retrofitted embankments.

As it was aforementioned, when implementing EPS (e.g., as the ones are shown in Figure 4.9) as embankment filling material revealed that the complete replacement of the soil with EPS increased significantly -up to five times- the vertical displacements of the embankment (Lyratzakis et al., 2019). On the other hand, as illustrated in Figure 4.19, the optimal placement of a limited number of EPS46 blocks on the inclined part of the embankment did not alter the vertical displacement levels compared to the initial geostructure. It is concluded that both EPS19 and EPS46 adequately mitigate the developed vibrations by Thalys HST passage without causing problems in the operation of the HSR.

4.6.4. *Comparison with thresholds of international guidelines*

In the sequence, the efficacy of the proposed mitigation approach is compared with international guidelines to investigate the effectiveness of the potential protection of human health and buildings. According to the German Institute for Standardization (DIN

(Deutsches Institut für Normung), 1999a), a PPV threshold of 3 mm/s is proposed in order to protect sensitive buildings from potential damages. Herein, the PPV of the soil embankment at distances from 15m to 35m from the track is significantly lower than this limit. Figure 4.20a illustrates the vibrations propagation at distances from 15 m to 35 m from the track in the examined scenario of the initial soil embankment and the mitigated embankment with EPS46 and EPS19 blocks at the slope. It is evident that the PPV is lower than the DIN threshold, and these values are even lower after the mitigation with EPS19 and EPS46 blocks. Hence, the construction of sensitive buildings across the track is feasible.

Apart from the potential damages to nearby buildings, the residents discomfort from the passage of the HST should be assessed. As has detailed presented in Chapter 2, several parameters have been proposed to estimate the level of the residents disturbance (DIN (Deutsches Institut für Normung), 1999b; ISO (International Organization for Standardization), 2003). According to the United States Department of Transportation (USDT, 1998), the highest value of the root mean square amplitude of the velocity time-hibase (v_{rms}) to avoid the discomfort of the residents is 0.10 mm/s for infrequent passages of HST (<70 passages per day). This value is increased to 0.26 mm/s for more than 70 passages per day. In the regular soil embankment case, the v_{rms} values are lower than the USDT lower limit for frequent passages of HST at distances greater than 21m from the track. The installation of EPS46 blocks on the embankment slope contributes to reducing the v_{rms} below this limit for all the distances between 15 and 35 m from the track (see Figure 4.20b). Furthermore, the USDT proposes a decibel scale to assess the impact of HST-induced vibrations.

The World Health Organization (WHO/Europe, 2018) noted that vibrations above 55 dB are quite dangerous for public health. More specifically, most of the residents could experience detrimental health effects as they become annoyed and sleep-disturbed, increasing the risk of cardiovascular diseases. Figure 4.20c compares the initial and mitigated embankments at increasing distances from the track in terms of V_{dB}. Note that in the case of the soil embankment, the V_{dB} is higher than the 55 dB threshold for the whole examined range. The implementation of EPS46 blocks reduces the V_{dB} values to below the 55 dB limit for distances greater than 23 m. The German Institute for Standardization (DIN4150-2, 1999) proposes the comparison between the maximum level of the weighted time-averaged signal ($KB_{F,max}$) and the limit of 0.15 mm/s for residential areas. The DIN

limit value for $KB_{F,max}$ has not been exceeded for distances greater than 21m after the mitigation with EPS blocks.
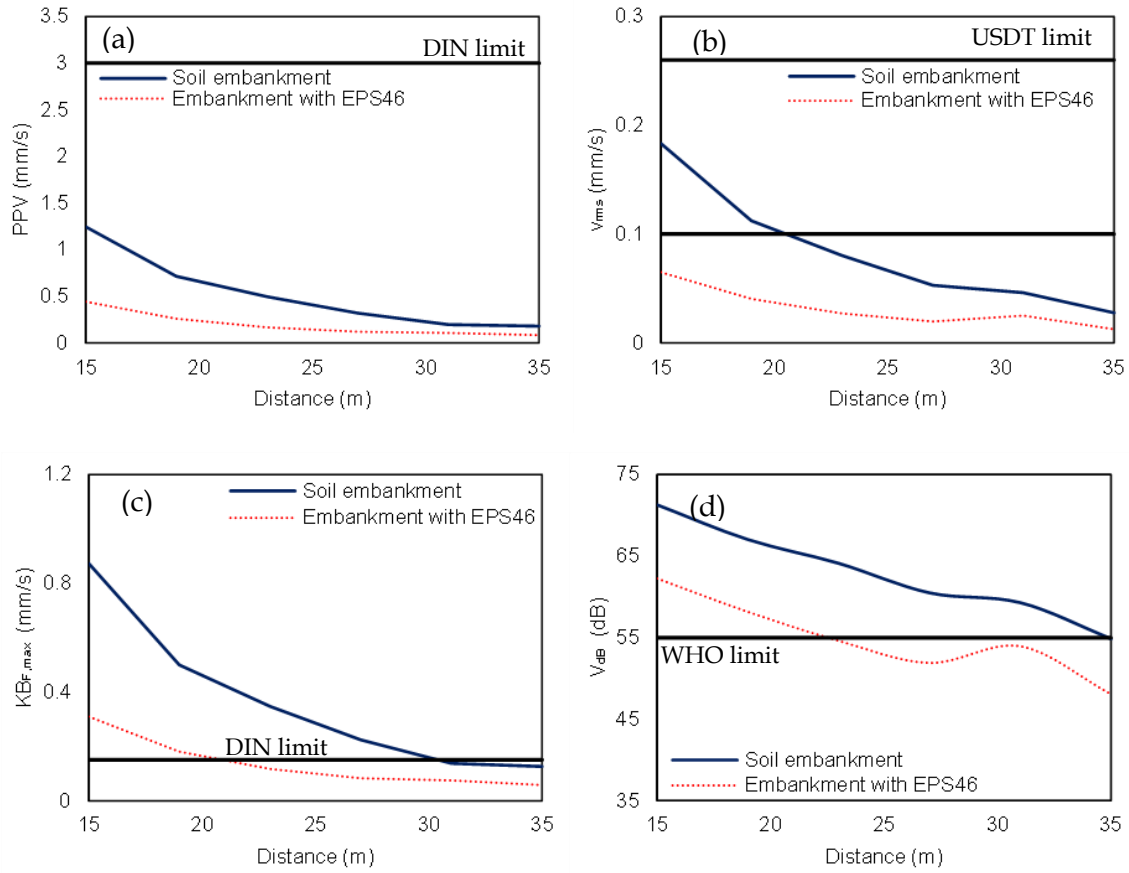
Figure 4.20 Comparison of soil and EPS-retrofitted embankments with slope at increasing distance from the track in terms of: (a) PPV, (b) v_{rms}, (c) V_{dB}, (d) $KB_{F, max}$.

4.7. *Impact of embankment geometry*

In this Section, the explicit time-domain 3D finite element (FE) model validated in Chapter 3 has been modified in order to examine the effect of the embankment geometrical properties on the vibrations propagation. The impact of the embankment geometry on the vibrations levels has been investigated. For this purpose, several embankments between 3.5m and 5.5m high and with a slope inclination between 20° and 45° are assessed. Furthermore, the induced vibrations have been mitigated with EPS46 blocks to investigate the efficiency of this mitigation measure with respect to the embankment geometry. The typical soil profile (e.g., Site 1, see Chapter 3) of the Paris-Brussels railway line has been used to investigate the induced vibrations.

4.7.1. *Impact of embankment height*

In order to examine the effect of the embankment height on the efficiency of the examined mitigation measure, five embankment cross-sections are examined and compared. All the embankments have a slope angle of 30° and their height varies between 3.5 and 5.5 m (Figure 4.21a). The five investigated embankment configurations are constructed from the same soil as the first layer of the underlying soil. Subsequently, the embankments are mitigated with the placement of EPS46 blocks at their slopes (Figure 4.21b). Each EPS block is 1.0 m wide and 1.0 m high. The total number of EPS block, implemented in each case, is 2H, where H is the embankment height. For each embankment, the far-field vibrations at various locations from the track/embankment structure are studied to determine the potential damage to structures and infrastructure in close proximity to the railway and the level of the vibrations mitigation achieved due to the implementation of EPS blocks.
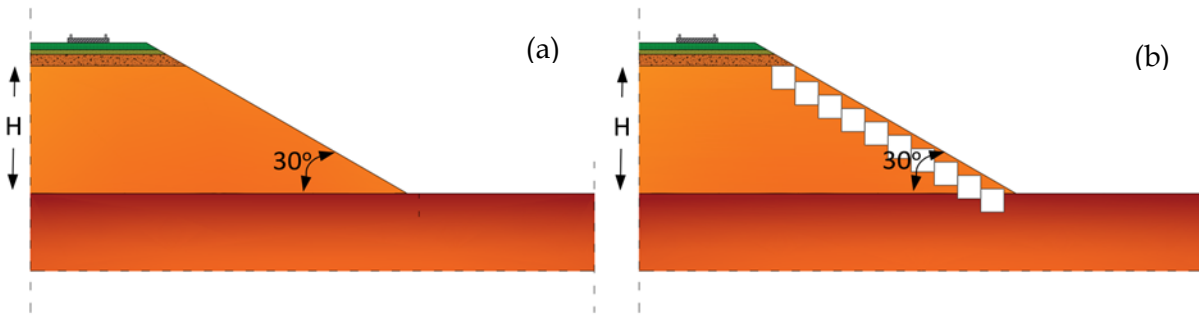
Figure 4.21 Cross-section with various heights of: (a) the soil embankment, (b) the mitigated embankment with EPS46 blocks.

The mitigation of the vibrations induced by Thalys passage from embankment sites with several heights at 15m from the track is illustrated in Figure 4.22. The first vertical velocity time hibase (see Figure 4.22a) shows the improvement of soil response in the case of the lower embankment with a height equal to 3.5m. The peak vertical velocity has been reduced from 1.1mm/s to 0.75mm/s. A higher reduction is observed at the beginning and the ending of the time hibase. On the other hand, the amplitude at the center of the time hibase has been slightly increased. The same observations are made in the case of an embankment with a height equal to 4m. As the height of the embankment increases, the level of the vibrations reduction is higher. More specifically, the peak vertical velocity has been reduced from 1.1mm/s to 0.67mm/s and 0.55mm/s, respectively, for embankments with heights equal to 4m and 4.5m. The same trend is observed for the highest examined embankment, as shown in Figure 4.22d. In this case, the peak vertical velocity has been minimized under 0.5mm/s.
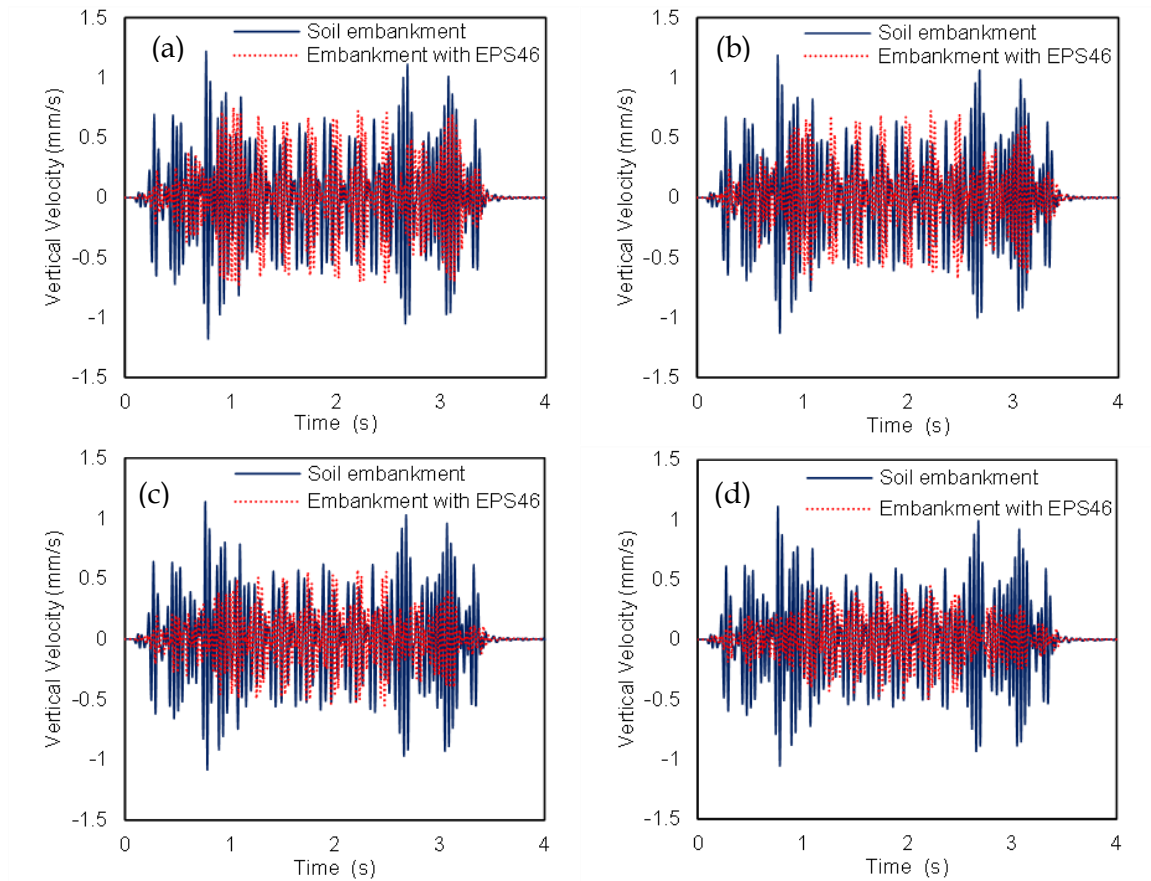
Figure 4. 22 Comparison of soil and EPS-retrofitted embankments in terms of vertical velocity time histories at 15m from the track for embankment height equal to: (a) 3.5m, (b) 4.0m, (c) 4.5m, (d) 5.0m.

Figure 4.23 illustrates the Fourier spectra at 15 m from the track. In the case of the soil embankment, the impact of its height on the vibrations induced by the Thalys HST passage is marginal. This mitigation measure is more effective for higher embankments. For instance, in the case of the highest embankment, with a height of 5m, the effect of the EPS blocks is more significant, as the vibrations peaks in the range from 10 to 28 Hz are successfully mitigated. More specifically, the main frequencies at 21.4 Hz and 25.2Hz, close to the most important frequencies of the nearby buildings and infrastructure, are successfully attenuated. In the case of higher frequencies, the vibrations remain at the same level. Furthermore, the peaks at several frequencies between 10 and 28 Hz are successfully reduced with the use of EPS blocks for all the examined embankments. However, the peaks at 29.6Hz and 34.0Hz are increased as the embankment height decreases. For the lower height embankments, the peak at 29.6 Hz is significantly increased.
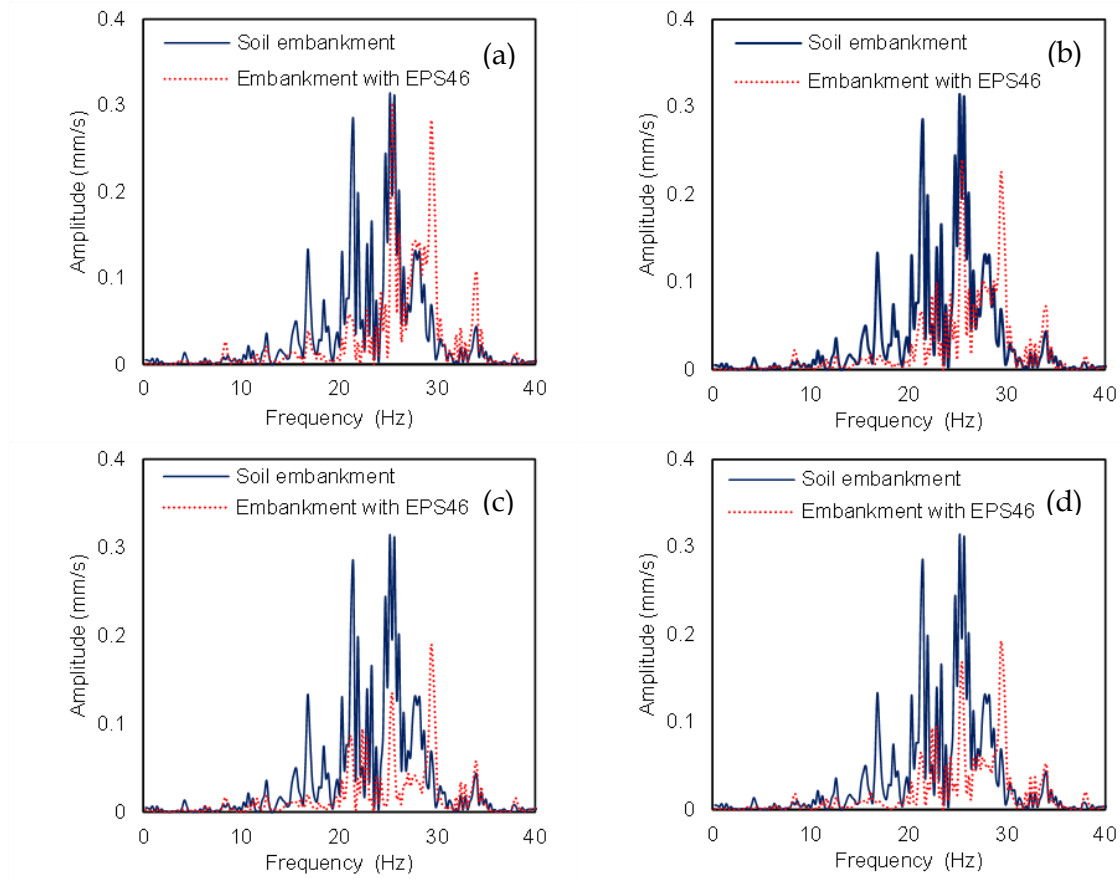
Figure 4.23 Comparison of soil and EPS-retrofitted embankments in terms of vertical velocity Fourier spectra at 15m from the track for embankment height equal to: (a) 3.5m, (b) 4.0m, (c) 4.5m, (d) 5.0m.

Figure 4.24 presents the effect on vibrations propagation at 35m from the track for both the soil and the EPS-retrofitted embankments. As expected, all the peaks are lower than those of the previously examined point (at 15m from the track). At 35 m from the track, there are no significant changes in the vibrations level in the case of the soil embankment, whereas the implementation of EPS blocks successfully reduces the developed vibrations at that point for all heights. For embankments with heights ranging from 4.5 m to 5 m, the vibrations peaks are attenuated by the EPS blocks for the whole low-frequency range between 0 and 40 Hz. However, in the case of the lower embankments (<4.5 m), the peaks at 29.6 and 34.0 Hz are slightly increased, although the amplitude of the vibrations is reduced for the rest of the examined frequencies.
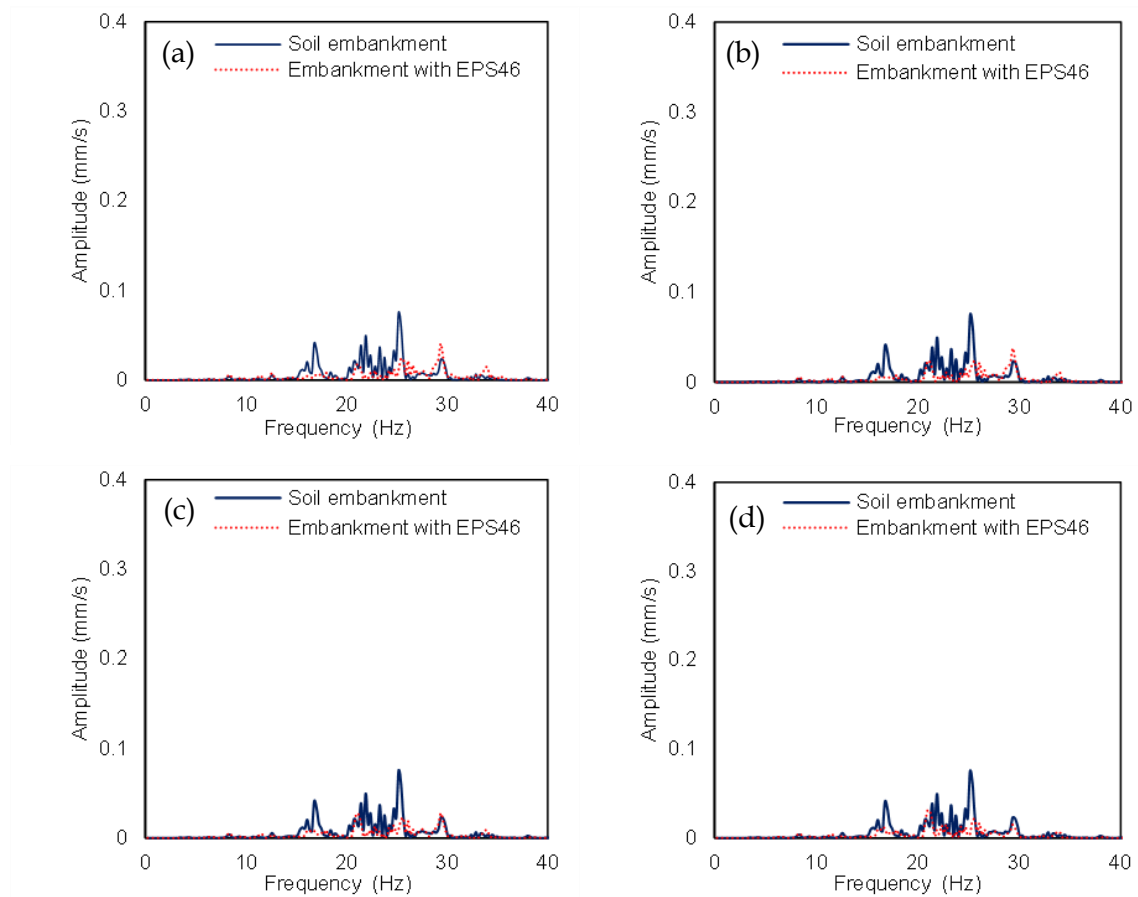
Figure 4.24 Comparison of soil and EPS-retrofitted embankments in terms of vertical velocity Fourier spectra at 35m from the track for embankment height equal to: (a) 3.5m, (b) 4.0m, (c) 4.5m, (d) 5.0m.

In the sequence, the level of the decibel reduction at 15m and 35m from the track is demonstrated in Figure 4.25. The most dominant octave bands are those with central frequencies 16Hz, 20Hz and 25Hz for both observation points. According to Figure 4.25a, at the first 4 octave bands, the level of decibel reduction is higher in the cases of the lower embankment at 15m from the track. The implementation of EPS46 geofoam slightly increases the vibrations level at the octave bands with central frequencies higher than 31.5Hz. Furthermore, the implementation of EPS geofoam at the embankment with a height higher than 5m, the decibel level remains the same or is reduced for all the examined octave bands. Figure 4.25b demonstrates the decibel level at the second observation position, at 35m from the track. The level of reduction is still higher for higher embankments. It is evident that in this case, the decibel level for all the examined octave bands has been minimized below 50dB, independently from the embankment height.
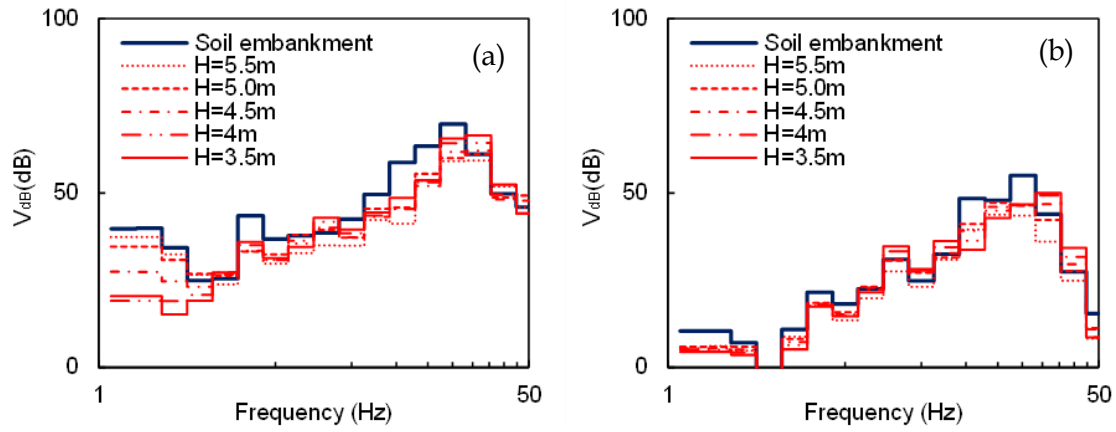
Figure 4.25 Comparison of soil and EPS-retrofitted embankments in terms of velocity decibels (V_{db}): (a) at 15m from the track, (b) at 35m from the track.
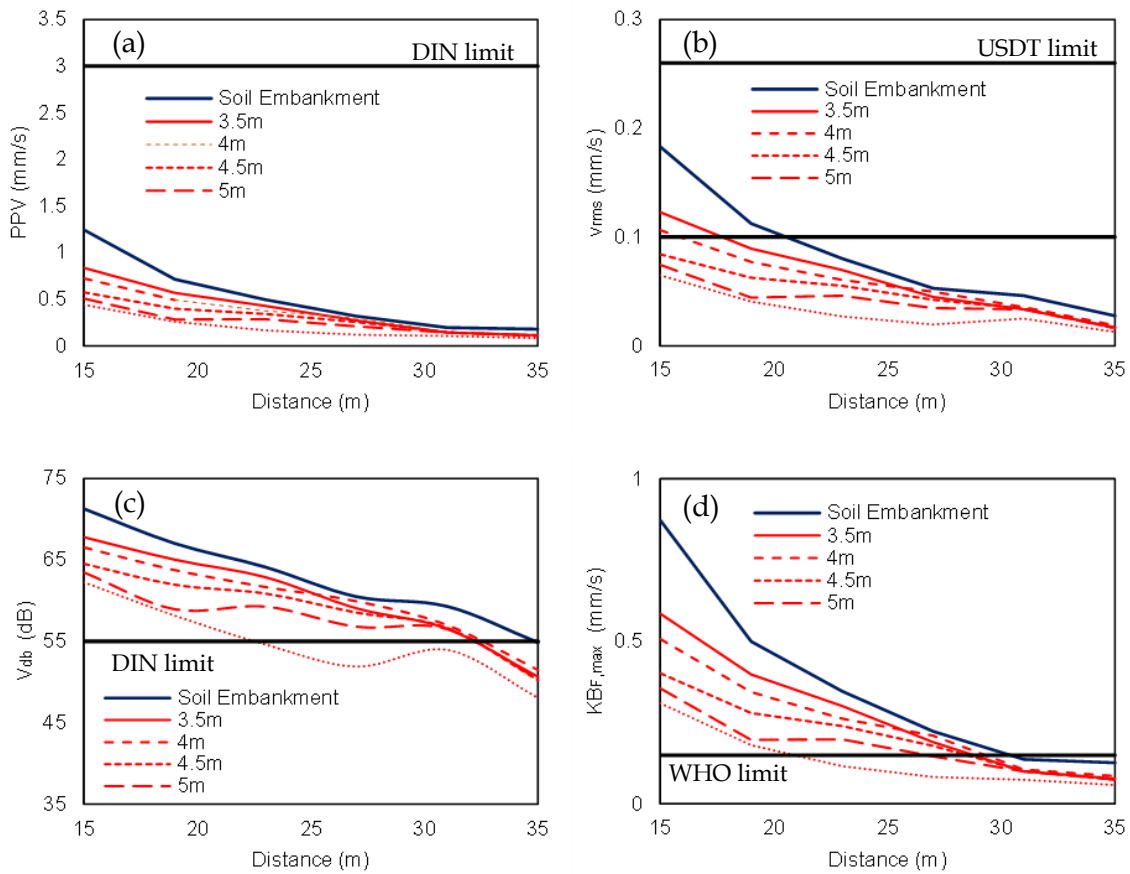
Figure 4.26 Comparison of soil and EPS-retrofitted embankments at increasing distance from the track in terms of: (a) PPV, (b) v_{rms}, (c) V_{dB}, (d) $KB_{F,max}$.

Figure 4.26a illustrates the peak partial velocity at six equally spaced observation points between 15 m and 35 m from the rails of the track/embankment structure. As previously mentioned, the PPV is reduced with distance from the track. Moreover, PPV is significantly decreased for all the examined embankment heights at all the observation

points after the mitigation with a small number of EPS blocks. In particular, the mitigation is more pronounced for the higher embankments. In the case of the soil embankment, the v_{rms} values for distances between 15m and 20m are higher than the USDT lower limit (Figure 4.26b). The implementation of the EPS blocks contributes to the reduction of these high values. Especially for embankments with heights from 4.5 m to 5.5 m, the v_{rms} values are acceptable for all the examined frequencies.

Values of V_{dB} exceed 55 dB for all the examined distances, in the case of the standard soil embankment. The mitigation with EPS blocks has not reduced those values significantly, except for the case of the highest embankment (5.5m), where the vibrations level is lower than 55 dB for distances between 22m and 35m from the track (see Figure 4.26c). Figure 4.26d shows that the $KB_{F,max}$ values in the case of the soil embankment are above 0.15mm/s for most of the examined cases. The implementation of EPS46 blocks significantly reduces the level of $KB_{F,max}$ for all the examined heights. Note that in the case of the highest embankment (5.5m), the level of $KB_{F,max}$ is lower than 0.15mm/s when the distance is between 21m and 35m.

4.7.2. *Impact of embankment slope inclination*

The impact of the inclination of the embankment slope on HST-induced vibrations is described in this Section. Several soil embankments with a constant height of 5.5 m and a slope angle ranging from 20° to 45° are investigated. Similarly, the same soil as the first underlying layer is used as embankment fill material (Figure 4.27a) for the initial embankment. Then, EPS46 blocks are placed at the embankment slope to mitigate the developed vibrations (Figure 4.27b). The vibrations level at distances ranging from 15m to 35m from each embankment are investigated to determine the contribution of the embankment slope inclination to the vibrations propagation.
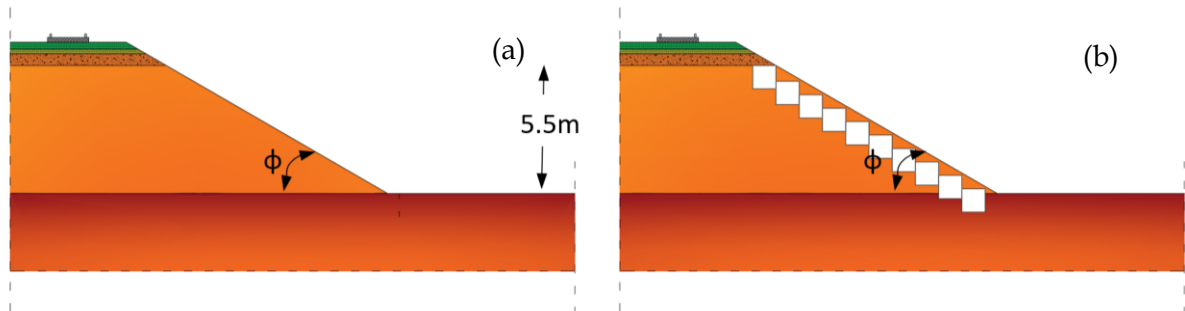
Figure 4.27 Cross-section of: (a) the soil embankment, (b) the mitigated embankment with EPS46.

Figure 4.28 depicts the PPV of all the examined cases, and an increase in slope inclination can significantly influence the propagation of the vibrations. As expected, a steeply inclined embankment causes a significant decrease in vibrations levels, while embankments with lower inclination show a corresponding increase. More specifically, at 15m from the track, the PPV level in the case of the embankment with a slope inclination of 20° is increased by about 120%, in contrast to the embankment with a 45° slope. Hence, the construction of embankments with high inclination leads to a reduction of far-field vibrations. On the other hand, the construction of embankments with a low slope inclination should be avoided.
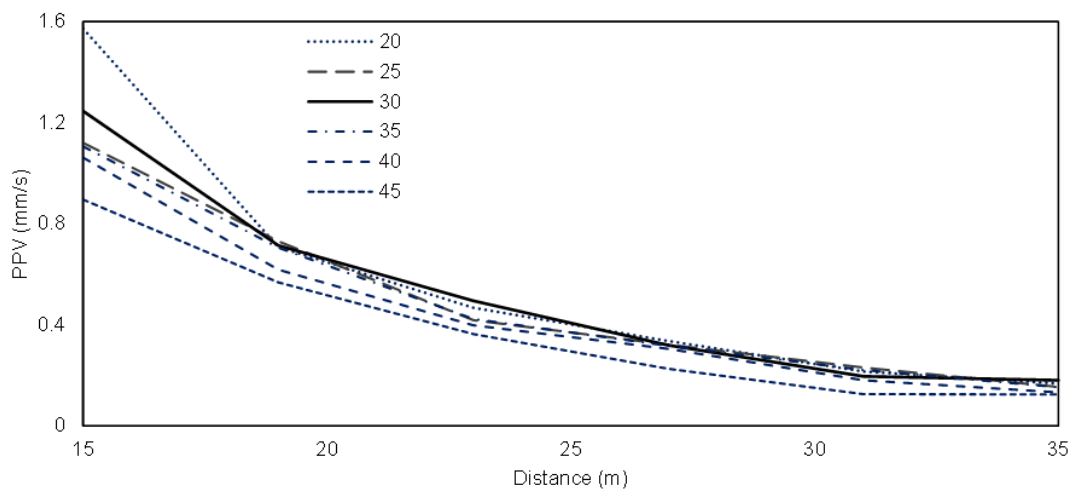
Figure 4. 28 Comparison of soil embankments with various slope inclination, vibration level in terms of PPV at increasing distance from the track.

Figure 4.29 illustrates a comparison between the soil embankment and the embankment mitigated with EPS46 blocks for two embankment slope inclinations: (a) 20°, (b) 45°. Similar to the PPV results, an increase of the slope inclination contributed to a reduction of the vibration levels. The two dominant vibration peaks at 21.4Hz and 25.2Hz are notably reduced in the case of the higher inclination. The vibration peak at 25.2Hz is reduced from 0.47mm/s in the case of 20° inclination to 0.31mm/s in the case of the initial embankment inclination (30°). This reduction is even higher in the case of the 45° slope, where the vibrations peak at 25.2 Hz is equal to 0.25 mm/s. The efficiency of the examined mitigation system is shown in Figure 4.27. In the case of a 20° inclination, the vibrations peak at 25.2 Hz is almost disappeared. Furthermore, the vibration peaks at 18.1, 21.4, and 28.1 Hz are significantly reduced. The same results are observed for 45° inclination. The two dominant vibrations peaks are reduced from 0.19mm/s and 0.25mm/s to 0.08mm/s and 0.14mm/s at 21.4Hz and 25.2Hz, respectively, in the case of a 45° inclination.

The same trend is observed at 35m from the track (Figure 4.28). In the case of the soil embankment, the vibrations level is higher for the milder slope. The most dominant peak at 25.2Hz is 0.12mm/s for a 20° inclination, in contrast to a 45° inclination. The same observation is made for all the peaks at the low-frequency range between 0Hz and 40Hz. The implementation of EPS blocks on the embankment slope significantly reduces the vibrations induced by the Thalys HST at 35m from the track. In the modeling scenario of a 20° slope inclination, all the vibrations peaks at 18.1Hz, 21.4Hz, 25.2Hz, and 28.1Hz has been almost disappeared.
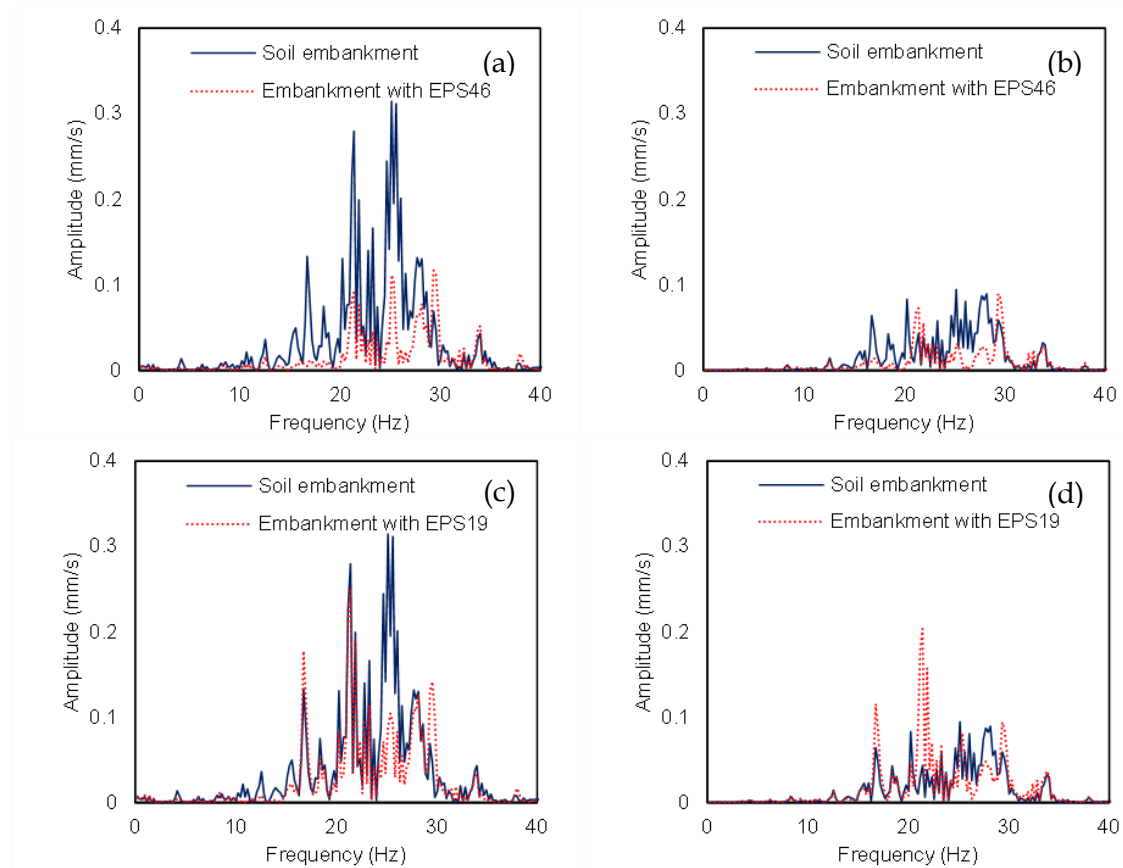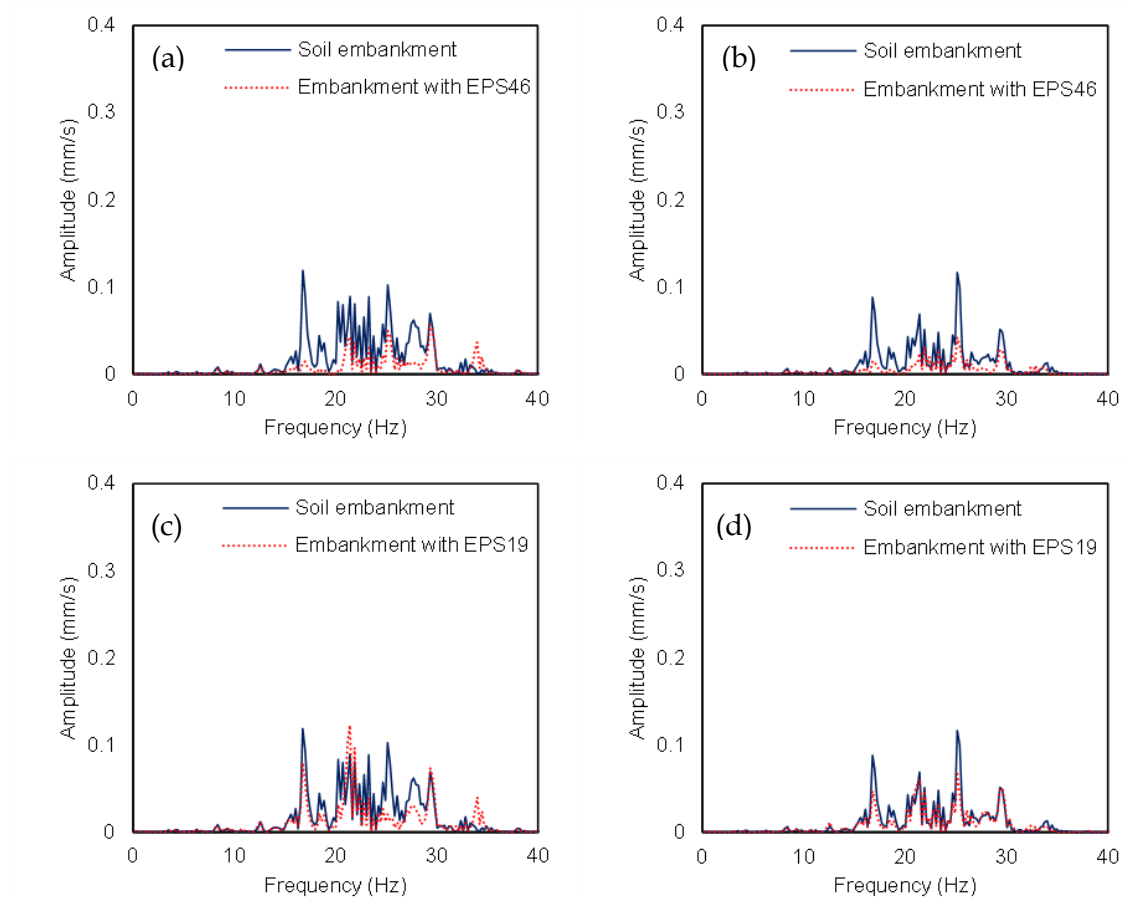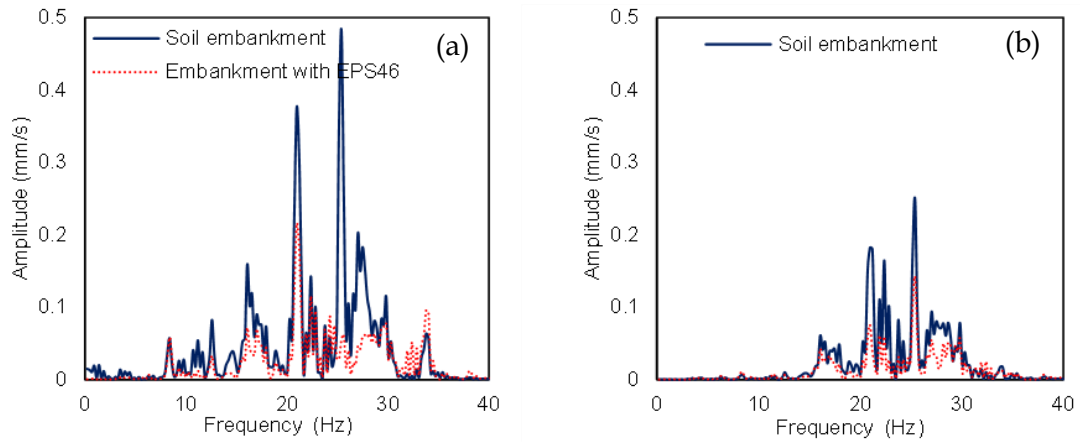

Figure 4.29 Comparison of soil and EPS-retrofitted embankments in terms of vertical velocity Fourier spectra at 15m from the track for embankment slope inclination equal to: (a) 20°, (b) 45°.

Furthermore, in the case of 45° inclination (Figure 4.30b), the proposed mitigation scheme reduces the vibrations across the whole examined frequency range (0 to 40 Hz). In the case of the soil embankment, the vibrations level is higher for the milder slope. The most dominant peak at 25.2 Hz is 0.12mm/s for a 20° inclination, in contrast to 0.04mm/s for a 45° inclination. The same observation has been made for all the peaks at the low-frequency range between 0 and 40Hz. The implementation of EPS blocks on the embankment slope significantly reduces the vibrations induced by the Thalys HST at 35m from the track. In the modeling scenario of a 20° slope inclination, all the vibrations peaks at 18.1Hz, 21.4Hz, 25.2Hz and 28.1 Hz have been almost disappeared. Furthermore, in the case of 45° inclination, the proposed mitigation approach contributes to a reduction of the vibrations across the whole examined frequency range (0 to 40 Hz).

The soil response at 15m from the track due to the developing vibrations are summarized in the 1/3 octave bands of Figure 4.31a. The most dominant octave bands are the 13th, 14th and 15th, where the V_{dB} varies between 65dB and 70dB in the case of the regular

embankment. Those values have been successfully minimized below 60dB after the implementation of EPS geofoam. In some cases, such as the last two octave bands, the decibel level has been slightly increased. However, the beneficial role of the proposed mitigation approach is substantial, as, in the majority of the octave bands, the decibel level is reduced.
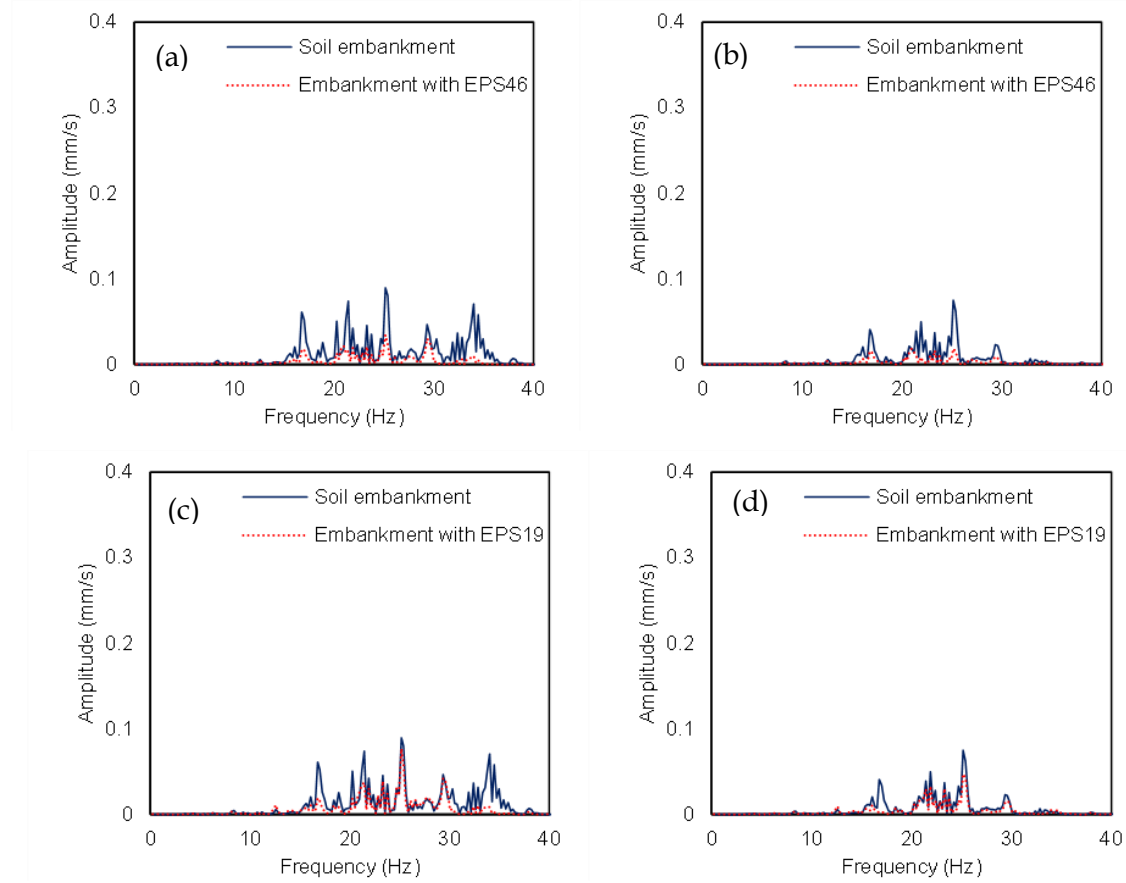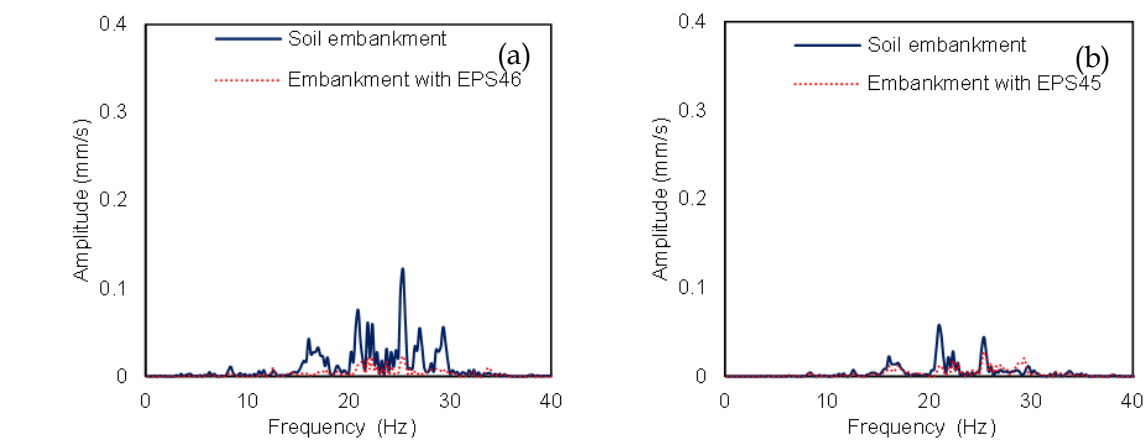

Figure 4.30 Comparison of soil and EPS-retrofitted embankments in terms of vertical velocity Fourier spectra at 35m from the track for embankment slope inclination equal to: (a) 20°, (b) 45°.

Figure 4.31b depicts the regular and retrofitted embankment velocity decibel level with a slope inclination of 45°. It is evident that the decibel level of the initial embankment is reduced compared to the embankment with a slope inclination equal to 20°. For instance, the decibel level at the first five octave bands is almost half compared to the previous case (see Figure 4.31a). However, the decibel level at the most dominant octave bands (e.g., 13th, 14th, 15th) remains higher than 60dB. Hence, the implementation of EPS geofoam does not significantly alter the amplitude of the vibrations at the octave bands with the lower centre frequencies. On the other hand, its beneficial role in the reduction of the vibrations is evident at the most dominant octave bands.

At the second observation position, the decibel level at 35m from the track is presented in the sequence. Figure 7.32a compares the vibrations level of the regular embankment and the embankment with EPS46 on each low-frequency octave band for embankments with 20° of slope inclination. In the case of the regular embankment, the decibel level is higher than 60dB at the octave bands with central frequencies 12.5Hz, 16Hz, 20Hz and 25Hz. The reduction of those values after the implementation of EPS46 success is substantial, as it ranges between 11dB and 14dB. In general, all the velocity decibels values are significantly reduced at all the examined octave bands. More specifically, the decibel

level remains lower than 47dB at the whole frequency range. In the case of embankment with 45° of slope inclination, the initial decibel level is lower than 51dB, as illustrated in Figure 4.32b. Furthermore, the implementation of EPS46 further decreases the decibel level. The decibel reduction is marginal at the lower octave bands, although it is higher than 3dB at the most dominant octave bands.
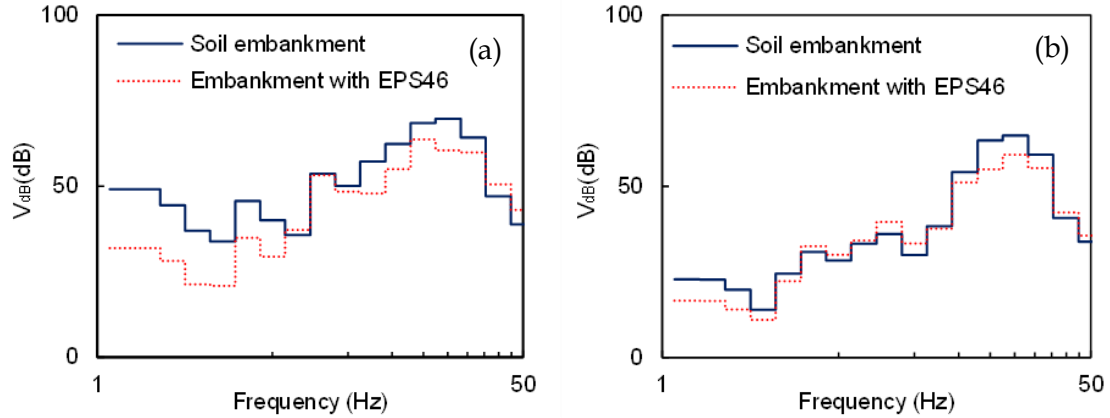
Figure 4.31 Comparison of soil and EPS-retrofitted embankments in terms of velocity decibels (V_{db}) at 15m from the track: (a) 20° of inclination, (b) 45° of inclination.
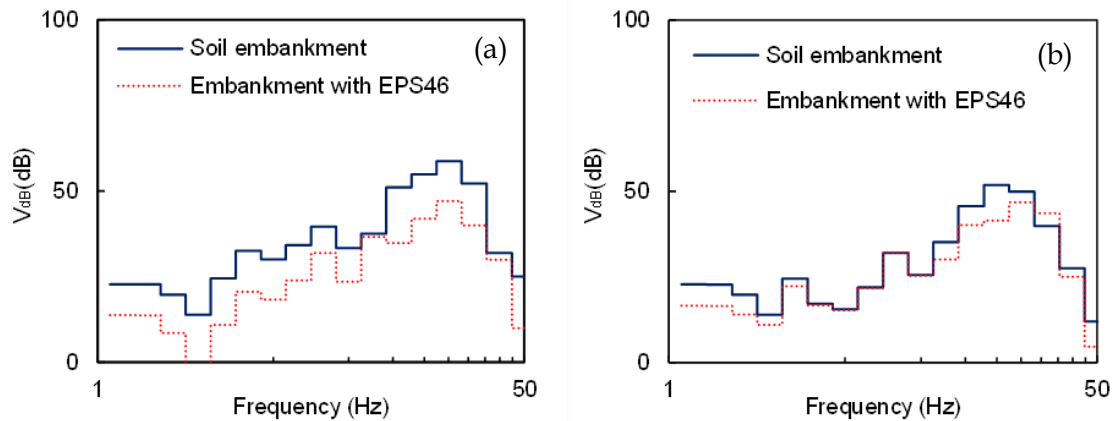
Figure 4.32 Comparison of soil and EPS-retrofitted embankments in terms of velocity decibels (V_{db}) at 35m from the track: (a) 20° of inclination, (b) 45° of inclination.

Figure 4.33 presents the vibrations levels in terms of PPV, V_{dB}, v_{rms}, and $KB_{F,max}$ at six equally spaced positions, ranging between 15 m and 35 m from the track in the case of the embankment with a slope inclination of 20°. As expected, these values are decreasing with distance from the embankment. The PPV at all the examined distances from the track has not exceeded the DIN limit for potential damage to sensitive nearby buildings (Figure 4.33a). Furthermore, the v_{rms} of the soil embankment is higher than the USDT lower limit for frequent passages of HST at distances between 15 m and 21 m from the track. The examined mitigation approach contributes to the decrease of the v_{rms} value to under

0.10mm/s for all the examined distances. In addition, the V_{dB} level is reduced to below 55dB for distances greater than 28m from the track after the mitigation with EPS blocks. The same trend is observed for $KB_{F,max}$ values (Figure 4.33d). The implementation of EPS blocks reduces the $KB_{F,max}$ to below the DIN limit for distances between 26m and 35m from the track.
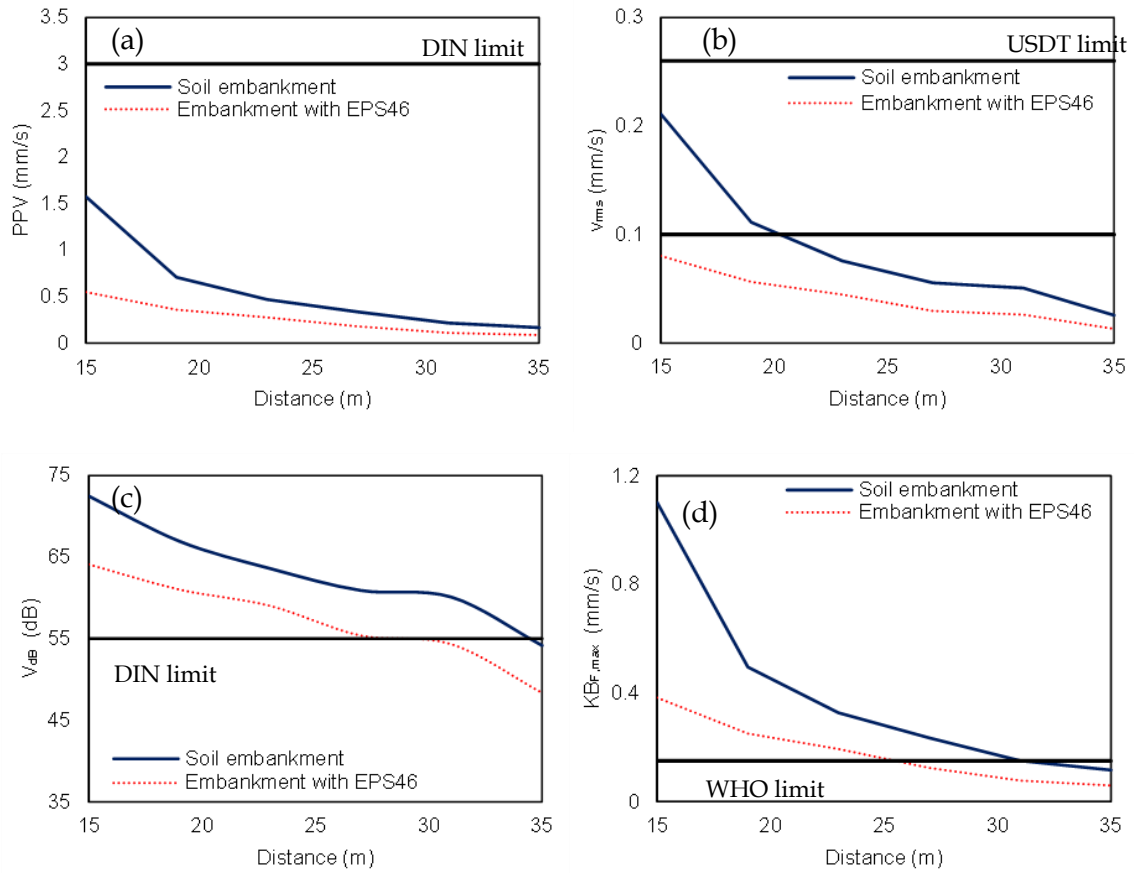
Figure 4.33 Comparison of soil and EPS-retrofitted embankments with slope inclination 20° at increasing distance from the track in terms of: (a) PPV, (b) v_{rms}, (c) V_{dB}, (d) KBF,max.

Figure 4.34 presents the vibrations level in terms of PPV, V_{dB}, v_{rms}, and $KB_{F,max}$ at increasing distances from the track in the case of an embankment with a 45° slope inclination. In the case of the soil embankment, the PPV and v_{rms} values are shallow. In particular, the v_{rms} value is lower than the USDT limit of 0.10 mm/s and the PPV is lower than the DIN limit of 3 mm/s for almost all the examined distances from the track. The implementation of EPS blocks has led to even lower values of v_{rms} and PPV. The V_{dB} level of the soil embankment is under 55 dB for distances greater than 26 m from the track. Furthermore, the mitigation of the embankment with EPS block contributes to further reducing the vibrations level. In this case, the V_{dB} level is lower than 55 dB for remote

distances between 23m and 35m from the track (Figure 4.34c). The same trend is observed for $KB_{F,max}$ values, which did not exceed the DIN limit value of 0.15 mm/s for remote distances (i.e.,>21 m) from the track.
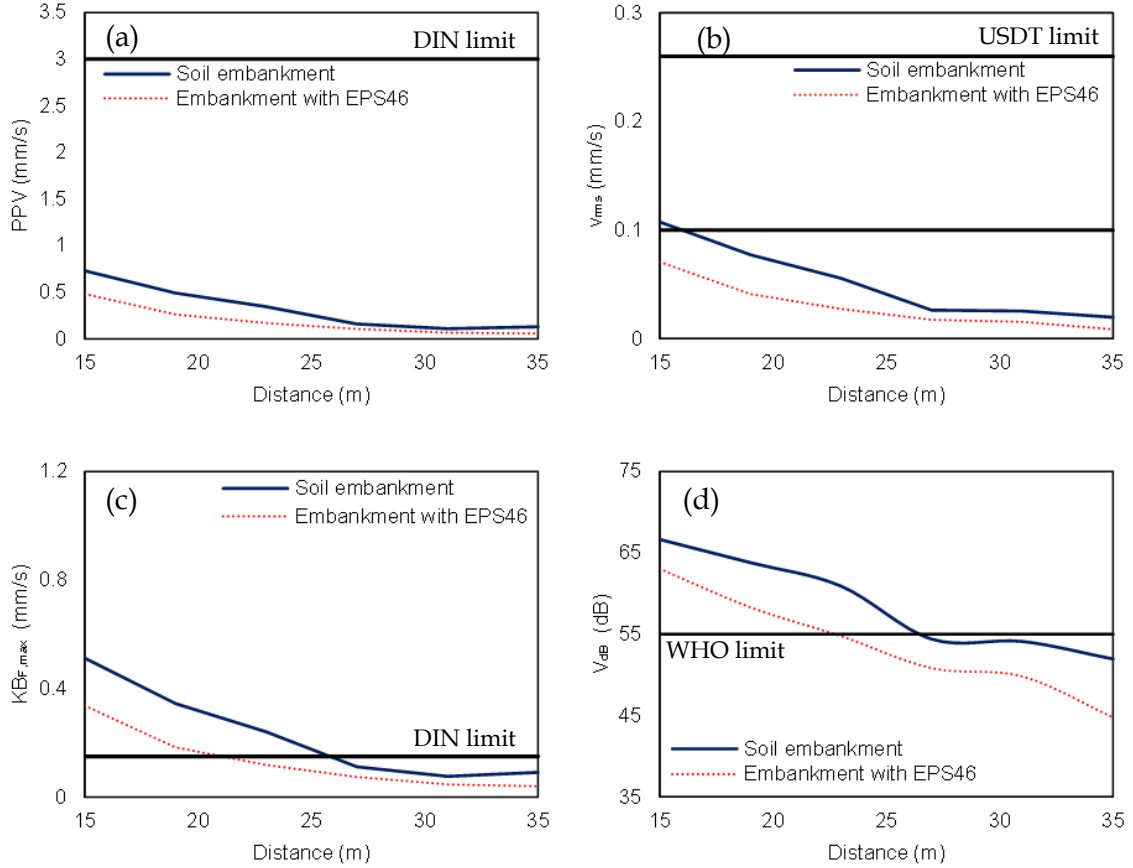
Figure 4.34 Comparison of soil and EPS-retrofitted embankments with slope inclination 45° at increasing distance from the track in terms of: (a) PPV, (b) v_{rms}, (c) V_{dB}, (d) $KB_{F,max}$.

4.8.   *Comparison with non-optimal configurations*

It is also worth noting that the rejected configuration illustrated in Figure 4.9a (i.e., a full EPS embankment) leads to substantial mitigation of the developed vibrations due to HST passage. Fig 4.35a shows that the vibrations level at 15 m from the track is almost half compared to the proposed scheme. The same observation has been made in the case of 35 m from the track, as depicted in Figure 4.35b. Nevertheless, in this case, the deflections are increased from 0.26mm to 1.27mm at HST moving axle. The vertical displacements of the rejected solution remain at high levels at all points in the surface of the embankment, as displayed in Figure 4.35c. These higher displacements could cause the derailment of the HST. However, the increased mitigation level of the vibrations necessitates further

investigating this configuration, perhaps in conjunction with other mitigation measures (e.g., trenches).
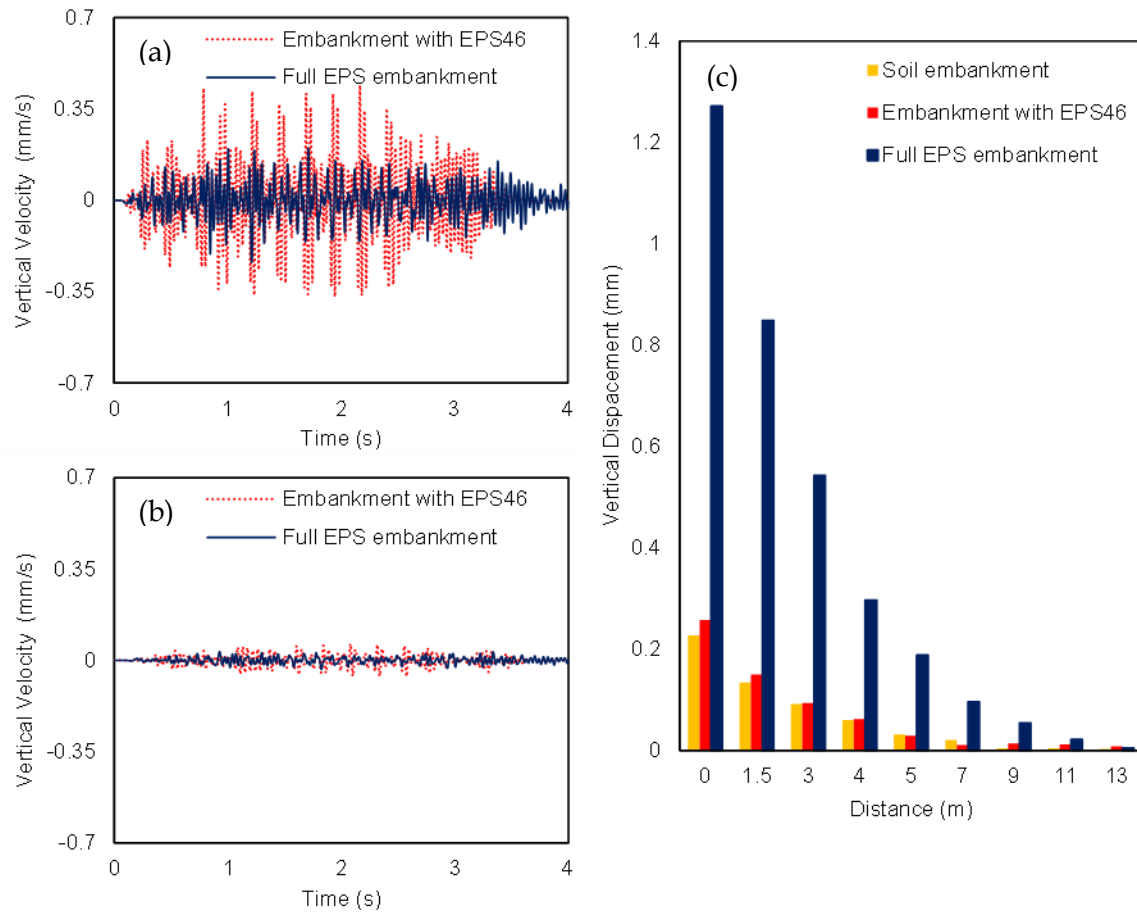
Figure 4.35 Comparison of full EPS (Figure 4.7a) and optimally EPS-retrofitted embankments (Figure 4.9): (a) vertical velocity time-histories at 15 m from the track, (b) vertical velocity time-histories at 35 m from the track, (c) vertical displacements at increasing distances from the track.

As mentioned earlier, several mitigation techniques have been investigated to reduce the developed vibrations due to HST passage. Over the last decades, EPS has been applied in many engineering applications, including normal speed railway embankments (Li, 2014; Neupane, 2015). In this Section, the focus is given on the comparison of the proposed application of EPS blocks (Model 2) with the most commonly used mitigation approach, the in-filled trench (Model 3), across the railway, which is compared. Furthermore, the hybrid implementation of both EPS-filled trenches along with EPS blocks at the slope of the embankment is investigated. Furthermore, the use of EPS46 blocks as trench filling material has also been examined as it has been proven that it is the optimal geofoam. After a preliminary investigation regarding the optimal dimensions and location, a single trench has been placed at 14m from the middle of the railway embankment, having a 50cm width

and 3m depth (see Figure 4.36c). Finally, it is assumed that using EPS blocks at the slopes of the embankment and as filling material in the trench could further decrease the HST-induced vibrations. Hence, the hybrid mitigation scenario, depicted in Figure 4.36d (Model 4), has also been studied.
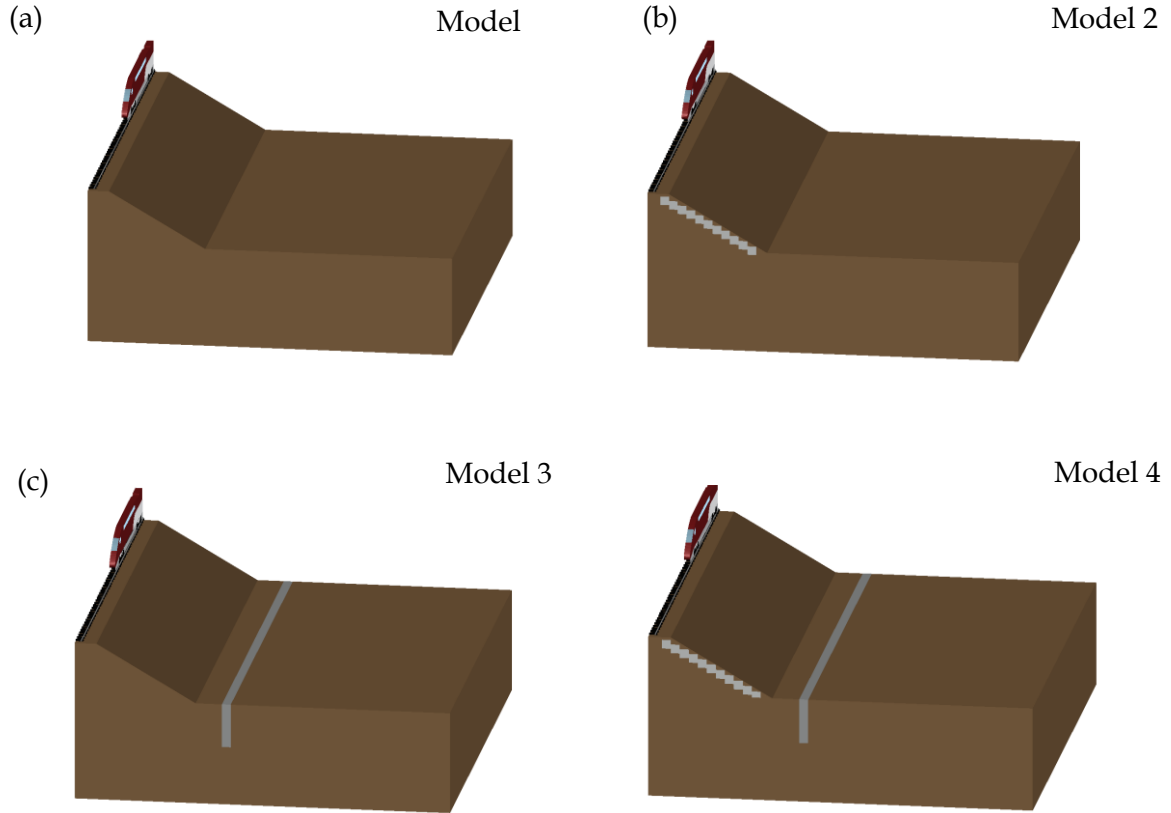
Figure 4. 36 HSR embankment cross-section: (a) Model 1 refers to the soil embankment, (b) Model 2 refers to the mitigated embankment with EPS blocks at the slopes, (c) Model 3 refers to the mitigated embankment with an EPS-filled trench, (d) Model 4 refers to the embankment with both mitigation measures.

The mitigation of the vibrations induced by HST passage using the three examined EPS configurations at 15m from the track is demonstrated in Figure 4.37. More specifically, Figure 4.37a shows the vertical velocity time-histories in the case of Model 2. As was aforementioned, the implementation of EPS blocks at the embankment slope minimizes the peak amplitude of the time hibase from 1.1mm/s to 0.45mm/s. Furthermore, the implementation of an EPS-filled trench at the base of the embankment has a beneficial role in reducing the induced vibrations as the reduction of the vibrations level reaches close to 35% (see Figure 4.37b). It is evident that the reduction of the decibel level is higher in the case of Model 2 in comparison with Model 3. The hybrid method

(e.g., Model 4) further reduces the vibrations level compared with Model 2, as shown in Figure 4.37c. However, the difference between Model 2 and 4 is marginal, Model 1 is the optimal solution in terms of implementation costs.

Figure 4. 37 Comparison of soil and EPS-retrofitted embankments at 15m from the track in terms of vertical velocity time-histories: (a) Model 1, (b) Model 2, (c) Model 3, (d) Model 4.

Figure 4.38 illustrates the vertical velocity time histories at the higher examined distance from the track, at 35m from the track. As it has arisen from Figures 4.38a and 4.38b, Model 2 still mitigates the HST-induced vibrations more successfully than Model 3. The implementation of the EPS-filled trench reduces marginal the vibrations level at the far-field. However, it is evident that Model 2 and Model 4 minimize the vibrations level more effectively. In these cases, the peak vertical velocity has been reduced below 0.05mm/s. It could be concluded that the proposed configuration with the implementation of EPS geofoam at the slope of the embankment (e.g., Model 2) is the optimal solution if the constructor takes into consideration both the efficacy and the cost of implementation.

Figure 4. 38 Comparison of soil and EPS-retrofitted embankments at 15m from the track in terms of vertical velocity time-histories: (a) Model 1, (b) Model 2, (c) Model 3, (d) Model 4.

In the sequence, the effectiveness of the proposed scheme is compared with Model 3. In Figure 4.39, the insertion loss calculated for Model 3 is compared with the corresponding one for the side-filled with EPS46 blocks embankment. Calculations have been made for the one-third octave band with centre frequency from 1.25 to 50Hz. Subsequently, the results are averaged into one-third octave bands, as presented in Figure 4.39. The insertion loss is calculated as follows (Coulier et al., 2013):

$$\text{IL} = 20 \log_{10} \frac{v_{rms,soil}}{v_{rms,0,mit}} \tag{4.1}$$

where:

$v_{rms,soil}$: the root mean square of the spectral velocity at the centre frequency of each 1/3 octave band of the initial soil embankment,

$v_{rms,mit}$: the root mean square of the spectral velocity at the centre frequency of each 1/3 octave band of the mitigated geostructure for each of the two examined approaches.

119

It is evident from Figure 4.39 that the implementation of EPS46 blocks at the slope is much more efficient from the EPS in-filled trench at the low frequencies between 3.15Hz and 25Hz. On the other hand, for higher frequencies (> 30 Hz), the insertion loss is increased in the case of the EPS-filled trench. More specifically, the insertion loss is close to 10dB at 4Hz, 12.5Hz and 25Hz, while a maximum insertion loss, equal to 16dB, is achieved at 20Hz. It is worth mentioning that according to several studies (e.g., (Thompson et al., 2016b)) the maximum insertion loss even for an open trench (i.e., filled with air) varies in the range of 10dB to 20dB. Hence, the reductions of the vibration levels in the low-frequency range using this efficient mitigation scheme are comparable even to those achieved by open trenches.
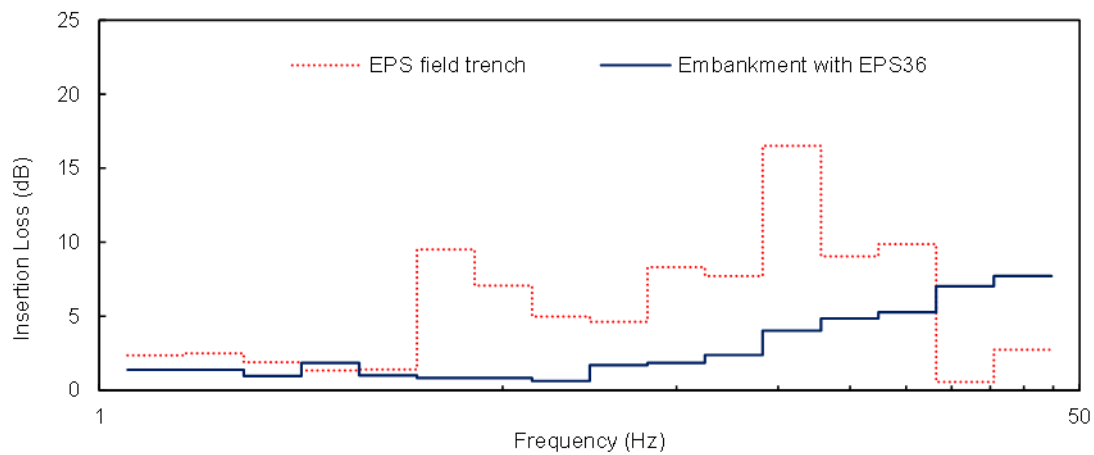
Figure 4.39 Comparison of insertion loss at 15 m from the track for embankment with EPS46 with EPS-filled trench.

4.9. *Investigation of HST passing velocity*

As detailed in Chapter 2, the passing velocity of the HST plays a crucial role in the induced vibrations. Thalys and TGV HST peak operation velocity, commonly used in the examined Paris-Brussels HSR line, is equal to 300km/h. For this reason, the assumption has been made that Thalys may pass from Site 1 with velocities from 0km/h to 300km/h. Hence, the vibrations level and the efficacy of the proposed mitigation approach for the passage of Thalys with several frequencies lower than 300km/h are examined. Figure 4.40 demonstrates the peak partial velocity for several passing velocities in the regular embankment case compared with the retrofitted embankment with EPS46. It is evident that for lower velocities, the amplitude of the peak vertical velocity is significantly reduced. For instance, the PPV level is just 0.3mm/s, in the case of Thalys passage with

100km/h from the regular soil embankment. This amplitude gradually increases close to 1.3mm/s, for Thalys passage with 200km/h.

Furthermore, the PPV remains at the same level for passing velocities between 200km/h and 300km/h. The implementation of EPS geofoam at the embankment slope reduces the vibrations level in low-speed passage marginally. On the other hand, the efficacy of the proposed mitigation scheme is even more pronounced for speeds higher than 150km/h. It should be mentioned that the Rayleigh waves velocity of the surface layer soil is equal to 132m/s (475.2km/h), as it is calculated from Eq. (2.7). Hence the examined speeds are significantly lower than the critical speed on this site, as Thalys HST cannot reach this speed.
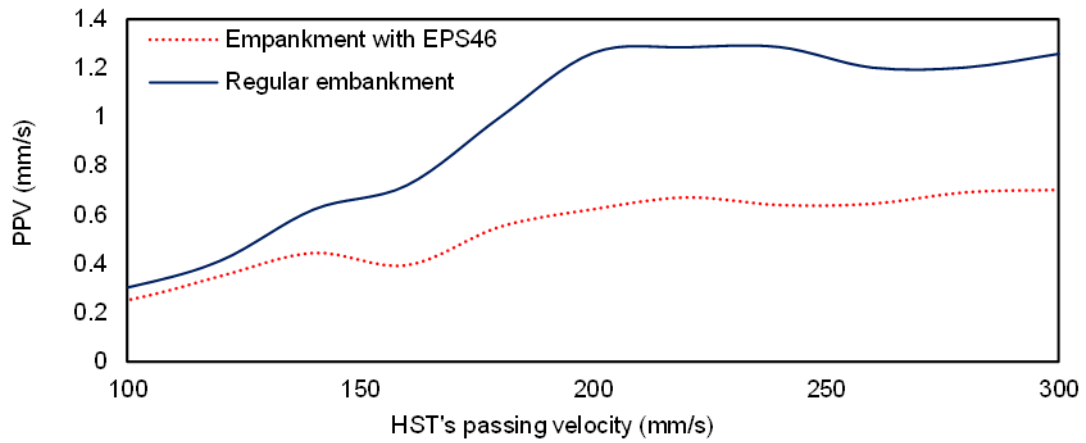
Figure 4.40 PPV level for several Thalys HST passing velocities.
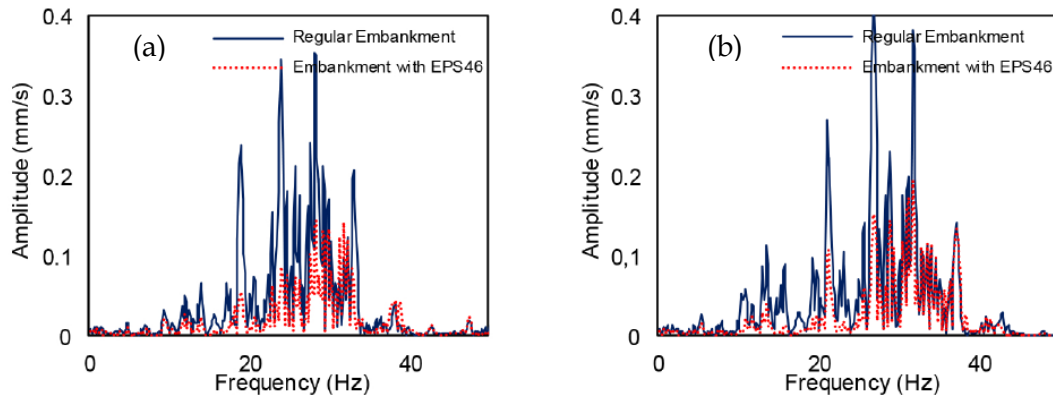
Figure 4.41 Comparison of soil and EPS-retrofitted embankments in terms of vertical velocity Fourier spectra for increased Thalys passing speed: (a) 320 km/h, (b) 360 km/h.

Nowadays, the operation speed of Thalys at the examined site is between 280 km/h and 300 km/h. There are even faster HST worldwide; for instance, Shanghai Maglev maximum speed reaches 430 km/h (Zhang and Huang, 2019) maximum speed is equal to 350 km/h (Sun et al., 2018). It should be noted that Thalys is operating since 1996; thus,

it may be replaced by a faster train in the future. Hence, the capability of the proposed mitigation approach to reduce HST vibrations level for even higher speeds should be investigated. Accordingly, the Fourier spectra at 15m from the track are indicatively shown in Figure 4.41, illustrating the decrease of the induced vibrations in the cases of higher passing speeds equal to 320 km/h and 360 km/h. Note that although the spectral values at the dominant frequencies are higher as the passing speed increases from 284 km/h, the vibrations level is always significantly reduced in the whole low-frequency range due to the presence of a few EPS blocks at the sides of the embankment.

4.10. *Investigation of embankment subsoil conditions*

In this Section, the varying soil conditions are investigated in order to examine the efficiency of the aforementioned EPS-based mitigation measure more thoroughly since the underlying soil and the embankment fill soil strongly influence the developed vibrations. In addition, the proposal of using EPS material as a mitigation measure is further expanded by examining its application as trench filling material, either alone or in conjunction with the placement of EPS blocks at the slopes of the railway embankment. Four different typical soil types, classified as rock, dense sand with gravels, stiff and soft clay, have been examined for this purpose.

In addition, the material properties of the embankment have been altered to assess to what extent they affect the propagation of HST vibrations and the effectiveness of the application of EPS blocks for their mitigation. The mechanical properties of the examined soils are shown in Table 4.1. The single soil layer under the embankment has been modeled as a solid section with dimensions equal to 30m, 50m and 50m (depth, width and length, respectively). Rayleigh damping has been used, in which the damping matrix [C] is analogous to the mass matrix [M] and the stiffness matrix [K] (Nakamura, 2017). In the present investigation, the damping ratio of the examined soils is set equal to 5%. In order to achieve a damping ratio of 5% within the frequency range of 5 to 60Hz, parameters α and b have been set equal to 4.901s^{-1} and 0.0003s, respectively.

In the sequence, a comparison between the conventional and the three mitigated embankments is presented for the four hypothetical soil scenarios in terms of velocity time-histories and Fourier spectra. Note that the scales in the plots are kept constant in order to illustrate that -as expected- the HST vibrations are increasing as underlying soil gets softer. The results are given for two characteristic locations, i.e., d=15m and d=35m

from the track, to illustrate the impact of the proposed mitigation measures both near-field and far-field from the track. These locations are often used in field measurements (Connolly et al., 2014; Kouroussis et al., 2011) and are also used in the validation of the applied numerical modeling approach in Chapter 3.

Table 4.1. Parameters of the examined four soil types.

	Soil type	Density (kg/m³)	Young's Modulus E_s (MPa)	Poisson's ratio	Damping ξ (%)
A	Rock	2150	10000	0.15	5
B	Dense sand with gravels	2100	1000	0.20	5
C	Stiff clay	2000	600	0.25	5
D	Soft clay	1850	170	0.35	5
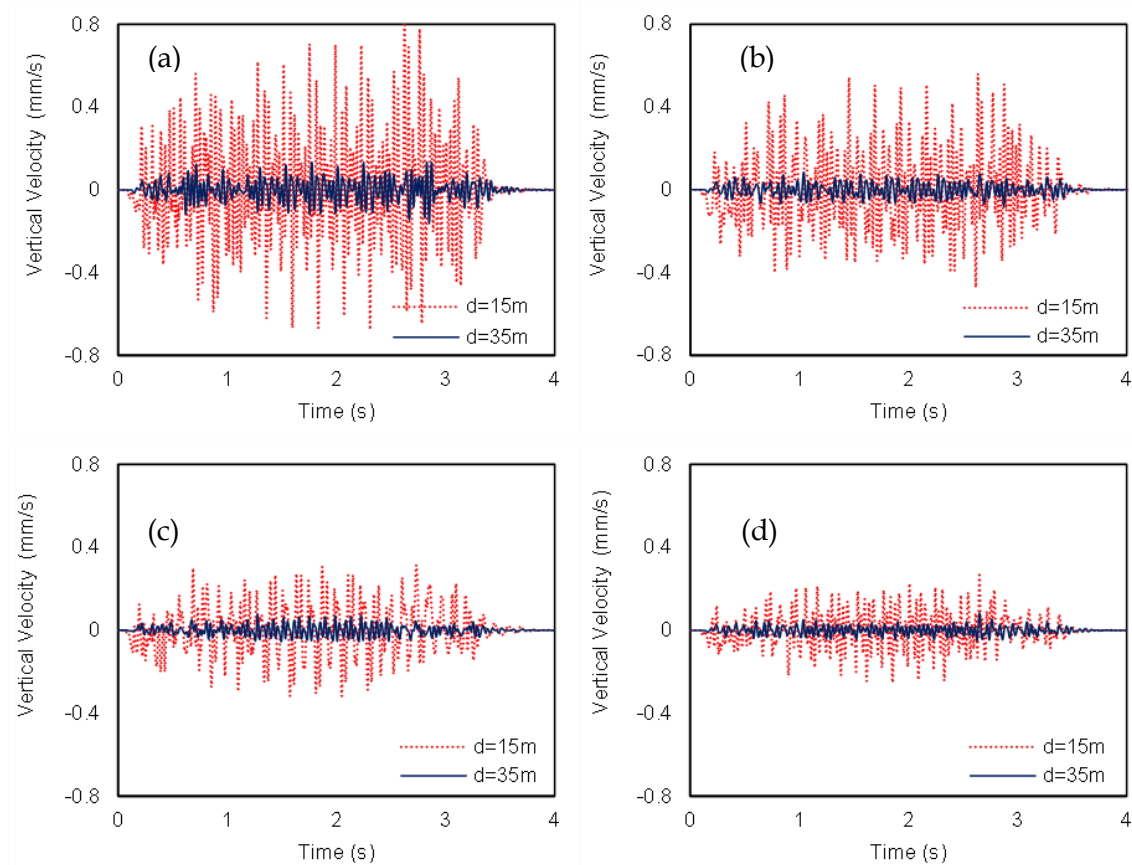
Figure 4.42 Comparison of soil and EPS-retrofitted embankments on soft clay in terms of vertical velocity time-histories: (a) Model 1, (b) Model 2, (c) Model 3, (d) Model 4.

4.10.1. Soft clay

A loose soil, classified as soft clay, is the first scenario that has been examined in this Chapter. The implementation of a limited number of EPS blocks (Model 2) in such soils plays a very beneficial role in the mitigation of the induced HST vibrations. The maximum vertical velocity has been decreased from 0.8mm/s to 0.35mm/s at the near-field location

(at 15m). The same trend is observed for Model 3, where the maximum vertical velocity has been decreased from 0.8mm/s to 0.5mm/s (the reduction is less than the corresponding one for Model 2). Lastly, as it can be noticed from Figure 4.42d, the decrease of the vibrations levels is even higher in the case of Model 4.
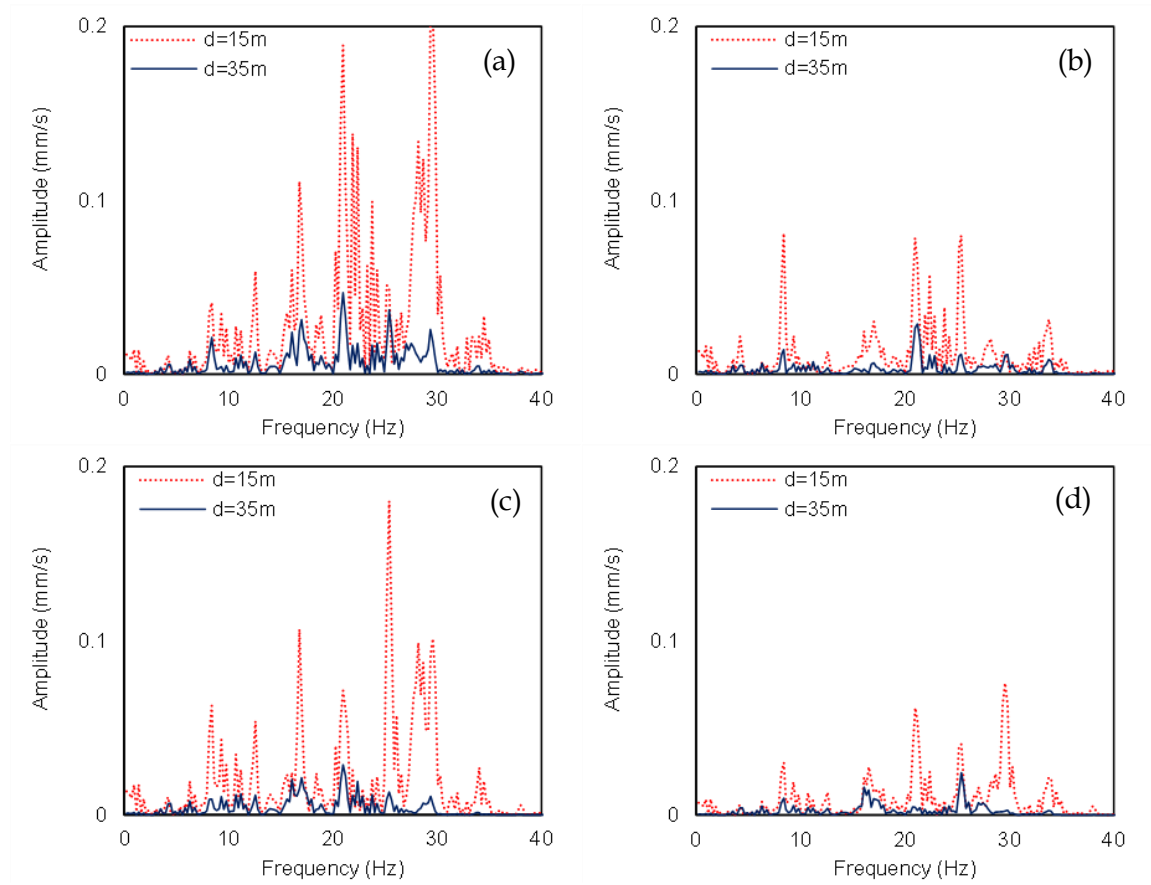
Figure 4.43 Comparison of soil and EPS-retrofitted embankments on soft clay in terms of vertical velocity Fourier spectra: (a) Model 1, (b) Model 2, (c) Model 3, (d) Model 4.

The most critical vibrations are the vibrations in the low-frequency range (Kouroussis et al., 2011). Accordingly, Figure 4.43 presents the impact of the examined mitigation measures on the velocity spectra at the low-frequency range (0-40Hz). In the case of Model 1, three frequencies (21.4Hz, 25.4Hz and 29.3Hz) can be spotted in Figure 4.43a. The plot in Figure 4.43b displays the improvement of the soil response in the whole low-frequency range in the case of Model 2. For example, the peak of the most dominant frequency (29.3Hz) is reduced from 0.2mm/s to almost 0 mm/s. In contrast, Figure 4.43c illustrates that the EPS-filled trench (Model 3) implementation has led to a slight reduction of the vibrations peaks in the whole examined frequency range (0 to 40Hz). It is obvious from Figure 4.43d that regarding near-field vibrations (i.e., at 15m), Model 4 has led to a

remarkable improvement of the soil response. The same observation can be drawn at 35m, where the examined measures mitigate the HST vibrations effectively.

In the sequence, the velocity decibels (V_{dB}) of the four examined Models are illustrated in Figure 4.44. More specifically, the response of the soil at 15m from the track to the passage of Thalys HST is demonstrated in Figure 4.44a. The most dominant octave bands are the 13th, 14th and 15th, where the vibrations levels in the case of the regular soil embankment range between 60dB and 64dB. Model 2 manages to reduce those values successfully. For instance, the decibel level is reduced from 64dB to 48dB at the octave band with a centre frequency 31.5Hz. Furthermore, the implementation of the EPS-filled trench at the base of the embankment (e.g., Model 3) has managed to reduce the vibrations level slightly. However, this approach is less effective in comparison with Model 2. The most effective mitigation approach is the most effective; hence it minimizes the decibel level below 52dB for all the dominant octave bands.
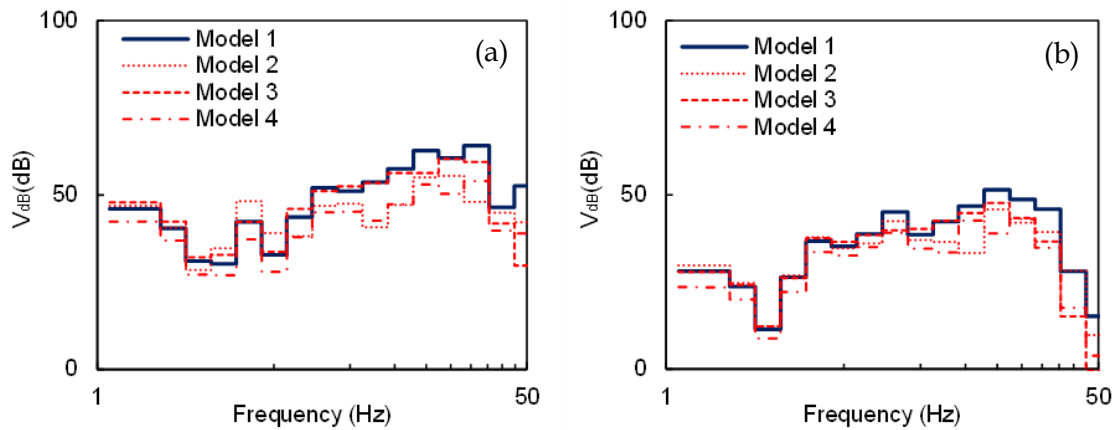
Figure 4. 44 Comparison of soil and EPS-retrofitted embankments on soft clay in terms of decibel level a: (a) at 15m from the track, (b) at 35m from the track.

Figure 4.44b illustrates the decibel level on each octave band with centre frequencies between 1.25Hz and 50Hz for the three examined mitigation scenarios. The decibel level of the regular soil embankment is significantly lower in comparison with the near field. The most dominant octave bands are those with centre frequencies between 16Hz and 31Hz. Furthermore, the decibel level remains below 52dB for the whole examined frequency range. All three examined mitigation schemes successfully minimize the vibrations level. More specifically, Model 2 and Model 3 reduces the decibel level of all the examined octave bands below 46dB. The most effective mitigation approach remains the hybrid (e.g., Model 4), as it manages to reduce the decibel level below 42dB.

4.10.2. Stiff clay

As shown in Figure 4.45, the beneficial influence of the mitigation with EPS46 blocks is also significant for stiff clay. In this case, Young's Modulus of the soil is 3.5 times higher than in the previous scenario. This results in lower vertical velocities than soft clay, e.g., at 15m, the maximum vertical velocity is equal to 0.4mm/s (see Figure 4.45a), almost half than previously (see Figure 4.42a). Figure 4.45b depicts the significant vibrations mitigation in the case of Model 2. The maximum vertical velocity is close to 0.19mm/s, 50% lower than for Model 1. Similarly, the vertical velocities have also been reduced in Model 3, in which the maximum vertical velocity is 0.18mm/s at 15m. The same observations can be made at 35m; in this case, all the examined mitigation measures contribute to a 50% reduction of the vertical velocity. For example, the maximum vertical velocity is decreased from 0.11mm/s to 0.06mm/s after the implementation of the EPS-filled trench (Model 2).
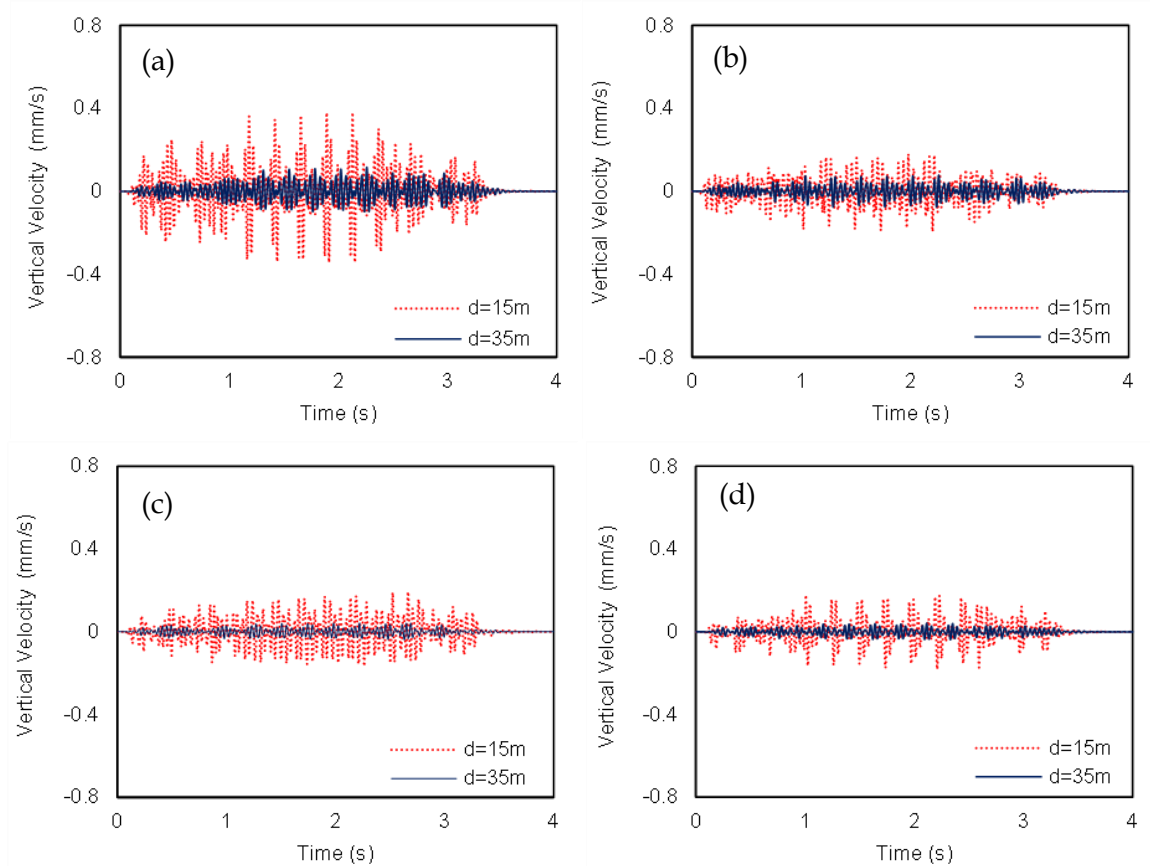
Figure 4.45 Comparison of soil and EPS-retrofitted embankments on stiff clay in terms of vertical velocity time-histories: (a) Model 1, (b) Model 2, (c) Model 3, (d) Model 4.

Figure 4.46 displays the comparison between the Fourier spectra of the four examined models for stiff clay. As it is clearly illustrated, the most critical frequencies remain the same as in the case of soft clay, while the peak values are decreased. For instance, the peak at 25.4Hz is equal to 0.12mm/s at 15m (about 50% of the peak for soft clay). The proposed measures are efficiently mitigating the HST vibrations within the low-frequency range. It can be noticed that Model 3 is more effective in the frequency range from 40Hz to 60Hz, while Model 2 reduces the vibrations significantly in the lower frequency range (0 to 40Hz). Figure 4.39d illustrates that Model 4 leads to the maximum mitigation of the vibrations. Similarly, at 35m, the proposed mitigation measures contribute to the spectral velocity reduction in the whole low-frequency range.
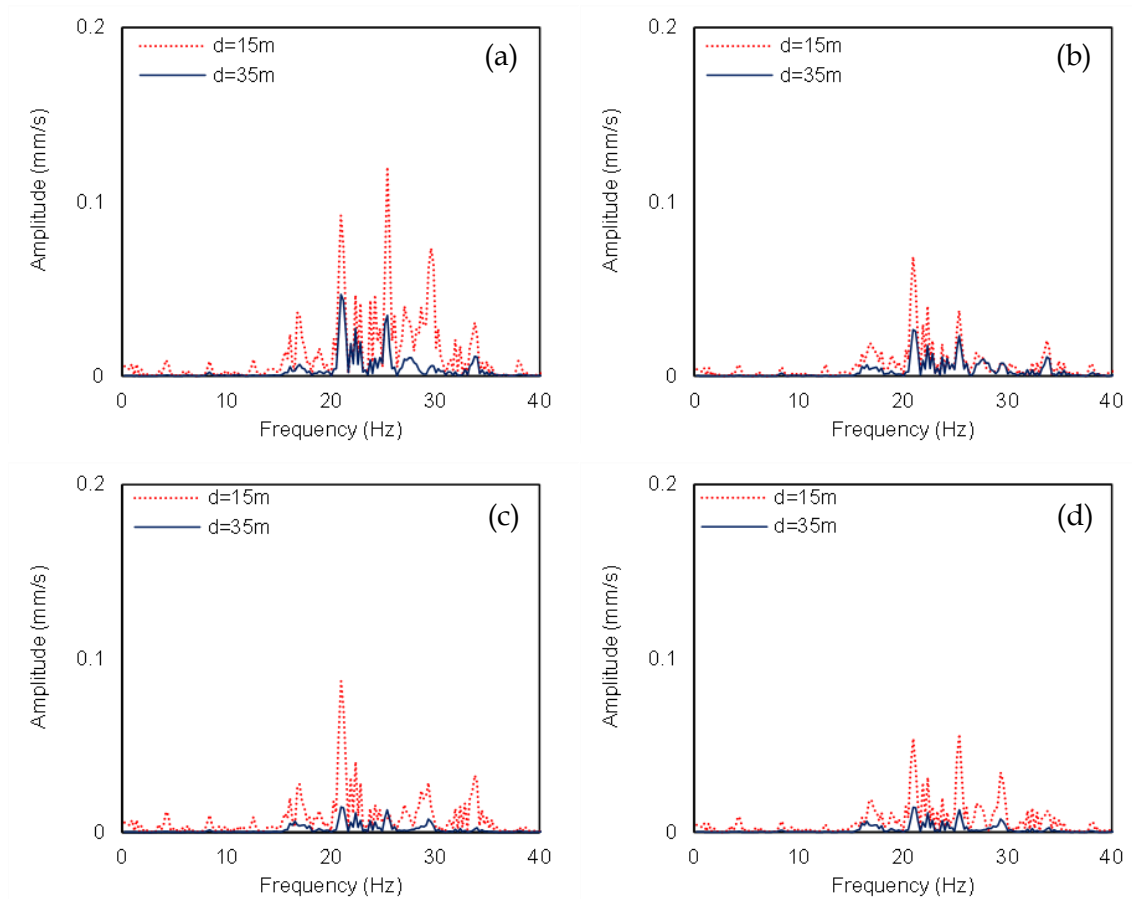
Figure 4.46 Comparison of soil and EPS-retrofitted embankments on stiff clay in terms of vertical velocity Fourier spectra: (a) Model 1, (b) Model 2, (c) Model 3, (d) Model 4.

To further illustrate the beneficial role of the examined mitigation approaches, the decibel level of each low-frequency octave bands is presented in Figure 4.47. In the case of the regular embankment, the decibel level ranges between 55dB and 57dB at the most dominant octave bands with central frequencies 20Hz, 25Hz and 31.5Hz at 15m from the

track. These values have been significantly reduced after the implementation of EPS at the slope of the embankment. In this case, the highest reduction of decibel level has been observed. The decibel level at the 15th octave band has been reduced from 55dB to 43dB. Furthermore, the most effective mitigation approach is Model 4, as it manages to reduce the decibel level below 50dB for all the examined octave bands. Figure 4.47b compares the decibel level at far-field (e.g., 35m from the track) of the four examined models. The decibel level has been substantially reduced below 20dB for the octave bands with centre frequencies below 12.5Hz. Furthermore, the decibel level at the most dominant octave bands (e.g., 13th and 14th) has been reduced below 50dB. In this case, the hybrid approach reduces the vibrations level below 40Hz for all the examined low-frequency octave bands.
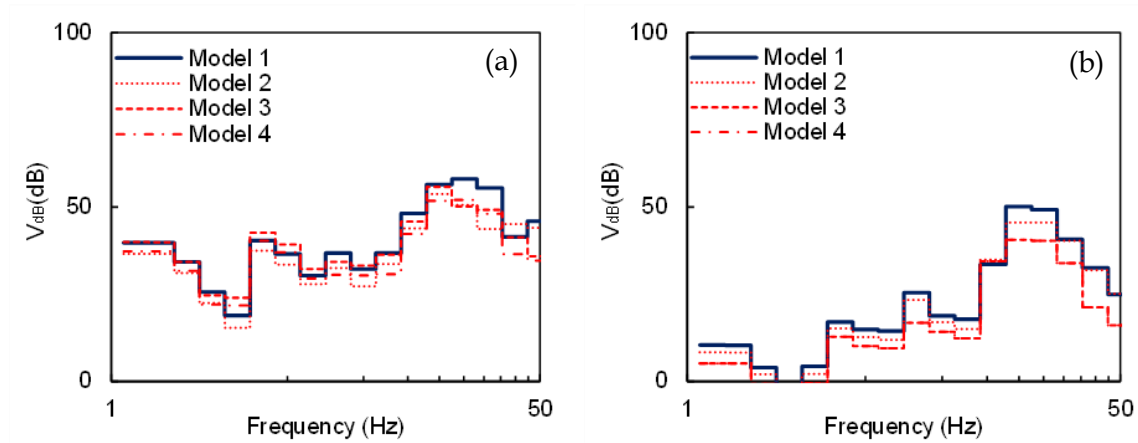
Figure 4.47 Comparison of soil and EPS-retrofitted embankments on stiff clay in terms of decibel level a: (a) at 15m from the track, (b) at 35m from the track.

4.10.3. Dense sand with gravels

Figure 4.48 illustrates the vertical velocity time-histories when the embankment is located on stiff soil (dense sand with gravels), where there is a significant decrease in the vibrations compared to stiff clay, while the beneficial impact of EPS is not so pronounced as in the previous cases of softer soils. More specifically, the maximum vertical velocity of the soil embankment model at 15m is equal to 0.2mm/s. Due to the higher weight of the first and the last locomotive bogies, higher near-field soil response has been observed when these carriages pass. As shown in Figure 4.48b, Model 2 has slightly reduced the vibrations induced by Thalys HST at both examined locations. Furthermore, Model 3 results in a higher decrease of the developed vibrations. Lastly, Model 4 leads to the optimum mitigation of the vibrations since the maximum vertical velocity is less than 0.16mm/s (see Figure 4.48d).
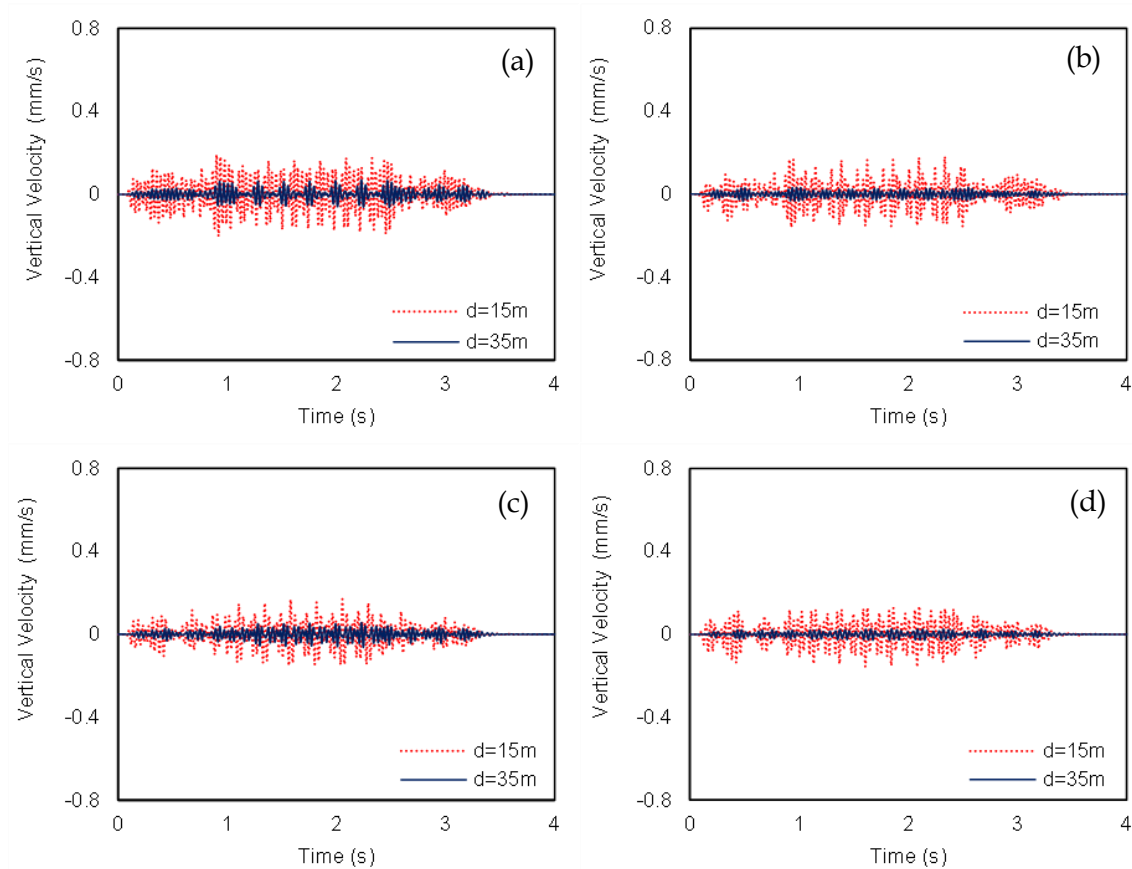
Figure 4.48 Comparison of soil and EPS-retrofitted embankments on dense sand with gravels in terms of vertical velocity time-histories: (a) Model 1, (b) Model 2, (c) Model 3, (d) Model 4.

The primary vibrations peaks at 25.4Hz and 29.3Hz in the soil embankment (Model 1) at 15m are equal to 0.06mm/s and 0.08mm/s, respectively is clearly illustrated in Figure 4.49. Furthermore, two lower peaks have been observed at 21.4Hz and 33.8Hz. Model 2 has contributed to the reduction of the most dominant peak at 29.3Hz from 0.08mm/s to 0.03mm/s. In addition, the vibrations peak at 25.4Hz has been reduced to 0.04mm/s. On the other hand, the peak at 21.4Hz has been slightly increased. Furthermore, in Model 3, the vibrations peaks at 15m are slightly reduced. Model 4 exhibits the higher reduction of the vibrations peak at 29.3Hz. However, the reduction of the vibrations level at the other peaks is marginal. Similar observations are made for the examined models at the far-field location (35m from the track). Figure 4.50a illustrates the 1/3 octave bands at 15m from the band of the four examined models when the HST passes through a site with dense sand with gravels. Obviously, in this case, the decibel level of the regular embankment is significantly lower compared to the pre-examined softer soils. More specifically, the peak decibel level, in this case, is equal to 53dB in comparison with the 64dB in the case of the soft clay. Hence, the implementation of any mitigation measure, in this case, is not

necessary. It is evident that according to Figure 4.37a, the reduction of the decibel level at the most dominant octave bands is marginal for all the examined mitigation approaches. Nevertheless, in general, the vibrations level remains close to the regular embankment at the whole examined frequency range. At the far-field, the level of the vibrations reduction is higher, although there is still no need for mitigation measures as the initial vibrations level is lower than 50dB.
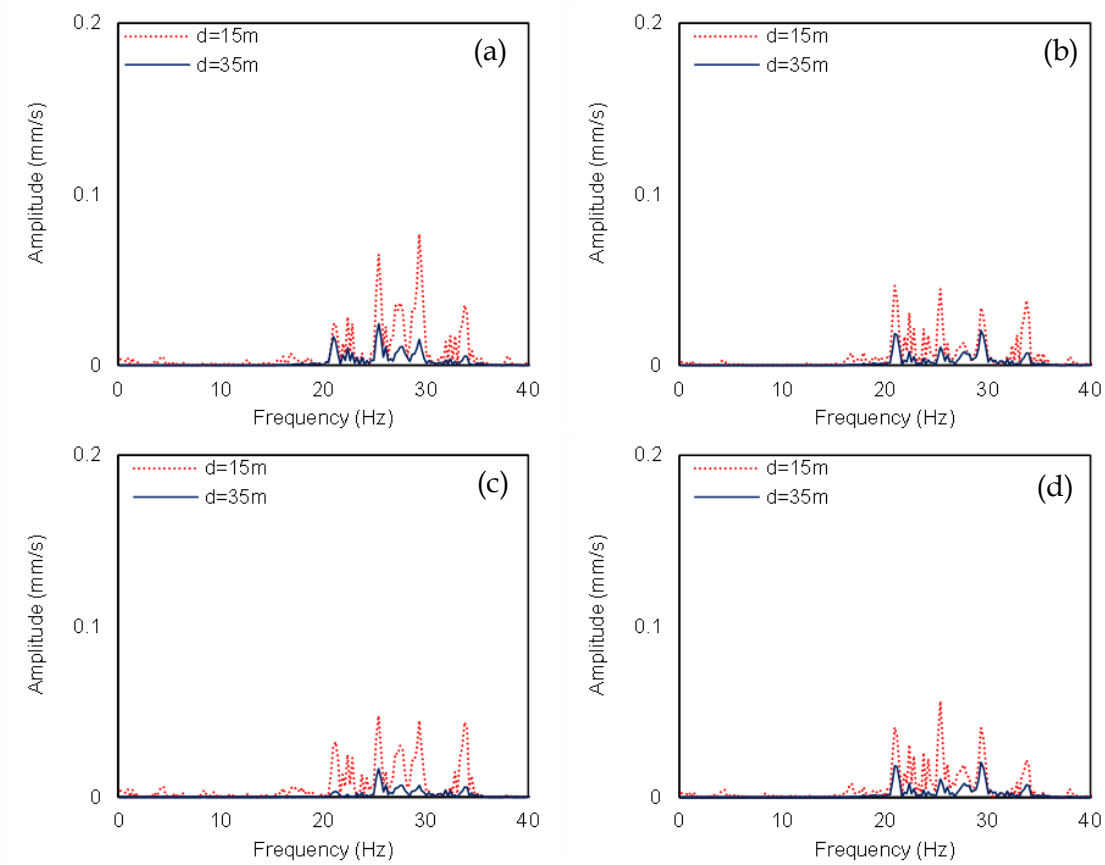
Figure 4.49 Comparison of soil and EPS-retrofitted embankments on dense sand with gravels in terms of vertical velocity Fourier spectra: (a) Model 1, (b) Model 2, (c) Model 3, (d) Model 4
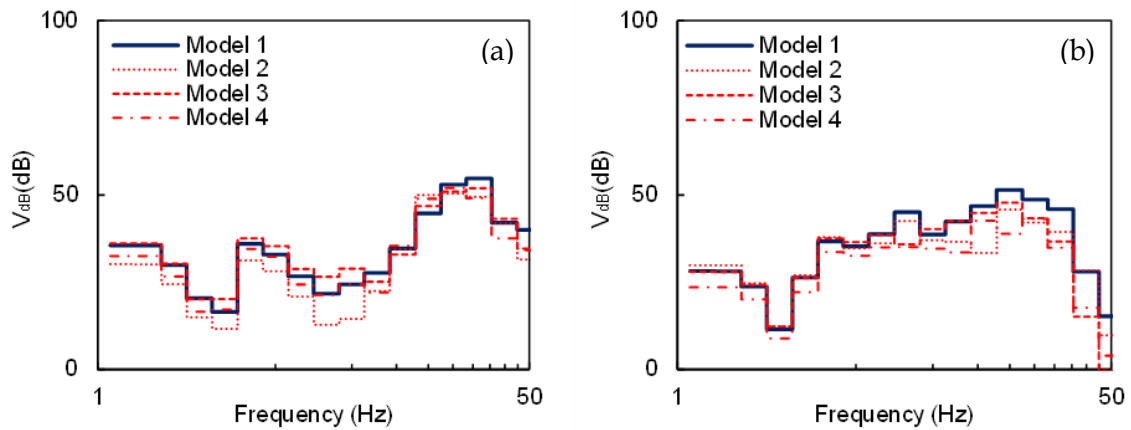
Figure 4.50 Comparison of soil and EPS-retrofitted embankments on dense sand with gravels in terms of decibel level a: (a) at 15m from the track, (b) at 35m from the track.

4.10.4. Rock

In the last soil scenario, the passage of Thalys HST over a very stiff soil layer has been investigated. The examined soil has been classified as rock. Figure 4.51 depicts a comparison between the initial soil embankment and the EPS-retrofitted embankments regarding the velocity time-histories at 15m and 35m from the track. According to Figure 4.51, in this case, the vibration level is almost zero for all the examined models. Hence, it is obvious that there is no need for the implementation of any mitigation approach. In order to present the difference of the vibrations level in comparison with the previously examined soil, the same limits of the vertical velocity axle have been used in Figure 4.51.
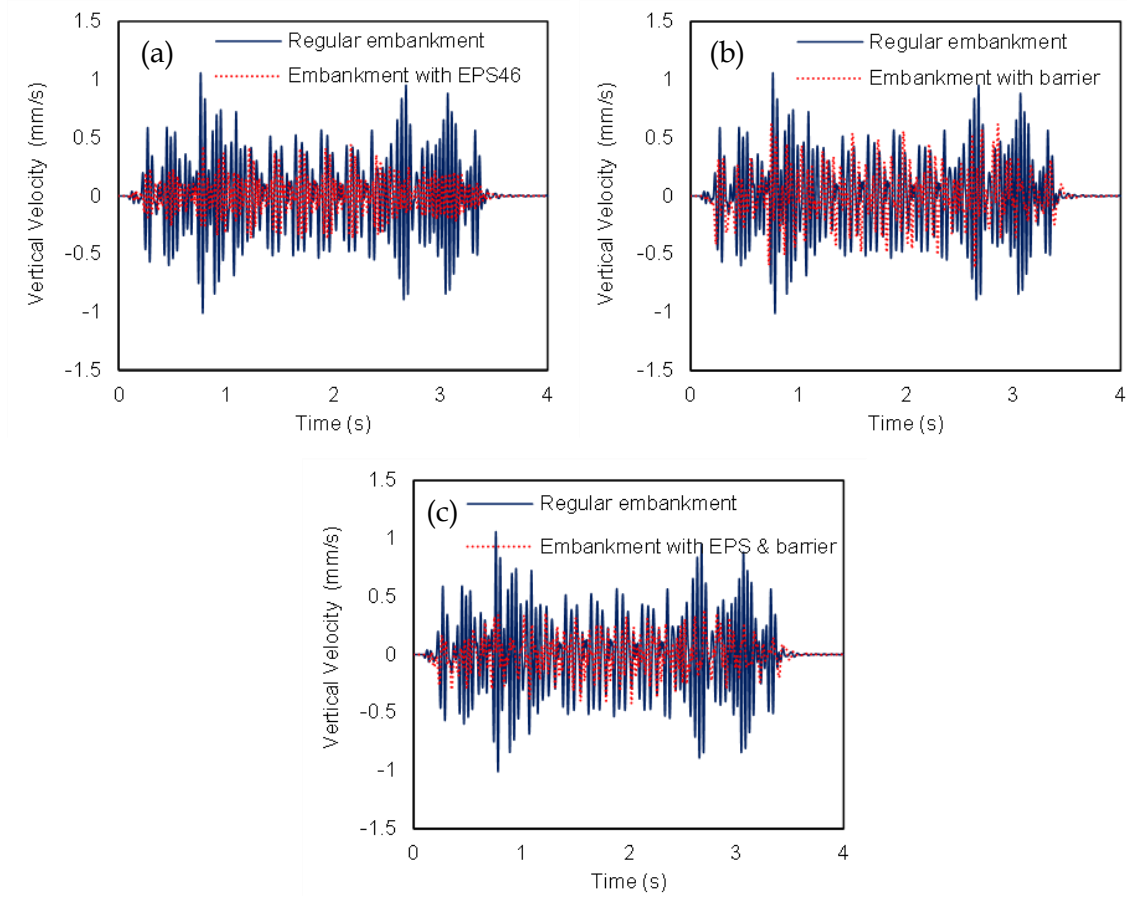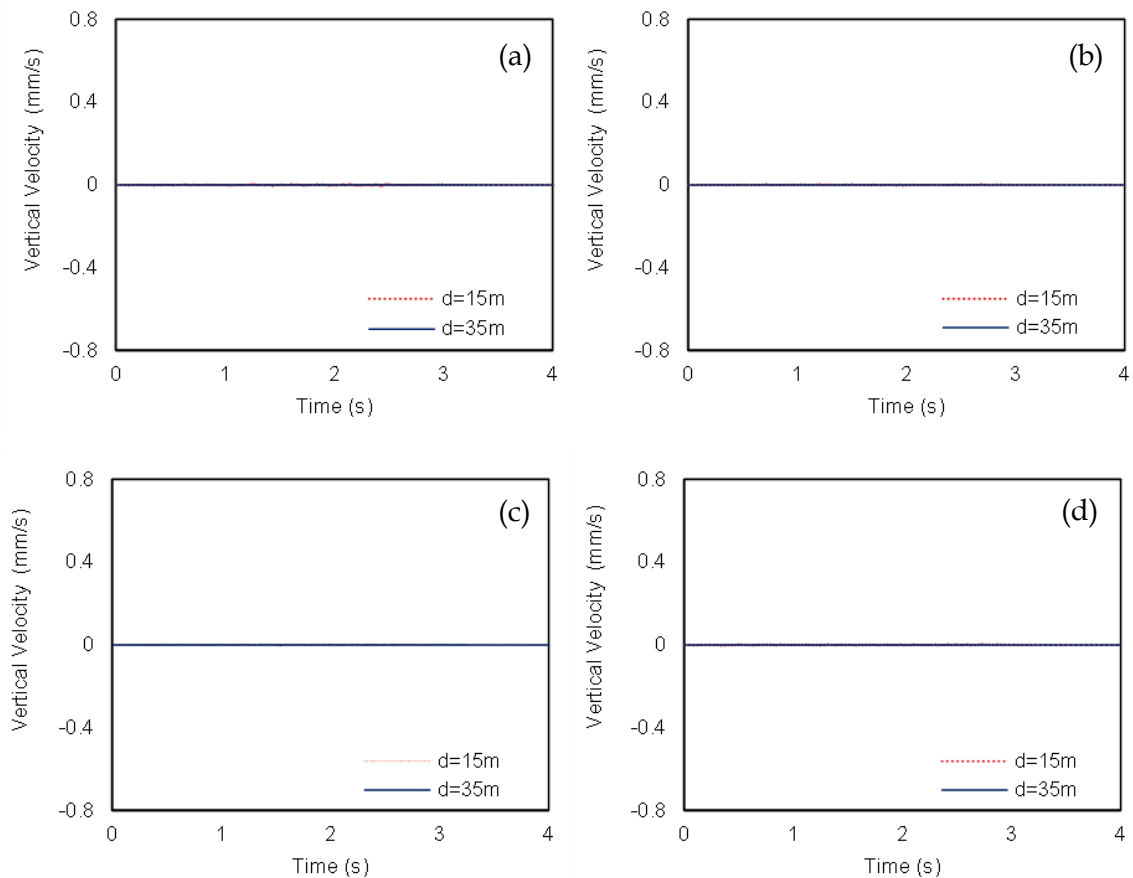

Figure 4.51 Comparison of soil and EPS-retrofitted embankments on rock in terms of vertical velocity time histories: (a) Model 1, (b) Model 2, (c) Model 3, (d) Model 4.

Accordingly, Figure 4.52 presents the influence of the examined mitigation measures on the velocity spectra when the HST is passing by a rocky site. As it was aforementioned, the HST ground-borne vibrations on the examined site are extremely low. Furthermore, there are some vibrations peaks at frequencies higher than 40Hz. For this purpose, the Fourier spectra' limits have been alerted to be all the vibrations peaks observable. At the

near field, there are numerous vibrations peaks at frequencies between 0 and 55Hz. Those peaks have been virtually disappeared at the far-field. Furthermore, the application of the examined mitigation measures is not effective enough. Hence, the use of EPS geofoam block on rocky sites is not recommended.
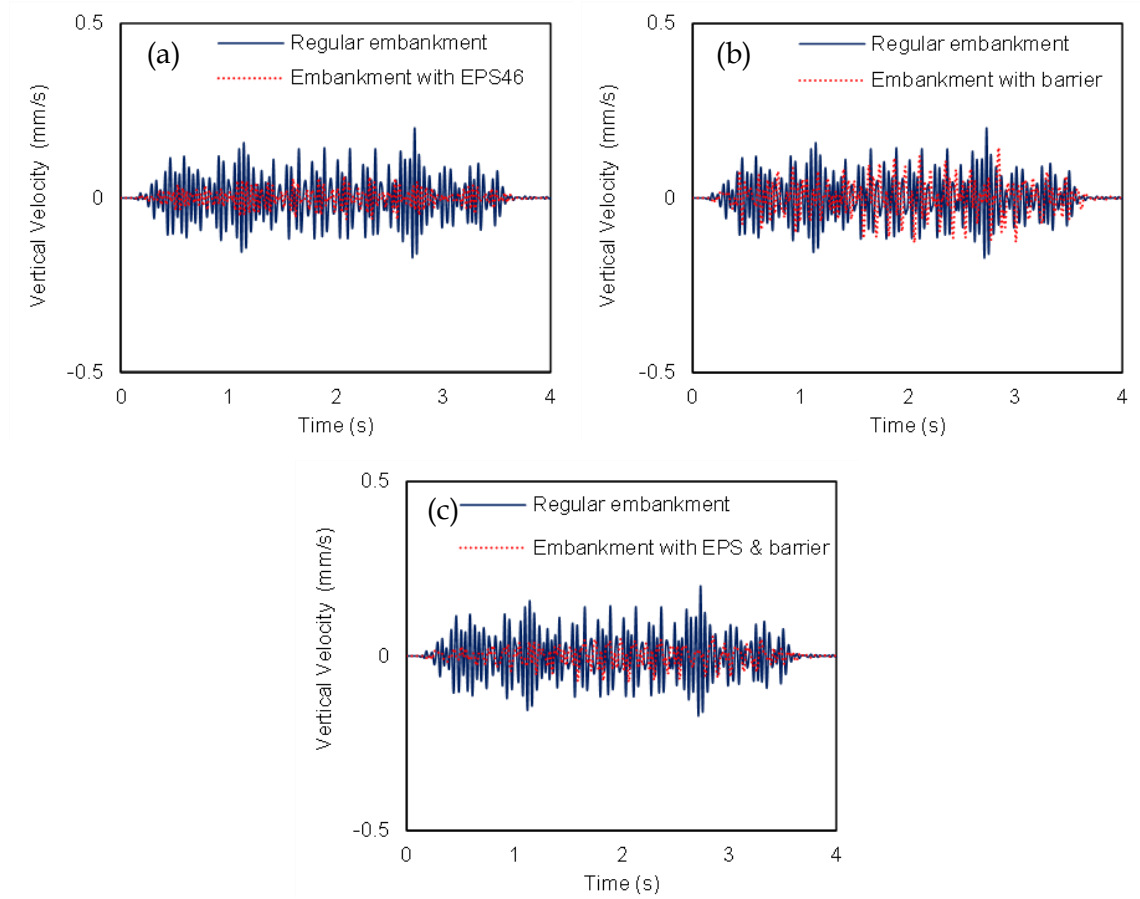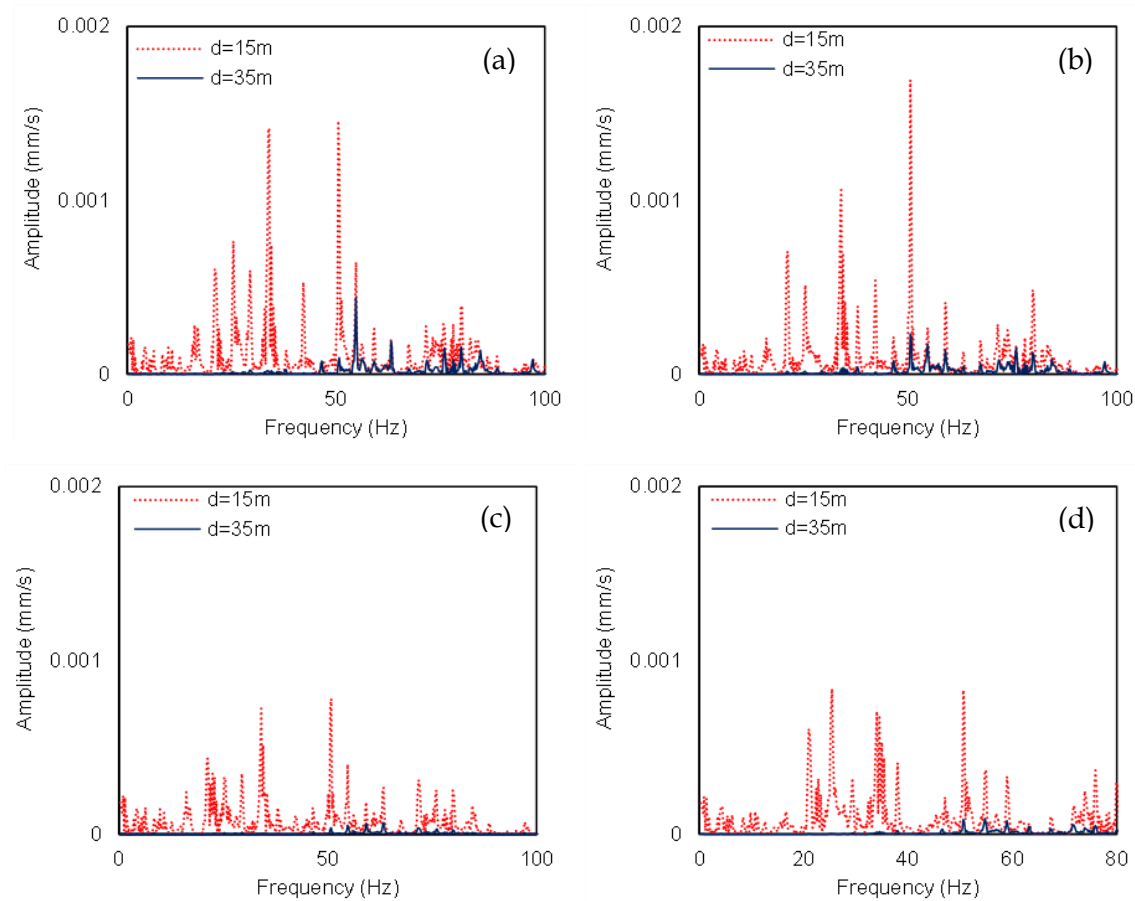

Figure 4.52 Comparison of soil and EPS-retrofitted embankments on rock in terms of vertical velocity Fourier spectra: (a) Model 1, (b) Model 2, (c) Model 3, (d) Model 4.
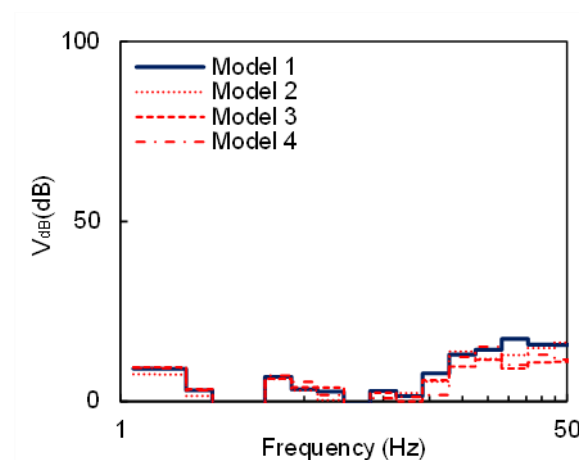
Figure 4.53 Comparison of soil and EPS-retrofitted embankments on rock in terms of decibel level at 15m from the track.

Figure 4.53 demonstrates the decibel level at 15m from the track at the centre of each low-frequency octave band. The vibrations level is significantly lower in comparison with previously examined soils. More specifically, the decibel level is lower than 18dB at all the examined octave bans. It is evident that those values are significantly lower than the acceptable WHO threshold (e.g., 55dB). The implementation of the examined mitigation measures is unnecessary, although they manage to reduce even further the vibrations level. It should also be mentioned that the decibel level at 35m from the track is zero; in this case, just the near field vibrations are presented.

4.10.5. Mitigation measures efficiency

The efficiency of the examined mitigation measures, i.e., Models 2, 3 and 4, which are compared with the reference case of the initial railway embankment (Model 1), is summarized in Figure 4.54. More specifically, the attenuation in terms of PPV for dense sand with gravels, stiff and soft clay at 15m is illustrated in this chart. In all soil types, the proposed mitigation measures have reduced the vibrations induced by Thalys HST passage. It is depicted that the most effective mitigation measure is Model 4 since the attenuation is close to 65% for the soft soil case, where it is noteworthy to observe that the side-fill (Model 2) is much more efficient compared to EPS-filled trench (Model 3).
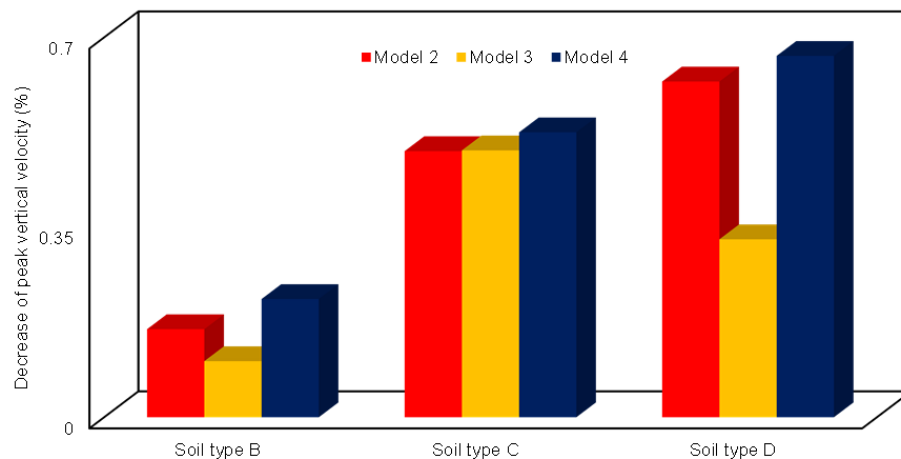
Figure 4. 54 Attenuation of PPV for soil type B, C and D at d=15m.

Figure 4.55 illustrates the effectiveness of the examined mitigation approaches in terms of PPV and $KB_{F,max}$. More specifically, the PPV in the modeling scenario of dense sand with gravels without any mitigation measure (Model 1) has been compared with Model 4 of the mitigated embankment laid on soft clay. As it is clearly shown in the plot, the PPV

at varying distances (from 15m to 35m) in the case of soft clay after the combined EPS mitigation (Model 4) is comparable with the corresponding ones of the soil embankment (Model 1) that is located on dense sand with gravels. In other words, by adopting this cost-effective intervention, the geotechnical conditions are notably upgraded and the HST can operate in a better and safer manner, even when it has to cross areas with soft soil layers.
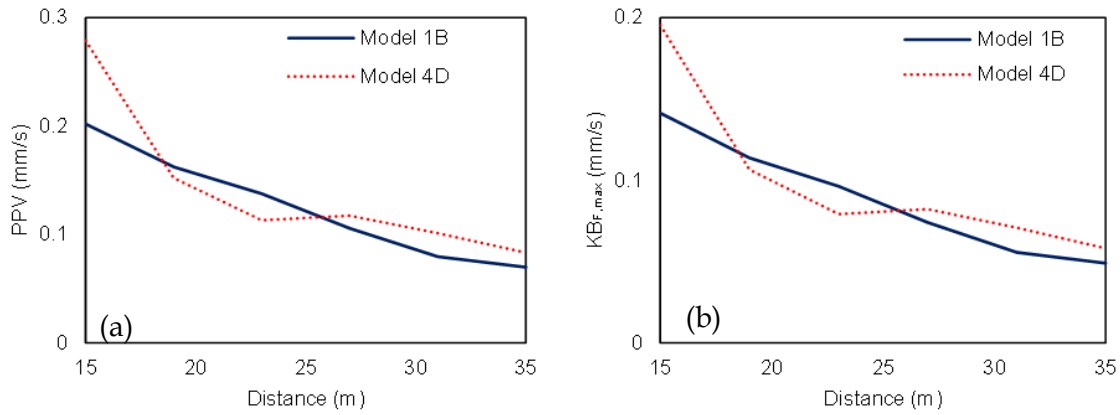
Figure 4.55 Comparison of (a) PPV and (b) KBF for the soil embankment (Model 1) on dense sand with gravels with the retrofitted embankment (Model 4) on soft clay.

Consequently, Figure 4.56 depicts the maximum level of KB_F at the six equally spaced observation points (15m to 35m) from the track. It is evident that $KB_{F,max}$ has been decreased with distance from the track. In addition, the $KB_{F,max}$ levels have been reduced after the implementation of all the examined mitigation measures for all soil scenarios. More specifically, as is clearly illustrated in Figure 4.56a, the hybrid mitigation technique is the most efficient for all soil types. As displayed in Figure 4.56c, in the case of dense sand with gravels, the $KB_{F,max}$ of Model 1 is lower than the threshold value of 15mm/s for distances between 17m and 35m. Hence, it can be deduced that the implementation of any mitigation is not necessary for such soil conditions, although the implementation of all the examined mitigation measures contributes to a substantial reduction of $KB_{F,max}$. The beneficial effect of the proposed mitigation approaches is more evident in the case of stiff clay, where initially $KB_{F,max}$ values are higher than the DIN limit for Model 1 for distances between 15m and 25m.

In contrast, the implementation of all EPS-based mitigation types has substantially decreased the $KB_{F,max}$ values below the limit of 15mm/s for almost all the examined distances. Finally, as expected, the highest values of $KB_{F,max}$ have been observed for soft clay, where $KB_{F,max}$ values are much higher (up to 4 times at near-field distances) than the DIN limit for all locations. Model 3 has reduced the values of $KB_{F,max}$, but they remain

above 15mm/s for most of the examined points (<29m from the track). On the other hand, Model 2 (and subsequently Model 4) has managed to reduce the $KB_{F,max}$ levels in all distances to acceptable levels effectively, apart from near-field (15m from the track), where it remains slightly higher than the limit.
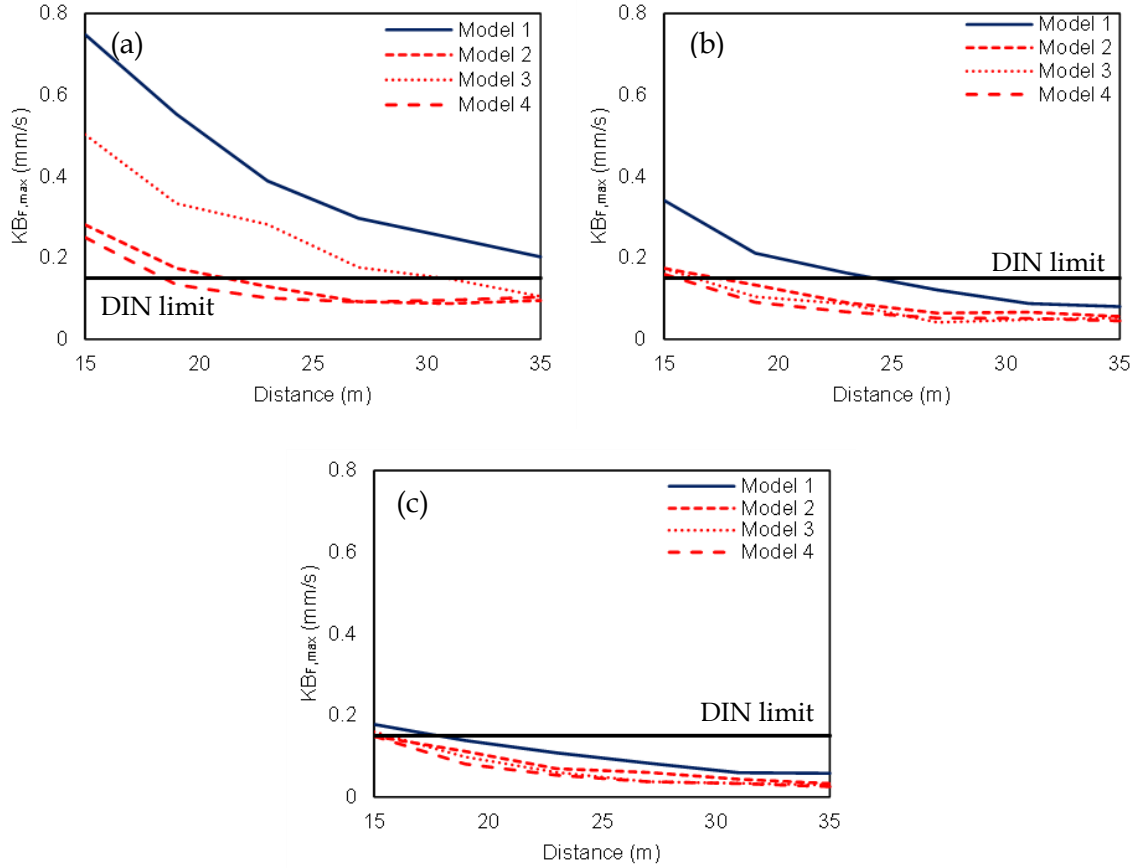
Figure 4.56 Comparison of soil and EPS-retrofitted embankments at increasing distance from the track in terms of $KB_{F,max}$: (a) soft clay, (b) stiff clay, (c) dense sand with gravels.

The insertion loss is illustrated for the three examined mitigation approaches in Figure 4.57. The calculations have been carried out at the center frequency of each one-third octave from 1.25Hz to 40Hz and the results are averaged to one-third octave bands. As it is illustrated in the plots of Figure 4.57, the insertion loss is higher for the softer soils for all the examined mitigation scenarios in the frequency range of interest (20Hz to 35Hz). It should be noted that according to Fourier spectral analysis, the dominant frequencies for all the examined soil layers are located at the 1/3 octave bands with center frequencies at 25Hz and 31.5Hz, in which the insertion loss curve is always positive. In particular, when the embankment is constructed on soft clay (Figure 4.57a),

Moreover, Model 4 reduces the vibrations level up to 5dB for the whole examined frequency range, while Model 2 and Model 3 are effective only for frequencies higher than 10Hz. When the embankment is located on stiff clay (Figure 4.58b), Model 2 exhibits a better performance in most frequencies. On the other hand, in the case of the stiffer soil (dense sand with gravels), the role of all mitigation measures is not beneficial. It is evident from Figure 4.57c that the addition of the trench (i.e., Model 3) increases the vibrations levels at the low octave bands from 1.25Hz to 8Hz. In contrast, Model 4 reduces the vibrations level for all the examined center frequencies, except for 20Hz, where the insertion loss is negative both for Model 2 and Model 4.
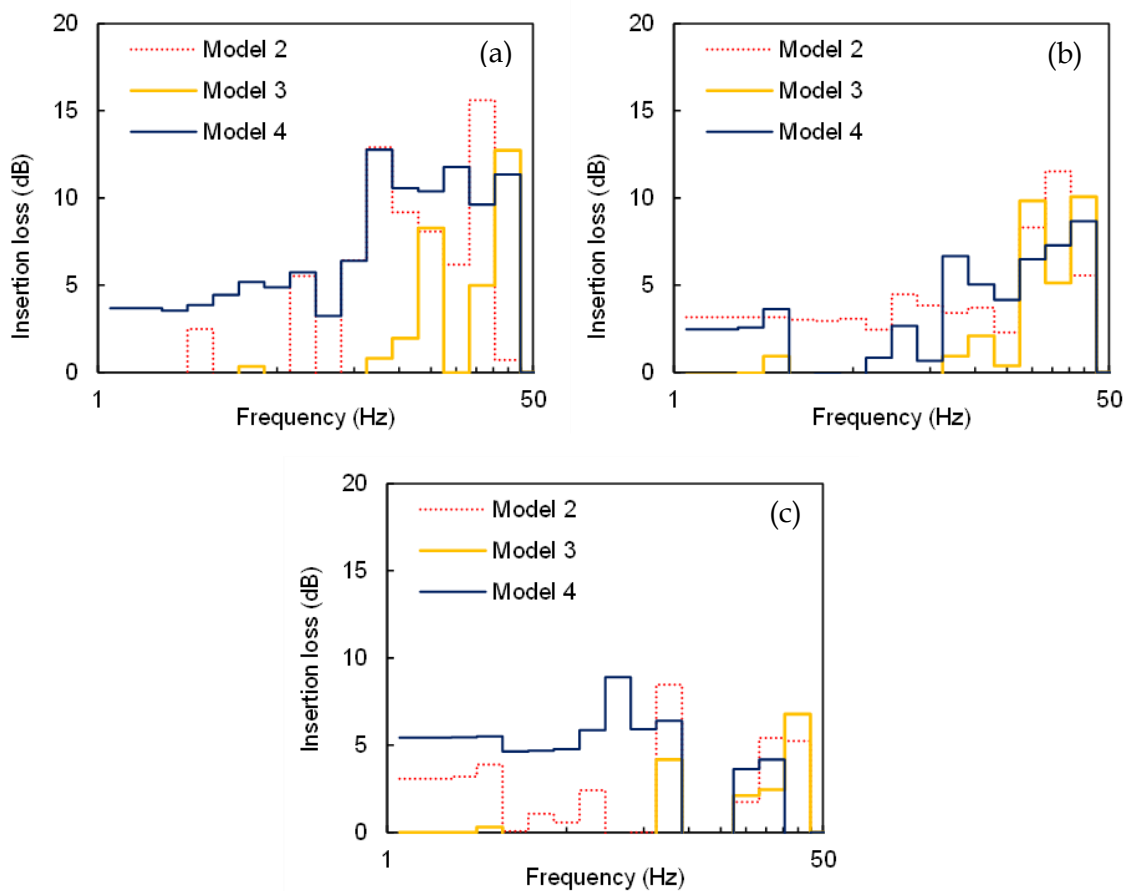
Figure 4.57 Comparison of insertion loss at 15 m from the track for the three mitigation approaches for: (a) soft clay, (b) stiff clay, (c) dense sand with gravels.

In existing HSR lines, residential buildings are commonly located at distances greater than 15m from the track. Thus, it is meaningful to also examine the IL curves at distances where buildings are usually cited. Nonetheless, in the future upgrading of existing normal speed railways, which pass through urban environments, the disturbance of adjacent buildings in much lower distances will become a common problem. Figure 4.58 depicts

the IL curves at 35m from the track, where the combined approach (Model 4) is, even more, the most effective mitigation scheme. More specifically, this scheme reduces the vibrations level from 3 dB to 16dB for all subsoil conditions within the whole examined frequency range. Furthermore, in the case of soft clay (Figure 4.58a), the higher IL is observed at the octave bands with centre frequencies higher than 20Hz, which are the most dominant ones according to the Fourier spectra. Similarly, the IL at the octave band with a centre frequency 20Hz is higher than 15dB when the embankment is based on stiff clay (Figure 4.58b). Lastly, in dense sand with gravels (Figure 4.58c), the higher IL is again observed at the octave band with a centre frequency 20Hz.
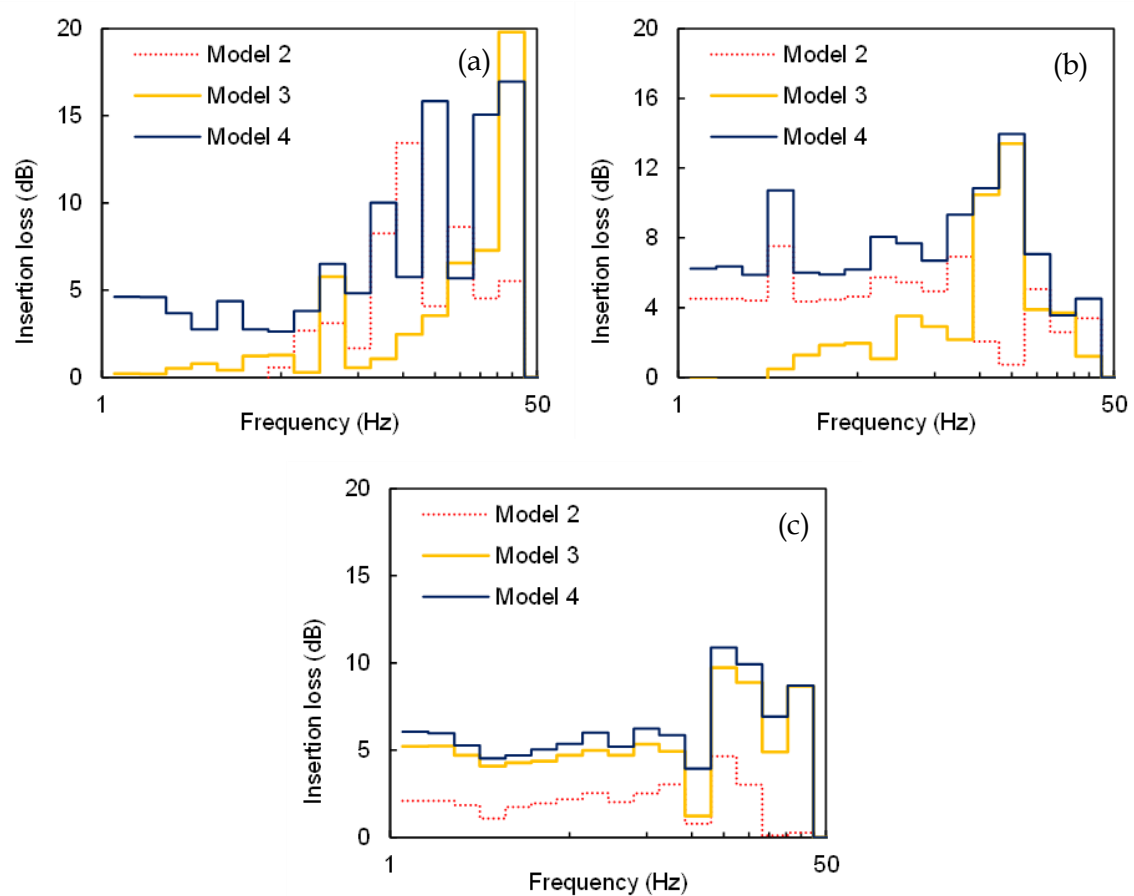
Figure 4.58 Comparison of insertion loss at 35 m from the track for the three mitigation approaches for: (a) soft clay, (b) stiff clay, (c) dense sand with gravels.

4.11. *Impact of embankment fill material*

Initially, the embankment has been constructed by the same silty soil -as described in the previous Sections- for all the examined soil scenarios in order to investigate the subsoil response for the same conditions. However, in engineering practice, the surface soil is commonly used as railway embankment fill material. Hence, the vibrations during the

passage of Thalys have been calculated when the subsoil (dense sand with gravels, stiff or soft clay) has been used as embankment fill material and the corresponding models are presented in Table 4.2.

Table 4.2. Models with different embankment soil material.

Embankment fill material	Regular embankment	Embankment with hybrid EPS mitigation
Dense sand with gravels	Model 1B	Model 4B
Stiff clay	Model 1C	Model 4C
Soft clay	Model 1D	Model 4D
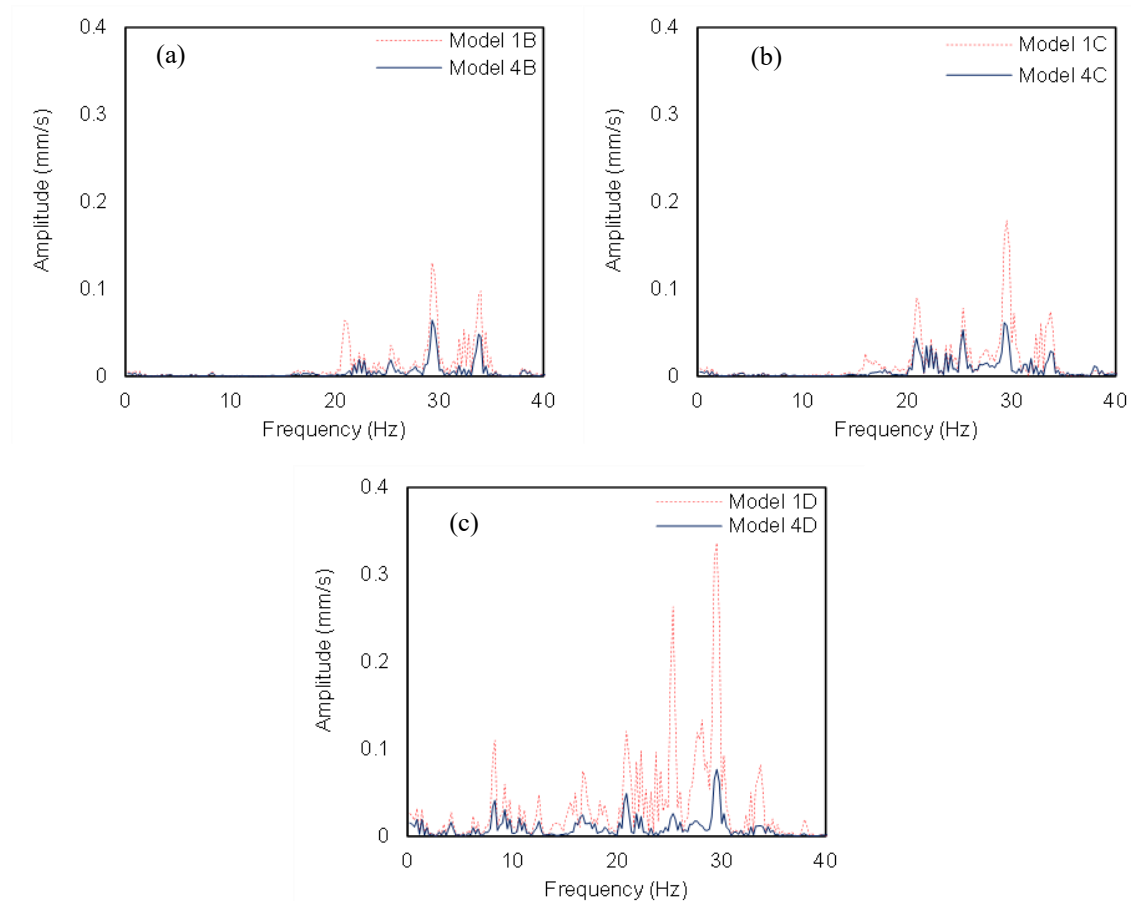
Figure 4. 59 Comparison of soil and EPS-retrofitted embankments in terms of vertical velocity Fourier spectra for: (a) dense sand with gravels, (b) stiff clay, (b) soft clay.

Figure 4.59a illustrates the vertical velocity Fourier spectra of Model 1B. In this case, the hybrid mitigation (Model 4B) implementation has reduced the vibrations peaks within the whole frequency range (0 to 40Hz). More specifically, the two dominant peaks at

29.3Hz and 33Hz have been reduced from 0.13mm/s and 0.1mm/s to 0.06mm/s and 0.04mm/s, respectively. The same observation can be made when the embankment has been constructed with soil obtained from the underlying stiff clay (see Figure 4.59b). The most dominant peak is at 29.3Hz and it is decreased from 0.18mm/s (Model 1C) to 0.06mm/s (Model 4C). Furthermore, all the other peaks between 0 and 60Hz have been substantially reduced. As it is clearly illustrated in Figure 4.59c, the vibrations peaks are much higher for soft clay compared to the other two soil types. In this scenario, the most critical frequency range is between 0 and 40Hz. The most dominant peaks at 25.4Hz and 29.3Hz have been significantly reduced by applying the proposed hybrid mitigation technique, similar to the behavior observed for the silty embankment for soft clay.

Figure 4.60 presents the IL curves of the three examined backfill embankments. The proposed mitigation approach contributes to the reduction of the vibrations level from 1 dB to 17dB for all the examined octave bands. In the case of soft clay, the IL is higher than 10dB for all octave bands with centre frequencies higher than 20Hz, where the vibrations peaks are observed in the Fourier spectra. The IL is lower in the cases of backfill embankment constructed from stiff clay or dense sand with gravels, although the vibrations level is again considerably reduced.
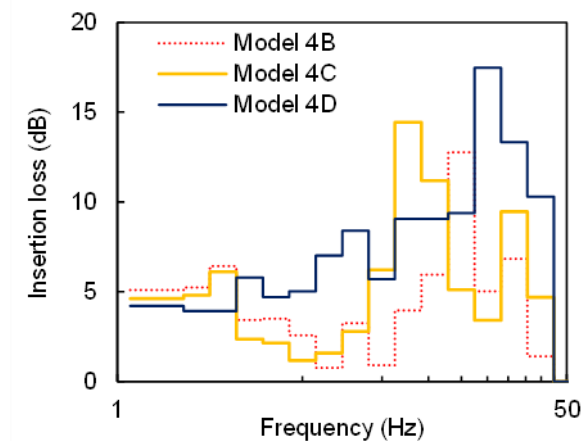
Figure 4.60 Comparison of insertion loss curves of the backfill embankment of the three examined subsoils.

Figure 4.61 illustrates how the $KB_{F,max}$ indicator evolves with increasing distance from the rail track for the examined cases. Note that the $KB_{F,max}$ levels are shown both for the initial silty soil and the embankment with dense sand with gravels, stiff or soft clay filling material. As shown in Figure 4.61a, the embankment material can significantly influence the HST-induced vibrations. The $KB_{F,max}$ for the embankment constructed from dense sand

with gravels (Model 1B) is increased compared to the initial silty embankment (Model 1) and it exceeds the DIN limit for distances between 15m and 25m. On the other hand, this indicator is less than the threshold value at all distances for the silty embankment. Nonetheless, the hybrid mitigation measure has a beneficial effect on the vibrations at all points, regardless of the embankment fill material.

Along the same lines, $KB_{F,max}$ values for stiff clay are displayed in Figure 4.61b. In this case, the $KB_{F,max}$ values for Model 1 are lower than Model 1C and exceed the limit from low to medium distances from the track. Furthermore, the proposed mitigation measure successfully reduces the $KB_{F,max}$ level, regardless of the embankment fill material. In the last scenario, the properties of the soft clay embankment (Model 1D) and the initial silty embankment (Model 1) are quite similar. Hence, the change of the embankment fill material has a minor impact on the $KB_{F,max}$ indicator values, which are remarkably reduced in both cases when applying the hybrid mitigation measure.
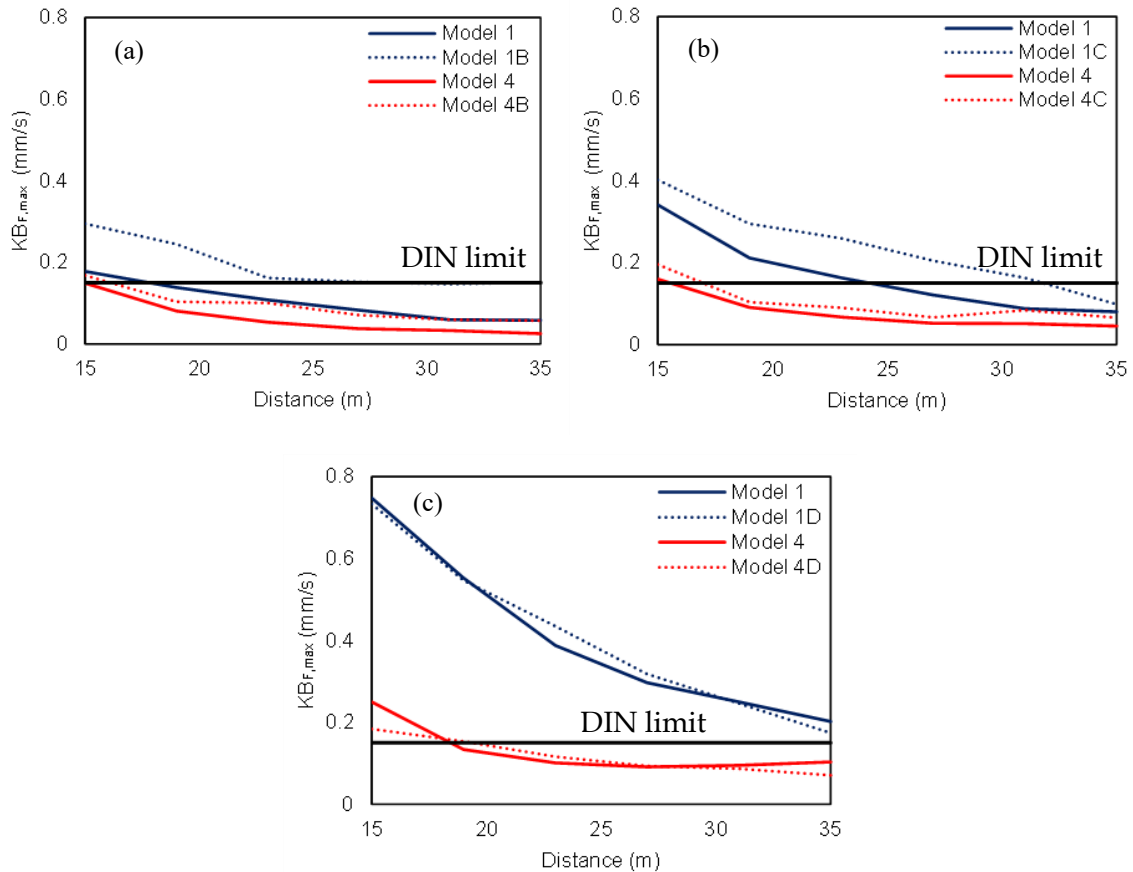
Figure 4.61 Comparison of $KB_{F,max}$ for different embankment filling material at increasing distance from the track for: (a) dense sand with gravels, (b) stiff clay, (b) soft clay.

According to the previous discussion, it can be deduced that the contrast between the subsoil and embankment material properties strongly influences the developed vibrations levels due to HST passage. The transmissions and reflections of the waves along the interface between the embankment and the underlying soil material can be determined via the so-called reflection coefficient (R), which is calculated as follows (Connolly et al., 2013):

$$R = \frac{\rho_S \cdot v_{S,S} - \rho_E \cdot v_{S,E}}{\rho_S \cdot v_{S,S} + \rho_E \cdot v_{S,E}} \tag{4.2}$$

where ρ_S is the subsoil density, $v_{S,S}$ is the shear wave velocity of the subsoil, ρ_E is the density of the embankment fill material, and $v_{S,E}$ is the shear wave velocity of the embankment.

As presented in Table 4.3, when the silty embankment (i.e., Model 1, with ρ_E = 200kg/m3 and $v_{S,E}$ =142m/s) is founded on stiff soil dense sand with gravels, then the interface has a high RC value equal to 62%. This causes wave energy to be reflected from the subsoil surface back into the embankment. In other words, the wave energy is trapped within the geostructure body, i.e., the embankment acts as a waveguide (Connolly et al., 2013). On the other hand, the value of RC is significantly lower for stiff clay, as it is only 26%. Lastly, the RC in the case of soft clay is very low (8%) due to the close shear wave velocity of the silty embankment and the underlying soil materials; thus, the HST vibrations are more easily propagated from the embankment to the surrounding soil.

Table 4.3. Reflection coefficient of the initial soil embankment (Model 1) for different subsoil conditions.

	Soil type	Density (kg/m³)	$v_{s,30}$ (m/sec)	RC (%)
B	Dense sand with gravels	2100	580	62
C	Stiff clay	2000	240	26
D	Soft clay	1850	180	8

4.12. *Discussion of the results*

In this Chapter, the application of EPS as an alternative material for mitigating the vibrations induced by HST passage has been investigated. Furthermore, the impact of

embankment height, the slope inclination, and the subsoil conditions on propagating traffic-induced vibrations by the passage of HST are investigated. The following conclusions can be drawn from the presented investigation:

- Implementing the new mitigation measure using EPS blocks as embankment partial slope fill material reduces the HST-induced vibrations.

- The use of stiffer EPS material leads to more effective mitigation of the developed vibrations.

- The investigated optimal configuration ensures safety against derailment of the HST as the embankment deflection is not significantly increased after the implementation of a limited number of EPS blocks. This observation is crucial since, as shown, a more extensive replacement of embankment soil with EPS blocks can lead to detrimental results.

- The soil embankment height has a relatively marginal impact on propagating the vibrations when the slope inclination is constant and the embankment fill material is the same as the upper subgrade layer. The implementation of EPS blocks contributes to the mitigation of the induced vibrations for all the examined embankment heights, especially at frequencies close to the fundamental frequencies of the adjacent buildings and infrastructure.

- The soil embankment slope inclination plays a more crucial role in the level of the HST-induced vibrations. A steeper slope leads to lower vibrations levels. However, the implementation of EPS blocks contributes to the mitigation of the vibrations for all the examined slope inclinations.

- PPV values are lower than the DIN limit for the protection of nearby buildings from potential damage. Nevertheless, PPV values have been reduced after the mitigation with EPS blocks for all the examined locations between 15 and 35 m from the track, while the mitigation technique is more effective for higher embankments.

- The mitigation of the embankment with EPS blocks has also led to a reduction of v_{rms} values below the USDT threshold for frequent passages of HST. The vibrations level in terms of V_{dB} and $KB_{F,max}$ have also been reduced.

- The vibrations induced by HST are decreased when the soil layer is stiffer, especially in the case of rock are marginal. Hence, mitigation measures are not required for firm soil conditions.

- The impact of the implementation of -a limited number of EPS blocks at the slopes of the embankment has led to the successful mitigation of the vibrations when the embankment is founded on dense sand with gravels, stiff or soft clay. More specifically, this mitigation measure is very effective in the frequency range of 0–40 Hz.

- The optimal mitigation measure is the implementation of both the EPS-filled trench and EPS blocks at the embankment slopes. In this case, the vibrations have been decreased within the whole low-frequency range.

- The embankment material also plays a vital role in the ground-borne vibrations, especially for stiffer soils. Depending on the difference between the subsoil and embankment soil properties, the waves may be trapped within the geostructure. Nonetheless, the proposed hybrid mitigation measure reduces the vibrations, regardless of the embankment fill material.

To summarize, the present work introduced a cost-efficient and straightforward approach in order to mitigate the induced vibrations due to HST passage. The proposed scheme involves the application of a limited number of EPS blocks and can be easily applicable to constructing new and upgrading existing embankments. Indeed, further investigation is required in order to examine more thoroughly this mitigation measure under different conditions. For instance, the use of EPS at HSR sites located in softer soils will be investigated, where the need for mitigation of HST-induced vibrations is even more pronounced.

HSR CUTTINGS MITIGATION WITH EPS GEOFOAM

5.1. Introduction

This chapter aims to investigate several mitigation configurations in order to present an optimal mitigation measure of ground vibrations induced by high-speed trains (HST) at cutting sites. As mentioned in the previous chapters, it is very important to propose such mitigation measures against soil vibrations due to various negative impacts on the population, structures, and railway infrastructure. This chapter examines the application of expanded polystyrene (EPS) blocks as an efficient mitigation measure against the ground vibrations induced by HST passage on the railway cutting. As mentioned, EPS is a high-performance geosynthetic fill material widely used due to its low weight and great compressibility. In the present numerical study, the three-dimensional (3D) model presented in Chapter 6 is used, utilizing the finite element software ABAQUS in conjunction with a user-developed subroutine to simulate the complex dynamic phenomenon accurately of soil response during the passage of HST. The use of different EPS schemes is investigated and compared to obtain an optimal geometrical configuration of EPS blocks that significantly reduces train-induced vibrations.

5.2. Mitigation with EPS at cutting slope

Since the developed numerical model can accurately replicate field data, it can be further expanded to include the proposed mitigation measures. The main aim of the present

chapter is to propose an efficient mitigation EPS-based approach capable of reducing the HST-induced vibrations in HSR cuttings as a continuation of the successful application of EPS blocks in HSR embankments, as presented in Chapter 4 (Lyratzakis et al., 2019, 2020, 2021b, 2021c). For this purpose, the EPS use has been investigated both in cutting slope and as filling material of a trench between the track and the slope. As it was aforementioned, EPS has been selected since it can be used for mitigating noise and vibrations mainly due to its mechanical properties. The EPS type used in the present investigation is EPS46 with 45.7 kg/m^3 density, elastic modulus equal to12800 kPa and very low Poisson's ratio (0.05) as in the previous Chapter the dense EPS46 has outperformed lighter EPS materials, it is also applied in this Chapter for HSR cuttings.

As reported in the related literature, when using a geofoam, the most common mitigation approach is to add it as trench fill material. For instance, Alzawi and EI-Naggar (2011) carried out a full-scale field test in order to compare the efficiency of open and geofoam-filled trenches and concluded that both types are more effective for a normalized depth greater than 0.6m. Furthermore, it was reported that the effectiveness of the geofoam barrier reached up to 68%. On the other hand, the impact of EPS-filled trenches depth and width has been studied via a centrifuge study by Bo et al. (2014), who concluded that a deep trench contributes to a higher reduction of the vibrations. Baziar et al. (2019) also performed centrifuge tests to investigate the performance of double EPS barriers and concluded that the mitigation efficiency of double EPS-filled trenches remains unchanged in various locations behind the trenches, while the effectiveness of a single trench decreased with increasing distance from the trench.

As mentioned in Chapter 4, the author has investigated an alternative configuration for HSR embankments, according to which a limited number of EPS blocks have been placed at the slope to minimize the HST-induced vibrations (Lyratzakis et al., 2021a). This configuration outperforms the standard approach of EPS-filled trench while combining the two measures increases the reduction of the vibration levels (Lyratzakis et al., 2021b). In this chapter, an EPS configuration is proposed for the case of cutting HSR sites (Lyratzakis et al., 2021c). Initially, the implementation of a limited number of EPS blocks at the cutting slope, identical to the proposed in the embankment site, has been investigated. In the sequence, the addition of an EPS-filled trench next to the cutting has also been examined. Furthermore, the upper layer of the cutting slope has been replaced

with a layer of EPS46 material. Several EPS blocks configurations have been examined, in which the abbreviations represent the thickness, t, of the EPS layer.
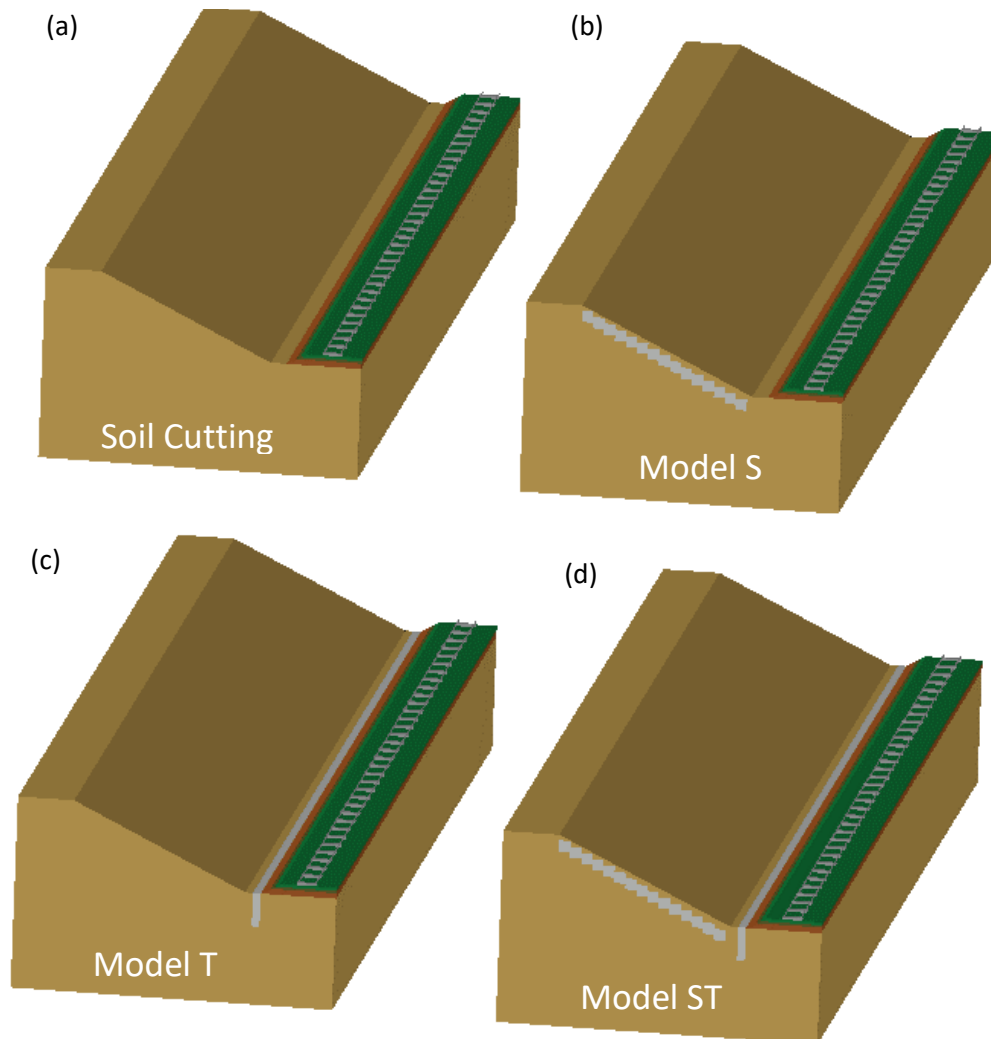
Figure 5.1 Sketches of EPS retrofitted cutting.

5.3.   *Implementation of a limited number of EPS blocks at the slope*

In this Section, the focus is given to modify the three examined applications of EPS blocks (Model 2) in the case of the embankment site in order to be implemented in the cutting site. Model S refers to the implementation of a limited number of EPS blocks at the cutting slopes. For this purpose, EPS blocks with a cross-section of 1mx1m have been placed and buried with 0.3m of soil, as shown in Figure 5.1b. Figure 5.1c presents the second examined mitigation scheme in the sequence, according to which an EPS-filled trench has been implemented across the track. In contrast with the embankment site, the trench implementation right next to the track is possible in this case. The examined trench is identical with the previously examined in Chapter 4, having a 0.5m width and a 3m depth.

Finally, the last examined model is based on the hybrid implementation of EPS both at the slopes of the embankment and as filling material in the trench (see Figure 5.1d). The efficiency of those approaches on the vibrations reduction at four critical positions is presented in the sequence. More specifically, the first examined position is located on the cutting slope at 15m from the track and the second at 19m close to the cutting top corner. Furthermore, the third position at 23m from the track represents the near field vibrations close to the cutting. The last observation point, at 35m from the track, has been selected in order to investigate the far-field vibrations. Figure 5.2 demonstrates the four examined positions.
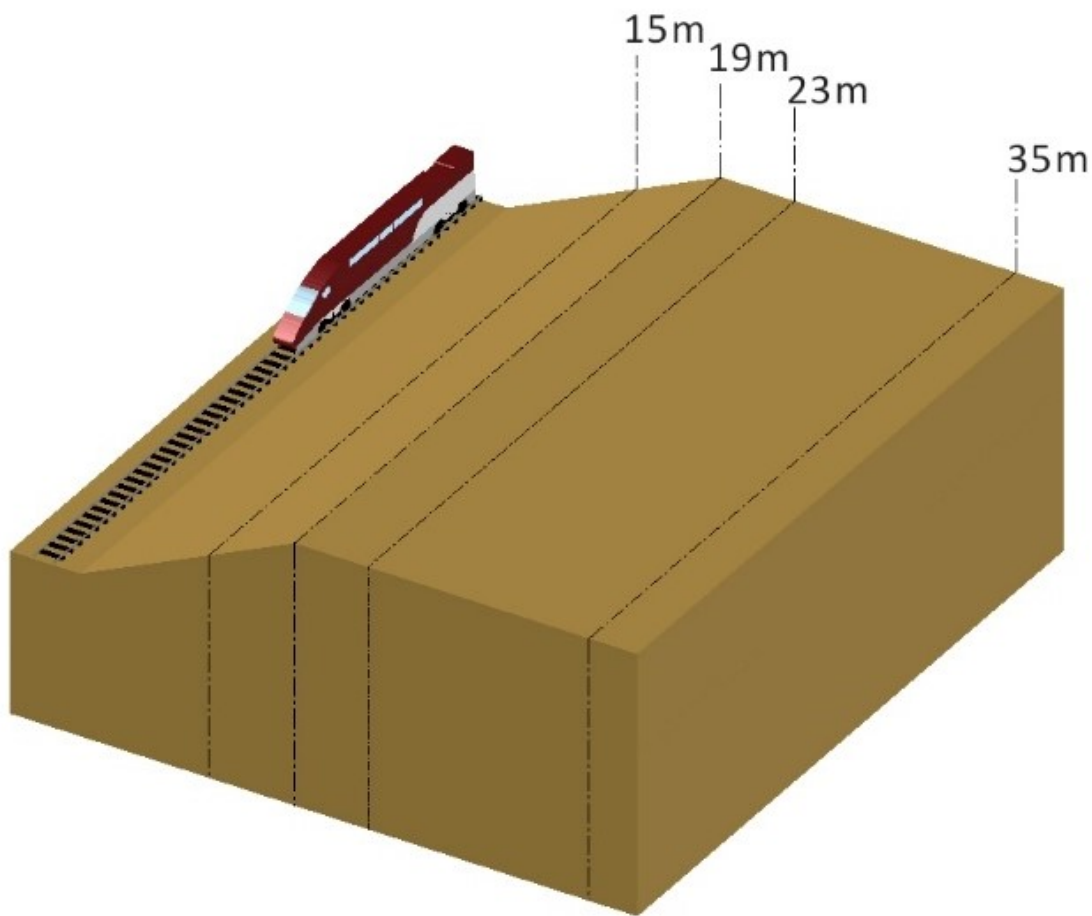
Figure 5.2 Sketch of the examined observation points.

The mitigation of the vibrations induced by Thalys passage from the HST cutting in the three mitigation scenarios at 15m from the track is depicted in Figure 5.3. The first vertical velocity time hibase (see Figure 5.3a) presents the vibrations level after implementing a limited number of EPS blocks at the slope (Model S). It is evident that this approach has not managed to reduce the vibrations level in this observation position;

conversely, it increases the vibrations level. More specifically, the peak vertical velocity has been increased from 1.45mm/s to 1.6mm/s. On the other hand, the second examined mitigation scheme, Model T, significantly reduces the vibrations level. Herein, the implementation of the EPS-filled trench has led to the decrease of the peak vertical velocity to 0.7mm/s, as illustrated in Figure 5.3b. Obviously, the efficacy of the hybrid mitigation scheme is lower than Model T. The peak vertical velocity has been minimized to 0.92mm/s in this case, according to Figure 5.3c.

Figure 5.3 Comparison of soil and EPS-retrofitted cutting in terms of vertical velocity time histories at 15m from the track: (a) Model S, (b) Model T, (c) Model ST.

The same observation is made at the second observation position, at 19m from the track. Figure 5.4 demonstrates the vertical velocity time histories close to the cuttings top corner. As it can be noticed in Figures 5.4a, Model S still increases the HST-induced vibrations significantly. More specifically, the increase of the vibrations is even more pronounced, as the peak vertical velocity, after the implementation of EPS blocks at the slope, reaches close to 2mm/s. On the other hand, the implementation of the EPS-filled trench has remarkably reduced the vibrations level, as the peak vertical velocity has been

minimized from 1.2mm/s to 0.5mm/s. Furthermore, Model ST slightly improves the vibrations level, as shown in Figure 5.4c. At the time hibase center, the level of reduction reaches close to 40%. However, the peak vertical velocity is not significantly altered. It could be concluded that the implementation of EPS blocks at the cutting slope (Model S and Model ST) is not proposed in order to mitigate the vibrations on the cutting slope. On the other hand, the EPS-filled trench is the most efficient.

Figure 5.4 Comparison of soil and EPS-retrofitted cutting in terms of vertical velocity time histories at 19m from the track: (a) Model S, (b) Model T, (c) Model ST.

Figure 5.5 illustrates the mitigation level at the first observation position in the free field, at 23m from the track. Herein, the efficacy of the first examined mitigation approach is remarkable in comparison with the previously examined positions. The peak vertical velocity has been minimized from 1mm/s to just 0.33mm/s, as illustrated in Figure 5.5a. Furthermore, the hybrid approach manages to further reduce the vibrations level to 0.31mm/s (See Figure 5.5c). Figure 5.5b presents the mitigation of the peak vertical velocity to 0.44mm/s after implementing the EPS-filled trench. It is evident that all the

examined mitigation approaches have managed to reduce the average vertical velocities up to 65% successfully.

Figure 5.5 Comparison of soil and EPS-retrofitted cutting in terms of vertical velocity time histories at 23m from the track: (a) Model S, (b) Model T, (c) Model ST.

Figure 5.6 depicts the vertical velocity time histories at the higher examined distances from the track. As shown in Figures 5.6a and 5.6b, the first approach (Model S) mitigates the HST ground-borne vibrations more effectively than the EPS-filled trench at the far-field. More specifically, Model T reduces the peak vertical velocity from 0.36mm/s to 0.27mm/s. The reduction is even more pronounced in the case of model S, as the peak vertical velocity has been minimized to 0.16mm/s. Once more, the implementation of the hybrid model is the most efficient approach, as the peak vertical velocity has been further reduced to 0.14mm/s. It could be concluded that the EPS-filled trench is the optimal approach in order to reduce the vibrations level at the observation positions located on the cutting slope. However, the other two mitigation approaches are most effective in the free field.

Figure 5.6 Comparison of soil and EPS-retrofitted cutting in terms of vertical velocity time histories at 35m from the track: (a) Model S, (b) Model T, (c) Model ST.

Figure 5.7 compares the velocity spectra between each examined EPS-retrofitted cutting at the slope (e.g., 15m from the track). At the closest examined distance, the most dominant peak at 26.4Hz is significantly decreased after the implementation of EPS blocks on the cutting slope, as demonstrated in Figure 5.7a. Furthermore, the second higher peak at 22.4Hz has not been significantly alerted. On the other hand, the peaks at 17.7Hz and 30.8Hz have been notably increased. The higher reduction, from 0.2mm/s to 0.45mm/s, has been observed at 30.8Hz.

Conversely, the beneficial role of the EPS-filled trench implementation has significantly reduced all the vibrations peaks in the examined frequency range between 10 to 40 Hz (see Figure 5.7b). The level of reduction at the dominant peaks at 22.4Hz and 30.8Hz is higher than 50%. The reduction is even more pronounced at the most dominant frequency. Herein, the vibrations level has been reduced from 0.45mm/s to just 0.19mm/s. In the last mitigation scenario (e.g., Model ST), most of the peaks in the low-frequency range (10 to 40 Hz) have been reduced, as shown in Figure 5.7c. However, the level of reduction is lower in comparison with the Model S. Hence, the assumption is made that

the EPS-filled trench is responsible for this reduction. On the other hand, the implementation of the EPS blocks at the slope has a negative role in this case.

Figure 5.7 Comparison of soil and EPS-retrofitted cuttings in terms of vertical velocity Fourier spectra at 15m from the track: (a) Model S, (b) Model T, (c) Model ST.

Figure 5.8 demonstrates the Fourier spectra at the second observation position, at the cuttings top corner. As mentioned, most of the peaks at the low-frequency range are increased after the implementation of Model S. More specifically, according to Figure 5.8a, the vibrations peaks at 22.4Hz, 26.4Hz and 30.8Hz reach values higher than 0.4mm/s. The vibrations peak, at the dominant frequency 17.7Hz, is the only exception. In this case, the amplitude of the vibrations has been significantly reduced. On the other hand, this trend changes in the case of Model T. The peaks at the range from 0Hz to 40Hz are sufficiently reduced in this case, as shown in Figure 5.8b. It is evident that all the vibrations peaks have been minimized below 0.15mm/s. Furthermore, Model ST has managed to reduce all the vibrations peaks, although the mitigation level is mediocre compared to Model T.

Figure 5.8 Comparison of soil and EPS-retrofitted cuttings in terms of vertical velocity Fourier spectra at 19m from the track: (a) Model S, (b) Model T, (c) Model ST.

The efficiency of Model S is drastically alerted at the free field. Accordingly, Figure 5.9 illustrates the impact of the examined mitigation measures on the velocity spectra at 23m from the track. In the case of Model S, the three dominant frequencies (17.7Hz, 22.4Hz and 26.4Hz), spotted in Figure 5.9a., are notably decreased. More specifically, the peak at 22.4Hz is reduced from 0.24mm/s to 0.11mm/s. Furthermore, all the other peaks have been minimized below 0.05mm/s. The plot in Figure 5.9b illustrates that the soil response is also improved in the whole low-frequency range in the case of Model T. The peak at 22.4Hz has been further reduced to just 0.08mm/s. However, the vibrations peaks at the frequency range between 25Hz and 40Hz are higher than Model S. It is obvious from Figure 5.9d that Model ST has led to the most remarkable improvement of the soil response. In this case, all the vibrations peaks are reduced below 0.1mm/s.

Figure 5.9 Comparison of soil and EPS-retrofitted cuttings in terms of vertical velocity Fourier spectra at 23m from the track: (a) Model S, (b) Model T, (c) Model ST.

Figure 5.10 demonstrates the Fourier spectra of the three examined mitigation scenarios at the far-field (e.g., 35m from the track). The primary vibrations peaks at 26.4Hz and 30.8Hz, in the case of the initial cutting, are equal to 0.12mm/s and 0.10mm/s. In addition, the other two dominant peaks, at 17.7Hz and 22.4Hz, are lower than 0.8mm/s. Model S has contributed to reducing the most dominant peak at 26.4Hz to 0.05mm/s (see Figure 5.10a). Furthermore, the vibrations peak at 30.8Hz has been virtually disappeared. In general, the implementation of EPS blocks on the cutting slope successfully mitigated the vibrations at the low-frequency range. Figure 5.10b presents the Fourier spectra in the case of the second examined mitigation approach, the implementation of EPS-filled barrier. This approach has also managed to decrease all the vibrations peaks, although the level of reduction is lower than Model S. Model ST exhibits the higher reduction of the vibrations peaks at the far-field. It is evident that the vibrations peaks remain below 0.035mm/s at the whole low-frequency range.

155

Figure 5.10 Comparison of soil and EPS-retrofitted cuttings in terms of vertical velocity Fourier spectra at 31m from the track: (a) Model S, (b) Model T, (c) Model ST.

The velocity decibels (V_{db}) of each examined mitigation scenario is compared with the initial decibel level in the sequence. In this case, the background vibrations levels are set equal to 5x 10^{-5} mm/s (USDT, 1998). Figure 5.11 demonstrates the velocity decibels at each examined 1/3 octave band with centre frequencies between 1.25Hz and 50Hz at the near field examined observation points. The most dominant octave bands are the 13th, 14th and 15th for all the examined observations positions. In the near field positions (e.g., 15m and 19m from the track), the implementation of a limited number of EPS blocks at the cutting slope reduces the decibel level octave bands with centre frequencies below 6.3Hz. However, it is obvious that the implementation of Model S has a negative role on the decibel level at the most dominant octave bands. For instance, the decibel level has been increased from 64dB to 70dB after the implementation of EPS block at the cutting slope (see Figure 5.11a). Furthermore, at 19m from the track, the decibel level at the 14th octave bands is increased to 72dB, as illustrated in Figure 5.11b.

On the other hand, the implementation of the EPS-field trench has led to an increase of the decibel level at the first eight octave bands. The most notable increase is observed

at the octave bands with central frequencies 4Hz and 5Hz. For instance, at the octave band, with a central frequency 5Hz, the is increased from 40 dB to 46 dB at 15m from the track, as illustrated in Figure 5.11a. On the other hand, the beneficial role of the EPS-filled trench is observed at the most dominant octave bands. It is evident that Model T has led to a decibel reduction equal to 6dB and 8dB at 15m and 19m from the track for all the dominant octave bands. Lastly, the hybrid approach (e.g., Model ST) is not the optimal approach as it has increased the decibel level at the first seven octave bands at 15m from the track. Furthermore, the reduction of the decibel level at the most dominant octave bands is lower in comparison with Model T.
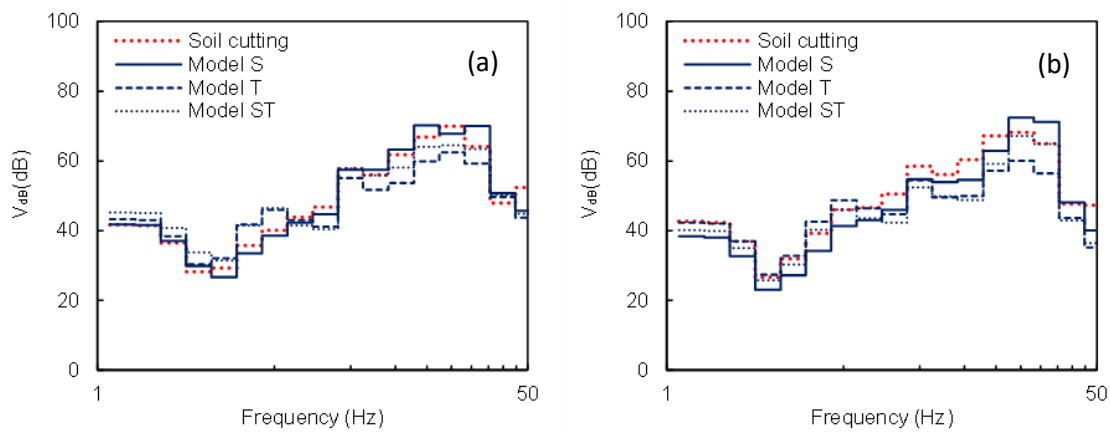
Figure 5.11 Comparison of the soil and the retrofitted cuttings at: (a) 15m, (b) 19m from the track.

The effectiveness of the examined approaches is remarkably altered at the far-field positions (e.g., 23m and 35m from the track), as demonstrated in Figure 5.12. At 23m from the track, all the examined mitigation approaches manage to reduce the examined octave bands vibrations level. It is evident that, in contrast with the near field positions, herein, Model S is more efficient than Model T. For instance, the decibel level at the 12th octave band has been reduced from 50dB to 48dB and 42dB, in the case of Model T and Model T, respectively. Furthermore, the reduction level of the hybrid method is comparable with Model S. Hence, Model ST is not the optimal choice for reducing the vibrations level at 23m from the track, taking into consideration both the implementation cost and the mitigation level. Figure 5.12b shows the reduction of the decibel level at the low-frequency range at 35m from the track. Herein, Model T is the less efficient mitigation approach, as it manages to reduce the decibel level from 58dB to 54dB at the most dominant octave band. On the other hand, the decibel level at the same octave band has been reduced to 51dB and 45dB, in the case of Model S and Model ST, respectively.

As it was aforementioned in the case of the initial soil cutting, the peak vertical velocity declines with distance from the track. The implementation of EPS blocks at the cutting slope gradually increases the vibrations level on the slope (e.g., for distances lower than 19m). In the sequence, model S rapidly reduces the vibrations level to values lower than 0.5mm/s. The same trend is observed in the case of Model ST. In this case, the vertical velocities remain lower than the initial soil cutting for all the examined distances from the track. However, the vertical velocity reaches values close to the initial model at the cuttings top corner. This approach reaches the lower velocities compared to the other two approaches at distances higher than 19m. Nevertheless, at the near field positions, on the cutting slope, the most efficient approach is the EPS-filled trench (e.g., Model T). However, for higher distances from the track, Model T is the less effective mitigation approach.
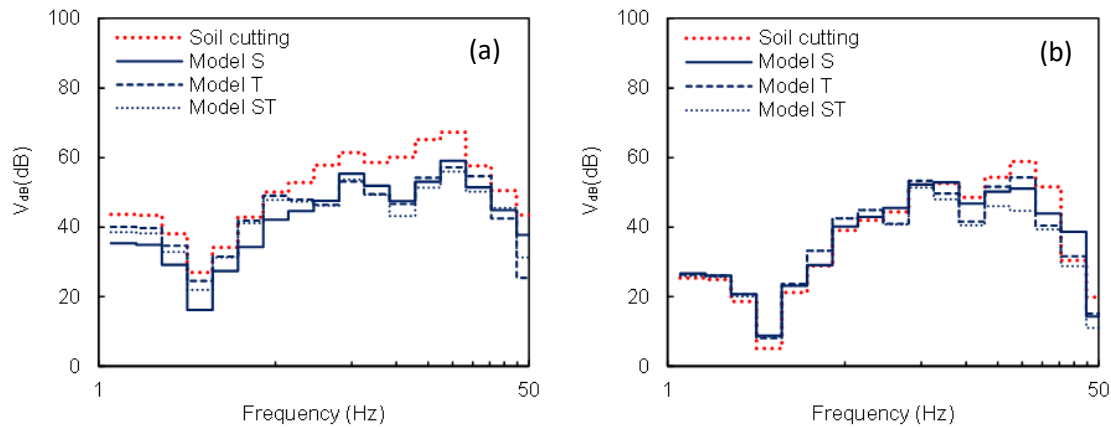
Figure 5.12 Comparison of the soil and the retrofitted cuttings at: (a) 23m, (b) 35m from the track.
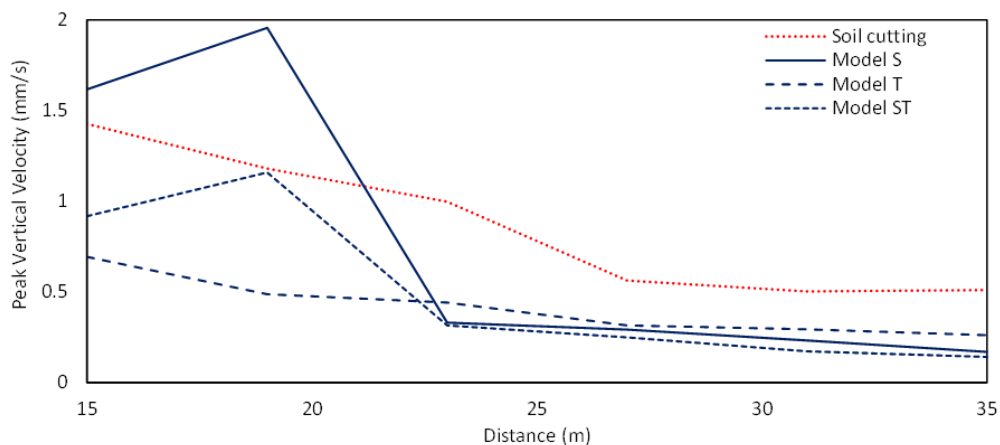
Figure 5.13 Peak vertical velocity at i Figure 5.13 summarizes the peak vertical velocity at several examined distances from the track, between 15m–35m from the track.

5.4. *Implementation of water-filled trench*

According to the previous Section, an EPS-filled trench is a reliable option for reducing the vibrations level. In order to further investigate the efficacy of the in-filled trench across the track at the cutting base, an alternative fill material has been investigated. More specifically, in this chapter, the fill of the trench with water has been studied. The geometrical properties and the location of the trench are the same as Model T (see Figure 5.1c). Figure 5.14a compares the vertical velocity time hibase of the initial cutting soil and the mitigated with a water-filled trench (e.g., Model W) at 15m from the track. Obviously, Model W remarkably reduces the vertical velocities in comparison with the previously examined models. More specifically, the peak vertical velocity has been minimized below 0.4mm/s. The beneficial role of the water-filled trench is even more pronounced at 35m from the track. According to Figure 5.14b, this approach manages to reduce the vertical velocities below 0.12mm/s.
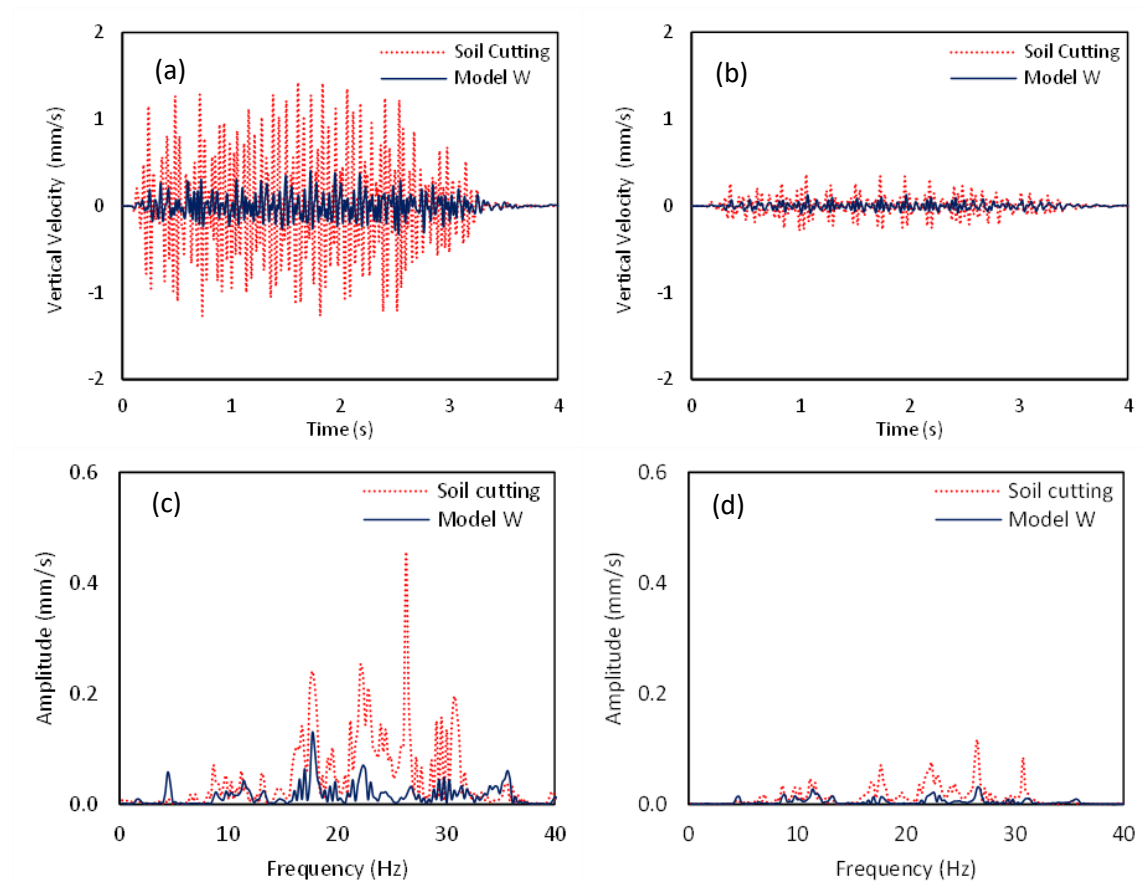
Figure 5.14 Comparison of soil cutting and Model W in terms of vertical velocity time histories (at (a) 15m, (b) 35m) and Fourier spectra (at (c) 15m, (d) 35m).

Figure 5.14c demonstrates the vertical velocity Fourier spectra at 15m and 35m from the track. All the vibrations peaks have been minimized below 0.2mm/s at the whole low-

frequency range. More specifically, the peak at 17.7Hz has been halved and at the other three (22.4Hz, 30.8Hz, 26.4Hz) has been reduced below 0.08mm/s. Two new peaks have been appeared at 4.5Hz and 35.8Hz, although their amplitude is below 0.05mm/s. At the most remote position of the track, the implementation of the water-filled trench virtually disappeared the majority of the vibrations peaks, as shown in Figure 5.14b.

In order to further illustrate the effectiveness of the water-filled trench, the velocity decibels at the low-frequency octave bands are presented in Figure 5.15. Model W minimizes the decibel level of all the examined octave bands below 60dB at 15m from the track. More specifically, the level of decibel reduction at the most dominant octave bands with centre frequencies 16Hz, 20Hz and 25Hz, is between 8dB and 15dB. On the other hand, the implementation of the water-filled trench significantly increased the decibel level at several low-frequency octave bands. For instance, the velocity decibel at the octave band with centre frequency increased from 40dB to 56dB, as illustrated in Figure 5.15a. The same observation is made at 35m from the track. Herein, the peaks at the most dominant octave bands have been reduced below 47dB. The implementation of the water-filled trench is a great alternative solution for the reduction of traffic-induced vibrations. However, several construction issues should be arranged before the implementation of this measure.
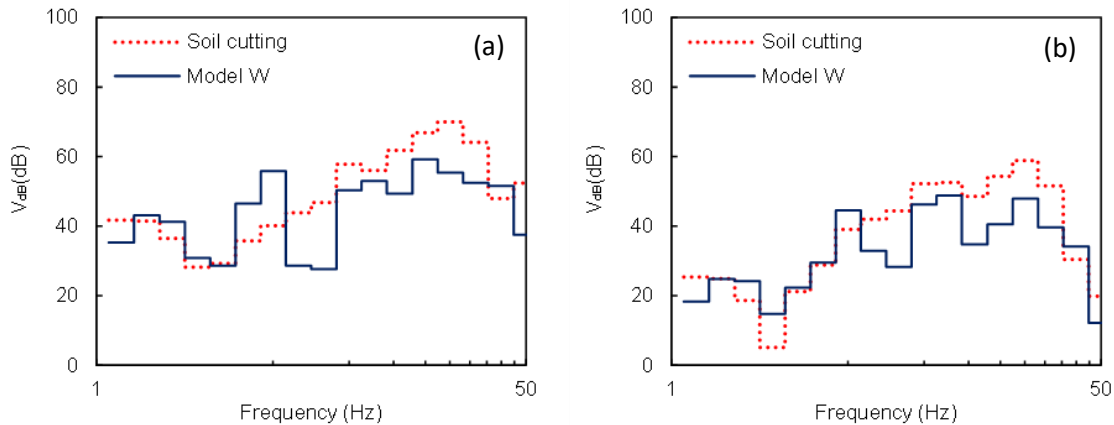
Figure 5.15 Comparison of the soil and Model W at: (a) 15m, (b) 35m from the track.

5.5. *Optimal approach*

5.5.1. *Description of the mitigation approach*

It is evident that none of the examined EPS configurations is optimal, as the EPS-filled trench is more effective for the vibrations reduction on the cutting slope. However, the other two approaches are more effective in the free field. For this purpose, the reason for

vibrations increase at the slope after the implementation of Model S should be examined. Hence, in the sequence, the approach could be modified to be effective at all the examined distances. This increased velocity level has one primary cause, the EPS to soil material interface has a seismic reflection coefficient (R_c) (Eq. 4.2) of 0.95, thus causing wave energy to be reflected from the EPS back into the cover soil layer, thus trapping energy within its structure. This effect causes a waveguide effect. Hence, the higher percentage of the induced vibrations is "trapped" on the backfill soil, which covers the EPS blocks, leading to increased vibrations level. According to this observation, an approach has been investigated to retain the beneficial role of Model S on the far-field vibrations reduction and resolve the issue of the increased vibrations at the cutting slope. More specifically, the upper layer of the cutting slope has been replaced with a layer of EPS46 material to avoid the waveguide effect on the backfill soil. Several EPS layer thicknesses have been investigated in order to examine the effect of its thickness on the mitigation level. More specifically, four layers thicknesses between 0.5m and 2m have been examined, as illustrated in Figure 5.16.
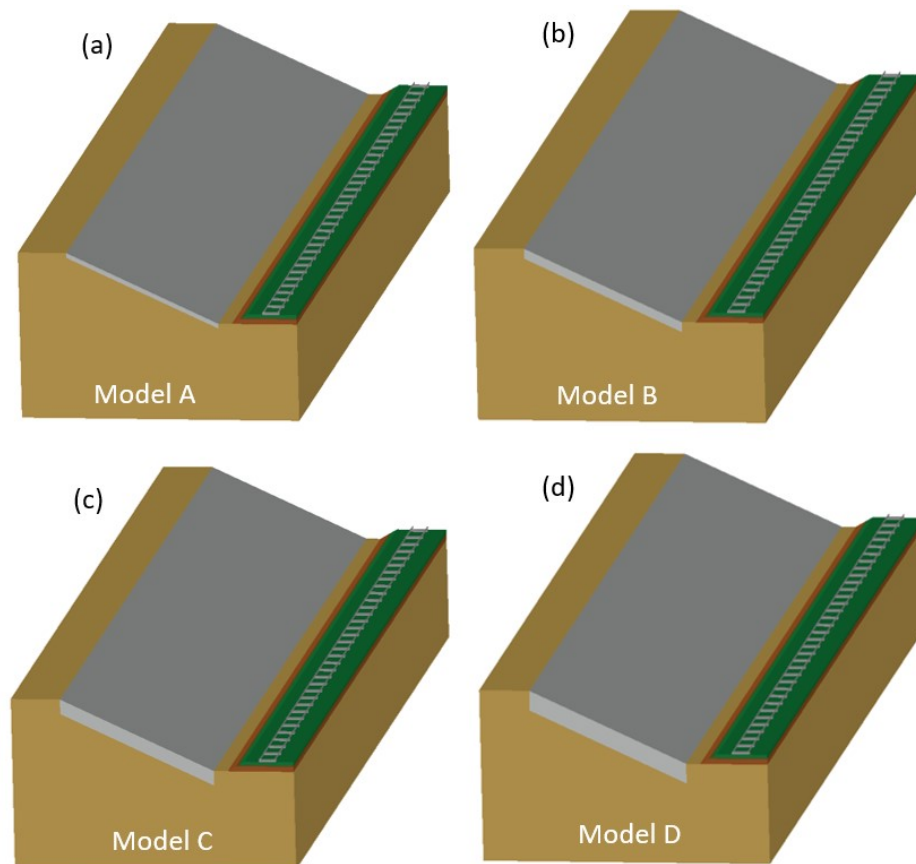
Figure 5.16 Sketches of EPS layer on the cutting slope with thickness, t, equal to: (a) 0.5 m, (b) 1.0 m, (c) 1.5 m, (d) 2.0 m.

5.5.2. *Vertical velocity time histories*

The vertical velocities at several distances from the track have been used to represent the vibrations levels for the various schemes. The impact of the depth of the EPS layer is illustrated in Figure 5.17, where the vertical velocity time histories on the EPS layer at 15m from the track are depicted both for the existing soil cutting and the retrofitted ones. As it is evident from Figure 5.17a, the addition of a thin layer with depth equal to 0.5m of EPS at the cutting slope (Model A) has a marginal impact on the vertical velocity time hibase. The peak vertical velocity has been reduced from 1.4mm/s to 1.05mm/s. By observing the other plots of Figure 5.17, it is evident that the efficiency of the proposed mitigation measure is increased when the depth of the EPS layer is increased. For instance, in the intermediate width scenarios of Model B and Model C, the peak vertical velocity has reduced to 0.78mm/s and 0.64mm/s, respectively. The most efficient examined depth is the thicker EPS layer (Model D).
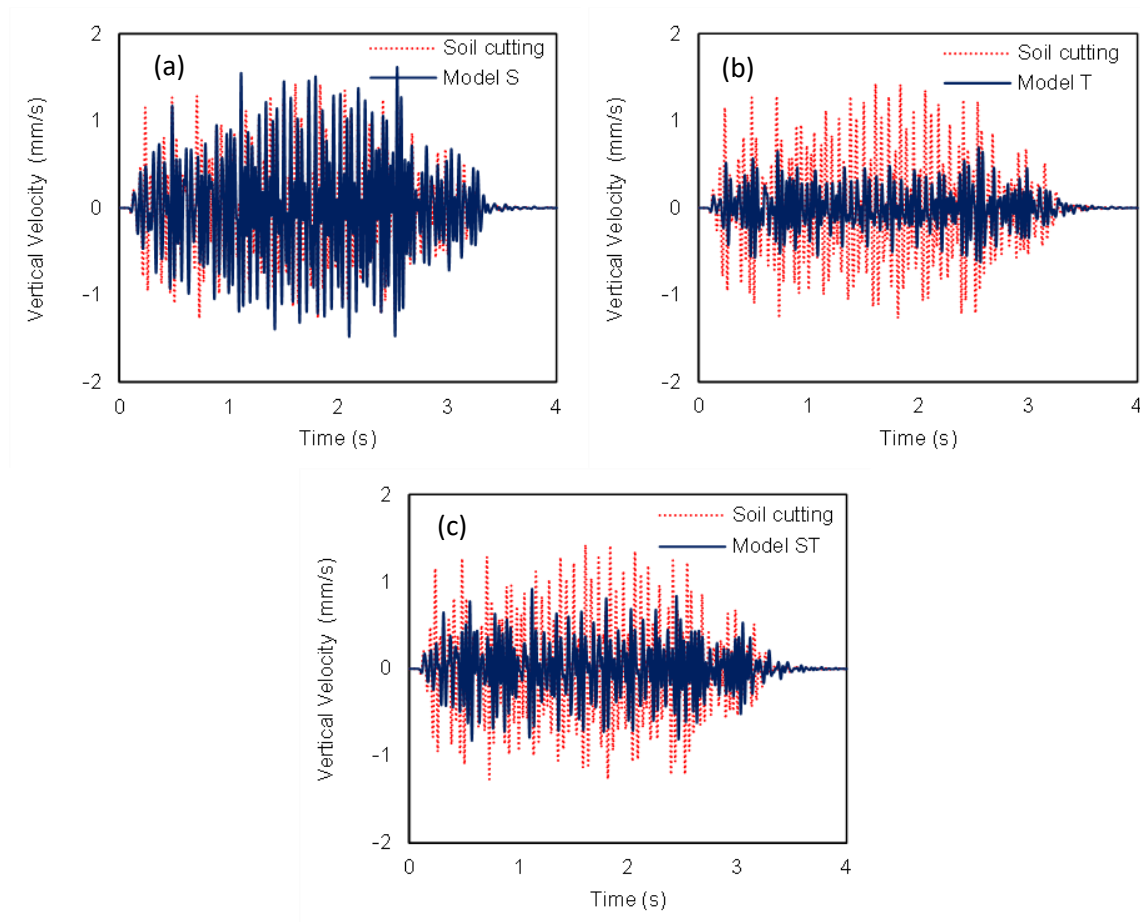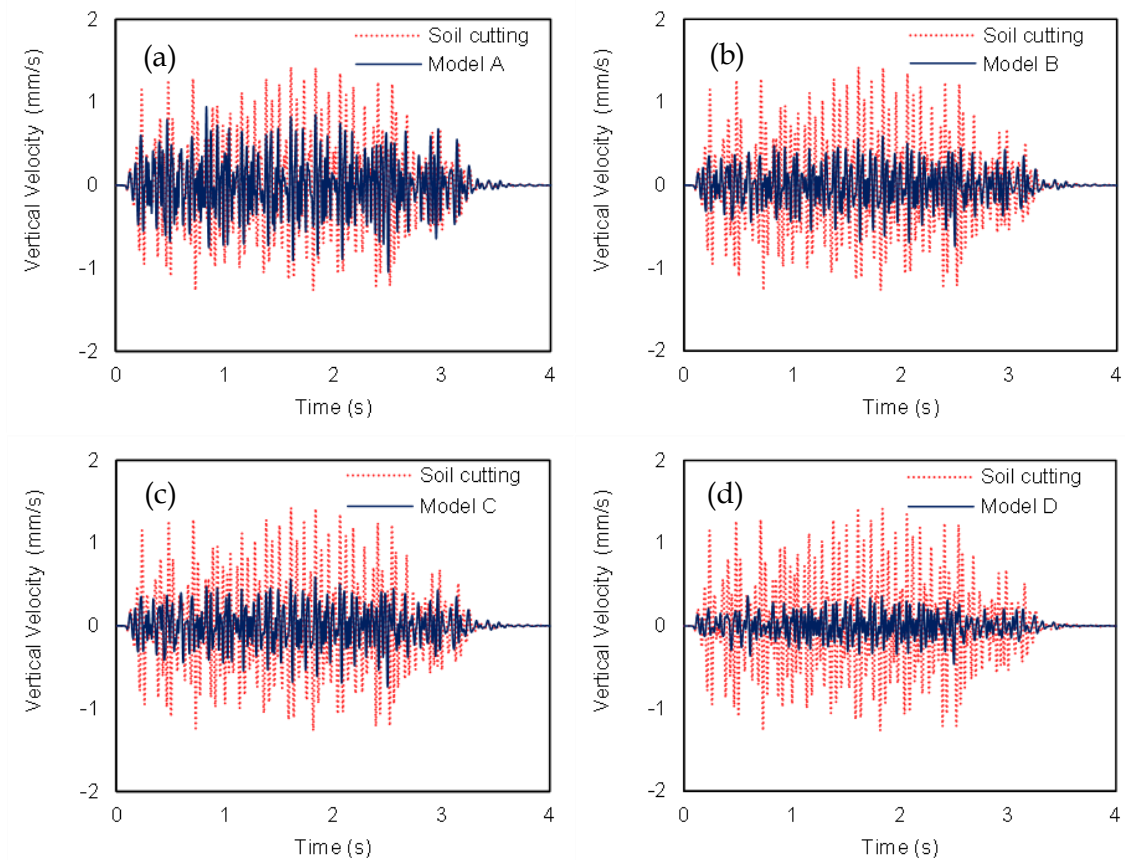

Figure 5.17 Comparison of soil and EPS-retrofitted cutting in terms of vertical velocity time histories at 15m from the track: (a) Model A, (b) Model B, (c) Model C, (d) Model D.

Similar trends have been observed for increasing distances from the track. Figure 5.18 illustrates the vertical velocity time histories at the top corner of the cutting slope (e.g.,

19m from the track). At this observation position, the implementation of the thinner layer of EPS46 (e.g., Model A) slightly reduces the vibrations level, as the reduction of the vibration level reaches in some cases over 40%. The reduction is higher at the center of the time hibase. On the other hand, at the start and the end of the time hibase, the vibrations level remains the same, as depicted in Figure 5.18a. The reduction of the vertical velocities is increasing gradually for incasing EPS layer height. More specifically, the peak vertical velocity has been reduced from 1.2mm/s to 0.47mm/s and 0.44mm/s, respectively, for Model B and Model C. The most effective mitigation approach is the last examined (e.g., Model D) according to Figure 5.18d. In this case, the level of the reduction is higher than 70%. Hence, the proposed approach is effective at the whole slope of the cutting.
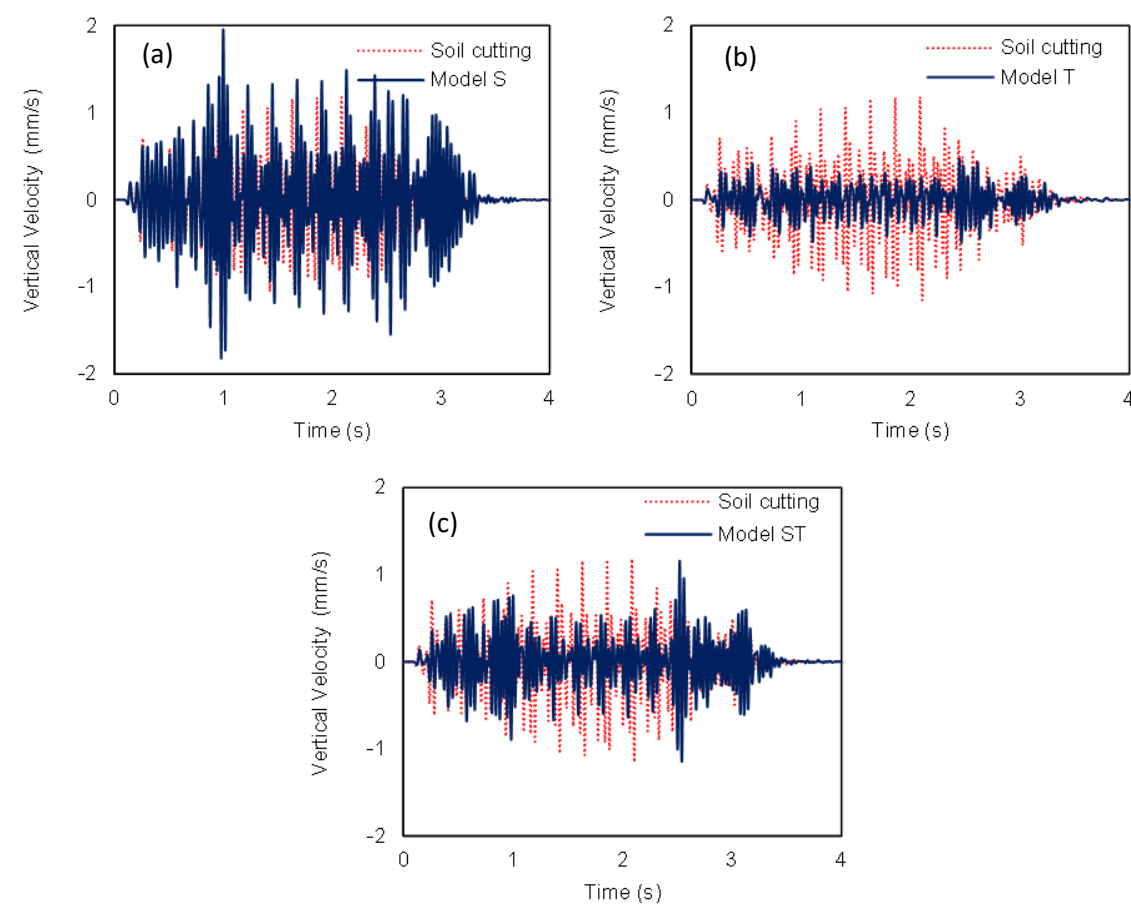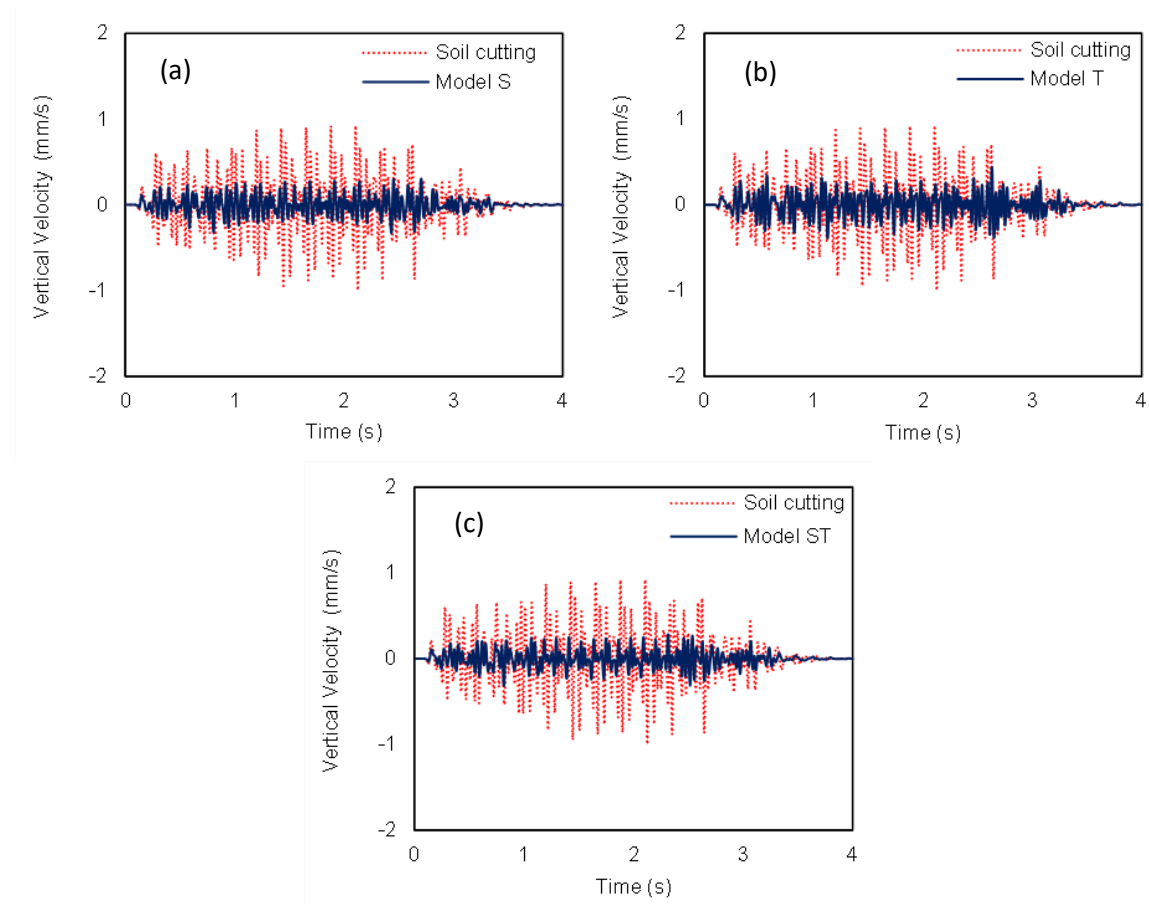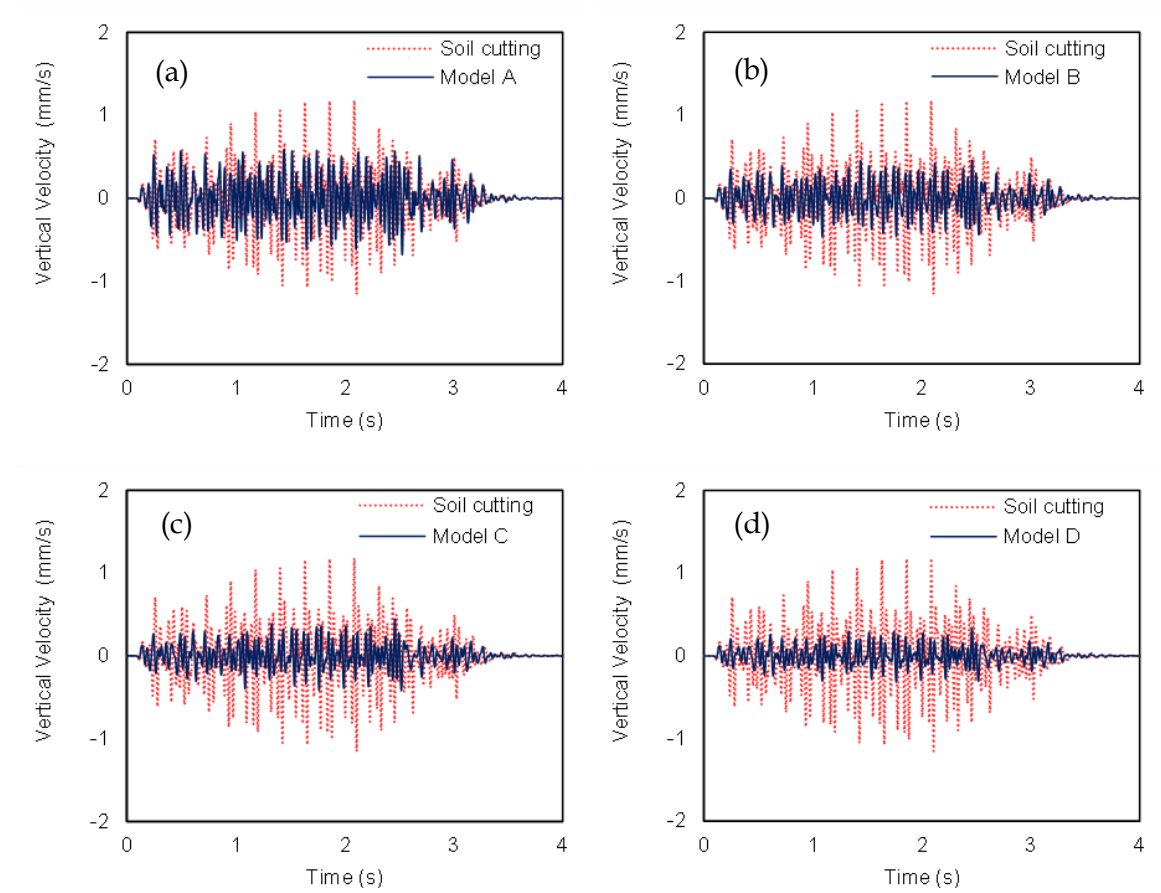

Figure 5.18 Comparison of soil and EPS-retrofitted cutting in terms of vertical velocity time histories at 19m from the track: (a) Model A, (b) Model B, (c) Model C, (d) Model D.

Apart from the cutting slope, the investigation of the examined mitigation approach effectiveness at greater distances from the top corner of the cutting, where a building could be constructed, should be examined. Figure 5.17 illustrates the vertical velocity time histories at 8m from the cutting slope (e.g., 23m from the track). It is evident that the vertical velocity at this observation position of the initial soil cutting is lower than the

previously examined observation points. More specifically, the peak vertical velocity is just 1mm/s compared with 1.2mm/s at 19m from the track. The implementation of the proposed mitigation approach still minimizes the vibrations level. For instance, the peak vertical velocity is minimized from 1mm/s to 0.5mm/s after the implementation of 0.5m EPS. This value is even more reduced for higher EPS layer thickness. The thicker EPS layer is still optimal, as it achieves the reduction of this value to 0.33mm/s.
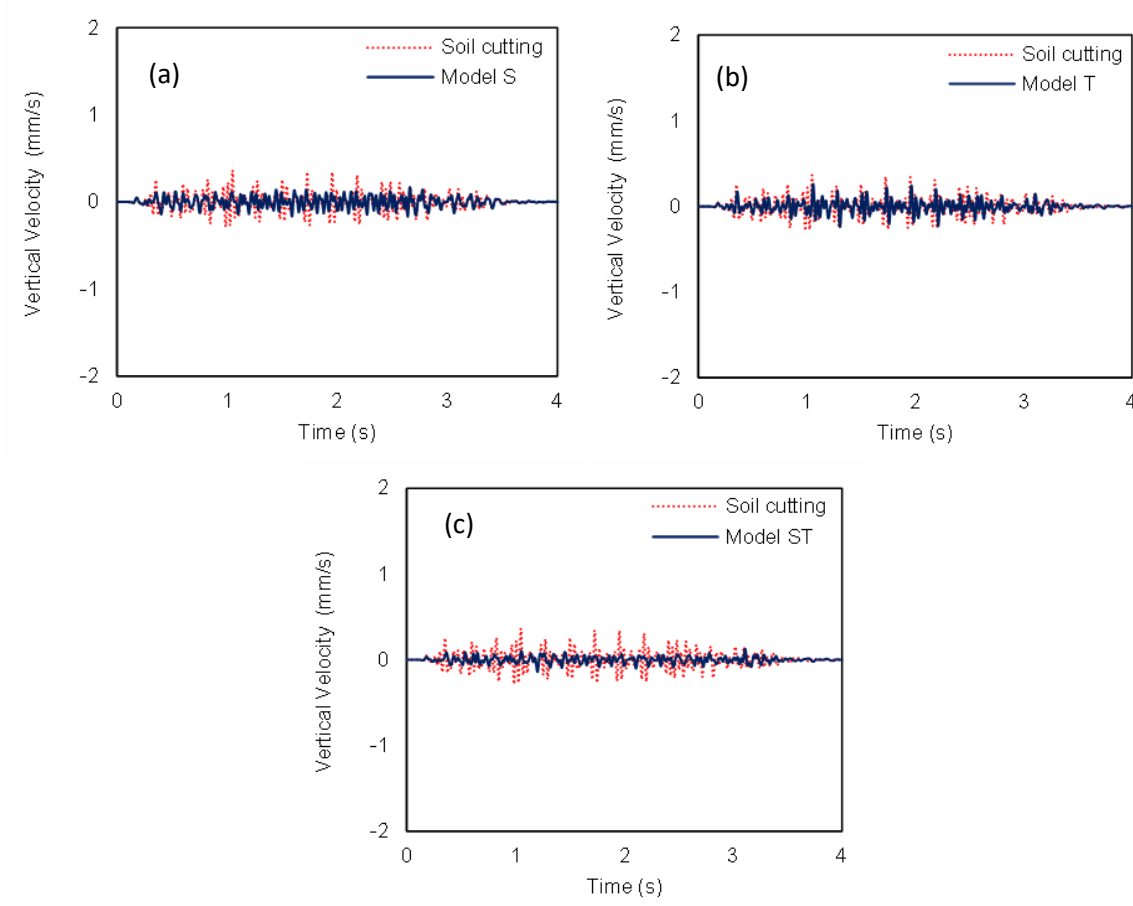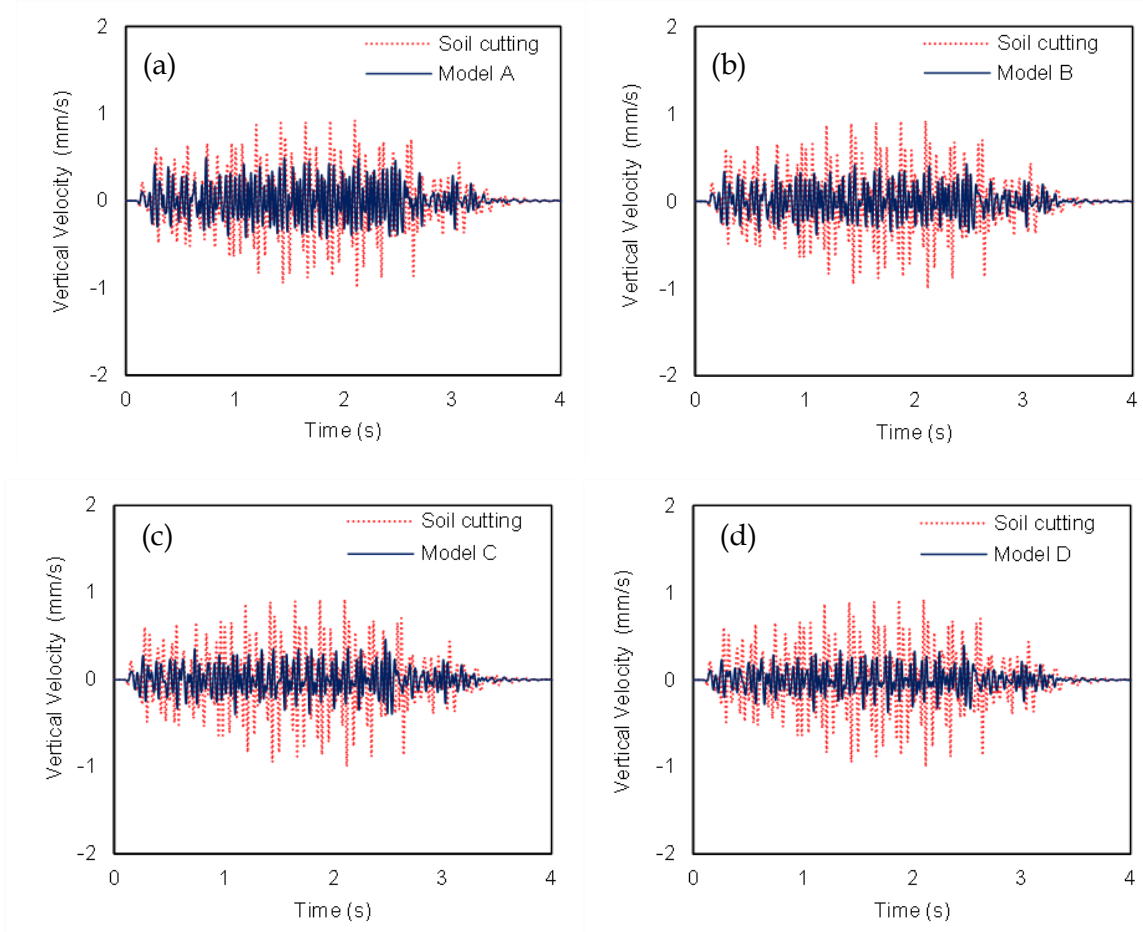

Figure 5.19 Comparison of soil and EPS-retrofitted cutting in terms of vertical velocity time histories at 23m from the track: (a) Model A, (b) Model B, (c) Model C, (d) Model D.

The same observation is made at the most remote observation position, at 35m from the track. According to Figure 5.20, the reduction of the vertical velocity is higher than 50% for all the examined mitigation approaches. More specifically, the implementation of an EPS layer with 0.5m height has led to the reduction of the peak vertical velocity from 0.36mm/s to 0.19mm/s. The reduction reaches the value of 0.17mm/s and 0.165mm/s for Model B and Model C, respectively. The peak vertical velocity of Model D remains the same with Model C. Hence the assumption could be made that Model B is the optimal

option for the reduction of the far-field vibrations, as layers with the higher thickness could not further reduce the vertical velocities.
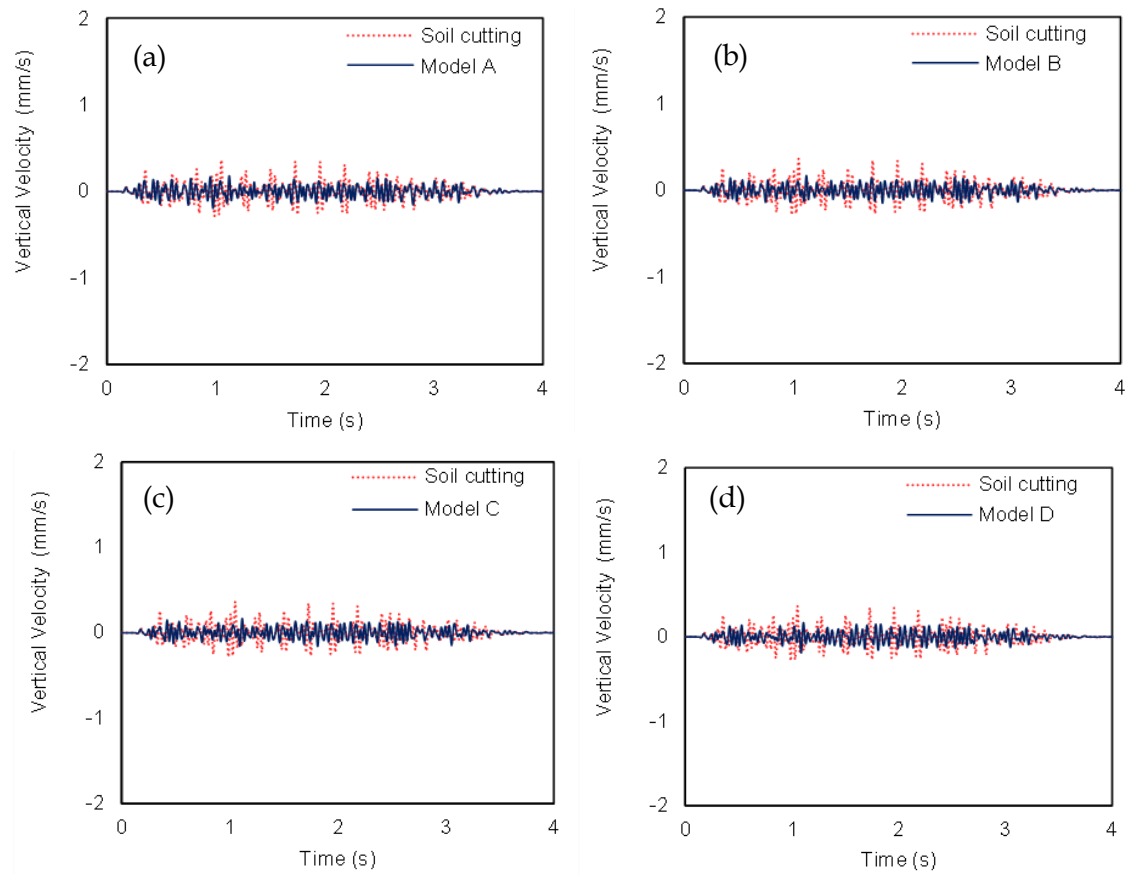
Figure 5.20 Comparison of soil and EPS-retrofitted cutting in terms of vertical velocity time histories at 35m from the track: (a) Model A, (b) Model B, (c) Model C, (d) Model D.

Similar observations can be derived by comparing the vertical velocity Fourier spectra in Figure 5.21. As illustrated, all the peaks in the frequency range between 0 and 40Hz, have been significantly reduced. More specifically, the most dominant peak at 26.32Hz is reduced from 0.46mm/s to 0.25mm/s and 0.1mm/s for Model A and Model D, respectively, at 15m from the track. Furthermore, the other three vibrations peaks at 17.7Hz, 21Hz and 30Hz are also reduced for all mitigation scenarios. Note that only some secondary peaks between 45Hz and 55Hz have been slightly increased after the implementation of a thin (0.5m depth) EPS layer. Therefore, it is obvious that for all the examined EPS widths; the proposed mitigation approach plays a beneficial role at all peaks in the low-frequency range at the surface of the embankment slope, which is close to the fundamental periods of common buildings and infrastructure (i.e., close to 20Hz).
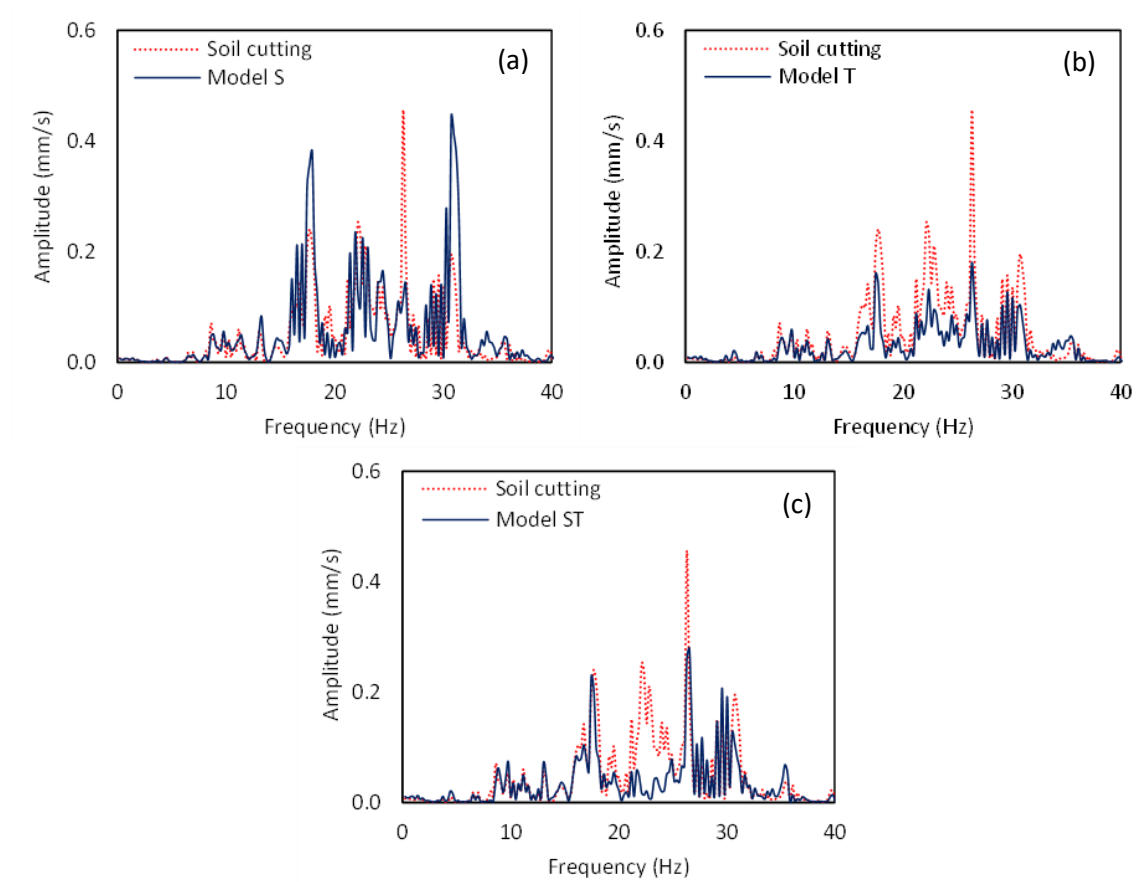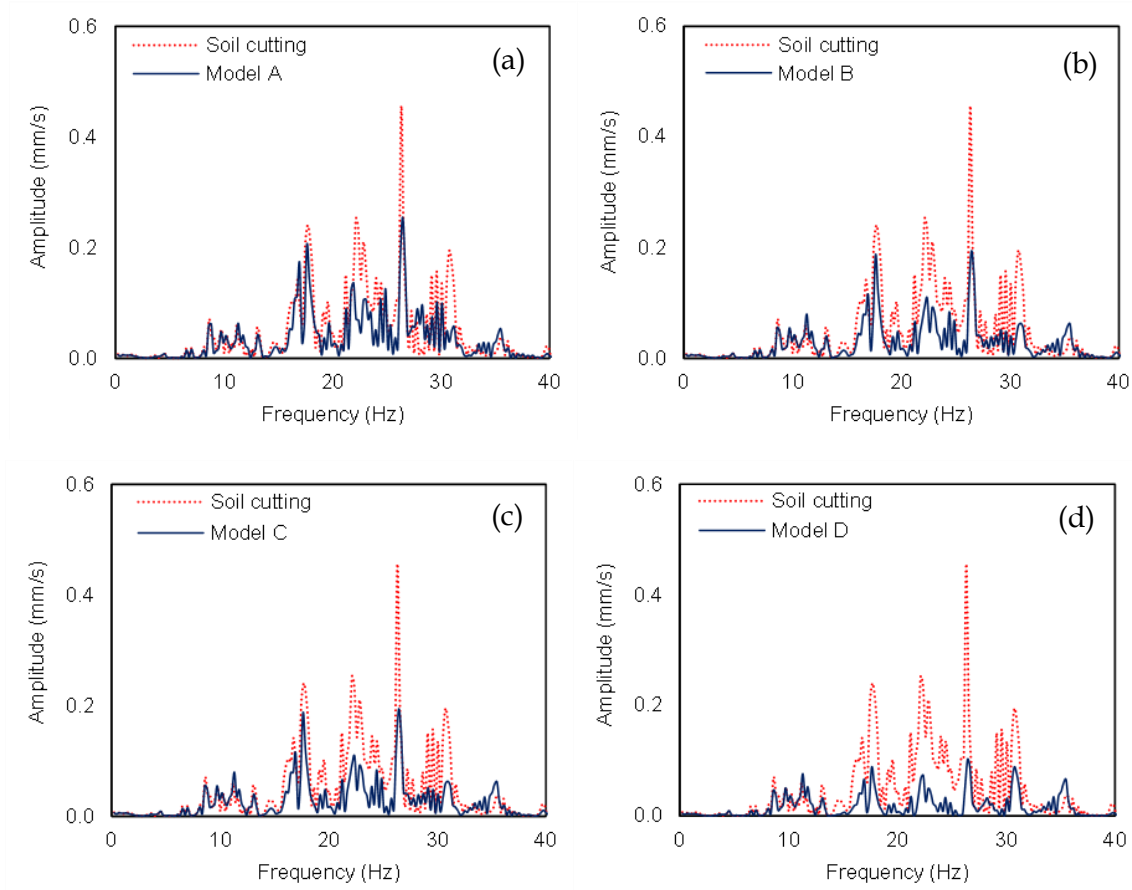
Figure 5.21 Comparison of soil and EPS-retrofitted cuttings in terms of vertical velocity Fourier spectra at 15m from the track: (a) Model A, (b) Model B, (c) Model C, (d) Model D.

This is further presented in the comparative Fourier spectrum of Figure 5.22 at the top corner of the cutting slope, in which the beneficial role of the subsoil response by replacing the upper soil layer of the cutting with EPS geofoam is presented. The vibrations peaks remain the same (e.g., 17.7Hz, 21Hz, 26.3Hz, 30Hz) at the low-frequency range. The most dominant vibrations peak is not significantly altered in the case of Model A. Howeve, the reduction at 17.7Hz and 21Hz is higher than 35%. Furthermore, the reduction of the spectral amplitude is extraordinary at the vibrations peak at 30Hz, where the spectral velocity is minimized from 0.2mm/s to 0.06mm/s. The implementation of a thicker EPS layer further decreases the vibrations peak. More specifically, the increase of the layer thickness manages to halve the spectral velocity at 26.3Hz successfully. The efficacy of the last examined mitigation scheme (e.g., EPS layer of 2m EPS is implemented) is remarkable. Figure 5.22d clearly illustrates that in this case, the vibrations peaks at all the examined low-frequency range is lower than 0.1mm/s.
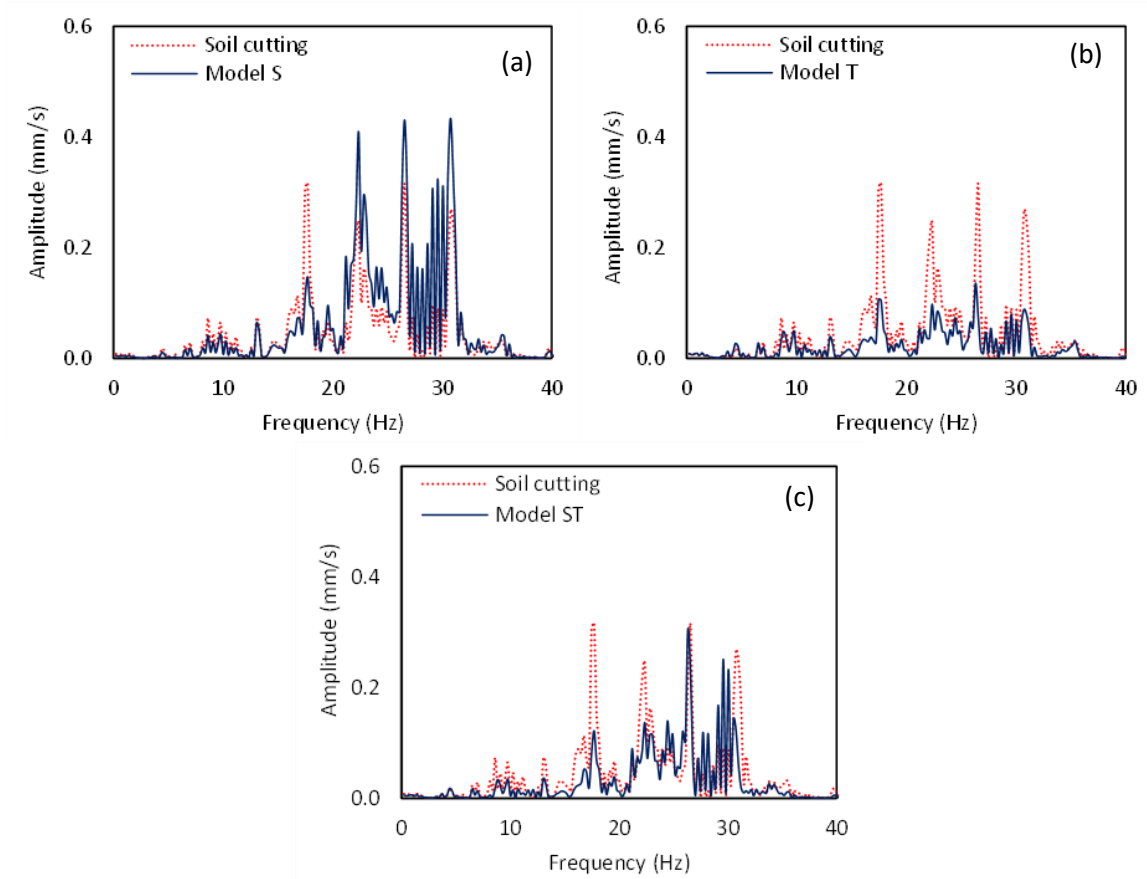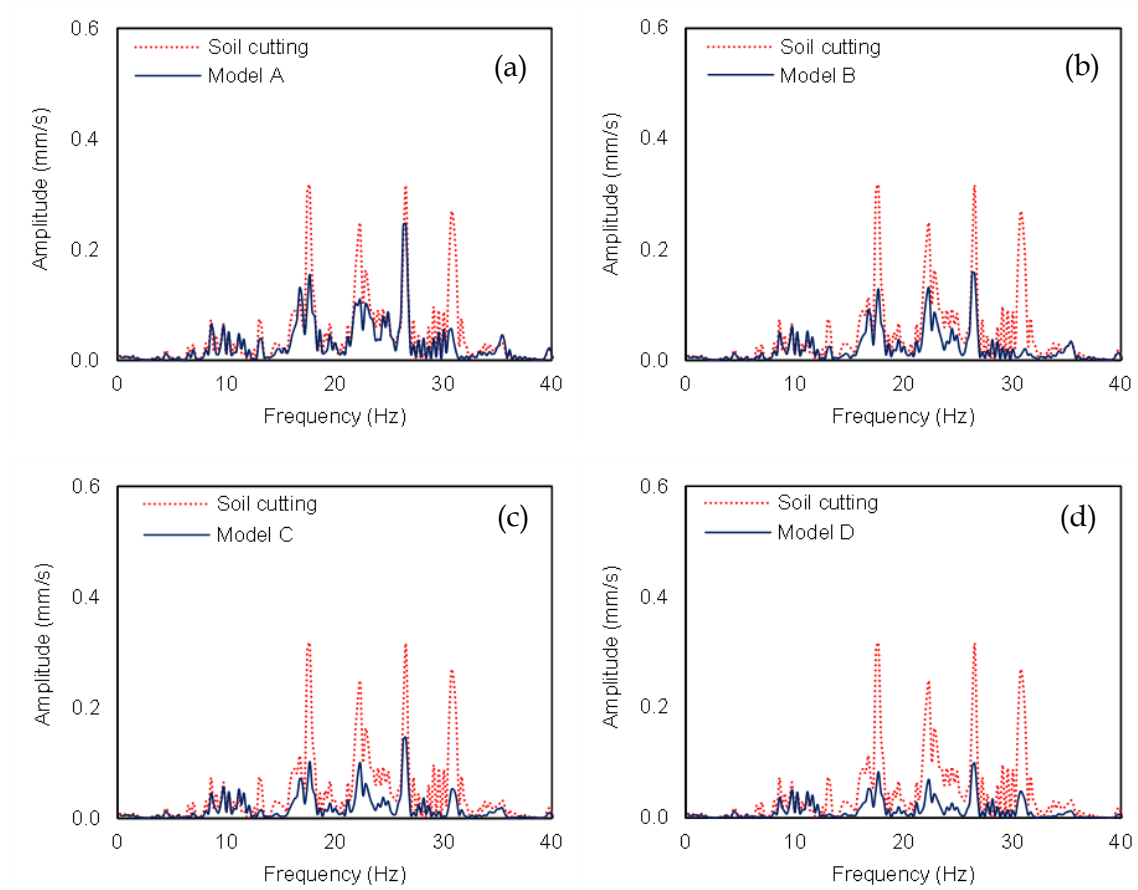
Figure 5.22 Comparison of soil and EPS-retrofitted cuttings in terms of vertical velocity Fourier spectra at 19m from the track: (a) Model A, (b) Model B, (c) Model C, (d) Model D.

Figure 5.23 illustrates the Fourier spectra at the closest examined distance from the top corner of the cutting slope (e.g., 23m from the track). At this observation point, as it was aforementioned, the beneficial role of the EPS geofoam at the cutting slope has been clearly depicted from the vertical velocity time histories (see Figure 5.19). Herein, it is obvious that the implementation of EPS geofoam manages to minimize all the vibrations peaks at the low-frequency range. It should be mentioned that the level of reduction at 21Hz is not significantly altered irrespective of the EPS thickness. Model A successfully minimizes all the peaks below 0.15mm/s, except for the most dominant peak at 26.3Hz, which remains at the same level after implementing just 50cm geofoam. As expected, as the EPS layer thickness increases, the level of reduction is even higher. Hence, the optimal approach is Model D, which manages to reduce the vibrations level below 0.1mm/s.
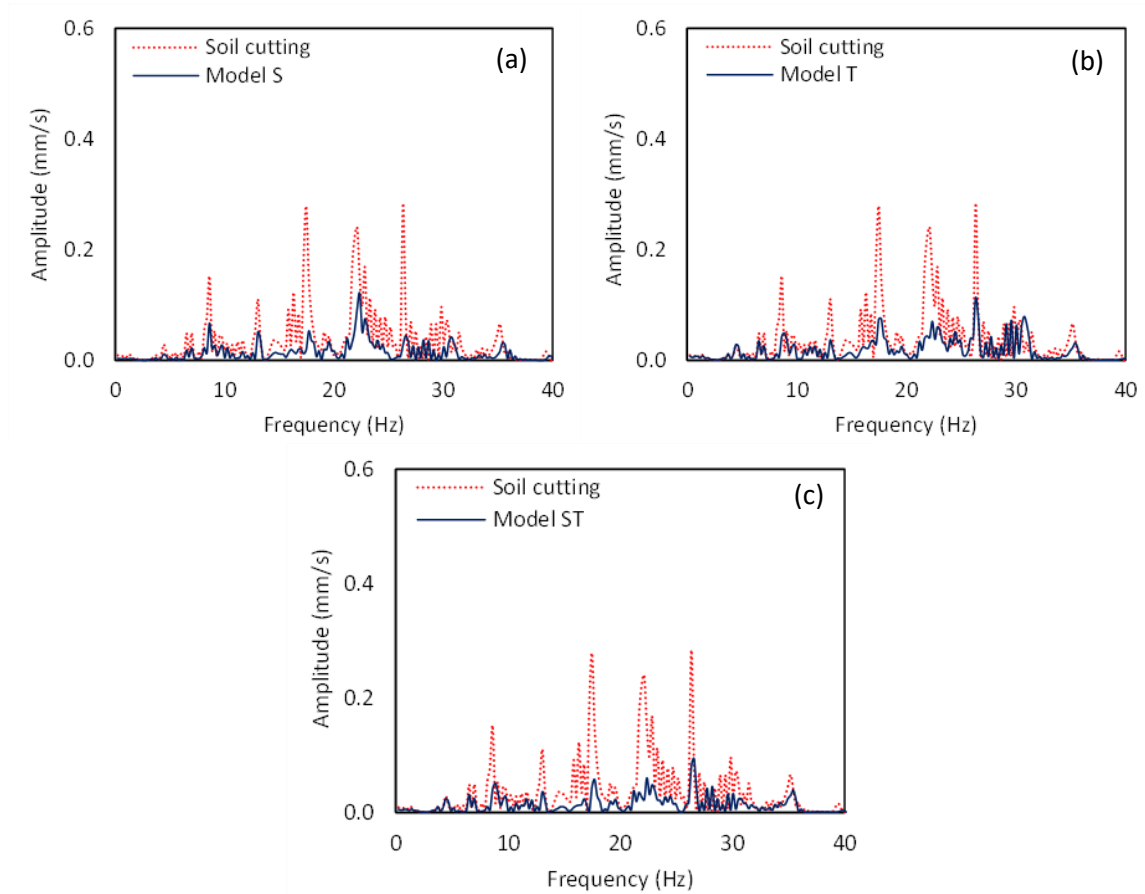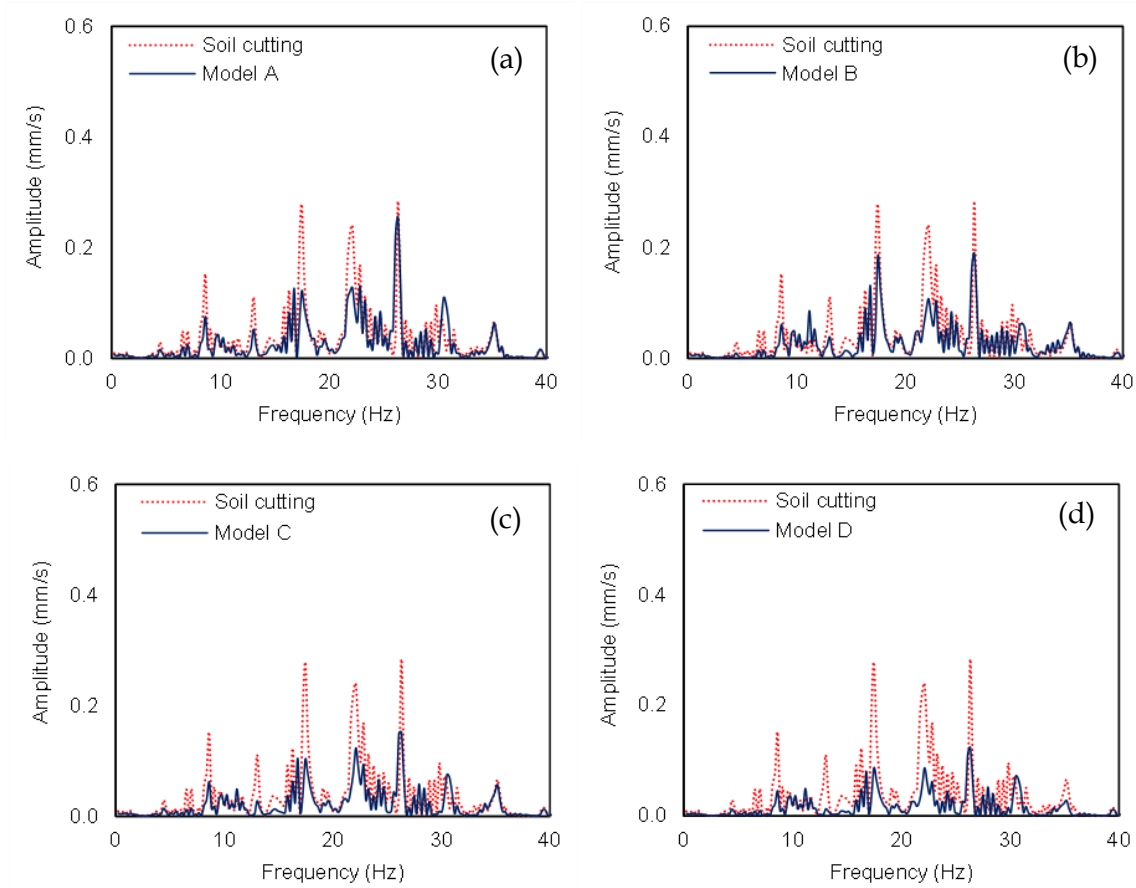
Figure 5.23 Comparison of soil and EPS-retrofitted cuttings in terms of vertical velocity Fourier spectra at 23m from the track: (a) Model A, (b) Model B, (c) Model C, (d) Model D.

Figure 5.24 compares the cutting efficacy before and after the implementation of the EPS layer at the slope at 35m from the track. In this case, the initial vibrations peaks are already relatively low, although the implementation of EPS geofoam further reduces the spectral velocity. In this case, the spectra could be divided in two parts (e.g. (0, 20Hz) and (20, 40Hz)). The level of reduction at the vibrations peak at the first part of the spectra (0, 20Hz) has been slightly reduced. More specifically, the level of reduction reaches in some cases close to 40% for all the examined layer thicknesses. The mitigation level is even more pronounced at the second part of the spectra (20, 40Hz). For instance, in the case of Model D, the vibrations peak at 30Hz has been virtually disappeared.
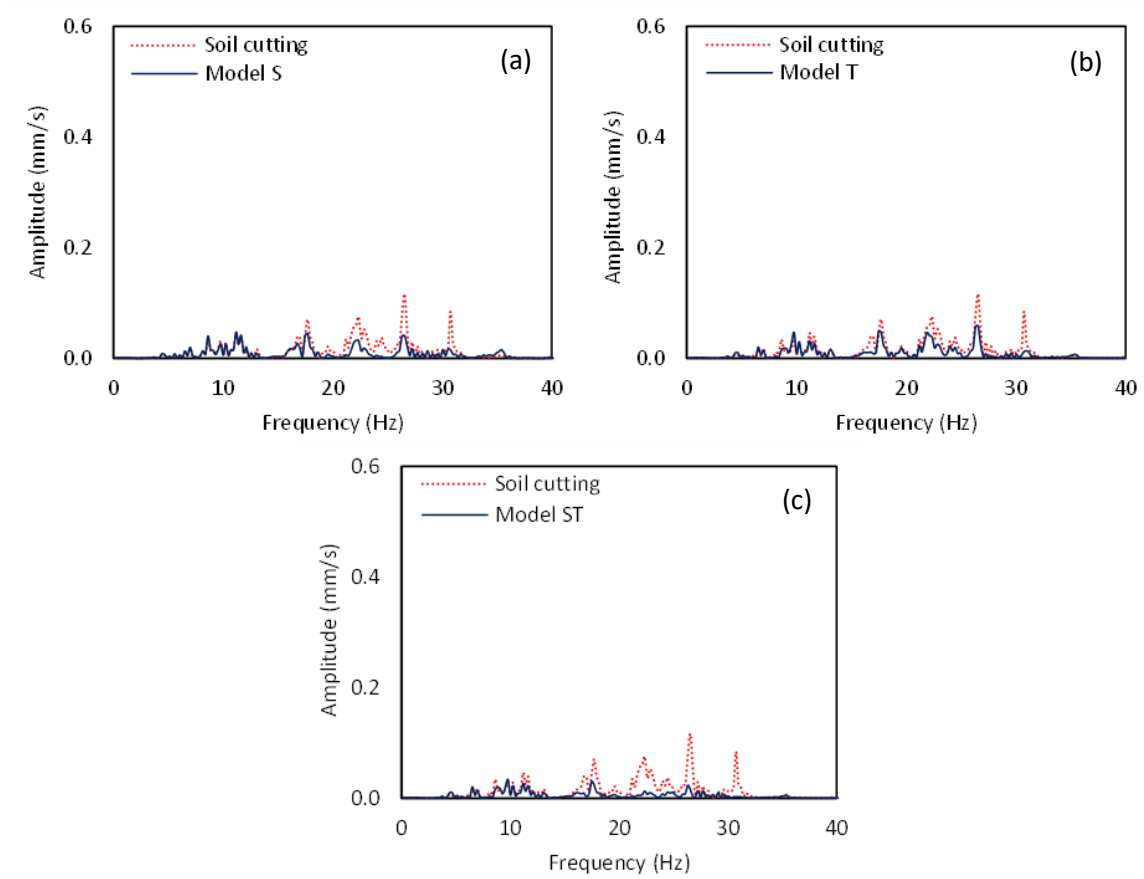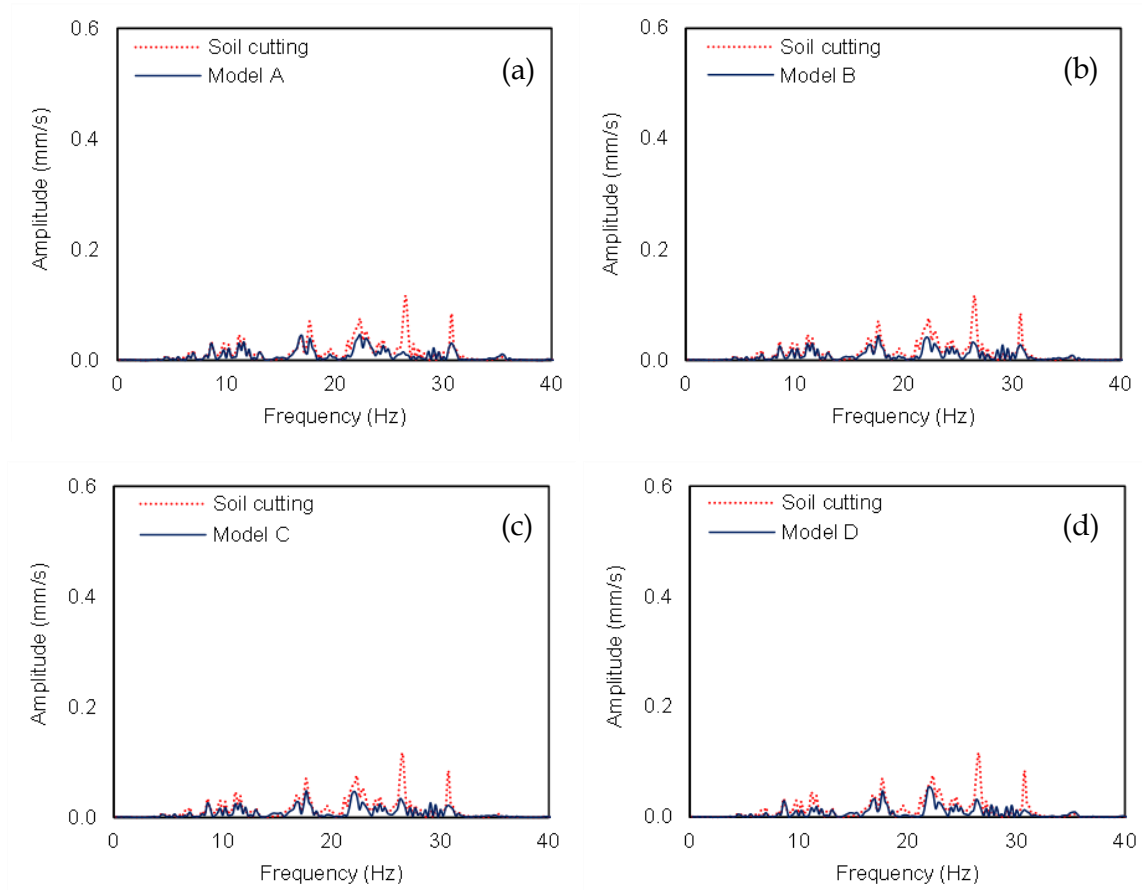
Figure 5.24 Comparison of soil and EPS-retrofitted cuttings in terms of vertical velocity Fourier spectra at 35m from the track: (a) Model A, (b) Model B, (c) Model C, (d) Model D

Figure 5.25 depicts the contour plots of vertical velocities at the soil surface, at 0.6s from the beginning of the analysis, aiming to illustrate further the impact of the EPS layer thickness on reducing HST-induced vibrations. The more intense contours represent the zones having vertical velocities with absolute values above 0.5mm/s. This value has been selected as an indicative threshold to illustrate the propagation of the vibrations along the soil surface for both models. As shown in Figure 5.23, the maximum absolute value is 0.73mm/s and 0.42mm/s at 23m from the track for Model A and Model D, respectively. It can be observed that the surface waves are more pronounced in the case of Model A, reaching peak values higher than 0.5mm/s at the top of the cutting slope. In contrast, the velocities and the scattering of the waves are much lower for Model D. Hence, it can be easily concluded that the efficiency of this mitigation approach depends on the thickness of the EPS layer, which of course, also increases the cost. Nevertheless, the cost of EPS material is generally low and varies depending on the material type, required quantities for large-scale projects, transportation costs, etc.
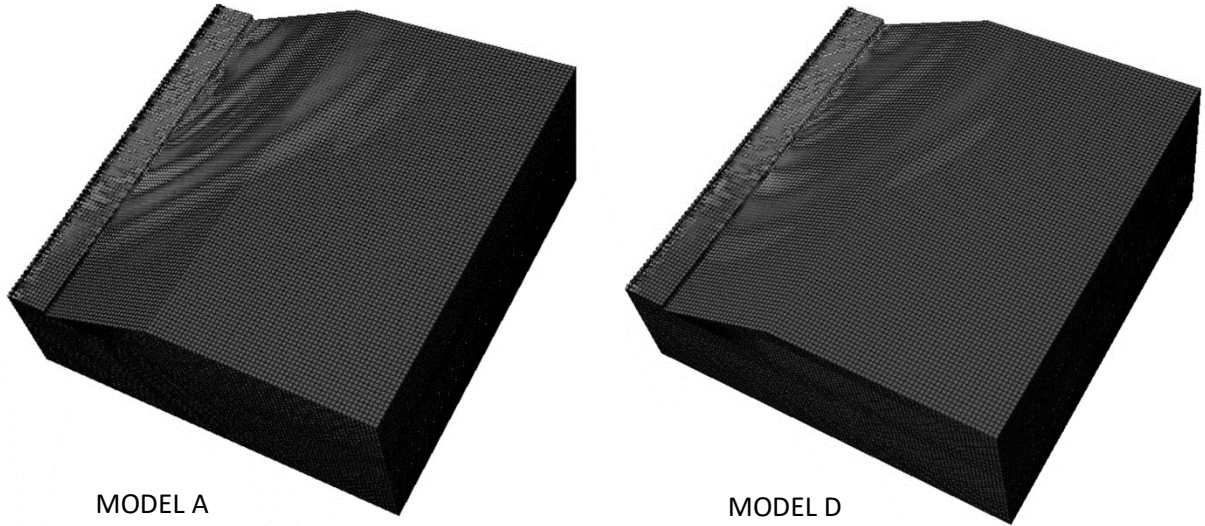
MODEL A   MODEL D

Figure 5.25 Contour plots of vertical velocities at soil surface for Model A and Model D.

In order to further illustrate the beneficial role of the examined mitigation scheme, the traffic-induced vibrations level in terms of velocity decibels (V_{dB}) are also compared. Figure 5.26 compares V_{dB} levels at the center frequency of each 1/3 octave band of the soil cutting and the retrofitted scenarios of Model A and Model D at 15 m and 19 m from the track. Compared to soil cutting, Model A at 15 m from the track reduces the V_{dB} levels in most of the examined octave bands with center frequencies between 0Hz and 50Hz, apart from a slight increase at 4Hz and a local spike at 50Hz, which diminishes in Model D. Moreover, Model D has contributed to the reduction of the V_{dB} levels within the low-frequency range, ranging from 1.5dB to 16dB.
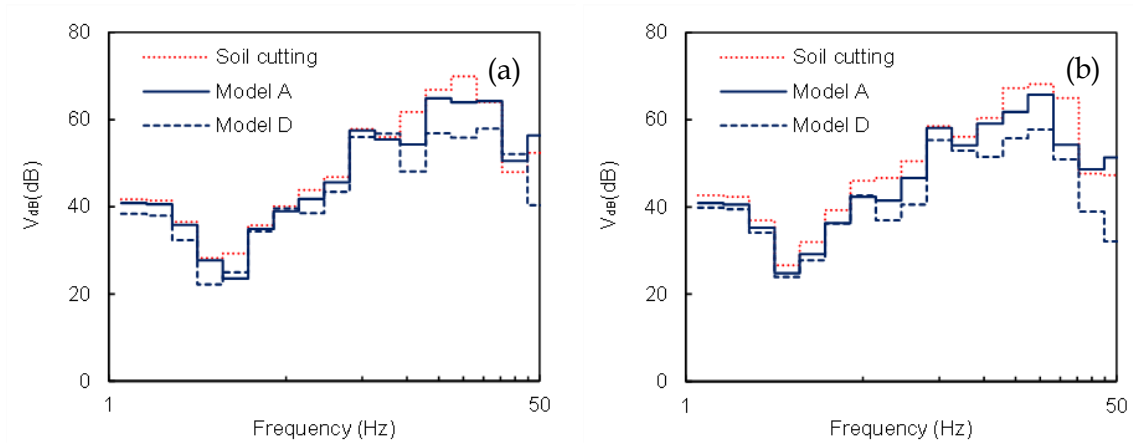
Figure 5.26 Comparison of the soil and the retrofitted Model A and Model D cuttings in terms of V_{dB}: (a) at 15m, (b) at 19m from the track.

Furthermore, at far-field (35m from the track), both retrofitting scenarios have reduced the V_{dB} level in all frequencies. Similarly, at near-field locations, Model D outperforms Model A, especially in the frequency range of interest. Figure 5.27a

demonstrates the velocity decibel at each of the low-frequency octave bands at 23m from the track. Model A manages to reduce the vibrations level at all the examined octave bands. For instance, at the octave band with a centre frequency 20Hz, the vibrations level has been reduced from 65dB to 59dB. On the other hand, in the most dominant octave band with a centre frequency 25Hz, the decibel level has not been significantly altered. The level of decibel reduction is even more pronounced in the case of Model D. This Model has managed to capture a decibel reduction higher than 3.5dB at all the examined octave bands. Furthermore, the decibel level at the most dominant octave bands with centre frequencies 20Hz and 25Hz has been reduced below 56dB. On the other hand, the decibel reduction of Model A and Model D is comparable at the far-field position, at 35m from the track. In this case, both models reduce the decibel level of all the examined bands below 53dB.
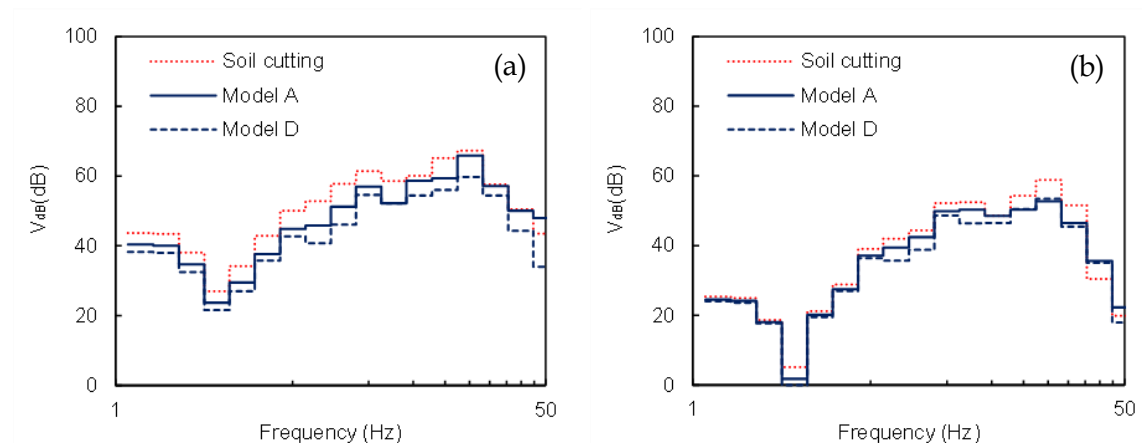
Figure 5.27 Comparison of the soil and the retrofitted Model A and Model D cuttings: (a) at 27m, (b) at 35m from the track.

As mentioned in Chapter 4, according to World Health Organization (WHO/Europe, 2018), vibrations higher than the threshold of 55 dB are dangerous for public health since they can cause annoyance, sleep disturbance, increasing the risk for cardiovascular diseases. At 15m from the track, the implementation of Model D significantly reduces the vibration levels at crucial center frequencies; however, it has not managed to reduce the V_{dB} levels below the 55dB limit. On the other hand, at 35m from the track, both models have achieved V_{dB} values lower from 55dB -much lower in the case of Model D- within the whole low-frequency range. It has to be noted that there are not many buildings - especially residential- at distances very close (e.g., at 15 m from the track) to operating HSR lines. On the other hand, in the future, upgrading existing normal speed railways, which often passes through urban environments, adjacent residential buildings in closer

distances will be more common. Note that apart from buildings, there are also other structures very close to HSR lines (e.g., overpass and nearby bridges), and their users could also be affected by HST vibrations.

5.6.   *Comparison between Model T and Model D*

As mentioned, Model D has been proposed to overpass the low efficacy of Model S at the cutting slope and achieve a lower vibrations level than the EPS-filled trench. Figure 5.28 compares the peak vertical velocity of Model D, Model T and Model ST at increasing distances from the track. It is obvious that the peak vertical velocity of the soil cutting model is gradually reduced from 1.4mm/s to 0.5mm/s with increasing distance from the track. The implementation of a single EPS-filled trench (e.g., Model T) has led to a notable reduction of the peak vertical velocities. More specifically, the level of reduction ranges between 42% and 58% for all the examined positions.
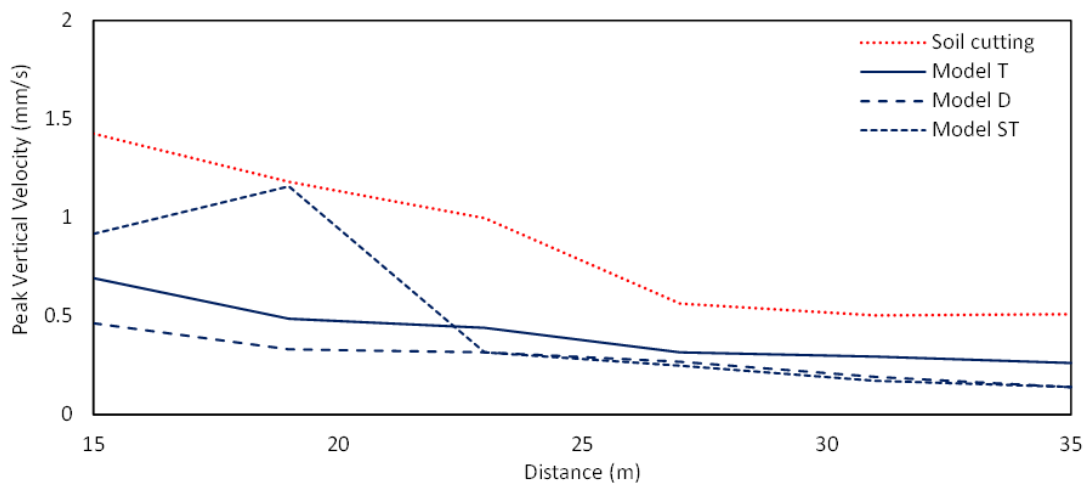
Figure 5.28 Peak vertical velocity at increasing distance from the track.

The implementation of the hybris model (e.g., Model ST) at the near field position is less effective than Model T. It is evident that the level of velocity reduction at 15m from the track is just 35%. Furthermore, at 19m from the track, this mitigation approach has not altered the peak vertical velocity. On the other hand, this approach is remarkably more effective at the upper flat of the cutting than the single EPS-filled trench. More specifically, at distances higher than 23m from the track, the implementation of the hybrid method increases the reduction of the peak vertical velocity up to 60%. For instance, the reduction is equal to 48% and 73% at 35m from the track for Model T and Model ST, respectively. The beneficial role of Model D is clearly illustrated in Figure 5.28. This mitigation scheme

is more effective than the EPS-filled trench at the cutting slope. Furthermore, it manages to capture the same velocity reduction with Model ST at the upper flat of the cutting. It is obvious that Model D is the optimal approach, as it captures a reduction of around 70% in the majority of the observation positions.

In order to further examine the efficacy of Model D, it is compared with the pre-examined Model T and Model S in terms of insertion loss (IL) curves. In the sequence, the commonly used IL curves have been used to compare the two approaches since they are commonly used to characterize the efficiency of each mitigation approach (Li et al., 2020; Ngamkhanong et al., 2020). The IL levels have been calculated for the center frequencies of the 1/3 octave bands between 1.25Hz and 50Hz according to Eq. 4.1. More specifically, the IL of Model D is compared with the second most effective scheme at each examined position (e.g., Model T at the cutting slope at the cutting slope (15m and 35m from the track) and Model ST at the upper flat positions (23m and 35m from the track)).

Figure 5.29 illustrates the IL curves of Model D and Model T at the slope of the cutting. The insertion loss of Model T ranges between 0dB to 7dB for all the examined octave bands at 15m from the track. Furthermore, the three peak values of insertion loss, reaching higher than 6dB, are located at the 1/3 octave bands with centre frequencies 8Hz, 16Hz and 25Hz. Furthermore, it is evident that the EPS-filled trench is more effective than Model D at the octave bands with frequencies between 8Hz and 12.5Hz. On the other hand, Model D is more effective at all the others 1/3 octave bands. Model D has significantly reduced the decibel level at the octave bands with centre frequency below 5Hz, in contrast with Model S, which is not effective in this range. Furthermore, the decibel reduction of Model D is even more pronounced at the most dominant octave bands with centre frequencies 16Hz, 20Hz and 25Hz. For instance, IL at the 14th octave band is close to 14dB. The same trend is observed at the cutting top corner, at 19m from the track. The IL at all the dominant frequencies is close to 8dB in the case of Model T at this observation position. However, Model D increases even higher IL, reaching in some cases close to 15dB.

Obviously, the volume of EPS material used to cover the cutting slope is greater than the EPS volume used for filling the trench. Nonetheless, EPS geofoam is not a very expensive construction material and this increase is not expected to substantially affect the total construction or upgrading cost of an HSR project. On the other hand, this layer can be constructed faster and avoids other costs (excavation, stabilization, etc.) needed to

make the EPS-filled trench. Thus, in order to compare the total cost of the two mitigation approaches, a detailed study is required, taking into account the conditions at the specific site. Nonetheless, what is more important is the increased mitigation efficiency of the proposed approach, provided that the EPS layer has an adequate thickness (e.g., as presented in Figure 5.29, the reduction of the dB levels achieved by Model D is considerably higher compared to the EPS-filled trench, especially within the most dominant octave bands). Lastly, if there exist budget constraints on the cost of any mitigation measures, the proposed scheme could be applied only at critical zones of existing or new HSR lines (e.g., close to "sensitive" buildings).
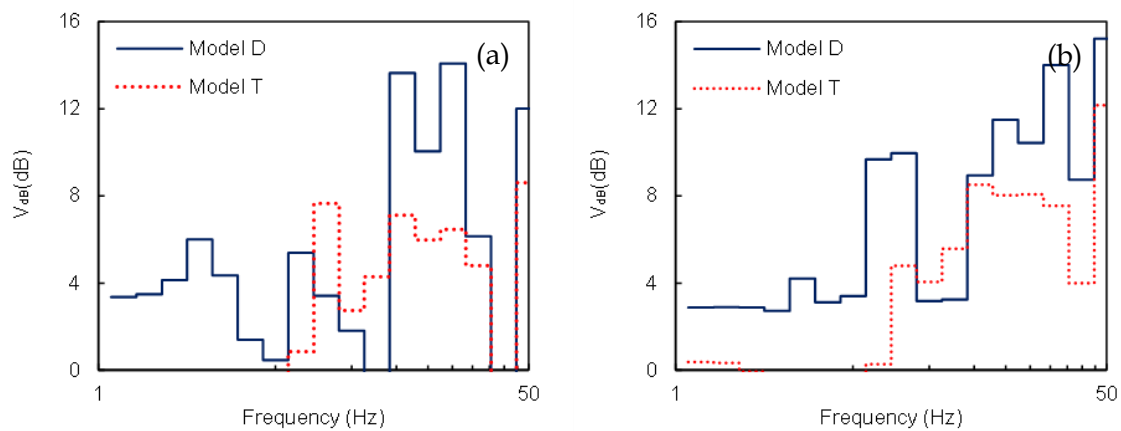
Figure 5.29 Comparison of insertion loss curves of Model D and Model T (a) at 15m, (b) at 19m from the track.

In the sequence, the efficacy of Model D is compared with the effective, at the far-field, Model S. Figure 5.30a demonstrates the IL at the low frequency 1/3 octave bands at 23m from the track. The efficacy of Model S at this observation position is remarkable, as the decibel reduction is higher than 6dB at all the examined octave bands. Furthermore, IL reaches slightly below 12dB at the 12th and 13th octave bands. In the case of Model D, the IL is also satisfactory at 23m from the track, although the decibel reduction, in general, is lower than Model S. On the other hand, at the most remote position, at 35m from the track, Model D is undoubtedly more effective than model S, as shown in Figure 5.30b. The decibel reduction of the two mitigation schemes is almost identical at the most dominant octave bands, reaching close to 8dB at the 14th and 15th octave bands. However, in contrast to model S, Model D is effective at the octave bands with centre frequencies below 12.5dB.
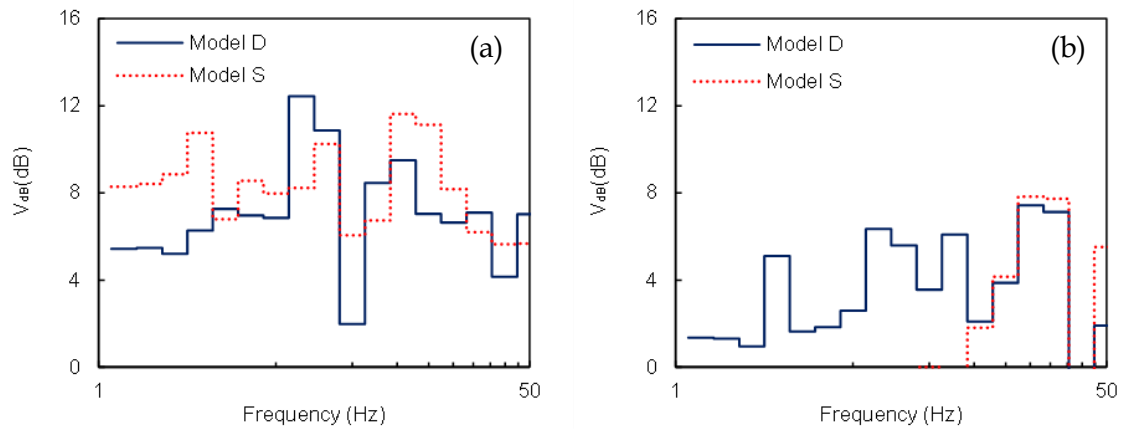
Figure 5.30 Comparison of insertion loss curves of Model D and Model S (a) at 23m, (b) at 35m from the track.

5.7. *Influence of subsoil properties*

In the previous sections, the efficiency of the proposed mitigated approach has been investigated for an existing layered soil profile in Belgium with specific properties to validate the accuracy of the numerical model with field measurements. Certainly, it is important to study further the effectiveness of this scheme for different soil sites. For this purpose, three additional hypothetical subsoil scenarios with homogenous underlying soil have been examined. More specifically, dense sand with gravels a stiff and soft clay have been simulated in a similar manner as the initial cutting site. Table 5.1 summarizes the mechanical properties of the examined soils.

The efficiency of the proposed mitigation approach is displayed in Figure 5.31, where the PPV levels at several distances are illustrated for the three different subsoil scenarios. By comparing the PPV values of the initial cuttings, it can be easily noticed that the stiffer subsoil exhibits lower vibrations levers. In addition, vibrations decrease with increasing distance from the track. Nonetheless, they have a slightly less linear reduction pattern in the case of the stiff clay compared to the other two subsoil cases, which are smoothened with the application of EPS (see Figure 5.31b). It is also clear that the proposed mitigation scheme reduces the vibrations levels for all soil types, especially at near-field locations (15 m to 23 m from the track). Furthermore, it is evident that in all cases, the increased EPS layer thickness provides better results. As it can be seen in Figure 5.31a, the PPV for the HSR track on dense sand with gravels is reduced 2 to 3.5 times when using the thick EPS layer (Model D) compared to the retrofitted cutting. Similar reductions can be observed for the other two subsoil types, as shown in Figures 5.31b and 5.31c.
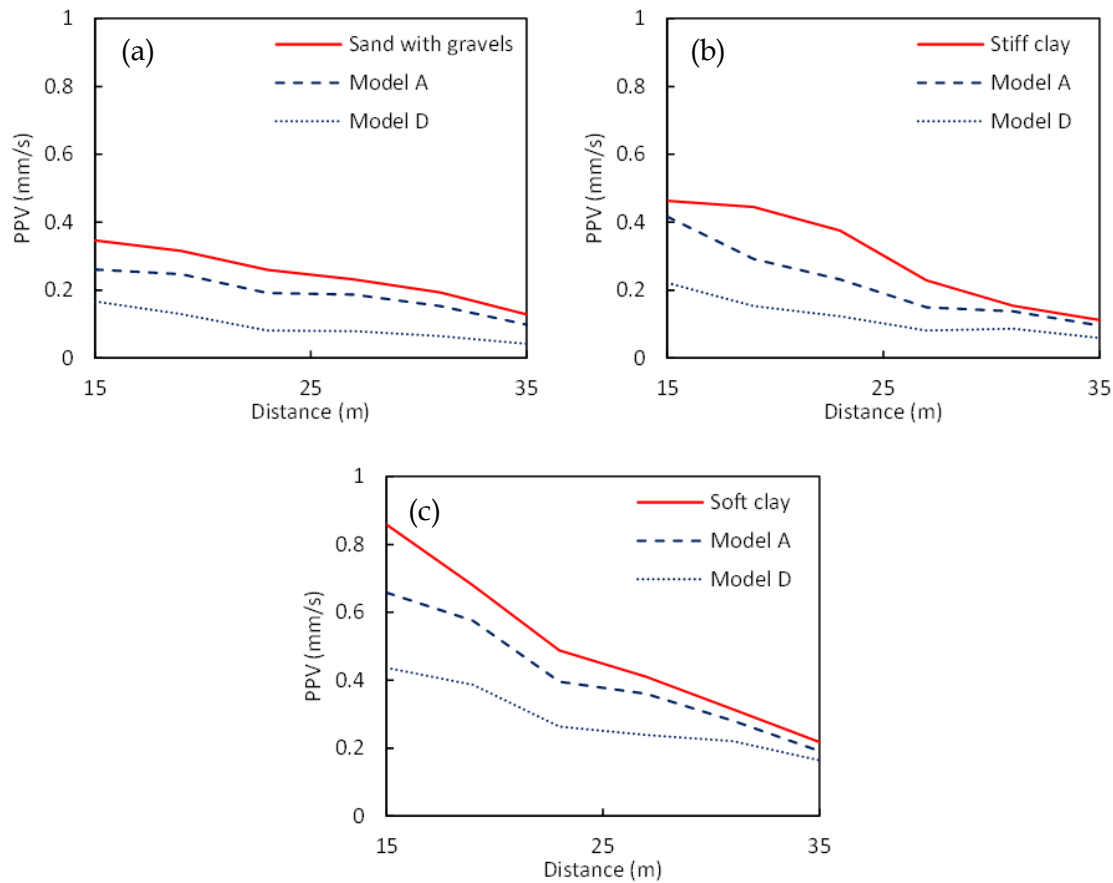
Figure 5.31 Comparison of initial and mitigated cutting vibration levels in terms of PPV at increasing distance from the track for a homogeneous soil site: (a) dense sand with gravels, (b) stiff clay, (c) soft clay.

Table 5.1. Properties of the examined subsoil scenarios.

Subsoil type	Density (kg/m³)	Young's Modulus (GPa)	Poisson's ratio	Damping (%)
Dense sand with gravels	2100	1.00	0.20	5
Stiff clay	2000	0.60	0.25	5
Soft clay	1850	0.15	0.30	5

Lastly, by comparing the non-retrofitted cutting in the case of the stiffer soil in Figure 5.31a with the retrofitted one with the thick EPS layer (Mode D) in the case of soft clay, it is worth noting that the proposed mitigation scheme has successfully reduced the PPV levels in similar values. In other words, with this relatively low-cost and easy-to-implement scheme, a substantial "upgrading" of a soft soil site can be achieved, which can have an "equivalent" response to HST-induced vibrations as a much stiffer site. Hence, this can expand the decision-making choices when the routing of new HSR is planned or when the upgrading of existing railway lines is examined.

As it was presented in Chapter 2, the German Institute for Standardization (DIN4150-2, 1999) proposes the threshold of 0.15 mm/s of $KB_{F,max}$ for residential areas. Figure 5.32 demonstrates the $KB_{F,max}$ values at distances between 15m and 35m from the track. In the case of a track based on the stiffer subsoil (e.g., dense sand with gravels), the $KB_{F,max}$ level of the initial unretrofitted model is the lowest among the three examined subsoils. More specifically, $KB_{F,max}$ is equal to 0.25mm/s at 15m from the track and reduces to 0.09mm/s at 35m from the track. Furthermore, it is observed that $KB_{F,max}$ is reduced below the DIN limit values for distances greater than 29m from the track, as shown in Figure 5.32α. The implementation of a thin EPS layer (e.g., Model A) reduces the $KB_{F,max}$ below 0.15mm/s, for distances higher than 21m from the track. However, the beneficial role of the thickest EPS layer is clearly illustrated in Figure 5.32a, as Model D minimizes $KB_{F,max}$ below DIN limit value at all the examined distances from the track.
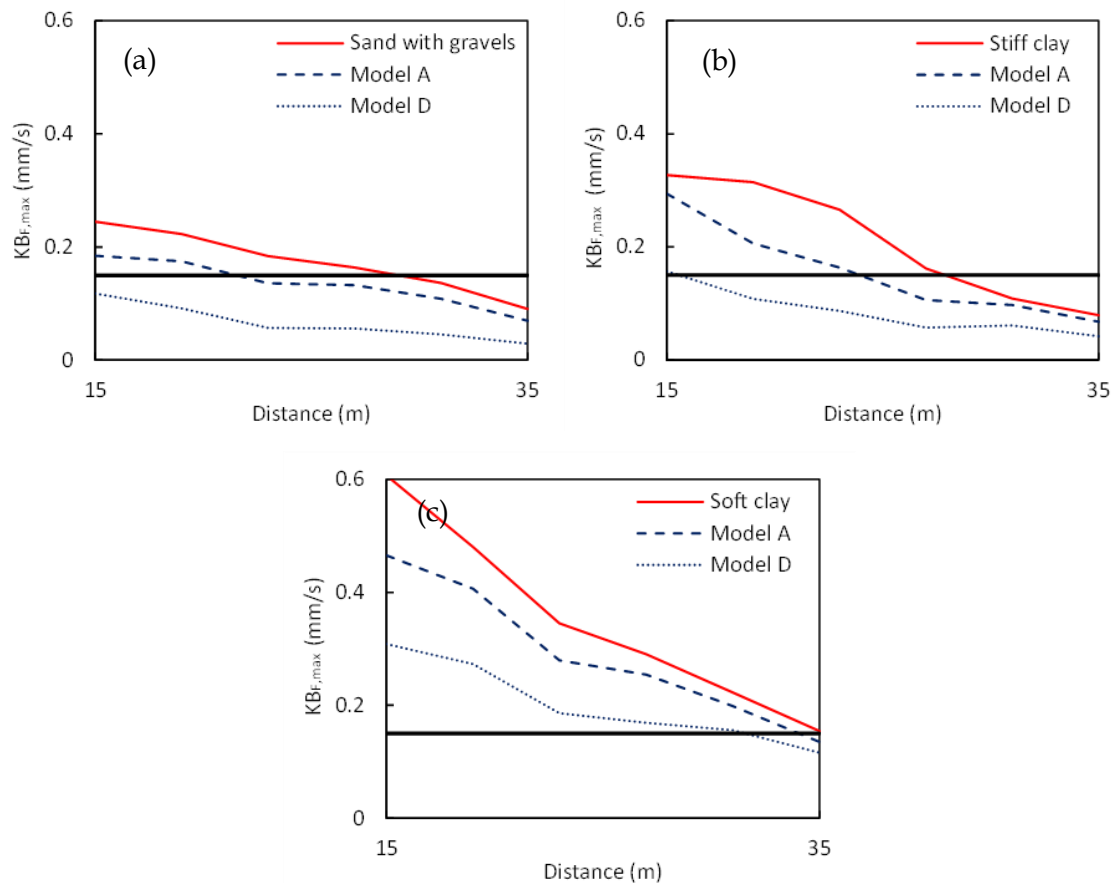
Figure 5.1. Comparison of initial and mitigated cutting vibration levels in terms of $KB_{F,max}$ at increasing distance from the track for a homogeneous soil site: (a) dense sand with gravels, (b) stiff clay, (c) soft clay.

Figure 5.32b illustrates the $KB_{F,max}$ in the modeling scenario for which the track is passing from a site consisted of stiff clay. The initial $KB_{F,max}$ value is significantly higher

than the previously examined soil at the near-field locations. For instance, at 15m from the track, $KB_{F,max}$ is equal to 0.33mm/s. However, $KB_{F\ max}$ has been minimized below the DIN threshold at a closer distance from the track than dense sand with gravels. Model A slightly reduces the $KB_{F,max}$ values, especially at the middle-field positions. However, Model D is more effective in this case, as it manages to minimize $KB_{F,max}$ below 0.15mm/s at the whole examined distance range. Lastly, $KB_{F,max}$ is higher than the DIN threshold at all the examined distances, in the case of the track constructed on soft clay. The proposed mitigation measures significantly reduce the $KB_{F,max}$ values, although the reduction level is not capable of minimizing the vibration levels below the DIN threshold.

5.8. *Discussion of the results*

A detailed numerical study has been conducted in this work to investigate and mitigate the HST-induced vibrations at HSR cuttings. Several mitigation approaches have been implemented to the HSR cutting in order to investigate their effectiveness. A new mitigation scheme for reducing vibrations using EPS blocks layer at the cutting slope has been proposed in the sequence. The efficacy of this approach has been compared with the other examined mitigation schemes. Furthermore, the captured mitigation level in several subsoil conditions has been investigated. The main conclusions that can be derived from the presented numerical investigation can be summarized as follows:

- The implementation of an EPS-filled trench across the track is a great countermeasure for the HST-induced vibrations at cutting sites. This approach is capable of reducing the vibrations level up to 10dB in some cases.

- The implementation of a limited number of EPS blocks at the cutting slope increases the vibrations level at the cutting slope due to the waveguide effect. However, at the upper flat part of the cutting, the level of reduction is higher than the eps-filled trench. Furthermore, if this approach is combined with an EPS-filled trench, the reduction level at the far-field is even higher.

- A high vibrations reduction has been observed after the implementation of a water-filled trench. However, several issues, such as maintaining the trench initial geometry, should be investigated and a more detailed simulation of the water dynamic response should be performed in order to better assess this alternative mitigation approach.

- The replacement of the upper soil layer of the cutting with EPS has overpassed the issues related to the waveguide effect and successfully reduces the HST-induced vibrations at both the slope and the upper flat positions, while a thicker EPS layer leads to a higher reduction of the vibrations.

- Furthermore, V_{dB} values are lower than the allowable limit of 55dB at 35m from the track, which is crucial for protecting public health.

- The efficiency of the mitigation using a thin EPS layer is comparable to the reduction achieved using an EPS-filled trench at the cutting slope, while it is further increased in the case of higher EPS layer thickness.

- The developed vibrations due to HST passage are increased in the case of soft subsoil. Nevertheless, the proposed mitigation approach reduces the vibrations levels substantially, regardless of the soil properties, especially at closer distances from the track.

The present investigation has shown that the proposed mitigation approach can substantially reduce HST-induced vibrations in HSR cuttings. Nonetheless, further investigation is required for different cutting geometries and HST types and train speed. In addition, it has to be noted that the adopted modelling approach has assumed that the track is smooth since scheduled maintenance has taken place before the field measurements. Hence, the efficiency of the proposed mitigation approach has to be further verified by taking into account potential track irregularities. In addition, a detailed investigation should be performed to simulate more accurately and examine the role of the potential kinematic mechanisms between EPS blocks as well as with EPS geofoam and the soil.

BURIED PIPELINES PROTECTION WITH EPS GEOFOAM

6.1. Introduction

As mentioned in Chapter 3, the HST-induced vibrations are propagated on the underlying soil surface in the form of surface Rayleigh waves. The growth of researchers knowledge on numerical and analytical methodologies in the past few years has contributed to the accurate prediction of the response of the railway tracks and the subsoil surface when subjected to HST-induced vibrations. The vast majority of the relevant investigations focus on the propagation of the surface vibrations (Celebi, 2006; Gao et al., 2019; Singh and Seth, 2017) and their mitigation (Gao et al., 2020; Lyratzakis et al., 2020b; Yao et al., 2019). On the other hand, only a few studies examine the effects of the developing vibrations by the HST passage on the subsoil and the underground infrastructure (Liolios et al.,2002; Saboya et al., 2020). Hence, in this Chapter, a first attempt is made to investigate the dynamic response of buried pipelines crossing an HSR line vertically and aiming to protect them by using EPS geofoam.

Recently, Tafreshi et al. (2020) presented a series of full-scale tests on underground pipelines subjected to traffic-induced loading and examined the reinforcement of the pipelines by implementing EPS geofoam and geocell as backfill layers. According to this study, the use of EPS blocks with height equal to 0.3D and width 1.5D (where D is the pipe diameter) over the pipeline is proposed as the most practical solution. Furthermore, the beneficial role of implementing EPS backfills for the protection of buried pipelines

subjected to other types of loading has been investigated. Choo et al. (2007) investigated the effectiveness of EPS geofoam backfill for the remediation of buried pipelines subjected to permanent ground deformation (e.g., surface faulting, land sliding, seismic settlement, lateral spreading due to soil liquefaction). Furthermore, in the case of strike-slip fault rupture, geofoam blocks decrease the axial tensile strain of the non-pressurized pipeline from 4.16% to 0.75% in the case of a crossing angle equal to 135° (Rasouli and Fatahi, 2020). Bartlett et al. (2015) examined several technics of protecting underground pipelines and culverts in transportation infrastructure by implementing EPS blocks such as cover layer or embankment constructed over the pipe, "imperfect trench method" with compressible inclusion EPS block placed the above, slot-trench light-weight cover system with EPS block placed in slot and EPS post and beam system with headspace void.

As mentioned, numerous studies have investigated the protection of underground pipes or culverts using EPS geofoam (Kim et al., 2010; Witthoeft and Kim, 2016). However, there is a lack of an international bibliography related to the traffic loads effect on the buried pipelines. Thus, aiming to contribute to this research direction, the present Chapter investigates the dynamic response of the pipeline under HST-induced vibrations and their potential protection with EPS geofoam. Firstly, the numerical model has been validated with pre-available experimental data for repeated equivalent traffic loads. In the sequence, the effect of the geofoam layers thickness and the buried depth of the pipeline on the vibrations level on the top of the pipeline has been investigated for three typical HST passing speeds. Furthermore, the optimal geofoam layer has been used to protect PVC and steel pipelines with several thicknesses between 3mm and 10mm to investigate the displacement level at the top of the pipe (Lyratzakis et al., 2021e).

6.2. *Validation with Experimental data*

6.2.1. *Pre-available field data*

As mentioned, there is no relevant bibliography related to experimental data or in-situ measurements investigating the response of buried pipelines to the HST-induced vibrations. However, there is a series of experimental tests simulating the response of buried pipes due to traffic loads, presented recently by Tafreshi et al. (2020) and Khalaj et al. (2020). Tafreshi et al. (2020) used a full-scale model to simulate the repeating loading of heavy traffic. More specifically, 14 tests were carried out on a high-density polyethylene pipe (HDPE 100) in unreinforced and reinforced soil with EPS geofoam blocks and

geocells. The model has been constructed on a test pit with a floor plan of 2.2m × 2.2m and a depth of 1m. Furthermore, the test trench has a 0.75m x 0.75m floor-plan and 1.75m depth, as illustrated in Figure 6.1.

A circular plate is repeatedly loading and unloading the test trench, aiming to simulate the traffic loads. The loading plate has a diameter of 250mm, while a pressure equal to 800kPa has been applied in order to simulate the half axle of a heavy vehicle. Furthermore, 150 repeated loading cycles have been carried out. Khalaj et al. (2020) presented a similar full-scale model. The floor plan of the test pit was slightly smaller in this case, although the same pipe and a similar soil were used. Compared with the first test, in this case, instead of repeated traffic-loads, a gradually increasing load has been placed on the plate. More specifically, the load is increasing linear from 0kPa to 800kPa in 5s. Furthermore, in this study, the experimental results were used in order to validate a numerical model. Those two investigations have been used in the present section to validate an initial numerical model capable of accurately representing the traffic loads.
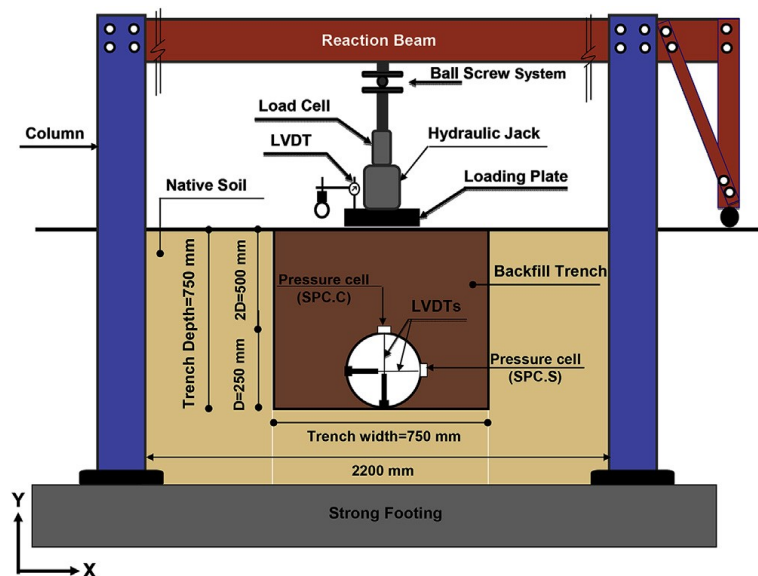
Figure 6.1 Schematic view of the test setup, instrumentation positions and geometric parameters (adopted by (Tafreshi et al., 2020)).

6.2.2. Description of the numerical model

The field test material properties and dimensions have been simulated via the commercial finite-element software ABAQUS (2014) to provide a numerical model capable of predicting the buried pipes response to traffic-induced vibrations. Figure 6.2 illustrates the numerical geometry of the used FE model. Hexahedral linear elements with a reduced integration formulation (C3D8R), with size 50mm, have been used to simulate the Backfill

trench and the native soil. The pipeline has been modelled with linear four-node shell elements (S4R). Furthermore, the interaction type between a loading plate and the ground surface has been assumed to be frictionless and "hard contact" for normal and tangential behavior.
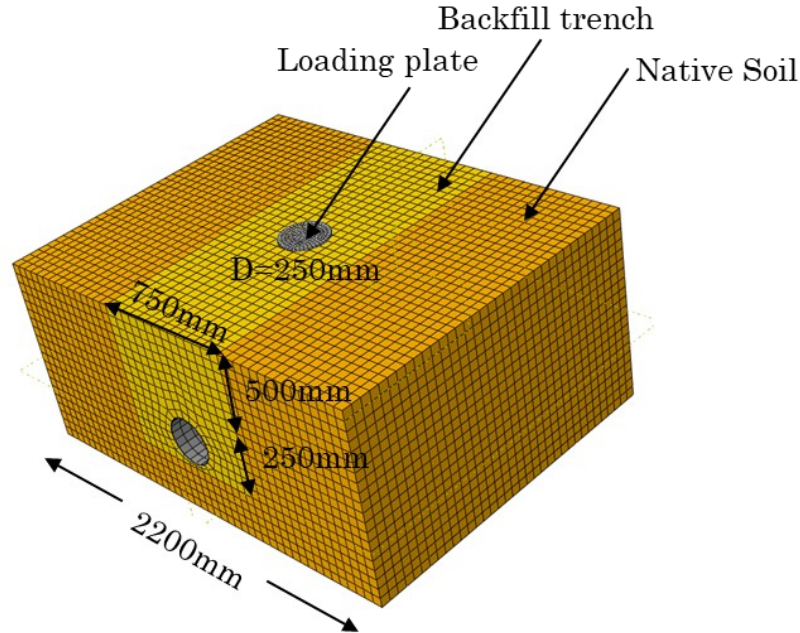
Figure 6.2 3D FE model, used for validation.

In the first analysis step, the geostatic pressure mass has been applied to the model parts. Then, the pressure has been applied to the rigid circular plate at the soil surface in the next step. In the sequence, the pressure on the loading plate has been applied in the second step in order to replicate the load of the two pressure plate tests. More specifically, in order to simulate the repeated loading cycles of Tafreshi et al. model, a pressure equal to 800kPa has been applied 150 times on the pressure plate with a frequency of 0.33Hz. Furthermore, a second loading scenario has been investigated, aiming to replicate the load of Khalaj et al. model. According to this, the pressure has been gradually increased from 0kPa to 800kPa. For the analysis, the explicit dynamic method has been used in order to capture accurate results. It should be mentioned that the dynamic implicit or static method is significantly faster than the explicit dynamic method, although their accuracy is significantly lower.

In order to simulate Khalaj et al. model accurately, Young's Modulus and Poisson's ratio of soil have been adopted equal to 45 MPa and 0.3, respectively. Furthermore, the soil angle of internal friction angle and the Cohesion have been set at 59.86° and 0.1kPa, respectively. The soil plastic behavior has been simulated by using a Mohr-Coulomb

model. Furthermore, the density of the soil is equal to 2062kg/m³. On the other hand, the internal friction angle and the density of the soil used to validate Tafreshi et al. model have been set equal to 1972kg/m³ and 40.5°, respectively. The mechanical properties of the HDPE 100 pipe have also been adopted by Khalaj et al. (2020). The pipeline has a density equal to 560kg/m³. Furthermore, Young's Modulus and Poisson's ratio of the pipeline are equal to 1000MPa and 0.45, respectively.
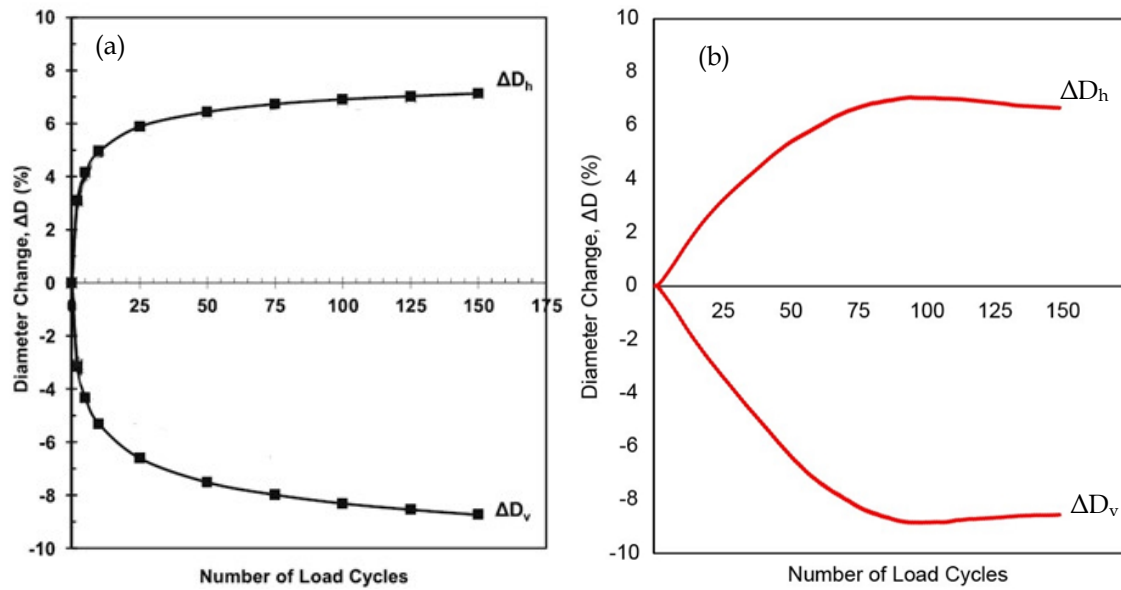
Figure 6.3 Vertical (ΔD_v) and horizontal (ΔD_h) diametric change according to (a) the experimental data adopted by Tafreshi et al. (2020), (b) the FE Model.

6.2.3. Validation of the numerical model

Figure 6.3 presents the verification of the numerical model with the first experimental test (e.g., Tafreshi et al. model) in which the combined behavior of the soil and the pipe against the applied traffic load is investigated. More specifically, the vertical and horizontal diameter change of the pipeline adopted by Tafreshi et al. (2020) is illustrated in Figure 6.3a. According to the experimental results, the level of the diameter change is rapidly increased from 0 to values higher than 6% after 25 loading cycles. In the sequence, the increase of the horizontal and vertical diameter changes is decreased, reaching up to 7% and 8%, respectively, after 150 loading cycles. The numerical model manages to capture the peak diameter change level accurately after 150 loading cycles, as shown in Figure 6.3b. On the other hand, the numerical results show a slight discrepancy from the experimental results at the inclination of the diagram. It is evident that 50 cycles are needed in order to reach 6% diameter change compared to the experimental results, which need just 25 cycles.

However, in general, these results show that the numerical model is relatively reliable to investigate the response of buried pipelines.
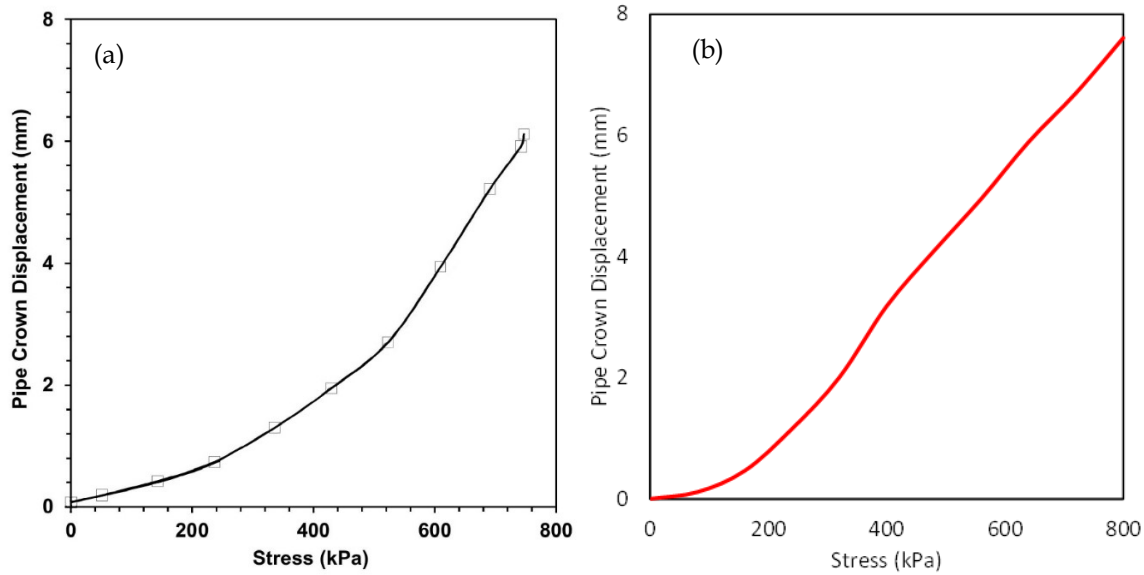
Figure 6.4 Pipe top displacement according to (a) the experimental data adopted by Khalaj et al. (2020), (b) the FE Model.

In the sequence, the numerical results are compared to the experimental data adopted by Khalaj et al. (2020). As mentioned, in this case, the applied load is gradually increased from 0 to 800kPa. Figure 6.4a presents the pipe top displacement according to the pre-available experimental data in terms of pipe top displacement. The pipe top displacement is slightly increased from 0 to 2mm when half of the total load is applied to the pipe. The increase of the pipe top displacement is increased more rapidly from 2mm to 6mm when the total load is applied to the model. The numerical model slightly overestimates the pipe top displacements compared to the experimental data, as it is depicted in Figure 6.4b. However, the shaping of the diagram is well captured and the numerical results are of the same order of magnitude as the experimental results.

6.3. *Imperfect trench method*

In the sequence, as it has been ensured in the previous section, the numerical model is partially validated; the model has been used to investigate the protection of the buried pipelines with EPS geofoam. Figure 6.5 illustrates the examined mitigation scheme with the use of EPS geofoam. This approach has been based on the so-called "imperfect trench method", which is proposed by the Norwegian Public Roads Administration (NPRA) (2010). According to NPRA, a horizontal trench filled with EPS geofoam is placed at 0.2D

above the top of the pipe, where D is the diameter of the pipe. Furthermore, the EPS layer has 1.5D width.
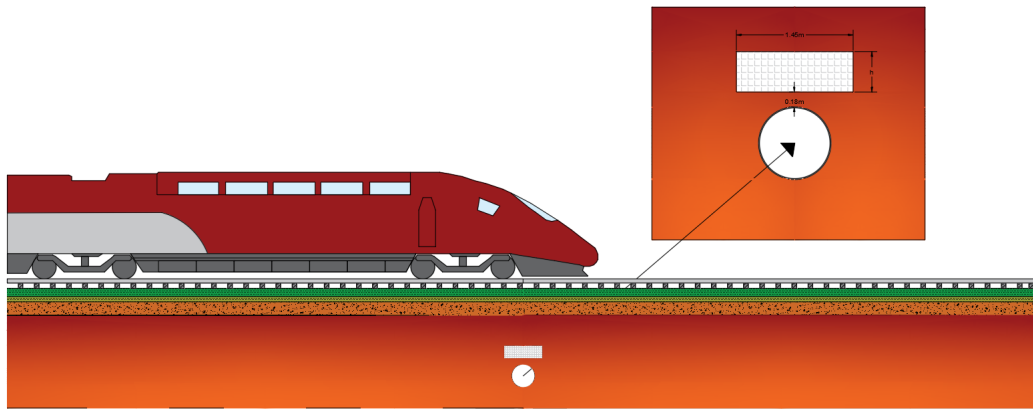
Figure 6.5 Recommended pipe and EPS layout for imperfect trench method from Handbook 16 (NPRA, 2010).
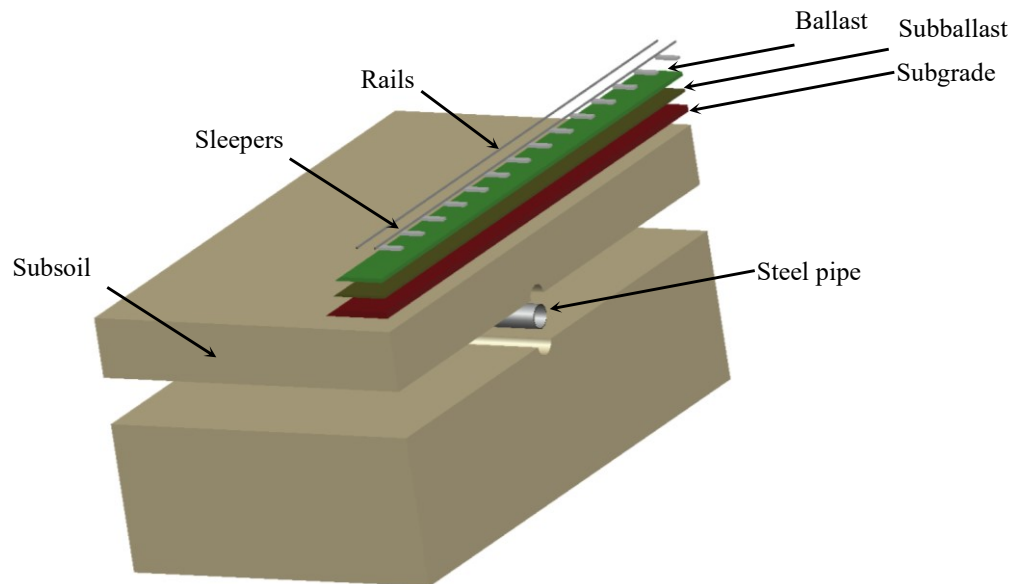
Figure 6.6 Sketch of the track components, soil and pipeline.

6.4. *Protection of steel pipe from HST induced vibrations*

Initially, the validated model from Section 6.2 has been combined with the HST-moving load model of Site 3 (see Chapter 3) in order to investigate the dynamic response of a steel pipeline to the HST-induced vibrations. Herein, this combined theoretical model has been considered in order to simulate a theoretical site of a railway track, where the HST is passing over a buried pipeline for the passage of Thalys HST. The steel pipeline has been embedded in the tracks subsoil. The numerical simulation has been separated into two steps in order to illustrate the field conditions better. Firstly, the gravity load has been

applied to the whole model to capture the pipe response due to the soil weight. Subsequently, the pass of Thalys HST has been implemented to the railway track as multiple moving loads. Figure 6.6 depicts a sketch of the examined theoretical site. The mechanical properties of the single-layered subsoil are summarized in Table 6.1. In this section, three passing velocities have been studied, a low (240km/h), a typical (300km/h) and a high (360km/h) velocity.

Table 6.1 Mechanical properties of subsoil adopted in the current investigation.

Subsoil property	Unit	Value
Density	kN/m³	18
Poisson's ratio	-	0.3
Young's Modulus	MPa	40
Friction angle	°	30
Cohesion	kPa	10

6.4.1. Modelling of the pipeline

A commonly-used X-65 steel pipeline has been investigated in the present section. Steel pipe section outside diameter and thickness are equal to 914mm and 12.7mm, respectively. Table 6.2 summarizes the parameters of the numerical simulation. Figure 6.7b illustrates the corresponding mesh for the soil/track part and Figure 6.7a for the steel pipeline. 4-noded reduced-integration shell elements have been used to model the steel pipeline, along with the large-strain Von Mises yield criterion for the steel pipe element. The burial depth of the pipeline has been chosen to be equal to double the pipe diameter, as it is commonly proposed (Mohitpour et al., 2007). As normal behavior, the parameter "hard contact" has been selected, which allows the separation of the pipeline from the subsoil. Furthermore, the friction parameter (μ) of the soil-pipeline interface has been assumed to be equal to 0.3. This value is commonly used by several relevant investigations (Emre et al., 2018; Vazouras et al., 2010).

Table 6.2 Properties of X65 steel pipe adopted in the current investigation.

X65 steel pipe property	Unit	Value
Diameter	mm	914
Thickness	mm	12.7
Tensile yield stress	MPa	450
Ultimate strength	MPa	560
Young's Modulus	GPa	210
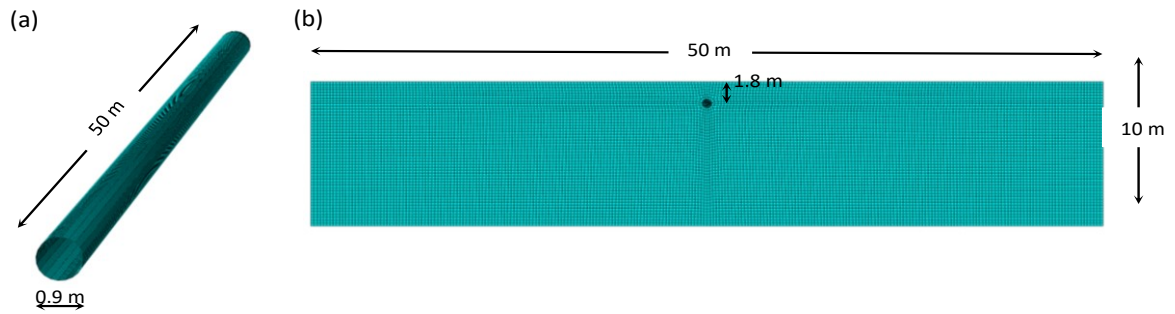
Figure 6.7 Finite element part of the (a) steel pipe cross-section, (b) soil cross-section.

The Imperfect trench method has been used to investigate its efficacy in reducing the HST-induced vibrations in the sequence. In this case, the EPS layer width and the distance from the pipe have been set equal to 1371 mm and 182.8 mm, respectively. The recommended height of the EPS block according to NPRA is equal to 50cm, although, in the present investigation, the effectiveness of EPS layer with several thicknesses between 12.5cm and 50cm has been examined.

6.4.2. *Investigation of the unprotected pipeline response*

The dynamic response on the top of the buried pipeline is examined for three typical HST passage speeds: a low speed (240 km/h), the typical Thalys operation speed (300 m/s) and a high speed (360 km/h). Figure 6.8 illustrates the vertical velocity time histories of the pipeline top for the three examined HST speeds. The peak vertical velocity at the low passing speed is equal to 10mm/s. The amplitude of the peak vertical velocity increases to 14mm/s and 17mm/s when the HST is passing with 300km/h or 360km/h, respectively. As expected, the time hibase length has been reduced as the passing speed is increased from 3.2s for 240km/h to 2.1s for 360km/h.

Figure 6.9 illustrates the Fourier spectra on the top of the pipeline for the three examined passing speeds. In the sequence, the peak frequencies of each spectrum are derived via the Dominant Frequency Method (DFM) (Kouroussis et al., 2015). According to DFM, the Fourier spectrum is strongly dependent on the train velocity and the geometry of its bogies. Hence, those parameters are responsible for the most dominant vibrations peaks, as presented in Chapter 3. The dominant frequencies are summarized in Table 6.3 for the three examined speeds. Those frequencies are well captured from the model, as it is illustrated in Figure 6.9. The first six bogies passing frequencies have been captured quite accurately by the numerical model. Furthermore, the dominant peaks are placed at

higher frequencies as the HST velocity increases from 240km/h to 360km/h. In the case of HST passing with low speed (240km/h), the most dominant frequencies are 3.5Hz ($f_{b,1}$), 7.2Hz ($f_{b,2}$), 46.4Hz ($f_{b,13}$), 49.9Hz ($f_{b,14}$) and the vibrations peaks vary between 1.3mm/s and 2mm/s. The peak at the axle passing frequency, close to 20Hz, is also dominant, as it reaches over 1mm/s. Furthermore, the peak at the sleeper passing frequency has been captured by the model, although it is quite low (3mm/s).
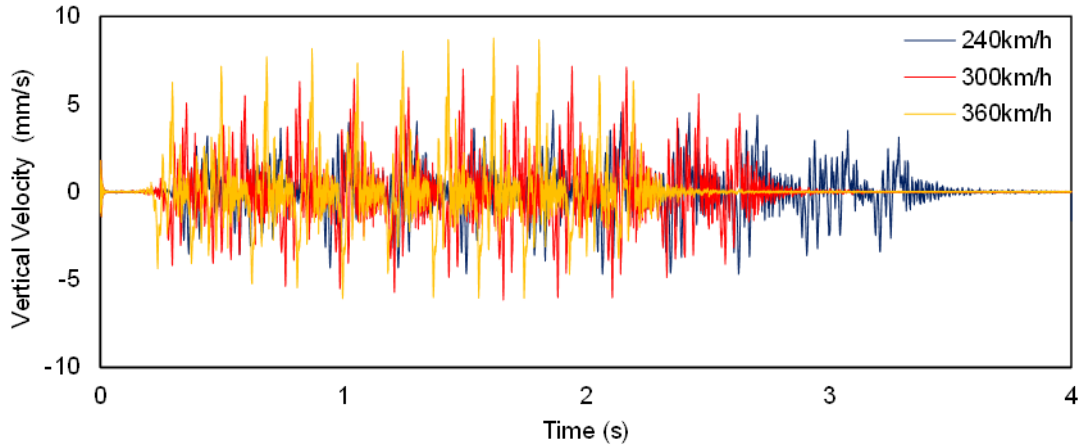
Figure 6.8 Vertical velocity time histories of pipeline top for several velocities.
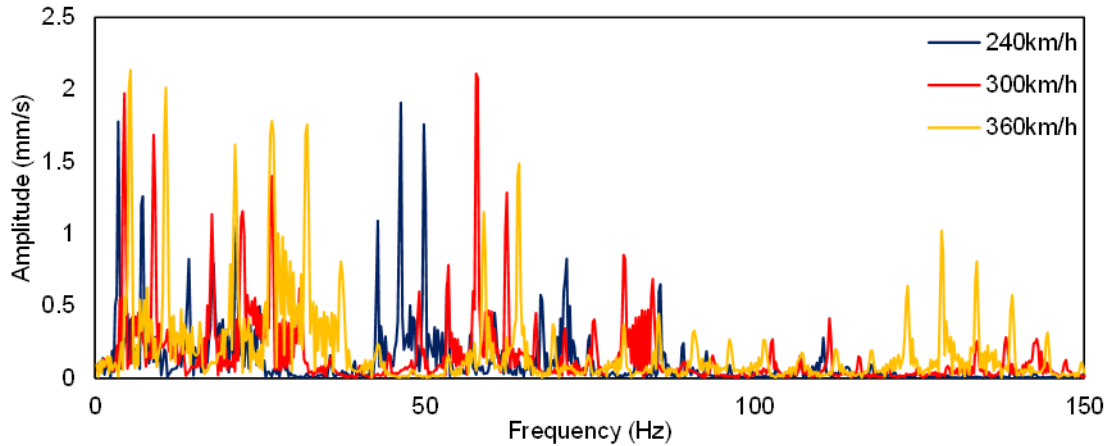
Figure 6.9 Fourier spectrum of the pipeline top for HST passage with (a) 240km/h, (b) 300km/h, (c) 360km/h.

The same observation is made in the modelling scenario, for which Thalys is running with its commonly operation velocity (300km/h). In this case, all the dominant peaks have been slightly moved to the right as expected (see Figure 6.9b). The first, the second and the thirteenth passing frequencies of the bogies have been the most dominant in the frequency range. Those peaks have been significantly increased in comparison with the passage with 240km/h. For instance, the vibration peak at $f_{b,1}$ has been increased from

18mm/s to 20mm/s. The peaks at axle and sleeper passing frequencies have also been slightly increased. Figure 6.5c shows the Fourier spectrum when the train passes with 360km/h. For this passing velocity, except for the same dominant frequencies at lower speeds, there have been several dominant peaks at other frequencies. More specifically, at $f_{b,1}$ (5.4Hz) and $f_{b,2}$ (10.7Hz), the amplitude of the peaks is almost double, compared to the same values, in the case of Thalys runs with 240km/h. It should be mentioned that the sleeper passing frequency has not been captured as it is quite high in this case (over 150Hz).

Table 6.3 Dominant frequencies.

Speed (m/s)	$f_{b,1}$ (Hz)	$f_{b,2}$ (Hz)	$f_{b,3}$ (Hz)	$f_{b,4}$ (Hz)	$f_{b,5}$ (Hz)	f_a (Hz)	f_s (Hz)
66.7	4	7	11	14	18	20	111
83.3	4	9	13	18	22	25	139
100.0	5	11	16	21	27	30	167

6.4.3. Investigation of EPS layer thickness effect on HST-induced vibrations

6.4.3.1. Case 1: Implementation of EPS with 12.5cm thickness

In the first modeling scenario, an EPS layer with 12.5cm thickness is implemented above the buried pipeline in order to reduce the HST-induced vibrations. Figure 6.10a compares the Fourier spectra on the pipeline top before and after the implementation of the EPS blocks in the modeling scenario of HST passage with 240km/h. The EPS layer beneficial role is clearly illustrated, as all the dominant vibrations peaks from 0Hz to 100Hz have been significantly reduced. For instance, the most dominant peak at 46.4Hz has been reduced from 1.9mm/s to 1.2mm/s. Furthermore, the peaks at other dominant frequencies (e.g., 3.5Hz, 7.2Hz, 49.9Hz) have a reduction equal to 40%. In the sequence, the effectiveness of the examined EPS layers has been investigated at the passage of Thalys with its common operation speed, 300km/h. In this case, the high level of vibrations peaks reduction remains at the lower frequency range (0, 30Hz).

Furthermore, EPS (see Figure 6.10b) is still effective at the whole examined frequency range. On the other hand, the examined mitigation scheme is not effective at the medium frequencies between 30Hz and 75Hz. In this range, the most dominant frequency is located at 58Hz, as the EPS blocks implementation slightly reduces the peak from 2.1mm/s to 2mm/s. The examined mitigation approach has a beneficial role at the higher frequencies

(>75Hz). The same observation could be made in the high passing velocity modeling scenario (360km/h), as shown in Figure 6.10c. A high reduction of all the vibrations peaks at the low and the high-frequency range has been observed. In this case, the most dominant frequencies are spotted at low frequencies (e.g., 5.4Hz, 10.7Hz, 26.5Hz, 31.9Hz). The peaks of those frequencies have a reduction of over 40%.
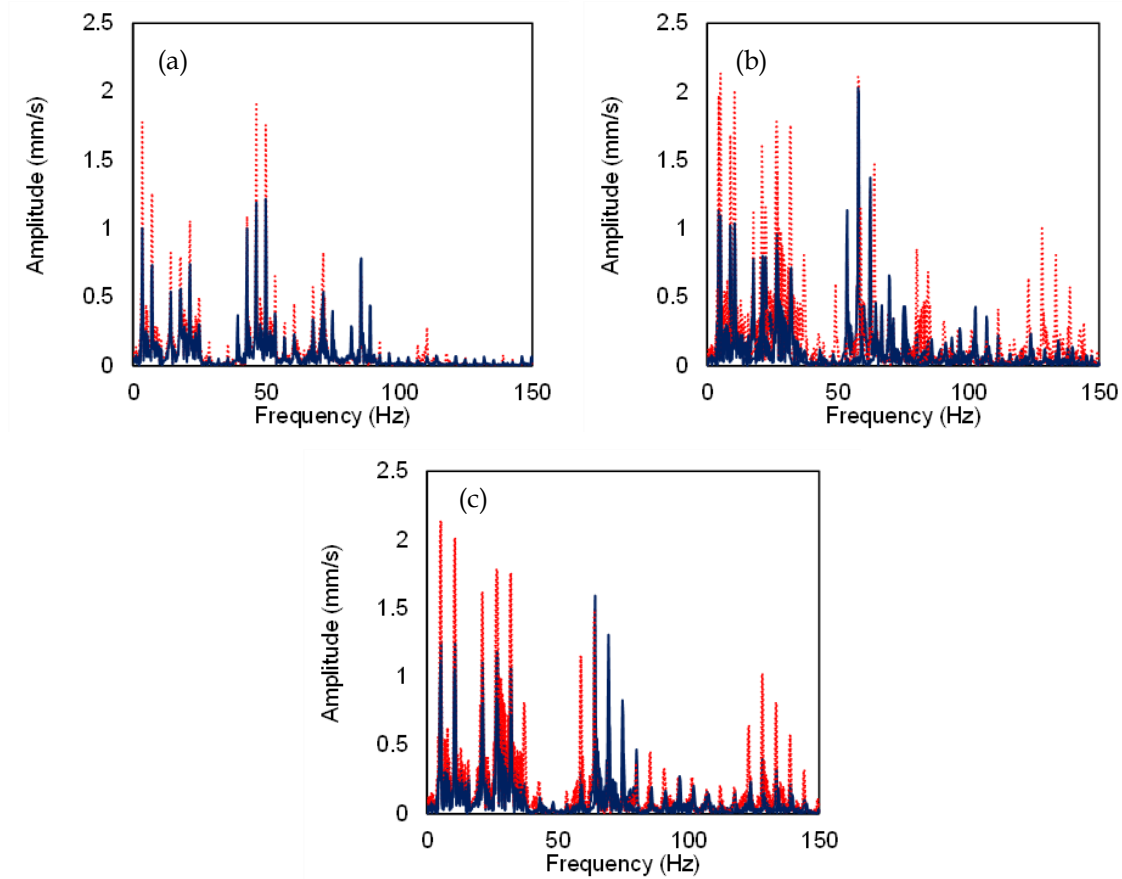
Figure 6.10 Fourier spectrum of the pipeline top for HST passage (a) with 240km/h, (b) with 300km/h, (c) with 360km/h with 50cm thickness.

6.4.3.2. *Case 2: Implementation of EPS with 25cm thickness*

According to the previous section, the implementation of EPS blocks between the track and buried pipeline minimizes the HST-induced vibrations successfully. However, the level of vibrations reduction is relatively low, thus in this section, the implementation of a thicker layer of EPS is investigated. More specifically, the thickness has been duplicated; thus, the impact of an EPS layer with a thickness of 25cm has been examined. As expected, the vibrations peaks remain at the same frequencies as the previous section, although the amplitude of the vibrations is significantly lower. For instance, the dominant peak at 46Hz has been minimized to 0.8mm/s in contrast to the 1.2mm/s in the case of the layer with a height of 12.5cm for HST running with 240km/h (see Figure 6.10a).

The same observation is made for all the dominant frequencies, with amplitude reduction of up to 50%. Figure 6.12b illustrates the Fourier spectra when the HST runs with 300km/h. The peak vibrations level is reduced to 1.5mm/s at 58Hz for EPS19. Furthermore, it should be mentioned that all the other vibrations peaks at the modeling scenario of EPS19 have been minimized under 1mm/s. The reduction of the vibrations level is remarkable when the HST runs at high speed (360km/h), as all the vibrations peaks have been successfully reduced under 1mm/s (see Figure 6.11c). It should be mentioned that vibrations peaks at the high-frequency range are almost zero after implementing EPS blocks.
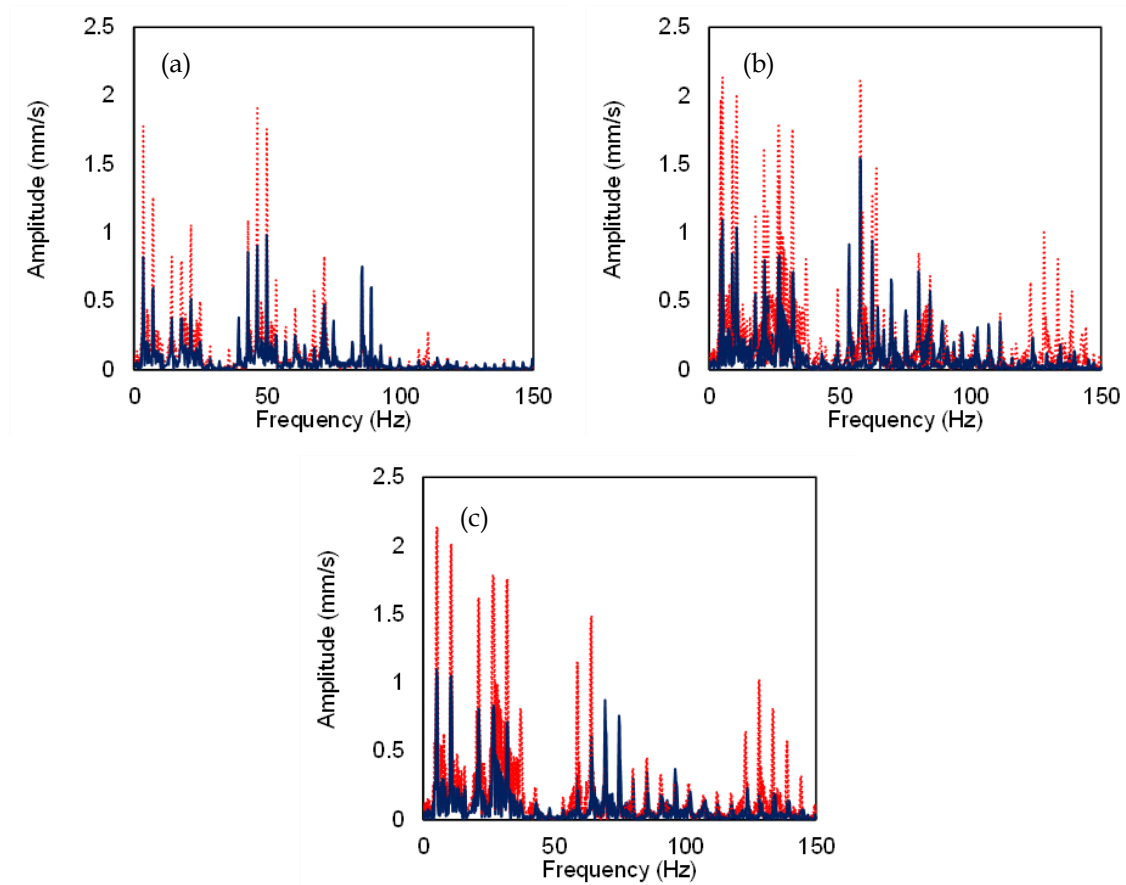
Figure 6.11 Fourier spectrum of the pipeline top for HST passage (a) with 240km/h, (b) with 300km/h, (c) with 360km/h with 25cm thickness.

6.4.3.3. Case 3: Implementation of EPS with 50cm thickness

In this section, the height of the examined EPS layer has been increased to 50cm to reduce the vibrations level further. Figure 6.12 depicts the Fourier spectra in this case. Obviously, the thicker EPS layer (50cm) effectively reduces the HST-induced vibrations for all the examined cases. For low HST-passing velocity, the vibrations peaks have been limited

under 0.8mm/s (see Figure 6.12a). The same observation is made in the case of the typical operation speed of Thalys, 300km/h, as the reduction reaches over 60% in some cases (e.g., $f_{b,1}$, $f_{b,2}$) when EPS19 is used, as shown in Figure 6.12b. Lastly, the effectiveness of the examined mitigation approach is remarkable for the highest examined passing speed. For instance, the vibrations peaks at the most dominant frequencies ($f_{b,1}$, $f_{b,2}$) have been reduced from 2.2mm/s and 2mm/s to just 0.8mm/s and 0.9mm/s, respectively, as is illustrated in Figure 6.12c.
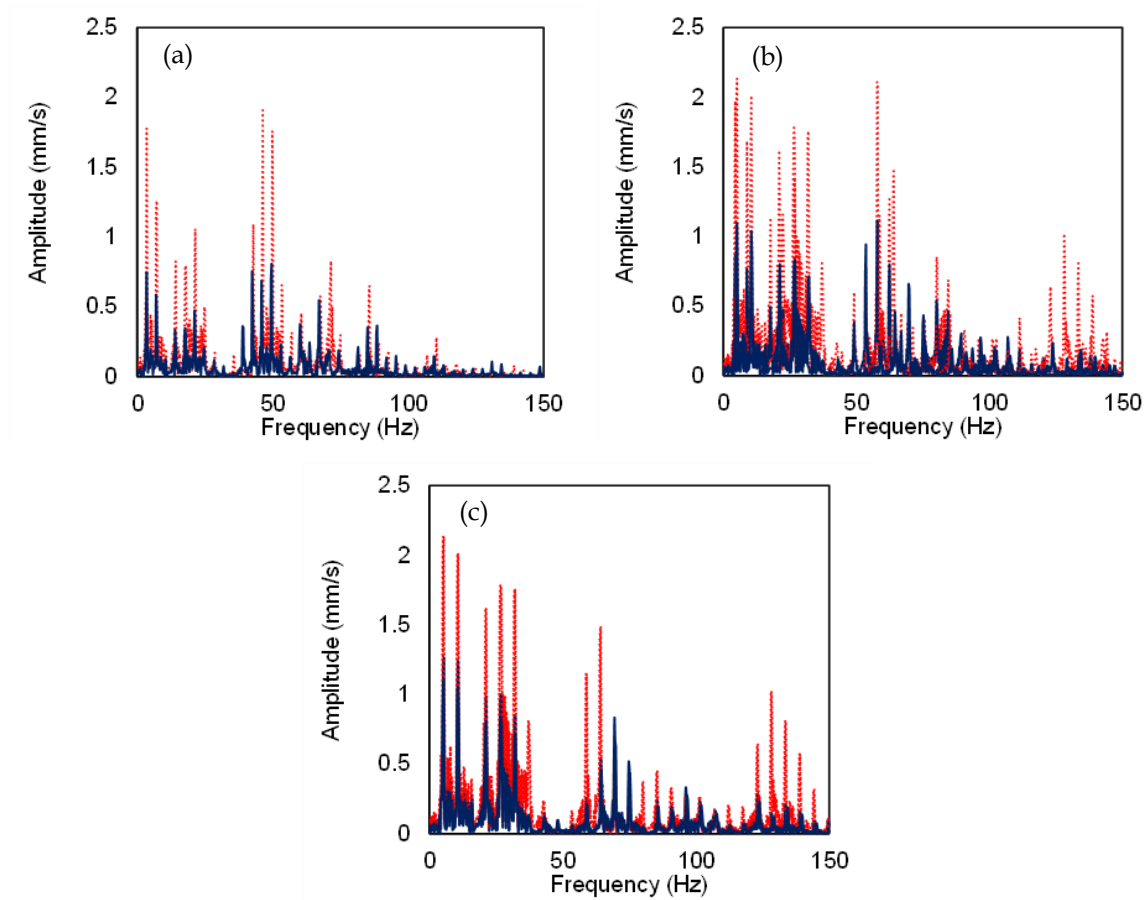
Figure 6.12 Fourier spectrum of the pipeline top for HST passage (a) with 240km/h, (b) with 300km/h, (c) with 360km/h with 50cm thickness.

Figure 6.13 illustrates the insertion loss (IL) of the examined mitigation measure in the cases of HST speed equal to 240km/h, 300km/h and 360km/h. IL has been computed at the centre frequency of each one-third octave band, from 1.25 to 125 Hz and the results have been averaged to one-third octave bands. In the case of the implementation of an EPS-filled trench with 12.5cm of thickness, the insertion loss remains at the same level for all the examined speeds at all the octave bands with central frequencies lower than 31.5Hz. More specifically, the insertion loss is close to 4.8dB at those central. At the higher

examined octave bands, the insertion loss is unstable, fluctuating between extremely low or high values. In general, the use of an EPS layer with 12.5cm thickness slightly reduces the vibrations level at the top of the pipeline, although this reduction is not satisfactory.
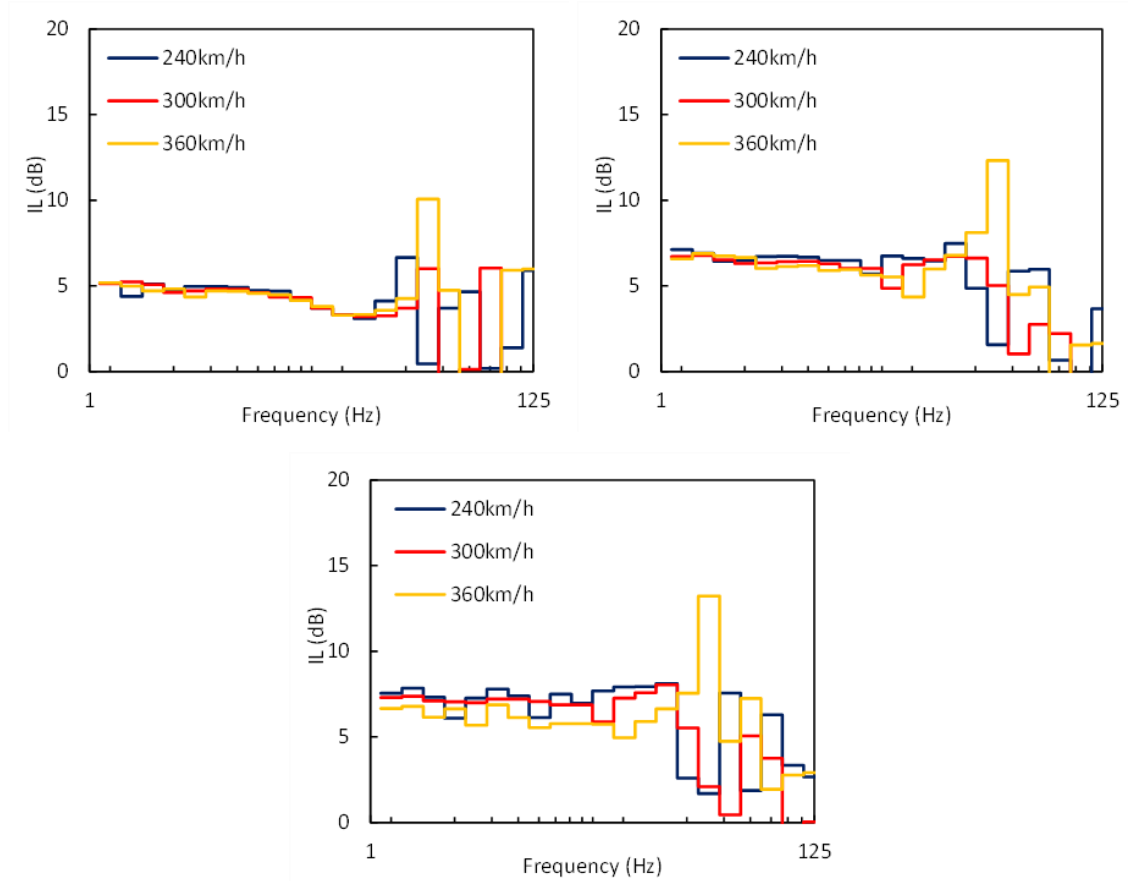
Figure 6.13 Insertion loss curves of the pipeline top for HST passage for EPS layer with a thickness equal to (a) 12.5cm (b) 25cm, (c) 50cm.

Figure 6.13b illustrates the IL curves in the case of a 25mm EPS layer. In this case, the insertion loss has been increased compared to the previous case. Herein, the amplitude of insertion loss at the octave bands with a centre frequency below 31.5Hz is close to 6.7dB for all the examined HST passing speeds. The insertion loss reaches its peak value of 12dB at the 1/3 octave band with centre frequency 40Hz after implementing EPS19 when Thalys passes with 360km/h. Figure 6.13c illustrates the insertion loss curve for the thicker examined EPS layer in the present investigation. The insertion loss is increased in comparison with the cases of thinner EPS layers. IL ranges around 7.3dB for the octave bands with centre frequencies lower than 31.5Hz. Those values remain at the same level for all the examined frequencies. It should be mentioned that the insertion loss is again unstable for the higher 1/3 octave bands.

6.4.4. *Investigation of pipelines-buried depth effect on HST-induced vibrations*

In order to examine the role of the pipelines- buried depth in vibrations level, the response of the initial shallow buried pipeline has been compared to the same value of a deeper buried pipeline. The deep-buried pipeline has the same mechanical properties as the initial pipeline and has been placed one meter deeper, at 2.8m from the subsoil surface. Figure 6.14 illustrates the Fourier spectra of the vertical velocity of all the examined speeds for the shallow-buried pipeline (as introduced previously) compared to the deep-buried pipeline. As seen in Figure 6.14a, the placement of the pipeline deeper can strongly influence the vibrations level. More specifically, in the modelling scenario, for which Thalys is passing with 240km/h, all the dominant frequencies in the examined range have been reduced. The peaks at the first and the second bogie passing frequencies have been reduced from 18mm/s and 13mm/s to 13mm/s and 6.5mm/s, respectively. The same observation is made for the higher dominant frequencies. For instance, the peak at 49.9Hz ($f_{b,14}$) has been halved from 18mm/s to 9mm/s. The peaks on the frequency range between 50Hz and 80Hz have been practically zeroed.

This reduction is even more pronounced as the HST passing speed is increased. As it is clearly illustrated in Figure 6.14b and Figure 6.14c, the reduction of the vibrations peak at $f_{b,1}$ reaches 25% and 36%, for passing velocities equal to 300km/h and 360km/h, respectively. Furthermore, the reduction for all the other vibrations peaks is over 50% when Thalys passes with its common operation speed, 300km/h. This trend has also been observed in the case of passing speed equal to 360km/h, except for 64.4Hz. In this case, the vibrations peak is not altered.

The effect of the pipeline buried depth on the developing vibrations is even more pronounced in terms of insertion loss. Figure 6.15 depicts the insertion loss curves in the case of which, as a mitigation approach, the pipe has been moved one meter deeper in the subsoil. The insertion is lower than 5dB at the one-third octave bands with central frequencies lower than 8Hz for all the examined passing velocities. However, at the higher octave bands, in some cases, the insertion loss is up to 10dB. For instance, insertion loss reaches 14dB at the 1/3 octave band with a centre frequency equal to 63Hz. It should be mentioned that there is a constant peak of 11.6dB, which is moving one octave band higher when the passing speed is increased. More specifically, this peak is located at the 1/3 octave band with a centre frequency 16Hz when the HST passing velocity is equal to

240km/h and moves to the 1/3 octave band with centre frequency 20Hz and 25Hz when the HST speed is 300km/h and 360km/h, respectively.
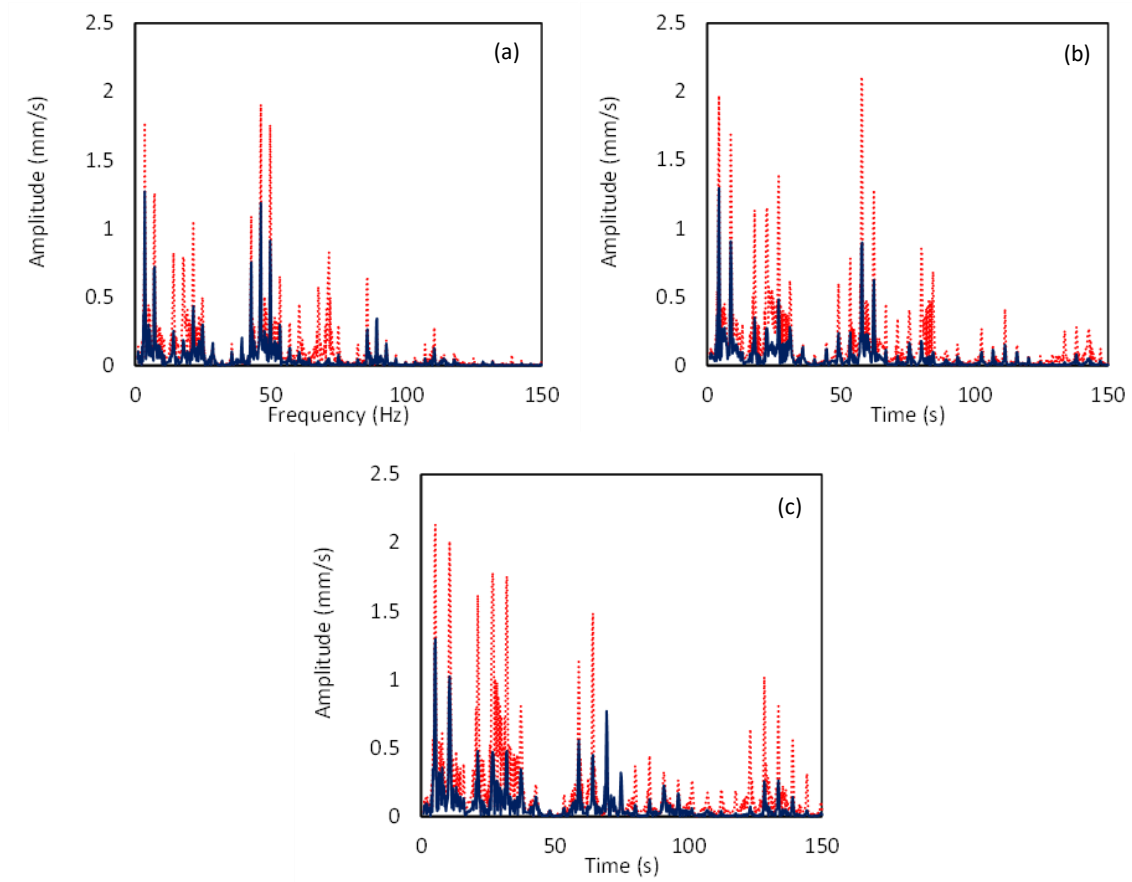
Figure 6.14 Comparison of deep and shallow buried pipeline response for HST passage with (a) 240km/h, (b) 300km/h, (c) 360km/h.
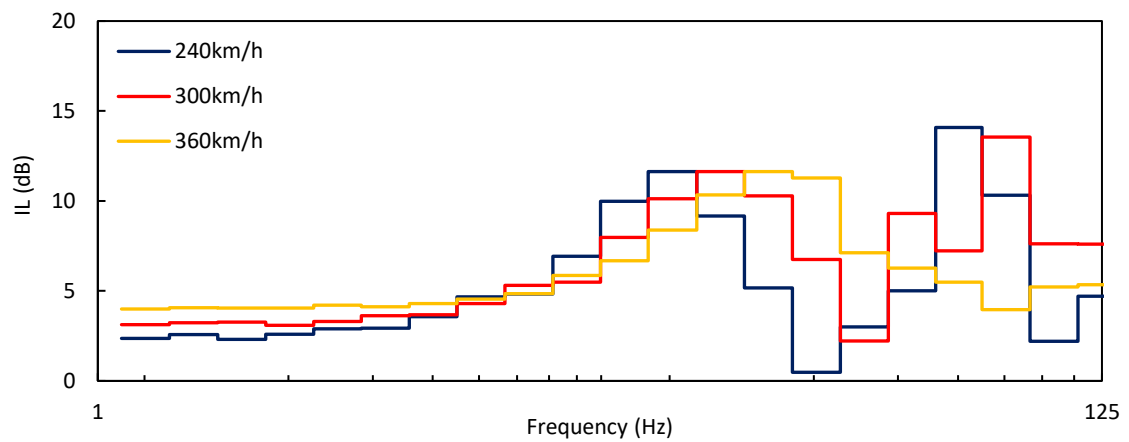
Figure 6.15 Insertion loss curves of the deep-buried pipeline top.

In this section, the effect of the buried depth on the examined mitigation approach effectiveness is investigated. As it was aforementioned, 50cm (case 3) is the most effective layer thickness. Herein, for the sake of brevity, only the optimal thickness, 50cm, has been

examined. Figure 6.16a compares the insertion loss curves of the shallow and deep buried pipeline in the modelling scenario for which Thalys passes with low speed (240km/s). In this case, the insertion loss is slightly reduced compared to the shallow-buried pipeline at all the low 1/3 octave bands. Therefore, it is concluded that, in general, the insertion loss is not significantly dependent on the buried depth of the pipeline when the HST passes with 240km/h. Figure 6.16b illustrates the insertion loss curves in the most common scenario when Thalys passes with its operation speed, 300km/h. The mean insertion loss at the 1/3 octave bands with central frequencies lower than 16Hz, has been decreased about 0.6dB. It should be mentioned that the reduction of the vibrations level has been increased at the higher octave bands when the pipeline is buried deeper. For instance, the insertion loss at the 1/3 octave band with centre frequency 63Hz has been increased from 5.1dB to 9.1dB.
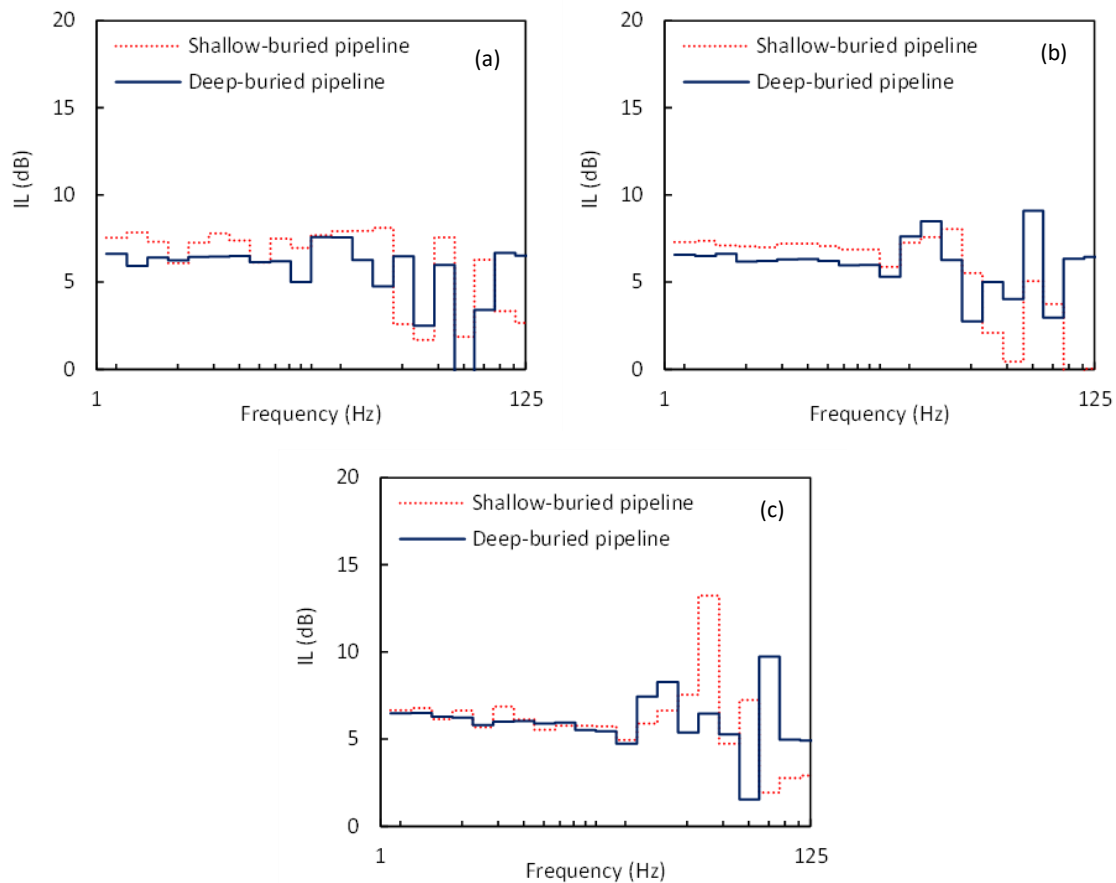
Figure 6.16 Comparison of insertion loss curves of the deep and shallow-buried pipeline top for HST passage with (a) 240km/h, (b) 300km/h, (c) 360km/h.

In the modelling scenario in which Thalys passing velocity is equal to 360km/h, the insertion loss has not been significantly altered at the 1/3 octave bands with centre frequencies lower than 16Hz (see Figure 6.16c). On the other hand, insertion loss is

significantly lower at the 1/3 octave band with a centre frequency 40Hz for both examined layer fill material. However, the deep-buried pipeline has higher insertion loss for the centre frequency at the octave bands with centre frequency higher than 80Hz. In general, it is concluded that the effectiveness of the examined mitigation schemes is not significantly altered with the depth of the buried pipeline.
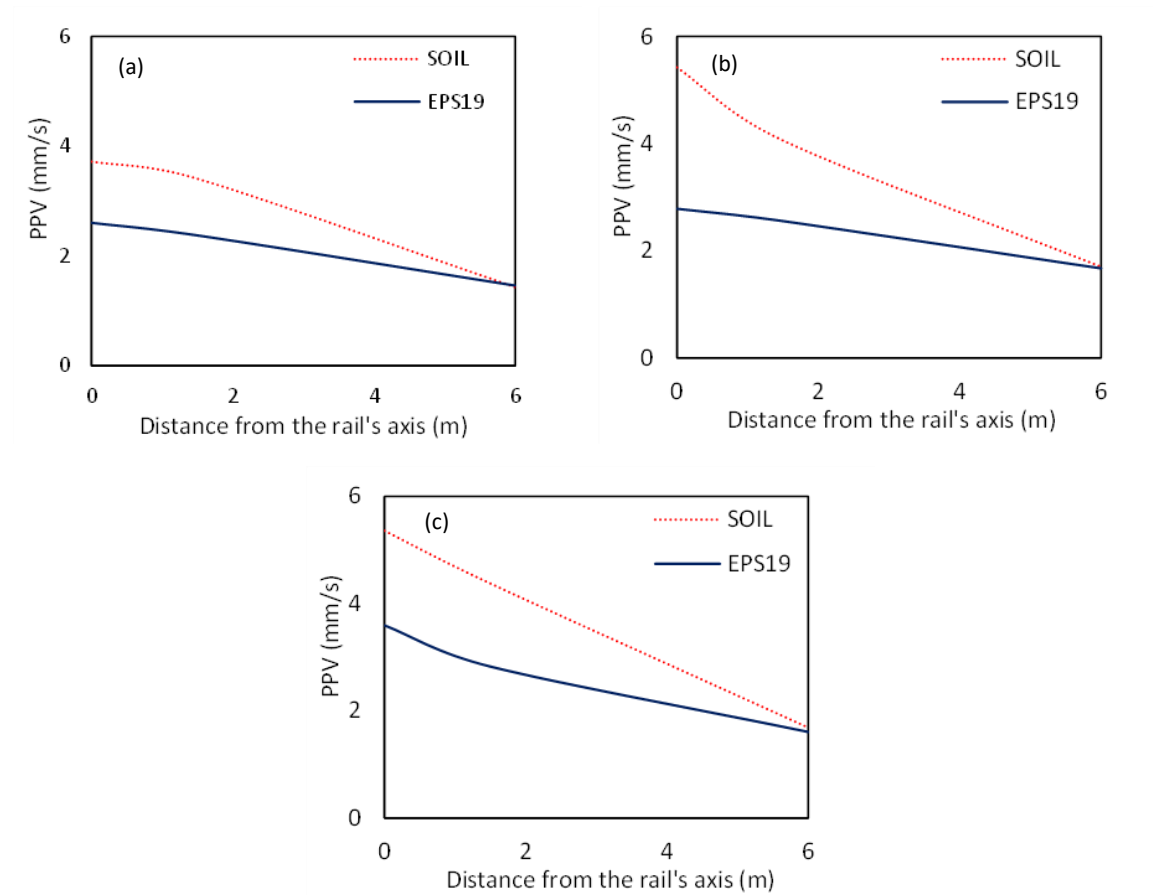
Figure 6.17 PPV at increasing distance from the rail axis for passing speed equal to (a) 240km/h, (b) 300km/h, (c) 360km/h.

Figure 6.17 depicts the PPV on the top of the pipeline at an increasing distance from the HST passing axis. As expected, the PPV values are slightly reduced with the distance from the track. Furthermore, the PPV on the top of the unprotected pipeline is reduced rapidly for all the examined passing speeds. When Thalys passes with 240km/h, the PPV of the unprotected pipeline has been reduced from 3.7mm/s to 1.4mm/s at 6m from the track. The same value has been decreased to 1.4mm/s from 2.6mm/s after the implementation of the EPS layer. The same observation is made in the case of a passing HST with 300km/h (see Figure 6.17b) and 360km/h (see Figure 6.17c), where PPV of the unprotected pipeline has been rapidly reduced from 5.4mm/s to 1.6mm/s. At 6m from

the rail axis, the PPV on the top of the unprotected pipeline is identical to the protected pipeline. It is obvious that the proposed mitigation meter has not affected the vibrations level at distances higher than 6m from the rail axis.

6.5. *Investigation of steel and PVC pipe diameter change*

In the previous section, the EPS geofoam significantly reduced the vibrations level on the pipe surface in terms of several commonly used indicators in the field of HST-induced vibrations. However, it is vital to investigate the effect of the HST-loads on the diameter change of the pipeline. As mentioned, the level of the diameter change is crucial for the response and the life cycle of the pipelines. The examined pipeline in the previous section is very thick (e.g., 12.7mm) and stiff; hence, its diameter change is negligible, as it is illustrated in Figure 6.18. It is evident that the horizontal diameter change of the unprotected pipeline is equal to 0.3mm at the passage of each HST bogie (see Figure 6.18a). This value is reduced to below 0.2mm after the implementation of an EPS19 layer with a thickness of 50mm. The same observation is made at the horizontal diameter change, as it is illustrated in Figure 6.18b. Furthermore, the vertical and horizontal residual deformations after the HST passage are almost zero. For this reason, the assumption is made that the pipeline is safe, independent of the EPS layers implementation.
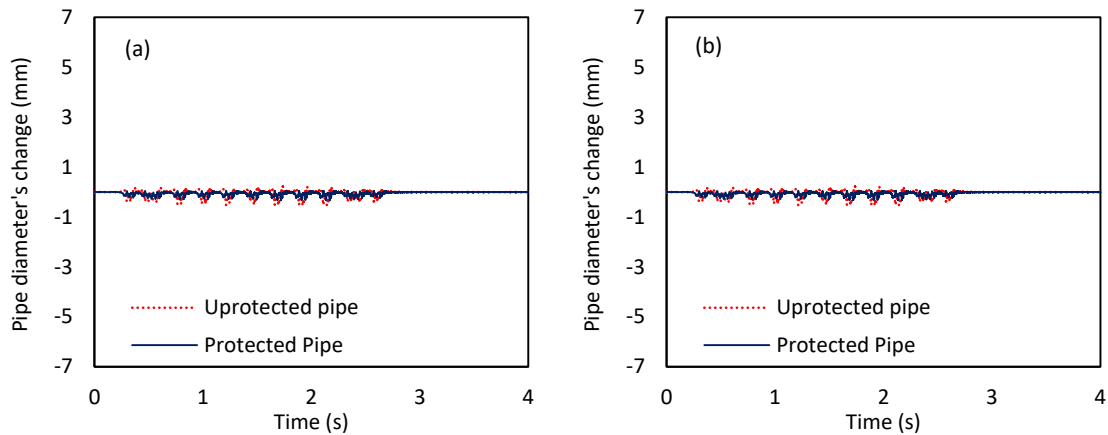
Figure 6.18. X-65 pipe diameter change.

The assumption is made that pipelines with lower thickness and buried at lower depths are more prone to deformation. For this reason, the HDPE 100 pipe, which has been used for the validation, has been implemented at 0.5m depth, and its diameter change due to the passage of Thalys has been investigated. In the sequence, the pipeline has been protected with the use of a 250mm EPS layer. In order to investigate the effect of pipe

thickness on the response of the pipeline, an identical pipe with a higher thickness (9mm) has also been investigated. Furthermore, two steel pipelines with 250mm and thicknesses of 3mm and 9mm have been studied. The mechanical properties of those pipes are identical to the X-65 pipe.
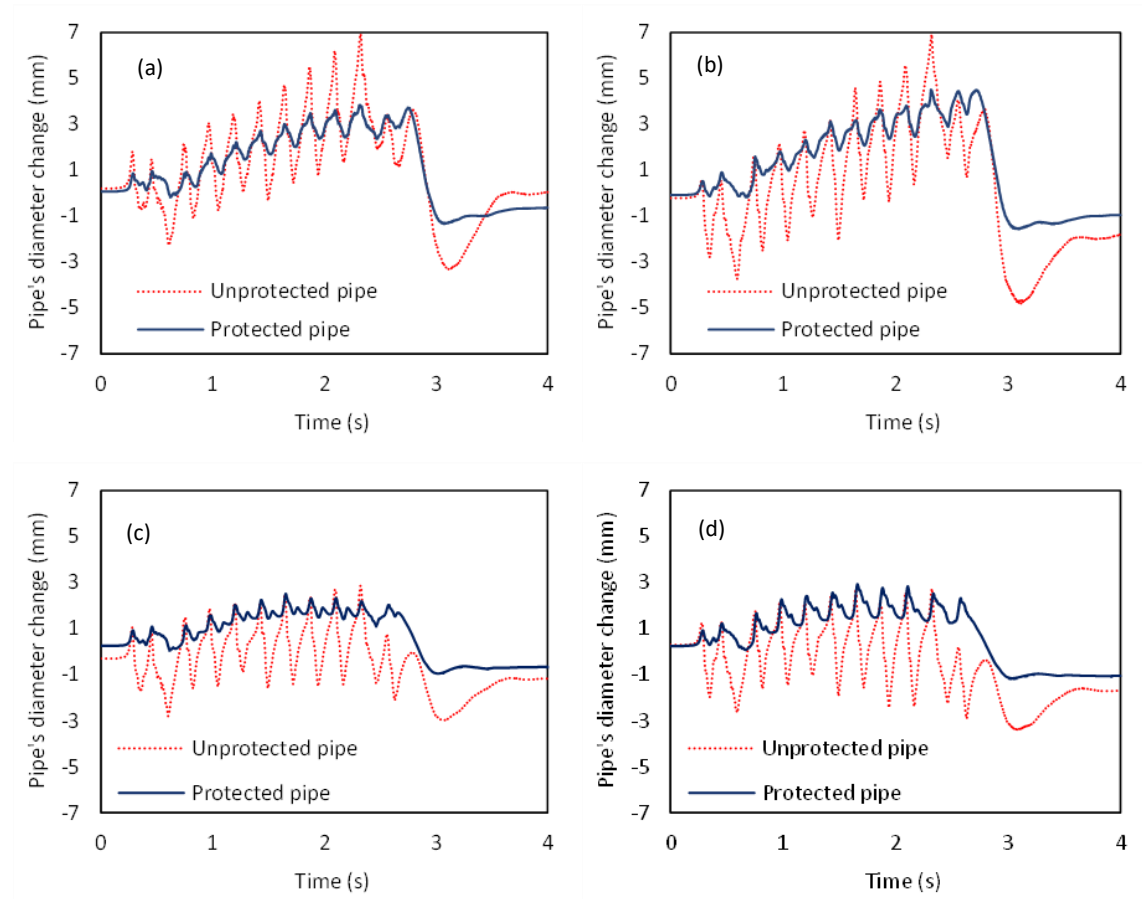
Figure 6.19. (a) vertical and (b) horizontal diameter change pf 3mm PVC pipe and (c) vertical and (d) horizontal diameter change pf 10mm PVC pipe.

Figure 6.19 demonstrates the effect of the HST passage on the diameter of the plastic pipelines with a diameter equal to 3mm and 9mm. It is evident that the diameter change of the pipeline is significantly higher in comparison with the X-65 pipe. At the first HST axle passage, the vertical diameter change of the unprotected pipe with 3mm thickness is equal to 1.6mm. The deformation is gradually increased, reaching the maximum value of 7mm at the passage of the last boogie. Furthermore, after the HST passage, a vertical residual deflection equal to 0.8mm is observed, it should be mentioned that the peak deformation oscillation width is close to 6mm. The EPS layer has a beneficial impact in the reduction of the pipe diameter change. It is evident that the implementation of the EPS layer has reduced the peak vertical deformation from 7mm to 3mm. Furthermore, the

oscillation width is minimized to 1mm. The same observation is made for the horizontal diameter change, as shown in Figure 6.19b. However, the horizontal residual deformation is significantly higher than the vertical, reaching higher than 2mm. Therefore, the implementation of the EPS layer minimized the horizontal residual deformation close to 1mm. Figures 6.19c and 6.19d compare the response of a thicker PVC pipe (10mm) before and after the implementation of the EPS layer. The increase of the pipeline thickness reduces the pipe vertical and horizontal deformations to below 3mm. Furthermore, the oscillation width is equal to 5mm and 5.5mm, for the vertical and horizontal deformation, respectively. The residual deformation at both dimensions is equal to 1.3mm. The beneficial role of the EPS layer implementation is obvious in this case. Especially in the vertical dimension, the peak oscillation width has been reduced to below 0.4mm and the residual deformation is below 1mm.
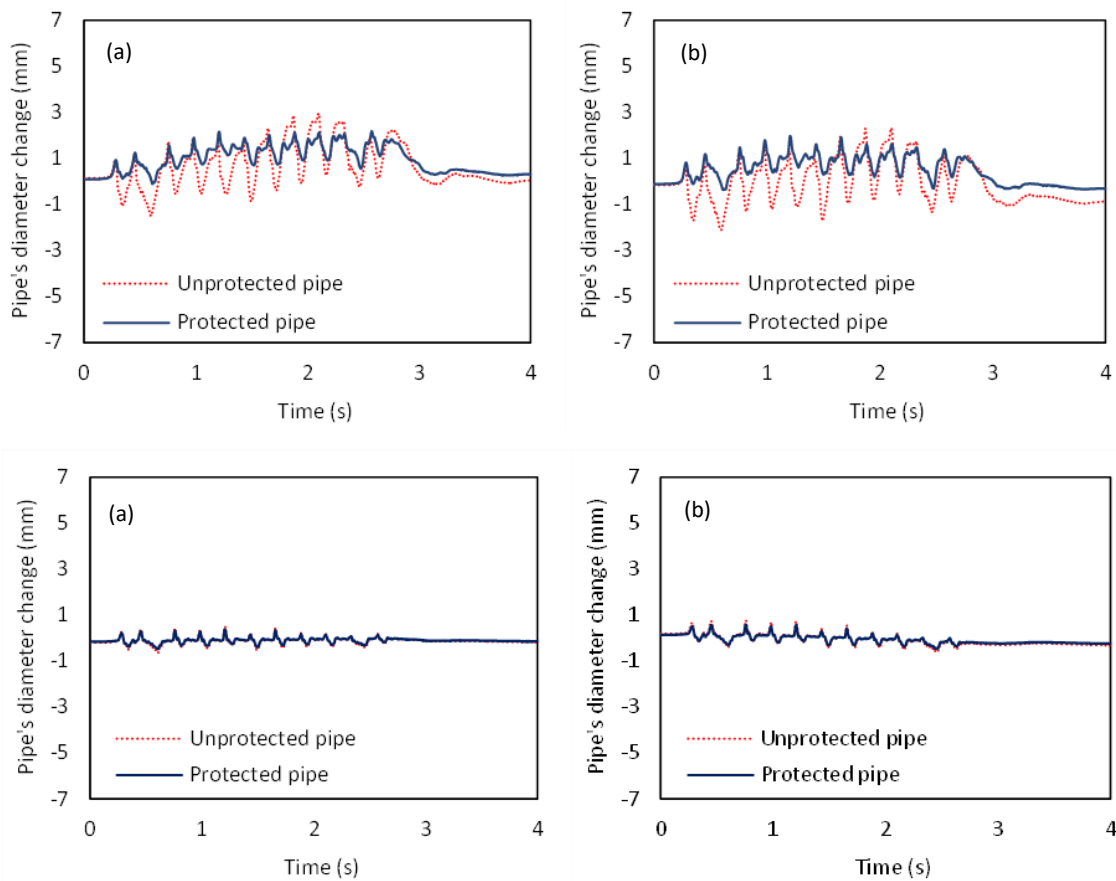
Figure 6.20. (a) vertical and (b) horizontal diameter change pf 3mm steel pipe and (c) vertical and (d) horizontal diameter change pf 10mm steel pipe.

In the sequence, the steel pipes diameter change is presented in Figure 6.20. The peak deformation of the unprotected steel pipe with 3mm thickness is equal to 3mm and 2.8mm at the vertical and horizontal coordinate, respectively, as shown in Figures 6.20a and 6.20b.

Furthermore, oscillation width is equal to 3mm. The horizontal and vertical residual deformations are equal to 0.8mm and 0.2mm, respectively. It is obvious that the steel pipe is significantly more resistant to HST-induced vibrations in comparison with the PVC pipe. Furthermore, it is evident that the examined protection scheme significantly reduces the induced deformations. Furthermore, the vertical residual deformation is reduced to almost zero. In addition, the horizontal residual deformation has been decreased from 0.8mm to 0.2mm, as it is illustrated in Figure 6.20b. The effect of the HST passage to the thicker steel pipe is marginal, as expected. More specifically, the vertical peak deformation remains below 0.3mm for a pipe with a 3mm thickness (see Figure 6.20c). The same observation is made at the horizontal dimension, as it is demonstrated in Figure 6.20d. Furthermore, the residual deformation of the 10mm steel pipe is almost zero. Furthermore, the reduction of the diameter change is marginal after the implementation of the EPS layer.

6.6.   *Discussion of the results*

A mitigation approach utilizing low-density backfill for buried pipelines subjected to vibrations induced by HST passage has been examined in the present Chapter. The numerical model has been partially validated with pre-available experimental data of equivalent traffic loads. The implementation of the low-density backfill has contributed to reducing the vibrations level on the top of the pipelines. The low-density EPS19 has been used as a backfill material. In order to examine the efficiency of the examined mitigation approach, the passage of Thalys HST with three different velocities has been investigated. Furthermore, the effect of the pipe material and thickness on the diameter change has been investigated by comparing steel and PVC pipelines. The main conclusions of the present investigation could be summarized as follows:

- As mentioned earlier, the presented numerical models have been successfully validated in Chapter 3, and it is capable of capturing the HST-induced vibrations on the model surface accurately. Herein, to ensure that the numerical model is also accurate at the subgrade, the results have been compared to pre-available experimental data for road traffic loads. Hence, the model is partially validated in order to investigate the effect of the HST-induced vibrations in the subgrade.

- Implementing an EPS layer between the track and the buried pipeline could reduce the HST-induced vibration. The level of reduction strongly depends on the

thickness of the EPS layer. The thickest layer reduces the developing vibrations more effectively at the top of the pipeline.

▪ The insertion loss at the centre frequencies of the lower 1/3 octave bands is constant and independent from the HST passing velocity and the buried depth of the pipeline.

▪ Except for the commonly used indicators in the field of the traffic-developing vibrations, the vertical and horizontal deformation of the pipe has been investigated. The effect of the proposed mitigation approach on several types of pipes has been presented. The residual deformation of the PVC pipes is higher compared to steel pipes. Furthermore, thicker pipes could minimize the dimeter changes. The EPS layer successfully reduces the diameter change of all the examined pipes.

▪ The implementation of an EPS layer above a thick and stiff steel pipe is unnecessary, as the pipe deformation is low.

Several researchers have used the examined mitigation approach in order to protect buried pipelines subjected to permanent ground deformation. The present investigation concludes that the implementation of the examined mitigation approach could successfully protect the buried pipelines from traffic loads. It should be mentioned that this is a first attempt to investigate the use of EPS geofoam between an HSR line and a buried pipe. Hence, further investigation is proposed in order to ensure the effectiveness of the examined measure. For instance, several soil conditions, train geometry or pipeline depth should be examined in future investigation.

PROTECTION OF BUILDINGS WITH EPS GEOFOAM

7.1.   Introduction

In recent years, one of the most critical environmental issues worldwide is the traffic-induced vibrations in nearby structures and infrastructure. The developing vibrations due to high-speed trains (HST) passage are commonly dominated by surface waves, which are propagating on upper soil layers and may affect nearby buildings. Hence, the realistic assessment of the vibrations in conjunction with the dynamic structural response is essential in order to prevent possible malfunctioning of sensitive equipment in the buildings, annoyance and discomfort of the residents or even damages in extreme cases. The mitigation of the induced vibrations is a factor of paramount importance both for new railway projects or the upgrading of existing railway lines to serve high-speed trains, especially in railways passing through urban areas close to buildings with many residents. Therefore, it is crucial: (a) to investigate the propagation of the induced vibrations from the railway track through the soil to the adjacent buildings, and (b) to propose mitigation schemes to minimize vibrations levels.

Several standards and guidelines have been published in recent years regarding train-induced vibrations in buildings. In United States, Federal Transit Administration (Hanson et al., 2006a) provisions propose the values of -2dB and -1dB per story for the estimation of story-to-story attenuation of the vibrations, for the first five lower stories and the next five stories, respectively. The International Standardization Organization (ISO) has

proposed recommendations for estimating human exposure to the induced vibrations, which are split into two parts: the first (ISO, 1997) investigates the vibrations felt by the passengers, while the second (ISO, 2003) is focused on nearby buildings and their residents. In Germany, DIN guidelines assess the impact of traffic vibrations in buildings with respect to human exposure (DIN, 1999b) as well as to structures (DIN, 1999a). According to DIN, the peak particle velocity (PPV) (e.g., the maximum value of the velocity time-history) is recommended as the primary indicator to evaluate both human exposure and structural damage. Similar to DIN guidelines, the Swiss standard (1992) has also adopted PPV as proper indicator factor. In addition, the US Department of Transportation (1998) adopted a decibel (dB) scale in order to estimate the impact of the developing vibrations.

The investigation of the complicated problem of the dynamic track-soil-structure interaction is highly demanding, both in terms of computational complexity and cost. Several relevant studies have been conducted in order to predict the vibrations levels utilizing numerical models (Kontoni and Farghaly, 2020; López et al., 2020; Pyl et al., 2007; Ribes et al., 2017). The structural vibrations on railway-side buildings are excessively increased if the train passing speed is close to Rayleigh-wave velocity of surface soil; thus, in such cases the train should reduce its speed in order to minimize potential adverse effects on the nearby buildings. For instance, Zou et al. (2021, 2017) investigated the impact of metro induced vibrations on over-track buildings and concluded that the vibrations levels are amplified by up to 6dB on the structures compared to the surrounding soil vibrations.

Sanayei et al. (2014) presented a full-scale test and the corresponding impedance-based analytical model in order to examine the response of a 4-story building with respect to the induced vibrations due to a city-train passage in Boston. It was reported that the use of a "blocking" ground story, i.e., with thickened floor slab, could reduce the vibrations at the upper stories of the building. Sadeghi and Vasheghani (2021) reported that top slab thickness has a greater impact, while other structural and non-structural parameters (e.g., story height, concrete compressive strength as well as the infill walls thickness) do not play a significant role. Hesami et al. (2016) examined the effect of train-induced vibrations in an urban environment close to Qaemshahr railway in Iran and proposed an optimal distance from the track equal to 18m for the construction of buildings. Connolly et al. (2019) used a 2.5D time-frequency domain model to investigate the impact of railway

defects as well as train speed and building height on the vibrations levels and concluded that different defect types (e.g., joints, switches, crossings) present a complex correlation with vibrations both in the surface soil and the nearby buildings.

In this Chapter, a numerical investigation of buildings response to the High-Speed Train passage is presented. The effect of the HST-induced vibrations on the neighboring buildings close to the railway is a vital environmental issue related to the residents comfort. The validated 3D FEM model in the case of the at grade site (see Chapter 3) from the Paris-Brussels railway line has been modified in order to investigate the structural response of nearby masonry and RC buildings. Several buildings (e.g., multi-story RC office buildings and low-rise masonry buildings) have been investigated as an application of the model in order to evaluate its response to the developing vibrations by Thalys HST passage with 240km/h. In the sequence, the implementation of mitigation technics has been studied, aiming to minimize the vibrations level at crucial buildings positions.

Consequently, the implementation of several mitigation configurations using EPS geofoam has been investigated to reduce the induced vibration on the buildings. In the sequence, the optimal configuration has been proposed for each building. Furthermore, the effect of the distance from the track to the building structural response has been investigated to determine in which distance the buildings could be constructed without causing health issues to the residents. In the last Section, the implementation of EPS geofoam between the building foundation and the surrounding soil has been examined to investigate the seismic protection level of a typical 2-story masonry building.

7.2. *RC multistory buildings*

7.2.1. *Numerical model modification*

In the present section, the vibrations from a HST passing at a relatively close distance from multi-story reinforced concrete (RC) buildings has been investigated. The previously validated in Chapter 3, three-dimensional finite element numerical model has been used in order to examine the propagation of the developing vibrations from the HST passage. The nearby RC buildings response to the HST-induced vibrations has been examined in the case of building constructed at 10m, 20m and 30m from the track. The implementation of single or double EPS-filled trenches across the track to reduce the structural vibrations at the buildings floors has been investigated in the sequence (Lyratzakis et al., 2021d).

The previously validated in Chapter 3, Site 3 (at grade) of the Paris-Brussels line, at 4km south of Leuze-en-Hainaut, Belgium, has been used as a case study (Connolly et al., 2014). The examined track is a classical ballasted track consisted of ballast, sub-ballast and subgrade. Figure 7.1 depicts the numerical model with the configuration of the track layers, including the building which has been added in the sequence. It should be mentioned that though rail irregularities can play a significant role, they are not considered herein, since prior to field measurements a track maintenance was performed at this site (Kouroussis et al., 2016). In general, maintenance of HSR lines is more often and more meticulous compared to ordinary railways to ensure smooth HST operation and passengers comfort.
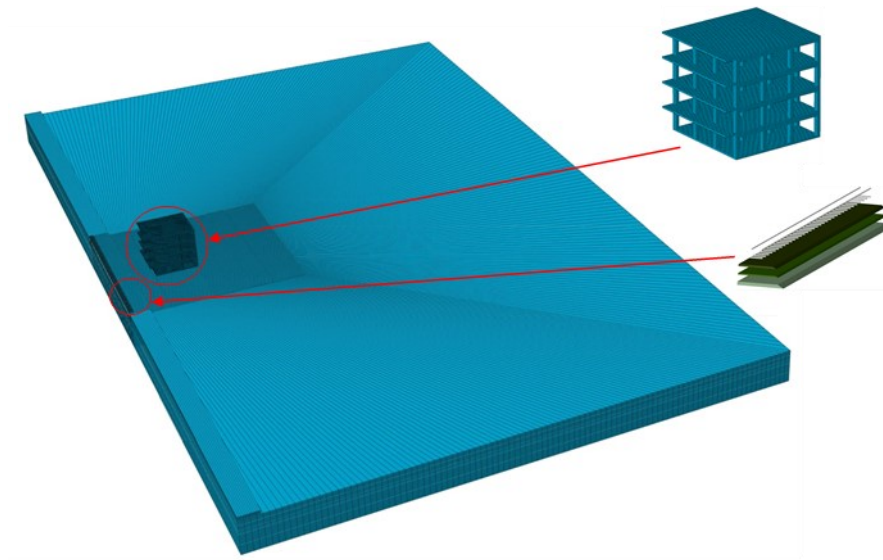
Figure 7.1 Finite/infinite element model.

Two symmetrical reinforced concrete (RC) (4-story and 8-story) building have been chosen for the investigation. The buildings are founded on a uniform RC slab and each story has 3m height (including slabs with 0.2 m thickness) resulting in a total height of 12m and 24m, respectively. The examined buildings have a rectangular floor plan with dimensions 12m x 12m. As presented in Figure 7.2, the structure comprises of concrete columns and beams with dimensions of 0.6m x 0.4m and 0.4m x 0.2m, respectively. At the front face of the building there is also a cantilever slab at each story, with a length equal to 1.5m. The mechanical properties of the reinforced concrete material are as follows: density ρ=2400kg/m3, Young's Modulus E=20GPa, Poisson's ratio v=0.2, damping ξ=5%. The columns, beams and slabs of the structure have been discretized using 4-noded solid finite elements. The buildings have been placed at a varying distance from the track (i.e.,

10m, 20m and 30m), in order to find the distance where the HST-induced vibrations impact is insignificant, by investigating the vibrations levels at all stories of the building. The induced vibrations due to HST passage can affect the health of the population; however, the possibility to cause structural damages is low. Hence, the behavior of the building is expected to be linear visco-elastic.
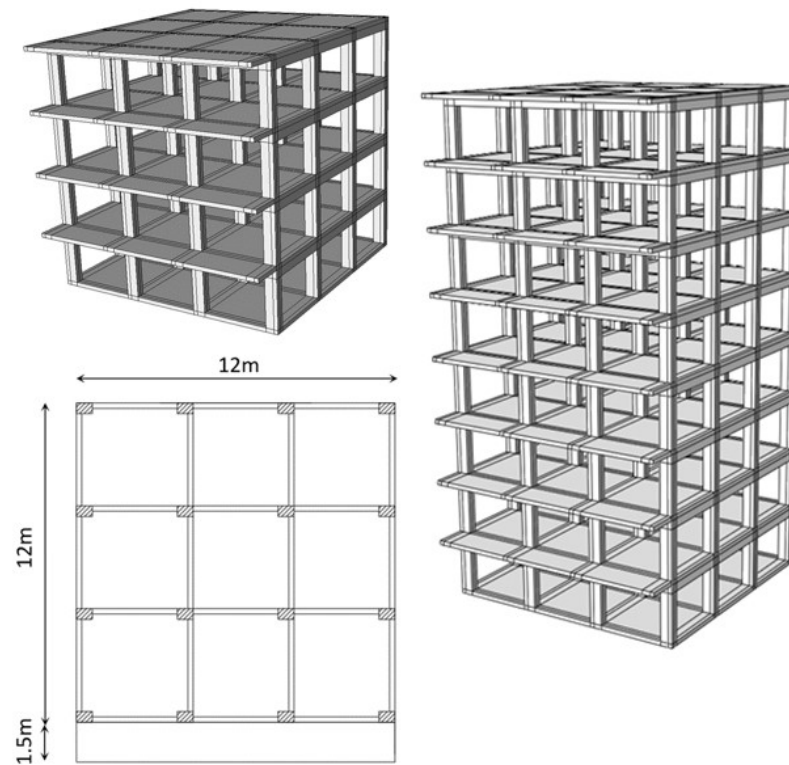
Figure 7.2 Building layouts.

Table 7.1. Properties of RC building adopted in the current investigation.

Material Properties	Unit	Value
Density	kg/m³	2400
Young's Modulus	GPa	20
Poisson's ratio	-	0.2
Damping	%	5

7.2.2. Examined EPS geofoam blocks configuration

In the present Chapter, the low density (18.4 kg/m³) EPS19 has been used. Figure 7.3a illustrates the first examined mitigation scheme using EPS geofoam to protect the building against HST-induced vibrations. The EPS-filled trench has been applied across the track. The applied trench has 60cm depth, which is the optimal value proposed recently by Alzawi et al. (2011) for geofoam in-filled trenches. According to Yarmohammadi et al. (2019), the double trench increases the level of vibrations reduction compared to the single

trench. Hence, according to the second mitigation scenario (see Figure 7.3b), a second trench has been implemented at 3m from the first trench to reduce the vibrations level further. The two EPS-filled trenches have the same geometrical properties as the first mitigation approach.
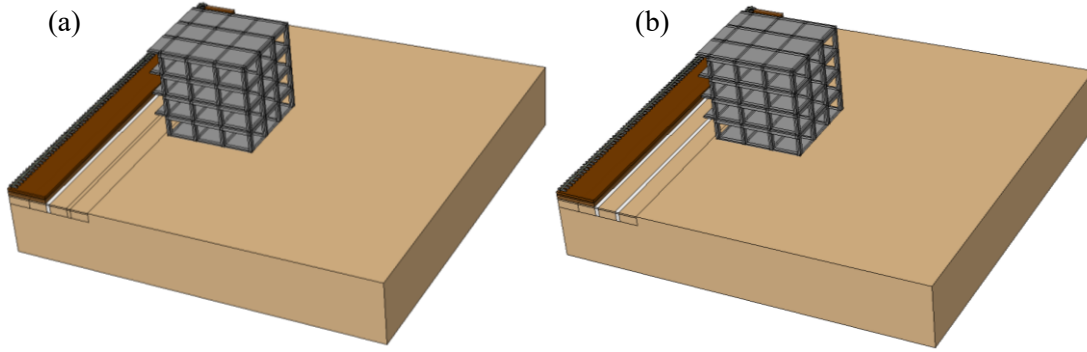
Figure 7.3 Mitigation schemes (a) single and (b) double EPS-filled trench across the track.
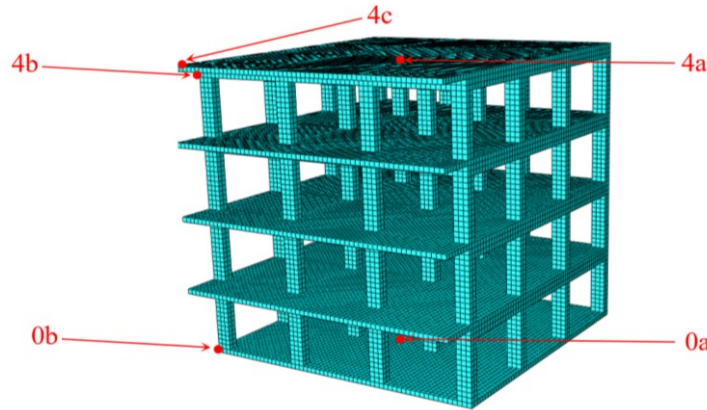
Figure 7.4 Observation points.

7.2.3. *4-story building*

7.2.3.1. *4-story building structural response*

Velocity decibels (V_{dB}) have been used in the present study as an indicator of the vibrations level due to the HST- induced vibrations at several examined positions on the building. The building responses have been investigated for five observation positions, two at the base and three at the 4th floor of the building. The center of the bases slab (0_a) and the base of the front corner column (0_b) have been chosen as the two observation points at the base level. On the 4th floor, the edge of the cantilever (4_c) has been examined in addition of the slab center (4_a) and the front column top (4_b). The five chosen observation positions are presented in Figure 7.4.

Figure 7.5 illustrates the effect of the HST passage on the vertical structural response on the building base and the top floor of the 4-story building at the positions 0_a and 4_a. It is obvious from the 1/3 octave bands that the vibrations response has been higher than the same value in the foundation level for all the examined bands. The most dominant octave band is the 14th. On the other hand, the 13th octave band vibrations level has been significantly increased at the 4th floor for all the examined distances from the track. In the modeling scenario for which the building has been constructed at 10m from the track (see Figure 7.5a), the response at the 12th and 13th octave bands have been increased to 68dB and 76dB, respectively, which is approximately 9dB greater than the maximum soil response of the 12th octave band, and 12dB greater than the soil response at 13th octave bands.

The same trend has been observed in the case of a building constructed at higher distances from the track. Figure 7.5b displays the 1/3 octave band of the central slab in the modeling scenario for which the building has been constructed at 20m from the track. As expected, the peak dB level at the 13th octave bands is significantly reduced compared to the first case from 76dB to 64 dB on the 4th floor. Furthermore, as shown in Figure 7.5b, the dB level of the lower octave bands is significantly reduced on the base level. The vibration level at the octave bands with centre frequencies from 1.25dB to 5dB is approximately 15dB. This value is significantly increased, reaching values between 23dB and 28 dB at the top of the building.

Figure 7.5c depicts the octave bands at the base and the 4th floor of the building in the case of a building constructed at the higher examined distance from the track (e.g., 30m). The vibrations level is the lowest of all the examined distances at both the 4th and base levels. The vibrations level has been decreased at values lower than 47dB at all the examined octave bands. Furthermore, the vibrations level is increased at the whole examined frequency range at the top of the building. The peak value of dB is equal to 55dB and remains at the 13th octave band. The decibel level is lower than 6dB of all the octave bands, with centre frequencies lower than 5 dB at the base level. The decibel level is equal to zero at the octave bands with centre frequencies 1.6dB and 2dB. The same indicators have values close to 17dB on the 4th floor.
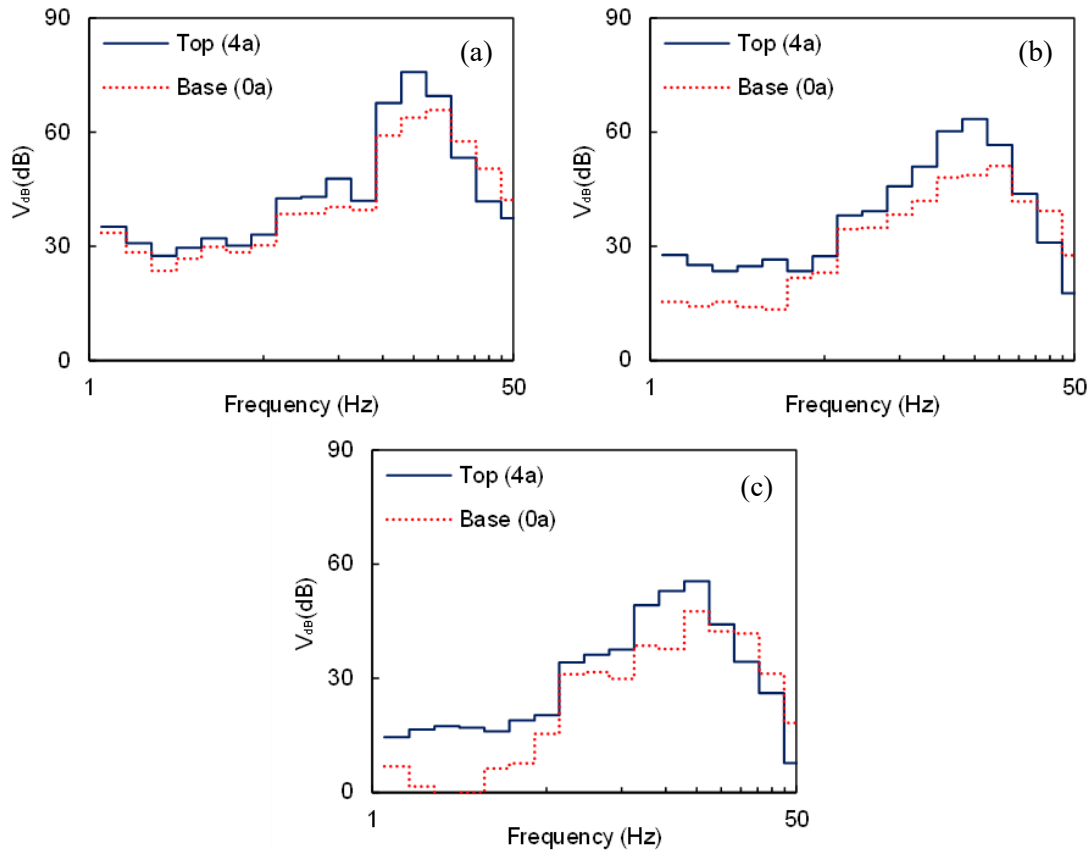
Figure 7.5 Central slab response of the 4-story building in terms of 1/3 octave bands when the building is constructed at (a) 10m from the track, (b) 20m from the track, (c) 30m from the track.

In the sequence, the vibrations level at the front corner column of the building has been examined at the base (position 0_b) and the top (position 4_b) of the building. Figure 7.6a illustrates the column response at the base and the 4th floor level when the 4-story building has been constructed at 10m from the track. It is clear that the decibel level has not been significantly altered at the top of the building compared to the base. The peak values of the vibrations level are observed at the 12th, 13th and 14th octave bands, equal to 68dB, 72dB and 67dB, respectively, at the base level. Those values are increased by 2dB on the 4th floor. The highest increase of dB level is located at the octave band with a centre frequency 10Hz. This indicator has been increased from 46dB in the base of the column to 51dB on the 4th floor. The peak vibrations level is slightly lower at the top of the column compared to the middle of the slab (position 4_a).

The same observation has been made when the building is constructed at 20m (see Figure 7.6b) and 30m (see Figure 7.6c) from the track. In those cases, the peak decibel level is located again at the 13th octave band. Furthermore, the decibel level is no significantly

altered between the base and the top of the building. The peak decibel level is equal to 63dB and 55dB for building constructed at 20m and 30m from the track, respectively.
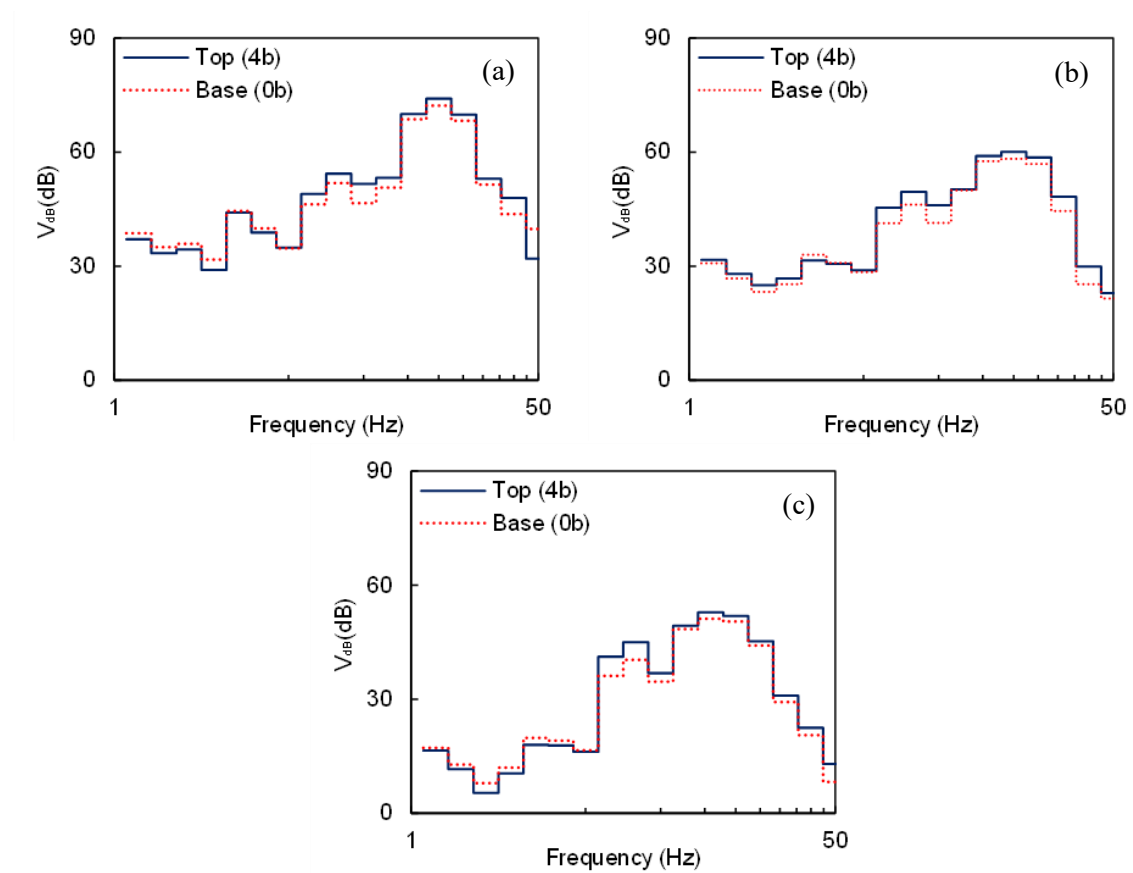
Figure 7.6 Column response of the 4-story building in terms of 1/3 octave bands when the building is constructed at (a) 10m from the track, (b) 20m from the track, (c) 30m from the track.

The last examined position is the corner of the 4th story cantilever (4c). As expected, the dB level has been increased compared to the top of the corner column and the central slab. Figure 7.7a illustrates the response of the cantilever when the building is constructed at 10m from the track. In this modelling scenario, the peak dB level has been observed at the 13th and the 14th octave band, and it is equal to 83dB and 81dB, respectively. Furthermore, the dB level is higher than 40dB at the whole examined frequency range. When the building has been constructed at 20m from the track, the dB level remains relatively high. For instance, the higher dB level, equal to 71dB, is located at the octave band with a centre frequency 25Hz (see Figure 7.7b).

Furthermore, the dB level of the middle range octave bands has not been significantly decreased compared to the modelling scenario for which the building has been constructed at 10m from the track. On the other hand, at the octave bands with centre

frequencies lower than 5Hz, the dB level has been significantly decreased to values lower than 31dB. The vibration level is even lower when the building has been located at 30m from the track, as it is clearly illustrated in Figure 7.7c. More specifically, the dB level is lower than 60dB at the whole examined frequency range.
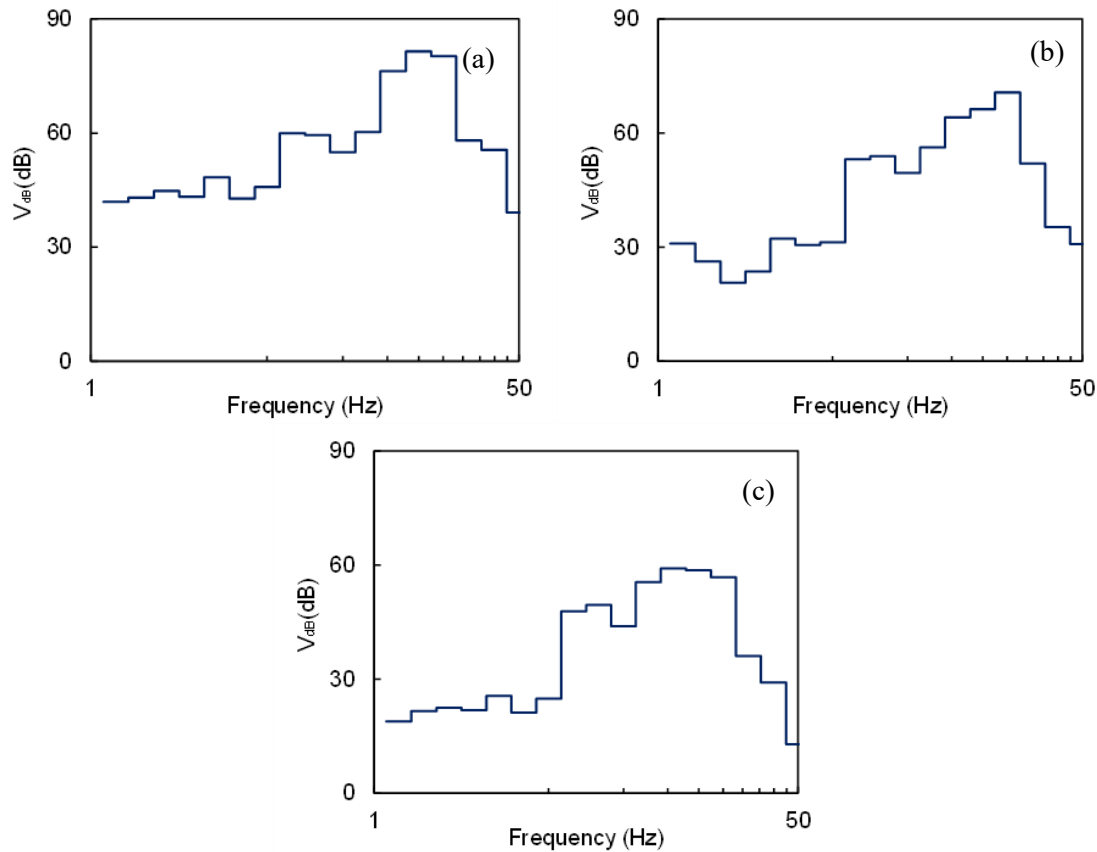
Figure 7.7 Cantilever response of the 4-story building in terms of 1/3 octave bands when the building is constructed at (a) 10m from the track, (b) 20m from the track, (c) 30m from the track.

7.2.3.2. *4-story building protection with the use of single EPS–filled trench.*

Figure 7.8 illustrates some contour plots of the vertical velocity on the soil surface and the building in order to depict the level of the vibrations reduction after the implementation of the single protecting barrier. The effect that this mitigation approach has on wave propagation is clearly illustrated in Figure 7.8. More specifically, Figure 7.8a demonstrates the wide spreading of the waves and their effect on the building. The implementation of the single EPS-filled trench has contributed to reducing the surface waves scattering, as depicted in Figure 7.8b. Furthermore, the implementation of the trench has minimized the vibrations level at the nearby building at 10m from the track. In the sequence, Figures 7.8c and 7.8d depict the scattering of the surface waves in the modelling scenario for which the building has been constructed at 20m from the track, before and after the implementation

of a single EPS-filled trench. The amount of the induced vibrations reaching the building has been significantly lower after the implementation of the in-filled trench.

In order to further illustrate the effectiveness of the single EPS-filled trench, a commonly used vibrations indicator, insertion loss (IL), has been used (Li et al., 2020; Ngamkhanong and Kaewunruen, 2020). Figure 7.9 demonstrates the IL curves of the EPS-filled trench at the three observation points on the 4th floor of the building for the three examined construction distances of the 4-story building. In the case of a building located at 10m from the track, high IL values have been observed for all the examined positions for the octave bands with centre frequencies higher than 16Hz. On the other hand, the decibel reduction is lower than 4dB for the first 11 octave bands, as illustrated in Figure 7.9a. At the centre of the slab, the peak decibel reduction, equal to 10dB, has been observed at the 16th octave band. Furthermore, at the most dominant octave bands (e.g., 11th, 12th and 13th, according to Figure 7.9a), the decibel reduction varies between 4dB and 6dB. At the second examined position, the top of the front corner column, the higher values of decibel reduction have been observed. More specifically, the reduction of the vibrations level reached the 11dB and the 13dB at the 14th and 15th octave bands, respectively. At the edge of the cantilever, the insertion loss is slightly lower than the other two observation points. However, at the 16th octave band, the decibel reduction reaches over 10dB.
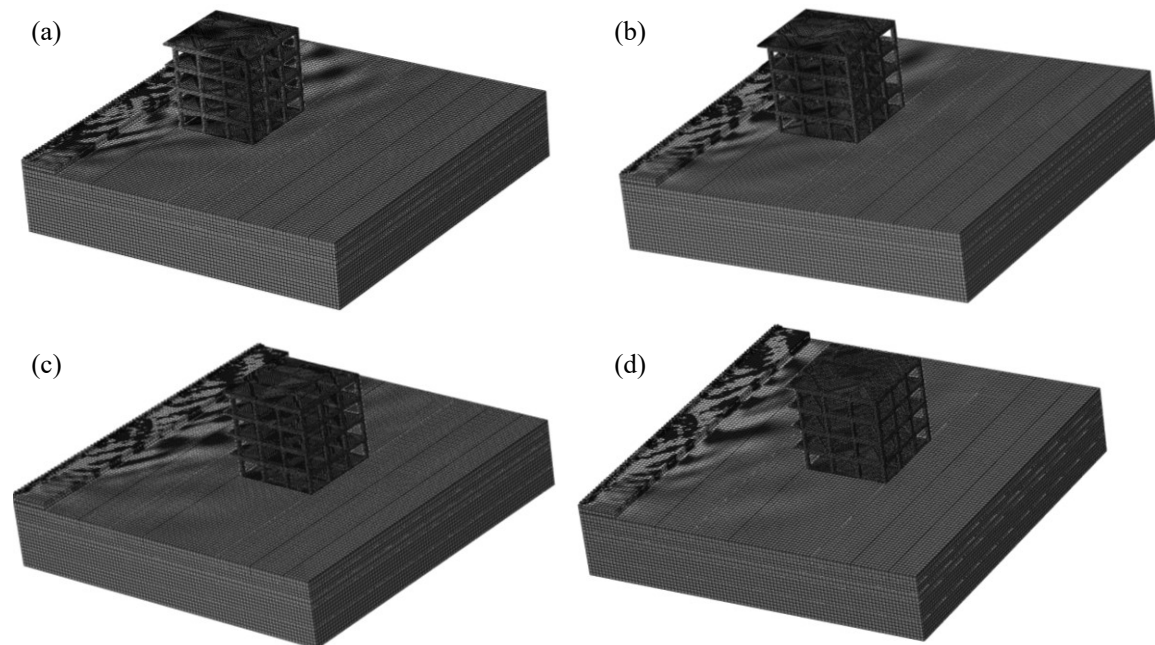
Figure 7.8 Typical contour plots of vertical velocity at soil surface: (a) building at 10m from the rails without trench, (b) building at 10m from the rails with trench, (c) building at 20m from the rails without trench and (d) building at 20m from the rails with trench.

Figure 7.9b shows the IL curves for the modelling scenario for which the RC building has been constructed at 20m from the track. The reduction of the vibrations level at the octave bands with centre frequencies lower than 5dB is higher than the previous case for all the examined observation positions. In some cases, the IL at the lower frequencies is higher than 5dB. On the other hand, the decibel levels reduction is slightly lower than the modelling scenario for which the building has been constructed at 10m from the track. However, in some cases, the IL reaches over 9dB; for instance, the IL level reaches the peak value of 10dB at the octave band with a centre frequency 25Hz at the observation points 4_b and 4_c. The same trend is observed in the case of a building constructed at the higher distance (30m from the track), as illustrated in Figure 7.9c. In this case, the level of decibel reduction remains close to 5dB for all the low frequencies. On the other hand, the dB reduction is minimized compared to the previously examined positions at the higher octave bands in the modelling scenario for which the building has been constructed closer to the track.
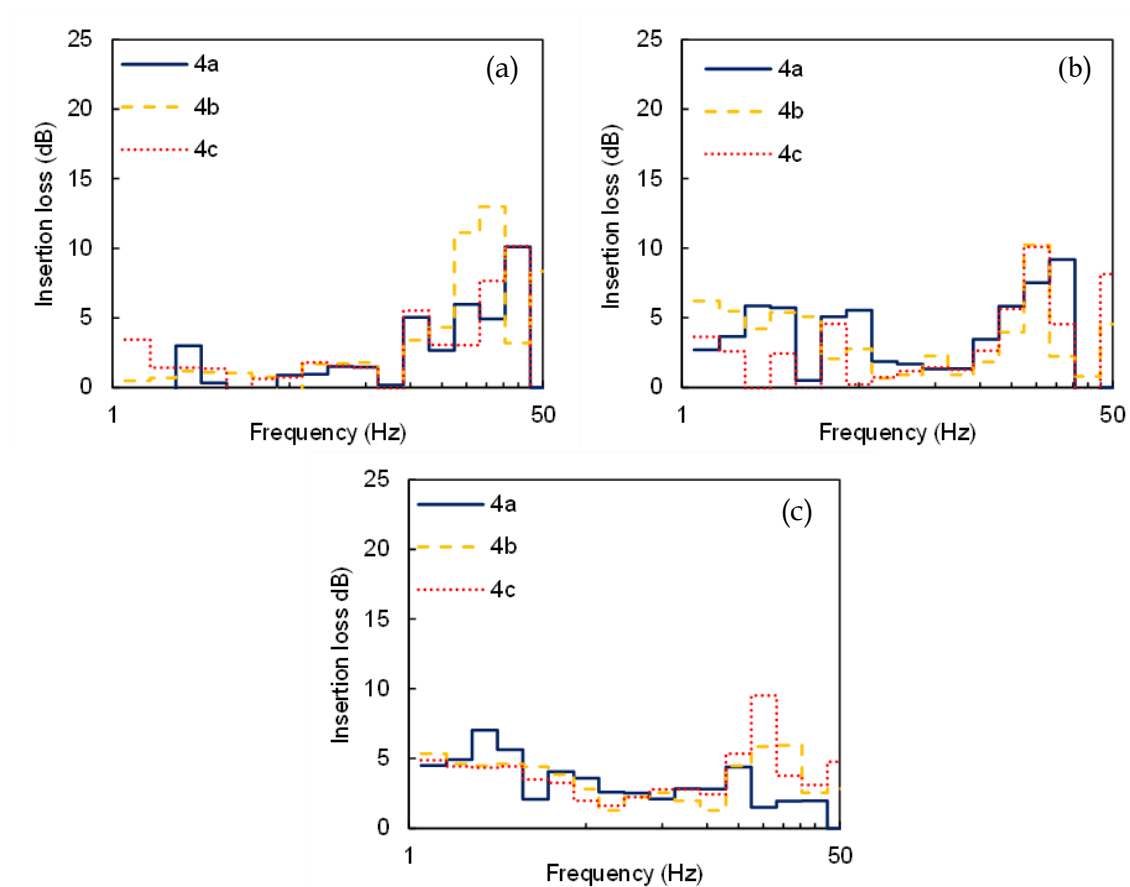
Figure 7.9 IL curves at the top of the building at (a) 10m from the track, (b) 20m from the track, (c) 30m from the track.

In the sequence, in order to depict the effectiveness of the implementation of the EPS trench, it is vital to compare this indicator with proposed thresholds. According to the environmental noise guidelines for the European region, the World Health Organization (WHO) strongly recommends reducing the induced vibrations levels below 54 dB, aiming to protect the users of the building from problems associated with adverse health effects. Furthermore, this value is reduced to 44dB at night hours in order to avoid disturbance associated with adverse effects on sleep (WHO/Europe, 2018). Table 7.2 summarizes the decibel level of the most dominant octave bands before and after implementing the EPS-filled trench. The reduction of the decibel level is not enough to minimize the vibrations level under the threshold of 54dB. For this reason, the construction of the RC building at 10m from the track is not recommended. The decibel level in several cases has been reduced below 54dB when the building is constructed at 20m from the track. However, the mitigation scheme is not capable of achieving this threshold for all the examined positions. On the other hand, at 30m from the track, the implementation of the EPS-filled trench manages to reduce the decibel level below 54dB for all the examined positions.

Table 7.2. The decibel level of the most dominant octave bands.

Observation position	Centre Frequency (Hz)	10m from the track		20m from the track		30m from the track	
		Initial V_{dB} (dB)	Mitigated V_{dB} (dB)	Initial V_{dB} (dB)	Mitigated V_{dB} (dB)	Initial V_{dB} (dB)	Mitigated V_{dB} (dB)
	16	68	64	60	58	53	51
4a	20	76	72	63	59	55	50
	25	70	59	56	46	44	39
	16	70	65	59	55	53	50
4b	20	74	71	60	54	52	48
	25	70	64	58	51	45	43
	16	76	70	64	61	58	54
4c	20	82	79	66	61	58	53
	25	80	77	70	60	57	47

7.2.3.3. 4-story building protection with the use of double EPS–filled trenches

The implementation of the single EPS-filled trench across the track reduces the vibrations level. However, the level of reduction is not capable of protecting the building users from possible health issues. In order to further reduce the vibrations level, a second identical trench has been placed at 2.5m from the first one. The contour plots of vertical velocities at the surface, as illustrated in Figure 7.10, aim to compare the effectiveness of the single and the double EPS-filled trench. More specifically, the surface waves have been more

widely spread in the case of the single trench (see Figure 7.10a) in comparison with the double EPS-filled trench, as it is illustrated in Figure 7.10b. Accordingly, the assumption could be made that the implementation of a second trench increases the reduction of the vibrations level.

(a)   (b)
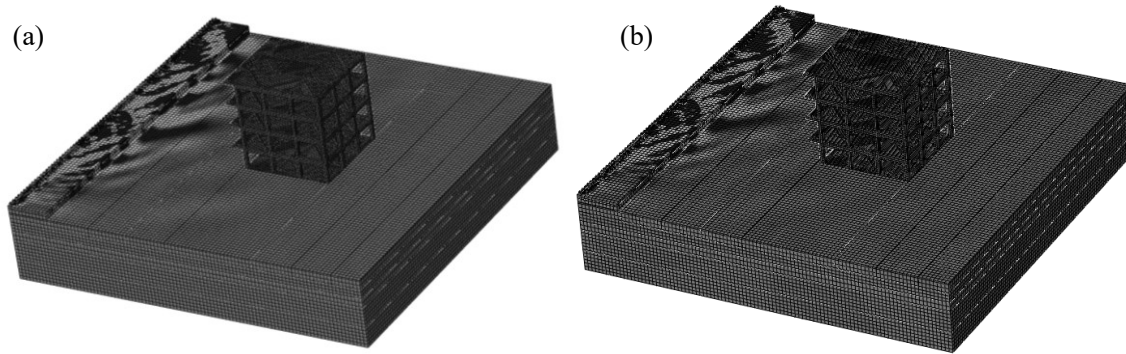
Figure 7.10 Typical contour plots of vertical velocity at the soil surface in the modeling scenario for which the building is constructed at 20m from the rails: (a) single and (b) double EPS-filled trench.

Figure 7.11 illustrates the insertion loss of the double EPS-filled trench. The vibrations reduction has been increased in comparison with the single trench. In the modelling scenario for which the building has been constructed at 10m from the track, the insertion loss at the most dominant octave bands (e.g., 12th, 13th, 14th) is significantly higher than the single trench. More specifically, at the top of the front corner column, the insertion loss reaches values close to 15dB and 12dB at the octave bands with centre frequencies 20Hz and 25Hz, respectively. The high level of vibrations reduction has also been observed at the other two observation points at the dominant octave bands as the insertion loss takes values between 9dB and 12dB. Furthermore, the insertion loss is significantly higher than the single in-filled trench.

The highest values of insertion loss have been observed in the case of a building constructed at 20m from the track, as depicted in Figure 7.11b. More specifically, the insertion loss at the dominant octave band with a centre frequency 20Hz is equal to 19dB and 22dB at the central slab and the edge of the cantilever, respectively. Additionally, the reduction of the decibel level at the lower frequencies is extraordinary. For instance, the vibrations reduction reaches values close to 9dB at the 4th octave band. Figure 7.11c demonstrates the insertion loss in the case of a building constructed at 30m from the track. The reduction of the decibel level is slightly lower than the previous two cases. The highest level of reduction has been observed at the edge of the cantilever, at the octave band with

20Hz centre frequency. Furthermore, the insertion loss is higher than 5dB at the three dominant octave bands for all the examined observation points. Considering the relatively high distance from the track, the decibel level has already been low before the implementation of the double trench. Hence the assumption could be made that the decibel reduction is satisfactory.
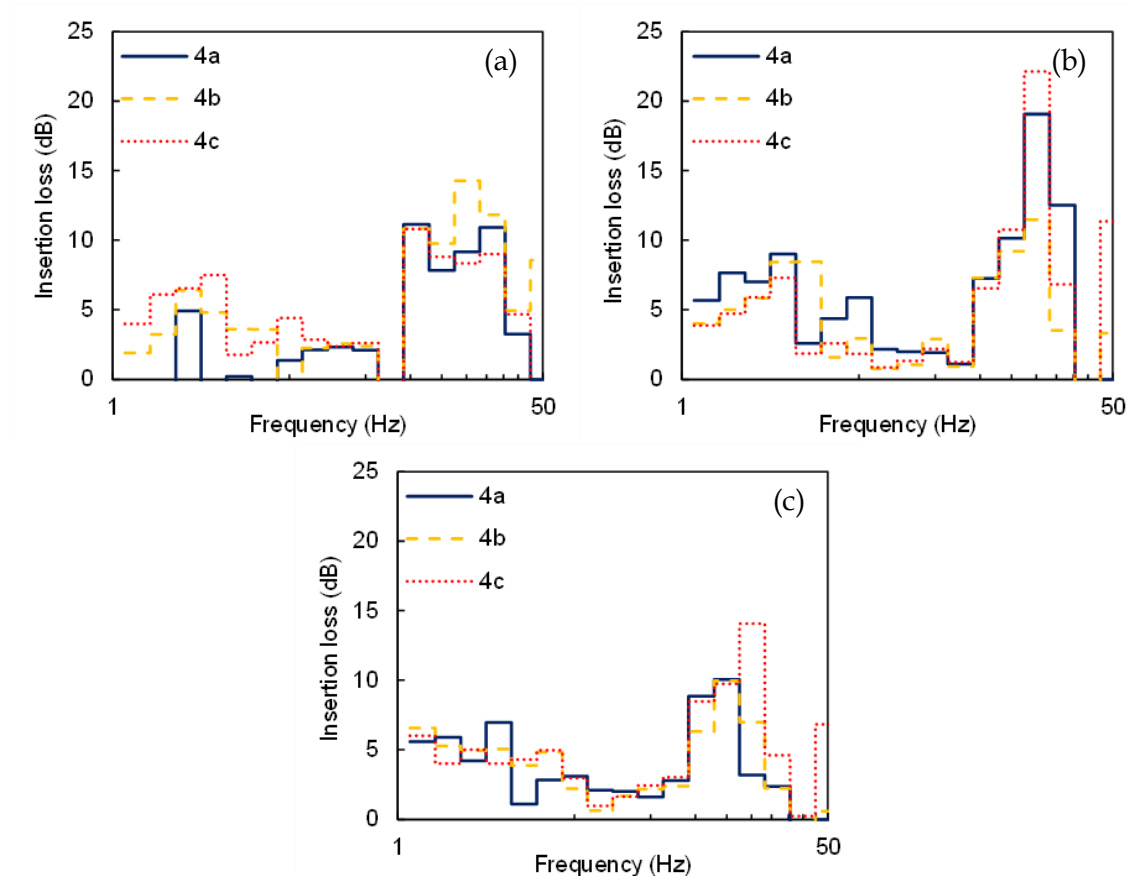
Figure 7. 11 IL curves at the top of the building at (a) 10m from the track, (b) 20m from the track, (c) 30m from the track.

Table 7.3 summarizes the decibel level at the most dominant octave bands before and after the implementation of the double in-filled trench. In the modeling scenario for which the building has been constructed at 10m from the track, the notable reduction of the decibel level is not enough in order to reduce the vibration level below the WHO threshold of 54dB. However, in contrast with the single trench, the decibel level at the top of the front corner column and the central slab of the 4th floor has been reduced below 66dB at the three dominant octave bands. The protection of the building is even more pronounced in the modeling scenario for which the building has been constructed at 20m from the track.

The dB level has been reduced under the WHO threshold of 54dB at the observation points 4_a and 4_b. Nevertheless, at the edge of the cantilever, the decibel level is slightly higher than 54dB at the octave bands with centre frequencies 16Hz and 20Hz. The assumption could be made that after the implementation of double EPS-filled trenches, the 20m from the track is a vital distance to construct a building, although the construction of a cantilever should be avoided. As mentioned, in the case of a building constructed at 30m from the track, the implementation of a single trench successfully reduces the decibel level under 54dB. Hence the implementation of a second trench is not necessary, although the double trench has further reduced the decibel level.

Table 7.3. The decibel level of the most dominant octave bands.

Observation position	Centre Frequency (Hz)	10m from the track		20m from the track		30m from the track	
		Initial V_{dB} (dB)	Mitigated V_{dB} (dB)	Initial V_{dB} (dB)	Mitigated V_{dB} (dB)	Initial V_{dB} (dB)	Mitigated V_{dB} (dB)
4a	16	68	58	60	53	53	47
	20	76	66	63	54	55	45
	25	70	56	56	45	44	37
4b	16	70	59	59	52	53	44
	20	74	66	60	50	52	42
	25	70	61	58	39	45	42
4c	16	76	66	64	57	58	50
	20	82	73	66	55	58	48
	25	80	72	70	48	57	43

7.2.3.4. Side by side comparison of single and double EPS – filled trench

As aforementioned, insertion loss is a great indicator of the mitigation measures effectiveness. Insertion loss curves depict the reduction of the decibel level at the examined frequency range. Obviously, except for the decibel reduction, the reduction of the most dominant vibrations peaks should be examined. For this purpose, the reduction of the vibrations level after implementing the examined mitigation approaches is examined in terms of vertical velocity Fourier Spectra. More specifically, in this Section, a side-by-side comparison of the single and the double trench configurations efficiency is presented at the low-frequency range between 0Hz and 40Hz at all the examined observation points.

Figure 7.12 demonstrates the vertical velocity Fourier spectra of the examined mitigation approaches at the central slab of the base and 4th floor (e.g., positions a_0 and a_4, respectively), in the modelling scenario for which the building has been constructed at 10m from the track. The most dominant vibrations peaks are located at the same

frequencies (e.g., 17.8 Hz, 21.5 Hz, 23.9 Hz and 28.5Hz) for both observation points 0_a and 4_a. It should be mentioned that the most dominant peak at 21.5 Hz is significantly increased from 0.14mm/s at 0_a to 0.81mm/s at 4_a. A lower increase is observed at the other two dominant frequencies (e.g., 17.8Hz and 23,9Hz), where the vibrations level increases up to 50% on the 4th floor. On the other hand, the amplitude of the induced vibrations is reduced from 0.14mm/s to 0.08mm/s at 28.5Hz.

Figure 7.12 Fourier spectra at the central slab at 10m from the track in the modeling scenario of a single trench ((a) base, (b) 4th floor), double trench ((a) base, (b) 4th floor).

In the case of the single trench, all the vibrations peaks are significantly minimized at both observation points. As it is clearly illustrated in Figure 7.12a, the most dominant vibrations peak at 21.5 Hz has been reduced from 0.81mm/s to 0.42mm/s. Furthermore, the vibrations peaks at the higher frequencies, 23.9 Hz and 28.5Hz, have been virtually disappeared. A slight reduction equal to 27% is observed at 17.8 Hz. The same observation is made at the central slab of the base, as is illustrated in Figure 7.12c. More specifically, all the vibrations peaks have been minimized under 0.1mm/s. The level of the vibrations reduction reaches in some cases over 60%.

The level of mitigation is even more pronounced in the case of the double EPS-filled trenches implementation. At the central slab of the 4th floor (see Figure 7.12b), the reduction of the vibrations amplitude at the most dominant frequency, 21.5 Hz, remains at the same level as the single trench. On the other hand, the reduction of the vibrations peak at 17.8 Hz is remarkably higher after implementing the second trench, as the level of reduction has been increased from 27% to 62%. Furthermore, the last two dominant vibrations peaks are reduced to almost zero. Figure 7.12d depicts the vertical velocity Fourier spectra at the central slab of the base in the case of double EPS-filled trenches implementation. It is evident that the implementation of a second trench has led to further reduction at this observation position, as the level of reductions reaches up to 70% at almost all the dominant frequencies.

Figure 7.13 presents the vertical velocity Fourier spectra of the examined mitigation approaches at the second observation position, the front corner column at the base and the 4th floor, in the case of a 4-story building constructed at the closest examined distance from the track (e.g., 10m). The most dominant vibrations peaks are slightly different from the previously examined observation position, although they remain at frequencies close to 20Hz. In this case, three dominant vibrations peaks are observed at 17.8 Hz, 21.2 Hz and 23.4 Hz at both observation points 0_b and 4_b. In this case, the most dominant peak at 17.8 Hz is slightly increased from 0.62mm/s 0.75mm/s at the base and the 4th floor levels, respectively. The same observation has been made at the other two dominant frequencies, where the vibrations level increased up to 25% on the 4th floor.

The vibrations peaks at the 4th floor are significantly reduced after implementing the single or double trench across the railway line, as illustrated in Figure 7.13a and 7.13b, respectively. The most dominant peak at 17.8Hz has been reduced from 0.72mm/s to 0.48mm/s for the single trench and 0.38mm/s for the double trench. In addition, the peak at 23.4 Hz has been disappeared for both examined mitigation approaches. On the other hand, the reduction of the vibrations peak at 17.8 Hz is marginal and a new vibrations peak has been observed in the case of the single trench at 28.5 Hz. The same observation is made at the base of the front corner column, as both mitigation approaches minimize the vibrations level (see Figures 7.13c-7.13d). In this case, the vibrations peaks are reduced from 0.68mm/s to under 0.4mm/s for both examined mitigation approaches. On the other hand, the peak at 21.2Hz is not significantly altered after the implementation of a single or double trench.
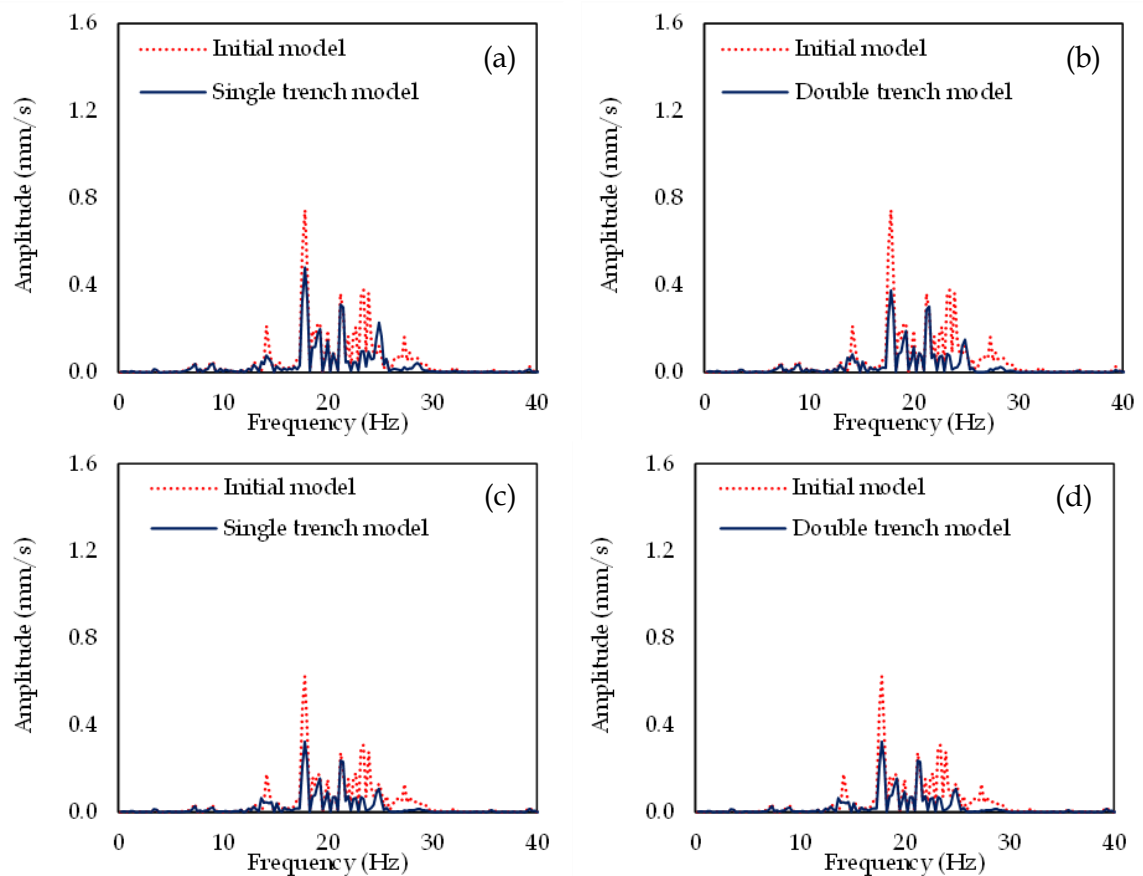
Figure 7.13 Fourier spectra at the front corner column at 10m from the track in the modeling scenario of a single trench ((a) base, (b) 4th floor), double trench ((a) base, (b) 4th floor).
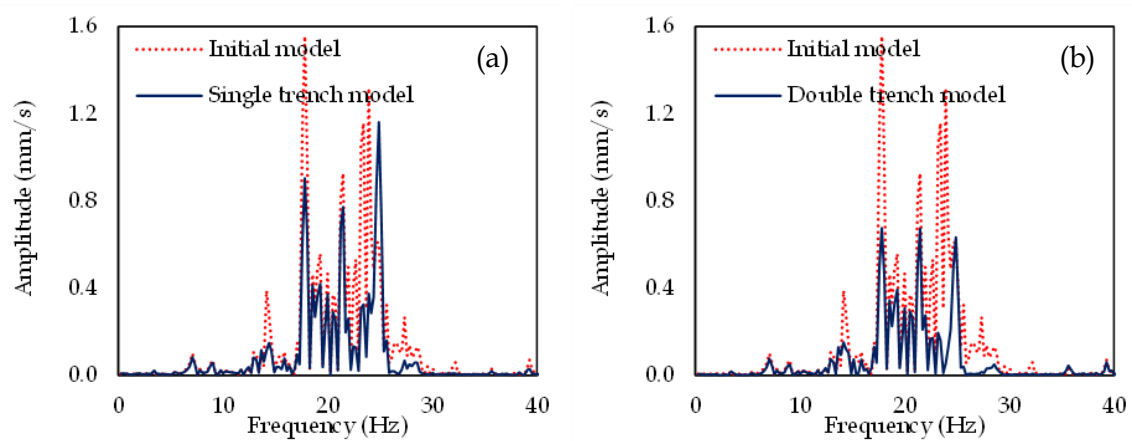
Figure 7.14 Fourier spectra at the cantilever of the 4th floor at 10m from the track in the modeling scenario of a single trench and double trench.

As aforementioned, the last observation position is located at the edge of the 4th floor cantilever. According to Figure 7.14, the three dominant peaks remain at the same frequencies (e.g., 17.8 Hz, 21.2 Hz and 23.4 Hz) with 4_b. It is evident that the amplitude of the vibrations at this observation point is significantly higher than all the other presented observation positions. The most dominant peak, equal to 1.56mm/s, is located at 17.8Hz.

Furthermore, the peaks at 21.2 Hz and 23.4 Hz are equal to 0.93mm/s and 1.3mm/s, respectively. The implementation of a single EPS-filled trench has reduced the dominant peaks at 17.8 Hz and 21.2Hz from 1.56mm/s and 0.93mm/s to 0.9mm/s and 0.78mm/s, respectively, as it is depicted in Figure 7.14a. On the other hand, the implementation of the EPS-filled trench duplicates a secondary vibrations peak at 24.9Hz. Figure 7.14b illustrates the reduction of the EPS level after the implementation of the double trench. In this modeling scenario, all the vibrations peaks have been minimized under 0.7mm/s at the whole low-frequency range. Furthermore, the vibrations peak at 24.9Hz has not been altered.
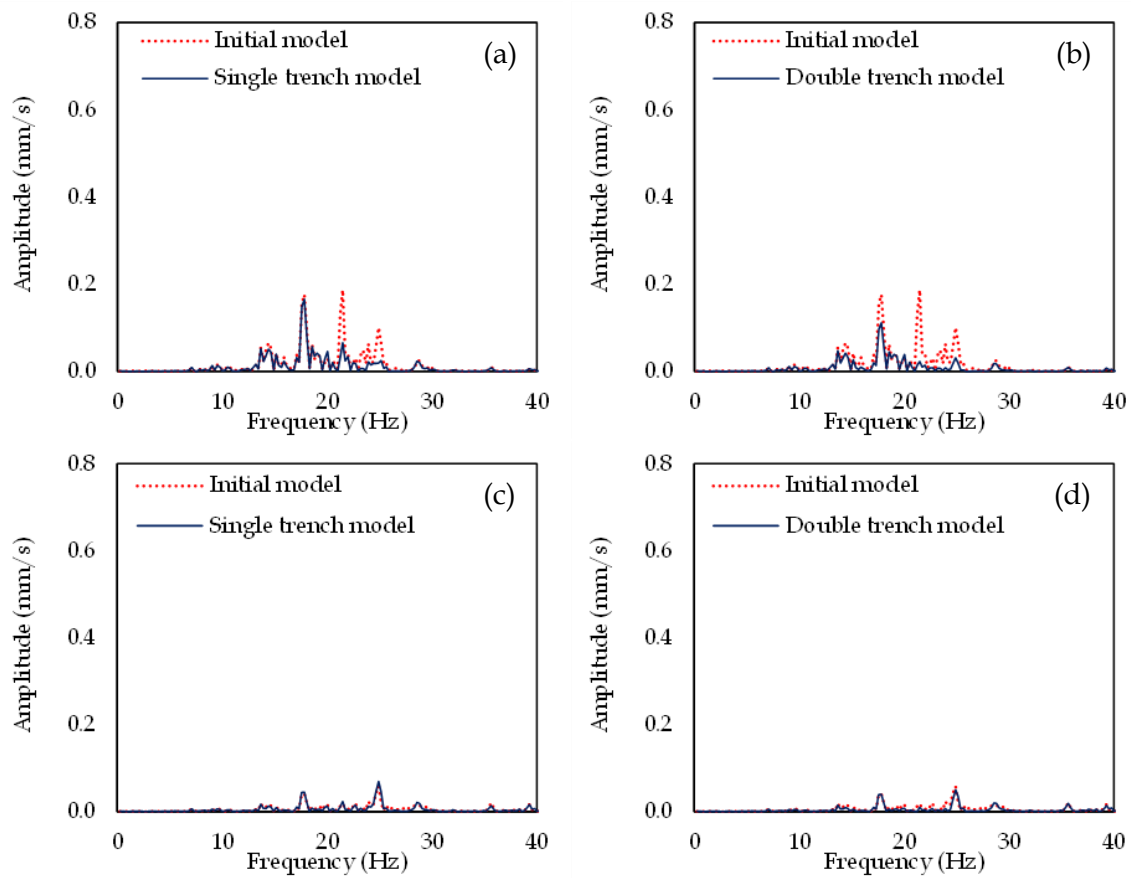
Figure 7.15 Fourier spectra at the central slab at 20m from the track in the modeling scenario of a single trench ((a) base, (b) 4th floor), double trench ((a) base, (b) 4th floor).

In the sequence, the vertical velocity time histories are presented in the case of a building placed at 20m from the track. Figure 7.15 presents the Fourier spectra at the first two observation positions (e.g., 0_a, 4_a). The initial vibrations level is significantly reduced compared to the case of a building constructed at 10m from the track, although they remain at the same frequencies (e.g., 17.8 Hz, 21.5 Hz and 23.9 Hz). The vibrations peaks remain lower than 0.2mm/s and 0.06mm/s at the central slab of the 4th floor and the base,

respectively. The vibrations level is already low; hence, the implementation of a single EPS-filled trench has not significantly altered the vibrations peaks, as illustrated in Figure 7.15c. On the other hand, the implementation of the double trench slightly reduces the vibrations level (see Figure 7.15d).

The effectiveness of the proposed mitigation measures is even more pronounced on the 4th floor of the building. Figure 7.15a shows the reduction of the vibrations level in the modeling scenario of the single trench. In this case, the vibrations peak at 17.8Hz remains at the same level. However, the vibrations peaks at 21.5 Hz and 23.9 Hz are reduced to 0.05mm/s and 0.02mm/s, respectively. The second trench implementation has managed to reduce the peak at 17.8Hz from 0.18mm/s to 0.14mm/s, as illustrated in Figure 7.15b. Furthermore, the other two vibrations peaks have been virtually disappeared.

Figure 7.16 compares the vibrations level at the low-frequency range at the front corner column when the 4-story building is constructed at 20m from the track. The vibrations peaks at the base of the structure are higher than the previously examined observation position. It could be explained by taking under consideration the distance of each observation position from the track. More specifically, the observation position 0_b is located at 20m from the track compared to the previously examined position, 0_a, which is located at 26m from the track. The vibrations peaks remain at the same frequencies (e.g., 14.2 Hz, 17.8 Hz, 21.5 Hz and 23.9 Hz) at the base and the 4th floor of the building. All the vibrations peaks range around 1.2mm/s and 1mm/s at the 4th floor and the base, respectively. Obviously, the increase of the vibrations level at the top of the building is significantly lower than the previously examined position (see Figure 7.15).

The implementation of a single trench across the track has led to the reduction of the vibrations peaks at 17.8 Hz and 23.9 Hz, close to 35% at the top of the building. Furthermore, a lower reduction of the vibrations peak at 14.2 Hz is observed, and the vibrations peak at 21.5 Hz has been disappeared (see Figure 7.16a). In addition, the implementation of two trenches halves the vibrations peak at 17.8Hz and reduces to zero the peaks at 21.5Hz and 23.9Hz at the 4th floor, as it is depicted in Figure 7.16b. At the base of the building, the implementation of the single trench seems to be a more practical approach for the reduction of the vibrations peaks below 20Hz, as it is illustrated in Figure 7.16c, in comparison with the double trench, which is more effective for the vibrations peaks at the higher examined frequencies (see Figure 7.16d).
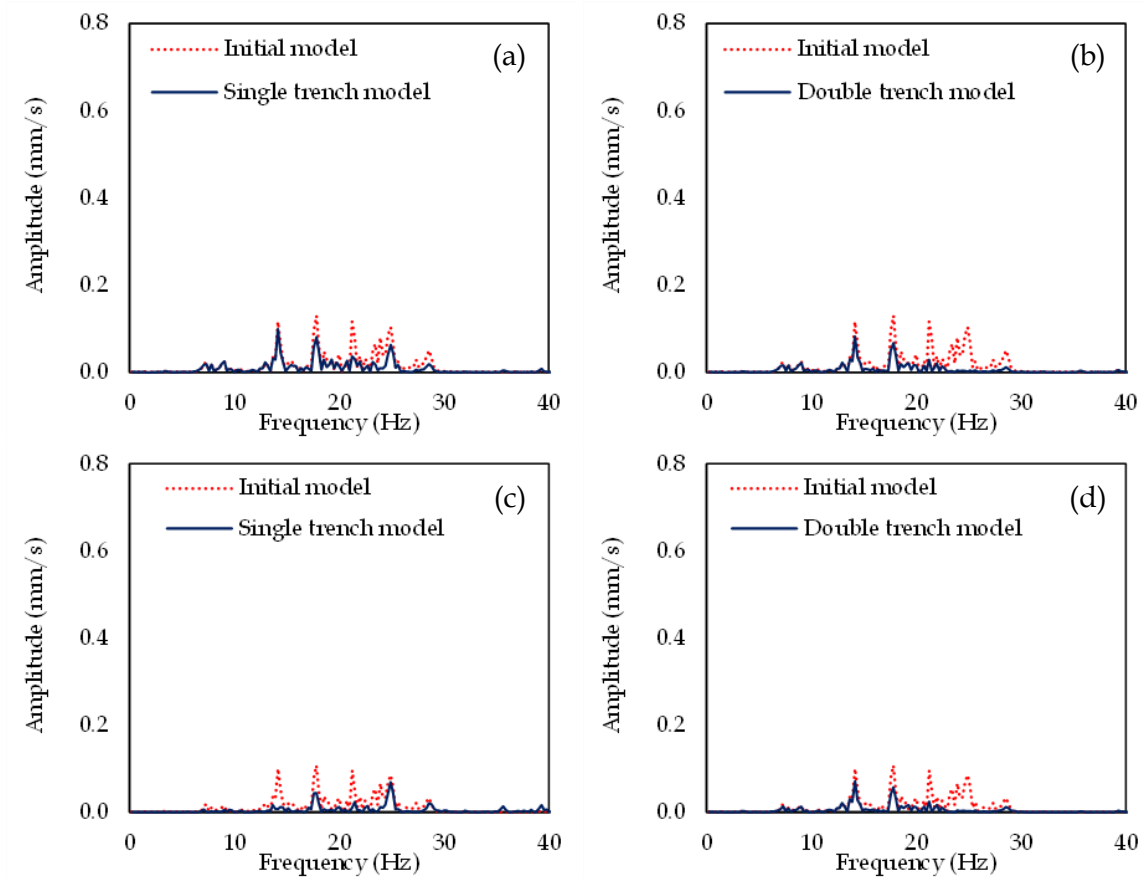
Figure 7.16 Fourier spectra at the front corner column at 20m from the track in the modeling scenario of a single trench ((a) base, (b) 4th floor), double trench ((a) base, (b) 4th floor).
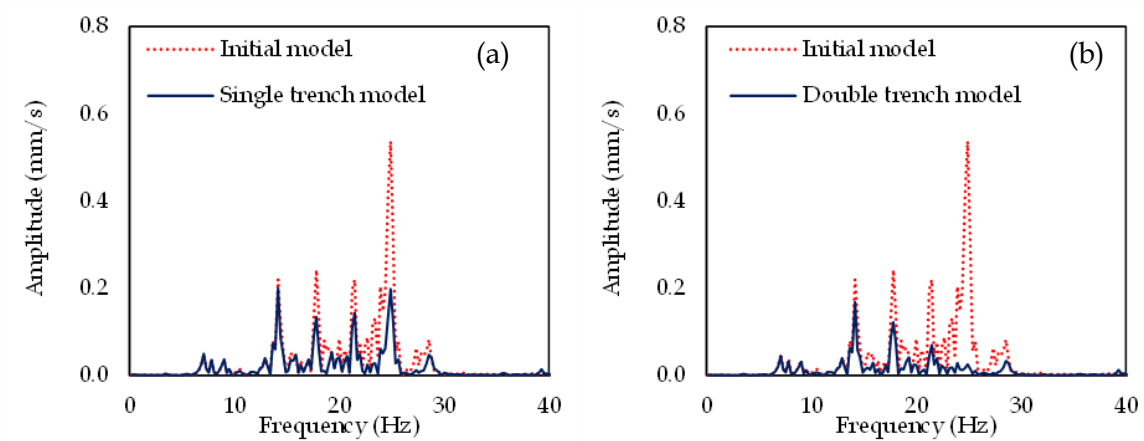
Figure 7.17 Fourier spectra at the cantilever of the 4th floor at 20m from the track in the modeling scenario of a single trench and double trench.

Figure 7.17 depicts the vertical velocity Fourier Spectra at the last observation position, the edge of the front cantilever of the 4th floor. As it was expected, in this position, the highest amplitudes of vibrations peaks are observed. In comparison with the previously examined distance from the track (e.g., 10m), in this case, the peak at 24.9Hz is undoubtedly the most dominant, reaching close to 0.6mm/s. Furthermore, there are three

more secondary peaks at 14.2Hz, 17.8Hz and 21.5Hz with amplitude slightly lower than 0.2mm/s.

It is evident from Figure 7.17a that the single trench manages to reduce the vibrations peaks at 14.2Hz and 24.9Hz close to 0.19mm/s. The mitigation level of vibrations peak reaches close to 45% and 35%, at 17.8 Hz and 21.5 Hz, respectively. On the other hand, the double trench implementation has managed to reduce those peaks up to 50%, as depicted in Figure 7.17b. Furthermore, the efficacy of the double trench on the most dominant peak reduction at 24.9Hz is remarkable, as it has been reduced from 0.9mm/s to almost 0mm/s.
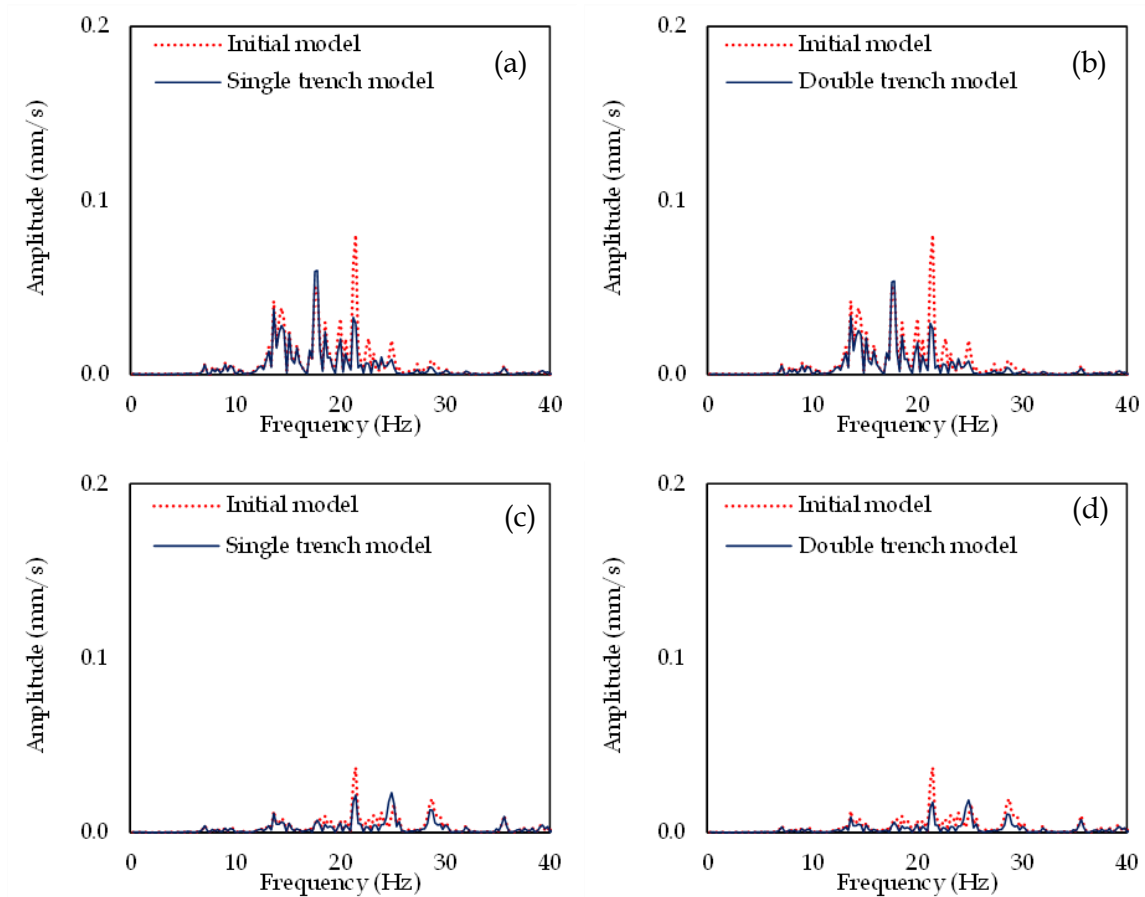
Figure 7.18 Fourier spectra at the central slab at 30m from the track in the modeling scenario of a single trench ((a) base, (b) 4th floor), double trench ((a) base, (b) 4th floor).

The Fourier spectra at the farthest location are presented at 30m from the track in the sequence. In this case, the vibrations level has been significantly reduced compared to the buildings constructed closer to the track. For instance, the vibrations peaks are lower than 0.04mm/s and 0.08mm/s at the base and the 4th floor levels central slab, as illustrated in Figure 7.18. The peak value of the vibration is located at 21.8Hz at both the base and the 4th floor of the building. However, at 0_a, all the other secondary peaks are located at

frequencies above 21.8Hz (e.g., 24.9 Hz, 28.5Hz) compared with 4_a, where the secondary peaks are located lower than 21.8Hz (e.g., 14.2Hz, 17.8Hz). In this case, the single and the double trench efficacy are pretty similar, as both examined mitigation approaches managed to reduce the peak at the most dominant frequency below 0.03mm/s at the 4th floor and 0.02mm/s at the base of the building.

Figure 7.19 illustrates the response at the second observation position, the front corner column in the case of a 4-story RC building, constructed at 30m from the track. The most dominant vibrations peaks are located at 14.2Hz, 17.8Hz, 21.5Hz and 24.9Hz. The amplitude of those peaks is gradually decreasing for higher frequencies. More specifically, on the 4th floor of the building, the vibrations peak at 14.2Hz is equal to 0.075mm/s and is gradually reduced to 0.03mm/s. The same observation is made at the building base, although the amplitude is slightly lower in this position. For instance, in this position, the vibrations peaks at 14.2Hz and 17.8Hz are equal to 0.06mm/s and 0.04mm/s, respectively.

According to Figures 7.19a-7.19b, the implementation of a second trench has not significantly contributed to further reducing the vibrations level at the top of the building. For instance, the implementation of a single trench decreases the most dominant vibrations peak at 14.2Hz from 0.075mm/s to 0.06mm/s (see Figure 7.19a). The same amplitude is equal to 0.053mm/s in the case of the double trench, as it is depicted in Figure 7.19b. Figure 7.19c demonstrates the vibrations level at the base of the building after the implementation of the single trench across the railway line. Herein, the examined mitigation approach slightly minimizes the peaks at 14.2Hz and 17.8Hz from 0.06mm/s and 0.04mm/s to 0.05mm/s and 0.03mm/s, respectively. The reduction of those peaks is even higher after implementing the double trench, as illustrated in Figure 7.19d. It should be mentioned that both examined approaches remarkably mitigate over 70% of the amplitude of the vibration peak at 21.5Hz.

Figure 7.20 depicts the vibrations peaks of the most critical observation position of the 4th floor, the edge of the front cantilever. In this case, the vibrations peaks are located at the same frequency as the previously examined position (4_b), although their values are significantly higher. For instance, the vibrations peaks at 14.2 Hz and 24.9 Hz are the only peaks (of all the examined observation positions when the building is constructed at 30m from the track), with amplitude higher than 0.1mm/s.
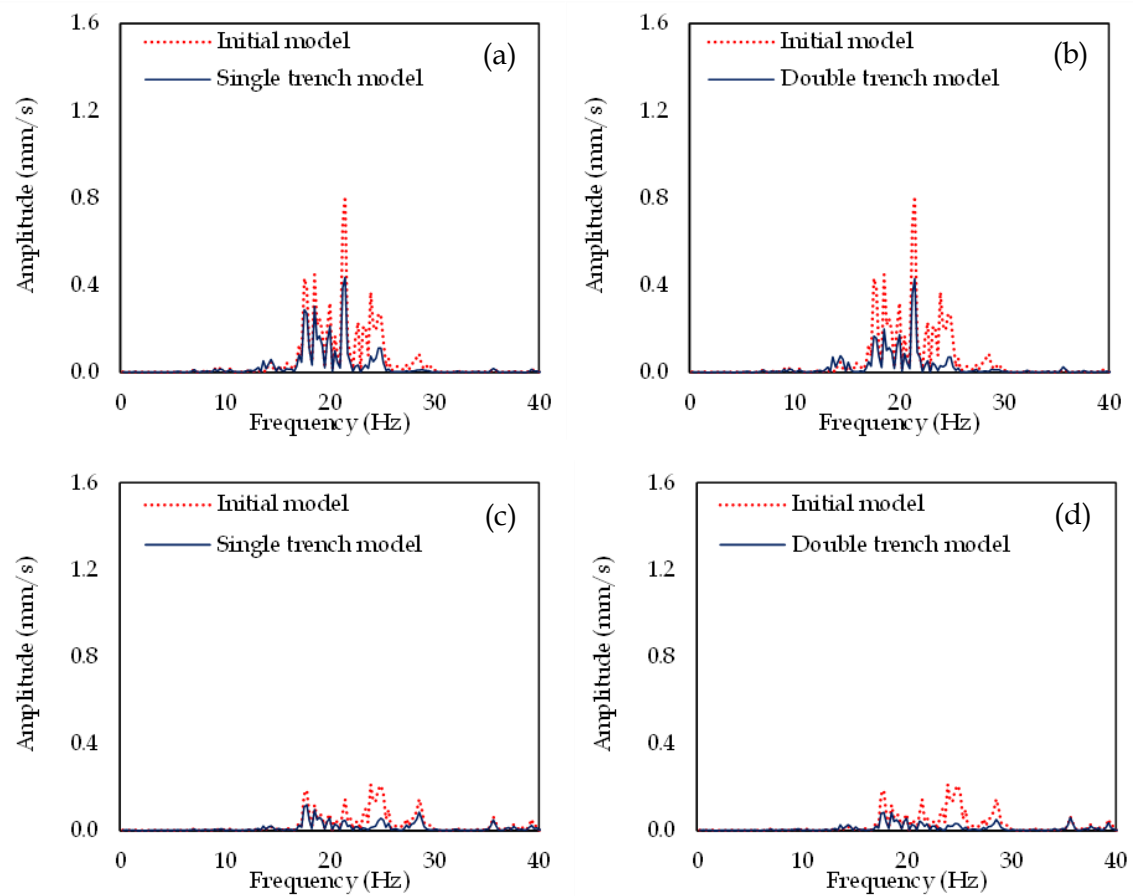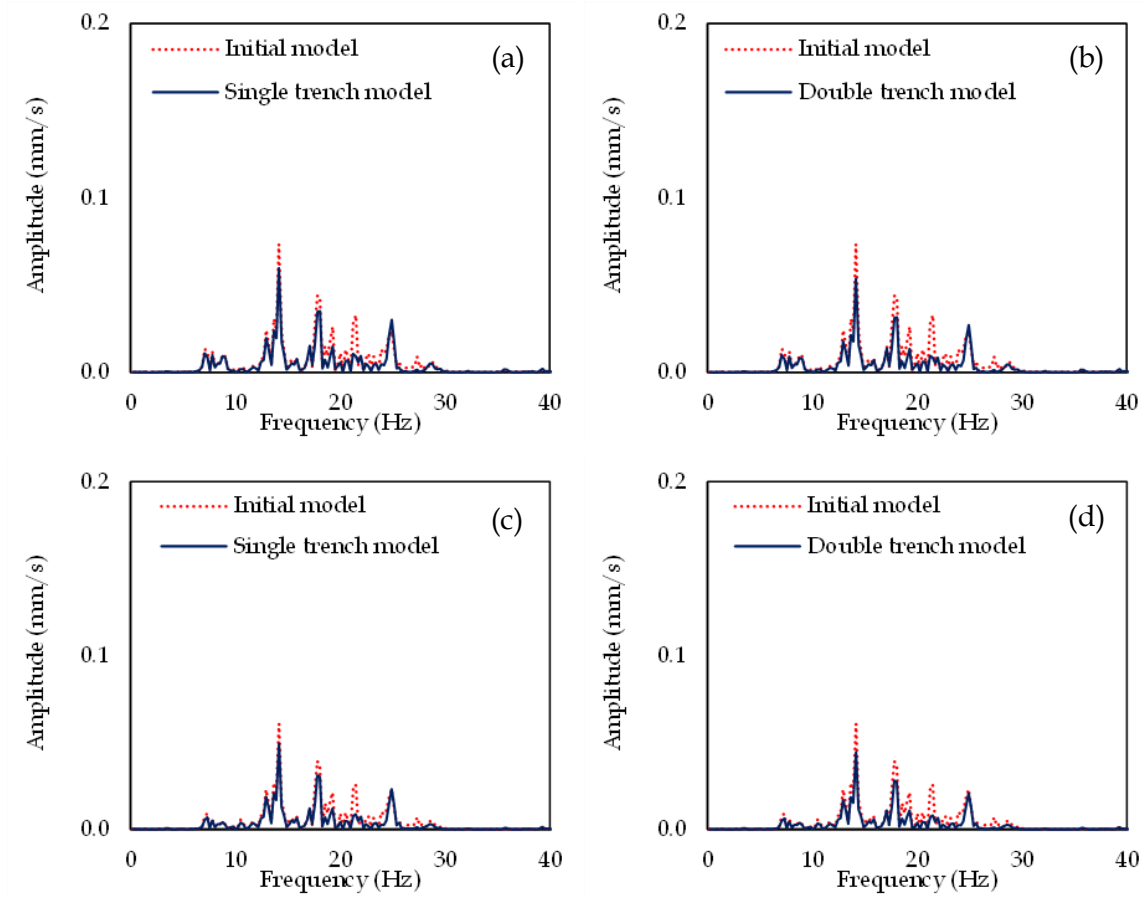
Figure 7.19 Fourier spectra at the front corner column at 30m from the track in the modeling scenario of a single trench ((a) base, (b) 4th floor), double trench ((a) base, (b) 4th floor).
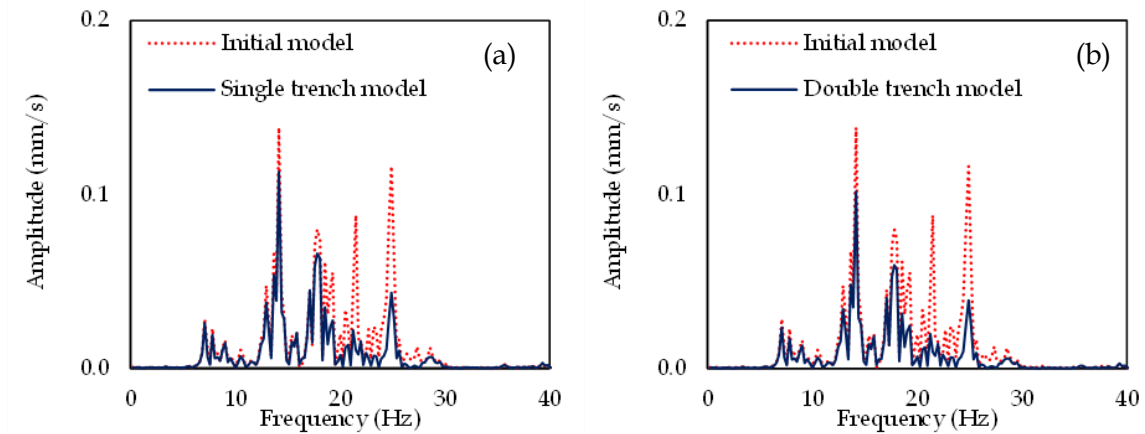
Figure 7.20 Fourier spectra at the cantilever of the 4th floor at 20m from the track in the modeling scenario of a single trench and double trench.

Furthermore, the other two vibrations peaks at 17.8Hz and 21.5Hz are close to 0.085mm/s. The single trench implementation across the track reduces the most dominant vibrations peak from 0.13mm/s to 0.11mm/s. In addition, the level of vibrations reduction is equal to 70% at 24.9Hz. In general, this mitigation approach is more effective for frequencies higher than 20Hz. The same observation has been made for the double EPS–

filled trench, as illustrated in Figure 7.20b. In this case, the reduction level is even higher, as this approach manages to reduce all the vibrations peaks below 0.1mm/s.

7.2.4. 8-story building

7.2.4.1. 8-story building structural response

In previous section, the 4-story building response to HST-induced vibrations has been examined and the efficacy of the single or double trench implementation has been compared. In general, the main remark of this investigation is that the double trench is the most efficient mitigation approach. Herein, the study is expanded by investigating the response of an 8-story building with an identical typical floor with the previously examined 4-story building (see Figure 7.2).
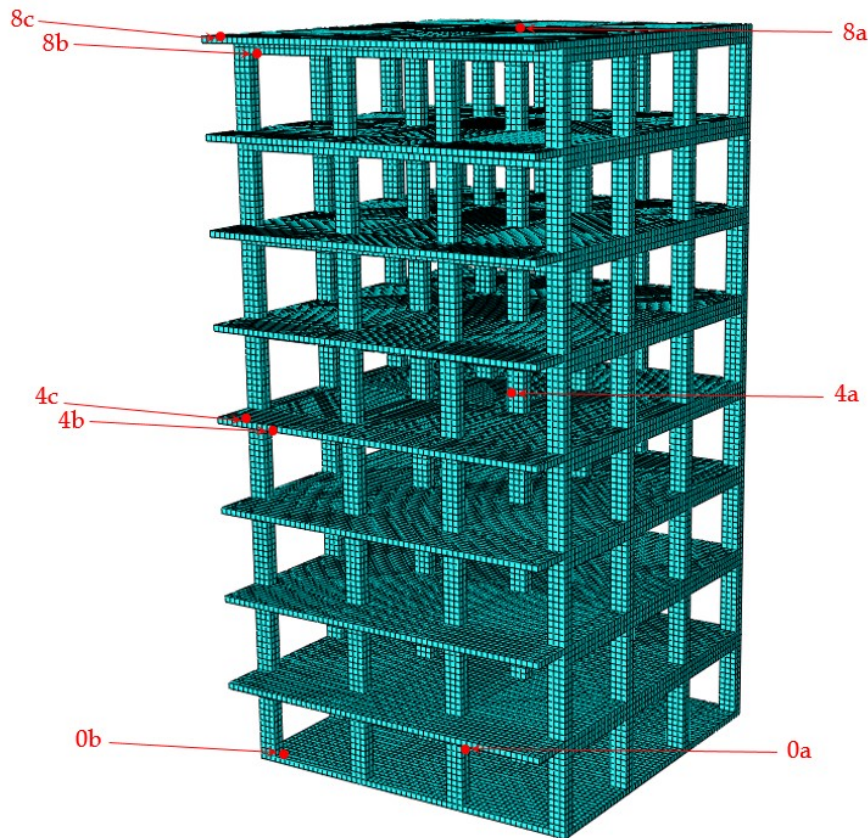
Figure 7.21 Observation points.

Initially, the commonly used indicator of the vibrations amplitude from the HST passage, velocity decibels (V_{dB}) is examined at the same with the previous case, five observation positions (two at the base and three at the 4th floor of the building) and three more new observation position at the 8th floor of the building. Hence, the three positions,

which have been examined on each floor, are the center of the bases slab (a_i), the front corner column (b_i) and the edge of the cantilever (c_i), where i is the number of the building floor. Figure 7.21 summarizes all the examined observation positions.

The response of the 8-story building due to the developing vibrations at each floor center by the passage of Thalys HST with 240km/h are summarized in the 1/3 octave bands of Figure 7.22. The most dominant octave band is the 13th, where the V_{dB} is equal to 62dB at the base level when the building is constructed at 10m from the track. This value is increased to 66dB and 70dB on the 4th and 8th floor, respectively. In general, the decibel level increases gradually on the upper floors at all the octave bands with central frequencies between 1.25Hz and 25Hz. On the other hand, the decibel level of the last three examined octave bands is significantly reduced on the upper floors, as shown in Figure 7.22a. Figure 7.22b illustrates the low-frequency octave bands at the same observation positions when the building is constructed at 30m from the track. The most dominant octave band remains the 13th, although the amplitude is significantly lower. In this case, the decibel level increases for the octave bands with central frequencies between 4 Hz and 25Hz. On the other hand, the decibel level is reduced at the octave bands with frequencies lower than 4Hz or higher than 25Hz.
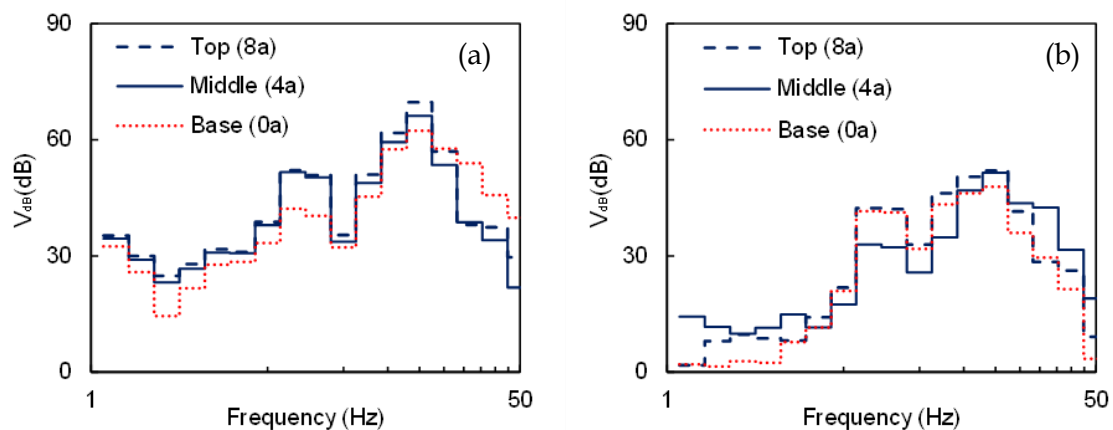
Figure 7.22 Central slab response of the 4-story building in terms of 1/3 octave bands when the building is constructed at (a) 10m from the track, (b) 30m from the track.

In the sequence, the decibel level at the second observation position, the front corner column is presented. Figure 7.23a compares the vibrations level on each low-frequency octave band at the three examined floors in the modeling scenario for which the building is located at 10m from the track. At the base, the decibel level is higher than 60dB at the octave bands with central frequencies 16Hz, 20Hz and 25Hz. In general, the vibrations level is slightly increased on the 4th floor, except for the last 4 octave bands, where the

decibel level is reduced. On the 8th floor, the decibel level is even higher. Herein, the decibel level is higher than the building base for all the examined octave bands. In the modeling scenario for which the building is constructed at 30m from the track, the decibel level remains below 50dB at the whole frequency range, as illustrated in Figure 7.23b. The decibel level is not significantly increased on the 4th and the 8th floor of the building. In some cases, such as at the octave band with central frequency 2Hz, the vibrations level is reduced. On the other hand, several octave bands, such as the 12th, where the decibel level, are increased.
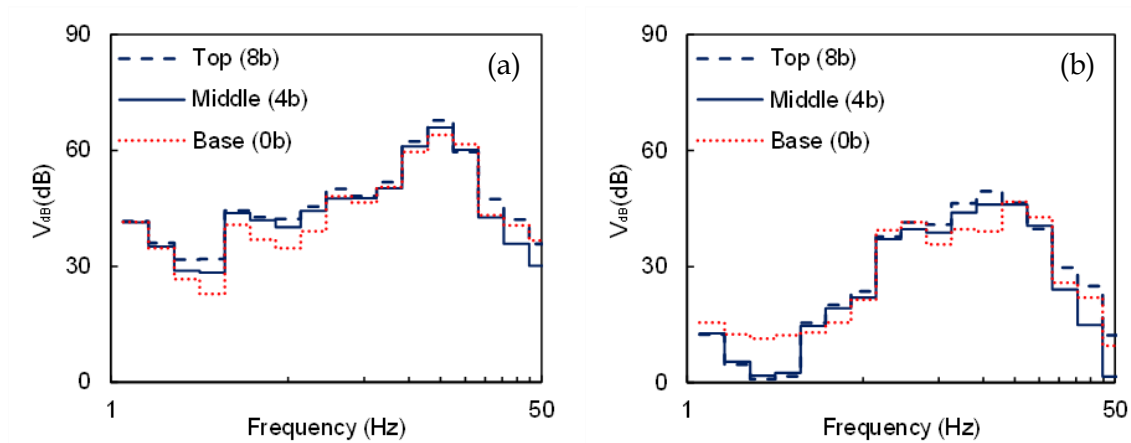
Figure 7.23 Column response of the 4-story building, constructed at (a) 10m from the track, (b) 30m from the track, in terms of 1/3 octave bands.
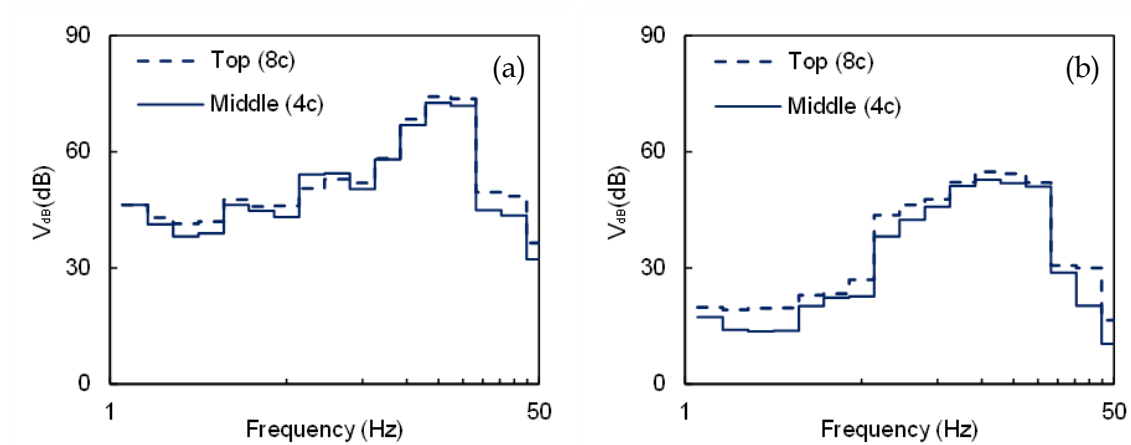
Figure 7.24 Cantilever response of the 4-story building, constructed at (a) 10m from the track, (b) 30m from the track, in terms of 1/3 octave bands.

Figure 7.24 depicts the last examined observation positions at the edge of the 4th and 8th floors cantilevers. As mentioned, this position is the most critical, as the higher decibel level is observed there. The most dominant octave bands are the 13th and 14th in the case of a building constructed at 10m from the track, as illustrated in Figure 7.24a. More specifically, the decibel level at those octave bands on the 4th floor is close to 74dB. The

same value is 2dB higher on the 8th floor. The same trend has been observed in the building case at 30m from the track (see Figure 7.24b). In this case, the decibel level is increased between 1dB and 10dB on the 8th floor for all the examined octave bands. Furthermore, at the octave bands with central frequencies 16Hz, 20Hz and 25Hz, the decibel level is higher than 50dB.
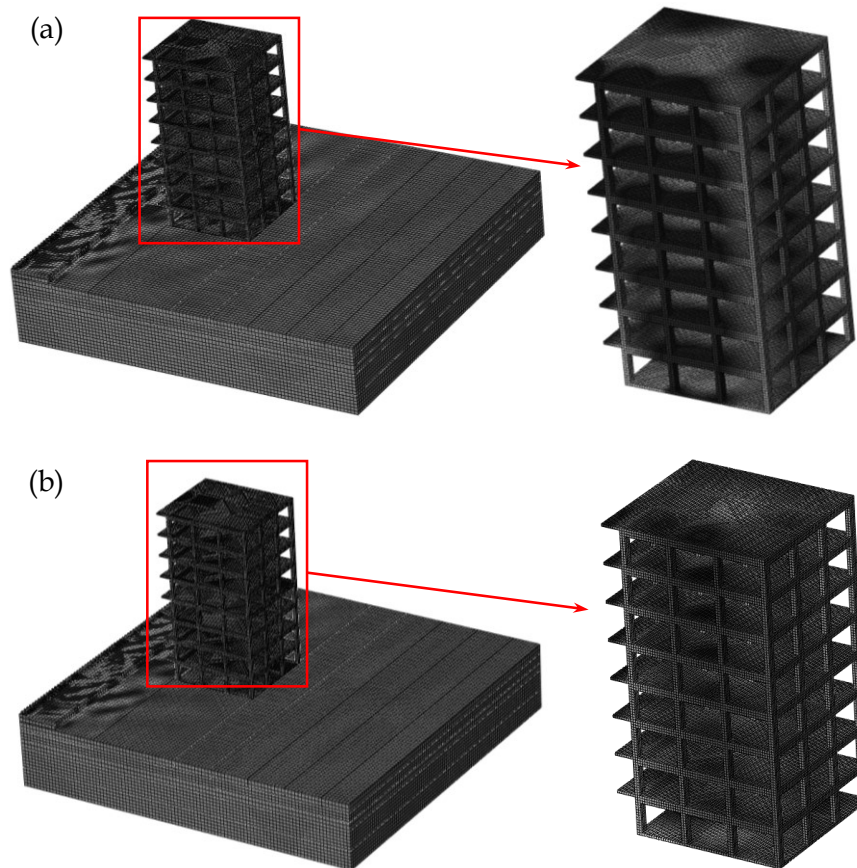
Figure 7.25 Typical contour plots of vertical velocity at the soil surface in the modeling scenario for which the 8-story building is constructed at 10m from the rails (a) without trenches and (b) with double EPS-filled trenches.

7.2.4.2. *8-story building protection with the use of double EPS–filled trench*

As it has been presented in the case of the 4-story building, the implementation of double EPS-filled trenches is the most effective mitigation approach compared to the implementation of just one trench. In the present Section, the protection of the 8-story building with the use of a double EPS-filled trench is examined. Initially, some contour plots of the vibrations propagation in terms of vertical velocity are demonstrated in Figure 7.25, aiming to depict the beneficial role of the double in-filled trenches. The first contour plot shows the propagation of the vibrations in the modelling scenario for which no mitigation measures have been applied to the track (see Figure 7.25a). In this case, a wide

spreading of the waves is observed at the surrounding soil surface and the effect on the 8-story building is significant. Figure 7.25b depicts the spread of the vibrations after implementing the double EPS-filled trench, which leads to the decrease of the vibrations scattering.

Consequently, the insertion loss curves have been drawn in order to present the effectiveness of the proposed mitigation approach. Figure 7.26a presents the IL curves at the three examined observation positions on the 4th floor in the case of an 8-story building constructed at 10m from the track. At the lower examined octave bands with central frequencies between 1.25Hz and 5Hz reaches in some cases higher than 5dB. For instance, the IL is close to 6dB at the 5th octave band at the front corner column and at the 6th octave band at the edge of the cantilever.
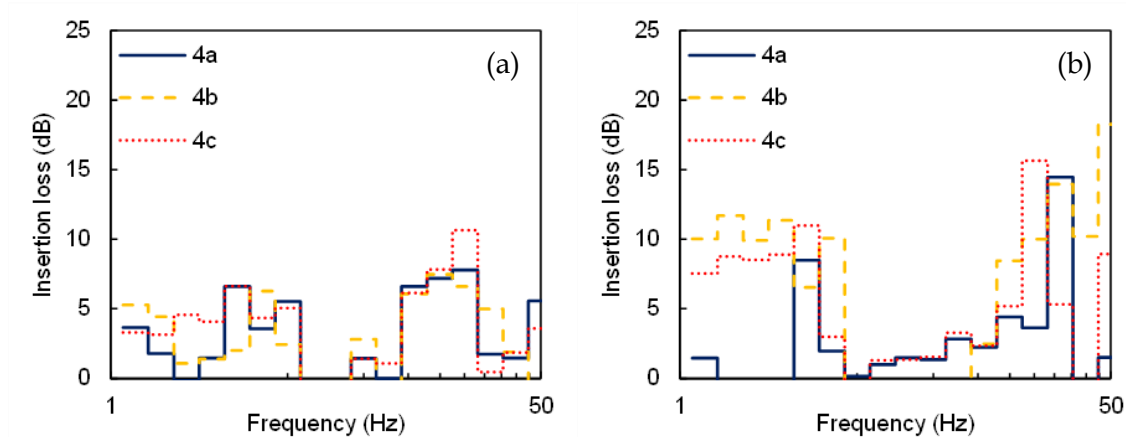
Figure 7.26 IL curves on the 4th floor of the building at (a) 10m from the track, (b) 30m from the track.

On the other hand, the double trench is not effective at the middle range octave bands with centre frequencies between 6.3Hz and 12.5Hz. As it was aforementioned, the most dominant vibrations are located in the octave bands with centre frequencies 16Hz, 20Hz, 25Hz. It is evident that the implementation of the double EPS-filled trench has led to remarkably high values of insertion loss. Thus, the insertion loss at those octave bands ranges between 7dB and 9dB at the first two observation positions (e.g., 4_a and 4_b). Furthermore, the insertion loss is higher than 11dB at the 14th octave band at the edge of the cantilever.

The same observation has been made at 30m from the track, as illustrated in Figure 7.26b. At the first 6 octave bands, the insertion loss ranges between 8dB and 12dB at the observation points 4_b and 4_c. In addition, the insertion loss is significantly increased at the

higher octave bands, reaching in some cases values higher than 15dB. More specifically, the insertion loss at the 15th octave band is equal to 15dB at the central slab and the front corner column of the 4th floor. Furthermore, it should be mentioned that the insertion loss is equal to 17dB at the most dominant octave band (e.g., 14th) at the edge of the cantilever. In general, the implementation of the double trench across the track has a beneficial role in the reduction of the structural vibrations on the 4th floor of the building.

Figure 7.27 presents the insertion loss of the double EPS-filled trench at the top floor of the building. It is evident that the vibrations reduction is slightly lower than the 4th floor of the building. If the building has been placed at 10m from the track (see Figure 7.27a), the insertion loss at the most dominant octave bands (e.g., 12th, 13th, 14th) is higher than 5dB at all the examined observation positions. Furthermore, at the edge of the cantilever, the insertion loss reaches close to 10dB at the 14th octave band. In general, the insertion loss level is decent, although it is slightly lower than the same values on the 4th floor. The highest values of insertion loss have been observed in the modelling scenario for which the building has been constructed at 30m from the track, as illustrated in Figure 7.27b. More specifically, at the edge of the cantilever, the insertion loss at the octave band with low centre frequencies ranges between 10dB and 15dB. Additionally, the reduction of the decibel level at the most dominant frequencies (e.g., 13th, 14th) reaches over 9dB.
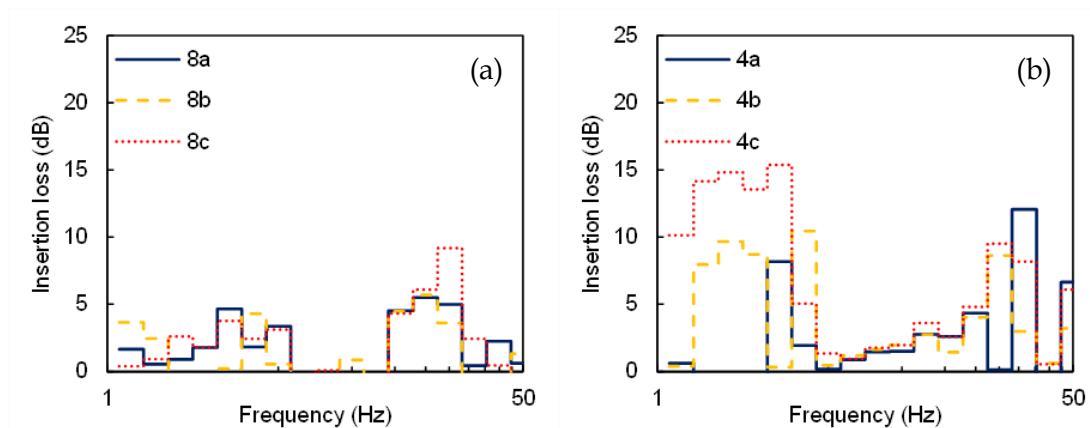
Figure 7.27 IL curves on the 8th floor of the building at (a) 10m from the track, (b) 30m from the track.

Table 7.4 summarizes decibel level at the most dominant octave bands, before and after the implementation of the double EPS-filled trench on the 4th floor of the 8-story building. Similar to the 4-story building, the vibrations level has been compared to the proposed thresholds by WHO to protect the residents from adverse health issues (54dB) and adverse effects on sleep (44dB). In the modelling scenario for which the building is

constructed at 10m from the track, the vibrations level exceeds the WHO threshold at all dominant frequencies for all the three examined observation points before implementing the double trench.

The implementation of the mitigation measure has led to a significant reduction of the vibrations level. Thus, in some cases, the vibrations level has been minimized under the limit value of 54dB. However, the decibel level remains high at some dominant octave band; hence the building construction at 10m from the track is not recommended. On the other hand, when the building is constructed at 30m from the track, the initial decibel level is significantly lower, as it remains lower than 54dB at all the examined octave bands, although the implementation of the double trench leads to further reduction. Hence, in several cases, the decibel level has reduced below 44dB.

Table 7.4. The decibel level of the most dominant octave bands on the 4th floor.

Observation position	Centre Frequency (Hz)	10m from the track		30m from the track	
		Initial V_{dB} (dB)	Mitigated V_{dB} (dB)	Initial V_{dB} (dB)	Mitigated V_{dB} (dB)
	16	59	51	47	47
4a	20	66	57	51	45
	25	55	51	44	37
	16	61	54	46	44
4b	20	66	57	46	42
	25	60	54	41	42
	16	67	59	53	48
4c	20	73	54	52	42
	25	72	61	51	48

In the sequence, the most dominant frequencies decibel level at the top of the building are summarized in Table 7.5. The decibel level at the top floor remains higher than 54dB and it is from 1dB to 3dB higher than the same value at the 4th floor (see Table 7.4), in the modelling scenario for which the building is constructed at 10m from the track. The implementation of the double trench, has significantly reduced the vibrations level, although it could not minimize the decibel level at all the dominant octave bands below 54dB. On the other hand, the initial decibel level is below 54dB at all dominant octave bands except the octave band with a centre frequency 16Hz at the edge of the cantilever. After the mitigation, the decibel level ranges between 28dB and 51dB.

Table 7.5. The decibel level of the most dominant octave bands on the 8th floor.

Observation position	Centre Frequency (Hz)	10m from the track		30m from the track	
		Initial V_{dB} (dB)	Mitigated V_{dB} (dB)	Initial V_{dB} (dB)	Mitigated V_{dB} (dB)
	16	62	57	50	45
4a	20	69	64	52	48
	25	57	51	42	28
	16	62	57	49	44
4b	20	68	62	46	41
	25	61	54	40	30
	16	68	63	55	51
4c	20	74	67	54	49
	25	74	64	52	42

Figure 7. 28 Typical building near the Paris – Brussels HSR in Belgium: (a) two story building, (b) single story building, (c) buildings constructed close to the line.

7.3. *Masonry infrastructure buildings*

7.3.1. *Numerical model modification*

In the previous sections, the response of multi-story RC buildings to the passage of HST has been presented to examine the optimal construction distance to protect the resident from problems associated with adverse health effects. It is evident that the use of EPS trenches has significantly mitigated the developing vibrations. For this reason, throughout an investigation into the existing buildings across the Paris-Brussels HSR line has been carried out to investigate such types of buildings protection with the use of EPS geofoam.

Figure 7.28 demonstrates some typical buildings constructed at small distances from the track, close to the southwest borders of Belgium.

In this area, the majority of the buildings are masonry or RC single (see Figure 7.28a) or double (see Figure 7.28b) story residential buildings with rectangular floor plans. Furthermore, the HSR line passes from residential areas at distances between 30m and 35m from the track, as illustrated in Figure 7.28b. Furthermore, except for the residential buildings, several masonry single story buildings are constructed at distances between 10m and 15m from the track. Figure 7.29 presents one of those buildings constructed at 12m from the track, which might be a part of the HSR lines infrastructure.

Figure 7.29 HSR infrastructure building at a distance of around 15m from the track.

In this Section, the propagation of the HST-induced vibrations to the nearby masonry buildings is investigated and the use of EPS geofoam has been proposed in order to reduce the structural vibrations on the buildings (Lyratzakis et al., 2020f). For this purpose, the pre-validated model of the at-grade site of the Paris-Brussels line has been modified by adding the examined masonry buildings at 10m from the track. The properties of the proposed numerical model are adequately described in Chapter 3.

Two typical masonry buildings, a single and a double story have been selected for the study. Each story of the buildings has a height equal to 3m and 10m x 5m floor-plan. For the building foundation, the masonry walls have been extended at 0.5m in the soil. The building roof has 30º degrees of inclination and is constructed from wooden beams with 3m spacing. The thickness of the building has been set equal to 40cm. The buildings have been discretized using 4-noded solid finite elements, as it is illustrated in Figure 7.30.
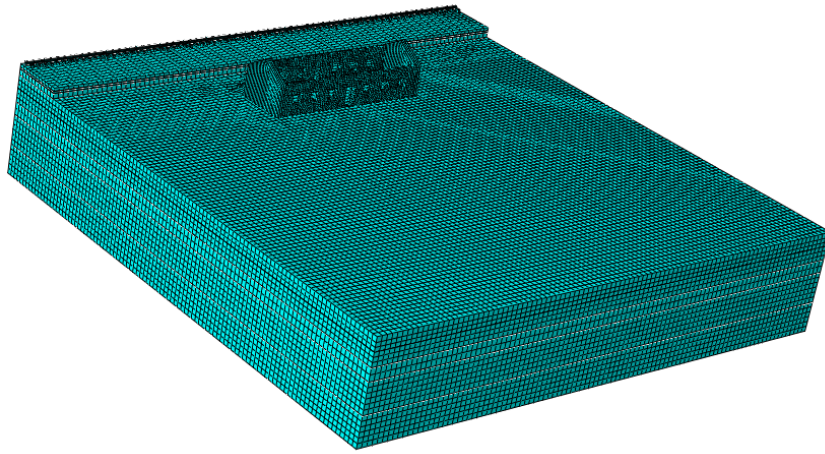
Figure 7.30 Single-story masonry building numerical model.

7.3.1.1. *Description of mechanical properties of the masonry buildings*

One of the main issues in numerical modeling and assessment of masonry buildings is the availability of reliable mechanical parameters. Reference values of the main mechanical parameters of masonry (elastic modulus, shear and compressive strength) are provided in the literature for various stone and brick types, based on available data that can be found in norms (e.g., Eurocode 6) or experimental tests. The calculation of the compressive strength, f_k, of masonry with standard mortar us derived according to Eurocode 6 (EC6, 2005):

$$f_k = \kappa f_b^{0.7} f_m^{0.3} \qquad (7.1)$$

where coefficient κ is derived from EC6 for manufactured natural stones and standard mortar to be equal to 0.45. For the compressive strength of stones, f_b, and mortar, f_m, two rather conservative values were used: 35 and 0.5 MPa, respectively, which are within the typical range of values for real masonry buildings. The compressive design strength has been computed using a safety coefficient of γ_m = 2. Based on these values, the compressive strength of the masonry is equal to 2.2 MPa. The tensile strength of the load-bearing masonry is calculated based on the compressive strength of the mortar. The tensile strength of the masonry along the joints is equal to ¼ of f_m, while with respect to the vertical direction it is equal to ½ f_m. Therefore, the tensile strength of the masonry parallel and perpendicular to the joints is $f_{t//}$ = 0.125 MPa and $f_{t\perp}$ = 0.25 MPa, respectively.

Young's modulus of the load-bearing masonry is calculated analogous to the compressive strength (E = 1000 f_k) and is equal to E = 2.2 GPa [EC6 (3.7.2.)]. For Poisson's ratio, the typical value of v = 0.3 is used. Wooden members in the models are assumed to

be constructed by wood material of type C24, according to Eurocode 5 guidelines. The mechanical properties of this material are as follows: the tensile strength parallel and perpendicular to the fibers is $f_{t//} = 14$ MPa and $f_{t\perp} = 0.5$ MPa, respectively; the compressive strength parallel and perpendicular to the fibers is $f_{c//} = 21$ MPa and $f_{c\perp} = 2.5$ MPa, respectively; Poisson's ratio is $v = 0.4$; Young's modulus is $E = 11$ GPa; density is $\rho = 350$ kg/m³.

7.3.2. Single story masonry building

7.3.2.1. Masonry buildings structural response

In the sequence, the velocity decibels (V_{dB}) are presented at four observation points on each of the buildings. The building front wall center and corner at the levels of the foundation and the roof have been chosen for the investigation. Figure 7.31a depicts the response to the passage of Thalys HST on the corner of the front wall. The most dominant octave bands are the 12th, 13th, 14th and 16th, where the vibrations levels at the soil range between 70dB and 80dB. As expected, the vibrations level at the most dominant octave bands has been increased at the top of the building compared to the same position at the base. The increase is lower than the pre-examined RC buildings due to the low height of the building.
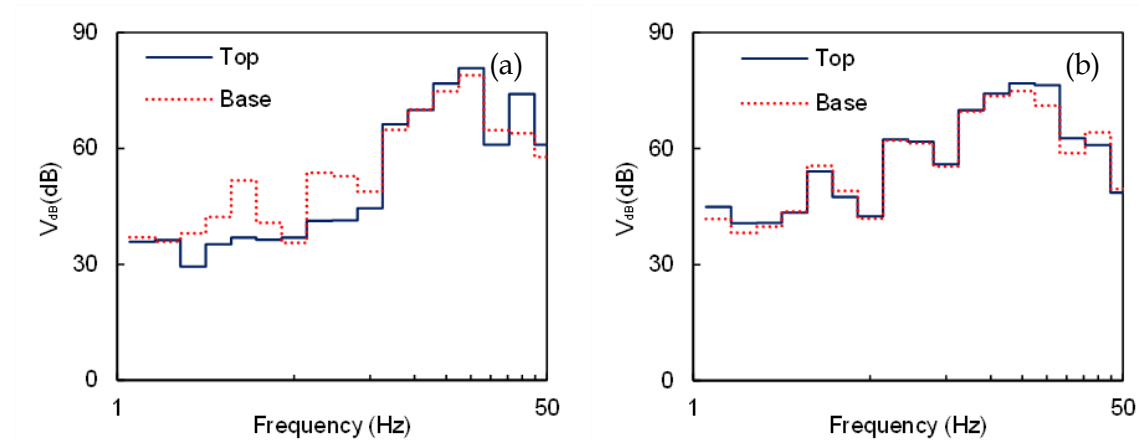
Figure 7.31 Masonry infrastructure building response in terms of 1/3 octave bands (a) at the center of the front wall, (b) at the corner of the front wall.

Furthermore, the decibel level at octave bands with centre frequencies lower than 10Hz is significantly lower than the higher octave bands and is reduced at the top of the building. The decibel level ranges between 35dB and 60dB at the foundation level for all the first 10 octave bands. Those values are significantly decreased at the top of the building. The level of reduction in some of those cases reaches close to 11dB. Figure 7.31b

shows the structural response of the single-story masonry building in terms of 1/3 octave bands at the corner of the front wall. In this case, the 1/3 octave bands with centre frequencies 16Hz, 20Hz and 25Hz are again the most dominant, as the vibrations level is higher than 70dB at the base of the building. Those values are slightly increased at the top of the buildings. For instance, the decibel level at the 14th octave band is increased from 70dB to 75dB. In general, the decibel level at this observation position has not significantly changed at the top of the building.

7.3.2.2. *Single-story masonry building protection with the use of EPS – geofoam*

In order to protect pre-existed masonry buildings, several mitigation configurations with the use of EPS geofoam have been investigated. In this Section, the double trench has not been examined, in contrast with the previous sections, where the implementation of double trenches has led to a remarkable reduction of RC buildings structural vibrations. Herein, the assumption has been made that the implementation of a double trench at pre-existed buildings is not a realistic option due to space limitation, as in most cases, roads are running between the buildings and the HSR.
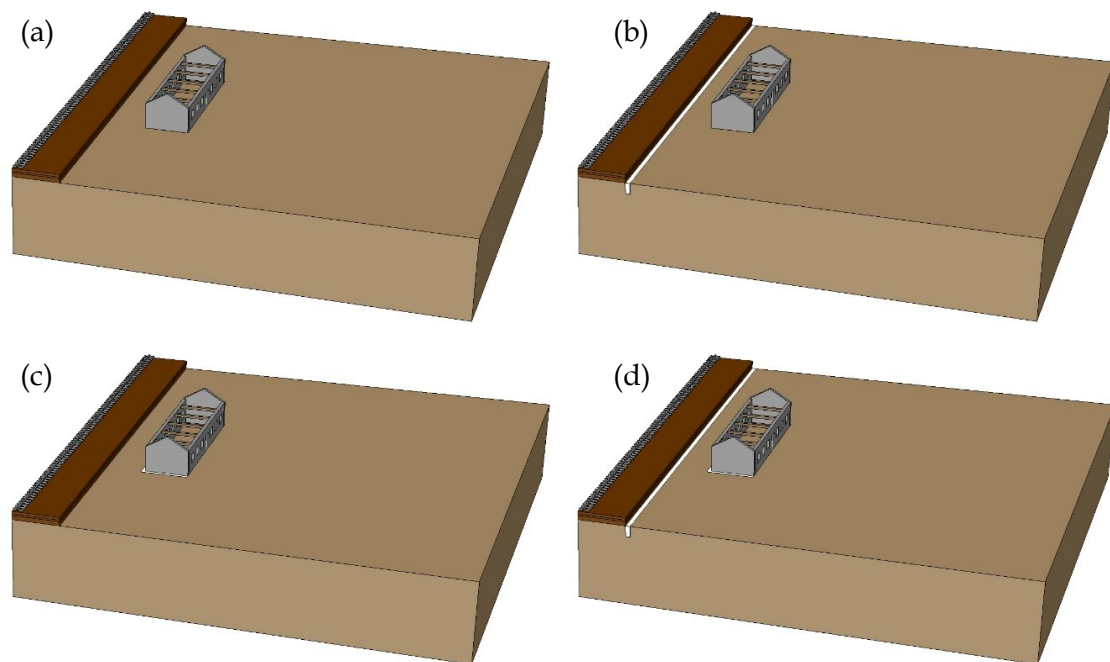
Figure 7.32 (a) Unretrofitted building, (b) protected building with single trench across the track, (c) protected building with trench across the building foundation, and (d) protected building with hybrid trench method.

Figure 7.32b demonstrates the first mitigation approach, according to which a single EPS-filled trench has been constructed across the HSR line. The EPS-filled trench has the

same geometrical properties as the single barrier, which has been investigated previously in the case of the 4-story RC building. According to the second mitigation approach (see Figure 7.32c), the EPS-filled trench has been placed in front of the building foundation. The last mitigation scenario is a hybrid approach, merging the first two examined mitigation measures, as illustrated in Figure 7.32d.
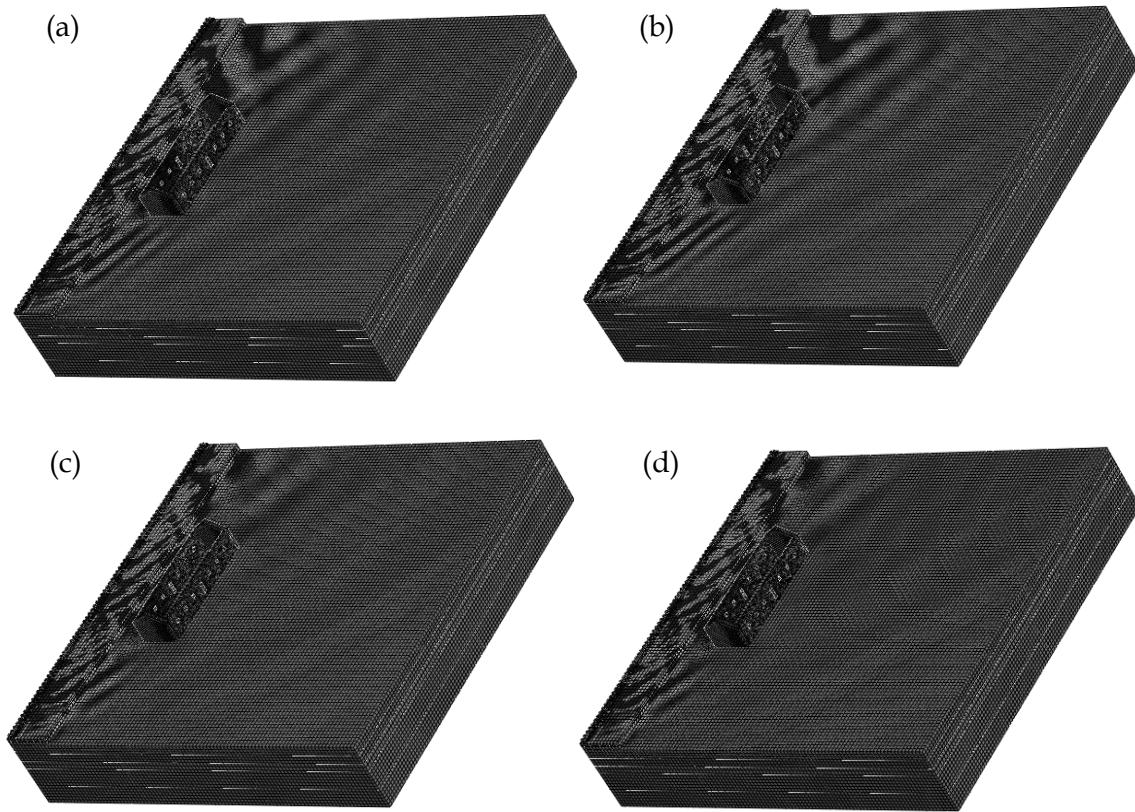
Figure 7.33 Typical contour plots of vertical velocity at the soil surface in the modeling scenario of a single store building constructed at 15m from the rails (a) initial model, (b) EPS-filled trench around the foundation of the building, (c) EPS-filled trench across the track, (d) double EPS-filled trench.

Figure 7.33. depicts four contour plots of the surface waves propagation, aiming to compare the efficacy of the three proposed mitigation approaches. Initially, no mitigation measures have been applied to the model. In this case, the surface waves are widely spread, reaching distances further than the building position, as illustrated in Figure 7.33a. The same trend has been observed after implementing the trench in front of the building foundation (see Figure 7.33c). In this case, the waves spread has been slightly reduced, especially around the building, although the level of reduction is low. On the other hand, the implementation of the single EPS-filled trench across the track led to a remarkable reduction of the propagated waves. It is evident from Figure 7.33b that the spread of the

waves at the back of the building has been virtual disappeared. The reduction of the vibrations level is even more pronounced in the hybrid mitigation approach, as demonstrated in Figure 7.33d.

In order to further illustrate the mitigation level of the examined configurations, the insertion loss curves of each approach are presented. Figure 7.34 shows the IL curves at the first observation position, the center of the front wall. At the lower examined octave bands with central frequencies between 1.25Hz and 5Hz, the insertion loss in the case of the implementation of a trench across the track reaches substantially high values at both foundation and roof levels. For instance, the insertion loss at the second octave band is equal to 11dB at the building base, as illustrated in Figure 7.34a. Furthermore, the insertion loss reaches 10dB and 8dB at the 4th and 5th octave bands at the level of the building roof (see Figure 7.34b). As it was aforementioned, the octave bands with centre frequencies higher than 12.5Hz are the most critical. The insertion loss at the octave bands with centre frequencies between 12.5Hz and 25Hz ranges from 3dB to 5dB and from 4dB to 7dB at the level of foundation and roof, respectively. The insertion loss is even more pronounced in the case of the octave band with a central frequency 31.5Hz is close to 15dB at the top of the building.
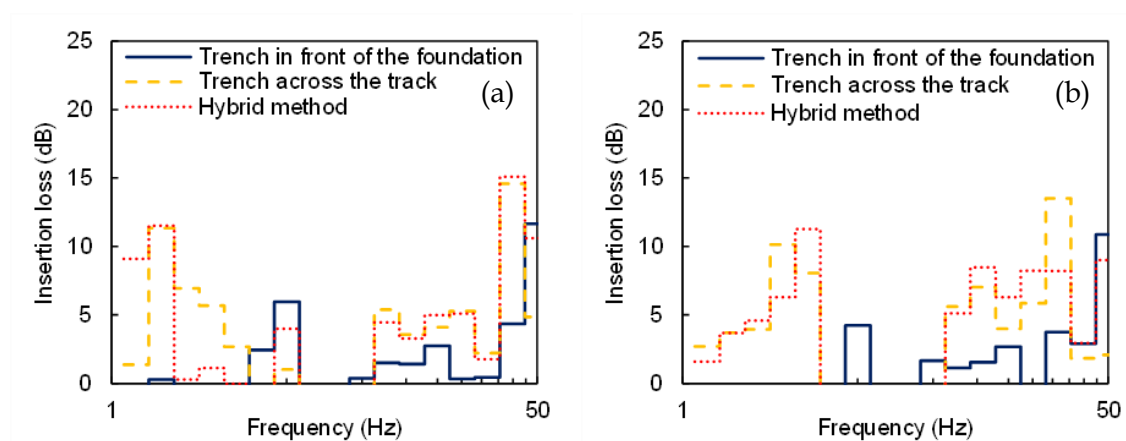
Figure 7.34 IL curves at the level of the (a) base, (b) top of the building at the center of the front wall.

On the other hand, the efficiency of the EPS-trench implementation in front of the building foundation is not as effective as the previously examined approach. It is evident that the insertion loss is zero or almost zero for all the low-frequency bands at both examined nodes. Furthermore, the insertion loss at the top of the building at the most dominant octave bands is lower than 3dB. The highest insertion loss, equal to 11dB, is observed at the last octave band, although this value is not essential as the initial decibel

level of this octave band is already low. The last examined EPS configuration (e.g., the hybrid method) has led to insertion losses comparable to implementing a single trench in front of the track. Hence, this approach is practical, although it is not recommended.

The same observation is made at the second position, at the corner of the front wall, as depicted in Figure 7.35. Implementing a trench around the building foundation has led to a mediocre level of insertion loss. In some cases, at the top of the building, especially at the lower octave bands, the insertion loss reaches values higher than 5dB. However, this mitigation approach has not significantly reduced the decibel level of the most dominant octave bands. For instance, the insertion loss remains lower than 4dB at both observation points for the octave bands with central frequencies between 12.5Hz and 25Hz, which are the most critical. Hence, the assumption could be made that the implementation of EPS around the building foundation is not the optimal mitigation approach.
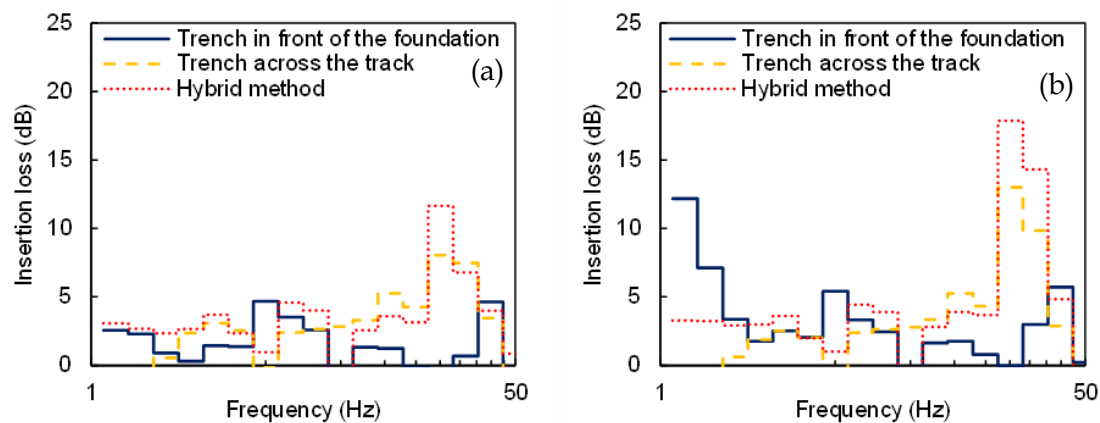
Figure 7.35 IL curves at the level of the (a) base, (b) top of the building at the corner of the front wall.

On the other hand, implementing a single EPS-filled trench across the track is significantly more efficient, especially at the most dominant octave bands. More specifically, the insertion loss reaches close to 8dB and 11dB at the octave band with centre frequency 25Hz, at the base and the top of the building, respectively. The use of the hybrid method increases, even more the insertion loss at the 14th octave band, reaching the top value of 18dB at the top of the building. In the case of the single-store masonry building, the implementation of the examined mitigation approaches could not manage to reduce the vibrations level below the WHO threshold, although the constructed buildings at those distances from the track are not commonly residential. Therefore, the reduction of vibrations might be acceptable for HSR infrastructure building in order to protect sensitive equipment in the building.

7.3.3. 2-story masonry building

7.3.3.1. 2-story masonry building structural response

The last examined case is a 2-story masonry building with the same floor-plan as the single-story building. Figure 7.36 illustrates the velocity decibel level at the octave bands with central frequencies between 1.25Hz and 50Hz for all the observation positions (e.g., the center and the corner of the front wall of the building at the levels of the soil and the roof). The most dominant 1/3 octave bands at the center of the front floor are those with central frequencies higher than 12.5Hz. The decibel level is higher than 55dB at those octave bands at both the base and the 2nd floor, as illustrated in Figure 7.36a. Furthermore, the decibel level is increased at the top of the building at most high-frequency octave bands. For instance, the vibrations level increase reaches 6dB and 15dB at the 13th and 15th octave bands, respectively. On the other hand, the decibel level at the octave bands with centre frequencies lower than 11Hz remains below 50dB. Furthermore, some of those values are increased and others are reduced at the top of the building. Hence, in general, the decibel level remains the same in those octave bands.
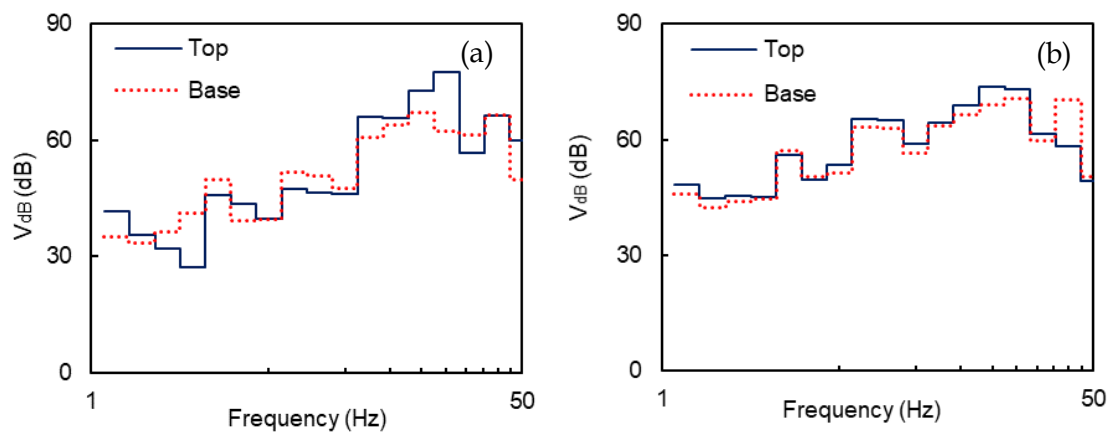
Figure 7.36 Masonry infrastructure building response in terms of 1/3 octave bands (a) at the center of the front wall, (b) at the corner of the front wall.

Figure 7.36b depicts the vertical decibel at the second observation position (e.g., the front corner of the building), at the foundation and the roof levels. In this case, the decibel level is increased at the octave bands with higher centre frequencies, although the difference with the decibel level of the octave bands with lower frequencies is even more negligible. The most dominant octave bands are the 13th, the 14th and the 15th, where the decibel level is close to 70dB. The decibel level in the majority of the octave bands increases between 1dB and 4dB. The highest increase is observed at the 13th octave band. On the other hand, the decibel level is reduced from 59dB to 69dB at the 15th octave band.

However, in general, the octave bands remain at a comparable level at both examined positions.

7.3.3.2. *2-story masonry building protection with the use of EPS – geofoam*

In the sequence, the examined mitigation approaches in the case of the single-story building (e.g., single EPS-filled trench across the track, EPS-filled trench around the building foundation and hybrid method) are implemented at the 2-story masonry building. The contour plots of the surface waves scattering in the case of the 2-story building before and after the implementation of the examined mitigation configurations are illustrated in Figure 7.37. The spread of the surface waves is significantly higher in the initial model (see Figure 7.37a) than the models after implementing the EPS configurations.
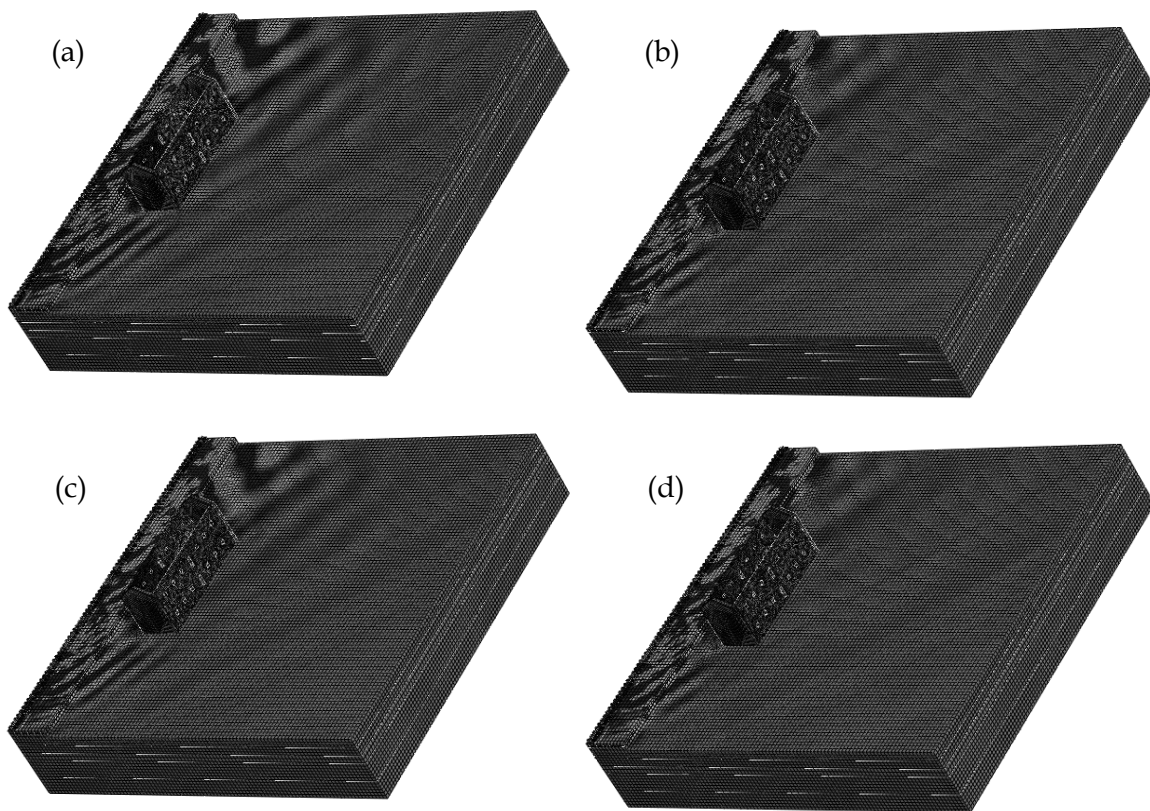
Figure 7.37 Typical contour plots of vertical velocity at the soil surface in the modeling scenario of a double store building constructed at 15m from the rails (a) initial model, (b) EPS-filled trench around the foundation of the building, (c) EPS-filled trench across the track, (d) double EPS-filled trench.

The implementation of EPS geofoam around the building foundation has slightly reduced the vibrations level compared to the previous case, as demonstrated in Figure

7.37c. On the other hand, in the modeling scenario for which a single EPS-filled trench has been applied across the track, the spread of the waves has been significantly reduced, as much lower vibrations are observed at distances higher than 25m (see Figure 7.37b). In this case, both of the pre-described mitigation schemes have been applied, the vibrations level's reduction is even higher, as depicted in Figure 7.37d.

Figure 7.38 shows the insertion loss curves of the three examined mitigation approaches at the first examined observation position, at the base and on the second floor. The implementation of EPS-trench around the building foundation has led to a remarkable reduction of the vibrations level compared to the single-story building. At several octave bands, the insertion loss is higher than 7dB and the highest decibel reduction, equal to 10dB, is observed at the 8th octave band. However, the implementation of a trench across the track reaches significantly higher insertion loss. The highest level of decibel reduction is located at the 4th octave band, as the insertion loss reaches values higher than 15dB at both the single trench and hybrid method.
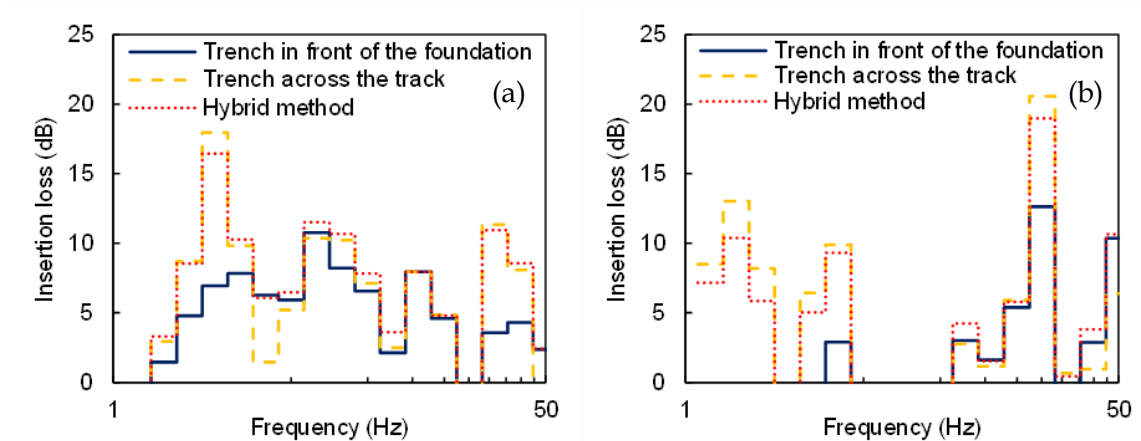
Figure 7.38 IL curves at the level of the (a) base, (b) 2nd floor of the building at the center of the front wall.

On the other hand, at the top of the building, the implementation of a trench in front of the foundation has not managed to reduce the vibrations level at the lower examined octave bands. However, this mitigation approach successfully reduces the vibrations level at the octave bands with central frequencies higher than 12.5Hz, which are the most dominant. As illustrated in Figure 7.38b, the higher insertion loss, equal to 13dB, is observed at the 14th octave band. The other examined mitigation approaches have led to higher insertion loss values at the first six octave bands. Furthermore, the insertion loss is even higher at the most dominant octave bands, with central frequencies between 12.5Hz and 25Hz, as at the 14th octave band, the insertion loss is close to 20dB.

The results are expanded to the second observation position, at the corner of the front wall, as illustrated in Figure 7.39. At the building base, the implementation of the EPS-filled trench in front of the building foundation has led to the insertion loss of around 5dB at the first six octave bands. The hybrid method reaches in comparable decibel reduction with the first examined mitigation approach at those octave bands, in contrast with the EPS-filled trench across the track, as depicted in Figure 7.39a. On the other hand, the implementation of the EPS-filled trench across the track is more effective at the higher (more dominant) octave bands. For instance, at the octave band with a centre frequency 25Hz, this mitigation approach has reduced the decibel level by 7.5dB. The same observation is made at the top of the building, as illustrated in Figure 7.38b. In general, the hybrid method reaches the optimal insertion loss at the whole examined frequency range.
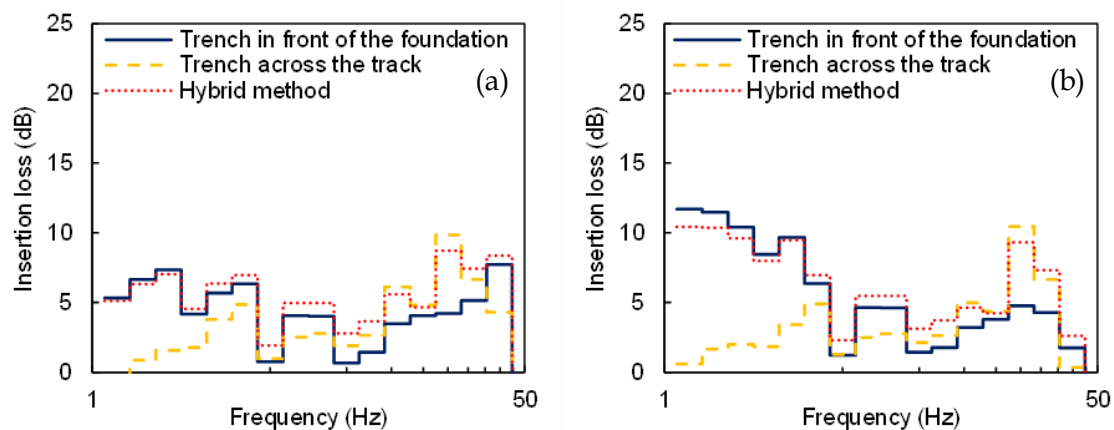
Figure 7.39 IL curves at the level of the (a) base, (b) 2nd floor of the building at the corner of the front wall.

7.4. *Seismic protection of masonry building with EPS geofoam*

As earlier mentioned, the implementation of an EPS-filled trench in front of the masonry building foundations is not the ideal approach to protect them from train-induced vibrations. However, the effect of the approach on the seismic protection of old masonry buildings has also been investigated. For this purpose, the methodology of Performance through Limited Duration Rehabilitation Interventions (LDRI), which aims to assess the seismic risk of monumental structures (Spyrakos, 2018; Spyrakos and Maniatakis, 2016), has been used. This methodology attempts to provide a framework that quantifies the "safe" duration (i.e., the nominal life) of an intervention that upgrades structural integrity in a specified manner. The nominal life of an intervention is defined as the period for

which this action ensures that the structure fulfills selected performance level(s) for a specific seismic scenario (e.g., probability of exceedance 10% and 20% in 50 years, respectively for Significant Damage and Damage Limitation Levels).

For this purpose, a typical Greek two-story URM building (Lyratzakis and Tsompanakis, 2018a, 2018b), is selected as a case study to perform the LDRI methodology also presented the effectiveness of the implementation of EPS filled the trench around the buildings foundation. As an extension to the use of EPS geofoam to minimize the HST-induced vibration, the present Section proposes the application of a new mitigation method capable of also improving the dynamic structural response, depending on the soil saturation level. As mentioned, an EPS-filled trench is placed between the surrounding soil and the outer side at the perimeter of the building foundation, acting as a compressible "shield." This simple, economical and fast intervention, which does not cause any structural or functional disturbance, aims to isolate the structure from ground shaking and absorb most of the seismic energy.

7.4.1. *Performance-based design/assessment: Theoretical background*

Modern seismic design norms/guidelines for the seismic design of new structures and the assessment of interventions in existing buildings have included state-of-the-art methodologies for assessing the structural response based on performance-based assessment for certain limit states (design levels). The Greek norm for structural interventions for existing reinforced concrete structures (Greek Code for Structural Interventions (CSI, 2012)) has adopted two seismic hazard levels:

- Seismic excitation with an exceedance probability of 50% in 50 years.

- Seismic excitation with an exceedance probability of 10% in 50 years.

In addition, CSI defines three performance levels, namely: Damage Limitation, Significant Damage, and Near Collapse, for structures with a conventional lifetime of T_L=50 years. Accepting that the cultural heritage structures belong to importance classes III and IV, CSI defines three performance levels:

- A1: Limited damage for seismic excitation with exceedance probability 10% in 50 yrs.
- A2: Limited damage for seismic excitation with an exceedance probability of 50% in 50 yrs.

- B1: Important damage for seismic excitation with exceedance probability 10% in 50 yrs.

It is noteworthy that CSI does not consider the performance level "Near Collapse" as acceptable for important monumental structures. Greek Earthquake Planning and Protection Organization (EPPO) has more recently released a draft regulation: Code for the Assessment and Interventions of Masonry Structures (CASIM), aiming to establish criteria for the assessment of the bearing capacity of existing masonry structures (CASIM, 2014), and a draft with specialized guidelines for monuments (EPPO, 2011). In general, CASIM follows the same principles and performance levels as CSI. Eurocode 8 -Part 1 (EC8-1, 2004) and Part 3 (EC8-3, 2004)- follows similar principles as CSI, while it provides an additional seismic hazard level:

- Seismic excitation with an exceedance probability of 20% in 50 years.
- Seismic excitation with an exceedance probability of 50% in 50 years.
- Seismic excitation with an exceedance probability of 10% in 50 years.

The target performance level results from the combination of acceptable damage level and seismic risk scenario and the important class of the structure. It has to be noted that EC8 does not refer to specific guidelines for the cases of high historical or artistic value monumental structures (Spyrakos, 2018). However, its principles can be followed for structural assessment and retrofitting in such cases as well.

Furthermore, according to US guidelines FEMA 349, the following four performance levels are defined for masonry structures (FEMA 349, 2000):

- Slight Damage State.
- Moderate Damage State.
- Extensive Damage State.
- Complete Collapse.

Similarly to EC8, FEMA 349 adopts three seismic hazard levels (FEMA 349, 2000):

- Seismic excitation with an exceedance probability of 50% in 50 years.
- Seismic excitation with an exceedance probability of 10% in 50 years.
- Seismic excitation with an exceedance probability of 2% in 50 years.

In addition, FEMA 349 proposes limit drift values for each performance level. The proposed values in Table 7.6 change according to the construction materials and the design norm of the structure. Note that for historic structures, the limit values of the URM buildings correspond to design level "Low-Code."

Table 7.6. Structural Damage State thresholds per Performance Level.

| Performance Level | Average Inter-Base Drift Ratio | | | | | |
| | Capacity Curve Control Points | | Structural Damage State Thresholds (Fragility Medians) | | | |
	Yield	Plastic	Slight	Moderate	Extensive	Complete
Special High - Code	0.0057	0.1371	0.005	0.015	0.05	0.125
High – Code	0.0038	0.0913	0.004	0.012	0.04	0.1
Moderate – Code	0.0029	0.0514	0.004	0.0099	0.0306	0.75
Low – Code	0.0019	0.0343	**0.004**	**0.0099**	0.0306	0.75
Pre – Code	0.0019	0.0343	0.0032	0.0079	0.0245	0.06

7.4.2. *Limited Duration Rehabilitation Intervention*

Improvement of dynamic structural response by applying the so-called "Limited Duration Rehabilitation Interventions" (LDRI) (Spyrakos, 2018; Spyrakos and Maniatakis, 2016) aims to implement mitigation measures for a specified period and a predefined limit state, after which a re-assessment of the building must be performed and depending on the results to revise the mitigation measures. According to this conceptual methodology, the time for which the operation ensures a predetermined performance level is defined as the nominal life of an intervention (T_Δ).

This methodology uses the following Equations for each of the three seismic hazard zones in Greece (Z1, Z2, Z3) for the calculation of the return period (T_{RL}) with respect to reference peak ground acceleration (a_{gR}):

$$\log a_{gR} \approx 0.277 \log T_{RL} + 1.579 \tag{7.2}$$

$$\log a_{gR} \approx 0.264 \log T_{RL} + 1.739 \tag{7.3}$$

$$\log a_{gR} \approx 0.240 \log T_{RL} + 2.015 \tag{7.4}$$

The code-imposed acceleration values a_{gRL} for the three Greek seismic hazard zones are 0.16g, 0.24g and 0.36g, respectively (ELOT, 2005). The return period T_{RL} related to the corresponding a_{gR} is calculated using the proper attenuation relationship among (7.2) - (7.4), for which a 20% reduction, i.e., $a_{gR} = 0.8 a_{gRL}$, is also considered (Spyrakos, 2018). Adopting a Poissonian distribution for the occurrence of seismic events, T_Δ is related to the return period T_{RL} and the probability of occurrence P_R as follows:

$$T_{RL} = -\frac{T_\Delta}{\ln(1 - P_R)} \tag{7.5}$$

If the seismic action is defined in terms of the reference peak ground acceleration a_{gR}, the value of the importance factor γ_I multiplying the reference seismic action to achieve the same probability of exceedance in T_Δ years as in the $T_{\Delta R}$ years for which the seismic reference action is defined can be computed by:

$$\gamma_I = (\frac{T_{\Delta R}}{T_\Delta})^{-1/k} \tag{7.6}$$

where exponential parameter k is in the order of 3 (EC8-1, 2004) and relates the nominal life of the examined intervention with the importance class (Spyrakos, 2018).
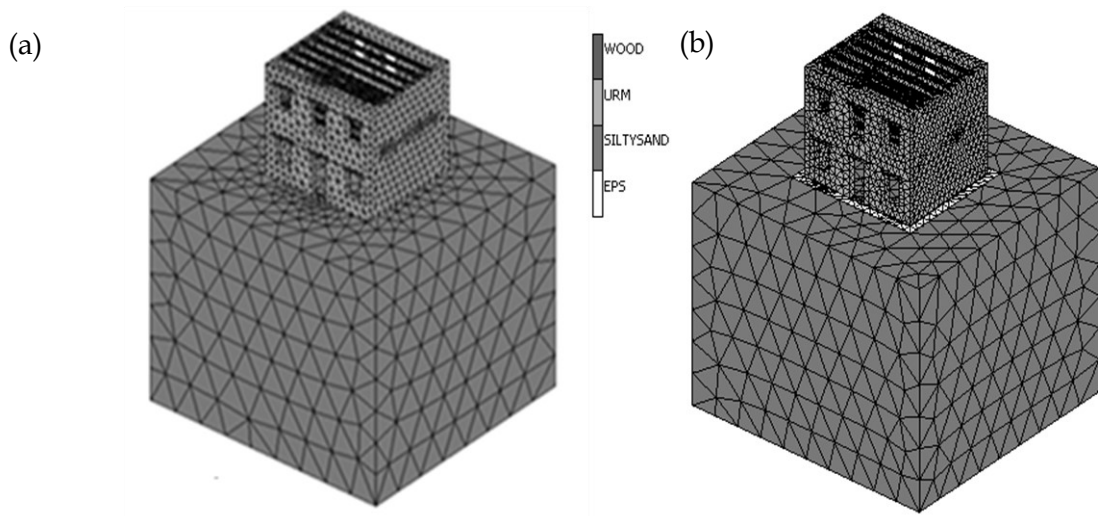
Figure 7.40 (a) Model in its initial state, (b) Retrofitted model with EPS geofoam.

7.4.3. Numerical model

In comparison with the previous sections, in this case, the general-purpose finite element software MSC Marc (2014) has been used to investigate the building seismic response. The mechanical characteristics of masonry walls are calculated according to EC6, while the parabolic Drucker-Prager yield criterion (Stavroulaki and Liarakos, 2008) is used to describe the inelastic behavior of the masonry walls. The structure is constructed on unsaturated silty sand, the mechanical properties of which with respect to the degree of saturation are taken from the study of Byun et al. (1996). Regarding the inelastic behaviour of the soil, the Cam-Clay yield criterion, according to the Critical State theory for unsaturated soils, is used (Casini et al., 2008). For the nonlinear dynamic analyses, the multiple-stripe dynamic analysis (MSDA) procedure has been repeated for eight different soil saturation conditions (8%, 12%, 16%, 20%, 32%, 54%, 63% and 80%) and ten seismic intensity levels. The twenty seismic records (Table 7.7) which have been used in this study

have been selected from the PEER database (PEER, 2015) and have been scaled utilizing EC8 guidelines as implemented in ISSARS software (Katsanos and Sextos, 2013).

7.4.3.1. *Description of mechanical properties of the masonry buildings*

The examined structural model is a typical form of a two-storey, symmetrical URM building (the so-called "neoclassical" buildings) that were constructed in Greece from the nineteenth century and later on. Typically, they have been used as residences and their volume is closed and cubic, while a basic tripartite separation is used to ensure symmetry in the faces. On the facade of the building, this typology is formed via the axially positioned entrance and the symmetrically located openings that imply the different function of the three parts of the house. The mechanical properties of the examined building are identical to the previous section (see 7.3.1.1.). For the description of the non-linear behavior of the masonry the parabolic Drucker-Prager yield criterion is used. The parameters σ and β of the yield criterion are determined by the uniaxial tensile and compressive strength of the material ($\sigma = 680$ kPa, $\beta = 2.98$).
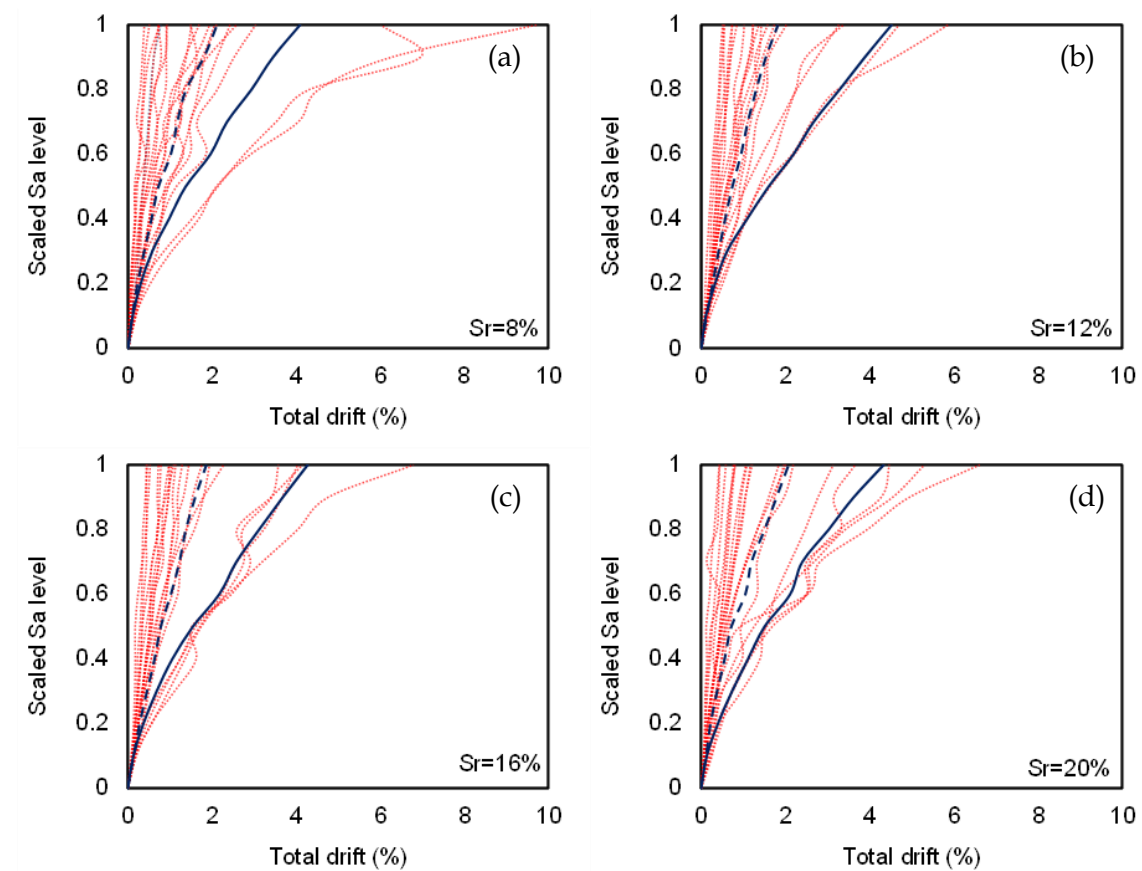
Figure 7.41 Total drift MSDA curves for the retrofitted building model, while bold dashed curves correspond to median values, while the bold continuous curves present median values for the initial building.

The original building is slightly retrofitted with EPS blocks, with a height equal to 1m and width of 0.50m (Figure 7.40), which are placed at the exterior of the foundation, aiming to improve the seismic response of the building and to minimize the impact of soil saturation conditions. This cost-effective intervention can enhance the dynamic behaviour of the building, as this EPS layer acts as a damper (due to its high compressibility), absorbing most of the dynamic distress, thus, protecting the structure, especially for lower S_r (<32%) values. This is evident by examining Figures 7.41 and 7.42, which depict the total drift MSDA curves for the retrofitted building, by comparing median curves of initial and retrofitted models, i.e., bold continuous vs. dashed curves, respectively.
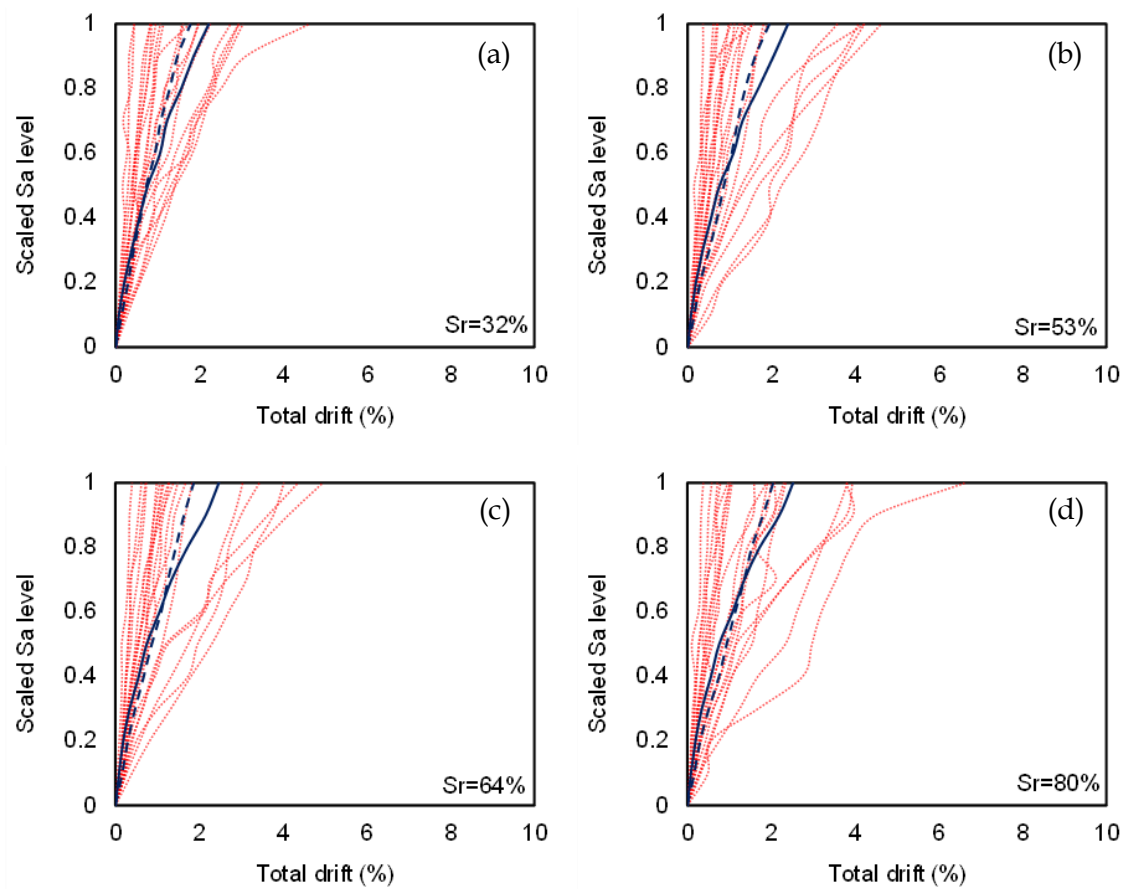
Figure 7.42 Total drift MSDA curves for the retrofitted building model, while bold dashed curves correspond to median values, while the bold continuous curves present median values for the initial building.

7.4.4. *Building nominal life for constant soil saturation level*

As aforementioned, the MSDA curves of the retrofitted model have been used to assess its performance following the LDRI principles. For this purpose, two performance levels: Slight and Moderate Damage States, as defined in FEMA 356, have been used. Accordingly, the values for URM buildings and Performance level "Low-Code" are taken

from Table 7.6. Firstly, the calculation of the nominal life is performed considering that the building is based on soil with a constant saturation level, i.e., not varying with time. Figure 7.43 depicts the average dynamic resistance curve and the limits (vertical lines) of the two performance levels for the examined building for eight different saturation conditions (Sr= 8%, 12%, 16%, 20%, 32%, 54%, 63% and 80%).

Table 7.7. Characteristics of the ground motion records.

No	Region	Station name	Magnitude	Epicentral distance (km)	PGA (g)
1		Bonds Corner		6.2	0.686
2	Imperial Valley	El Centro Array #5	6.53	27.8	0.448
3		El Centro Array #7		27.64	0.42
4		El Centro Array #8		28.09	0.538
5	Mammoth Lakes	Convict Creek	6.06	1.43	0.419
6	Coalinga	Pleasant Valley P.P	6.36	9.98	0.571
7	N. Palm Springs	North Palm Springs	6.06	10.57	0.59
8		Whitewater Trout Farm		4.24	0.602
9	Chalfant Valley	Zack Brothers	6.19	14.33	0.425
10	Loma Prieta	Capitola	6.93	9.78	0.48
11		Gilroy Array #3		31.4	0.462
12	Cape Mendocino	Rio Dell Overpass	7.01	22.64	0.424
13	Big Bear	Big Bear Lake - Civic	6.46	10.15	0.503
14		Beverly Hills		13.39	0.459
15		Canyon Country		26.49	0.436
16		LA Obregon Park		39.39	0.467
17	Northridge	Newhall - Fire Sta	6.69	20.27	0.698
18		Pardee – SCE		25.65	0.505
19		Rinaldi Receiving		10.91	0.634
20		S. Monica City Hall		22.45	0.591

In the comparative plot of Figure 7.43, there is a clear trend that the selected retrofitting intervention in most cases leads to a substantial improvement of the structural response. However, it has to be noticed that during the first scaling steps, the MSDA curves of the original and the retrofitted building are identical. In other words, for low seismic intensity levels, the soil saturation conditions do not play a crucial role. Furthermore, for higher saturation levels (Sr>32%), the structural response is not improved in the first steps of record scaling. On the other hand, for higher seismic intensity levels, in all cases, the

application of this retrofitting scheme drastically improves the response of the structure, depending on the saturation level. In particular, the improvement of the response of the retrofitted structure is even more pronounced at lower saturation levels.

In addition, the results of the original building seem to be grouped, i.e., to have slight variations for low (Sr=8% to 20%) and high (Sr=32% to 80%) saturation levels. This is due to the variation of soil stiffness for these soil conditions since, according to the experimental data, the impact of saturation level substantially affects the basic mechanical parameters of the soil in this specific manner. In contrast, the application of EPS geofoam at the foundation level alleviates this scattering and groups the curves in a more uniform way irrespective of the saturation conditions.
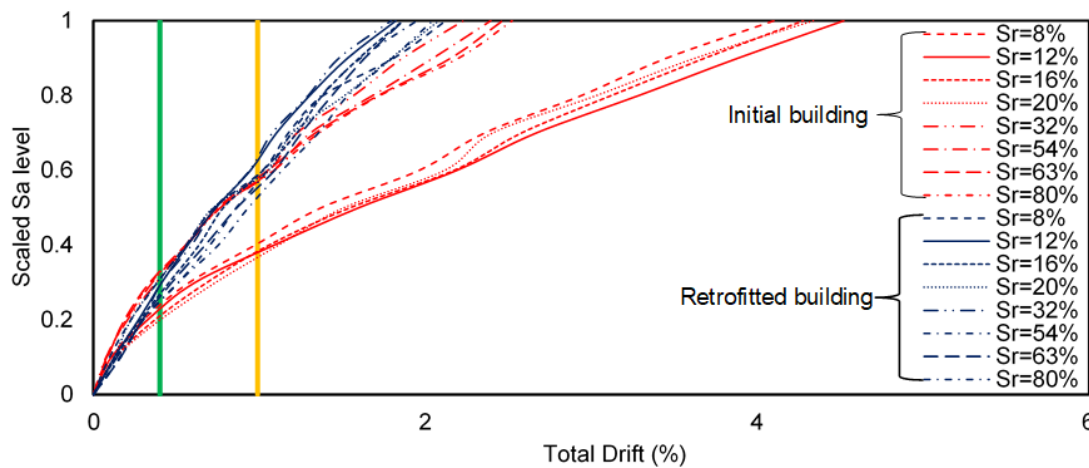
Figure 7.43 Comparison of initial and retrofitted model IDA curves.

Regarding the calculations of nominal life of the retrofitted and initial models utilizing LDRI approach, it is assumed that the building is located at seismic zone Z2; thus, T_{RL} return period is calculated via Equation (7.2). The nominal life for all examined models is calculated using Equation (7.4), and the results are presented in Table 7.8. As a consequence of the building response varies according to the degree of saturation, the nominal life of the structure varies considerably depending on the soil conditions.

The response of the initial building has proven to be directly dependent on the degree of soil saturation. More specifically, it is observed that the increase of soil saturation (Sr >32%) contributes to the increase of the building nominal life. When the building is founded on soil with a Sr < 32%, the nominal life of the building varies from 7 to 14 years for A2 design level and from 11 to 16 years for B1 design level. Conversely, when the building is founded on soil with higher Sr, the nominal life increases significantly,

reaching between 39 and 48 years for A2 design level and from 58 to 62 years for B1 design level. The nominal life of the original building is extremely small for low soil saturation levels. Moreover, the nominal life varies considerably depending on the degree of subsoil saturation. In particular, the nominal life is altered between 9 and 49 years for A2 design level and from 11 to 62 years for B1 design level. Therefore, it is obvious that a reliable prediction of the initial building nominal life is not a straightforward task.

Table 7.8. Nominal Life (in years) for each model for A2 and B1 design levels.

Design Level	A2		B1	
Soil Saturation	Original Building	EPS Retrofitted Building	Original Building	EPS Retrofitted Building
Sr=8%	14	**38**	16	**67**
Sr=12%	12	**30**	12	**84**
Sr=16%	9	**22**	13	**65**
Sr=20%	7	**38**	11	**63**
Sr=32%	**39**	30	61	**88**
Sr=54%	**44**	16	**58**	58
Sr=63%	**48**	19	**62**	53
Sr=80%	**46**	16	**59**	44

Since the scattering of the initial structure nominal life is quite high, retrofitting of the structure is deemed necessary from this viewpoint as well. Nonetheless, even after the selected retrofitting with EPS blocks at the foundation, the nominal life of the structure varies depending on the degree of soil saturation. However, the variation is less compared to the structure in its initial state. As presented in Table 7.8, when the building is founded on soil with Sr<32%, the nominal life of the building is significantly higher than the original building for both A2 and B1 performance levels. On the other hand, when the building is founded on soil with a Sr>32%, a decrease of the nominal life is observed, especially for the lower (i.e., A2) performance level.

7.4.5. *Building nominal life for varying soil saturation level*

In the preceding section, the calculation of nominal life has been performed separately for each soil saturation level. In other words, it is assumed that the degree of soil saturation remains constant. In reality, the degree of saturation varies within each year, i.e., usually, it is higher in winter than in summer months. Thus, the response of the building is different, which should be considered in the calculation of the building nominal life. The

accurate calculation of the nominal life as a function of the soil saturation variation requires data representing the annual change of Sr. Unfortunately, there are no accurate related measurements (which strongly depend on the location and the climate). Thus, an assumption is made that the annual change of Sr follows a sinusoidal curve and the degree of saturation takes values between the two extreme values of the selected Sr bounds, namely 8% and 80%. The minimum and maximum values correspond to the summer and winter months, as shown in Figure 7.44. Based on this simplifying assumption, it is considered that during a year, the change in the soil saturation level is given by:

$$S_r = 44 + 36 \cos \frac{\pi T}{6} \tag{7.7}$$

where: T denotes month number (January=1, February=2,.., December=12).
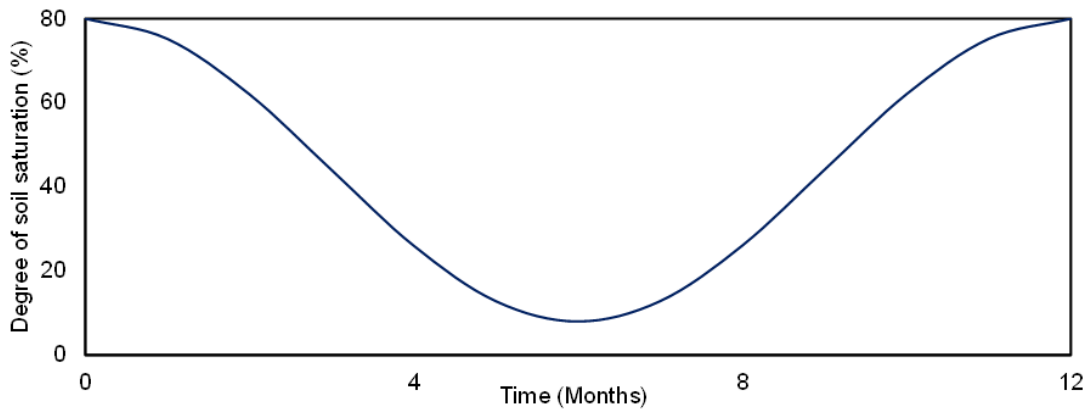
Figure 7.44 Change of soil saturation level during one year.
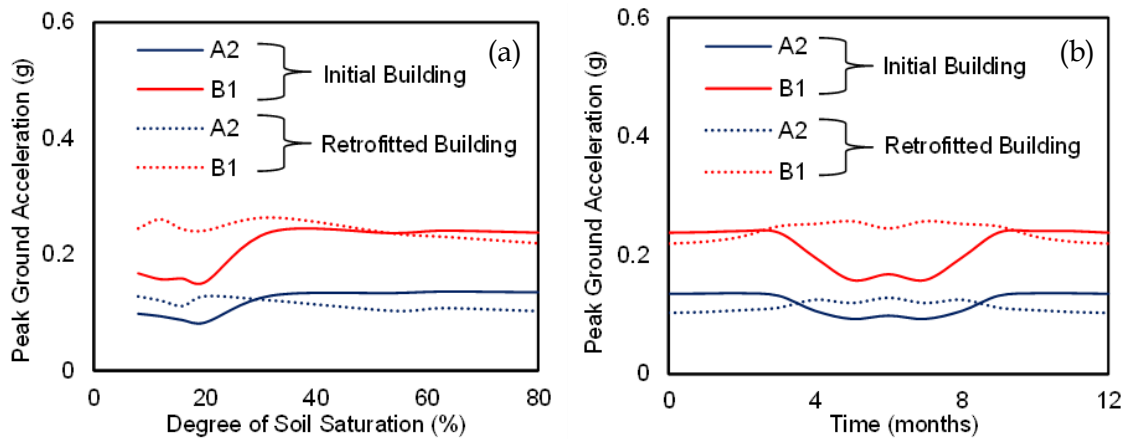
Figure 7.1. (a) Change of peak ground acceleration for various saturation levels; (b) Peak ground acceleration annual variation.

The change of peak ground acceleration to achieve A2 and B1 performance levels as a function of Sr are shown in Figure 7.45a for the initial and the retrofitted buildings. The curves for the two models are constructed based on a_{gR} values according to the MSDA

curves shown in Figure 7.43. Firstly, the degree of saturation for each month has been calculated according to Equation (7.6). Subsequently, the peak ground acceleration for each month has been calculated by linear interpolation and the results are displayed in Figure 7.45b.

Table 7.9. T_Δ and P_a calculations per month for each design level.

| Month | S_r (%) | Initial Building | | | | EPS Retrofitted Building | | | |
| | | Design level A2 | | Design level B1 | | Design level A2 | | Design level B1 | |
		$T_{\Delta r}$ (years)	P_a (%) in 11 years	$T_{\Delta r}$ (years)	P_a (%) in 13 years	$T_{\Delta r}$ (years)	P_a (%) in 16 years	$T_{\Delta r}$ (years)	P_a (%) in 44 years
1	75.2	46	15.14	60	2.25	17	47.71	46	9.55
2	62	47	14.94	62	2.19	19	43.98	53	8.31
3	44	42	16.65	60	2.28	22	39.50	70	6.37
4	26	18	34.01	28	4.71	34	27.77	75	6.03
5	12.8	**11**	50.00	**13**	10.00	29	32.20	80	5.62
6	8	14	42.87	16	8.28	38	25.56	67	6.73
7	12.8	**11**	50.00	**13**	10.00	29	32.20	80	5.62
8	26	18	34.01	28	4.71	34	27.77	75	6.03
9	44	42	16.65	60	2.28	22	39.50	70	6.37
10	62	47	14.94	62	2.19	19	43.98	53	8.31
11	75.2	46	15.14	60	2.25	17	47.71	46	9.55
12	80	46	15.26	59	2.29	**16**	50.00	**44**	10.00

Table 7.9 presents on a monthly basis the values of the degree of saturation and peak ground acceleration. Considering that each month a_{gr} remains constant all years throughout the life of the structure, the relevant nominal life ($T_{\Delta r}$) is determined. Under this perspective, twelve different nominal lives are obtained (one per month) and the most critical equivalent nominal life ($T_{\Delta cr}$) is defined. For instance, the initial building critical equivalent nominal life is presented at the fifth and seventh month when the building is founded on soil with Sr=12.8%. The critical equivalent nominal life is equal to 11 and 13 years for performance levels A2 and B1, respectively. On the other hand, when the building is slightly retrofitted, $T_{\Delta cr}$ is calculated for the twelfth month (December), when the building is founded on soil with an 80% degree of saturation. The retrofitted model critical equivalent nominal life is equal to 16 and 44 years for performance levels A2 and B1, respectively.

Subsequently, the probability (P_a) to exceed the drift limits of the chosen performance levels is determined within the specific $T_{\Delta cr}$ for all months (e.g., $T_{\Delta cr}$=11 years for A2 performance level for the initial building, as shown in the 4th column of Table 7.9). The average probability during $T_{\Delta cr}$ and the final nominal life of the initial and the retrofitted

buildings for performance levels A2 and B1 are calculated (considering that the probability of an earthquake during the year is the same for all months) using the following formula:

$$T_\Delta = \frac{P_a T_{\Delta cr}}{P_{AV}}$$ (7.8)

According to the results of the adopted procedure, by taking into account in a realistic manner the annual changes in the soil saturation level, the nominal life is increased when retrofitting the foundation with EPS blocks. As presented in Table 7.10, the nominal life notably increases from 29 to 60 years for performance level B1 when the building is slightly retrofitted with EPS geofoam. In contrast, the nominal life for design level A2 is only slightly increased from 20 to 21 years. In any case, since the nominal life is increased for the more crucial design level B1, the use of EPS blocks improves the overall behavior of the building.

Table 7.10. Calculation of final nominal life (in years).

Model	Design Level	P_a	$T_{\Delta cr}$	P_{av}	T_Δ
Original Building	A2	50	11	26.63	20
	B1	10	13	4.45	29
EPS Retrofitted Building	A2	50	16	38.16	21
	B1	10	44	7.37	60

7.5. *Discussion of the results*

In the present Chapter, the mitigation of the dynamic vibrations on buildings with the use of EPS geofoam has been examined. Initially, the effect of the HST-induced vibrations on the structural response of nearby buildings has been examined via three-dimensional numerical analysis. The efficiency of several mitigation schemes with the application of EPS geofoam has been investigated in order to reduce the vibration level on the floors of masonry and RC buildings and the optimal measures in each case are proposed. The vibrations level at several observation positions on the RC buildings has been compared with the proposed threshold by WHO in order to determine the optimal distance from the track for the construction of new RC buildings. The building has been placed at several distances from the rack to examine the effect of the distance on the vibrations level. Furthermore, the single and double EPS-filled trench efficacy has been investigated. In the sequence, the numerical results have been expanded in the case of low-rise masonry buildings. The last aim of this Chapter is to investigate the seismic vulnerability of masonry buildings taking into account the impact of seismic soil-structure interaction

(SSI) and the mitigation level of the implementation of an EPS-filled trench around the building foundation.

Based on the presented results, the main findings of the application of EPS for the protection of buildings from dynamic vibrations are as follows:

- The level of HST-induced vibrations has been increased at the building top floor compared to the base of the building for all the examined buildings.

- At the closer distance from the track, the vibrations level has reached in some cases over 80dB. On the other hand, in the case of RC buildings constructed at 30m from the track, the decibel level has been reduced below 60dB. A higher level of dB has been obtained at the front cantilever edge at all the examined distances from the track.

- Implementing a single EPS-filled trench to minimize the HST-induced vibrations on the top of RC buildings has contributed to the reduction of the vibrations level up to 10dB at some octave bands. The decibel reduction is higher when the building is constructed closer to the track. The implementation of a double EPS-filled trench is more effective than the single one. In this case, the reduction of the vibrations level is significantly higher. It is evident that the insertion loss in some cases is higher than 20dB.

- The implementation of both single and double EPS-filled trenches cannot reduce the vibration level below the WHO threshold of 54dB when the building has been constructed at 10m from the track. The single trench is effective when the building has been constructed at 30m from the track. On the other hand, the double EPS-filled trench made the construction of buildings possible, even at 20m from the track.

- The implementation of both EPS-filled trenches across the track and around the building foundation is the most effective mitigation approach in the case of masonry buildings close to the track. Especially in the case of a single-story masonry building, the implementation of just an EPS trench in front of the foundation has not managed to mitigate the vibrations level successfully at the top of the building. On the other hand, the trench across the track reaches comparable insertion loss with the hybrid method.

▪ By applying an EPS-filled trench, this light intervention scheme improved the seismic response of a typical masonry building and increased the building nominal life and limited the scattering of the results due to varying soil saturation conditions, especially for the B1 performance level. Certainly, alternative retrofitting approaches, either as single or combined schemes, e.g., by applying EPS blocks at the foundation together with RC structural elements, should be investigated in order to examine their effectiveness in similar soil conditions.

CONCLUSIONS

8.1. Conclusions

This chapter summarizes the main conclusions that can derived from the present Doctoral Thesis as described in the previous chapters. In the sequence, ideas for further investigation are presented. Many analytical numerical and experimental investigations have been carried in recent decades, aiming to study the HST-induced vibrations. Furthermore, several mitigation approaches have been proposed in order to reduce the developing vibrations level. The majority of those studies investigate the efficiency of open or in-filled trenches. The present Ph.D. Thesis numerically investigates alternative mitigation approaches based on EPS geofoam in order to reduce the HST-induced vibrations via validated elaborate 3D FE models.

Initially, a low computational-cost numerical model capable to accurately investigate the HST-induced vibration has been presented. In order to achieve the balance between the computational cost and the efficacy of the model, the usage of several numerical tools has been investigated. Accordingly, the three-dimensional FE modelling approach via the commercial software Abaqus has been selected to simulate this complex phenomenon. Furthermore, a user-defined subroutine has been developed for the input of the train moving loads. This approach has been validated by comparing the numerical results with pre-available field data from three Sites from Paris-Brussels HSR. According to this investigation, the following aspects are highlighted:

- The most dominant vibrations peaks have been well captured by the FE model, according to the rail dominant frequencies derived from field data. The numerical

models successfully capture the bogies, axles and sleepers passing frequency for all the examined sites.

- The patterns of the vertical velocity time histories are in good agreement with the data from the in-situ measurements. There is a high accuracy of the vertical velocities at the nearest examined positions from the track for all the examined sites. In the case of site 3, the vertical velocity is underestimated at the far-field. However, the model reliability is still high at the most remote positions in the case of the embankment and cutting sites.

- According to the experimental data, the most dominant vibrations peaks are located at the low-frequency range between 0Hz and 40Hz. The numerical model manages to capture the location and the amplitude of those peaks.

- There is a high correlation between the dominant frequencies at the low-frequency range between 0Hz and 40Hz for all the examined cases, which is even more pronounced in the case of Site 1.

- The most dominant octave bands are the same for all the examined sites at all the examined distances from the track. More specifically, the most dominant bands are those with centre frequency from 16Hz to 31.5Hz. The peak dB level is located at the octave band with a centre frequency 25Hz, equal to 75dB for all the examined sites. Furthermore, the decibel level is decreased to below 63dB at the most remote position. The decibel level is notably similar to the field data at 15m from the track.

- There is a high correlation between the numerical results and the field data in terms of PPV and $KB_{F,max}$. The trend of those indicators at increasing distance from the track follows the in-situ measurements.

- Some deviations between the numerical and the experimental data are reasonable due to the examined phenomenon complexity and the uncertainties in reproducing the real conditions during the measurements. However, the discrapancies are limited compared with other numerical approaches. Hence, the developed FE-based methodology is capable of accurately predicting the HST-induced vibrations.

In the sequence, the numerical methodology has been used to investigate several configurations using EPS geofoam to reduce the HST-induced vibrations at embankment sites. An optimal configuration with the use of a limited number of EPS-geofoam is proposed. Lastly, the effect of the embankment height, the slope inclination, the subsoil conditions and the HST passing speed in the effectiveness of the optimal approach has been investigated. The main findings of this investigation are summarized as follows:

- The construction of a whole EPS-filled embankment remarkably reduces the vibrations level in comparison with a common soil embankment. However, there are increased rail deflections, which lead to a high possibility of HST derailment. On the other hand, the replacement of the fill soil at the whole embankment slope with EPS-geofoam slightly reduces the induced vibrations. However, the stability of the embankment should be further examined.

- The implementation of a limited number of EPS-geofoams at the embankment slope is proposed as the optimal mitigation measure. This approach leads to a considerable reduction of the vibrations and ensures safety against derailment of the HST.

- The effectiveness of several types of EPS geofoam has been compared. It is concluded that the stiffest EPS46 is the optimal fill material in order to mitigate the induced vibrations.

- The combination of the proposed mitigation approach with the commonly used EPS-filled trench across the embankment further reduces the vibrations level.

- When the slope inclination is constant and the embankment fill material is the same as the upper subgrade layer, the height of the soil embankment has a minor effect on vibrations propagation. EPS blocks have helped to reduce the induced vibrations at all of the examined embankment heights between 3.5m and 5.5m, especially at the most dominant frequencies.

- The inclination of the soil embankment slope is essential in influencing the level of HST-induced vibrations. The vibrations level is reduced when the slope is steeper. The use of EPS blocks decreases the vibrations level for all of the examined slope inclinations between 20° and 45°.

- The vibrations level has been compared with several thresholds in terms of PPV, v_{rms}, V_{dB} and $KB_{F,max}$. It has been observed that PPV is already below the DIN threshold to protect nearby buildings from potential damage. However, PPV values are minimized even further with the implementation of EPS blocks for all the examined locations. Furthermore, the proposed mitigation approach is more effective for higher embankments. The implementation of EPS blocks has reduced the v_{rms} to values lower than the USDT limit for frequent passages of HST.

- The Ground-borne vibrations are low when the HSR is located at a firm soil layer. Especially in the case of rock, the vibrations level is almost zero. Hence, mitigation measures are not required for the location of stiff soils.

- The beneficial role of the limited number of EPS blocks at the embankment slope is obvious, in the case of embankment based on dense sand with gravels, stiff or soft clay.

- The level of HST-induced vibrations is also influenced by embankment fill material, especially in sites with stiffer subsoil, as the waves are trapped within the embankment depending on the differences in subsoil and embankment soil properties. Regardless of the embankment fill material, implementing the proposed mitigation approach along with an EPS-filled trench reduces the induced vibrations.

The mitigation of the induced vibrations with several configurations at cuttings sites has been presented in the sequence. In contrast to the HSR embankments, the cuttings have not been extensively investigated by researchers in the field. This investigation has led to the following conclusions:

- The most commonly used mitigation measure, the EPS-filled trench, significantly reduces the HST-induced vibrations. The level of reduction in some octave bands reaches up to 10dB. This approach is more effective in cutting sites compared to embankments, as the trench construction right next to the track is feasible.

- Due to the waveguide effect, using a small number of EPS blocks at the cutting slope raises the vibrations level at the cutting slope. On the other hand, the beneficial role of this mitigation approach is obvious at the cutting upper flat part. Herein, the mitigation level is higher than the EPS-filled barrier. In addition, the

combination of this approach with an EPS-filled trench across the track leads to an even higher reduction of the HST-induced vibrations at the cutting upper flat part.

- The waveguide effect is overcome by replacing the upper soil layer of the cutting with EPS, which successfully reduces HST-induced vibrations at both the slope and upper flat positions. Furthermore, a thicker EPS layer results in a greater reduction of vibrations.

- The mitigation efficiency using a thin EPS layer is comparable to the reduction achieved using a common EPS-filled trench across the track. However, the level of reduction is significantly higher than the EPS-filled trench if the EPS layer has a high thickness.

- When the HST passes sites with soft subsoil, the induced vibrations are increased. However, regardless of soil properties, the proposed mitigation solution reduces the vibrations levels significantly, especially at closer distances from the track.

In addition, the main findings of the research regarding HST-buried pipe interaction and protection via EPS can be summarized as follows:

- The numerical results have been compared to pre-existed experimental measurements of equivalent heavy traffic loads. According to this procedure, the numerical results have been partially validated in order to investigate the pipe response to HST-induced vibrations.

- The level of the developed vibrations on the top of the buried pipeline has been successfully reduced after the implementation of an EPS-filled layer between the track and the pipe. The EPS-filled layer thickness is an important factor that influences the efficiency of the proposed method. More specifically, the thicker the layer, the higher the reduction of the induced vibrations.

- The depth of the buried pipe and the HST passing speed impact on the insertion loss at the low-frequency range is marginal.

- In comparison to steel pipes, PVC pipes have a larger residual deformation. In addition, thicker pipelines have lowed diameter changes. All of the pipes evaluated had their diameter changes reduced after the implementation of the EPS layer.

- The placement of an EPS layer over a thick and rigid steel pipe is not necessarily due to the pipe low deformation.

The efficiency of single and multiple EPS-filled trenches in protecting buildings against HST-induced vibrations and seismic loads has been presented as a part of the current Ph.D. Thesis. The numerical investigation of the protection of RC and masonry building with EPS-geofoam has led to the following conclusions:

- The vibrations level due to the HST passage of all the examined buildings constructed between 10m and 30m from the track has been increased at the top floor in comparison with the building base.

- Cantilevers are the most crucial positions of an RC building, as in those positions, the highest decibel level has been observed. It is evident that the decibel level of the most dominant octave bands reaches values up to 80dB at the top floor in the case of buildings constructed at 10m from the track. This value is minimized below 60dB if the building is constructed at 30m from the track.

- The vibrations level at the top of the buildings in several octave bands has been reduced up to 10dB after implementing a single EPS-filled trench across the track. The efficacy of this mitigation approach is even more pronounced for buildings constructed at the nearest positions from the track. The EPS-filled trench is a great countermeasure, although the efficacy of a double EPS-filled trench is even higher. In this case, the dB reduction reaches peak values higher than 20dB.

- The construction of RC and masonry buildings at 10m from HSR tracks should be avoided, as the decibel level at the building floors is high. More specifically, the decibel reduction after the implementation of a single or double EPS-filled trench has been significantly reduced. However, this reduction is not enough in order to minimize the vibrations level below the WHO threshold for residents health protection. On the other hand, the single trench achieves to reduce the decibel level below the WHO limit if the building is constructed at 30m from the track. In addition, the construction of some types of buildings is possible even at 20m from HSRs, after the implementation of the double EPS trench.

- In the case of masonry buildings along the track, the most efficient mitigation scheme is the construction of two EPS-filled trenches, the first across the track and the second around the building base. On the other hand, the implementation of a

single EPS trench in front of the building foundation has not been effective enough in order to decrease the vibrations level at the top floor of the building.

In conclusion, it is evident that several configurations have been investigated to reduce the HST-induced vibration at the surrounding soil surface, especially at the embankment and cutting sites in the present Ph.D. Thesis. Furthermore, the optimal proposed approaches lead to remarkable vibrations reductions. In addition, the EPS geofoam has been used in order to protect buildings close to the HSR and pipes crossing below the track. Obviously, the implementation of an EPS-filled trench between the source (e.g., rails) and the receiver (e.g., buildings or pipes) leads to a notable reduction of the developing vibrations.

8.2. *Contribution to the advancement of engineering science*

It should be mentioned that the present Ph.D. Thesis is the first attempt to investigate the complex phenomenon of HST-induced vibrations in Greece. The knowledge and results gathered in the last four years are a great database for future researchers in the field. The main contributions to engineering practice, derived by the present doctoral thesis are listed as follows:

- Fully validated numerical models have been presented capable of predicting the HST-induced vibrations accurately.

- A commonly used material in several geotechnical applications, such as EPS geofoam, has been investigated as an alternative option for reducing the developing vibrations.

- Several new mitigation configurations have been extensively investigated and proposed at the embankment and cutting sites.

- A first attempt has been carried out in order to investigate the response of buried pipelines to HST-induced vibrations.

- Lastly, the effect of the HST-induced vibrations has been studied to propose the optimal countermeasures to minimize the vibrations level at the top of the buildings.

8.3. *Contribution to the advancement of engineering practice*

In recent decades many new HSR lines have been constructed worldwide. Furthermore, more and more regular railways are upgraded in order to serve HSTs. As a result, it is evident that, by the end of 2020, close to 38,000 km HSR operates in China. Furthermore, this railway-building boom continues, as the operating lines are predicted to reach close to 70,000 km in the next 15 years. In Centre Europe, the HST serve up to 40% of the medium-distance trips. It should be mentioned that there are several popular routes such as London-Paris or Paris-Brussels, where this rate is even higher. In easter Europe and Greece, the construction projects of HSR lines are still limited. However, a rapid growth of HSR lines is expected in the near future due to their economic and social advantages, e.g., to cover increasing traveling needs of tourism.

Obviously, decision-makers are looking for HSR track modifications capable of reducing the induced vibrations with low implementation cost. The proposed low-cost mitigation approaches at embankment or cutting sites could significantly reduce the vibrations level at loose soil sites, where the induced vibrations are high. In those locations, the construction of HST could be impossible without the implementation of any mitigation scheme. Furthermore, in order to upgrade the existing railway lines to serve HST, nearby existing buildings and infrastructure should be firstly protected. The proposed approaches that can be applied in order to protect pipelines and buildings enable the conventional railway upgrading.

8.4. *Recommendations for future extensions*

It is obvious that any research is impossible to fully cover a complex and multi-parametric phenomenon such as HST-induced vibrations. A doctoral dissertation can contribute to the understanding of some scientific issues but at the same time be the trigger for further development in this field of research. For example, based on the above findings of the present work, could include the following future extensions:

- Since this is the first time to use EPS geofoam material in such configuration, further investigations need to be conducted to investigate the proposed scheme by conducting a full-scale experimental work setup. That would be great if experimental or in-situ measurements could verify the proposed configurations.

- In the present study, only HST are investigated. However, several other types of trains, such as freights, regular speed trains or tram-trains, could be investigated. Furthermore, there are HSR lines that are serving more than one type of HST. Hence, the investigation of the proposed schemes effectiveness at different types of trains is proposed.

- Nowadays, in the case of HSR lines, defects such as rail irregularities or unevenness have been minimized due to the extensive use of continuous welded rails and the high level of maintenance. However, the effect of rail irregularities and unevenness on the efficacy of the proposed mitigation approaches could be investigated.

- It should be noted that in the present investigation the velocity time-histories have been used as measured in the field, i.e., no filters have been used in order to remove any external noise. In order to further improve the accuracy of the proposed numerical methodology, field data could be properly filtered.

- Except for the EPS geofoam, a first attempt has been carried out in order to investigate the effectiveness of a water-filled trench at the mitigation of the developing vibrations. A more detailed investigation of this approach could be carried out as an extension of the present study.

- In the present investigation, the EPS layers have been assumed to be monolithic and fixed to the subsoil. This is valid, as joints could be used in order to fix the EPS blocks. However, in the future, a detailed investigation could be performed to simulate more accurately the soil/EPS interface and examine the role of the potential kinematic mechanisms between EPS blocks.

8.5. *Publications*

The following papers in scientific journal and international conferences have been published after review as a part of the research effort in the preparation of the present dissertation.

8.5.1. *Refereed Journal Publications*

- Lyratzakis A, Tsompanakis Y, Psarropoulos P (2020). Efficient mitigation of high-speed trains induced vibrations of railway embankments using expanded

polystyrene blocks. Transportation Geotechnics, 22(2020), 100312. https://doi.org/10.1016/j.trgeo.2019.100312.

- Lyratzakis A, Tsompanakis Y, Psarropoulos PN (2021). Mitigation of HST-induced vibrations by EPS blocks applied in railway embankments. Invited paper for Special Issue "Noise and Vibration from Transportation". Journal of Zhejiang University-SCIENCE A, 22, 6–20. https://doi.org/10.1631/jzus.A1900680.

- Lyratzakis A, Tsompanakis Y, Psarropoulos PN (2021). Mitigating high-speed train vibrations for various soil conditions. Soil Dynamics and Earthquake Engineering, 141(2021), 106482. https://doi.org/10.1016/j.soildyn.2020.106482.

- Lyratzakis A, Tsompanakis Y, Psarropoulos PN (2021). Mitigation of vibrations in high-speed railway cuttings using expanded-polystyrene blocks. Transportation Geotechnics, 29 (2021), 100572. https://doi.org/10.1016/j.trgeo.2021.100572.

- Lyratzakis A, Tsompanakis Y, Psarropoulos PN (2021). Efficient mitigation of high-speed train vibrations on adjacent reinforced concrete buildings. Construction and Building Materials, 125653, https://doi.org/10.1016/j.conbuildmat.2021.125653.

- Lyratzakis A, Tsompanakis Y, Psarropoulos PN (2021). Protection of buried pipelines from high-speed trains vibrations with EPS geofoam (under review).

8.5.2. *Conference Publications*

- Λυρατζάκης Α, Τσομπανάκης Γ (2017). Αποτίμηση και ενίσχυση κτιρίου από φέρουσα τοιχοποιία με μη-γραμμική προσαυξητική δυναμική ανάλυση λαμβάνοντας υπόψη τον βαθμό κορεσμού του υπεδάφους. Ημερίδα ΕΤΑΜ: Η Αντισεισμική Μηχανική μέσα από την επιστημονική ματιά Νέων Ερευνητών και Μηχανικών, 3 Νοεμβρίου 2017, Αθήνα.

- Lyratzakis A, Tsompanakis Y (2018). Dynamic response of masonry buildings considering the time-dependent soil saturation conditions. 9th GRACM International Congress on Computational Mechanics, Chania, 4-6 June, 2018, paper 37.

- Lyratzakis A, Tsompanakis Y, Psarropoulos PN (2019). Assessment of high-speed train induced vibrations using efficient numerical models. In: Sapountzakis EJ, Banerjee M, Biswas P, Inan E (eds), Proceedings of the 14th International Conference on Vibration Problems, Hersonisos Crete, 1-4 September 2019. Lecture

Notes in Mechanical Engineering. Springer. https://doi.org/10.1007/978-981-15-8049-9_7.

- Λυρατζάκης Α, Τσομπανάκης Γ, Ψαρόπουλος Π (2019). Κραδασμοί σε σιδηροδρομικά επιχώματα κατά τη διέλευση τρένων υψηλής ταχύτητας: Αριθμητική προσομοίωση του φαινομένου και διερεύνηση μέτρων αντιμετώπισης. 8ο Πανελλήνιο Συνέδριο Γεωτεχνικής Μηχανικής, Αθήνα, 6-8 Νοεμβρίου 2019.

- Lyratzakis A, Tsompanakis Y, Psarropoulos PN (2021). Mitigating the impact of high-speed train vibrations on adjacent buildings. 10th GRACM International Congress on Computational Mechanics, Athens, 5-7 June, 2021.

REFERENCES

ABAQUS. (2014). Analysis user's manual Ver. 6.14. Providence, RI, USA: Simulia Corp.

Adam, M., Von Estorff, O. (2005). Reduction of train-induced building vibrations by using open and filled trenches. *Computers & Structures*, *83*(1), 11–24. https://doi.org/https://doi.org/10.1016/j.compstruc.2004.08.010

Al-Hussaini, T. M., Ahmad, S. (1996). Active Isolation of Machine Foundations by In-Filled Trench Barriers. *Journal of Geotechnical Engineering*, *122*(4), 288–294. https://doi.org/10.1061/(ASCE)0733-9410(1996)122:4(288)

Alzawi, A., Hesham El Naggar, M. (2011). Full scale experimental study on vibration scattering using open and in-filled (GeoFoam) wave barriers. *Soil Dynamics and Earthquake Engineering*, *31*(3), 306–317. https://doi.org/https://doi.org/10.1016/j.soildyn.2010.08.010

Andersen, L., Nielsen, S.R.K. (2005). Reduction of ground vibration by means of barriers or soil improvement along a railway track. *Soil Dynamics and Earthquake Engineering*, *25*(7), 701–716. https://doi.org/https://doi.org/10.1016/j.soildyn.2005.04.007

Antes, H., Von Estorff, O. (1994). Dynamic response of 2D and 3D block foundations on a halfspace with inclusions. *Soil Dynamics and Earthquake Engineering*, *13*(5), 305–311. https://doi.org/https://doi.org/10.1016/0267-7261(94)90022-1

Arlaud, E., Costa, S., & Balmes, E. (2020). Receptance of railway tracks at low frequency : Numerical and experimental approaches Elodie Arlaud , Sofia Costa d ' Aguiar , Etienne Balmes To cite this version : HAL Id : hal-02569120 experimental approaches. https://doi.org/10.1016/j.trgeo.2016.06.003

Astley, R. J. (2000). Infinite elements for wave problems: a review of current formulations and an assessment of accuracy. *International Journal for Numerical Methods in Engineering*, *49*(7), 951–976. https://doi.org/https://doi.org/10.1002/1097-

0207(20001110)49:7<951::AID-NME989>3.0.CO;2-T

ASTM D6817. (2017). Standard Specification for Rigid Cellular Polystyrene Geofoam. West Conshohocken, PA: ASTM International. Retrieved from www.astm.org

Auersch, L. (2008). The effect of critically moving loads on the vibrations of soft soils and isolated railway tracks. *Journal of Sound and Vibration*, *310*(3), 587–607. https://doi.org/https://doi.org/10.1016/j.jsv.2007.10.013

Barbosa, J. M. de O., Park, J., Kausel, E. (2012). Perfectly matched layers in the thin layer method. *Computer Methods in Applied Mechanics and Engineering*, *217–220*, 262–274. https://doi.org/10.1016/j.cma.2011.12.006

Bartlett, S.F., Lingwall, B.N., Vaslestad, J. (2015). Methods of protecting buried pipelines and culverts in transportation infrastructure using EPS geofoam. *Geotextiles and Geomembranes*, *43*(5), 450–461. https://doi.org/10.1016/j.geotexmem.2015.04.019

Baziar, M. H., Kazemi, M., Shahnazari, H. (2019). Mitigation of ground vibrations induced by high speed railways using double geofoam barriers: Centrifuge modeling. *Geotextiles and Geomembranes*, *47*(6), 712–728. https://doi.org/https://doi.org/10.1016/j.geotexmem.2019.103482

Beskos, D. E., Dasgupta, B., Vardoulakis, I. G., Engineering, M. (1986). Vibration isolation using open or filled trenches. *Computational Mechanics*, *1:43*, 1975–1976. https://doi.org/https://doi.org/10.1007/BF00298637

Bettess, P., Zienkiewicz, O. C. (1977). Diffraction and refraction of surface waves using finite and infinite elements. *International Journal for Numerical Methods in Engineering*, *11*(8), 1271–1290. https://doi.org/https://doi.org/10.1002/nme.1620110808

Bian, X., Cheng, C., Jiang, J., Chen, R., Chen, Y. (2016). Numerical analysis of soil vibrations due to trains moving at critical speed. *Acta Geotechnica*, *11*(2), 281–294. https://doi.org/10.1007/s11440-014-0323-2

Bo, Q., Ali, L., Irini, D.-M. (2014). Numerical study of wave barrier and its optimization design. *Finite Elements in Analysis and Design*, *84*, 1–13. https://doi.org/https://doi.org/10.1016/j.finel.2014.02.002

Byun, Y. H., Cho, S. H., Yoon, H. K. (1996). Evaluation of void ratio and elastic modulus of unsaturated soil using elastic waves, 1089–1092.

Cao, Z. G., Cai, Y. Q., Sun, H. L., Xu, C. J. (2011). Dynamic responses of a poroelastic half-space from moving trains caused by vertical track irregularities. *International Journal for Numerical and Analytical Methods in Geomechanics*, *35*(7), 761–786. https://doi.org/https://doi.org/10.1002/nag.919

CASIM. (2014). Draft code for the assessment and structural interventions on masonry structures. Athens, Greece: Earthquake Planning Protection Organization (EPPO) and European Centre on Prevention and Forecasting of Earthquakes (ECPFE).

Casini, F., Vassallo, R., Mancuso, C., Desideri, A. (2008). *Application to a compacted soil of a Cam Clay model extended to unsaturated conditions*. https://doi.org/10.1201/9780203884430.ch82

Celebi, E. (2006). Three-dimensional modelling of train-track and sub-soil analysis for surface vibrations due to moving loads. *Applied Mathematics and Computation*, *179* (1), 209–230. https://doi.org/https://doi.org/10.1016/j.amc.2005.11.095

Çelebi, E., Göktepe, F. (2012). Non-linear 2-D FE analysis for the assessment of isolation performance of wave impeding barrier in reduction of railway-induced surface waves. *Construction and Building Materials*, *36*, 1–13. https://doi.org/https://doi.org/10.1016/j.conbuildmat.2012.04.054

Chew, J. H., Leong, E. C. (2019). Field and numerical modelling of sand-rubber mixtures vibration barrier. *Soil Dynamics and Earthquake Engineering*, *125*, 105740. https://doi.org/https://doi.org/10.1016/j.soildyn.2019.105740

Clark, R., Dean, P. A., Elkins, J., Newton, S. G. (1982). An Investigation into the Dynamic Effects of Railway Vehicles Running on Corrugated Rails. *Archive: Journal of Mechanical Engineering Science 1959-1982 (Vols 1-23)*, *24*, 65–76.

Connolly, D., Giannopoulos, A., Forde, M. C. (2013). Numerical modelling of ground borne vibrations from high speed rail lines on embankments. *Soil Dynamics and Earthquake Engineering*, *46*, 13–19. https://doi.org/10.1016/j.soildyn.2012.12.003

Connolly, D. P., Galvín, P., Olivier, B., Romero, A., & Kouroussis, G. (2019). A 2 .5D time-frequency domain model for railway induced soil-building vibration due to railway defects, *120* (January), 332–344. https://doi.org/10.1016/j.soildyn.2019.01.030

Connolly, D.P., Kouroussis, G., Laghrouche, O., Ho, C.L., Forde, M.C. (2015). Benchmarking railway vibrations - Track, vehicle, ground and building effects. *Construction and Building Materials*, *92*, 64–81. https://doi.org/10.1016/j.conbuildmat.2014.07.042

Connolly, D.P., Kouroussis, G., Woodward, P.K., Alves Costa, P., Verlinden, O., Forde, M. C. (2014). Field testing and analysis of high speed rail vibrations. *Soil Dynamics and Earthquake Engineering*, *67*, 102–118. https://doi.org/https://doi.org/10.1016/j.soildyn.2014.08.013

Corbridge, C., Griffin, M.J., Harborough, P.R. (1989). Seat Dynamics and Passenger

Comfort. *Proceedings of the Institution of Mechanical Engineers, Part F: Journal of Rail and Rapid Transit*, 203(1), 57–64. https://doi.org/10.1243/PIME_PROC_1989_203_209_02

Corbridge M., Colins M., Griffin, M. (1991). Effects of vertical vibration on passenger activities: writing and drinking. *Ergonomics*, *34*(10), 1313–1332. https://doi.org/10.1080/00140139108964870

Costa, P. A., Colaço, A., Calçada, R., Cardoso, A. S. (2015). Critical speed of railway tracks. Detailed and simplified approaches. *Transportation Geotechnics*, *2*, 30–46. https://doi.org/https://doi.org/10.1016/j.trgeo.2014.09.003

Coulier, P, Cuéllar, V., Degrande, G., & Lombaert, G. (2015). Experimental and numerical evaluation of the effectiveness of a stiff wave barrier in the soil. *Soil Dynamics and Earthquake Engineering*, *77*, 238–253. https://doi.org/https://doi.org/10.1016/j.soildyn.2015.04.007

Coulier, P, Dijckmans, A., François, S., Degrande, G., Lombaert, G. (2014). A spatial windowing technique to account for finite dimensions in 2.5D dynamic soil–structure interaction problems. *Soil Dynamics and Earthquake Engineering*, *59*, 51–67. https://doi.org/https://doi.org/10.1016/j.soildyn.2014.01.006

Coulier, P, François, S., Degrande, G., Lombaert, G. (2013). Subgrade stiffening next to the track as a wave impeding barrier for railway induced vibrations. *Soil Dynamics and Earthquake Engineering*, *48*, 119–131. https://doi.org/https://doi.org/10.1016/j.soildyn.2012.12.009

Coulier, Pieter, Dijckmans, A., Jiang, J., Thompson, D., Degrande, G., Lombaert, G. (2013). *Stiff Wave Barriers for the Mitigation of Railway Induced Vibrations*. *Notes on Numerical Fluid Mechanics and Multidisciplinary Design* (Vol. 126). https://doi.org/10.1007/978-3-662-44832-8_63

CSI. (2012). Code of Structural Interventions. Final harmonized text, English temporary version V1. Athens, Greece: Harmonization Team of Code of Interventions to Eurocodes. Earthquake Planning Protection Organization (EPPO).

Dahlberg, T. (2010). Railway Track Stiffness Variations – Consequences and Countermeasures. *IJCE*, *8*(1), 1–12. Retrieved from http://ijce.iust.ac.ir/article-1-420-en.html

Degrande, G., Schillemans, L. (2001). Free field vibrations during the passage of a thalys high-speed train at variable speed. *Journal of Sound and Vibration*, *247*(1), 131–144. https://doi.org/https://doi.org/10.1006/jsvi.2001.3718

Dijckmans, A., Coulier, P., Jiang, J., Toward, M.G.R., Thompson, D.J., Degrande, G.,

Lombaert, G. (2015). Mitigation of railway induced ground vibration by heavy masses next to the track. *Soil Dynamics and Earthquake Engineering*, *75*, 158–170. https://doi.org/https://doi.org/10.1016/j.soildyn.2015.04.003

Dijckmans, A., Ekblad, A., Smekal, A., Degrande, G., Lombaert, G. (2016). Efficacy of a sheet pile wall as a wave barrier for railway induced ground vibration. *Soil Dynamics and Earthquake Engineering*, *84*, 55–69. https://doi.org/https://doi.org/10.1016/j.soildyn.2016.02.001

DIN (Deutsches Institut für Normung). (1999a). Structural vibrations - Part 3: Effects of vibration on structures.

DIN (Deutsches Institut für Normung). (1999b). Structural vibrations – Part 2: Human exposure to vibration in buildings. National Standards of Germany (in German).

Drake, L. A. (1972). Love and Rayleigh waves in nonhorizontally layered media. *Bulletin of the Seismological Society of America*, *62*(5), 1241–1258. https://doi.org/10.1785/BSSA0620051241

EC8-1. (2004). Design of structures for earthquake resistance Part 1: General rules, seismic actions and rules for buildings. Brussels, Belgium: European Committee for Standardization.

EC8-3. (2004). Design of structures for earthquake resistance Part 3: Assessment and retrofitting of buildings. Brussels, Belgium: European Committee for Standardization.

Ekanayake, S. D., Liyanapathirana, D. S., Leo, C. J. (2014). Attenuation of ground vibrations using in- filled wave barriers. *Soil Dynamics and Earthquake Engineering*, *67*, 290–300. https://doi.org/10.1016/j.soildyn.2014.10.004

El Kacimi, A., Woodward, P. K., Laghrouche, O., Medero, G. (2013). Time domain 3D finite element modelling of train-induced vibration at high speed. *Computers and Structures*, *118*, 66–73. https://doi.org/10.1016/j.compstruc.2012.07.011

ELOT (2005). Greek National Annex to Eurocode 8: Design of structures for earthquake resistance - Part 1: General rules, seismic actions and rules for buildings. Athens, Greece: Hellenic Organization for Standardization.

Emre, H., Bhattacharya, S., Karamitros, D., Alexander, N. (2018). Experimental and numerical modelling of buried pipelines crossing reverse faults. *Soil Dynamics and Earthquake Engineering*, *114* (July), 198–214. https://doi.org/10.1016/j.soildyn.2018.06.013

EPPO. (2011). Draft Framework regulatory document for structural interventions and

seismic protection of monuments. Athens, Greece: Earthquake Planning Protection Organization (EPPO) and European Centre on Prevention and Forecasting of Earthquakes (ECPFE).

Federal Transit Administration. (1997). Wheel/Rail Noise Control Manual. Washington D.C: Transportation Research Board, National Research Council.

FEMA 349. (2000). Action plan for performance based seismic design. Washington, DC, USA: Federal Emergency Management Agency.

Feng, S. J., Zhang, X. L., Zheng, Q. T., Wang, L. (2017). Simulation and mitigation analysis of ground vibrations induced by high-speed train with three dimensional FEM. *Soil Dynamics and Earthquake Engineering*, *94*, 204–214. https://doi.org/10.1016/j.soildyn.2017.01.022

Feng, S., Li, J., Zhang, X., Chen, Z., Zheng, Q., Zhang, D. (2019a). Numerical analysis of buried trench in screening surface vibration. *Soil Dynamics and Earthquake Engineering*, *126*, 105822. https://doi.org/https://doi.org/10.1016/j.soildyn.2019.105822

Feng, S., Li, J., Zhang, X., Chen, Z., Zheng, Q., Zhang, D. (2019b). Numerical analysis of buried trench in screening surface vibration. *Soil Dynamics and Earthquake Engineering*, *126*(August), 105822. https://doi.org/10.1016/j.soildyn.2019.105822

Ferreira, P. A., López-Pita, A. (2015). Numerical modelling of high speed train/track system for the reduction of vibration levels and maintenance needs of railway tracks. *Construction and Building Materials*, *79*, 14–21. https://doi.org/https://doi.org/10.1016/j.conbuildmat.2014.12.124

François, S., Schevenels, M., Thyssen, B., Borgions, J., Degrande, G. (2012). Design and efficiency of a composite vibration isolating screen in soil. *Soil Dynamics and Earthquake Engineering*, *39*, 113–127. https://doi.org/https://doi.org/10.1016/j.soildyn.2012.03.007

Galavi, V., & Brinkgreve, R. (2014). *Finite element modelling of geotechnical structures subjected to moving loads*. https://doi.org/10.1201/b17017-44

Galvín, P., & Domínguez, J. (2009). Experimental and numerical analyses of vibrations induced by high-speed trains on the Córdoba–Málaga line. *Soil Dynamics and Earthquake Engineering*, *29*(4), 641–657. https://doi.org/10.1016/j.soildyn.2008.07.001

Galvín, P., François, S., Schevenels, M., Bongini, E., Degrande, G., Lombaert, G. (2010). A 2.5D coupled FE-BE model for the prediction of railway induced vibrations. *Soil Dynamics and Earthquake Engineering*, *30*(12), 1500–1512. https://doi.org/10.1016/j.soildyn.2010.07.001

Galvín, P., Mendoza, D. L., Connolly, D. P., Degrande, G., Lombaert, G., Romero, A. (2018). Scoping assessment of free-field vibrations due to railway traffic. *Soil Dynamics and Earthquake Engineering*, *114*, 598–614. https://doi.org/https://doi.org/10.1016/j.soildyn.2018.07.046

Gao, G., Bi, J., Chen, J. (2020). Vibration mitigation performance of embankments and cuttings in transversely isotropic ground under high-speed train loading. *Soil Dynamics and Earthquake Engineering*, 106478. https://doi.org/https://doi.org/10.1016/j.soildyn.2020.106478

Gao, G., Li, N., Gu, X. (2015). Field experiment and numerical study on active vibration isolation by horizontal blocks in layered ground under vertical loading. *Soil Dynamics and Earthquake Engineering*, *69*, 251–261. https://doi.org/https://doi.org/10.1016/j.soildyn.2014.11.006

Gao, G., Xu, C., Chen, J., Song, J. (2018). Investigation of ground vibrations induced by trains moving on saturated transversely isotropic ground. *Soil Dynamics and Earthquake Engineering*, *104*, 40–44. https://doi.org/10.1016/j.soildyn.2017.09.030

Gao, G. Y., Chen, Q. S., He, J. F., Liu, F. (2012). Investigation of ground vibration due to trains moving on saturated multi-layered ground by 2.5D finite element method. *Soil Dynamics and Earthquake Engineering*, *40*, 87–98. https://doi.org/10.1016/J.SOILDYN.2011.12.003

Gao, G., Yao, S., Yang, J., Chen, J. (2019). Investigating ground vibration induced by moving train loads on unsaturated ground using 2.5D FEM. *Soil Dynamics and Earthquake Engineering*, *124*, 72–85. https://doi.org/https://doi.org/10.1016/j.soildyn.2019.05.034

Gao, M., Tian, S. P., Wang, Y., Chen, Q. S., Gao, G. Y. (2020). Isolation of ground vibration induced by high speed railway by DXWIB : Field investigation. *Soil Dynamics and Earthquake Engineering*, *131* (January), 106039. https://doi.org/10.1016/j.soildyn.2020.106039

Garinei, A., Risitano, G., Scappaticci, L. (2014). Experimental evaluation of the efficiency of trenches for the mitigation of train-induced vibrations. *Transportation Research Part D: Transport and Environment*, *32*, 303–315. https://doi.org/https://doi.org/10.1016/j.trd.2014.08.016

Ghali, A., Neville, M., Brown, T. (2017). *Structural Analysis: A Unified Classical and Matrix Approach, Seventh Edition (7th ed.)*. CRC Press. Retrieved from https://doi.org/10.1201/b22004

Griffin, M. J., Hayward, R.A. (1994). Effects of horizontal whole-body vibration on reading. *Applied Ergonomics*, *25*(3), 165–169. https://doi.org/https://doi.org/10.1016/0003-6870(94)90014-0

Grossoni, I., Andrade, A. R., Bezin, Y., Neves, S. (2018). The role of track stiffness and its spatial variability on long-term track quality deterioration. *Proceedings of the Institution of Mechanical Engineers, Part F: Journal of Rail and Rapid Transit*, *233* (1), 16–32. https://doi.org/10.1177/0954409718777372

Hamdan, N. (2013). Two-Dimensional Numerical Modelling of Wave Propagation in Soil Media Nawras Hamdan Submitted for the degree of Doctor of Philosophy in Geotechnical Engineering Institute for Infrastructure & Environment, (September).

Hanazato, T., Ugai, K., Mori, M., Sakaguchi, R. (1991). Three-Dimensional Analysis of Traffic-Induced Ground Vibrations. *Journal of Geotechnical Engineering*, *117*(8), 1133–1151. https://doi.org/10.1061/(ASCE)0733-9410(1991)117:8(1133)

Hanson, C. E., Towers, D. A., Meister, L. D., Miller, H. M. (2006). *Transit noise and vibration impact assessment, relatório técnico.*

Heckl, M., Hauck, G., Wettschureck, R. (1996). Structure-Borne Sound and Vibration from Rail Traffic. *Journal of Sound Vibration*, *193*, 175–184. https://doi.org/10.1006/jsvi.1996.0257

Hesami, S., Ahmadi, S., Ghalesari, A. T. (2016). Numerical modeling of train-induced vibration of nearby multi-story building: A case study. *KSCE Journal of Civil Engineering*, *20* (5), 1701–1713. https://doi.org/10.1007/s12205-015-0264-9

Horvath, J. S. (1994). Expanded Polystyrene (EPS) geofoam: An introduction to material behavior. *Geotextiles and Geomembranes*, *13*(4), 263–280. https://doi.org/https://doi.org/10.1016/0266-1144(94)90048-5

Hung, H.H., Yang, Y.B., Chang, D.W. (2004). Wave Barriers for Reduction of Train-Induced Vibrations in Soils. *Journal of Geotechnical and Geoenvironmental Engineering*, *130*(12), 1283–1291. https://doi.org/10.1061/(ASCE)1090-0241(2004)130:12(1283)

ISO (International Organization for Standardization). (1997). *Mechanical vibration and shock - Evaluation of human exposure to whole-body vibration - Part 1: General requirements.* Geneva, Switzerland: International Organization for Standardization.

ISO (International Organization for Standardization). (2003). Mechanical vibration and shock - evaluation of human exposure to whole-body vibration - Part 2: Vibration in buildings (1-80Hz). Geneva, Switzerland: International Organization for Standardization.

Jalil, N. A. A., Griffin, M. J. (2007). Fore-and-aft transmissibility of backrests: Effect of backrest inclination, seat-pan inclination, and measurement location. *Journal of Sound and Vibration*, *299*(1–2), 99–108. https://doi.org/10.1016/j.jsv.2006.06.053

Jayawardana, P., Thambiratnam, D.P., Perera, N., Chan, T. (2019). Dual in-filled trenches for vibration mitigation and their predictions using artificial neural network. *Soil Dynamics and Earthquake Engineering*, *122*, 107–115. https://doi.org/https://doi.org/10.1016/j.soildyn.2019.04.006

Kanda, H., Ishii, H., Yoshioka, O. (2006). Use of Gas Cushions for Field Measurement and Analysis of Hybrid Vibration Isolation Wall. *Transportation Research Record*, *1983*(1), 42–50. https://doi.org/10.1177/0361198106198300107

Kargarnovin, M.H., Younesian, D., Thompson, D., Jones, C. (2005). Ride comfort of high-speed trains travelling over railway bridges. *Vehicle System Dynamics*, *43*(3), 173–197. https://doi.org/10.1080/00423110512331335111

Karlström, A., Boström, A. (2007). Efficiency of trenches along railways for trains moving at sub- or supersonic speeds. *Soil Dynamics and Earthquake Engineering*, *27*(7), 625–641. https://doi.org/https://doi.org/10.1016/j.soildyn.2006.12.005

Katsanos, E.I., Sextos, A.G. (2013). ISSARS: An integrated software environment for structure-specific earthquake ground motion selection. *Advances in Engineering Software*, *58*, 70–85. https://doi.org/https://doi.org/10.1016/j.advengsoft.2013.01.003

Khalaj, O., Azizian, M., Darabi, N. J., Tafreshi, S.N.M., & Jirková, H. (2020). The role of expanded polystyrene and geocell in enhancing the behavior of buried HDPE pipes under trench loading using numerical analyses. *Geosciences (Switzerland)*, *10*(7), 1–15. https://doi.org/10.3390/geosciences10070251

Khan, M.R., & Dasaka, S.M. (2019). Quantification of ground-vibrations generated by high speed trains in ballasted railway tracks. *Transportation Geotechnics*, *20* (March), 100245. https://doi.org/10.1016/j.trgeo.2019.100245

Khan, M. R., & Dasaka, S. M. (2020). EPS Geofoam as a Wave Barrier for Attenuating High-Speed Train-Induced Ground Vibrations: A Single-Wheel Analysis. *International Journal of Geosynthetics and Ground Engineering*, *6*(4), 43. https://doi.org/10.1007/s40891-020-00230-1

Khan, M. S., Sundstrom, J. (2007). Effects of Vibration on Sedentary Activities in Passenger Trains. *Journal of Low Frequency Noise, Vibration and Active Control*, *26*(1), 43–55. https://doi.org/10.1260/026309207781487448

Kim, H., Choi, B., Kim, J. (2010). Reduction of Earth Pressure on Buried Pipes by EPS Geofoam Inclusions. *Geotechnical Testing Journal*, *33*(4), 304–313. https://doi.org/10.1520/GTJ102315

Knothe, K. L., Grassie, S. L. (1993). Modelling of Railway Track and Vehicle/Track Interaction at High Frequencies. *Vehicle System Dynamics*, *22*(3–4), 209–262. https://doi.org/10.1080/00423119308969027

Kontoni, D. N., Farghaly, A.A. (2020). Mitigation of train-induced vibrations on nearby high-rise buildings by open or geofoam-filled trenches. *Journal of Vibroengineering*, *22*(2), 416–426. https://doi.org/10.21595/jve.2019.20523

Kouroussis, G., Verlinden, O. (2013). Prediction of railway induced ground vibration through multibody and finite element modelling. *Mechanical Sciences*, *4*(1), 167–183. https://doi.org/10.5194/ms-4-167-2013

Kouroussis, G., Verlinden, O., & Conti, C. (2011). Free field vibrations caused by high-speed lines: Measurement and time domain simulation. *Soil Dynamics and Earthquake Engineering*. https://doi.org/10.1016/j.soildyn.2010.11.012

Kouroussis, G., Anastasopoulos, Conti, C. (2011). Discrete modeling of vertical track–soil coupling for vehicle–track dynamics. *Soil Dynamics and Earthquake Engineering*, *31*, 1711–1723. https://doi.org/10.1016/j.soildyn.2011.07.007

Kouroussis, G., Connolly, D.P., Alexandrou, G., Vogiatzis, K. (2015). The effect of railway local irregularities on ground vibration. *Transportation Research Part D: Transport and Environment*, *39*, 17–30. https://doi.org/https://doi.org/10.1016/j.trd.2015.06.001

Kouroussis, G., Connolly, D. P., Forde, M. C., Verlinden, O. (2015). Train speed calculation using ground vibrations. *Proceedings of the Institution of Mechanical Engineers, Part F: Journal of Rail and Rapid Transit*, *229*(5), 466–483. https://doi.org/10.1177/0954409713515649

Kouroussis, G., Connolly, D.P., Olivier, B., Laghrouche, O., Costa, P.A. (2016). Railway cuttings and embankments: Experimental and numerical studies of ground vibration. *Science of the Total Environment*. https://doi.org/10.1016/j.scitotenv.2016.03.016

Kouroussis, G., Conti, C., Verlinden, O. (2014). Building vibrations induced by human activities : A benchmark of existing standards. *Mechanics and Industry*, *15*(5), 345–353. https://doi.org/10.1051/meca/2014041

Kouroussis, G., Verlinden, O., Conti, C. (2011). Finite-Dynamic Model for Infinite Media: Corrected Solution of Viscous Boundary Efficiency. *Journal of Engineering Mechanics*, *137*(7), 509–511. https://doi.org/10.1061/(ASCE)EM.1943-7889.0000250

Lakušić, S., Ahac, M. (2012). Rail traffic noise and vibration mitigation measures in urban areas. *Tehnicki Vjesnik*, *19*(2), 427–435.

Lamb, H. (1904). On the propagation of tremors over the surface of an elastic solid. *Philosophical Transactions of the Royal Society of London. Series A, Containing Papers of a Mathematical or Physical Character*, *203*(359–371), 1–42. https://doi.org/10.1098/rsta.1904.0013

Lee, J., Jin, B., & Ji, Y.G. (2009). Development of a Structural Equation Model for ride comfort of the Korean high-speed railway. *International Journal of Industrial Ergonomics*, *39*, 7–14. https://doi.org/10.1016/j.ergon.2008.09.003

Lesgidis, N., Sextos, A., Moschen, L., Gutierrez Gomez, J. S., Pistone, E. (2020). Rigorous vehicle-soil-track simulation of high-speed rail through optimization-based model order reduction. *Transportation Geotechnics*, *23*(March), 100350. https://doi.org/10.1016/j.trgeo.2020.100350

Li, S. (2014). *Evaluation and numerical modeling of deflections and vertical displacement of rail systems supported by eps geofoam embankments*. MSc Thesis, The University of Utah.

Li, T., Su, Q., Kaewunruen, S. (2020). Seismic metamaterial barriers for ground vibration mitigation in railways considering the train-track-soil dynamic interactions. *Construction and Building Materials*, *260*, 119936. https://doi.org/https://doi.org/10.1016/j.conbuildmat.2020.119936

Liolios, A., Profillidis, V., Christodoulidis, D., Tantanozis, N. (2002). A computational approach to the dynamic soil-pipeline interaction induced by high-speed railway traffic, 259–262.

Lo, L., Fard, M., Subic, A., Jazar, R. (2013). Structural dynamic characterization of a vehicle seat coupled with human occupant. *Journal of Sound and Vibration*, *332*(4), 1141–1152. https://doi.org/10.1016/j.jsv.2012.10.010

López-Mendoza, D., Connolly, D. P., Romero, A., Kouroussis, G., Galvín, P. (2020). A transfer function method to predict building vibration and its application to railway defects. *Construction and Building Materials*, *232*, 117217. https://doi.org/https://doi.org/10.1016/j.conbuildmat.2019.117217

Lyratzakis, A., Tsompanakis, Y. (2018a). Impact of soil saturation level on the dynamic response of masonry buildings, *4* (May), 1–14. https://doi.org/10.3389/fbuil.2018.00024

Lyratzakis A., Tsompanakis Y. (2018b). Dynamic response of masonry buildings considering the time-dependent soil saturation conditions. 9th GRACM International

Congress on Computational Mechanics, Chania, 4-6 June, 2018, paper 37.

Lyratzakis A., Tsompanakis Y., Psarropoulos P.N. (2019). Assessment of high-speed train induced vibrations using efficient numerical models. In: Sapountzakis EJ, Banerjee M, Biswas P, Inan E (eds), Proceedings of the 14th International Conference on Vibration Problems, Hersonisos Crete, 1-4 September 2019. Lecture Notes in Mechanical Engineering. Springer. https://doi.org/10.1007/978-981-15-8049-9_7.

Lyratzakis A., Tsompanakis Y., Psarropoulos P. (2020). Efficient mitigation of high-speed trains induced vibrations of railway embankments using expanded polystyrene blocks. Transportation Geotechnics, 22 (2020), 100312. https://doi.org/10.1016/j.trgeo.2019.100312.

Lyratzakis A., Tsompanakis Y., Psarropoulos P.N. (2021a). Mitigation of HST-induced vibrations by EPS blocks applied in railway embankments. Invited paper for Special Issue "Noise and Vibration from Transportation". Journal of Zhejiang University-SCIENCE A, 22, 6–20. https://doi.org/10.1631/jzus.A1900680.

Lyratzakis A., Tsompanakis Y, Psarropoulos P.N. (2021b). Mitigating high-speed train vibrations for various soil conditions. Soil Dynamics and Earthquake Engineering, 141(2021), 106482. https://doi.org/10.1016/j.soildyn.2020.106482.

Lyratzakis A., Tsompanakis Y, Psarropoulos P.N. (2021c). Mitigation of vibrations in high-speed railway cuttings using expanded-polystyrene blocks. Transportation Geotechnics, 29 (2021), 100572. https://doi.org/10.1016/j.trgeo.2021.100572.

Lyratzakis A., Tsompanakis Y., Psarropoulos P.N. (2021d). Efficient mitigation of high-speed train vibrations on adjacent reinforced concrete buildings. Construction and Building Materials, 125653, https://doi.org/10.1016/j.conbuildmat.2021.125653.

Lyratzakis A., Tsompanakis Y., Psarropoulos P.N. (2021e). Protection of buried pipelines from high-speed trains vibrations with EPS geofoam (under review).

Lyratzakis A., Tsompanakis Y., Psarropoulos P.N. (2021f). Mitigating the impact of high-speed train vibrations on adjacent buildings. 10th GRACM International Congress on Computational Mechanics, Athens, 5-7 June, 2021.

Lysmer, J., Drake, L. A. (1971). The propagation of Love waves across nonhorizontally layered structures. *Bulletin of the Seismological Society of America*, *61*(5), 1233–1251. https://doi.org/10.1785/BSSA0610051233

Majumder, M., Bhattacharyya, S. (2021). ANN-Based Model to Predict the Screening Efficiency of EPS Geofoam Filled Trench in Reducing High-Speed Train-Induced Vibration. https://doi.org/10.1007/978-981-15-9978-7_16

Massarsch, R. (2021, June 18). Vibration Isolation Using Gas-filled Cushions. *Soil Dynamics Symposium in Honor of Professor Richard D. Woods*. https://doi.org/doi:10.1061/40780(159)7

Mohitpour, M., Golshan, H., Murray, A. (2007). *Pipeline Design & Construction: A Practical Approach, Third Edition*. ASME Press. https://doi.org/10.1115/1.802574

Moliner, E., Museros, P., Martínez-Rodrigo, M.D. (2012). Retrofit of existing railway bridges of short to medium spans for high-speed traffic using viscoelastic dampers. *Engineering Structures*, *40*, 519–528. https://doi.org/https://doi.org/10.1016/j.engstruct.2012.03.016

MSC Marc. (2014). Marc 2014.2 software documentation. Newport Beach, California, USA: MSC Software Corporation.

Murillo, C., Thorel, L., Caicedo, B. (2009). Geotextiles and Geomembranes Ground vibration isolation with geofoam barriers: Centrifuge modeling. *Geotextiles and Geomembranes*, *27*(6), 423–434. https://doi.org/10.1016/j.geotexmem.2009.03.006

Nakamura, N. (2017). Time history response analysis using extended Rayleigh damping model. *Procedia Engineering*, *199*, 1472–1477. https://doi.org/https://doi.org/10.1016/j.proeng.2017.09.408

Neupane, R. (2015). *Expanded polystyrene geofoam embankment for support of railways and bridges*. MSc Thesis. The University of Utah.

Ngamkhanong, C., Kaewunruen, S. (2020). Effects of under sleeper pads on dynamic responses of railway prestressed concrete sleepers subjected to high intensity impact loads. *Engineering Structures*, *214*, 110604. https://doi.org/https://doi.org/10.1016/j.engstruct.2020.110604

NPRA. (2010). *Håndbok 016: Geoteknikk i vegbygging (in Norwegian)*.

Park, J., Kausel, E. (2004). Impulse response of elastic half-space in the wave number-time domain. *Journal of Engineering Mechanics-Asce*, *130*, 1211–1222. https://doi.org/10.1061/(ASCE)0733-9399(2004)130:10(1211)

Park Seismic. (2013). Multichannel analysis of surface waves.

PEER. (2015). PEER NGA-West2 ground motion database.

Pflanz, G., Hashimoto, K., Chouw, N. (2002). Reduction of structural vibrations induced by a moving load. *Journal of Applied Mechanics*, *5*, 555–563. https://doi.org/10.2208/journalam.5.555

Pierce, A. (1989). *Acoustics: An Introduction to Its Physical Principles and Applications*. *Physics Today - PHYS TODAY* (Vol. 34). https://doi.org/10.1063/1.2914388

Pita, A. L., Teixeira, P. F., & Robuste, F. (2004). High speed and track deterioration: The role of vertical stiffness of the track. *Proceedings of the Institution of Mechanical Engineers, Part F: Journal of Rail and Rapid Transit*, *218*(1), 31–40. https://doi.org/10.1243/095440904322804411

Pollard, M. G., Simons, N. J. A. (1984). Passenger Comfort—the Role of Active Suspensions. *Proceedings of the Institution of Mechanical Engineers, Part D: Transport Engineering*, *198*(3), 161–175. https://doi.org/10.1243/PIME_PROC_1984_198_143_02

Popp, K., Kruse, H., Kaiser, I. (1999). Vehicle-Track Dynamics in the Mid-Frequency Range. *Vehicle System Dynamics*, *31*(5–6), 423–464. https://doi.org/10.1076/vesd.31.5.423.8363

Pyl, L., Masoumi, H. R., Degrande, G. (2007). The influence of dynamic soil – structure interaction on traffic induced vibrations in buildings, *27*, 655–674. https://doi.org/10.1016/j.soildyn.2006.11.008

Rasouli, H., Fatahi, B. (2020). Geotextiles and Geomembranes Geofoam blocks to protect buried pipelines subjected to strike-slip fault rupture. *Geotextiles and Geomembranes*, *48*(3), 257–274. https://doi.org/10.1016/j.geotexmem.2019.11.011

Rayleigh, L. (1885). On Waves Propagated along the Plane Surface of an Elastic Solid. *Proceedings of the London Mathematical Society*, *s1-17*(1), 4–11. https://doi.org/https://doi.org/10.1112/plms/s1-17.1.4

Remington, P.J. (1976). Wheel/rail noise— Part I: Characterization of the wheel/rail dynamic system. *Journal of Sound Vibration*, *46*, 359–379. https://doi.org/10.1016/0022-460X(76)90861-0

Remington, P.J. (1988). Wheel/rail rolling noise: What do we know? What don't we know? Where do we go from here? *Journal of Sound and Vibration*, *120*(2), 203–226. https://doi.org/https://doi.org/10.1016/0022-460X(88)90430-0

Ribes-llario, F., Marzal, S., Zamorano, C., Real, J. (2017). Numerical Modelling of Building Vibrations due to Railway Traffic : Analysis of the Mitigation Capacity of a Wave Barrier. *Shock and Vibration*, *2017*, 11.

Rokhlin, S. I., Wang, L. (2002). Stable recursive algorithm for elastic wave propagation in layered anisotropic media: stiffness matrix method. *The Journal of the Acoustical Society of America*, *112*(3 Pt 1), 822–834. https://doi.org/10.1121/1.1497365

Rudd, M. J. (1976). Wheel/rail noise—Part II: Wheel squeal. *Journal of Sound Vibration*, *46*, 381–394. https://doi.org/10.1016/0022-460X(76)90862-2

Saboya, F., Tibana, S., Martins, R., Durand, A., Maria, C., & Rangel, D. A. (2020). Centrifuge and numerical modeling of moving tra ffi c surface loads on pipelines buried in cohesionless soil. *Transportation Geotechnics*, *23*(January), 100340. https://doi.org/10.1016/j.trgeo.2020.100340

Sadeghi, J., & Vasheghani, M. (2021). Safety of buildings against train induced structure borne noise. *Building and Environment*, *197*(February), 107784. https://doi.org/10.1016/j.buildenv.2021.107784

Sanayei, M., Kayiparambil P., A., Moore, J. A., Brett, C. R. (2014). Measurement and prediction of train-induced vibrations in a full-scale building. *Engineering Structures*, *77*, 119–128. https://doi.org/https://doi.org/10.1016/j.engstruct.2014.07.033

Sayeed, M.A., Shahin, M.A. (2016a). Three-dimensional numerical modelling of ballasted railway track foundations for high-speed trains with special reference to critical speed. *Transportation Geotechnics*, *6*, 55–65. https://doi.org/10.1016/J.TRGEO.2016.01.003

Schweizerische Normen-Vereinigung, S.-640312a. (1992). Les ´ebranlements – Effet des ´ebranlements sur les constructions (Swiss Standard on vibration effects on buildings).

Sheng, X., Jones, C. J. C., Thompson, D. J. (2006). Prediction of ground vibration from trains using the wavenumber finite and boundary element methods. *Journal of Sound and Vibration*, *293*(3–5), 575–586. https://doi.org/10.1016/j.jsv.2005.08.040

Singh, D. V, Seth, Y. (2017). 3D Modelling of Ground Surface Vibration Induced by Underground Train Movement. *Procedia Engineering*, *173*, 1580–1586. https://doi.org/https://doi.org/10.1016/j.proeng.2016.12.253

Sitharam, T. G., Sebastian, R., Fazil, F. (2018). Vibration isolation of buildings housed with sensitive equipment using open trenches – Case study and numerical simulations. *Soil Dynamics and Earthquake Engineering*, *115*, 344–351. https://doi.org/https://doi.org/10.1016/j.soildyn.2018.08.033

Spyrakos, C. (2018). Bridging Performance Based Seismic Design with Restricted Interventions on Cultural Heritage Structures. *Engineering Structures*, *160*. https://doi.org/10.1016/j.engstruct.2018.01.022

Spyrakos, C., & Maniatakis, C. (2016). *Seismic protection of monuments and historic structures – the seismo research project*. https://doi.org/10.7712/100016.2187.15540

Stark, T. D., Bartlett, S. F., Arellano, D. (2012). Expanded polystyrene (EPS) geofoam applications and technical data. *The EPS Industry Alliance*.

Stavroulaki, M., Liarakos, E. (Vagelis). (2008). *Parametric finite element analysis of masonry structures using different constitutive models*. https://doi.org/10.13140/RG.2.1.1519.1523

Stiebel, D. (2011). Protocol for free field measurement of mitigation. RIVAS—DeliverableD1.2.

Stiebel, D., Muller, R., Bongini, E., Ekbald, A., Coquel, G., & Alguacil, A. (2012). *Definition of reference cases typical for hot-spots in Europe with existing vibration problems*.

Sun, Y., Jiang, Z., Gu, J., Zhou, M., Li, Y., Zhang, L. (2018). Analyzing high speed rail passengers train choices based on new online booking data in China. *Transportation Research Part C*, *97*(February), 96–113. https://doi.org/10.1016/j.trc.2018.10.015

Suzuki, H., Shiroto, H., Tezuka, K. (2005). Effects of Low Frequency Vibration on Train Motion Sickness. *Quarterly Report of RTRI*, *46*(1), 35–39. https://doi.org/10.2219/rtriqr.46.35

Tafreshi, S. N. M., Darabi, N. J., Dawson, A. R. (2020). Geotextiles and Geomembranes Combining EPS geofoam with geocell to reduce buried pipe loads and trench surface rutting. *Geotextiles and Geomembranes*, *48*(3), 400–418. https://doi.org/10.1016/j.geotexmem.2019.12.011

Takemiya, H. (2004). Field vibration mitigation by honeycomb WIB for pile foundations of a high-speed train viaduct. *Soil Dynamics and Earthquake Engineering*, *24*(1), 69–87. https://doi.org/https://doi.org/10.1016/j.soildyn.2003.07.005

Talbot, J. P., Hunt, H. E. M. (2003a). Isolation of Buildings from Rail-Tunnel Vibration: A Review. *Building Acoustics*, *10*(3), 177–192. https://doi.org/10.1260/135101003322661998

Talbot, J. P., & Hunt, H. E. M. (2003b). The effect of side-restraint bearings on the performance of base-isolated buildings. *Proceedings of the Institution of Mechanical Engineers, Part C: Journal of Mechanical Engineering Science*, *217*(8), 849–859. https://doi.org/10.1243/095440603322310404

Thompson, D. J., Jiang, J., Toward, M. G. R., Hussein, M. F. M., Dijckmans, A., Coulier, P., Lombaert, G. (2015). Mitigation of railway-induced vibration by using subgrade stiffening. *Soil Dynamics and Earthquake Engineering*, *79*, 89–103. https://doi.org/https://doi.org/10.1016/j.soildyn.2015.09.005

Thompson, D. J., Jiang, J., Toward, M. G. R., Hussein, M. F. M., Ntotsios, E., Dijckmans, A., Degrande, G. (2016). Reducing railway-induced ground-borne vibration by using open trenches and soft-filled barriers. *Soil Dynamics and Earthquake Engineering*, *88*,

45–59. https://doi.org/https://doi.org/10.1016/j.soildyn.2016.05.009

Thornely-Taylor, R. (2004). The prediction of vibration, groundborne and structure-radiated noise from railways using finite difference methods-Part I-Theory. *Proc Inst Acoust*, *26*.

U.S. Department of Transportation. (1998). High-Speed Ground Transportation Noise and Vibration Impact Assessment.

Vazouras, P., Karamanos, S. A., Dakoulas, P. (2010). Finite element analysis of buried steel pipelines under strike-slip fault displacements. *Soil Dynamics and Earthquake Engineering*, *30*(11), 1361–1376. https://doi.org/10.1016/j.soildyn.2010.06.011

Vér, I. L., Ventres, C. S., Myles, M. M. (1976). Wheel/rail noise—Part III: Impact noise generation by wheel and rail discontinuities. *Journal of Sound and Vibration*, *46*(3), 395–417. https://doi.org/https://doi.org/10.1016/0022-460X(76)90863-4

Wathelet, M. (2008a). An improved neighborhood algorithm: Parameter conditions and dynamic scaling. *Geophysical Research Letters*, *35*(9). https://doi.org/https://doi.org/10.1029/2008GL033256

Wathelet, M. (2008b). www.Geopsy.org.

WHO/Europe. (2018). Environmental Noise Guidelines for the European Region. Copenhagen, Denmark: WHO Regional Office for Europe.

With, C., Bahrekazemi, M., Bodare, A. (2009). Wave barrier of lime–cement columns against train-induced ground-borne vibrations. *Soil Dynamics and Earthquake Engineering*, *29*(6), 1027–1033. https://doi.org/https://doi.org/10.1016/j.soildyn.2008.12.005

Witthoeft, A. F., Kim, H. (2016). Numerical investigation of earth pressure reduction on buried pipes using EPS geofoam compressible inclusions. *Geosynthetics International*, *23*(4), 287–300. https://doi.org/10.1680/jgein.15.00054

Woldringh, R. F., New, B. M. (1999). Embankment design for high speed trains on soft soils. *Geotechnical Engineering for Transportation Infrastructure. Proceedings of the 12th European Conference on Soil Mechanics and Geotechincal Engineering, Amsterdam, June 1999. Vol. 3.*, 1703–1712.

Woods, R. D. (1968). Screening of Surface Waves in Soils. *Journal of the Soil Mechanics and Foundations Division*, *94*, 951–979. https://doi.org/10.1061/JSFEAQ.0001180

Wook, Y., Abdoun, T. H., Rourke, M. J. O., Ha, D. (2007). Remediation for buried pipeline systems under permanent ground deformation, *27*, 1043–1055. https://doi.org/10.1016/j.soildyn.2007.04.002

Yang, J., Zhu, S., Zhai, W., Kouroussis, G., Wang, Y., Wang, K., … Xu, F. (2019). Prediction and mitigation of train-induced vibrations of large-scale building constructed on subway tunnel. *Science of The Total Environment*, *668*, 485–499. https://doi.org/https://doi.org/10.1016/j.scitotenv.2019.02.397

Yang, Y.-B., & Hung, H.-H. (1997). A parametric study of wave barriers for reduction of train-induced vibrations. *International Journal for Numerical Methods in Engineering*, *40*(20), 3729–3747. https://doi.org/10.1002/(SICI)1097-0207(19971030)40:20<3729::AID-NME236>3.0.CO;2-8

Yang, Y. B., Ge, P., Li, Q., Liang, X., & Wu, Y. (2018). 2.5D vibration of railway-side buildings mitigated by open or infilled trenches considering rail irregularity. *Soil Dynamics and Earthquake Engineering*, *106*, 204–214. https://doi.org/https://doi.org/10.1016/j.soildyn.2017.12.027

Yao, J., Zhao, R., Zhang, N., & Yang, D. (2019). Vibration isolation effect study of in-filled trench barriers to train-induced environmental vibrations. *Soil Dynamics and Earthquake Engineering*, *125*(May), 105741. https://doi.org/10.1016/j.soildyn.2019.105741

Yarmohammadi, F., Rafiee-Dehkharghani, R., Behnia, C., Aref, A. J. (2018). Topology optimization of jet-grouted overlapping columns for mitigation of train-induced ground vibrations. *Construction and Building Materials*, *190*, 838–850. https://doi.org/https://doi.org/10.1016/j.conbuildmat.2018.09.156

Yarmohammadi, F., Rafiee-Dehkharghani, R., Behnia, C., & Aref, A. J. (2019). Design of wave barriers for mitigation of train–induced vibrations using a coupled genetic-algorithm/finite-element methodology. *Soil Dynamics and Earthquake Engineering*, *121*, 262–275. https://doi.org/https://doi.org/10.1016/j.soildyn.2019.03.007

Zhang, L., Huang, J. (2019). Dynamic interaction analysis of the high-speed maglev vehicle / guideway system based on a fi eld measurement and model updating method. *Engineering Structures*, *180*, 1–17. https://doi.org/10.1016/j.engstruct.2018.11.031

Zhang, X., Thompson, D., & Sheng, X. (2020). Differences between Euler-Bernoulli and Timoshenko beam formulations for calculating the effects of moving loads on a periodically supported beam. *Journal of Sound and Vibration*, *481*, 115432. https://doi.org/https://doi.org/10.1016/j.jsv.2020.115432

Zhao, N., Sanayei, M., Moore, J., Zapfe, J., & Hines, E. (2010). Mitigation of Train-Induced Floor Vibrations in Multi-Story Buildings Using a Blocking Floor. https://doi.org/10.1061/41130(369)199

Zou, C., Moore, J. A., Sanayei, M., Wang, Y., & Tao, Z. (2021). Efficient impedance model for the estimation of train-induced vibrations in over-track buildings. *JVC/Journal of Vibration and Control*, *27*(7–8), 924–942. https://doi.org/10.1177/1077546320935285

Zou, C., Wang, Y., Moore, J. A., & Sanayei, M. (2017). Train-induced field vibration measurements of ground and over-track buildings. *Science of the Total Environment*, *575*, 1339–1351. https://doi.org/10.1016/j.scitotenv.2016.09.216